2013

Computational investigation of the mechanism of action of DNA glycosylases

Kellie, Jennifer L.

Lethbridge, Alta. : University of Lethbridge, Dept. of Chemistry and Biochemistry

COMPUTATIONAL INVESTIGATION OF THE MECHANISM OF

ACTION OF DNA GLYCOSYLASES

JENNIFER L. KELLIE
B. Sc. in Chemistry, University of Lethbridge, 2007
M. Sc. in Chemistry, University of Lethbridge, 2009

A Thesis
Submitted to the School of Graduate Studies
of the University of Lethbridge
in Partial Fulfillment of the
Requirements for the Degree

DOCTOR OF PHILOSOPHY
in Biomolecular Science

Department of Chemistry and Biochemistry
University of Lethbridge
LETHBRIDGE, ALBERTA, CANADA

COMPUTATIONAL INVESTIGATION OF THE
MECHANISM OF ACTION OF DNA GLYCOSYLASES

JENNIFER L. KELLIE

Approved:

(Signature)   (Rank)   (Highest Degree)   Date

_____   _____   _____   _____

Supervisor

_____   _____   _____   _____

Thesis Examination Committee Member

_____   _____   _____   _____

Thesis Examination Committee Member

_____   _____   _____   _____

Thesis Examination Committee Member

_____   _____   _____   _____

External Examiner

_____   _____   _____   _____

Chair, Thesis Examination Committee

Abstract

The integrity of the base pair sequence that makes up the information storage system of cells is under continual assault. Two of the most prevalent forms of nucleobase damage are conversion of cytosine to uracil, and guanine to 8-oxoguanine. Repair of these lesions is initiated by a specific glycosylase that hydrolyzes the N-glycosidic (sugar–nucleobase) bond of the damaged nucleotide. The present thesis uses advanced computational chemistry techniques to study the mechanism of action of three glycosylases, namely human uracil–DNA glycosylase (hUNG2), adenine–DNA glycosylase (MutY) and human 8-oxoguanine–DNA glycosylase (hOgg1). Truncated active-site models treated entirely with quantum mechanics, and reaction potential energy surfaces, provide detailed structural and energetic information regarding how these enzymes catalyze deglycosylation of their substrates. From these results, a novel and informative method for predicting the mechanism (e.g., degree of asychronicity) and relative rate is proposed.

Acknowledgements

I would like to thank my husband, Sean, and my family. Without their continued support throughout my academic career I would not have accomplished what I have.

Thanks to my supervisor, Dr. Stacey Wetmore for providing me with the opportunity to work in her lab and develop my teaching skills, and for supporting my efforts throughout the years. I also want to thank the Wetmore group for their insightful discussions, especially when I was having convergence issues and it looked like I would never get anywhere with hOgg1.

I would like to thank my committee members, Drs. Peter Dibble, Steven Mosimann and Brent Selinger, for their support and helpful comments about my research and studies.

I want to thank the Teaching Centre and everyone who attended the Talking about Teaching and Professional Development events. Our discussions inspired me to continue in my studies and helped me become a better student and teacher.

I would like to thank the University of Lethbridge and the Natural Sciences and Engineering Research Council (NSERC) for funding. I thank WestGrid, part of the Compute/Calcul Canada high-performance computing platform, and the URACIL computing cluster for computational resources.

Finally, I want to thank Tracey and the rest of the graduate students in the Chemistry and Biochemistry Department for sanity-instilling conversations.

Table of Contents

List of Figures

List of Tables

List of Abbreviations

AAG	Alkyl adenine–DNA glycosylase (EC # 3.2.2.21)
ACS	American Chemical Society
aDZ	Dunning's aug-cc-pVDZ basis set
AID	Activation-induced deaminase (EC # 3.5.4.5)
AlkA	3-Methyladenine–DNA glycosylase I (EC # 3.2.2.21)
APE1	AP-endonuclease 1 (EC # 4.2.99.18)
AP-site	Apurinic/apyrimidinic site, abasic site
B1B95	Becke 88 exchange with Becke 95 correlation density functional
B3LYP	Becke 88 exchange with Lee-Yang-Parr correlation density functional
B97-2	B97-2 exchange and correlation functionals
BB1K	Becke 88 exchange with Becke 95 correlation density functional
BER	Base excision repair
BP86	Becke 88 exchange with Perdew 86 correlation density functional
BSSE	Basis set superposition error
CBS	Complete basis set
CCSD(T)	Coupled-cluster method with singles, doubles and perturbative triples
DFT	Density functional theory
DNA	Deoxyribonucleic acid
dsDNA	Double-stranded DNA
εA	Ethenoadenine
EndoIII	Endonuclease III
eUDG	*Escherichia coli* uracil–DNA glycosylase (EC # 3.2.2.27)
FdA	2′-fluorodeoxyadenine
FEN1	Flap-endonuclease 1 (EC # 3.1.21.1)
FLRC	Lesion recognition complex of MutY bound to 2′-fluorodeoxyadenine
FPG	Formamidopurine–DNA glycosylase (a.k.a. MutM) (EC # 3.2.2.23)
HF	Hartree-Fock

hMYH	Human homologue of adenine–DNA glycosylase (EC # 3.2.2.–)
hOgg1	Human 8-oxoguanine–DNA glycosylase (EC # 3.2.2.–, 4.2.99.18)
hTDG	Human thymine–DNA glycosylase (EC # 3.2.2.29)
hUNG2	Human uracil–DNA glycosylase (EC # 3.2.2.27)
IEF-PCM	Integral-equation formalism polarizable continuum method
KIE	Kinetic isotope effect
Lig1	DNA ligase 1 (EC # 6.5.1.1)
LRC	Lesion recognition complex of MutY
M06-2X	Minnesota M06 functional with double HF exchange
MAP	hMYH-associated polyposis
MD	Molecular dynamics
meA	3-methyladenine
MM	Molecular mechanics
MMUE	Average of a set of mean unsigned errors
MP2	Møller-Plesset 2nd order perturbation theory
MPW1K	Modified Perdew-Wang91 exchange with Perdew-Wang91 correlation functional
MPWB1K	Modified Perdew-Wang91 exchange with Becke95 correlation functional
MUD	Mean unsigned deviation
MUE	Mean unsigned error
MUPD	Mean unsigned percent deviation
MutM	Formamidopurine–DNA glycosylase (a.k.a. FPG) (EC # 3.2.2.23)
MutT	8-oxoguanosine triphosphate hydrolase (EC # 3.6.1.55)
MutY	Adenine–DNA glycosylase (EC # 3.2.2.–)
NEIL1	Endonuclease VIII-like glycosylase (EC # 3.2.2.-, 4.2.99.18)
NER	Nucleotide excision repair
OG	7,8-dihydro-8-oxoguanine, 8-oxoguanine
ONIOM	Our-own N-layered integrated molecular orbital method
PES	Potential energy surface
PM3	Parameterized model 3 semi-empirical method

PM6	Parameterized model 6 semi-empirical method
Polβ	Repair DNA polymerase β (EC # 2.7.7.7)
Polε	DNA polymerase ε (EC # 2.7.7.7)
ψU	Pseudouridine
QM	Quantum mechanics
QST	Quadratic synchronous transit method
RI-MP2	Resolution of identity Møller-Plesset 2nd order perturbation theory
RMSD	Root mean square deviation
RNA	Ribonucleic acid
ROS	Reactive oxygen species
RSC	Royal Society of Chemistry
SCF	Self-consistent field
SE	Semi-empirical
S_N1	Unimolecular nucleophilic substitution
S_N2	Bimolecular nucleophilic substitution
ssDNA	Single-stranded DNA
TDG	Thymine–DNA glycosylase (EC # 3.2.2.29)
TS	Transition state
WC	Watson-Crick
ωB97X-D	ωB97X exchange and correlation with Grimme's –D correction
ZPVE	Zero-point vibrational energy

Nucleobase and Nucleoside Abbreviations

A	Adenine	dA	2′-deoxyadenosine
C	Cytosine	dC	2′-deoxycytidine
G	Guanine	dG	2′-deoxyguanosine
T	Thymine	dT	2′-deoxythymidine
U	Uracil	dU	2′-deoxyuridine
OG	8-oxoguanine	dOG	2′-deoxy-8-oxoguanosine

Single- and Triple-Letter Codes for the Amino Acids

A	Ala	Alanine
C	Cys	Cysteine
D	Asp	Aspartate, aspartic acid
E	Glu	Glutamate, glutamic acid
F	Phe	Phenylalanine
G	Gly	Glycine
H	His	Histidine
I	Ile	Isoleucine
K	Lys	Lysine
L	Leu	Leucine
M	Met	Methionine
N	Asn	Asparagine
P	Pro	Proline
Q	Gln	Glutamine
R	Arg	Arginine
S	Ser	Serine
T	Thr	Threonine
V	Val	Valine
W	Trp	Tryptophan
Y	Tyr	Tyrosine

List of Models and Mechanisms

Chapter Two

AS   Active-site optimization test set

HB   Hydrogen-bonding test set

PP   Stacking and T-shaped interaction test set

PT   Proton transfer test set

SN2 S_N2 hydrolysis test set

UNI   Unimolecular cleavage test set

Chapter Three

wat_{Asp}^{Pro} hUNG2 ONIOM model with water nucleophile interacting with D145 and P146 with a neutral H148.

$wat_{Asp}^{Pro}(+)$ hUNG2 ONIOM model with water nucleophile interacting with D145 and P146 with a cationic H148.

wat_{Asp}^{His} hUNG2 ONIOM model with water nucleophile interacting with D145 and H148.

Chapter Four

CS-Cap   MutY ONIOM model with D144 helix-capping interaction in place and new orientaiton of E188.

CS-NoCap   MutY ONIOM model with D144 helix-capping interaction broken and new orientaiton of E188.

CS-Y126F   MutY ONIOM model with D144 helix-capping interaction in place, new orientaiton of E188, and Y126F mutation.

X-WT   MutY ONIOM model with X-ray coordinates for D144 and E188.

X-D144N   MutY ONIOM model with X-ray coordinates for D144 and E188, and D144N mutation.

Mechanism A   Hydrolysis mechanism with Wat28 as the nucleophile.

Mechanism B   Hydrolysis mechanism with Wat50 as the nucleophile.

Mechanism C   Hydrolysis mechanism with contributions from D144 and Wat28.

Chapter Five

$D-N_RC_R$ Lyase mechanism with direct ring opening, proton transfer of $N–H_R$ and abstraction of $C–H_R$.

D-N$_R$C$_S$ Lyase mechanism with direct ring opening, proton transfer of N–H$_R$ and abstraction of C–H$_S$.

D-N$_S$C$_R$ Lyase mechanism with direct ring opening, proton transfer of N–H$_S$ and abstraction of C–H$_R$.

D-N$_S$C$_S$ Lyase mechanism with direct ring opening, proton transfer of N–H$_S$ and abstraction of C–H$_S$.

A-N$_R$C$_R$ Lyase mechanism with base-assisted ring opening, proton transfer of N–H$_R$ and abstraction of C–H$_R$.

A-N$_R$C$_S$ Lyase mechanism with base-assisted ring opening, proton transfer of N–H$_R$ and abstraction of C–H$_S$.

A-N$_S$C$_R$ Lyase mechanism with base-assisted ring opening, proton transfer of N–H$_S$ and abstraction of C–H$_R$.

A-N$_S$C$_S$ Lyase mechanism with base-assisted ring opening, proton transfer of N–H$_S$ and abstraction of C–H$_S$.

Chapter Six

K249–Nuc   hOgg1 monofunctional mechanism with K249 as nucleophile for deglycosylation, where the crosslink is immediately hydrolyzed.

D268–GB   hOgg1 monofunctional mechanism with a water nucleophile and D268 as the general base.

K249–GB   hOgg1 monofunctional mechanism with a water nucleophile and K249 as the general base.

Chapter Seven

BE_{Sum} Summation prediction method based on corrections from potential energy surface scans.

BE_{R1} Distance-dependent prediction method with the correction to vertical separation based on tilt angle.

BE_{Tilt} Tilt-dependent prediction method with corrections for vertical separation and tilt angle.

Chapter 1: Thesis Introduction

1.1 DNA Background

One of the primary classes of biological molecules is the nucleic acids, which can be divided into deoxyribonucleic acids (DNA) and ribonucleic acids (RNA). The basic structure of these two types differs in the substitution of the sugar unit (Figure 1.1), where the 2′-hydroxyl is absent in DNA. The only other difference in chemical composition between the two types of nucleic acids is the library of nitrogenous bases attached to the sugar. In DNA, the pyrimidine thymine (T) replaces uracil (U) found in RNA, which differs in chemical composition by a single methyl group; both nucleic acids use the purines, adenine (A) and guanine (G), and the pyrimidine cytosine (C) (Figure 1.1). These relatively small chemical modifications lead to different structures and function, which are outlined below.
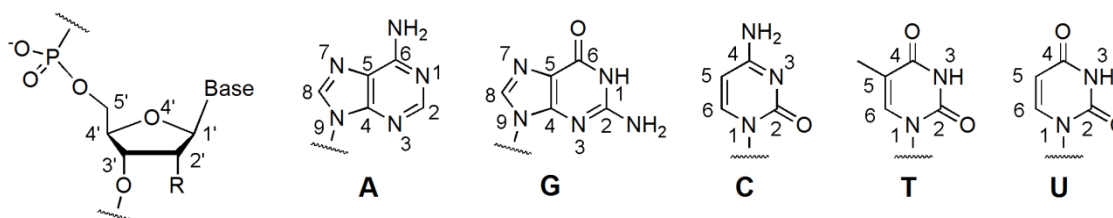
Figure 1.1. *The structural definition of a nucleic acid (R = H in DNA, R = OH in RNA), where a strand is generated by attaching the 5' phosphate of one nucleotide to the 3' end of the previous nucleotide. The base is attached to the sugar moiety via an N-glycosidic bond and can be one of the natural nucleobases, where adenine (**A**), guanine (**G**) and cytosine (**C**) are common to both DNA and RNA, thymine (**T**) occurs only in DNA and uracil (**U**) in RNA. The conventional numbering for the nucleobases and sugar moiety are included.*

RNA is relatively short lived, and its production is strictly monitored.[1] It is generally single stranded, although the secondary structure may involve self-pairing leading to double-stranded regions. Some of the instability of RNA can be attributed to the 2′-hydroxyl, which can act as a nucleophile and react with the nearby 3′-phosphate to self-cleave the backbone of the strand. The single-stranded nature of RNA introduces additional difficulties. For example, there is no way to tell if the sequence has become compromised due to damage to the nucleobases. Since

RNA has a wide variety of functions including coding for proteins, catalyzing reactions and signal regulation,[1] small changes in the sequence have large downstream effects. It is therefore beneficial that most RNA is short-lived and quickly recycled to prevent damage propagation.

In contrast to RNA, DNA has a single purpose: to store the genetic information an organism requires to survive in a sequence of nucleobases. There is only one copy of DNA in a cell, and therefore it is essential that the integrity of the nucleobase sequence is maintained throughout the life of the cell. Watson and Crick published the first description of the structure of DNA, which outlined the double-helical nature of the molecule.[2-3] The two strands of DNA run in antiparallel directions, with the phosphodiester linkages on the outside of the helix, and the nucleobases on the inside of the helix. The nucleobases form hydrogen-bonding pairs with G opposite C and A opposite T (Figure 1.2). This purine–pyrimidine pairing yields almost identical distances between the backbones of both pairs, which gives DNA a highly regular structure.[2-3]
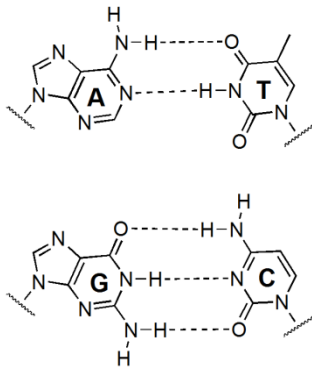
Figure 1.2. The Watson-Crick hydrogen-bonding pattern for the A:T (top) and G:C (bottom) pairs.

The specific base pairing (G:C and A:T) in DNA provides the genetic information stored in the nucleic acid sequence a level of redundancy. In their seminal paper on the structure of DNA, Watson and Crick proposed that the base pairing could be used as a template for copying DNA.[2] Furthermore, the redundancy inherent to double-stranded DNA implies that if a nucleobase becomes damaged, the correct replacement can be determined by reading the other strand. In contrast to the short life of RNA, the DNA nucleobases are protected by the double-

helical nature that decreases solvent accessibility through, for example, steric blocking of the hydrogen-bonding face. Additionally, the integrity of the nucleobase sequence is partially maintained by the stability of the solvent-accessible backbone. For example, the half-life to hydrolysis of the phosphate backbone is ~31,000,000 years at 25°C, 1 atm and pH 7,[4] and the glycosidic bond that connects the nucleobase to the sugar has a half-life between ~70 (G) and ~230 (C) years.[4–6]

1.2 DNA Damage

Despite the inherent stability of DNA, there are many ways the nucleobases can become damaged, which can roughly be separated into two categories: bulky damage and non-bulky damage. Bulky nucleobase lesions include damage such as intrastrand crosslinks[7] and addition products (e.g., involving phenoxyl radicals,[8] or polyaromatic systems[9]), and are often cytotoxic because they block DNA replication and/or transcription. In contrast, non-bulky damage, such as deamination, oxidation and alkylation, often leads to changes in less than three atoms, and are usually carcinogenic and/or cytotoxic.[10–13] This Thesis focuses on two of the most common forms of non-bulky damage: deamination of cytosine and oxidation of guanine, and these examples will be discussed in detail below.

1.2.1 Deamination of Cytosine to Uracil

Spontaneous hydrolytic degradation of deoxycytidine (dC) to deoxyuridine (dU, Figure 1.3) occurs with a half-life of ~120 years.[4] Cytosine can also be deaminated by a variety of small molecules such as bisulphite[14–15] and nitrous anhydride (N_2O_3).[16–17] Some protection from deamination is provided through hydrogen bonding of the exocyclic amine in C to G in double-stranded DNA (dsDNA) (Figure 1.2). Indeed, it has been found that the rate of spontaneous cytosine deamination is 140-fold faster in single-stranded DNA (ssDNA) than in dsDNA.[18] During replication and transcription, the DNA helix partially unwinds, which generates local

areas with single-stranded nature and increases the susceptibility of the nucleobases to deamination or other forms of attack. It has been shown that uracil appears in DNA at a rate of ~200 bases/cell/day,[19] where this value is dependent on the phase of the cell (e.g., higher during proliferation). Cytosine can additionally be deaminated to uracil by proteins, such as activation-induced deaminase (AID, EC# 3.5.4.5).[20] When cytosine is converted to uracil, a premutagenic U:G base pair is generated. Subsequently, during replication or transcription, U will be recognized as T and A will be placed opposite U, which leads to a C:G to T:A transversion mutation. As a testament to the importance of correcting this lesion, half of the identified human glycosylase repair proteins have uracil as a substrate.[21–22]
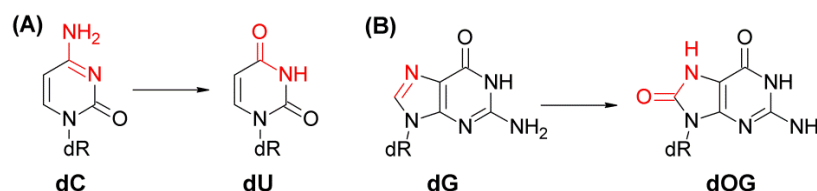
Figure 1.3. *The two most common forms of nucleobase damage in DNA: a) deamination of deoxycytidine (dC) to deoxyuridine (dU), and b) oxidation of deoxyguanosine (dG) to 8-oxo-deoxyguanosine (dOG).*

1.2.2 Oxidation of Guanine to 8-Oxoguanine

The unsaturated C8–N7 bond of guanine (Figure 1.3) is vulnerable to attack by reactive oxygen species (ROS),[23–24] naturally occurring metabolic intermediates and products such as $^{\bullet}$OH, and H_2O_2. Due to a combination of the prevalence of ROS, and the fact that the C8–N7 bond is unprotected in the double helix (does not take part in hydrogen bonding with C), oxidation of G to 8-oxoguanine (OG) is the most abundant form of DNA damage.[25] Specifically, it has been found that OG formation takes place an average of 1,000 times/cell/day,[26] which is five times more often than cytosine deamination.

The OG lesion is particularly problematic since it can form a Watson-Crick (WC) hydrogen-bond pair with C or, by rotating about the glycosidic bond, the OG Hoogsteen face can

interact with A (Figure 1.4). Neither of these two base pairs cause distortion to the helix,[27–30] and in fact, the main replicative polymerase (Polε, EC # 2.7.7.7) preferentially adds A opposite OG.[31] This preference for pairing with A leads to G:C to T:A transversion mutations, which are among the most common mutations in cancer cells (e.g., lung, breast, ovarian, colorectal and renal).[11]
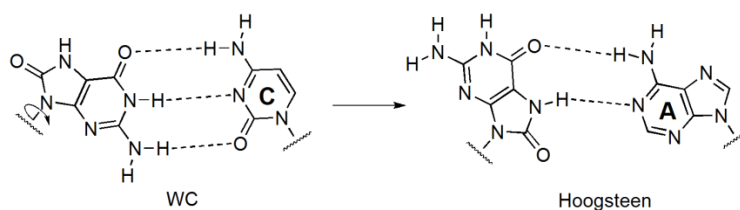
Figure 1.4. The 8-oxoguanine lesion can hydrogen bond either in a Watson-Crick (WC, anti orientation) fashion with cytosine (C) or in a Hoogsteen fashion (syn orientation) with adenine (A) by rotating about its glycosidic bond.

After OG is removed from nucleic acids (both DNA and RNA), it is excreted through the urine. Measurements of the level of urinary OG have found elevated concentrations in (lung) cancer patients, where this value increases during both radio and chemotherapy.[32] This connection has introduced OG as a biomarker for oxidative stress. However, it has not been shown whether the increased oxidative damage in cancer cells is a cause or an effect of the disease.[26]

1.3 DNA Repair

As mentioned above, despite the stability of the DNA helix, damage and errors in the 10^9 base pairs in the human genome (collection of all genes in the cell)[33] is unavoidable. In fact, damage to the genome is continuous, and therefore a broad spectrum of repair mechanisms has developed to prevent damage from persisting.[34] For example, the lesion can be repaired by directly reversing the damage, by removing the nucleobase (base excision repair, BER), or by removing a section of the DNA (nucleotide excision repair, NER).[35–38] The BER pathway repairs some of the most prevalent forms of damage to DNA,[39] including dU[40] and OG,[26] and is thus central to this Thesis.

1.3.1 Base Excision Repair

The BER pathway uses a collection of proteins to remove nucleobase damage from dsDNA and ssDNA. BER is responsible for the repair of non-bulky bases with potentially subtle alterations, generally without long-range effects such as changes in the helical structure. For example, the damaged nucleobase may differ from its natural counterpart by a simple substitution, such as a methyl replacing a proton. Furthermore, nucleobase lesions are relatively rare events, OG is the most common lesion and the ratio of damaged to undamaged base pairs is still only 1:1,000,000.[26] Therefore, the main obstacle that must be overcome by the BER pathway is substrate recognition. To overcome this problem, many BER initiating proteins (glycosylases) 'scan' the nucleic acid strand,[41] thus removing any dependence on diffusion to bring together the protein and substrate. The negatively charged phosphate backbone of DNA is bound at an ~22 Å cleft lined with cationic residues. In addition, the glycosylases often contain an *exo*-site that interrogates nucleotides so that only the substrate is introduced into the active site.[42] In this way, some BER glycosylases appear to catalyze reactions faster than the 3D diffusion limit permits.[41]

As discussed above, the BER pathway is initiated by a glycosylase (Figure 1.5) that scans the DNA backbone for a specific substrate or set of substrates. After a lesion has been found, the damaged nucleotide is flipped out of the DNA helix and into the glycosylase active site. Next, the N-glycosidic bond is cleaved. The chemical step of a monofunctional glycosylase involves a water nucleophile that is activated by an active-site general base, such as aspartate or glutamate. In contrast, bifunctional glycosylases use an active-site amine (such as lysine or N-terminal proline) as the nucleophile and additionally nick the phosphate backbone. For example, human 8-oxoguanine–DNA glycosylase (hOgg1, EC # 3.2.2.–, 4.2.99.18) exhibits β-lyase activity, where the product is a 5′-monophosphate and a modified apurinic/apyrimidinic site (AP-site). The resulting AP-site is highly cytotoxic due to its proclivity to mispair with A, as well as form crosslinks and strand breaks.[43–44] In general, glycosylases have a high affinity for the AP-site and

will stay associated until displaced by an AP-endonuclease (e.g., APE1, EC # 4.2.99.18), which cleaves the 5′ side of the damage and leaves a 3′-hydroxyl on the preceding nucleotide.[43] In short-patch repair, a repair polymerase, such as Polβ (EC # 2.7.7.7), adds one nucleotide to the 3′-end of the template and uses the AP-lyase activity exhibited by its N-terminal domain to remove the remaining extra sugar-phosphate unit.[45] During long-patch repair, the polymerase adds 2 − 8 nucleotides, and the displaced nucleotides and AP-site are removed by a flap-endonuclease (e.g., FEN1, EC # 3.1.21.1). In both cases, DNA ligase 1 (Lig1, EC # 6.5.1.1) closes the nick to regenerate the strand.[45] An overview of the mechanism of action of the monofunctional and bifunctional glycosylases studied in this Thesis will be provided in the next Section.
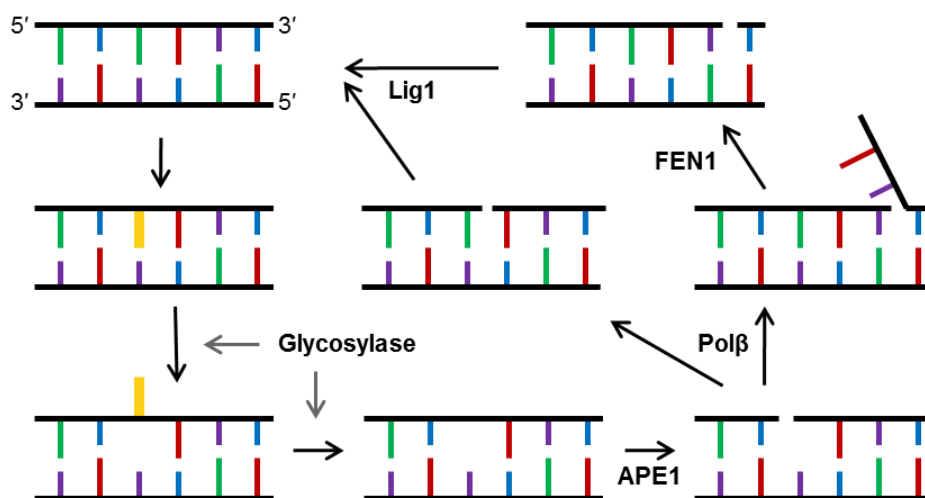
Figure 1.5. *Schematic of the base excision repair (BER) pathway. See Section 1.3.1 for description.*

1.4 Overview of Glycosylases Considered in this Thesis

This Thesis investigates the mechanism of action of three glycosylases that span both mono- and bifunctional activity. All three glycosylases are highly specific for their respective substrates and all three bind strongly to the product AP-site. The only other feature that all three enzymes have in common is an aspartate residue in close proximity to the sugar moiety. A brief

overview of the proposed mechanism of action of these enzymes is provided here, and a more detailed description can be found in the respective Chapters.

1.4.1 Uracil–DNA Glycosylase

The first enzyme modeled in this Thesis is uracil–DNA glycosylase, specifically the human nuclear form hUNG2 (EC 3.2.2.3). The *Escherichia coli* homologue (eUDG) was the first glycosylase discovered,[46] and therefore the largest body of research exists for this protein. Not only is eUDG (and hUNG2) the fastest glycosylase, it is also incredibly specific for uracil. The general proposed mechanism of action involves S_N1 hydrolysis of the dU glycosidic bond and two catalytically essential active-site residues (Figure 1.6). While the non-enzymatic hydrolysis of dU is acid catalyzed,[47–48] the hUNG2 active site is arranged to stabilize the uracil leaving group without protonation of the nucleobase.[49] Specifically, H268 is involved in a strong hydrogen bond with O2 of uracil, and thereby catalyzes the dissociation step of the mechanism.[50–51] The second catalytically essential residue is D145, which has been proposed to electrostatically stabilize the oxacarbenium cation and activate the water nucleophile.[52]
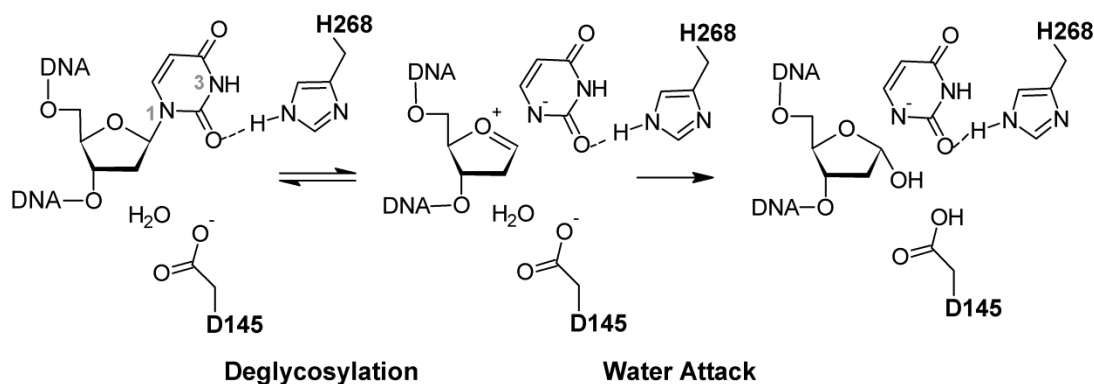
Figure 1.6. *Proposed mechanism of action of human uracil–DNA glycosylase. See Section 1.4.1 for a description.*

1.4.2 Adenine–DNA Glycosylase

Adenine–DNA glycosylase (MutY, EC 3.2.2.3) is a monofunctional glycosylase like hUNG2 that specifically removes adenine paired opposite an OG lesion.[53] MutY activity is an essential step in the process that converts A:OG base pairs to C:OG base pairs, and ensures that all instances of OG are corrected to G instead of T.[54] In contrast to hUNG2, the proposed mechanism of MutY involves protonation of the adenine leaving group (similar to the nonenzymatic depurination of dA)[55–56] by a nearby glutamate residue in the first step (Figure 1.7).[57] This activation step is then followed by S_N1 hydrolysis similar to hUNG2, with nucleophile activation by E43 or D144 (*Geobacillus stearothermophilus* numbering used throughout).[58]
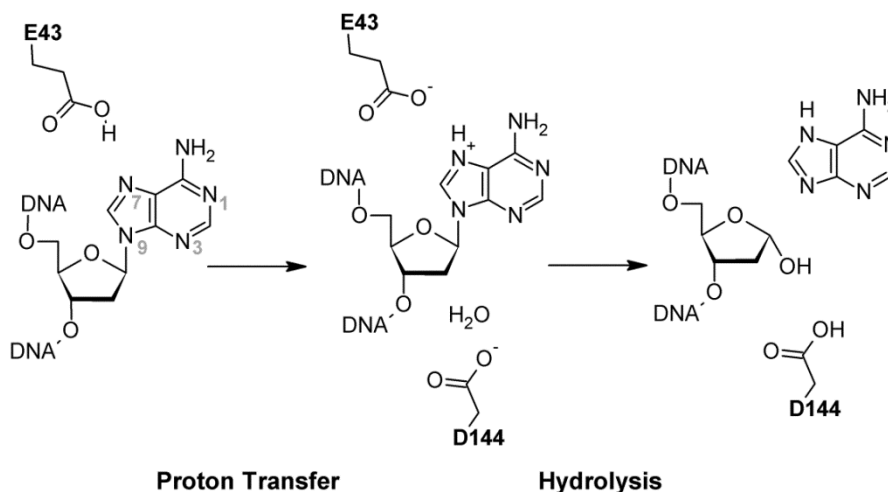
Figure 1.7. *Proposed mechanism of action of adenine–DNA glycosylase. See Section 1.4.2 for a description.*

1.4.3 8-Oxoguanine–DNA Glycosylase

The final enzyme examined in this Thesis is a bifunctional glycosylase, namely hOgg1. As discussed for hUNG2, the OG nucleobase is not protonated prior to deglycosylation. However, the chemical step for hOgg1 is very different from that of hUNG2 or MutY.[41,59] First, the accepted mechanism for hOgg1 involves S_N1 or S_N2 deglycosylation with K249 as the

nucleophile (Figure 1.8).[60] D268 is catalytically important, likely in the deglycosylation step, with

a proposed role of electrostatic stabilization of the oxacarbenium cation-like transition state.[61]

Next, the sugar ring opens and the DNA–protein covalent linkage rearranges to a Schiff base,

which is possibly catalyzed by the OG anion.[60] After rearrangement, the C3′–O3′ bond is broken

through β-elimination with abstraction of either the *pro–R* or the *pro–S* proton on C2′, and the

nucleobase as a cofactor.[60] Finally, the DNA–protein crosslink is hydrolyzed to release the

product and regenerate the enzyme. Recently, hOgg1 has been shown to exhibit monofunctional

activity *in vivo*, although the mechanistic details are as yet unknown.[61–63]
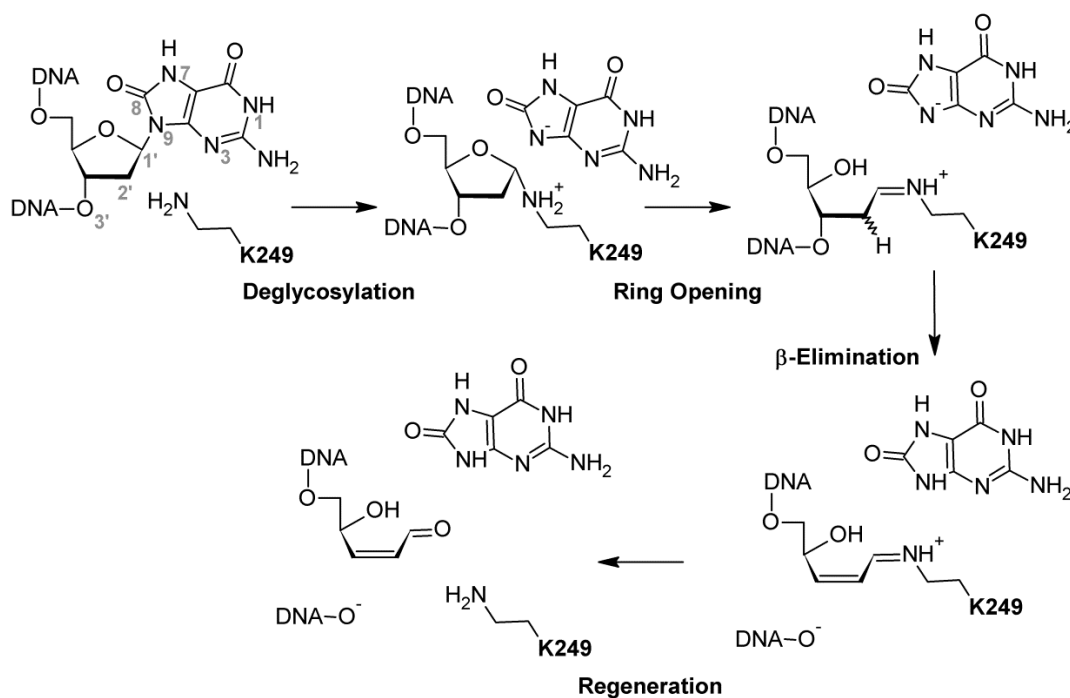
Figure 1.8. *Proposed mechanism of action of human 8-oxoguanine–DNA glycosylase. See Section 1.4.3 for a description.*

1.4.4 Previous Computational Studies

While a plethora of experimental research has been carried out on the glycosylases, there

are still questions regarding how they perform their essential function. For example, X-ray crystal

structures to date have not been obtained with a resolution high enough to accurately place

hydrogen atoms on a structure. Therefore, it is difficult to know the protonation state of many

active-site residues (and the substrate) at various points in the mechanism. Furthermore, it is experimentally challenging to definitively determine the role of the highly conserved active-site aspartate/glutamate residues (electrostatic stabilization and/or nucleophile activation). To this end, computational chemistry can be used to model different components of the various glycosylase mechanisms. In addition, modeling can modify the reaction in ways that may be difficult (or impossible) to replicate experimentally. In this Thesis, computational chemistry is used to compare the monofunctional mechanisms of three glycosylases (hUNG2, MutY and hOgg1) in order to learn the roles of various active-site residues and potentially develop a method of predicting mechanism and rate.

Most of the glycosylases with available protein X-ray crystal structures have been studied to some degree computationally. These studies can be separated into three broad categories based on their primary focus: (1) nucleotide flipping; (2) glycosidic bond and leaving group stability; and (3) deglycosylation mechanism. The computational systems have ranged from small, gas-phase models to full enzyme–substrate complexes. In addition to using a large number of model sizes, a wide variety of methodologies have been implemented. Since the focus of this Thesis is the chemical step, the nucleotide-flipping studies will not be further discussed here.

The chemical step catalyzed by monofunctional glycosylases is significantly less complicated than for the bifunctional glycosylases, and therefore more computational work has used a water nucleophile (activated to some degree). Studies on glycosidic bond stability and nucleobase (N1 for pyrimidines and N9 for purines) acidity have correlated an increased glycosidic bond length and nucleobase acidity with an increased depurination/depyrimidination rate.[64–82] Small model systems (< 100 atoms) have been used to investigate the mechanism of action of thymine–DNA glycosylase (TDG, EC # 3.2.2.29),[83–85] hUNG2,[86–87] MutY,[88] alkyladenine–DNA glycosylase (AAG, EC # 3.2.2.21),[89] hOgg1,[90–93] as well as generic (catalyzed) deglycosylation.[94–96] In addition, large model studies (> 100 atoms) that explicitly

treat the protein environment have been carried out on hUNG2,[97] hOgg1,[98] AAG,[99] and MutY.[100] These investigations into the deglycosylation mechanism have been contradictory in some cases, likely due to differences in computational approach and system contents. Therefore, in addition to modeling the mechanism of action of various glycosylases, a methodological study will be carried out in this Thesis to identify a level of theory that provides consistent results.

1.5 Thesis Overview

Many DNA glycosylases contain an aspartate or glutamate residue in close proximity to the sugar moiety of the bound substrate (See Section 1.4). The primary goal of this Thesis is to determine if there is a universally conserved role for this residue in the monofunctional activity of the DNA glycosylases. To this end, the mechanisms of action of three glycosylases are investigated with hybrid computational methods, density functional theory (DFT) and large enzyme–substrate models. Specifically, ONIOM(DFT:SE) is used to model the reactions, which allows a sizable system (~600 atoms) to be treated entirely with quantum mechanics. Reaction potential energy surfaces (PES) are generated for the various mechanisms to gain an understanding of the contribution of active-site residues along the reaction pathway, in addition to the stationary points. This methodology also permits the characterization of transition states that would be difficult (or impossible) to optimize using standard techniques due to size constraints.

Throughout the Thesis, initial geometries are generated based on X-ray crystal structures that contain no active-site mutations (a 2′-fluoro inhibitor is used) and resolutions ranging from 1.8 – 2.3 Å. Active-site models include a 10 Å sphere about the damaged nucleotide, which provides explicit treatment of the surrounding protein. The reaction center (nucleotide and nucleophile) and nearby (interacting) residues are treated with DFT, while the remainder of the model is constrained and treated with SE. A benefit of this approach over QM/MM techniques is that the high-level region is polarized by the low-level region. In addition, connectivity changes,

such as proton transfer, are permitted throughout the model, rather than being constrained to only the high-level region. Although many studies relax the reactant with molecular dynamics prior to studying the reaction, all conformational searches and reaction surfaces are carried out with QM on the truncated model in this Thesis. This approach allows for a consistent treatment of the active sites across the glycosylases studied, and permits direct comparison of energetics. In addition, since proteins are inherently dynamic, selecting a given geometry for the protein (whether it is constrained or minimized during the reaction phase) is arbitrary. A portion of the error introduced due to this choice should cancel when the energetics are determined.

In Chapter 2, a variety of density functional methods are compared to determine which functional provides the best treatment of the various features important to the deglycosylation mechanism, including reaction kinetics and noncovalent interactions. Chapters 3 and 4 model the monofunctional enzymes hUNG2 and MutY, respectively, taking care to introduce as little bias as possible into the model. Next, the bifunctional glycosylase hOgg1 is investigated. First the many possible mechanisms for glycosylase and β-lyase activity are studied with a small model (Chapter 5), and then a large model study is carried out on possible monofunctional mechanisms (Chapter 6). The active sites of many glycosylases, such as hUNG2 and hOgg1, contain π–π contacts, which require large basis sets and high levels of theory to properly determine the binding energy.[101–102] Since the active-site models used in this Thesis are too large for such a treatment, a method to predict the binding energy of nucleobase–amino acid contacts based on simple geometric variables is developed in Chapter 7. Finally, global conclusions regarding the mechanism of action of DNA glycosylases are presented in Chapter 8, as well as a few applications of the results from this Thesis.

1.6 References[a]

---

[a] Bibliography and citations in ACS (American Chemical Society) format.

(1)   Voet, D.; Voet, J. G., *Biochemistry*. 3 ed.; John Wiley & Sons: 2004.

(2)   Watson, J. D.; Crick, F. H. C., Molecular Structure of Nucleic Acids – A Structure for Deoxyribose Nucleic Acid. *Nature (London, U. K.)* **1953,** *171* (4356), 737–738.

(3)   Watson, J. D.; Crick, F. H. C., Genetical Implications of the Structure of Deoxyribonucleic Acid. *Nature (London, U. K.)* **1953,** *171* (4361), 964–967.

(4)   Schroeder, G. K.; Wolfenden, R., Rates of Spontaneous Disintegration of DNA and the Rate Enhancements Produced by DNA Glycosylases and Deaminases. *Biochemistry* **2007,** *46* (47), 13638–13647.

(5)   Lindahl, T.; Karlstro, O., Heat-Induced Depyrimidination of Deoxyribonucleic Acid in Neutral Solution. *Biochemistry* **1973,** *12* (25), 5151–5154.

(6)   Lindahl, T.; Nyberg, B., Rate of Depurination of Native Deoxyribonucleic Acid. *Biochemistry* **1972,** *11* (19), 3610–3618.

(7)   Rajski, S. R.; Williams, R. M., DNA Cross-Linking Agents as Antitumor Drugs. *Chem. Rev. (Washington, DC, U. S.)* **1998,** *98* (8), 2723–2796.

(8)   Manderville, R. A., Ambient Reactivity of Phenoxyl Radicals in DNA Adduction. *Can. J. Chem.* **2005,** *83* (9), 1261–1267.

(9)   Pfohl-Leszkowicz, A.; Manderville, R. A., An Update on Direct Genotoxicity as a Molecular Mechanism of Ochratoxin A Carcinogenicity. *Chem. Res. Toxicol.* **2011,** *25* (2), 252–262.

(10)   Bohr, V. A.; Ottersen, O. P.; Tonjum, T., Genome Instability and DNA Repair in Brain, Ageing and Neurological Disease. *Neuroscience* **2007,** *145* (4), 1183–1186.

(11)   Greenman, C.; Stephens, P.; Smith, R.; Dalgliesh, G. L.; Hunter, C.; Bignell, G.; Davies, H.; Teague, J.; Butler, A.; Edkins, S.*, et al.*, Patterns of Somatic Mutation in Human Cancer Genomes. *Nature (London, U. K.)* **2007,** *446* (7132), 153–158.

(12)   Kryston, T. B.; Georgiev, A. B.; Pissis, P.; Georgakilas, A. G., Role of Oxidative Stress and DNA Damage in Human Carcinogenesis. *Mutat. Res., Fundam. Mol. Mech. Mutagen.* **2011,** *711* (1-2), 193–201.

(13)   Ziech, D.; Franco, R.; Pappa, A.; Panayiotidis, M. I., Reactive Oxygen Species (ROS) – Induced Genetic and Epigenetic Alterations in Human Carcinogenesis. *Mutat. Res., Fundam. Mol. Mech. Mutagen.* **2011,** *711* (1-2), 167–173.

(14)   Sono, M.; Wataya, Y.; Hayatsu, H., Role of Bisulfite in Deamination and Hydrogen Isotope-Exchange of Cytidylic Acid. *J. Am. Chem. Soc.* **1973,** *95* (14), 4745–4749.

(15)   Chen, H.; Shaw, B. R., Kinetics of Bisulfite-Induced Cytosine Deamination in Single-Stranded-DNA. *Biochemistry* **1993,** *32* (14), 3535–3539.

(16)   Dedon, P. C.; Tannenbaum, S. R., Reactive Nitrogen Species in the Chemical Biology of Inflammation. *Arch. Biochem. Biophys.* **2004,** *423* (1), 12–22.

(17)   Rayat, S.; Qian, M.; Glaser, R., Nitrosative Cytosine Deamination. An Exploration of the Chemistry Emanating from Deamination with Pyrimidine Ring-opening. *Chem. Res. Toxicol.* **2005,** *18* (8), 1211–1218.

(18)   Frederico, L. A.; Kunkel, T. A.; Shaw, B. R., A Sensitive Genetic Assay for the Detection of Cytosine Deamination: Determination of Rate Constants and the Activation Energy. *Biochemistry* **1990,** *29* (10), 2532–2537.

(19)   Kavli, B.; Otterlei, M.; Slupphaug, G.; Krokan, H. E., Uracil in DNA – General Mutagen, but Normal Intermediate in Acquired Immunity. *DNA Repair* **2007,** *6* (4), 505–516.

(20)   Franca, R.; Spadari, S.; Maga, G., APOBEC Deaminases as Cellular Antiviral Factors: A Novel Natural Host Defense Mechanism. *Med. Sci. Monit.* **2006,** *12* (5), RA92–RA98.

(21)   Lindahl, T.; Wood, R. D., Quality Control by DNA Repair. *Science (Washington, DC, U. S.)* **1999,** *286* (5446), 1897–1905.

(22)   Visnes, T.; Doseth, B.; Pettersen, H. S.; Hagen, L.; Sousa, M. M. L.; Akbari, M.; Otterlei, M.; Kavli, B.; Slupphaug, G.; Krokan, H. E., Uracil in DNA and its Processing by Different DNA Glycosylases. *Phys. Trans. R. Soc., B* **2009,** *364* (1517), 563–568.

(23)   Barnett, R. N.; Bongiorno, A.; Cleveland, C. L.; Joy, A.; Landman, U.; Schuster, G. B., Oxidative Damage to DNA: Counterion-Assisted Addition of Water to Ionized DNA. *J. Am. Chem. Soc.* **2006,** *128* (33), 10795–10800.

(24)   Yadav, A.; Mishra, P. C., Carbonate Radical Anion as an Efficient Reactive Oxygen Species: Its Reaction with Guanyl Radical and Formation of 8-Oxoguanine. *Chem. Phys.* **2012,** *405*, 76–88.

(25)   Kamiya, H., Mutagenic Potentials of Damaged Nucleic Acids Produced by Reactive Oxygen/Nitrogen Species: Approaches using Synthetic Oligonucleotides and Nucleotides. *Nucleic Acids Res.* **2003,** *31* (2), 517–531.

(26)   Loft, S.; Danielsen, P. H.; Mikkelsen, L.; Risom, L.; Forchhammer, L.; Moller, P., Biomarkers of Oxidative Damage to DNA and Repair. *Biochem. Soc. Trans.* **2008,** *36*, 1071–1076.

(27)   Dodson, M. L.; Lloyd, R. S., Backbone Dynamics of DNA Containing 8-Oxoguanine: Importance for Substrate Recognition by Base Excision Repair Glycosylases. *Mutat. Res., DNA Repair* **2001,** *487* (3-4), 93–108.

(28)   Cheng, X. L.; Kelso, C.; Hornak, V.; de los Santos, C.; Grollman, A. P.; Simmerling, C., Dynamic Behavior of DNA Base Pairs Containing 8-Oxoguanine. *J. Am. Chem. Soc.* **2005,** *127* (40), 13906–13918.

(29)   Crenshaw, C. M.; Wade, J. E.; Arthanari, H.; Frueh, D.; Lane, B. F.; Nunez, M. E., Hidden in Plain Sight: Subtle Effects of the 8-Oxoguanine Lesion on the Structure, Dynamics, and Thermodynamics of a 15-Base Pair Oligodeoxynucleotide Duplex. *Biochemistry* **2011,** *50* (39), 8463–8477.

(30)   Singh, S. K.; Szulik, M. W.; Ganguly, M.; Khutsishvili, I.; Stone, M. P.; Marky, L. A.; Gold, B., Characterization of DNA with an 8-Oxoguanine Modification. *Nucleic Acids Res.* **2011,** *39* (15), 6789–6801.

(31)   Locatelli, G. A.; Pospiech, H.; Le Gac, N. T.; van Loon, B.; Hubscher, U.; Parkkinen, S.; Syvaoja, J. E.; Villani, G., Effect of 8-Oxoguanine and Abasic Site DNA Lesions on *in vitro* Elongation by Human DNA Polymerase ε in the Presence of Replication Protein A and Proliferating-Cell Nuclear Antigen. *Biochem. J.* **2010,** *429*, 573–582.

(32)   Crohns, M.; Saarelainen, S.; Erhola, M.; Alho, H.; Kellokumpu-Lehtinen, P., Impact of Radiotherapy and Chemotherapy on Biomarkers of Oxidative DNA Damage in Lung Cancer Patients. *Clin. Biochem.* **2009,** *42* (10-11), 1082–1090.

(33)   Blackburn, G. M.; Gait, M, J, *Nucleic Acids in Chemistry and Biology*. 2nd ed.; Oxford University Press: New York, 1996.

(34)   Lindahl, T., Instability and Decay of the Primary Structure of DNA. *Nature (London, U. K.)* **1993,** *362* (6422), 709–715.

(35)   Wood, R. D.; Mitchell, M.; Sgouros, J.; Lindahl, T., Human DNA Repair Genes. *Science (Washington, DC, U. S.)* **2001,** *291* (5507), 1284–1289.

(36)   Sedgwick, B.; Bates, P. A.; Paik, J.; Jacobs, S. C.; Lindahl, T., Repair of Alkylated DNA: Recent Advances. *DNA Repair* **2007,** *6* (4), 429–442.

(37)   Nouspikel, T., DNA Repair in Mammalian Cells. *Cell. Mol. Life Sci.* **2009,** *66* (6), 994–1009.

(38)   Morita, R.; Nakane, S.; Shimada, A.; Inoue, M.; Iino, H.; Wakamatsu, T.; Fukui, K.; Nakagawa, N.; Masui, R.; Kuramitsu, S., Molecular Mechanisms of the Whole DNA Repair System: A Comparison of Bacterial and Eukaryotic Systems. *J. Nucleic Acids* **2010,** (Copyright (C) 2012 American Chemical Society (ACS). All Rights Reserved.), 179594.

(39)   Zharkov, D. O., Base Excision DNA Repair. *Cell. Mol. Life Sci.* **2008,** *65*, 1544–1565.

(40)   Mosbaugh, D. W.; Bennett, S. E., Uracil-Excision DNA-Repair. In *Progress in Nucleic Acid Research and Molecular Biology, Vol 48*, 1994; Vol. 48, pp 315–370.

(41)   Stivers, J. T.; Jiang, Y. L., A Mechanistic Perspective on the Chemistry of DNA Repair Glycosylases. *Chem. Rev. (Washington, DC, U. S.)* **2003,** *103* (7), 2729–2759.

(42)   Banerjee, A.; Yang, W.; Karplus, M.; Verdine, G. L., Structure of a Repair Enzyme Interrogating Undamaged DNA Elucidates Recognition of Damaged DNA. *Nature (London, U. K.)* **2005,** *434* (7033), 612–618.

(43)   Wilson, D. M.; Barsky, D., The Major Human Abasic Endonuclease: Formation, Consequences and Repair of Abasic Lesions in DNA. *Mutat. Res., DNA Repair* **2001,** *485* (4), 283–307.

(44)   Kroeger, K. M.; Hashimoto, M.; Kow, Y. W.; Greenberg, M. M., Cross-Linking of 2-Deoxyribonolactone and its β-Elimination Product by Base Excision Repair Enzymes. *Biochemistry* **2003,** *42* (8), 2449–2455.

(45)   Dianov, G. L.; Allinson, S. L.; Budworth, H.; Sleeth, K., Mammalian Base Excision Repair. *Eukaryotic DNA Damage Surveill. Repair* **2004**, 27–48.

(46)   Lindahl, T.; Ljungquist, S.; Siegert, W.; Nyberg, B.; Sperens, B., DNA N-Glycosidases - Properties of Uracil-DNA Glycosidase from *Escherichia-coli*. *J. Biol. Chem.* **1977,** *252* (10), 3286–3294.

(47)   Garrett, E. R.; Seydel, J. K.; Sharpen, A. J., Acid-Catalyzed Solvolysis of Pyrimidine Nucleosides. *J. Org. Chem.* **1966,** *31* (7), 2219–2227.

(48)   Shapiro, R.; Danzig, M., Acidic Hydrolysis of Deoxycytidine and Deoxyuridine Derivatives. The General Mechanism of Deoxyribonucleoside Hydrolysis. *Biochemistry* **1972,** *11* (1), 23–29.

(49)   Dong, J.; Drohat, A. C.; Stivers, J. T.; Pankiewicz, K. W.; Carey, P. R., Raman Spectroscopy of Uracil DNA Glycosylase-DNA Complexes: Insights into DNA Damage Recognition and Catalysis. *Biochemistry* **2000,** *39* (43), 13241–13250.

(50)   Drohat, A. C.; Xiao, G. Y.; Tordova, M.; Jagadeesh, J.; Pankiewicz, K. W.; Watanabe, K. A.; Gilliland, G. L.; Stivers, J. T., Heteronuclear NMR and Crystallographic Studies of Wild-Type and H187Q *Escherichia coli* Uracil DNA Glycosylase: Electrophilic Catalysis of Uracil Expulsion by a Neutral Histidine 187. *Biochemistry* **1999,** *38* (37), 11876–11886.

(51)   Drohat, A. C.; Stivers, J. T., NMR Evidence for an Unusually Low N1 pK(a) for Uracil Bound to Uracil DNA Glycosylase: Implications for Catalysis. *J. Am. Chem. Soc.* **2000,** *122* (8), 1840–1841.

(52)   Drohat, A. C.; Jagadeesh, J.; Ferguson, E.; Stivers, J. T., Role of Electrophilic and General Base Catalysis in the Mechanism of *Escherichia coli* Uracil DNA Glycosylase. *Biochemistry* **1999,** *38* (37), 11866–11875.

(53)   Noll, D. M.; Gogos, A.; Granek, J. A.; Clarke, N. D., The C-terminal Domain of the Adenine-DNA Glycosylase MutY Confers Specificity for 8-Oxoguanine·Adenine Mispairs and May Have Evolved from MutT, an 8-Oxo-dGTPase. *Biochemistry* **1999,** *38* (20), 6374–6379.

(54)   Michaels, M. L.; Cruz, C.; Grollman, A. P.; Miller, J. H., Evidence That MutY and MutM Combine to Prevent Mutations by an Oxidatively Damaged Form of Guanine in DNA. *Proc. Nat. Acad. Sci. USA* **1992,** *89* (15), 7022–7025.

(55)   Zoltewicz, J. A.; Clark, D. F.; Sharples, T. W.; Grahe, G., Kinetics and Mechanism of Acid-Catalyzed Hydrolysis of Some Purine Nucleosides. *J. Am. Chem. Soc.* **1970,** *92* (6), 1741–1750.

(56)   McCann, J. A. B.; Berti, P. J., Transition State Analysis of Acid-Catalyzed dAMP Hydrolysis. *J. Am. Chem. Soc.* **2007,** *129* (22), 7055–7064.

(57)   McCann, J. A. B.; Berti, P. J., Transition-State Analysis of the DNA Repair Enzyme MutY. *J. Am. Chem. Soc.* **2008,** *130*, 5789–5797.

(58)   Brinkmeyer, M. K.; Pope, M. A.; David, S. S., Catalytic Contributions of Key Residues in the Adenine Glycosylase MutY Revealed by pH-dependent Kinetics and Cellular Repair Assays. *Chem. Biol.* **2012,** *19* (2), 276–286.

(59)   Berti, P. J.; McCann, J. A. B., Toward a Detailed Understanding of Base Excision Repair Enzymes: Transition State and Mechanistic Analyses of N-glycoside Hydrolysis and N-glycoside Transfer. *Chem. Rev. (Washington, DC, U. S.)* **2006,** *106* (2), 506–555.

(60)   Fromme, J. C.; Bruner, S. D.; Yang, W.; Karplus, M.; Verdine, G. L., Product-Assisted Catalysis in Base-Excision DNA Repair. *Nat. Struct. Biol.* **2003,** *10* (3), 204–211.

(61)   Dalhus, B.; Forsbring, M.; Helle, I. H.; Vik, E. S.; Forstrøm, R. J.; Backe, P. H.; Alseth, I.; Bjørås, M., Separation-of-Function Mutants Unravel the Dual-Reaction Mode of Human 8-Oxoguanine DNA Glycosylase. *Structure (Cambridge, MA, U. S.)* **2011,** *19* (1), 117–127.

(62)   Hill, J. W.; Hazra, T. K.; Izumi, T.; Mitra, S., Stimulation of Human 8-Oxoguanine-DNA Glycosylase by AP-endonuclease: Potential Coordination of the Initial Steps in Base Excision Repair. *Nucleic Acids Res.* **2001,** *29* (2), 430–438.

(63)   Vidal, A. E.; Hickson, I. D.; Boiteux, S.; Radicella, J. P., Mechanism of Stimulation of the DNA Glycosylase Activity of hOGG1 by the Major Human AP Endonuclease: Bypass of the AP Lyase Activity Step. *Nucleic Acids Res.* **2001,** *29* (6), 1285–1292.

(64)   Nguyen, M. T.; Chandra, A. K.; Zeegers-Huyskens, T., Protonation and Deprotonation Energies of Uracil - Implications for the Uracil-Water Complex. *J. Chem. Soc.-Faraday Trans.* **1998,** *94* (9), 1277–1280.

(65)   Chandra, A. K.; Nguyen, M. T.; Uchimaru, T.; Zeegers-Huyskens, T., Protonation and Deprotonation Enthalpies of Guanine and Adenine and Implications for the Structure and Energy of Their Complexes with Water: Comparison with Uracil, Thymine, and Cytosine. *J. Phys. Chem. A* **1999,** *103* (44), 8853–8860.

(66)   Jang, Y. H.; Sowers, L. C.; Cagin, T.; Goddard, W. A., III, First Principles Calculation of pKa Values for 5-Substituted Uracils. *J. Phys. Chem. A* **2001,** *105* (1), 274–280.

(67)   Chandra, A. K.; Uchimaru, T.; Zeegers-Huyskens, T., Theoretical Study on Protonated and Deprotonated 5-Substituted Uracil Derivatives and Their Complexes with Water. *THEOCHEM* **2002,** *605* (2-3), 213–220.

(68)   Di Laudo, M.; Whittleton, S. R.; Wetmore, S. D., Effects of Hydrogen Bonding on the Acidity of Uracil. *J. Phys. Chem. A* **2003,** *107* (48), 10406–10413.

(69)   Chandra, A. K.; Michalska, D.; Wysokinsky, R.; Zeegers-Huyskens, T., Theoretical Study of the Acidity and Basicity of the Cytosine Tautomers and Their 1:1 Complexes with Water. *J. Phys. Chem. A* **2004,** *108* (44), 9593–9600.

(70)   Miller, T. M.; Arnold, S. T.; Viggiano, A. A.; Miller, A. E. S., Acidity of a Nucleotide Base: Uracil. *J. Phys. Chem. A* **2004,** *108* (16), 3439–3446.

(71)   Whittleton, S. R.; Hunter, K. C.; Wetmore, S. D., Effects of Hydrogen Bonding on the Acidity of Uracil Derivatives. *J. Phys. Chem. A* **2004,** *108* (38), 7709–7718.

(72)   Lee, J. K., Insights into Nucleic Acid Reactivity Through Gas-Phase Experimental and Computational Studies. *Int. J. Mass Spectrom.* **2005,** *240* (3), 261–272.

(73)   McConnell, T. L.; Wheaton, C. A.; Hunter, K. C.; Wetmore, S. D., Effects of Hydrogen Bonding on the Acidity of Adenine, Guanine, and Their 8-Oxo Derivatives. *J. Phys. Chem. A* **2005,** *109* (28), 6351–6362.

(74)   Rios-Font, R.; Bertran, J.; Rodriguez-Santiago, L.; Sodupe, M., Effects of Ionization, Metal Cationization and Protonation on 2 '-Deoxyguanosine: Changes on Sugar Puckering and Stability of the N-glycosidic Bond. *J. Phys. Chem. B* **2006,** *110* (11), 5767–5772.

(75)   Hunter, K. C.; Wetmore, S. D., Environmental Effects on the Enhancement in Natural and Damaged DNA Nucleobase Acidity Because of Discrete Hydrogen-Bonding Interactions. *J. Phys. Chem. A* **2007,** *111* (10), 1933–1942.

(76)   Hunter, K. C.; Millen, A. L.; Wetmore, S. D., Effects of Hydrogen-Bonding and Stacking Interactions with Amino Acids on the Acidity of Uracil. *J. Phys. Chem. B* **2007,** *111* (7), 1858–1871.

(77)   Zheng, Y.; Xue, Y.; Yan, S. G., The Effects of Oxidation and Protonation on the N-glycosidic Bond Stability of 8-Oxo-2'-deoxyguanosine: DFT Study. *THEOCHEM* **2008,** *860* (1-3), 52–57.

(78)   Tehrani, Z. A.; Fattahi, A.; Pourjavadi, A., Interaction of Mg^{2+}, Ca^{2+}, Zn^{2+} and Cu^+ with Cytosine Nucleosides: Influence of Metal on Sugar Puckering and Stability of N-glycosidic Bond. A DFT Study. *THEOCHEM* **2009,** *913* (1-3), 117–125.

(79)   Zheng, Y.; Xue, Y.; Yan, G. S., The Influences of Oxidation and Cationization on the N-glycosidic Bond Stability of 8-Oxo-2'-deoxyadenosine - A Theoretical Study. *J. Theor. Comput. Chem.* **2009,** *8* (6), 1253–1264.

(80)   Michelson, A. Z.; Chen, M.; Wang, K.; Lee, J. K., Gas-Phase Studies of Purine 3-Methyladenine DNA Glycosylase II (AlkA) Substrates. *J. Am. Chem. Soc.* **2012,** *134* (23), 9622–9633.

(81)   Michelson, A. Z.; Rozenberg, A.; Tian, Y.; Sun, X.; Davis, J.; Francis, A. W.; O'Shea, V. L.; Halasyam, M.; Manlove, A. H.; David, S. S.*, et al.*, Gas-Phase Studies of Substrates for the DNA Mismatch Repair Enzyme MutY. *J. Am. Chem. Soc.* **2012,** *134* (48), 19839–19850.

(82)   Shakourian-Fard, M.; Fattahi, A.; Jamshidi, Z., Interaction of Cations with 2'-Deoxythymidine Nucleoside and Analysis of the Nature and Strength of Cation Bonds. *J. Phys. Org. Chem.* **2012,** *25* (2), 153–161.

(83) Chen, Z. Q.; Zhang, C. H.; Xue, Y., Theoretical Studies on the Thermodynamics and Kinetics of the N-Glycosidic Bond Cleavage in Deoxythymidine Glycol. *J. Phys. Chem. B* **2009,** *113* (30), 10409–10420.

(84) Chen, Z. Q.; Xue, Y., Theoretical Investigations on the Thermal Decomposition Mechanism of 5-Hydroxy-6-hydroperoxy-5,6-dihydrothymidine in Water. *J. Phys. Chem. B* **2010,** *114* (39), 12641–12654.

(85) Williams, R. T.; Wang, Y. S., A Density Functional Theory Study on the Kinetics and Thermodynamics of N-Glycosidic Bond Cleavage in 5-Substituted 2 '-Deoxycytidines. *Biochemistry* **2012,** *51* (32), 6458–6462.

(86) Millen, A. L.; Archibald, L. A. B.; Hunter, K. C.; Wetmore, S. D., A Kinetic and Thermodynamic Study of the Glycosidic Bond Cleavage in Deoxyuridine. *J. Phys. Chem. B* **2007,** *111* (14), 3800–3812.

(87) Kellie, J. L.; Navarro-Whyte, L.; Carvey, M. T.; Wetmore, S. D., Combined Effects of π–π Stacking and Hydrogen Bonding on the (N1) Acidity of Uracil and Hydrolysis of 2′-Deoxyuridine. *J. Phys. Chem. B* **2012,** *116* (8), 2622–2632.

(88) Tiwari, S.; Agnihotri, N.; Mishra, P. C., Quantum Theoretical Study of Cleavage of the Glycosidic Bond of 2'-Deoxyadenosine: Base Excision-Repair Mechanism of DNA by MutY. *J. Phys. Chem. B* **2011,** *115* (12), 3200–3207.

(89) Ebrahimi, A.; Habibi-Khorassani, M.; Bazzi, S., The Impact of Protonation and Deprotonation of 3-Methyl-2'-deoxyadenosine on N-glycosidic Bond Cleavage. *Phys. Chem. Chem. Phys.* **2011,** *13* (8), 3334–3343.

(90) Osakabe, T.; Fujii, Y.; Hata, M.; Tsuda, M.; Neya, S.; Hoshino, T., Quantum Chemical Study on Base Excision Mechanism of 8-Oxoguanine DNA Glycosylase: Substrate-Assisted Catalysis of the N-glycosidic Linkage Cleavage Reaction. *Chem-Bio Inf. J.* **2004,** *4* (3), 73–92.

(91) Schyman, P.; Danielsson, J.; Pinak, M.; Laaksonen, A., Theoretical Study of the Human DNA Repair Protein hOGG1 Activity. *J. Phys. Chem. A* **2005,** *109* (8), 1713–1719.

(92) Shim, E. J.; Przybylski, J. L.; Wetmore, S. D., Effects of Nucleophile, Oxidative Damage, and Nucleobase Orientation on the Glycosidic Bond Cleavage in Deoxyguanosine. *J. Phys. Chem. B* **2010,** *114* (6), 2319–2326.

(93) Šebera, J.; Trantírek, L.; Tanaka, Y.; Sychrovský, V., Pyramidalization of the Glycosidic Nitrogen Provides the Way for Efficient Cleavage of the N-Glycosidic Bond of 8-OxoG with the hOGG1 DNA Repair Protein. *J. Phys. Chem. B* **2012,** *116* (41), 12535–12544.

(94) Rios-Font, R.; Rodriguez-Santiago, L.; Bertran, J.; Sodupe, M., Influence of N7 Protonation on the Mechanism of the N-Glycosidic Bond Hydrolysis in 2'-Deoxyguanosine. A Theoretical Study. *J. Phys. Chem. B* **2007,** *111* (21), 6071–6077.

(95) Millen, A. L.; Wetmore, S. D., Glycosidic Bond Cleavage in Deoxynucleotides - A Density Functional Study. *Can. J. Chem.* **2009,** *87* (7), 850–863.

(96)   Rios-Font, R.; Bertran, J.; Sodupe, M.; Rodriguez-Santiago, L., On the Mechanism of the N-glycosydic Bond Hydrolysis of 2'-Deoxyguanosine: Insights from First Principles Calculations. *Theor. Chem. Acc.* **2011,** *128* (4-6), 619–626.

(97)   Dinner, A. R.; Blackburn, G. M.; Karplus, M., Uracil-DNA Glycosylase Acts by Substrate Autocatalysis. *Nature (London, U. K.)* **2001,** *413* (6857), 752–755.

(98)   Calvaresi, M.; Bottoni, A.; Garavelli, M., Computational Clues for a New Mechanism in the Glycosylase Activity of the Human DNA Repair Protein hOGG1. A Generalized Paradigm for Purine-Repairing Systems? *J. Phys. Chem. B* **2007,** *111* (23), 6557–6570.

(99)   Rutledge, L. R.; Wetmore, S. D., Modeling the Chemical Step Utilized by Human Alkyladenine DNA Glycosylase: A Concerted Mechanism Aids in Selectively Excising Damaged Purines. *J. Am. Chem. Soc.* **2011,** *133* (40), 16258–16269.

(100)   Brunk, E.; Arey, J. S.; Rothlisberger, U., Role of Environment for Catalysis of the DNA Repair Enzyme MutY. *J. Am. Chem. Soc.* **2012,** *134* (20), 8608–8616.

(101)   Rezac, J.; Riley, K. E.; Hobza, P., Evaluation of the Performance of Post-Hartree-Fock Methods in Terms of Intermolecular Distance in Noncovalent Complexes. *J. Comput. Chem.* **2012,** *33* (6), 691–694.

(102)   Riley, K. E.; Platts, J. A.; Rezac, J.; Hobza, P.; Hill, J. G., Assessment of the Performance of MP2 and MP2 Variants for the Treatment of Noncovalent Interactions. *J. Phys. Chem. A* **2012,** *116* (16), 4159–4169.

Chapter 2: DFT Method Testing[a]

2.1 Introduction

Over the past decade, computational studies of enzyme-catalyzed reactions have been progressing to larger and larger models, including truncated enzyme–substrate models of 70–200 atoms.[1–8] As a result, the use of ONIOM (Our-own N-layered Integrated molecular Orbital Method) and quantum mechanical/molecular mechanical (QM/MM) hybrid methodologies has become increasingly popular,[9–13] and such calculations on full enzyme–substrate systems have appeared in the literature (see, for example, references 14–22). In addition, the development of density functionals (methods) capable of treating both reactions and weak noncovalent interactions has increased the variety of active-site environments that can be studied.[23–26] However, due to the complexity of the systems being investigated and the vast number of density functionals available, selecting a method to describe the high-level region is a daunting task.

Despite evidence in the literature that B3LYP cannot reliably predict barrier heights or describe dispersion interactions,[27–28] B3LYP is still the most frequently used DFT functional. A survey of articles published in ACS, RSC and Elsevier journals from 2009–2012 indicates that B3LYP has dominated the field, accounting for 69% of the ONIOM calculations that used density functionals in the high-level region (Figure 2.1). The next most frequently used functionals are M06-2X and BP86 with approximately 4% each, and all other methods contribute less than 4% each. While the use of B3LYP has been declining (B3LYP had 61% usage in 2011, down from 86% in 2010), it is clear that there is no consensus in the literature regarding the DFT method that should replace B3LYP as the default functional or whether a replacement is even required.
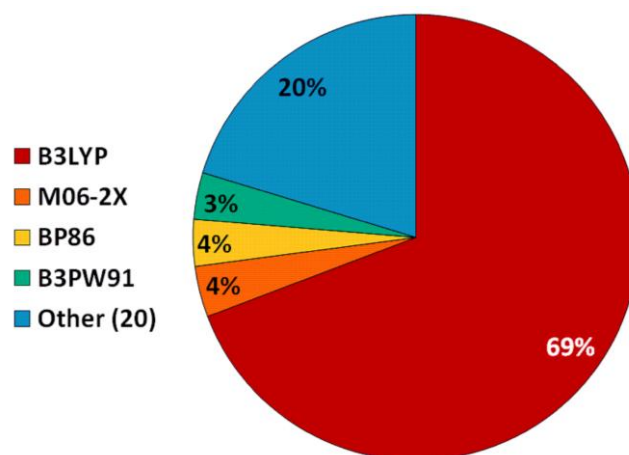
Figure 2.1. *Percentage use of various DFT methods in the high-level region of ONIOM calculations since 2009.*

The selection of a DFT method to treat the high-level region in an ONIOM model is further exacerbated by an overabundance of published benchmark tests that focus solely on high-level energetics. Indeed, while new method-testing studies are continually published (over 150 in 2011 and 130 in 2012),[b] few consider optimizations,[13,29–38] and fewer discuss the ability of functionals to accurately predict structure.[13,29–30,32–35,37] In addition, benchmarking studies rarely use double-ζ quality basis sets that are suitable for the optimization of enzyme active sites (for example, diffuse functions are often too expensive).[13,39] Instead, these studies generally rely on high-level (triple-ζ quality) energy calculations on benchmark geometries to evaluate the accuracy of a given technique. Although large basis set benchmarks are invaluable for selecting a method to determine accurate energetics,[27,40–48] this metric does not always indicate how well a given method can predict reliable structures (such as whether catalytically important contacts observed in protein X-ray crystal structures are maintained). As a result, methods that can successfully optimize enzyme systems are often tested and selected on a case-by-case basis.[13,49–53] Therefore, focus is placed on structure prediction in this work, and the reader is directed to high-quality benchmark studies to select a method for the corresponding single-point energy

[b] CAPLUS and MEDLINE search for 'DFT assessment OR DFT benchmark' run October 2012.

calculations.[27,40–48] Nevertheless, the importance of high-quality single-point energy calculations will be demonstrated in the present Chapter with a subset of functionals that performed well in previous benchmarks.

Modeling of enzyme-catalyzed reactions requires a variety of chemical phenomena to be accurately and simultaneously described. For example, this Thesis is interested in the mechanism of action of the DNA glycosylases, namely hUNG2, MutY and hOgg1. The active sites of the DNA glycosylases contain catalytic hydrogen-bonding and π–π (stacking and T-shaped) interactions, and the catalyzed reaction involves charge-separated species (sugar oxacarbenium cation and often a nucleobase anion) and proton transfer (for example, (water) nucleophile activation and/or nucleobase protonation). Therefore, a method that performs well for both noncovalent interactions and reaction kinetics is necessary to correctly model the mechanism of action of these crucial enzymes. Nevertheless, a variety of DFT functionals have been used by different groups to model the DNA glycosylases using hybrid methodologies.[20,54–56] Identifying a uniform method is important for comparing the function of the enzymes in the DNA glycosylase family, as well as for considering other non-metalloenzymes[22,57–60] for which these specifications are also important.

In the present Chapter, eight (hybrid, hybrid-meta, and dispersion-corrected) DFT methods were selected from a survey of the literature and their ability to characterize reactions and interactions with double-ζ quality basis sets that are suitable for large-scale ONIOM studies was tested. The test sets cover features commonly found in active sites of enzymes, such as the DNA glycosylases, that function without transition metals. Specifically, hydrogen-bonding interactions, π–π contacts (stacking and T-shaped orientations), proton transfer, S_N2 hydrolysis and unimolecular cleavage were investigated. From these tests, method and basis set combinations are proposed for use in ONIOM (or QM/MM) modeling of enzymatic systems with a large number (~100) of heavy atoms in the DFT region and will be used in the remainder of the

Thesis. As an example, the active site of hUNG2 bound to dU is optimized with each functional to demonstrate their ability to treat a combination of interactions in an enzymatic environment using ONIOM (DFT:SE). These results will aid the selection of a DFT method for a large array of systems beyond those of interest to this Thesis (glycosylases), including the hydrolases, glycosidases and other non-metalloenzymes.

2.2 Computational Details

2.2.1 Method Selection

In total, eight functionals (Table 2.1) were tested in this study with four entry-level sized Pople basis sets (6-31G(d), 6-31G(d,p), 6-31+G(d) and 6-31+G(d,p)). The methods were selected by combining the results of eleven benchmarking studies. Four of these studies reported data from a double-ζ quality basis set,[40,61–63] six benchmarks reported triple-ζ quality values,[40–41,61–62,64–65] and four reported the performance of Grimme's –D corrected functionals.[24,46–47,66] The double-ζ quality (6-31+G(d,p)) benchmarks examined the performance of 51 methods. The reported mean unsigned errors (MUE) were tabulated for all test sets, which span the binding energy of weak interactions and chemical kinetics. For the binding energies, only values without a counterpoise correction were included since ONIOM counterpoise-corrected calculations are impractical and fragment definitions along reaction mechanisms are often inconsistent. Of the 51 functionals reported, only 26 have MUE available for both weak interaction energies and barrier heights. From the 62 methods that used a triple-ζ quality basis set, 49 have MUE reported for both weak interactions and kinetics. In addition, the four benchmarks that include the Grimme –D type correction reported 42 methods, where 31 had values for both important categories. Thus, in total, the general performance of 88 density functional combinations was tabulated (see Tables A1 – A3, Appendix A).

Table 2.1. *Summary of the density functionals used in the present study.*

Method	Type	% HF Exchange	$\varepsilon_{Exchange}$ $\varepsilon_{Correlation}$	Reference
B3LYP	Hybrid	20	Becke88 Lee Yang Parr	67–69
B97-2	Hybrid	21	B97-2 exchange B97-2 correlation	70
MPW1K	Hybrid	42.8	modified Perdew-Wang91 Perdew-Wang91	71–72
MPWB1K	Hybrid-meta	44	modified Perdew-Wang91 Becke95	40
BB1K	Hybrid-meta	42	Becke88 Becke95	67,73–74
B1B95	Hybrid-meta	25	Becke88 Becke95	67,73
M06-2X	Hybrid-meta	56	M06-2X M06-2X	41
ωB97X-D	Hybrid, –D3	21	ωB97X ωB97X	75

Comparison of the double-ζ and triple-ζ benchmark results indicates that energetics display a strong basis set dependence. However, the goal of this work is to identify a method that can be used to optimize a large DFT region in an ONIOM calculation. Therefore, the double-ζ studies were used to select candidate functionals. The five functionals with the smallest total MUE from the double-ζ benchmarks were used in this study (barring XB1K and X1B95, where only the interaction energies for the parameterization set were reported). These methods include two hybrid-GGA functionals (MPW1K[71–72,76] and B97-2[70,77]) and three hybrid-meta-GGA functionals (BB1K,[70,74] MPWB1K,[40] and B1B95[67,73]). It should be noted that there are known self-consistent field (SCF) convergence issues with the B95 correlation functional (BB1K, MPWB1K, B1B95); however, the Truhlar group has reported a modification to the Gaussian program that corrects this problem.[62]

Since the ideal method must describe an enzyme active site that contains multiple noncovalent interactions (e.g., hydrogen bonding, π–π interactions) and perform well for chemical kinetics, additional functionals were included to account for different treatments of

dispersion. Specifically, the M06-2X functional was selected to represent the Minnesota functionals[41] since this was the best performer in the triple-ζ benchmarks for this type of functional (Table A2). Additionally, the ωB97X-D[75] functional was the best performer among the Grimme –D set (Table A3) and was therefore included in the test set. Finally, the B3LYP[67–69] functional was included for comparison due to its popularity (Figure 2.1).

2.2.2 Overview of Test Sets

As mentioned in the Introduction, most method testing studies do not conduct many (if any) optimizations, and rely on high-level energy calculations on benchmark geometries to determine the performance of a given method. This study focuses on practical applications of various density functionals by expanding the investigated criteria to include features important for modeling enzyme active sites with hybrid methods (e.g., ONIOM or QM/MM). Therefore, two of the evaluation tests focus on noncovalent interactions (hydrogen bonding (HB) and π–π contacts (PP)), three sets focus on reactions (proton transfer (PT), S_N2 hydrolysis (SN2), and unimolecular cleavage (UNI)) and the final set examines the ONIOM treatment of an active-site (AS). For the HB, PP and PT test sets, benchmark geometries were obtained with MP2 and the corresponding energies with CCSD(T)/CBS. CCSD(T)/CBS energies for the PT test set were calculated by adding a correction (determined with aug-cc-pVDZ, aDZ) to the MP2/CBS energy according to:

$$E_{CBS}^{CCSD(T)} = E_{CBS}^{MP2} + \left(E_{aDZ}^{CCSD(T)} - E_{aDZ}^{MP2} \right) \qquad [2.1]$$

where the MP2/CBS values were obtained using the Helgaker extrapolation scheme.[c,78–79,] The larger SN2 and UNI sets are compared to MP2/6-311+G(2df,p)//B3LYP/6-311+G(d,p) results and the AS results are compared across the various functionals tested starting from an

---

[c] The basis sets aug-cc-pVDZ and aug-cc-pVTZ, and values X = 2, Y = 3 and α = 1.43 were used in the Helgaker extrapolations to the CBS limit for the MP2 energies.

ONIOM(MPWB1K:PM3) geometry for hUNG2. The specific composition of each test set will be discussed in the relevant Results and Discussion section, and the reference structures and energetics are included in Appendix A (Table A4). In all cases, except for the ONIOM test, frequency calculations were run at the optimization level of theory to determine the nature of the stationary points and obtain (scaled) zero-point vibrational energy (ZPVE) corrections. As mentioned above, the basis set superposition error (BSSE) was not corrected since counterpoise calculations are not practical in ONIOM enzyme modeling.

All calculations were carried out in Gaussian 09[80] revisions A.02 or C.01. Some of the selected functionals are not immediately available and require the following IOp commands.

BB1K: # bb95/6-31+G(d,p) IOp(3/76=0580004200)

MPW1K: # mpwpw91/6-31+G(d,p) IOp(3/76=0572004280)

MPWB1K: # mpwb95/6-31+G(d,p) IOp(3/76=0560004400)

2.3 Results and Discussion

The primary focus of this Chapter is to identify accurate methods for the optimization of enzyme–substrate complexes. Structural deviations for the various tests will be considered first, followed by the accuracy of the energetics at the optimization level of theory. While it is recommended that high-quality single-point calculations be carried out on optimized geometries to obtain reliable energies, there are a number of situations where reporting the optimization energy is desirable. For example, the system may be too large to use a triple-ζ quality basis set. Alternatively, one may wish to report the entire potential energy surface (PES) for a reaction, which is only computationally feasible with smaller basis sets. Therefore, a summary of the MUE for the energies calculated with all method/basis set combinations can be found in Table 2.2, while data restricted to the basis sets most suitable for large model optimizations (i.e., no diffuse

functions) are summarized in Appendix A (Table A5). Next, the improvement provided by high-quality energies on double-ζ quality geometries will be demonstrated by re-evaluating the energetics using triple-ζ quality basis sets, which are known to be more accurate for energetics, and the recommended methods in the triple-ζ benchmarks.[41,47] Finally, the structure of a representative active-site complex optimized using different methods will be discussed.

Table 2.2. *Mean unsigned errors (MUE) of binding energies (ΔE_I), barrier heights (ΔE_a), and reaction energies (ΔE_R), as well as average MUE for energies (kJ mol^{-1}).[a]*

Method	Basis Set	ΔE_I			ΔE_a		ΔE_R		MMUE[d]
		HB	PP$_E$[b]	PP$_O$[c]	PT	SN2	PT	SN2	
B3LYP	6-31G(d)	1.4	20.0		5.8	*39.3*	6.1	50.7	20.5
B3LYP	6-31G(d,p)	**0.4**	19.9		*9.6*	*39.2*	3.5	55.3	*21.3*
B3LYP	6-31+G(d)	18.0	*25.0*		6.7	30.4	*6.5*	31.6	19.7
B3LYP	6-31+G(d,p)	17.8	*24.7*		6.5	30.9	4.3	29.2	18.9
B97-2	6-31G(d)	9.5	20.5		5.4	*33.3*	6.0	*57.6*	*22.1*
B97-2	6-31G(d,p)	8.1	20.4		9.1	32.9	3.2	*60.0*	*22.3*
B97-2	6-31+G(d)	*22.6*	*23.7*		6.3	23.9	*6.3*	37.8	20.1
B97-2	6-31+G(d,p)	*22.0*	23.4		5.8	24.1	3.7	34.4	18.9
MPW1K	6-31G(d)	1.7	17.8		5.9	16.8	3.6	*57.3*	17.2
MPW1K	6-31G(d,p)	1.8	17.8		5.1	16.3	**0.8**	54.4	16.0
MPW1K	6-31+G(d)	13.1	19.9		8.7	**5.6**	5.0	31.1	13.9
MPW1K	6-31+G(d,p)	11.3	19.8		6.0	**8.2**	1.6	30.6	12.9
MPWB1K	6-31G(d)	1.5	11.0	15.8	5.6	20.1	2.9	42.5	14.2
MPWB1K	6-31G(d,p)	**0.8**	11.1	15.5	**1.3**	18.7	**0.7**	39.4	12.5
MPWB1K	6-31+G(d)	13.9	12.8		*9.6*	**7.7**	4.4	**23.7**	12.0
MPWB1K	6-31+G(d,p)	12.7	12.7		**2.4**	12.0	**0.8**	26.1	11.1
BB1K	6-31G(d)	7.8	15.2	21.0	5.1	20.3	3.1	47.9	17.2
BB1K	6-31G(d,p)	6.9	15.1	20.2	**1.8**	20.0	0.8	45.8	15.8
BB1K	6-31+G(d)	19.7	17.0	22.6	8.1	9.8	6.2	25.9	15.6
BB1K	6-31+G(d,p)	18.3	16.6	22.6	2.7	10.0	1.5	23.7	13.7
B1B95	6-31G(d)	8.3	15.8	*23.0*	4.6	29.8	4.4	46.9	19.0
B1B95	6-31G(d,p)	7.2	15.6	22.8	*10.1*	29.3	1.7	52.4	19.9
B1B95	6-31+G(d)	*22.3*	17.9	*26.0*	5.1	20.8	4.8	27.7	17.8
B1B95	6-31+G(d,p)	21.3	17.6	*27.1*	6.4	20.5	2.2	24.8	17.2
M06-2X	6-31G(d)	5.2	**0.6**	2.7	5.2	25.6	1.4	50.5	13.0
M06-2X	6-31G(d,p)	6.3	**0.5**	2.3	7.5	25.4	2.9	48.8	13.4
M06-2X	6-31+G(d)	6.5	1.7	**1.6**	5.9	19.9	2.3	29.3	9.6
M06-2X	6-31+G(d,p)	6.1	1.4	1.9	6.3	20.6	1.2	26.9	**9.2**
ωB97X-D	6-31G(d)	10.1	3.3	**1.3**	5.3	22.1	5.7	40.7	12.6
ωB97X-D	6-31G(d,p)	11.8	3.7	2.1	4.8	22.4	3.0	38.9	12.4
ωB97X-D	6-31+G(d)	4.1	**1.2**	**1.5**	6.9	15.6	*7.1*	**15.0**	**7.3**
ωB97X-D	6-31+G(d,p)	**1.1**	1.5	1.9	3.4	16.0	3.9	**14.3**	**6.0**

[a] Lowest three values in bold and highest three values in italics for each measurement. [b] Binding energies calculated with database geometries. [c] Binding energies calculated on optimized geometries including scaled ZPVE corrections. [d] Average of the seven MUE in energies reported.

2.3.1 Noncovalent Interactions

In enzyme-catalyzed reactions, noncovalent interactions are essential for binding the substrate and aligning catalytic residues. Therefore, it is important that these interactions are properly treated both structurally (to predict the correct binding motifs) and energetically (to predict accurate binding energies and potential catalytic contributions of active-site residues). Two different kinds of noncovalent interactions were investigated in the present study: hydrogen-bonding and π–π interactions, which represent interactions ranging from electrostatic to dispersion dominated. Furthermore, both interactions are generally critical for substrate binding, where hydrogen bonds are orientation-specific contacts and π–π interactions are more structurally broad. Since these types of interactions are very different, each will be discussed separately below.

2.3.1.1 Hydrogen Bonding (HB)

The well-studied adenine$\cdots$thymine (A:T) and guanine$\cdots$cytosine (G:C) base pairs were used to test the ability of the DFT functionals to treat hydrogen-bonding interactions by comparing the optimized structures and corresponding energies to the RI-MP2/cc-pVTZ geometries and CCSD(T)/CBS energies (HB test set).[81] The deviation in the H$\cdots$Y distance and X–H$\cdots$Y angle are shown in Figure 2.2. No method deviates from the benchmark bond lengths by more than 0.080 Å, where the largest mean deviation was obtained with B97-2/6-31+G(d). While the basis set has a small effect on the distance MUE, the hydrogen-bond angle is generally improved by incorporating diffuse functions (with the exception of M06-2X). Nevertheless, all deviations in these important angles are small (< 2°). Overall, the method chosen does not significantly affect the geometries and all methods perform equally well. It should be noted that a cancellation of effects leads to the excellent results with the smallest basis sets tested (6-31G(d) and 6-31G(d,p)). Specifically, the absence of diffuse functions in the basis set leads to contacts

that are too loose and the lack of BSSE correction causes the interactions to be too tight. Therefore, diffuse functions may not be necessary to determine accurate hydrogen-bonded structures.
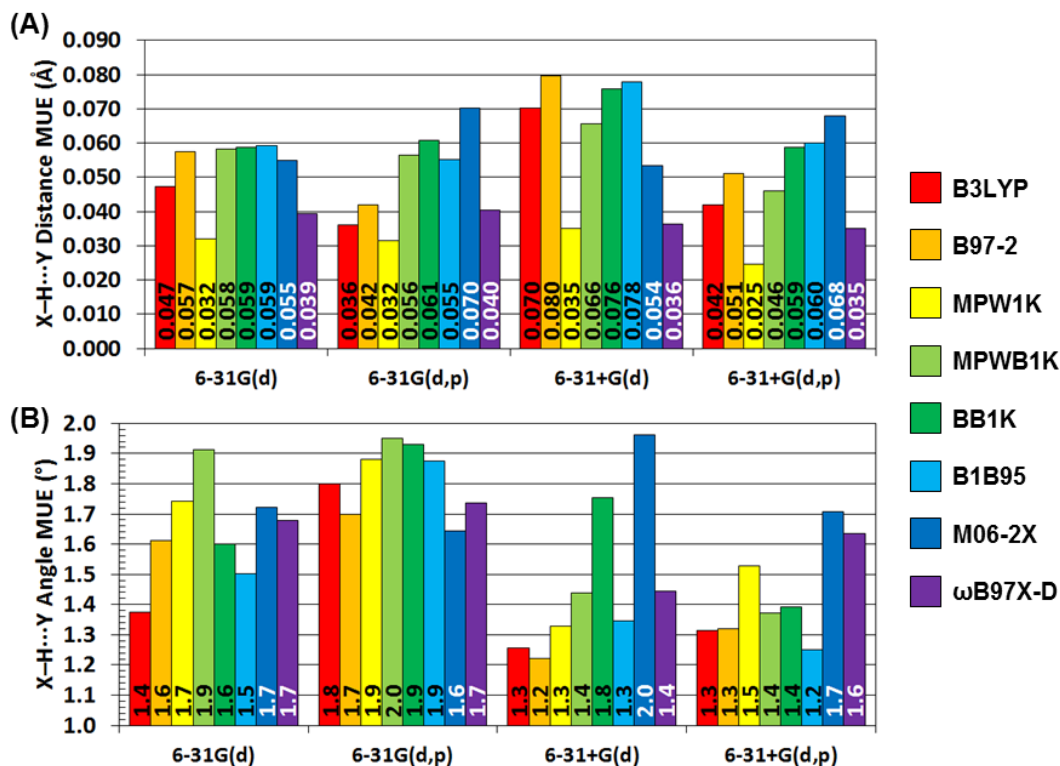
Figure 2.2. *MUE in (A) hydrogen-bond distances and (B) angles determined for the HB test set.*

The interaction energies calculated at the same level of theory as the optimization are presented in Table 2.2 (HB). Interestingly, the MUE for the binding energies are significantly smaller without diffuse functions for all methods except M06-2X and ωB97X-D. This is likely because of a cancellation of errors since BSSE was ignored due to the impractical nature of these calculations in large-scale ONIOM calculations. B3LYP and MPWB1K (with 6-31G(d,p)) predict the best binding energies (MUE < 1 kJ mol^{-1}). Similar accuracy can be obtained with ωB97X-D, but only if diffuse functions are included (MUE = 1.1 kJ mol^{-1} with diffuse functions and MUE = 10.1 − 11.8 kJ mol^{-1} without diffuse functions). M06-2X consistently yields an MUE of ~6 kJ mol^{-1} with all basis sets. Since all method combinations predicted similar hydrogen-bonding

structures, the best method combinations when considering both structure and energy are B3LYP or MPWB1K with 6-31G(d,p) or ωB97X-D with 6-31+G(d,p).

2.3.1.2 Stacking and T-shaped (PP)

Interactions with a large dispersion component were tested using different types of π–π contacts (PP test sets). It has been recently recognized that full optimization of stacking systems can lead to significant changes in binding energy,[82–83] and therefore two approaches were used for this test set. First, the binding energies of select systems from two databases were calculated to evaluate the ability of each functional to reproduce the energetics of weakly bound systems at the optimum geometry (PP$_E$ test set). These dimers included the stacking and T-shaped orientations of uracil–phenylalanine (modeled as uracil–benzene, U:F) and phenylalanine–tryptophan (modeled as benzene–indole, F:W). These examples were selected since U:F prefers the stacked structure, while F:W prefers the T-shaped orientation.[84–85] In addition, these dimers have T-shaped–stacking relative binding energies of 10.0 and –2.1 kJ mol^{-1}, respectively (Table A4), which will permit evaluation of the ability of each method to correctly predict the optimum orientation for nearly isoenergetic conformers. The benchmark geometries and CCSD(T)/CBS binding energies were taken from Hobza's S22 set (F:W)[84] and the Wetmore RW127 set (U:F).[85]

The M06-2X and ωB97X-D dispersion-corrected methods yield interaction energies with MUEs less than 4 kJ mol^{-1}, while all other method combinations yield MUEs greater than 10 kJ mol^{-1} (PP$_E$, Table 2.2). The M06-2X results are relatively consistent upon inclusion of diffuse functions (MUE < 2 kJ mol^{-1}), while the ωB97X-D results improve with the larger basis sets. The MPWB1K functional is the next best performing functional (MUE = 11.0 – 12.8 kJ mol^{-1}), with slightly poorer agreement upon basis set expansion. The hybrid functionals (B3LYP, B97-2 and MPW1K) incorrectly predict the U:F T-shaped geometry to be more stable than the stacked structure, while all method combinations correctly predict F:W to be preferentially T-shaped (see

energies reported in Table A4). This finding is especially interesting since the difference between the two benchmark conformations is significantly larger for U:F (10.0 kJ mol^{-1}) than F:W (–2.1 kJ mol^{-1}). The smallest deviations from the benchmark binding energies on benchmark geometries are obtained with M06-2X and the 6-31G(d) or 6-31G(d,p) basis set.

The second test for π–π contacts was the optimization of select systems and the evaluation of the corresponding binding energy. The sandwich stacked orientations of adenine with thymine (A:T) and the uracil dimer (U:U), and the stacked/T-shaped orientations of benzene–indole were considered. The benchmark geometries and CCSD(T)/CBS binding energies were taken from Hobza's S22 set (A:T, U:U, F:W).[84] Of the eight DFT functionals examined, only four consistently optimize parallel-displaced stacked geometries (Figures 2.3A and 2.3B), namely BB1K, M06-2X, ωB97X-D and B1B95 (although with distorted geometries). MPWB1K also maintains a stacked geometry when diffuse functions are not included in the basis set. However, the best stacking geometries are obtained with ωB97X-D and M06-2X, regardless of basis set. In contrast, T-shaped geometries (N–H⋯π) are generated with all methods, including B3LYP (Figures 2.3C and 2.3D). The major exception for the T-shaped geometries is the dispersion-corrected ωB97X-D functional, which biases parallel geometries and leads to highly distorted interplanar angles when used with any basis set (Figure 2.3D). The highly tilted geometries obtained with ωB97X-D have been reported upon optimization of the benzene–indole dimer with other –D type functionals.[86] Distorted T-shaped geometries are also observed for M06-2X with basis sets void of diffuse functions (Figure 2.3D). Consequently, the best T-shaped geometries are obtained with M06-2X with diffuse functions and MPWB1K without diffuse functions in the basis set. Therefore, when systems with both stacking and T-shaped π–π interactions are considered, M06-2X with basis sets containing diffuse functions is among the best combinations of those considered. Interestingly, the best geometries are obtained with M06-2X with diffuse functions, but the best energies (PP$_E$) are obtained without diffuse

functions, which highlights that energetics on benchmark geometries are not necessarily representative of the ability of a method to optimize these systems.
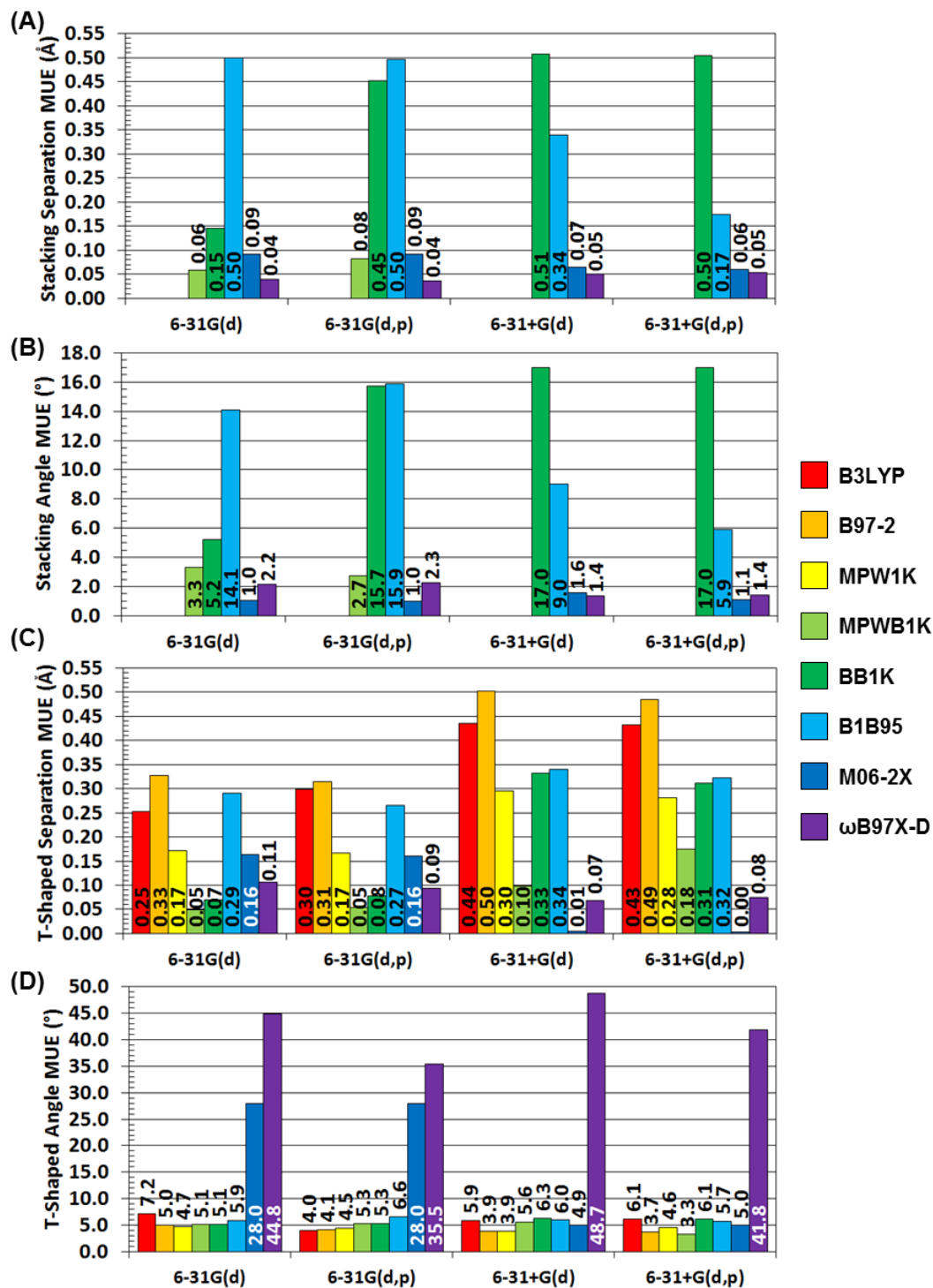
Figure 2.3. MUE in the stacking (a) vertical separation and (b) interplanar angle, and T-shaped (c) ring separation and (d) interplanar angle for the optimized geometries in the PP test set.

Following geometry optimization of the π–π contacts, the corresponding interaction energies were calculated at the optimization level of theory for those methods that predicted reasonable structures (PP$_O$, Table 2.2). In general, the resulting binding energies have slightly larger MUEs than those obtained using the benchmark geometries, but are consistent with other studies of stacking and T-shaped systems with various DFT functionals.[24,28,43,87] The excellent performance of ωB97X-D on the binding energies despite incorrect T-shaped geometries is likely due to a flat potential energy surface (PES). Indeed, the PES for vertical separation is known to be shallow, and the calculated MUE of ∼0.1 Å typically corresponds to a change in binding energy of less than 1 kJ mol^{-1}.[28,88] Nevertheless, M06-2X with diffuse functions, which yields much better geometries, also has MUE less than 2 kJ mol^{-1}, and therefore is likely the most reliable method for the optimization and energies of π–π contacts. Interestingly, MPWB1K with 6-31G(d) or 6-31G(d,p) performs exceptionally well in optimizing the PP test set (Figure 2.3), but yields large (11 – 16 kJ mol^{-1}) errors in the binding energy (PP$_E$ and PP$_O$, Table 2.2). These results emphasize that energies tell only part of the story and may not be predictive of the optimization potential of a given functional. Furthermore, the excellent geometries obtained with this functional and the entry-level basis sets may make this method combination the best choice for ONIOM optimizations of systems containing π–π contacts when computer resources limit the use of larger basis sets. Nevertheless, if MPWB1K is used for optimizing, then accurate binding energies must be obtained with a different functional (for example, M06-2X or ωB97X-D) and a larger basis set.

2.3.2 Reactions

As outlined in Section 2.1, a variety of simple reactions are commonly involved in the mechanism of action of enzymes that function without transition metals. For example, proton transfer frequently occurs in enzyme-mediated reactions, including protonation of the substrate to enhance reactivity or activating the nucleophile.[89] Therefore, the ability of various functionals to

describe proton transfer reactions was examined in the present study using cytosine tautomerization (PT test set). Mechanisms involving either an isolated cytosine nucleobase or a cytosine–water complex were characterized and compared to MP2/6-31+G(d,p) structures (which were re-optimized starting from the geometries reported in reference 90) and CCSD(T)/CBS energies (calculated as described in the Section 2.2.2). Since this Thesis is interested in the mechanism of action of DNA glycosylases, additional reaction tests include the hydrolytic or unimolecular deglycosylation, which covers S_N2 and the first step of S_N1-type mechanisms, respectively. The S_N2 hydrolysis of 2′-deoxyuridine with two different nucleophiles (OH$^-$ and an HCOO$^-$···H$_2$O complex) was used to test the treatment of nucleophilic substitution reactions (SN2 test set). The unimolecular dissociation of 2′-deoxyuridine (UNI test set) in the gas phase and in the presence of bulk (IEF-PCM water) solvent was used to examine how various methods characterize an inherently difficult transition state that has been previously shown to only be visible on the Gibbs energy surface.[91–92] MP2/6-311+G(2df,p)//B3LYP/6-311+G(2d,p) results were refined from initial structures reported in reference 93 for the SN2 test and reference 92 for the UNI test (d(C1′–N1) = 1.400 – 2.900 Å). B3LYP was used as the reference method in these tests since B3LYP with a large basis set is known to perform well for standard organic reactions.[29] The ability of a given method to optimize the correct structure of transition states is one of the most important tests included in this study since the correct prediction of early or late transition states is essential when investigating enzyme mechanisms. Finally, the pucker of the deoxyribose group was monitored by calculating the pseudorotational angle[94] since sugar pucker can have an impact on the catalytic mechanism and local structure of enzyme–substrate complexes through, for example, hyperconjugation effects. Although the specific example of the puckering of the deoxyribose ring is considered in the present work, which directly applies to DNA–enzyme complexes, these results can likely be extrapolated to other systems such as ribose rings and other carbohydrates. The results for the transition state geometries, sugar puckering, barrier heights and reaction energetics will be separately discussed below.

2.3.2.1 Transition State Distances

Figure 2.4 summarizes the deviations in the calculated transition state distances for the PT and SN2 tests, while the UNI test will be discussed in the barrier heights section due to the plateau in the TS region on the PES of this unimolecular dissociation.[91–92] All method combinations performed equally well for the PT test, with MUE of less than 0.040 Å. Significantly larger errors are observed for the SN2 reactions, especially without diffuse functions (MUE of up to 0.157 Å for M06-2X/6-31G(d,p)). However, the SN2 errors are greatly reduced when diffuse functions are included in the basis set, often by over 50%. Barring B3LYP, which was used to optimize the reference structures, B97-2 and ωB97X-D perform the best for the SN2 test set. Combined, these results support the use of B3LYP, B97-2 and ωB97X-D (as long as sugar pucker is not important, see below) for the optimization of similar transition states, with improved agreement obtained upon incorporation of diffuse functions. This conclusion is consistent with a recent study of the treatment of transition states by DFT methods.[23]
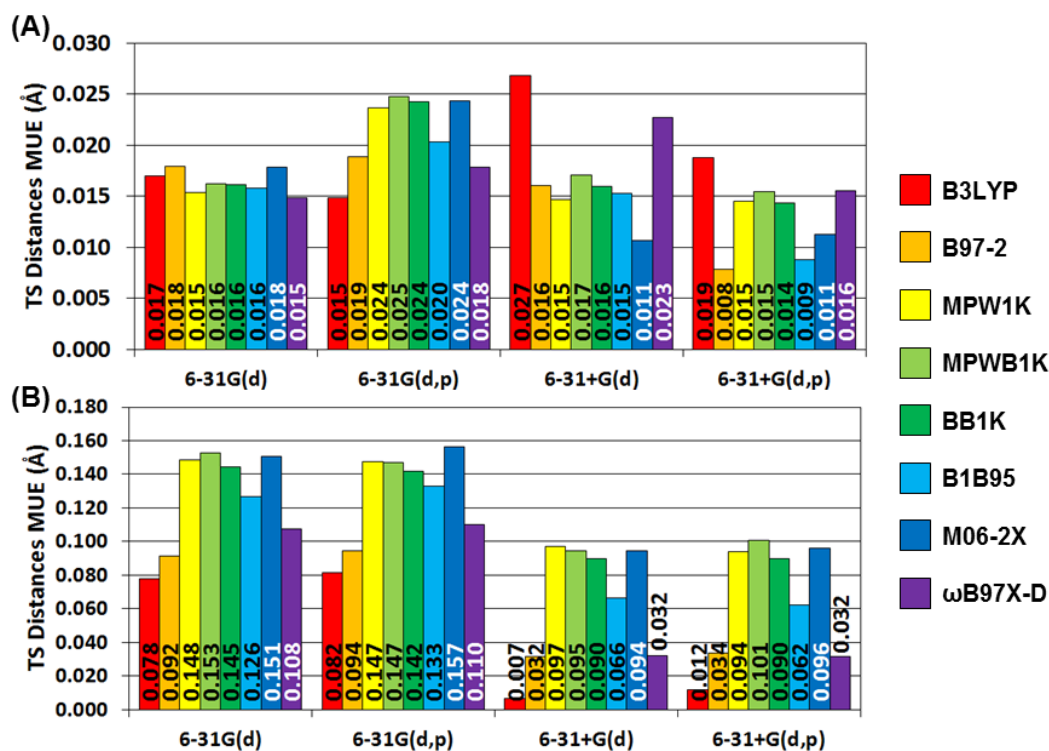
Figure 2.4. *MUE in transition state distances for the (a) PT and (b) SN2 test sets.*

2.3.2.2 Sugar Puckering

The large deviations in the transition state structures observed for the SN2 and UNI tests can be partially attributed to changes in the pucker of the deoxyribose ring throughout the reaction (Figure 2.5). For each basis set, the largest deviations in pucker are obtained with M06-2X (9.1° – 21.6°) and ωB97X-D (8.6° – 13.1°). These deviations are significant enough to change the structure from an envelope to a twisted geometry (for example, C2′-*endo* to C2′-*endo*/C3′-*exo* twist), but not large enough to change from North (e.g., C3′-*endo*) to South (e.g., C2′-*endo*) pucker.[94] Since sugar pucker results from chemical features such as hyperconjugation and the anomeric effect,[95] deviations of this magnitude could have dramatic effects on the energetics of the system. Therefore, care should be taken when using the M06-2X and ωB97X-D methods to monitor ring pucker. All other methods report mean deviations from the reference of less than 9° (less than 6° when the basis set contains diffuse functions), which is not large enough to appreciably alter the sugar geometry and are thus suitable for optimizing these types of systems.
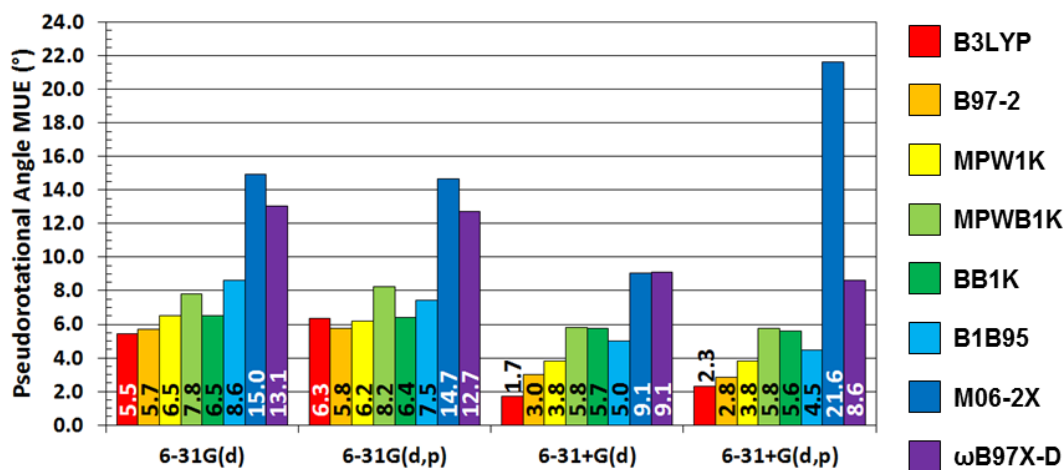
Figure 2.5. *MUE in the pseudorotational angle of the deoxyribose ring in the SN2 and UNI test sets.*

2.3.2.3 Barrier Heights

The three reaction test sets contain different degrees of freedom, and therefore exhibit errors in the barrier heights of varying magnitudes. For example, the largest system in the PT test contains a simple proton transfer through one explicit water molecule, and the largest MUE is 10.1 kJ mol^{-1}. In contrast, the largest model in the SN2 test includes a deoxynucleotide, a water molecule and a formate anion with many degrees of freedom, and thus the associated errors are larger (up to 39.3 kJ mol^{-1}). The UNI test similarly contains errors greater than 30 kJ mol^{-1}. Due to these differences, each test case will be discussed separately below.

All method combinations perform similarly for the barrier heights in the PT test (ΔE_a, Table 2.2), with MUE ranging from 1.3 kJ mol^{-1} (MPWB1K/6-31G(d,p)) to 10.1 kJ mol^{-1} (B1B95/6-31G(d,p)). The performance of most methods was improved upon incorporation of diffuse functions as expected for a transition state with charge separation (reductions in MUE were approximately 9 kJ mol^{-1}), with the exception of MPW1K and BB1K. However, any improvements were minimal and it is therefore not likely worth the computational expense to include diffuse functions, especially in large-scale ONIOM calculations. A significantly larger error range is obtained for the SN2 test set. The smallest MUE (5.6 kJ mol^{-1}) was obtained with MPW1K/6-31+G(d) and the largest MUE (39.3 kJ mol^{-1}) was obtained with B3LYP/6-31G(d), where most methods have MUE closer to 20 kJ mol^{-1}.

The results for the UNI test are presented in Figure 2.6. To demonstrate how the deviation from the reference changes over the course of the reaction for each functional, each point on the PES is averaged for the four basis sets. Sharp changes in the plot indicate that the different methods/basis sets predict the TS at a slightly different point on the surface. In the gas phase (Figure 2.6A), the best methods are MPWB1K and BB1K, which never deviate from the reference by more than 5 kJ mol^{-1}. All other methods show a steady increase in error (ranging

from $10 - 37$ kJ mol^{-1}) as the reaction progresses further from the minimum. Including (IEF-PCM) solvent effects in the optimization routine (Figure 2.6B) greatly improves the performance of M06-2X, but worsens the results for ωB97X-D and does not significantly affect the other methods.
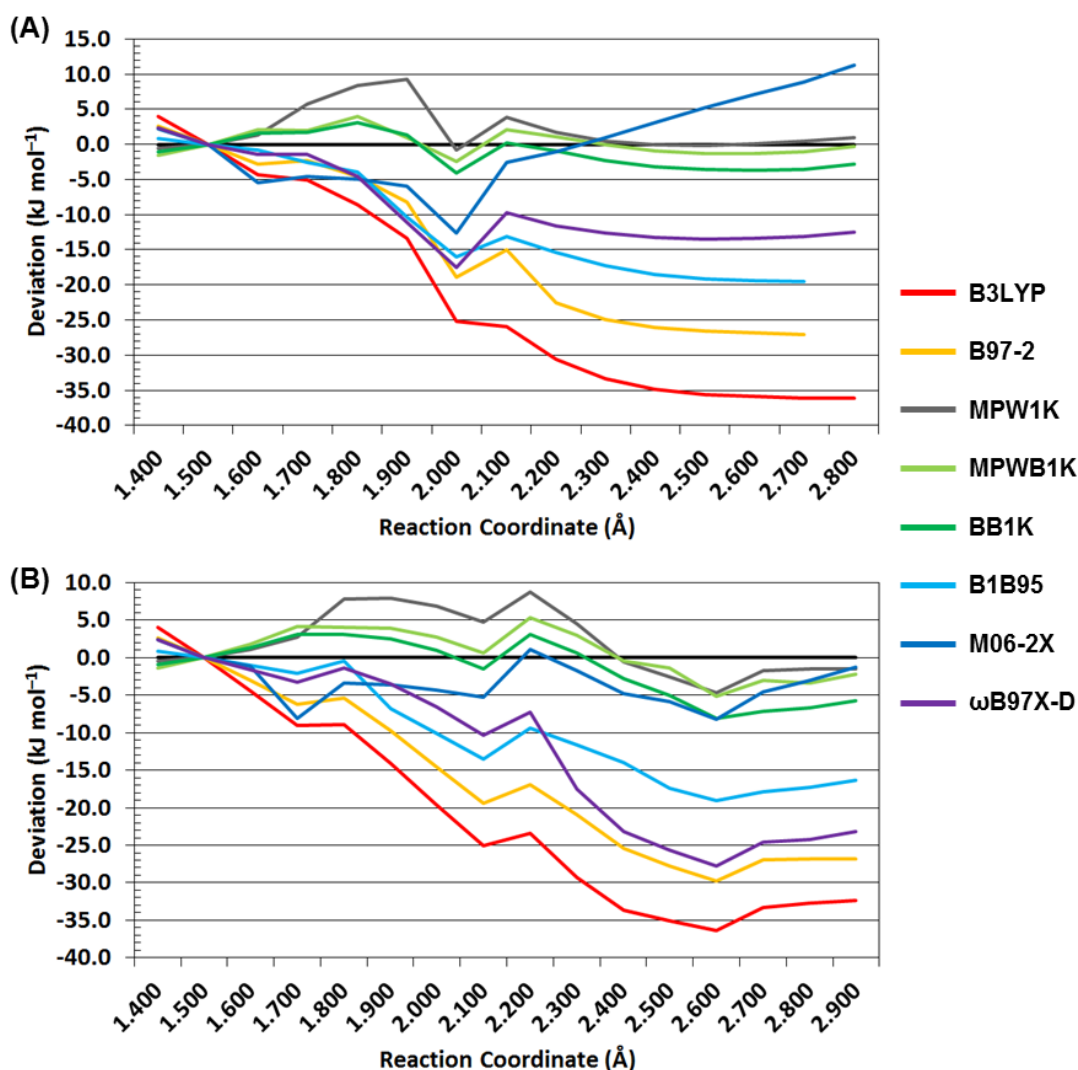
Figure 2.6. *Deviation in the relative energy along the dU unimolecular cleavage reaction coordinate (glycosidic bond) in the (a) gas phase and (b) solvent phase averaged over all basis sets compared to MP2/6-311+G(2df,p)//B3LYP/6-311+G(d,p) values (black line).*

2.3.2.4 Relative Energies

In addition to barrier heights, the PT and SN2 tests allow for a measure of the ability of various methods to predict relative energies and reaction energies, respectively. As can be seen

from Table 2.2 (ΔE_R), most methods yield MUE of less than 4 kJ mol^{-1} for the PT test. The largest errors occur for ωB97X-D, B3LYP and B97-2 with the 6-31+G(d) basis set. In most cases, the results for the PT and SN2 tests are improved (by ∼50%) when p-polarization functions are included in the basis set. MPW1K, MPWB1K and BB1K with the 6-31G(d,p) basis set lead to the lowest errors compared to CCSD(T)/CBS, which supports the use of entry-level basis sets for such processes.

As found for the barrier heights, the errors in the SN2 reaction energies are very large (14.3 − 60.0 kJ mol^{-1}). Inclusion of diffuse functions in the basis set reduces the MUE by approximately half in all cases, which is expected for a reaction with an overall anionic charge. The (M06-2X and ωB97X-D) dispersion-corrected methods optimize products with a lone-pair–π interaction between the uracilate anion and O5′ of the sugar, which causes errors in the energetics due to overstabilization of a product complex with significantly different structural characteristics. Based on MUE alone, ωB97X-D performs the best among all approaches considered; however, this is likely due to a cancellation of effects since the structure is significantly different from the reference geometry. This provides further evidence that energetics alone cannot be used to determine the structural accuracy of a method.

Overall, the best transition state geometries are obtained with B3LYP and B97-2. However, if the optimization energies are reported (for example, in the case of reaction PES), then MPWB1K/6-31+G(d) or M06-2X (with any double-ζ basis set and environmental effects) are recommended. In cases where diffuse functions are not feasible, then MPWB1K/6-31G(d,p) is the best method for reporting double-ζ quality reaction energetics (Table A5 in Appendix A).

2.3.3 High Quality Energies

While the errors reported for the energies of the SN2 and UNI tests are large, the focus of this study is to find a method to use for the *optimization* of large systems. It is expected that a

separate calculation with a triple-ζ quality basis set would be used to determine the corresponding energetics. To demonstrate that methods with large MUEs in energetics are appropriate for obtaining structures that can subsequently be used to evaluate the reaction energetics, the energetics of all systems were re-evaluated with M06-2X and ωB97X-D and the 6-311+G(2df,p) basis set since these functionals performed the best in triple-ζ quality benchmark studies.[41,47] The deviation across basis sets for a given method is small, and therefore Figure 2.7 shows the average MUE for each method combination (for example, M06-2X//B3LYP). In all cases, except the relative energy of the cytosine tautomers (E_R PT, Figure 2.7), the ωB97X-D high-level energies yield lower MUE than those determined with M06-2X. While the SN2 test still leads to large errors, these are much smaller than for the double-ζ quality energies (Table 2.2). When all test sets are combined into one MMUE (Total, Figure 2.7), M06-2X values cluster around 14 kJ mol^{-1} and ωB97X-D yields values near 9 kJ mol^{-1} regardless of the method used to optimize the geometries. Therefore, these calculations demonstrate that high-level single-point calculations should be used to determine energetics and a different method used to optimize the system, which is selected depending on the model composition.
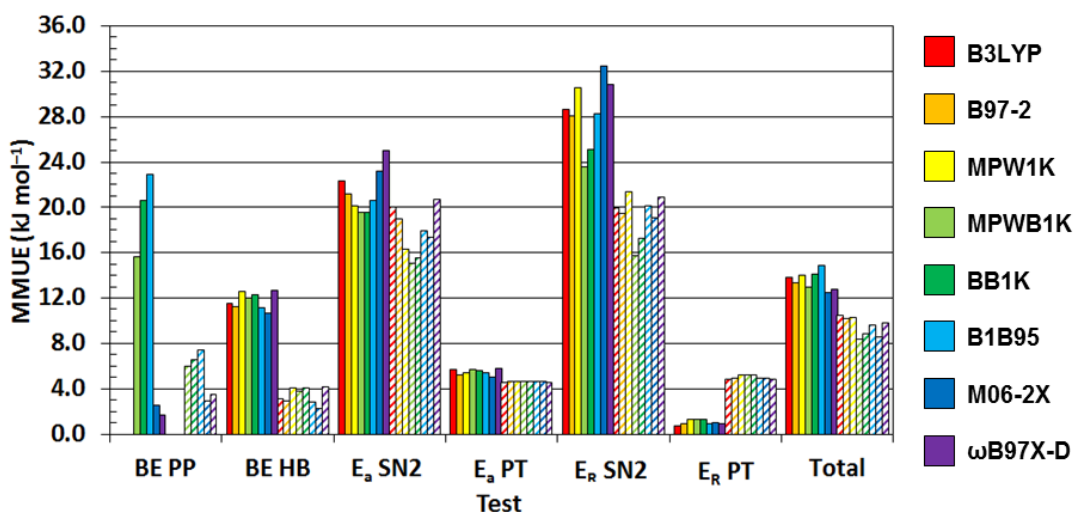
Figure 2.7. *Mean MUE (MMUE) averaged over all optimization basis sets for M06-2X (solid) and ωB97X-D (dashed) single-point energies with a 6-311+G(2df,p) basis set.*

2.3.4 ONIOM Optimization

The ability of DFT functionals to optimize a reasonable reactant complex involving an enzyme active site that contains hydrogen-bonding, π–π stacking and T-shaped interactions was examined using an ONIOM(MPWB1K/6-31G(d):PM3) model of human uracil–DNA glycosylase (hUNG2) bound to 2′-deoxyuridine. A semi-empirical method was used in the low-level region to ensure that the entire system was modeled with QM, and PM3 was selected due to its common use with biological systems (see, for example, references 10, 96–100). Due to the size of the system, only the 6-31G(d) and 6-31G(d,p) basis sets were considered. Table 2.3 summarizes important geometric characteristics obtained with each method. The glycosidic bond was found to be 1.557±0.035 Å and therefore is fairly consistent across the various methods. In contrast, the hydrogen-bond distances differ from the average by up to 0.174 Å (for M06-2X/6-31G(d,p)). Furthermore, all methods predict the same sugar pucker (P = −25.2±4.8°), with the exception of MPWB1K/6-31G(d), which more closely resembles the puckering of the pseudouridine inhibitor present in the crystal structure (P = −1.4°).[95] The M06-2X structures contain a different uracil–phenylalanine (U:F) stacking geometry and a weaker hydrogen-bond contact with a water molecule (O_W–O4, Table 3). The U:F vertical separation in the M06-2X structures is tighter by 0.08 – 0.33 Å and is accompanied by an increase in tilt angle (by 2–13°) compared to the average geometry due to steric constraints in the model (backbone frozen). However, a similar interaction exists in the human 8-oxoguanine–DNA glycosylase (hOgg1) reactant (PDB ID: 3KTU) and preliminary calculations indicate that deviations of this magnitude are not observed, even with M06-2X (see Appendix A, Table A6 and Figure A1). Therefore, as discussed earlier for sugar puckering, care should be taken with M06-2X to ensure that any dispersion interactions are not over emphasized. Interestingly, all methods maintain the active-site stacking and T-shaped interactions despite their performance on the PP set, which is likely due to the steric constraints enforced by the low-level region of the ONIOM calculation. Thus, it can be concluded that even

B3LYP can be used to optimize systems that contain noncovalent interactions as long as the model is large enough to capture steric constraints.

Table 2.3. *Summary of enzyme–substrate contacts and nucleotide conformation in the hUNG2 active site optimized using ONIOM(DFT:PM3) with various density functionals in the high level region.*

Method	BS[a]	P[b] (°)	N204–N3 Y···H (Å)	N204–N3 X–H···Y (°)	H268–O2 Y···H (Å)	H268–O2 X–H···Y (°)	dU–F58 Sep[c] (Å)	dU–F58 Tilt[d] (°)	dU–Y126 Sep[e] (Å)	dU–Y126 Tilt[d] (°)
B3LYP	d	−24.1	1.954	160.6	1.890	167.2	4.01	15.2	4.46	80.7
	d,p	−23.8	1.951	160.3	1.886	167.2	4.00	15.3	4.46	80.6
B97-2	d	−24.1	1.993	160.2	1.901	167.0	4.01	15.2	4.47	81.3
	d,p	−23.8	1.995	159.8	1.899	166.8	4.00	15.4	4.47	81.2
MPW1K	d	−20.7	1.987	159.7	1.946	164.8	4.05	16.3	4.60	85.8
	d,p	−20.5	1.990	159.4	1.946	164.7	4.04	16.5	4.60	85.9
MPWB1K	d	−10.7	1.869	162.1	1.960	158.8	4.07	14.0	4.50	83.0
	d,p	−26.7	1.866	162.2	1.962	158.6	4.06	13.9	4.51	83.3
BB1K	d	−26.6	1.872	162.2	1.957	159.3	4.07	14.0	4.52	83.2
	d,p	−25.0	1.867	162.2	1.957	159.0	4.07	13.9	4.52	83.3
B1B95	d	−26.4	1.977	160.9	1.935	160.0	3.94	17.3	4.43	81.4
	d,p	−26.0	1.973	160.7	1.944	159.8	4.02	16.3	4.42	81.2
M06-2X	d	−27.7	1.996	156.7	2.049	142.6	3.63	28.3	4.39	79.3
	d,p	−28.1	2.015	155.0	2.119	134.1	3.88	18.3	4.38	78.4
ωB97X-D	d	−27.6	1.955	159.9	1.889	163.6	3.77	11.0	4.42	80.5
	d,p	−27.1	1.948	159.8	1.887	164.0	3.76	11.0	4.42	80.5
Average[f]		−24.3	1.951	160.1	1.946	159.8	3.96	15.7	4.47	81.9

[a] Basis set: d, 6-31G(d); d,p, 6-31G(d,p). [b] Pseudorotational angle. [c] Separation between the plane of the dU nucleobase and center of the Phe ring. [d] Interplanar angle between the plane of U and the amino acid ring. [e] Separation between the plane of the Tyr ring and the center of the U ring. [f] Average value.

2.4 Conclusions

In this Chapter, eight density functionals with four Pople double-ζ quality basis sets were tested for their ability to optimize simple reactions (S_N2 hydrolysis, unimolecular cleavage and proton transfer) and non-covalent interactions (hydrogen bonding, π–π stacking and π–π T-shaped). The goal of this study was to identify a method combination that can be used to treat the high-level region in hybrid (ONIOM) optimizations of enzymatic reactions. Reaction

characteristics, such as transition state distances and sugar pucker, are best treated with the B3LYP and B97-2 hybrid methods, as well as the ωB97X-D dispersion corrected functional (TS distances only). In general, the inclusion of diffuse functions in the basis set improves the structural results for the reaction tests. In particular, the increasingly popular M06-2X only performs well when diffuse functions are included. The best π–π geometries are exhibited for hybrid-meta functionals (such as M06-2X and MPWB1K (without diffuse functions)) and the Grimme dispersion-corrected ωB97X-D, while all methods treat hydrogen-bonding systems equally well. In contrast to the reaction test sets, the effect of diffuse functions on the structure of π–π systems was minimal, with the exception of M06-2X where the larger basis set greatly improves the T-shaped interactions. Unfortunately, reaction energetics evaluated with the double-ζ basis sets can be poor. In addition, the functionals that predict the best geometries do not always yield the best energetics. However, improved agreement with reference data can be obtained when the energetics are determined with a higher-level calculation on structures optimized with an entry-level (6-31G(d)) basis set. Combined, these results emphasize that energetics alone are not predictive of the ability of a method to optimize a system. In the event that optimization energies must be reported, MPWB1K/6-31G(d,p) is recommended (in the top three for five of seven energy tests, Table A5 in Appendix A) or M06-2X/6-31+G(d,p).

Based on results for the various test sets, several factors must be weighed when selecting a density functional for the high-level region in ONIOM optimizations of enzymatic systems. Some general guidelines for choosing the DFT method are:

(1) When parallel stacking interactions are important and the model does not contain enough sterics to maintain the interaction, use MPWB1K (without diffuse functions), M06-2X, or ωB97X-D.

(2) When T-shaped interactions are important, avoid ωB97X-D (with any double-ζ quality basis set) and M06-2X (without diffuse functions). All other methods tested correctly

predict T-shaped (N–H⋯π) geometries, with MPWB1K/6-31G(d) yielding the best results.

(3) When sugar pucker is important, any method can be used, but the M06-2X and ωB97X-D functionals should be used with care.

(4) When TS distances are important use B3LYP, B97-2 or ωB97X-D, preferably with diffuse functions.

(5) When reporting optimization energies (for example, when generating PES for reactions) use MPWB1K or M06-2X (with implicit environmental effects, if the model is small).

In summary, no one density functional performs the best in all test sets implemented in the present work. Therefore, when selecting a functional for a system containing all of the components considered in this study (such as the active site of DNA glycosylases), one must identify the facet(s) of the system that is(are) the most important. Since the PES for π–π interactions are so flat, if the model contains sufficient sterics to constrain stacking interactions, then B3LYP is still an effective choice for enzyme modeling. However, it must be emphasized that this is for structure only, and another method should be used to determine accurate energetics. If the model does not contain enough sterics to maintain π–π interactions, then more expensive methods such as MPWB1K or M06-2X are required. In some cases, one may wish to report energies at the optimization level of theory, for example when generating a potential energy surface when a TS optimization is not possible due to the size of the system. In this case, the results support the use of MPWB1K when diffuse functions are not feasible or M06-2X if they are. Finally, calculated barrier heights, reaction energies and binding energies are greatly improved with the use of high quality (6-311+G(2df,p)) single-point calculations with a functional that performs well for energetics. Therefore, MPWB1K and M06-2X are used throughout the course of this Thesis to study the mechanism of action of hUNG2, MutY and hOgg1.

2.5 References[d]

(1)   Himo, F., Quantum Chemical Modeling of Enzyme Active Sites and Reaction Mechanisms. *Theor. Chem. Acc.* **2006,** *116* (1-3), 232–240.

(2)   Chen, S. L.; Fang, W. H.; Himo, F., Technical Aspects of Quantum Chemical Modeling of Enzymatic Reactions: The Case of Phosphotriesterase. *Theor. Chem. Acc.* **2008,** *120* (4-6), 515–522.

(3)   Liu, H. N.; Llano, J.; Gauld, J. W., A DFT Study of Nucleobase Dealkylation by the DNA Repair Enzyme AlkB. *J. Phys. Chem. B* **2009,** *113* (14), 4887–4898.

(4)   Georgieva, P.; Himo, F., Quantum Chemical Modeling of Enzymatic Reactions: The Case of Histone Lysine Methyltransferase. *J. Comput. Chem.* **2010,** *31* (8), 1707–1714.

(5)   Huang, W. J.; Llano, J.; Gauld, J. W., Redox Mechanism of Glycosidic Bond Hydrolysis Catalyzed by 6-Phospho-alpha-glucosidase: A DFT Study. *J. Phys. Chem. B* **2010,** *114* (34), 11196–11206.

(6)   Huang, W.; Bushnell, E. A. C.; Francklyn, C. S.; Gauld, J. W., The α-Amino Group of the Threonine Substrate as The General Base During tRNA Aminoacylation: A New Version of Substrate-Assisted Catalysis Predicted by Hybrid DFT. *J. Phys. Chem. A* **2011,** *115* (45), 13050–13060.

(7)   Liao, R. Z.; Yu, J. G.; Himo, F., Quantum Chemical Modeling of Enzymatic Reactions: The Case of Decarboxylation. *J. Chem. Theory Comput.* **2011,** *7* (5), 1494–1501.

(8)   Siegbahn, P. E. M.; Himo, F., The Quantum Chemical Cluster Approach for Modeling Enzyme Reactions. *Wiley Interdiscip. Rev.-Comput. Mol. Sci.* **2011,** *1* (3), 323–336.

(9)   Kukushkin, A. K.; Jalkanen, K. J., Role of Quantum Chemical Calculations in Molecular Biophysics with a Historical Perspective. *Theor. Chem. Acc.* **2010,** *125* (3-6), 121–144.

(10)   Lonsdale, R.; Ranaghan, K. E.; Mulholland, A. J., Computational Enzymology. *Chem. Commun.* **2010,** *46* (14), 2354–2372.

(11)   Lonsdale, R.; Harvey, J. N.; Mulholland, A. J., A Practical Guide to Modelling Enzyme-Catalysed Reactions. *Chem. Soc. Rev.* **2012,** *41* (8), 3025–3038.

(12)   Sousa, S. F.; Fernandes, P. A.; Ramos, M. J., Computational Enzymatic Catalysis - Clarifying Enzymatic Mechanisms with the Help of Computers. *Phys. Chem. Chem. Phys.* **2012,** *14* (36), 12431–12441.

(13)   Bushnell, E. A. C.; Gauld, J. W., An Assessment of Pure, Hybrid, Meta, and Hybrid-Meta GGA Density Functional Theory Methods for Open-Shell Systems: The Case of the Nonheme Iron Enzyme 8R-LOX. *J. Comput. Chem.* **2013,** *34* (2), 141–148.

---

[d] Bibliography and citations in ACS format.

(14)   Altun, A.; Yokoyama, S.; Morokuma, K., Spectral Tuning in Visual Pigments: An ONIOM(QM : MM) Study on Bovine Rhodopsin and Its Mutants. *J. Phys. Chem. B* **2008,** *112* (22), 6814–6827.

(15)   Imhof, P.; Fischer, S.; Smith, J. C., Catalytic Mechanism of DNA Backbone Cleavage by the Restriction Enzyme EcoRV: A Quantum Mechanical/Molecular Mechanical Analysis. *Biochemistry* **2009,** *48* (38), 9061–9075.

(16)   Krupička, M.; Tvaroška, I., Hybrid Quantum Mechanical/Molecular Mechanical Investigation of the β-1,4-Galactosyltransferase-I Mechanism. *J. Phys. Chem. B* **2009,** *113* (32), 11314–11319.

(17)   Li, X.; Chung, L. W.; Paneth, P.; Morokuma, K., DFT and ONIOM(DFT:MM) Studies on Co-C Bond Cleavage and Hydrogen Transfer in B-12-Dependent Methylmalonyl-CoA Mutase. Stepwise or Concerted Mechanism? *J. Am. Chem. Soc.* **2009,** *131* (14), 5115–5125.

(18)   Soliman, M. E. S.; Ruggiero, G. D.; Pernia, J. J. R.; Greiga, I. R.; Williams, I. H., Computational Mutagenesis Reveals the Role of Active-Site Tyrosine in Stabilising a Boat Conformation for the Substrate: QM/MM Molecular Dynamics Studies of Wild-Type and Mutant Xylanases. *Org. Biomol. Chem.* **2009,** *7* (3), 460–468.

(19)   Retegan, M.; Milet, A.; Jamet, H., Comparative Theoretical Studies of the Phosphomonoester Hydrolysis Mechanism by Purple Acid Phosphatases. *J. Phys. Chem. A* **2010,** *114* (26), 7110–7116.

(20)   Rutledge, L. R.; Wetmore, S. D., Modeling the Chemical Step Utilized by Human Alkyladenine DNA Glycosylase: A Concerted Mechanism Aids in Selectively Excising Damaged Purines. *J. Am. Chem. Soc.* **2011,** *133* (40), 16258–16269.

(21)   Kawatsu, T.; Lundberg, M.; Morokuma, K., Protein Free Energy Corrections in ONIOM QM:MM Modeling: A Case Study for Isopenicillin N Synthase (IPNS). *J. Chem. Theory Comput.* **2011,** *7* (2), 390–401.

(22)   Wu, R. B.; Gong, W. J.; Ting, L.; Zhang, Y. K.; Cao, Z. X., QM/MM Molecular Dynamics Study of Purine-Specific Nucleoside Hydrolase. *J. Phys. Chem. B* **2012,** *116* (6), 1984–1991.

(23)   Schenker, S.; Schneider, C.; Tsogoeva, S. B.; Clark, T., Assessment of Popular DFT and Semiempirical Molecular Orbital Techniques for Calculating Relative Transition State Energies and Kinetic Product Distributions in Enantioselective Organocatalytic Reactions. *J. Chem. Theory Comput.* **2011,** *7* (11), 3586–3595.

(24)   Grimme, S., Density Functional Theory with London Dispersion Corrections. *Wiley Interdiscip. Rev.-Comput. Mol. Sci.* **2011,** *1* (2), 211–228.

(25)   Zhao, Y.; Truhlar, D. G., Applications and Validations of the Minnesota Density Functionals. *Chem. Phys. Lett.* **2011,** *502* (1-3), 1–13.

(26)   Grimme, S.; Antony, J.; Schwabe, T.; Muck-Lichtenfeld, C., Density Functional Theory with Dispersion Corrections for Supramolecular Structures, Aggregates, and Complexes of (Bio)organic Molecules. *Org. Biomol. Chem.* **2007,** *5* (5), 741–758.

(27)   Sousa, S. F.; Fernandes, P. A.; Ramos, M. J., General Performance of Density Functionals. *J. Phys. Chem. A* **2007,** *111* (42), 10439–10452.

(28)   Rutledge, L. R.; Wetmore, S. D., The Assessment of Density Functionals for DNA-Protein Stacked and T-shaped Complexes. *Can. J. Chem.* **2010,** *88* (8), 815–830.

(29)   Simon, L.; Goodman, J. M., How Reliable are DFT Transition Structures? Comparison of GGA, Hybrid-Meta-GGA and Meta-GGA Functionals. *Org. Biomol. Chem.* **2011,** *9*, 689–700.

(30)   Steinmann, S. N.; Corminboeuf, C., Comprehensive Bench Marking of a Density-Dependent Dispersion Correction. *J. Chem. Theory Comput.* **2011,** *7* (11), 3567–3577.

(31)   Singh, R. K.; Tsuneda, T.; Hirao, K., An Examination of Density Functionals on Aldol, Mannich and α-Aminoxylation Reaction Enthalpy Calculations. *Theor. Chem. Acc.* **2011,** *130* (2-3), 153–160.

(32)   Antony, J.; Bruske, B.; Grimme, S., Cooperativity in Noncovalent Interactions of Biologically Relevant Molecules. *Phys. Chem. Chem. Phys.* **2009,** *11* (38), 8440–8447.

(33)   Zhao, Y.; Truhlar, D. G., Exploring the Limit of Accuracy of the Global Hybrid Meta Density Functional for Main-Group Thermochemistry, Kinetics, and Noncovalent Interactions. *J. Chem. Theory Comput.* **2008,** *4* (11), 1849–1868.

(34)   Leverentz, H. R.; Truhlar, D. G., Assessment of New Meta and Hybrid Meta Density Functionals for Predicting the Geometry and Binding Energy of a Challenging System: The Dimer of H_2S and Benzene. *J. Phys. Chem. A* **2008,** *112* (26), 6009–6016.

(35)   Xu, X. F.; Alecu, I. M.; Truhlar, D. G., How Well Can Modern Density Functionals Predict Internuclear Distances at Transition States? *J. Chem. Theory Comput.* **2011,** *7* (6), 1667–1676.

(36)   Yu, F., Assessment of *ab initio* MP2 and Density Functionals for Characterizing the Potential Energy Profiles of the S_N2 Reactions at N Center. *J. Comput. Chem.* **2012,** *33* (15), 1347–1352.

(37)   Mangiatordi, G. F.; Brémond, E.; Adamo, C., DFT and Proton Transfer Reactions: A Benchmark Study on Structure and Kinetics. *J. Chem. Theory Comput.* **2012,** *8* (9), 3082–3088.

(38)   Karton, A.; O'Reilly, R. J.; Radom, L., Assessment of Theoretical Procedures for Calculating Barrier Heights for a Diverse Set of Water-Catalyzed Proton-Transfer Reactions. *J. Phys. Chem. A* **2012,** *116* (16), 4211–4221.

(39)   Zheng, J. J.; Zhao, Y.; Truhlar, D. G., The DBH24/08 Database and Its Use to Assess Electronic Structure Model Chemistries for Chemical Reaction Barrier Heights. *J. Chem. Theory Comput.* **2009,** *5* (4), 808–821.

(40)   Zhao, Y.; Truhlar, D. G., Hybrid Meta Density Functional Theory Methods for Thermochemistry, Thermochemical Kinetics, and Noncovalent Interactions: The MPW1B95 and MPWB1K Models and Comparative Assessments for Hydrogen Bonding and Van der Waals Interactions. *J. Phys. Chem. A* **2004,** *108* (33), 6908–6918.

(41)   Zhao, Y.; Truhlar, D. G., The M06 Suite of Density Functionals for Main Group Thermochemistry, Thermochemical Kinetics, Noncovalent Interactions, Excited States, and Transition Elements: Two New Functionals and Systematic Testing of Four M06-Class Functionals and 12 Other Functionals. *Theor. Chem. Acc.* **2008,** *120* (1-3), 215–241.

(42)   Yang, K.; Zheng, J. J.; Zhao, Y.; Truhlar, D. G., Tests of the RPBE, revPBE, τ-HCTHhyb, ωB97X-D, and MOHLYP Density Functional Approximations and 29 Others Against Representative Databases for Diverse Bond Energies and Barrier Heights in Catalysis. *J. Chem. Phys.* **2010,** *132* (16), 164117.

(43)   Goerigk, L.; Kruse, H.; Grimme, S., Benchmarking Density Functional Methods against the S66 and S66x8 Datasets for Non-Covalent Interactions. *ChemPhysChem* **2011,** *12* (17), 3421–3433.

(44)   Zhao, Y.; Truhlar, D. G., Density Functional Theory for Reaction Energies: Test of Meta and Hybrid Meta Functionals, Range-Separated Functionals, and Other High-Performance Functionals. *J. Chem. Theory Comput.* **2011,** *7* (3), 669–676.

(45)   Theilacker, K.; Arbuznikov, A. V.; Bahmann, H.; Kaupp, M., Evaluation of a Combination of Local Hybrid Functionals with DFT-D3 Corrections for the Calculation of Thermochemical and Kinetic Data. *J. Phys. Chem. A* **2011,** *115* (32), 8990–8996.

(46)   Hujo, W.; Grimme, S., Comparison of the Performance of Dispersion-Corrected Density Functional Theory for Weak Hydrogen Bonds. *Phys. Chem. Chem. Phys.* **2011,** *13* (31), 13942–13950.

(47)   Goerigk, L.; Grimme, S., A Thorough Benchmark of Density Functional Methods for General Main Group Thermochemistry, Kinetics, and Noncovalent Interactions. *Phys. Chem. Chem. Phys.* **2011,** *13* (14), 6670–6688.

(48)   Mardirossian, N.; Parkhill, J. A.; Head-Gordon, M., Benchmark Results for Empirical Post-GGA Functionals: Difficult Exchange Problems and Independent Tests. *Phys. Chem. Chem. Phys.* **2011,** *13* (43), 19325–19337.

(49)   Alzate-Morales, J. H.; Caballero, J.; Gonzalez-Nilo, F. D.; Contreras, R., A Computational ONIOM Model for the Description of the H-bond Interactions Between NU2058 Analogues and CDK2 Active Site. *Chem. Phys. Lett.* **2009,** *479* (1–3), 149–155.

(50)   Garrec, J.; Sautet, P.; Fleurat-Lessard, P., Understanding the HIV-1 Protease Reactivity with DFT: What Do We Gain from Recent Functionals? *J. Phys. Chem. B* **2011,** *115* (26), 8545–8558.

(51)   de Farias Silva, N.; Lameira, J.; Alves, C. N., A Quantum Mechanical/Molecular Mechanical Study of the Aspartic Protease Plasmepsin IV Complexed with Allophenylnorstatine-Based Inhibitor. *Chem. Phys. Lett.* **2011,** *509* (4–6), 169–174.

(52)   Tian, B.; Strid, Å.; Eriksson, L. A., Catalytic Roles of Active-Site Residues in 2-Methyl-3-hydroxypyridine-5-carboxylic Acid Oxygenase: An ONIOM/DFT Study. *J. Phys. Chem. B* **2011,** *115* (8), 1918–1926.

(53)   Gómez, H.; Polyak, I.; Thiel, W.; Lluch, J. M.; Masgrau, L., Retaining Glycosyltransferase Mechanism Studied by QM/MM Methods: Lipopolysaccharyl-α-1,4-galactosyltransferase C Transfers α-Galactose via an Oxocarbenium Ion-like Transition State. *J. Am. Chem. Soc.* **2012,** *134* (10), 4743–4752.

(54)   Dinner, A. R.; Blackburn, G. M.; Karplus, M., Uracil-DNA Glycosylase Acts by Substrate Autocatalysis. *Nature (London, U. K.)* **2001,** *413* (6857), 752–755.

(55)   Calvaresi, M.; Bottoni, A.; Garavelli, M., Computational Clues for a New Mechanism in the Glycosylase Activity of the Human DNA Repair Protein hOGG1. A Generalized Paradigm for Purine-Repairing Systems? *J. Phys. Chem. B* **2007,** *111* (23), 6557–6570.

(56)   Brunk, E.; Arey, J. S.; Rothlisberger, U., Role of Environment for Catalysis of the DNA Repair Enzyme MutY. *J. Am. Chem. Soc.* **2012,** *134* (20), 8608–8616.

(57)   Perez, M. A. S.; Fernandes, P. A.; Ramos, M. J., Understanding the Mechanism for Ribonucleotide Reductase Inactivation by 2 '-Deoxy-2 '-methylenecytidine-5 '-diphosphate. *J. Chem. Theory Comput.* **2010,** *6* (9), 2770–2781.

(58)   Chung, L. W.; Hirao, H.; Li, X.; Morokuma, K., The ONIOM Method: Its Foundation and Applications to Metalloenzymes and Photobiology. *Wiley Interdiscip. Rev.-Comput. Mol. Sci.* **2012,** *2* (2), 327–350.

(59)   Carvalho, A. T. P.; Fernandes, P. A.; Ramos, M. J., The Catalytic Mechanism of RNA Polymerase II. *J. Chem. Theory Comput.* **2011,** *7* (4), 1177–1188.

(60)   Brás, N. r. F.; Fernandes, P. A.; Ramos, M. J., QM/MM Studies on the β-Galactosidase Catalytic Mechanism: Hydrolysis and Transglycosylation Reactions. *J. Chem. Theory Comput.* **2010,** *6* (2), 421–433.

(61)   Zhao, Y.; Pu, J. Z.; Lynch, B. J.; Truhlar, D. G., Tests of Second-Generation and Third-Generation Density Functionals for Thermochemical Kinetics. *Phys. Chem. Chem. Phys.* **2004,** *6* (4), 673–676.

(62)   Zhao, Y.; Truhlar, D. G., Benchmark Databases for Nonbonded Interactions and Their Use to Test Density Functional Theory. *J. Chem. Theory Comput.* **2005,** *1* (3), 415–432.

(63)   Zhao, Y.; Truhlar, D. G., How Well Can New-Generation Density Functional Methods Describe Stacking Interactions in Biological Systems? *Phys. Chem. Chem. Phys.* **2005,** *7* (14), 2701–2705.

(64)   Zhao, Y.; Gonzalez-Garcia, N.; Truhlar, D. G., Benchmark Database of Barrier Heights for Heavy Atom Transfer, Nucleophilic Substitution, Association, and Unimolecular Reactions and Its Use to Test Theoretical Methods. *J. Phys. Chem. A* **2005,** *109* (9), 2012–2018.

(65)   Zhao, Y.; Truhlar, D. G., Design of Density Functionals that are Broadly Accurate for Thermochemistry, Thermochemical Kinetics, and Nonbonded Interactions. *J. Phys. Chem. A* **2005,** *109* (25), 5656–5667.

(66)   Antony, J.; Grimme, S.; Liakos, D. G.; Neese, F., Protein-Ligand Interaction Energies with Dispersion Corrected Density Functional Theory and High-Level Wave Function Based Methods. *J. Phys. Chem. A* **2011,** *115* (41), 11210–11220.

(67)   Becke, A. D., Density-Functional Exchange-Energy Approximation with Correct Asymptotic-Behavior. *Phys. Rev. A* **1988,** *38* (6), 3098–3100.

(68)   Lee, C. T.; Yang, W. T.; Parr, R. G., Development of the Colle-Salvetti Correlation-Energy Formula into a Functional of the Electron-Density. *Phys. Rev. B* **1988,** *37* (2), 785–789.

(69)   Stephens, P. J.; Devlin, F. J.; Chabalowski, C. F.; Frisch, M. J., Ab-initio Calculation of Vibrational Absorption and Circular-Dichroism Spectra Using Density-Functional Force-Fields. *J. Phys. Chem.* **1994,** *98* (45), 11623–11627.

(70)   Hamprecht, F. A.; Cohen, A. J.; Tozer, D. J.; Handy, N. C., Development and Assessment of New Exchange-Correlation Functionals. *J. Chem. Phys.* **1998,** *109* (15), 6264–6271.

(71)   Adamo, C.; Barone, V., Exchange Functionals with Improved Long-Range Behavior and Adiabatic Connection Methods Without Adjustable Parameters: The mPW and mPW1PW Models. *J. Chem. Phys.* **1998,** *108* (2), 664–675.

(72)   Boese, A. D.; Handy, N. C., New Exchange-Correlation Density Functionals: The Role of the Kinetic-Energy Density. *J. Chem. Phys.* **2002,** *116* (22), 9559–9569.

(73)   Becke, A. D., Density-Functional Thermochemistry .4. A New Dynamical Correlation Functional and Implications for Exact-Exchange Mixing. *J. Chem. Phys.* **1996,** *104* (3), 1040–1046.

(74)   Zhao, Y.; Lynch, B. J.; Truhlar, D. G., Development and Assessment of a New Hybrid Density Functional Model for Thermochemical Kinetics. *J. Phys. Chem. A* **2004,** *108* (14), 2715–2719.

(75)   Chai, J. D.; Head-Gordon, M., Long-Range Corrected Hybrid Density Functionals with Damped Atom-Atom Dispersion Corrections. *Phys. Chem. Chem. Phys.* **2008,** *10* (44), 6615–6620.

(76)   Lynch, B. J.; Fast, P. L.; Harris, M.; Truhlar, D. G., Adiabatic Connection for Kinetics. *J. Phys. Chem. A* **2000,** *104* (21), 4811–4815.

(77)   Wilson, P. J.; Bradley, T. J.; Tozer, D. J., Hybrid Exchange-Correlation Functional Determined from Thermochemical Data and *ab initio* Potentials. *J. Chem. Phys.* **2001,** *115* (20), 9233–9242.

(78)   Halkier, A.; Helgaker, T.; Jorgensen, P.; Klopper, W.; Koch, H.; Olsen, J.; Wilson, A. K., Basis-set Convergence in Correlated Calculations on Ne, N-2, and H$_2$O. *Chem. Phys. Lett.* **1998,** *286* (3-4), 243–252.

(79)   Halkier, A.; Helgaker, T.; Jorgensen, P.; Klopper, W.; Olsen, J., Basis-set Convergence of the Energy in Molecular Hartree-Fock Calculations. *Chem. Phys. Lett.* **1999,** *302* (5-6), 437–446.

(80)   Frisch, M. J.; Trucks, G. W.; Schlegel, H. B.; Scuseria, G. E.; Robb, M. A.; Cheeseman, J. R.; Scalmani, G.; Barone, V.; Mennucci, B.; Petersson, G. A*., et al. Gaussian 09*, Revision A.02; Gaussian, Inc.: Wallingford CT, 2009.

(81)   Sponer, J.; Jurecka, P.; Hobza, P., Accurate Interaction Energies of Hydrogen-Bonded Nucleic Acid Base Pairs. *J. Am. Chem. Soc.* **2004,** *126* (32), 10142–10151.

(82)   McDonald, A. R.; Denning, E. J.; MacKerell, A. D., Impact of Geometry Optimization on Base–Base Stacking Interaction Energies in the Canonical A- and B-Forms of DNA. *J. Phys. Chem. A* **2013,** *117* (7), 1560–1568.

(83)   Parker, T. M.; Hohenstein, E. G.; Parrish, R. M.; Hud, N. V.; Sherrill, C. D., Quantum-Mechanical Analysis of the Energetic Contributions to π Stacking in Nucleic Acids versus Rise, Twist, and Slide. *J. Am. Chem. Soc.* **2013,** *135* (4), 1306–1316.

(84)   Jurecka, P.; Sponer, J.; Cerny, J.; Hobza, P., Benchmark Database of Accurate (MP2 and CCSD(T) Complete Basis Set Limit) Interaction Energies of Small Model Complexes, DNA Base Pairs, and Amino Acid Pairs. *Phys. Chem. Chem. Phys.* **2006,** *8* (17), 1985–1993.

(85)   Rutledge, L. R.; Durst, H. F.; Wetmore, S. D., Evidence for Stabilization of DNA/RNA-Protein Complexes Arising from Nucleobase-Amino Acid Stacking and T-Shaped Interactions. *J. Chem. Theory Comput.* **2009,** *5* (5), 1400–1410.

(86)   Biswal, H. S.; Gloaguen, E.; Mons, M.; Bhattacharyya, S.; Shirhatti, P. R.; Wategaonkar, S., Structure of the Indole-Benzene Dimer Revisited. *J. Phys. Chem. A* **2011,** *115* (34), 9485–9492.

(87)   Karthikeyan, S.; Nagase, S., Origins of the Stability of Imidazole-Imidazole, Benzene-Imidazole, and Benzene-Indole Dimers: CCSD(T)/CBS and SAPT Calculations. *J. Phys. Chem. A* **2012,** *116* (7), 1694–1700.

(88)   Sherrill, C. D.; Takatani, T.; Hohenstein, E. G., An Assessment of Theoretical Methods for Nonbonded Interactions: Comparison to Complete Basis Set Limit Coupled-Cluster Potential Energy Curves for the Benzene Dimer, the Methane Dimer, Benzene-Methane, and Benzene-H$_2$S. *J. Phys. Chem. A* **2009,** *113* (38), 10146–10159.

(89)   Stivers, J. T.; Jiang, Y. L., A Mechanistic Perspective on the Chemistry of DNA Repair Glycosylases. *Chem. Rev. (Washington, DC, U. S.)* **2003,** *103* (7), 2729–2759.

(90)   Gorb, L.; Podolyan, Y.; Leszczynski, J., A Theoretical Investigation of Tautomeric Equilibria and Proton Transfer in Isolated and Monohydrated Cytosine and Isocytosine Molecules. *THEOCHEM* **1999,** *487* (1-2), 47–55.

(91)   Baik, M. H.; Friesner, R. A.; Lippard, S. J., Theoretical Study on the Stability of N-Glycosyl Bonds: Why Does N7-Platination not Promote Depurination? *J. Am. Chem. Soc.* **2002,** *124* (16), 4495–4503.

(92)   Przybylski, J. L.; Wetmore, S. D., Designing an Appropriate Computational Model for DNA Nucleoside Hydrolysis: A Case Study of 2′-Deoxyuridine. *J. Phys. Chem. B* **2009,** *113* (18), 6533–6542.

(93)   Millen, A. L.; Archibald, L. A. B.; Hunter, K. C.; Wetmore, S. D., A Kinetic and Thermodynamic Study of the Glycosidic Bond Cleavage in Deoxyuridine. *J. Phys. Chem. B* **2007,** *111* (14), 3800–3812.

(94)   Altona, C.; Sundaral.M, Conformational-Analysis of Sugar Ring in Nucleosides and Nucleotides - New Description Using Concept of Pseudorotation. *J. Am. Chem. Soc.* **1972,** *94* (23), 8205–8206.

(95)   Parikh, S. S.; Walcher, G.; Jones, G. D.; Slupphaug, G.; Krokan, H. E.; Blackburn, G. M.; Tainer, J. A., Uracil-DNA Glycosylase-DNA Substrate and Product Structures: Conformational Strain Promotes Catalytic Efficiency by Coupled Stereoelectronic Effects. *Proc. Nat. Acad. Sci. USA* **2000,** *97* (10), 5083–5088.

(96)   Sklenak, S.; Yao, L. S.; Cukier, R. I.; Yan, H. G., Catalytic mechanism of yeast cytosine deaminase: An ONIOM computational study. *J. Am. Chem. Soc.* **2004,** *126* (45), 14879–14889.

(97)   Zhou, B. J.; Wong, C. F., A Computational Study of the Phosphorylation Mechanism of the Insulin Receptor Tyrosine Kinase. *J. Phys. Chem. A* **2009,** *113* (17), 5144–5150.

(98)   Ceron-Carrasco, J. P.; Zuniga, J.; Requena, A.; Perpete, E. A.; Michaux, C.; Jacquemin, D., Combined effect of stacking and solvation on the spontaneous mutation in DNA. *Phys. Chem. Chem. Phys.* **2011,** *13* (32), 14584–14589.

(99)   Lundberg, M., Understanding Cross-Boundary Events in ONIOM QM:QM' Calculations. *J. Comput. Chem.* **2012,** *33* (4), 406–415.

(100)   Treesuwan, W.; Hirao, H.; Morokuma, K.; Hannongbua, S., Characteristic Vibration Patterns of Odor Compounds from Bread-Baking Volatiles Upon Protein Binding: Density Functional and ONIOM Study and Principal Component Analysis. *J. Mol. Model.* **2012,** *18* (5), 2227–2240.

Chapter 3: Monofunctional Glycosylases Part 1:

Human Uracil–DNA Glycosylase (hUNG2)[a]

3.1 Introduction

Human uracil-DNA glycosylase and the *Escherichia coli* homologue have been extensively studied in the literature since their discovery decades ago.[1–2] As discussed in Chapter 1, hUNG2 catalyzes the hydrolysis of the N-glycosidic bond in 2′-deoxyuridine, a common form of DNA damage, in single- and double-stranded DNA.[3] There are two main steps involved in the catalytic deglycosylation mechanism: 1) flipping the damaged nucleotide out of the helix and into the active site; and 2) hydrolysis of the glycosidic bond through a general base mechanism.[4–6] Due to the high similarity between their sequences and activities, hUNG2 and eUDG have been used interchangeably to investigate the second (chemical) step in a broad variety of experiments, including Raman spectroscopy,[7] kinetic isotope effects (KIE),[8] X-ray crystallography,[9–14] NMR spectroscopy,[15–18] and mutational analysis,[10–11,15,19–21] as well as computational studies.[22–25]

Based on previous investigations, a step-wise dissociative pathway for the chemical step has been proposed.[4–6,26] In the first (rate-limiting) step of the proposed mechanism (Figure 3.1), uracil departs from the DNA backbone to form a uracilate anion. The glycosidic bond cleavage is believed to be catalyzed by a short, strong hydrogen bond between neutral H268[b] and the uracil moiety, while the resulting highly unstable oxacarbenium cation is most likely electrostatically stabilized by the uracilate anion and D145, as well as nearby phosphate groups. In the second step of the proposed mechanism, a nucleophilic water molecule irreversibly adds to the anomeric

---

[a] Reproduced in part with permission from Przybylski, J. L.; Wetmore, S. D. A QM/QM Investigation of the hUNG2 Reaction Surface: The Untold Tale of a Catalytic Residue *Biochemistry* **2011**, *50*, 4218–4227. Copyright 2011 American Chemical Society.
[b] Human uracil-DNA glycosylase numbering will be used throughout.

sugar carbon to form an apyrimidinic site (AP-site). During this step, the nucleophile must be activated by proton transfer to a general base,[27] a role assigned to D145.
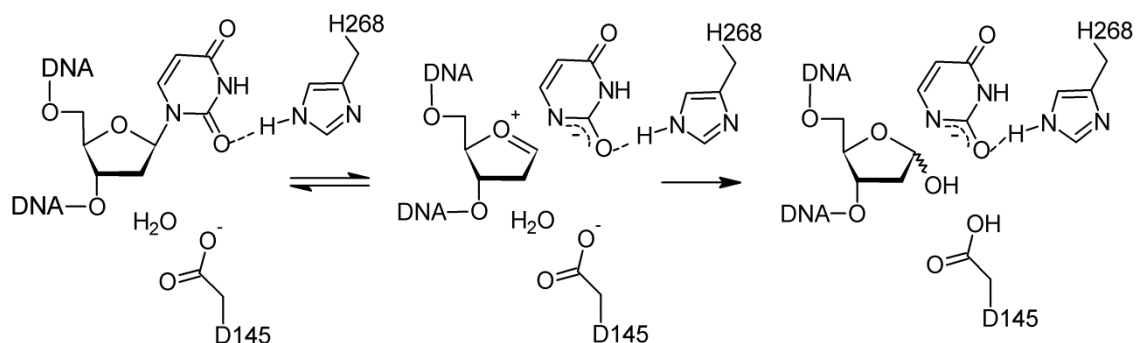
Figure 3.1. *General proposed hUNG2 mechanism. In the first step the N-glycosidic bond dissociates yielding a uracilate anion and oxacarbenium cation. In the second, irreversible step a water attacks the anomeric carbon with proton transfer to the D145 general base.*

Building on the essential involvement of H268 and D145 in the mechanism of hUNG2 action, a recent study by Parker and Stivers uncovered another important active-site residue, namely H148.[18] In addition to contributing to the nucleotide-flipping step,[18,28] it was revealed that H148 makes an important catalytic contribution late in the reaction. The study by Parker and Stivers also shows that H148 is neutral in the unbound protein and at the start of the reaction, but becomes protonated as the reaction proceeds.[18] Furthermore, mutation of this residue to alanine decreases binding of TS-mimics, which suggests that H148 provides transition state stabilization. Based on these results, it was proposed that H148 plays a role in the chemical step, possibly through orienting the nucleophilic water molecule and/or enhancing electrostatic stabilization by excluding solvent from the active site.[18] Interestingly, this absolutely conserved histidine is within hydrogen-bonding distance of the nucleophile,[13–14] and likely has an increased proton affinity due to interactions with a nearby phosphate group. Therefore, it is possible that the role of H148 in the chemical step of the hUNG2 mechanism is to activate the water nucleophile.

It is commonly believed that the general base in the hUNG2 mechanism is D145 since mutation of this residue effectively removes the catalytic activity of the enzyme.[10] Independent of

this role, it is accepted that D145 provides significant electrostatic stabilization to the dissociative transition state and oxacarbenium-cation intermediate.[20,26] Consequently, it is highly plausible that removing this residue prevents catalysis by destabilizing nucleobase departure rather than water activation. Indeed, bifunctional glycosylases (such as hOgg1, formamidopurine–DNA glycosylase (FPG), endonuclease III (EndoIII), and endonuclease VIII-like glycosylase (NEIL1)) that do not use a water nucleophile contain an essential carboxylate group (aspartate or glutamate residue) in a similar location with respect to the sugar moiety, and the primary role of this residue is electrostatic stabilization.[29–32] An essential carboxylate group with an electrostatic stabilization role is found in a comparable location in other monofunctional glycosylases (such as MutY, 3-methyladenine–DNA glycosylase (AlkA) and AAG).[33–35] Interestingly, there are two carboxylate groups in the MutY active site, where one is proposed to stabilize the sugar moiety and the other has been implicated in water activation.[34] Therefore, another residue may be responsible for water activation in hUNG2 without contradicting the key experimental findings regarding the importance of D145.

The above discussion suggests that the role of both H148 and D145 in the mechanism of hUNG2 action may not yet be fully revealed. Molecular modeling of the reaction is a useful way to further investigate how these residues are involved in the chemical step of the reaction. Among the computational investigations of hUNG2 to date,[22–25] the most in-depth used QM/MM techniques to model the reaction.[23] A detailed reaction potential energy surface was generated, primarily to investigate the dissociation step of the hUNG2 mechanism. However, this study was carried out before the initial protonation state of H148 was elucidated[18] and consequently this residue was modeled as cationic throughout the entire reaction. Furthermore, since H148 was treated at the low (MM) level of theory and the nucleophilic water at the high (QM) level of theory, interactions between these moieties were not accurately described in part because neither charge nor atom transfer can occur across a QM/MM boundary. Finally, only one avenue for

water activation was considered, which utilized D145. In addition to addressing these technical issues, a more thorough computational investigation of the hUNG2 reaction surface is required to account for, and explain, new experimental evidence that has identified the importance of H148 in the chemical step.

In the current study, the mechanism of hUNG2 action is investigated with a QM/QM active-site model. Detailed reaction potential energy surfaces for several models differing in the nucleophile hydrogen-bonding pattern are used to consider how the enzyme catalyzes uracil dissociation and activates the water nucleophile. Particular attention is placed on the roles of essential active-site residues including the involvement of H268 in base departure and, more importantly, the currently unclear function of D145 and H148 in nucleophile activation. In addition, the effect of the protonation state of H148 on the reaction is studied for comparison to previous computational work,[23] and *in silico* mutational analysis is used to calculate contributions of individual residues to the activation energy. The extensive calculations in this Chapter allow examination of the interdependence of nucleobase dissociation and nucleophile association during the mechanism, and clarify the function of important active-site residues. In this Chapter, a modified mechanism of hUNG2 action is proposed that is consistent with experimental research, clarifies the identity and role of essential active-site amino acids, and supports a unified primary purpose for active-site carboxylate groups present in many (monofunctional and bifunctional) glycosylases.

3.2 Computational Details

3.2.1 Model Generation

The initial geometry for all systems was taken from a crystal structure (PDB ID: 1EMH) of hUNG2 bound to a reactant mimic (pseudouridine, ψU).[13] First, a truncated model of the hUNG2 active site was generated that contained residues within 10 Å of the ψU glycosidic bond,

including 18 discrete water molecules. Within this model, the full ψU nucleotide (P2U5, with C1 bend maintained) was included, as well as the dT4 and dA6 nucleotides. The phosphate group of the dT7 nucleotide was also included due to its proximity to the reaction center. Subsequently, components of the model that are directed away from the reaction center were truncated because they are not believed to play a role in the chemical step. Specifically, several residues (Table B1, Appendix B) were modeled as glycine (i.e., only the backbone was included). Additionally, since most of the I173 side chain is within 10 Å of the reaction center, the backbone was truncated between C_α and C_β of the residue. Finally, the nucleobases in the nearby nucleotides were modeled as amino groups. Hydrogen atoms were added to the resulting model by inspection, where D145 was modeled as anionic and all other residues as neutral. The total charge of the system is –5.

The ONIOM(MPWB1K/6-31G(d):PM3) methodology[36–38] was used on the model system, which treats the low-level region with the PM3 semi-empirical method[39–40] and the high-level region with the MPWB1K density functional method[41] in conjunction with the 6-31G(d) basis set. The DFT region contains the 2′-deoxyuridine nucleoside, the water nucleophile (W600), an additional water molecule (W727), the full D145 residue, and the R-groups of Q144, Y147, H148, F158, N204, and H268 (Figure 3.2).[c] Thus, there are 63 heavy atoms in the DFT region, and 248 heavy atoms in the semi-empirical region with a charge of –1 and –5, respectively. A detailed description of all groups included in the high and low levels is provided in Appendix B (Table B1). Reactant geometries were obtained by initially relaxing all protons at the PM3 level of theory and subsequently relaxing the DFT region using the full ONIOM(MPWB1K/6-31G(d):PM3) method combination. Throughout the remainder of the study, the DFT region was

---

[c] The definition of the high-level region was tested by moving various groups (e.g., H148, 5′-phosphate, P146) into or out of the high-level region. Changing the definition did not affect the energetics ($\Delta\Delta E < 6$ kJ mol^{-1}), therefore the DFT region describes a large enough region.

free to optimize, while the semi-empirical region was held fixed to this original reactant geometry. The coordinates of the semi-empirical region were fixed since overlays of crystal structures of hUNG2 bound to reactant,[13] intermediate[14] and product[12–13] mimics are substantially similar for all residues included in the low-level region (RMSD > 0.7 Å). Finally, the reactant mimic was mutated to uracil and the DFT region was re-optimized.
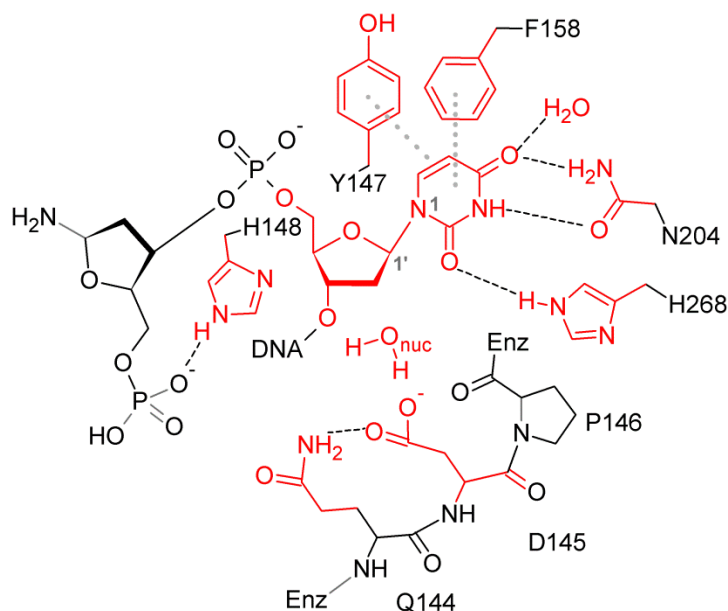
Figure 3.2. *Schematic of the DFT region (red) of the ONIOM(MPWB1K/6-31G(d):PM3) model.*

3.2.2 Surface Generation

Reaction potential energy surfaces were obtained by constraining the glycosidic (C1′–N1) and nucleophilic (C1′–O$_{nuc}$) distances (Figure 3.2). One coordinate was systematically altered by an increment of 0.200 Å, and the remainder of the DFT region was allowed to relax. This process was repeated until a stationary point was identified, or the change in energy between two points was greater than 40 kJ mol^{-1}. Specifically, the highly compressed region with glycosidic and nucleophilic distances less than 1.8 Å was not investigated. The (ONIOM(MPWB1K/6-31G(d):PM3)) relative energies (with respect to the corresponding reactant complex) are

presented as PES plots for each model (Figure 3.3), where the reactant well occurs on the bottom left and the product well on the top right.
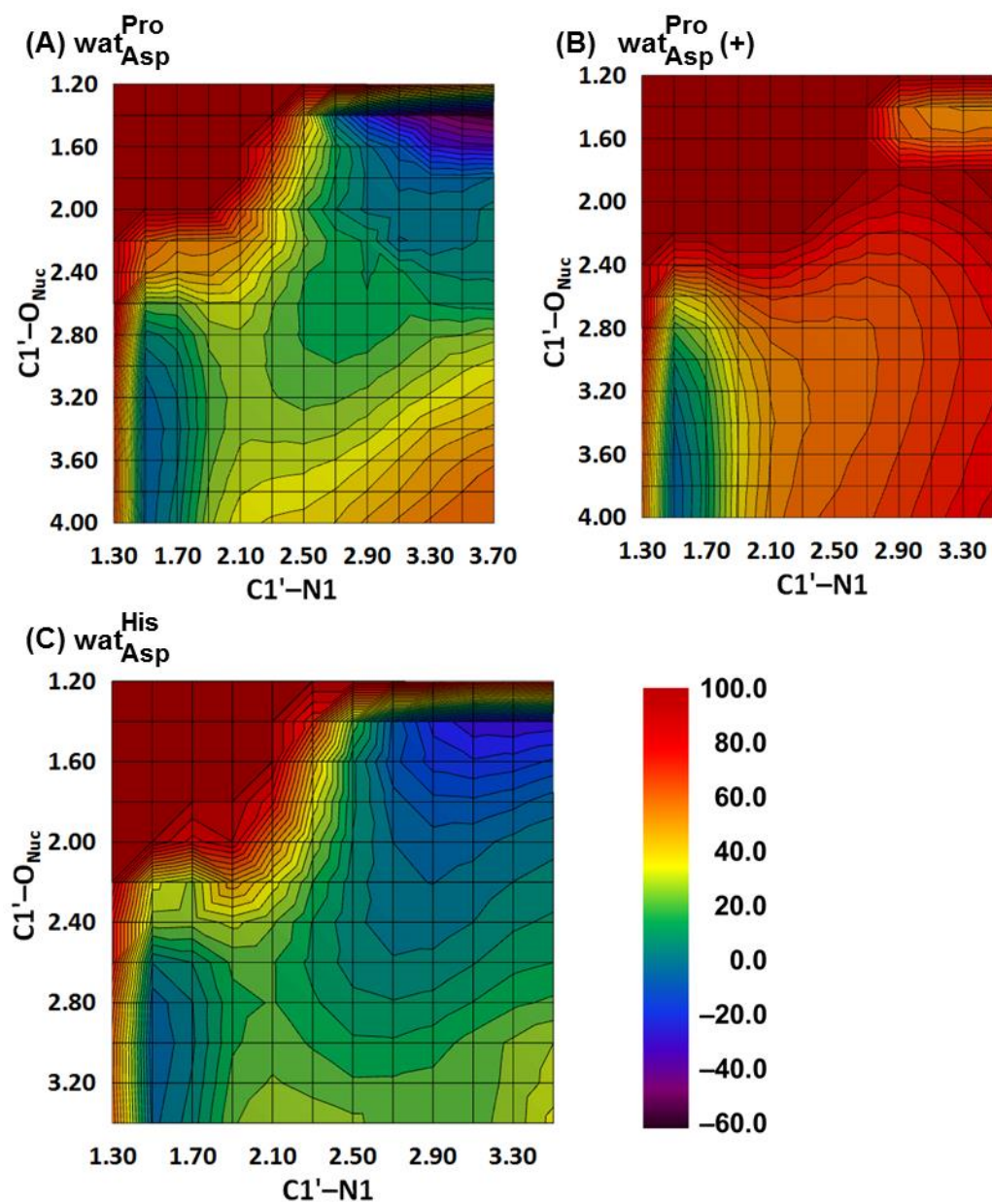
Figure 3.3. *ONIOM(MPWB1K/6-31G(d):PM3) reaction surfaces (Å) for the mechanism of hUNG2 action using the* ***wat$_{Asp}^{Pro}$*** *model (**A**), the* ***wat$_{Asp}^{Pro}$(+)*** *model (**B**) and the* ***wat$_{Asp}^{His}$*** *model (**C**). The relative energies (ΔE, kJ mol^{-1}) are reported relative to the respective reactant.*

3.2.3 Refinement of Stationary Points

The geometries of the reactant, transition state and product complexes identified from the PES of feasible reaction pathways were further relaxed. Specifically, the constraints to the reaction coordinates for the reactant and product complexes were removed and the system was optimized to a minimum with the ONIOM(MPWB1K/6-31G(d):PM3) level of theory. The transition state structure was refined using the Quadratic Synchronous Transit (QST) method, with the three complexes from the PES as input. The QST methodology has recently been found to be effective for large models of other biological systems.[42–45] The optimization was considered complete when the forces converged to default criteria and the displacement converged to loose criteria (< 0.002 Hartrees). Due to computational resource limitations, frequency calculations could not be run on the entire system. Therefore, as in a previous study,[46] the character of the fully-optimized stationary points was verified by visual inspection of the normal modes of the high-level region of a system with any atom further than 4 Å from a DFT heavy atom removed. Through this analysis, it is found that the fully optimized transition states contain a large imaginary frequency (190 – 240 cm^{-1}) corresponding to motion along the desired reaction coordinate. Since zero-point energy corrections could not be calculated, the reported relative energies are upper-bounds to the true ONIOM(MPWB1K/6-31G(d):PM3) barrier. Coordinates for all relaxed stationary points are provided in Appendix B. All calculations were carried out with Gaussian 09, revision A.02.[47]

3.3 Results

To ensure that all options for water activation were investigated, models corresponding to chemically-relevant orientations of the nucleophilic water molecule interacting with any residue within hydrogen-bonding distance were generated. Careful consideration of these active-site models led to reaction potential energy surfaces for three models, which encompass two water

nucleophile orientations (Figure 3.4) and two H148 protonation states. In the first ($\mathbf{wat_{Asp}^{Pro}}$) model, the nucleophile is involved in hydrogen bonds with the functional group of D145 and the backbone carbonyl of P146. In the second model ($\mathbf{wat_{Asp}^{Pro}(+)}$), the nucleophile orientation is the same as in $\mathbf{wat_{Asp}^{Pro}}$, but H148 is protonated for comparison to previous computational work,[23] which adds an N_δ–H$\cdots$O hydrogen bond between H148 and the water nucleophile. Finally, in the $\mathbf{wat_{Asp}^{His}}$ model, the nucleophile acts as a proton donor to both H148 and D145.
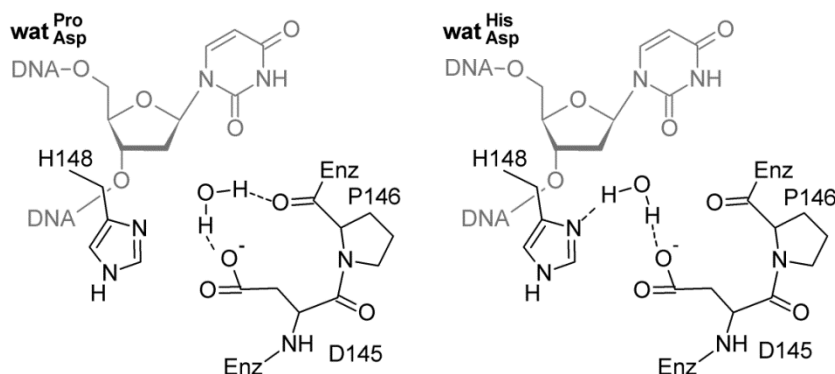
Figure 3.4. *Orientation of the water nucleophile in the various models used in this study.*

The reaction potential energy surfaces corresponding to the three nucleophile models are presented in Figure 3.3. In the graphs, the reactant complex occurs on the bottom left, and the product complex on the top right. Furthermore, a dissociative mechanism will progress along the bottom of the plot, while an associative mechanism will occur near the top of the plot. A table of energies corresponding to each surface can be found in the Appendix B (Tables B2–B4). In the following sections, each model will be described individually, and subsequently, results from point mutations on the most viable models will be presented.

3.3.1 Wat_{Asp}^{Pro} Model

In the $\mathbf{wat_{Asp}^{Pro}}$ model, the nucleophilic water molecule acts as a hydrogen donor to both the carboxylate group of D145 and the backbone carbonyl of P146 (Figure 3.4). On the

constrained PES (Figure 3.3A), the reactant occurs at a glycosidic bond length of 1.500 Å and a nucleophile distance of 3.000 Å. A transition state (TS) with a barrier of 25.4 kJ mol^{-1} (Table 3.1) can be identified with C1′–N1 and C1′–O$_{nuc}$ distances of 2.100 and 2.600 Å, respectively. The TS is highly dissociative and slowly falls to an exothermic product (–24.7 kJ mol^{-1}, relative to the reactant) with a C1′–N1 distance of 3.300 Å and a C1′–O$_{nuc}$ distance of 1.400 Å.

Table 3.1. *Barrier heights and reaction energies for the mechanism of hUNG2 action.*[a]

Model	Constrained[b]		Relaxed[c]	
	$\Delta E^{\ddagger}$	ΔE_R	$\Delta E^{\ddagger}$	ΔE_R
wat$_{Asp}^{Pro}$	25.4	–24.7	26.7	–25.2
wat$_{Asp}^{Pro}$(+)	97.0	59.0	–[d]	–[d]
wat$_{Asp}^{His}$	32.8	–56.1	34.8	–57.8

[a] Energies (kJ mol^{-1}) calculated at the ONIOM(MPWB1K/6-31G(d):PM3) level of theory. [b] From constrained potential energy surfaces (see Figure 3.3). [c] From fully optimized stationary points. [d] Not determined (see text).

The relaxed stationary points for this mechanism have reaction coordinate distances similar to the constrained geometries (Figure 3.5, Table B5 in Appendix B). Furthermore, removing the constraints only slightly increases the barrier to 26.7 kJ mol^{-1} (Table 3.1). In the relaxed transition state (TS, Figure 3.5), the sugar moiety is nearly planar, which reflects oxacarbenium cation character. The planar sugar, combined with a relatively large C1′–O$_{nuc}$ distance (2.727 Å), indicates that this mechanism is dissociative in nature. In addition, attack of the water at C1′ is delayed with respect to dissociation of the nucleobase, where the hydrogen-bond distance between the nucleophile and the general base, D145, is large (2.176 Å) in the transition state. A tightening of the N$_{\varepsilon}$–H···O2 hydrogen bond with H268 from 1.950 Å in the reactant to 1.880 Å in the transition state is observed in the relaxed complexes (Figure 3.5), which stabilizes the formation of the uracilate anion. The electrophilic C1′ migrates 0.793 Å towards the water nucleophile between the reactant and product complex, where the majority of this motion occurs after the transition state.
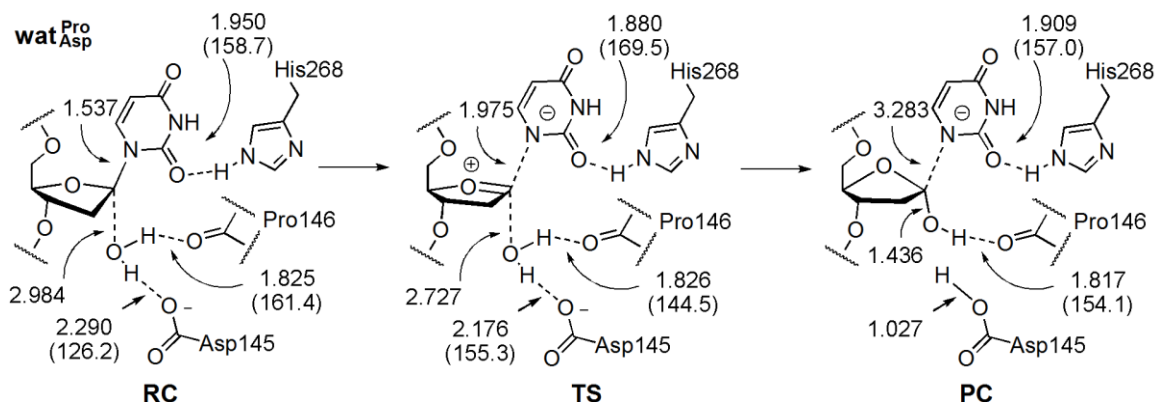
Figure 3.5. *Important distances (Å) and angles (°, in parentheses) for the relaxed stationary points from the* ***wat$_{Asp}^{Pro}$*** *model in which D145 is the general base and H148 neutral (ONIOM(MPWB1K/6-31G(d):PM3) optimized geometries).*

Throughout the reaction, F158 (Figure 3.2) remains in a near parallel (π–π stacked) orientation with respect to the uracil moiety, with an inter-ring distance of ~4.1 Å. The phenyl ring is positioned above C4/N3 of uracil in the (relaxed) reactant and TS geometries, but is centered over the pyrimidine ring in the product. The N3–H$\cdots$O$_\delta$ hydrogen bond to Asn204 increases from 1.839 to 1.851 Å between the reactant and product complexes, respectively. The N$_\delta$–H$\cdots$O4 interaction between Asn204 and uracil compresses by 0.013 Å in the transition state before returning to a length of 1.917 Å in the product. Finally, the hydrogen bond between a water molecule and O4 of uracil is reduced from 1.949 Å in the reactant to 1.925 Å in the TS and 1.889 Å in the product complex.

3.3.2 Wat$_{Asp}^{Pro}$(+) Model

The **wat$_{Asp}^{Pro}$(+)** model has the same nucleophile orientation as **wat$_{Asp}^{Pro}$**, but H148 is protonated at N$_\delta$ (Figure 3.4). In the (constrained) reactant, H148 interacts with the nucleophile via a tight (1.705 Å) N$_\delta$–H$\cdots$O$_{nuc}$ hydrogen bond. This contact greatly reduces the nucleophilicity of the water molecule, and results in a large barrier (97.0 kJ mol^{-1}) for addition to C1$'$ (Figure 3.3B, Table 3.1). Furthermore, the C1$'$–O$_{nuc}$ distance in the transition state is very short (1.800 Å), which is in contrast to experimental evidence suggesting a highly dissociative reaction pathway.

Therefore, it is very unlikely that the reaction will proceed with a cationic H148 residue, and this reaction will not be further refined through stationary point relaxation.

3.3.3 Wat_{Asp}^{His} Model

The final model employed in this study bridges the nucleophilic water between H148 and D145 ($\mathbf{wat_{Asp}^{His}}$, Figure 3.4). This water orientation has been previously proposed, based on a crystal structure of hUNG2 bound to an intermediate mimic.[14] The surface generated with this model (Figure 3.3C) is very similar in appearance to the $\mathbf{wat_{Asp}^{Pro}}$ PES (Figure 3.3A). The constrained reactant complex has glycosidic and nucleophilic distances of 1.500 and 3.600 Å, respectively. A TS can be observed at a C1′–N1 distance of 2.100 Å and a nucleophile distance of 3.200 Å, and leads to an activation energy of 32.8 kJ mol^{-1}. This is close to the $\mathbf{wat_{Asp}^{Pro}}$ transition state in both geometry and energy (Table 3.1 and Table B5 in Appendix B). After the TS, the surface steps down to an exothermic product (–56.1 kJ mol^{-1} relative to the reactant), which is significantly more stable than that on the $\mathbf{wat_{Asp}^{Pro}}$ surface. Interestingly, while this model allows for transfer to either D145 or H148 and thus does not explicitly bias nucleophile activation, proton transfer occurs from the nucleophile to H148 rather than D145.

There is very little change in geometry after releasing the reaction coordinate constraints on the reactant and transition state complexes. Therefore, when the constraints are removed from the $\mathbf{wat_{Asp}^{His}}$ stationary points, the barrier increases only slightly (to 34.8 kJ mol^{-1}). A notable difference upon full optimization is an increase in the C1′–N1 distance from 3.900 to 4.261 Å in the product (Table B5 in Appendix B); however, there is only a very small change in the reaction energy (ΔE_R = –57.8 kJ mol^{-1}). Similar to the electrophile migration observed with the $\mathbf{wat_{Asp}^{Pro}}$ model, C1′ drifts 1.325 Å during the reaction, and the sugar moiety adopts a C1′-exo pucker at the end of the reaction.

The N_ε–H$\cdots$O2 hydrogen bond between H268 and uracil reduces from 1.965 Å in the reactant to 1.876 Å in the transition state. In contrast to the $\mathbf{wat_{Asp}^{Pro}}$ model, the interplanar distance between the uracil group and F158 decreases from ~4.1 to ~3.6 Å as the reaction proceeds. This is accompanied by tightening of the hydrogen bonds to O2 and O4 of the uracilate anion. For example, the O–H$\cdots$O4 interaction between an active-site water molecule and uracil reduces from 1.967 Å in the reactant to 1.892 Å in the product. Similarly, the N–H$\cdots$O4 interaction with N204 decreases by 0.080 Å, and the N3–H$\cdots$O$_\delta$ distance decreases from 2.015 to 1.844 Å from reactant to product. In addition, the N–H$\cdots$O2 hydrogen bond between O2 of uracil and the backbone amine of Q144 significantly shortens from 2.265 Å in the reactant to 1.981 and 1.788 Å in the transition state and product, respectively.

3.3.4 Point Mutations

Mutations involving D145, H148, N204 and H268 were performed on the two viable models ($\mathbf{wat_{Asp}^{Pro}}$ and $\mathbf{wat_{Asp}^{His}}$) to allow for comparison of calculated (Table 3.2) and experimental[10,19] changes in the barrier height. The mutations were carried out on the constrained PES geometries to ensure that the transition state did not collapse to a minimum (reactant or product) when an essential residue was removed. The new R-group was positioned to have maximum overlap with the original R-group, this residue was optimized, and then the entire DFT region was relaxed (with the exception of the C1′–N1 and C1′–O$_{nuc}$ constraints). While it is understood that the complex may rearrange in experimental studies to fill the vacancy created by mutations, this approach permits an investigation of the energetic (rather than structural) contribution of the mutations. The largest increase in barrier height (32.8 kJ mol^{-1}) occurs for the D145N mutant with the $\mathbf{wat_{Asp}^{Pro}}$ model, which is partially due to a steric conflict between N145 and Q144 (Figure 3.2), since the hydrogen-bond acceptor on D145 has been replaced with a

hydrogen-bond donor. Otherwise, the largest effects are seen for the H268A and H268L mutations, which are likely the result of the loss of the N_ε–H$\cdots$O2 hydrogen bond.

Table 3.2. *Changes in calculated barrier heights due to single mutations.*[a]

Mutation	wat_{Asp}^{Pro}	wat_{Asp}^{His}	Mutation	wat_{Asp}^{Pro}	wat_{Asp}^{His}
D145N	32.8	8.3	Q144G	0.6	–2.8
H148L	7.6	7.0	D145G	19.2	12.1
N204V	2.3	7.1	H148G	5.5	15.7
H268A	18.6	13.1	F158G	–1.8	–0.2
H268L	15.5	12.3	N204G	–[b]	7.2
H268Q	5.2	6.8	H268G	18.7	13.2
			Water[c]	7.1	6.9

[a] Relative energies (kJ mol^{-1}) calculated at the ONIOM(MPWB1K/6-31G(d):PM3) level of theory, where a positive value represents an increase in barrier height. [b] A stable structure could not be found. [c] Water molecule hydrogen bound at O4 of uracil was removed.

The contributions of various residues (Q144, D145, H148, F158, N204, and H268) to the calculated dissociation barrier were determined by replacing individual R-groups with a hydrogen atom (i.e., mutation to glycine) (Table 3.2). Removing the residue that acts as the general base from each model leads to significant changes in barrier height. Specifically, removing D145 from the **wat_{Asp}^{Pro}** model increases the barrier by 19.2 kJ mol^{-1}. Similarly, a 15.7 kJ mol^{-1} contribution of H148 is calculated for the **wat_{Asp}^{His}** model. In addition, D145 lowers the **wat_{Asp}^{His}** barrier by 12.1 kJ mol^{-1}, which is similar to the contribution from the general base (H148). Two other groups yield large changes in the calculated activation energy. First, H268 contributes substantially to the catalytic effect of hUNG2, lowering the **wat_{Asp}^{Pro}** barrier by 18.7 kJ mol^{-1} and the **wat_{Asp}^{His}** barrier by 13.2 kJ mol^{-1}. Second, the water molecule hydrogen bound to O4 of uracil contributes nearly 7 kJ mol^{-1} to both the **wat_{Asp}^{Pro}** and **wat_{Asp}^{His}** barriers (Table 3.2), where the effect of this water molecule was ascertained through deletion of the entire molecule. No other significant changes to the barrier height were calculated with either model for any other mutation considered (Table 3.2).

3.4 Discussion

3.4.1 Protonation State of H148

The mechanism of hUNG2 action was examined with different water nucleophile interactions to thoroughly characterize both the uracil dissociation and water activation aspects of the reaction. While models containing a neutral H148 yield an activation energy (~30 kJ mol^{-1}) appropriate for enzyme catalysis, the reaction potential energy surface for the model with protonated H148 produces a comparatively large barrier (~100 kJ mol^{-1}, Table 3.1). This finding supports experimental evidence that H148 is neutral as the nucleobase dissociates,[18] but contradicts a previous QM/MM study on hUNG2 that characterized a (~60 kJ mol^{-1}) barrier consistent with enzyme catalysis when H148 is protonated.[23] The discrepancy in the two computational studies is likely due to different partitioning schemes between the high- and low-level regions, where the current model treats more active-site residues at the high (QM) level of theory (e.g., H268). Therefore, single-point calculations were carried out on the $\mathbf{wat_{Asp}^{Pro}(+)}$
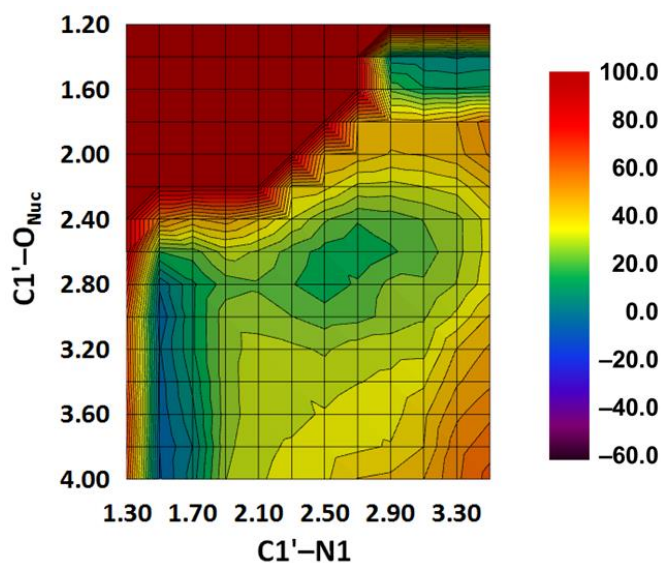
Figure 3.6. *ONIOM(MPWB1K/6-31G(d):PM3) reaction surfaces (Å) for the mechanism of hUNG2 action using the $\textbf{wat}_{\textbf{Asp}}^{\textbf{Pro}}$(+) model and a reduced high-level region. The relative energies (ΔE, kJ mol^{-1}) are reported relative to the respective reactant.*

geometries with the high-level region defined as in previous work (Figure 3.6). These calculations yield an overall reaction pathway and energetics similar to those previously reported, which indicates that the earlier results were most likely obtained due to the use of an inappropriately small high-level region. The importance of selecting an appropriate model size can also be seen by comparing the barrier height obtained with ONIOM (34.8 kJ mol^{-1}) to that obtained with just the DFT region (87.8 kJ mol^{-1}) for the $\mathbf{wat^{His}_{Asp}}$ model. Furthermore, the large barrier calculated in the presence of a cationic H148 is more consistent with an anticipated decrease in the nucleophilicity of the water molecule upon protonation of this residue, as well as an increase in electrostatic repulsion between cationic H148 and the positive charge developing on the sugar moiety. Since the current model predicts a high barrier when H148 is protonated, and experimental evidence suggests this residue is neutral in the reactant,[18] only the $\mathbf{wat^{Pro}_{Asp}}$ and $\mathbf{wat^{His}_{Asp}}$ models will be discussed further.

3.4.2 Comparison of Point Mutations to Experiment

The experimental trend in activity for a selection of mutant enzymes (H148L > N204V > H268L > D145N)[10] is predicted by both models containing neutral H148 (Table 3.2), within the error of the methodology implemented. With respect to specific residues, the calculated effect of H268 on both models (Table 2) is consistent with the experimentally predicted contribution of this residue (9 – 20 kJ mol^{-1}).[7,17,20] Furthermore, the relatively small calculated effect (7.0 – 7.6 kJ mol^{-1}) of a H148L mutation on both barriers is in line with mutational analysis reporting an 8 kJ mol^{-1} effect on the barrier.[18] Most importantly, the calculated catalytic contribution of the previously proposed general base, D145, was found to be 19.2 and 12.1 kJ mol^{-1} for the $\mathbf{wat^{Pro}_{Asp}}$ and $\mathbf{wat^{His}_{Asp}}$ models, respectively. This is remarkably similar to the proposed transition state stabilization provided by D145 (12 kJ mol^{-1}) determined using intermediate mimics.[20]

3.4.3 Catalytic Effect of Nucleotide Conformation

As mentioned in Section 3.2, all hUNG2 active-site models were generated from a crystal structure (PDB ID: 1EMH) of the enzyme bound to DNA containing pseudouridine.[13] In this starting structure, C1 of ψU is bent ~40° out of the C1′–C2–C6 plane towards an sp^3-hybridized geometry. When ψU is mutated to uracil to generate the reactant geometries, the bend is greatly reduced (< 20°), but does not entirely disappear. Optimization of the nucleoside configuration found in the current work with no enzyme present removes the bend at N1 of uracil, which eliminates the possibility that the kink is an artifact of the DFT method implemented. In addition, the χ dihedral angle about the glycosidic bond in the relaxed enzyme-bound deoxyuridine reactant (170 – 180°) deviates by ~40° from the free nucleoside optimized at the same level of theory. Thus, both geometric features are likely due to steric constraints in the active site (Figure 3.2), particularly the close proximity of F158, as well as strong hydrogen-bonding interactions with N204 and H268.[21,48] Although the altered conformation of the reactant was originally reported for a substrate mimic (ψU),[13] these calculations show that these deformations persist with 2′-deoxyuridine. As suggested in previous work, these geometrical changes to the dU nucleotide likely have a significant contribution to the catalytic effect of hUNG2 by lowering the barrier to deglycosylation through hyperconjugation and anomeric effects.[13,48] This change in conformation requires over 10 kJ mol^{-1}.[d] Therefore, while the activation energies calculated using the two viable models in this Chapter (26.7 and 34.8 kJ mol^{-1}, for $\mathbf{wat^{Pro}_{Asp}}$ and $\mathbf{wat^{His}_{Asp}}$, respectively) are lower than the experimental value (50.6 kJ mol^{-1}),[49–50] at least some of this difference can be attributed to bending of the nucleotide to fit into the active site.

---

[d] Calculated at the MPWB1K/6-31G(d) level of theory by fixing the N1 out-of-plane angle in the bare dU nucleoside in the gas phase.

3.4.4 hUNG2 Mechanism Highly Dissociative

Calculations on both of the viable models suggest that the reaction has a single transition state that is highly dissociative in nature. Specifically, the transition state for both the $\text{wat}_{\text{Asp}}^{\text{Pro}}$ and $\text{wat}_{\text{Asp}}^{\text{His}}$ models exhibits a glycosidic bond length of ~2 Å, and a considerably longer nucleophile distance (> 2.6 Å). After the transition state, the potential energy surface has a flat plateau corresponding to further stretching of the glycosidic bond. Once the glycosidic bond is sufficiently elongated, C1′ electrophile migration towards the water nucleophile and barrierless addition of water to the anomeric carbon occurs. While it has been proposed that a stable intermediate exists along the reaction pathway, the present calculations support a transition state that is highly dissociative and has substantial oxacarbenium ion character as suggested by KIE experiments.[8] In addition, the shape of the calculated PES following the transition state is supported by evidence that nucleophilic addition to oxacarbenium cations is often barrierless.[51–52] Regardless, the models implemented in this Chapter indicate that the nucleophile is deprotonated before, rather than after, addition to the anomeric carbon, and therefore nucleophile activation likely plays a role in the barrierless addition in this particular reaction. Taken together, the comparisons in the above paragraphs support the use of both the $\text{wat}_{\text{Asp}}^{\text{Pro}}$ and $\text{wat}_{\text{Asp}}^{\text{His}}$ active-site models and allows us to examine other aspects of the chemical step of the hUNG2 mechanism with confidence.

3.4.5 Trade-Off of Leaving Group Stabilization

A benefit to carrying out reaction PES scans is the ability to observe how substrate interactions change during the course of the reaction, which in turn permits predictions about the role of active-site residues. The most important finding from this analysis is that several amino acid residues share the responsibility of stabilizing the negative charge building up on the uracil moiety throughout the reaction despite emphasis on only H268 in the literature. Furthermore,

each group provides stabilization at slightly different stages of the reaction. The interactions involving O4 of uracil are at their strongest earlier in the reaction (C1′–N1 = 2.1 – 2.5 Å) since this site has the largest proton affinity in the neutral nucleobase.[53] Specifically, the hydrogen bond between N204 and O4 of the uracil moiety is shortest immediately following the TS (Table B7 in Appendix B). The interactions involving O2 are strongest later in the reaction since the negative charge in the uracilate anion is delocalized over N1/O2. Indeed, the interaction between the catalytic H268 residue and O2 is strongest when the C1′–N1 distance is around 2.7 – 2.9 Å. Interestingly, interactions between O4 and an active-site water molecule also change during the reaction, where these interactions are strongest just before the product complex. The above effects are observed for both the $\text{wat}_{\text{Asp}}^{\text{Pro}}$ and $\text{wat}_{\text{Asp}}^{\text{His}}$ models; however, the changes in hydrogen-bond length throughout the reaction are more pronounced for the $\text{wat}_{\text{Asp}}^{\text{His}}$ model (see Appendix B, Table B7). For both models, changes in the interactions between uracil and any other active-site amino acid residues are insignificant.

3.4.6 D145 Mutations Can Mask Effects of Other Residues

As mentioned in the Results section, the D145G mutation to both the $\text{wat}_{\text{Asp}}^{\text{Pro}}$ and $\text{wat}_{\text{Asp}}^{\text{His}}$ models leads to a significant change in barrier height (19.2 and 12.1 kJ mol^{-1}, respectively, Table 3.2). Since the TS is highly dissociative, this is consistent with suggestions that D145 electrostatically stabilizes the sugar moiety in the TS.[20,26] Furthermore, since association of the water nucleophile is barrierless (Figure 3.3), mutations that remove D145 can conceal the effects of residues on processes that occur later along the reaction pathway, such as the role of H148 in activation of the nucleophile. For example, the H148L effect on the barrier for both models is ~7.0 kJ mol^{-1} (Table 3.2), which indicates a smaller dependence of the dissociative TS on this residue, despite being the general base in one of the models. This suggests that the contribution of H148 occurs after the rate-limiting step, and therefore may not be observed in mutations (e.g.,

D145N) that disrupt dissociation of the nucleobase. Based on this discussion, it may not be possible to conclusively determine the role of D145 as the general base or the role of other residues (i.e., H148) in the chemical step of the hUNG2 mechanism following base departure by point mutations alone.

3.4.7 H148 is the Preferred General Base

Deletion of the acting general base from either the $\textbf{wat}_{\textbf{Asp}}^{\textbf{Pro}}$ or $\textbf{wat}_{\textbf{Asp}}^{\textbf{His}}$ models (D145 and H148, respectively) causes the nucleophile to reorient to interact with the other potential activator. Therefore, in the absence of H148, D145 can act as the general base and *vice versa*. When coupled with similar calculated reaction barriers (26.7 and 34.8 kJ mol^{-1}, Table 3.2), this finding suggests that either D145 or H148 may activate the water nucleophile depending on the orientation the water is bound in the active site. However, the preference for proton transfer from the nucleophile to one base over the other can be ascertained by examining the $\textbf{wat}_{\textbf{Asp}}^{\textbf{His}}$ model, which allows for water activation by either H148 or D145. In the relaxed $\textbf{wat}_{\textbf{Asp}}^{\textbf{His}}$ reactant complex (RC, Figure 3.6), the hydrogen-bond distances between the nucleophile and the two potential general bases (H148 and D145) are almost identical. Nevertheless, the contact to H148 tightens and that to D145 loosens in the transition state. In addition, the nucleophilic water fully transfers a proton to H148 in the product complex, which contrasts the incomplete transfer in the $\textbf{wat}_{\textbf{Asp}}^{\textbf{Pro}}$ product (PC, Figure 3.5). This demonstrates that proton transfer to histidine is preferred, which is consistent with proposals that hydrogen bonds formed between groups with matching pK_a's can provide a large contribution to enzyme catalysis[54] since the pK_a of water is closer to histidine than aspartate. Therefore, while either D145 or H148 can act as the general base in the mechanism of hUNG2 action, proton transfer to histidine is more likely.
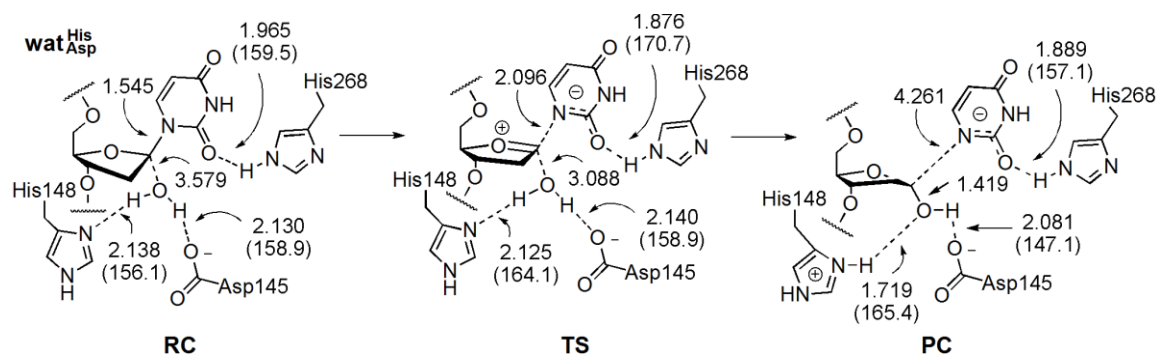
Figure 3.7. *Important distances (Å) and angles (°, in parentheses) for the relaxed stationary points from the* **wat$_{Asp}^{His}$** *model in which H148 is the general base (ONIOM(MPWB1K/6-31G(d):PM3) optimized geometries).*

3.4.8 Roles of D145 and H148

The calculations in this Chapter suggest that both D145 and H148 are required for maximum efficiency of the chemical step. During the early stages of the reaction, the water nucleophile is held in place by an anionic D145 and a neutral H148, which confirms this previously hypothesized function of H148.[18] However, the role of H148 is further expanded to include activation of the nucleophile (i.e., catalyzes AP-site formation). This newly proposed function is supported by the work of Parker and Stivers[18] who found that H148 is initially neutral, but becomes protonated during the reaction, and has a catalytic contribution late in the chemical step. Furthermore, they proposed that H148 should be added to the list of important active-site groups for transition state stabilization, potentially through positioning the substrate and catalytic water or producing a favourable reaction environment (solvent exclusion). These results agree that H148 is an important catalytic residue, and reveal for the first time that its primary role in the chemical step is likely activation of the water nucleophile. This new function for H148 does not exclude possible significant contributions to earlier events such as nucleotide flipping or active-site reorganization.[18,28] Finally, in agreement with previous proposals,[20] the primary role of D145 is defined as electrostatic stabilization of the cationic sugar moiety formed as the reaction proceeds (i.e., catalyzes glycosidic bond cleavage). Recently, it has been proposed that the role of

the catalytically essential lysine in hOGG1 as the nucleophile is secondary to its role in substrate recognition and binding, and is the direct result of its proximity to the sugar.[55] When this concept is applied to D145 in hUNG2, the proximity of the D145 residue to the water nucleophile resulting from its primary role of electrostatic stabilization of the TS allows participation in proton transfer as a possible secondary role.

3.5 Conclusions

In this Chapter, ONIOM(QM:QM) calculations were utilized to study the reaction potential energy surfaces of the mechanism of hUNG2 action. Unlike previous computational work that treated fewer active-site residues with a high (QM) level of theory, the present study determined that H148 must be neutral during dissociation of the nucleobase, which is consistent with recent experimental evidence. The reaction PES generated using two models with neutral H148 residues are both consistent with an abundance of experimental data, including mutational studies. This supports the use of active-site models and allows me to confidently examine different aspects of the chemical step catalyzed by hUNG2.

For the first time, a complete mechanism is presented for the chemical step of hUNG2 action where H268, D145 *and* H148 are catalytic. Specifically, it is proposed that the primary function of D145 is electrostatic stabilization of the cationic charge forming on the sugar moiety. Therefore, this residue catalyzes glycosidic bond cleavage in conjunction with H268. Although this role for H268 has been previously proposed, this Chapter demonstrates that N204 and a water molecule are also involved in stabilization of the negative charge on uracil, where the importance of these interactions changes throughout the course of the reaction. In addition, while D145 can act as the general base, this Chapter reveals for the first time that H148 preferentially activates the water nucleophile in the chemical step. By classifying water activation, as well as nucleophile orientation, as a potential secondary function of D145, the primary (electrostatic stabilization)

role of this residue becomes aligned with that of active-site carboxylate groups in other glycosylases. Most importantly, this Chapter supports the incorporation of H148 into the list of residues (D145 and H268) essential to the chemical step of the hUNG2 mechanism, and explains the experimental observation that this residue contributes to the catalysis of the chemical step.

3.6 References[e]

(1)   Lindahl, T., An N-Glycosidase from *Eschirichia coli* that Releases Free Uracil from DNA Containing Deaminated Cytosine Residues. *Proc. Nat. Acad. Sci. USA* **1974,** *71* (9), 3649–3653.

(2)   Krokan, H.; Wittwer, C. U., Uracil DNA-Glycosylase from HeLa-Cells - General-Properties, Substrate-Specificity and Effect of Uracil Analogs. *Nucleic Acids Res.* **1981,** *9* (11), 2599–2613.

(3)   Kavli, B.; Sundheim, O.; Akbari, M.; Otterlei, M.; Nilsen, H.; Skorpen, F.; Aas, P. A.; Hagen, L.; Krokan, H. E.; Slupphaug, G., hUNG2 is the Major Repair Enzyme for Removal of Uracil from U:A Matches, U:G Mismatches, and U in Single-Stranded DNA, with hSMUG1 as a Broad Specificity Backup. *J. Biol. Chem.* **2002,** *277* (42), 39926–39936.

(4)   Blackburn, G. M.; Walcher, G., "No Strain, No Gain": Studies in the Mechanism of a DNA Repair Enzyme. *Pol. J. Chem.* **2001,** *75* (8), 1183–1194.

(5)   Stivers, J. T.; Jiang, Y. L., A Mechanistic Perspective on the Chemistry of DNA Repair Glycosylases. *Chem. Rev. (Washington, DC, U. S.)* **2003,** *103* (7), 2729–2759.

(6)   Berti, P. J.; McCann, J. A. B., Toward a Detailed Understanding of Base Excision Repair Enzymes: Transition State and Mechanistic Analyses of N-glycoside Hydrolysis and N-glycoside Transfer. *Chem. Rev. (Washington, DC, U. S.)* **2006,** *106* (2), 506–555.

(7)   Dong, J.; Drohat, A. C.; Stivers, J. T.; Pankiewicz, K. W.; Carey, P. R., Raman Spectroscopy of Uracil DNA Glycosylase-DNA Complexes: Insights into DNA Damage Recognition and Catalysis. *Biochemistry* **2000,** *39* (43), 13241–13250.

(8)   Werner, R. M.; Stivers, J. T., Kinetic Isotope Effect Studies of the Reaction Catalyzed by Uracil DNA Glycosylase: Evidence for an Oxocarbenium Ion-Uracil Anion Intermediate. *Biochemistry* **2000,** *39* (46), 14054–14064.

(9)   Mol, C. D.; Arvai, A. S.; Sanderson, R. J.; Slupphaug, G.; Kavli, B.; Krokan, H. E.; Mosbaugh, D. W.; Tainer, J. A., Crystal Structure of Human Uracil-DNA Glycosylase in Complex with a Protein Inhibitor: Protein Mimicry of DNA. *Cell (Cambridge, MA, U. S.)* **1995,** *82* (5), 701–708.

[e] Bibliography and citations in ACS format.

(10)   Mol, C. D.; Arvai, A. S.; Slupphaug, G.; Kavli, B.; Alseth, I.; Krokan, H. E.; Tainer, J. A., Crystal Structure and Mutational Analysis of Human Uracil-DNA Glycosylase: Structural Basis of Specificity and Catalysis. *Cell (Cambridge, MA, U. S.)* **1995,** *80* (6), 869–878.

(11)   Slupphaug, G.; Mol, C. D.; Kavli, B.; Arvai, A. S.; Krokan, H. E.; Tainer, J. A., A Nucleotide-Flipping Mechanism from the Structure of Human Uracil-DNA Glycosylase Bound to DNA. *Nature (London, U. K.)* **1996,** *384* (6604), 87–92.

(12)   Parikh, S. S.; Mol, C. D.; Slupphaug, G.; Bharati, S.; Krokan, H. E.; Tainer, J. A., Base Excision Repair Initiation Revealed by Crystal Structures and Binding Kinetics of Human Uracil-DNA Glycosylase with DNA. *EMBO J.* **1998,** *17* (17), 5214–5226.

(13)   Parikh, S. S.; Walcher, G.; Jones, G. D.; Slupphaug, G.; Krokan, H. E.; Blackburn, G. M.; Tainer, J. A., Uracil-DNA Glycosylase-DNA Substrate and Product Structures: Conformational Strain Promotes Catalytic Efficiency by Coupled Stereoelectronic Effects. *Proc. Nat. Acad. Sci. USA* **2000,** *97* (10), 5083–5088.

(14)   Bianchet, M. A.; Seiple, L. A.; Jiang, Y. L.; Ichikawa, Y.; Amzel, L. M.; Stivers, J. T., Electrostatic Guidance of Glycosyl Cation Migration Along the Reaction Coordinate of Uracil DNA Glycosylase. *Biochemistry* **2003,** *42* (43), 12455–12460.

(15)   Drohat, A. C.; Xiao, G. Y.; Tordova, M.; Jagadeesh, J.; Pankiewicz, K. W.; Watanabe, K. A.; Gilliland, G. L.; Stivers, J. T., Heteronuclear NMR and Crystallographic Studies of Wild-Type and H187Q *Escherichia coli* Uracil DNA Glycosylase: Electrophilic Catalysis of Uracil Expulsion by a Neutral Histidine 187. *Biochemistry* **1999,** *38* (37), 11876–11886.

(16)   Drohat, A. C.; Stivers, J. T., *Escherichia coli* Uracil DNA Glycosylase: NMR Characterization of the Short Hydrogen Bond from His187 to Uracil O2. *Biochemistry* **2000,** *39* (39), 11865–11875.

(17)   Drohat, A. C.; Stivers, J. T., NMR Evidence for an Unusually Low N1 pK(a) for Uracil Bound to Uracil DNA Glycosylase: Implications for Catalysis. *J. Am. Chem. Soc.* **2000,** *122* (8), 1840–1841.

(18)   Parker, J. B.; Stivers, J. T., Uracil DNA Glycosylase: Revisiting Substrate-Assisted Catalysis by DNA Phosphate Anions. *Biochemistry* **2008,** *47* (33), 8614–8622.

(19)   Drohat, A. C.; Jagadeesh, J.; Ferguson, E.; Stivers, J. T., Role of Electrophilic and General Base Catalysis in the Mechanism of *Escherichia coli* Uracil DNA Glycosylase. *Biochemistry* **1999,** *38* (37), 11866–11875.

(20)   Jiang, Y. L.; Drohat, A. C.; Ichikawa, Y.; Stivers, J. T., Probing the Limits of Electrostatic Catalysis by Uracil DNA Glycosylase Using Transition State Mimicry and Mutagenesis. *J. Biol. Chem.* **2002,** *277* (18), 15385–15392.

(21)   Shaw, R. W.; Feller, J. A.; Bloom, L. B., Contribution of a Conserved Phenylalanine Residue to the Activity of *Escherichia coli* Uracil DNA Glycosylase. *DNA Repair* **2004,** *3* (10), 1273–1283.

(22) Luo, N.; Mehler, E.; Osman, R., Specificity and Catalysis of Uracil DNA Glycosylase. A Molecular Dynamics Study of Reactant and Product Complexes with DNA. *Biochemistry* **1999,** *38* (29), 9209–9220.

(23) Dinner, A. R.; Blackburn, G. M.; Karplus, M., Uracil-DNA Glycosylase Acts by Substrate Autocatalysis. *Nature (London, U. K.)* **2001,** *413* (6857), 752–755.

(24) Ma, A.; Hu, J.; Karplus, M.; Dinner, A. R., Implications of Alternative Substrate Binding Modes for Catalysis by Uracil-DNA Glycosylase: An Apparent Discrepancy Resolved. *Biochemistry* **2006,** *45* (46), 13687–13696.

(25) Millen, A. L.; Archibald, L. A. B.; Hunter, K. C.; Wetmore, S. D., A Kinetic and Thermodynamic Study of the Glycosidic Bond Cleavage in Deoxyuridine. *J. Phys. Chem. B* **2007,** *111* (14), 3800–3812.

(26) Jiang, Y. L.; Cao, C.; Stivers, J. T.; Song, F.; Ichikawa, Y., The Merits of Bipartite Transition-State Mimics for Inhibition of Uracil DNA Glycosylase. *Bioorg. Chem.* **2004,** *32* (4), 244–262.

(27) Wolfenden, R., Degrees of Difficulty of Water-Consuming Reactions in the Absence of Enzymes. *Chem. Rev. (Washington, DC, U. S.)* **2006,** *106* (8), 3379–3396.

(28) Parker, J. B.; Bianchet, M. A.; Krosky, D. J.; Friedman, J. I.; Amzel, L. M.; Stivers, J. T., Enzymatic Capture of an Extrahelical Thymine in the Search for Uracil in DNA. *Nature (London, U. K.)* **2007,** *449* (7161), 433–438.

(29) Norman, D. P. G.; Chung, S. J.; Verdine, G. L., Structural and Biochemical Exploration of a Critical Amino Acid in Human 8-oxoguanine Glycosylase. *Biochemistry* **2003,** *42* (6), 1564–1572.

(30) Fromme, J. C.; Verdine, G. L., DNA Lesion Recognition by the Bacterial Repair Enzyme MutM. *J. Biol. Chem.* **2003,** *278* (51), 51543–51548.

(31) Fromme, J. C.; Verdine, G. L., Structure of a Trapped Endonuclease III-DNA Covalent Intermediate. *EMBO J.* **2003,** *22* (13), 3461–3471.

(32) Doublie, S.; Bandaru, V.; Bond, J. P.; Wallace, S. S., The Crystal Structure of Human Endonuclease VIII-Like 1 (NEIL1) Reveals a Zincless Finger Motif Required for Glycosylase Activity. *Proc. Nat. Acad. Sci. USA* **2004,** *101* (28), 10284–10289.

(33) Lau, A. Y.; Wyatt, M. D.; Glassner, B. J.; Samson, L. D.; Ellenberger, T., Molecular Basis for Discriminating Between Normal and Damaged Bases by the Human Alkyladenine Glycosylase, AAG. *Proc. Nat. Acad. Sci. USA* **2000,** *97* (25), 13573–13578.

(34) Fromme, J. C.; Banerjee, A.; Huang, S. J.; Verdine, G. L., Structural Basis for Removal of Adenine Mispaired with 8-Oxoguanine by MutY Adenine DNA Glycosylase. *Nature (London, U. K.)* **2004,** *427* (6975), 652–656.

(35) Bowman, B. R.; Lee, S.; Wang, S. Y.; Verdine, G. L., Structure of *Escherichia coli* AlkA in Complex with Undamaged DNA. *J. Biol. Chem.* **2010,** *285* (46), 35783–35791.

(36)   Humbel, S.; Sieber, S.; Morokuma, K., The IMOMO Method: Integration of Different Levels of Molecular Orbital Approximations for Geometry Optimization of Large Systems: Test for n-Butane Conformation and S_N2 Reaction: RCl+Cl. *J. Chem. Phys.* **1996,** *105* (5), 1959–1967.

(37)   Dapprich, S.; Komaromi, I.; Byun, K. S.; Morokuma, K.; Frisch, M. J., A New ONIOM Implementation in Gaussian98. Part I. The Calculation of Energies, Gradients, Vibrational Frequencies and Electric Field Derivatives. *THEOCHEM* **1999,** *462*, 1–21.

(38)   Lundberg, M.; Kawatsu, T.; Vreven, T.; Frisch, M. J.; Morokuma, K., Transition States in a Protein Environment - ONIOM QM:MM Modeling of Isopenicillin N Synthesis. *J. Chem. Theory Comput.* **2009,** *5* (1), 222–234.

(39)   Stewart, J. J. P., Optimization of Parameters for Semiemperical Methods. 1. Method. *J. Comput. Chem.* **1989,** *10* (2), 209–220.

(40)   Stewart, J. J. P., Optimizations of Parameters for Semiemperical Methods. 2. Applications. *J. Comput. Chem.* **1989,** *10* (2), 221–264.

(41)   Zhao, Y.; Truhlar, D. G., Hybrid Meta Density Functional Theory Methods for Thermochemistry, Thermochemical Kinetics, and Noncovalent Interactions: The MPW1B95 and MPWB1K Models and Comparative Assessments for Hydrogen Bonding and Van der Waals Interactions. *J. Phys. Chem. A* **2004,** *108* (33), 6908–6918.

(42)   Cisneros, G. A. s.; Perera, L.; Schaaper, R. M.; Pedersen, L. C.; London, R. E.; Pedersen, L. G.; Darden, T. A., Reaction Mechanism of the ε Subunit of *E. coli* DNA Polymerase III: Insights into Active Site Metal Coordination and Catalytically Significant Residues. *J. Am. Chem. Soc.* **2009,** *131* (4), 1550–1556.

(43)   Parks, J. M.; Guo, H.; Momany, C.; Liang, L.; Miller, S. M.; Summers, A. O.; Smith, J. C., Mechanism of Hg−C Protonolysis in the Organomercurial Lyase MerB. *J. Am. Chem. Soc.* **2009,** *131* (37), 13278–13285.

(44)   Tao, P.; Gatti, D. L.; Schlegel, H. B., The Energy Landscape of 3-Deoxy-d-manno-octulosonate 8-Phosphate Synthase. *Biochemistry* **2009,** *48* (49), 11706–11714.

(45)   Lonsdale, R.; Harvey, J. N.; Mulholland, A. J., Compound I Reactivity Defines Alkene Oxidation Selectivity in Cytochrome P450cam. *J. Phys. Chem. B* **2010,** *114* (2), 1156–1162.

(46)   Tao, P.; Fisher, J. F.; Shi, Q.; Mobashery, S.; Schlegel, H. B., Matrix Metalloproteinase 2 (MMP2) Inhibition: DFT and QM/MM Studies of the Deprotonation-Initialized Ring-Opening Reaction of the Sulfoxide Analogue of SB-3CT. *J. Phys. Chem. B* **2010,** *114* (2), 1030–1037.

(47)   Frisch, M. J.; Trucks, G. W.; Schlegel, H. B.; Scuseria, G. E.; Robb, M. A.; Cheeseman, J. R.; Scalmani, G.; Barone, V.; Mennucci, B.; Petersson, G. A*., et al. Gaussian 09*, Revision A.02; Gaussian, Inc.: Wallingford CT, 2009.

(48)   Werner, R. M.; Jiang, Y. L.; Gordley, R. G.; Jagadeesh, G. J.; Ladner, J. E.; Xiao, G. Y.; Tordova, M.; Gilliland, G. L.; Stivers, J. T., Stressing-Out DNA? The Contribution of

Serine-Phosphodiester Interactions in Catalysis by Uracil DNA Glycosylase. *Biochemistry* **2000,** *39* (41), 12585–12594.

(49) Wittwer, C. U.; Krokan, H., Uracil-DNA Glycosylase in HeLa S3 Cells: Interconvertibility of 50 and 20 kDa Forms and Similarity of the Nuclear and Mitochondrial Form of the Enzyme. *Biochim. Biophys. Acta, Protein Struct. Mol. Enzymol.* **1985,** *832* (3), 308–318.

(50) Slupphaug, G.; Eftedal, I.; Kavli, B.; Bharati, S.; Helle, N. M.; Haug, T.; Levine, D. W.; Krokan, H. E., Properties of a Recombinant Human Uracil-DNA Glycosylase from the *Ung* Gene and Evidence That *Ung* Encodes the Major Uracil-DNA Glycosylase. *Biochemistry* **1995,** *34* (1), 128–138.

(51) Richard, J. P., A Consideration of the Barrier for Carbocation-Nucleophile Combination Reactions. *Tetrahedron* **1995,** *51* (6), 1535–1573.

(52) Richard, J. P.; Williams, K. B.; Amyes, T. L., Intrinsic Barriers for the Reactions of an Oxocarbenium Ion in Water. *J. Am. Chem. Soc.* **1999,** *121* (36), 8403–8404.

(53) Di Laudo, M.; Whittleton, S. R.; Wetmore, S. D., Effects of Hydrogen Bonding on the Acidity of Uracil. *J. Phys. Chem. A* **2003,** *107* (48), 10406–10413.

(54) Cleland, W. W.; Kreevoy, M. M., Low-Barrier Hydrogen-Bonds and Enzymatic Catalysis. *Science (Washington, DC, U. S.)* **1994,** *264* (5167), 1887–1890.

(55) Dalhus, B.; Forsbring, M.; Helle, I. H.; Vik, E. S.; Forstrøm, R. J.; Backe, P. H.; Alseth, I.; Bjørås, M., Separation-of-Function Mutants Unravel the Dual-Reaction Mode of Human 8-Oxoguanine DNA Glycosylase. *Structure (Cambridge, MA, U. S.)* **2011,** *19* (1), 117–127.

Chapter 4: Monofunctional Glycosylases Part 2:

Adenine–DNA Glycosylase (MutY)[a]

4.1 Introduction

As outlined in Section 1.2.2, the integrity of the genetic code must be continually protected from various damaging mechanisms including oxidative stress,[1] which has been linked to cancer[2–5] and neurodegenerative diseases.[6–8] One of the most prevalent and mutagenic forms of oxidative damage is OG, due to Polε generating OG:A mispairs during replication.[9] In bacteria, the deleterious effects of the OG lesion are prevented by a collection of proteins that form the GO system, namely MutM (FPG), MutY and MutT (EC # 3.6.1.55).[10–12] MutM and MutY are both glycosylases,[13–14] while MutT is a nucleotide sanitization protein.[15–16] Specifically, MutM catalyzes deglycosylation of OG when base-paired with cytosine.[11] In the event that one round of replication has occurred and an OG:A pair has formed, MutY selectively removes the adenine residue (to be replaced with cytosine by a BER polymerase) in preparation for MutM.[17] However, repairing all adenine mismatches in this way assumes that OG should always be replaced with guanine. Another possibility involves misincorporation of an OG nucleotide opposite adenine, in which case MutY repair would lead to a T:A → G:C transversion. Therefore, a third repair protein, MutT, hydrolyzes the OG nucleotide triphosphate to remove it from the nucleotide pool.[15] Due to their interplay, if any one of these proteins is disrupted, serious downstream implications arise. For example, a common polymorphism of hMYH (the human homologue of MutY) removes OG specificity and is associated with multiple diseases, such as MYH-associated polyposis (MAP), and has been linked to a predisposition to colorectal cancer.[18–19]

The mechanism of action of MutY has been studied with a variety of methods including kinetics,[17,20–27] alternative substrates,[28–37] kinetic isotope effects,[38] and X-ray crystallography.[20,23,39–43] Mutational studies have identified two essential catalytic residues: E43 and D144 (*geobacillus stearothermophilis* numbering).[20–21,27] Analysis of a crystal structure of OG:A bound to MutY(D144N) (referred to as the lesion recognition complex, LRC, Figure 4.1A) indicates that E43 is aligned with N7 of adenine, while D144 is near the deoxyribose ring.[39,42] The LRC led to the generally accepted mechanism whereby E43 acts as a general acid (via a bridging water molecule) in the first protonation step and as a general base in the second hydrolysis step (Figure 4.1C). However, due to the lack of direct contacts between MutY and adenine, Verdine *et*
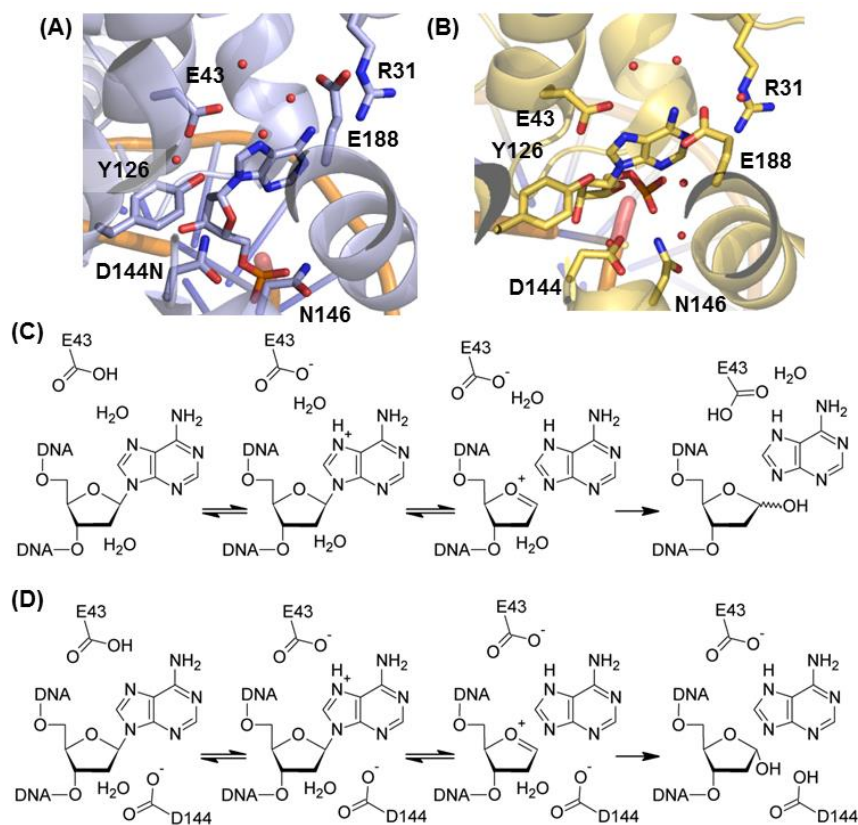
Figure 4.1. *(A) Active site of bsMutY(D144N) with OG:A bound (LRC, PDB ID: 1RRQ). (B) Active site of bsMutY with OG:FA bound (FLRC, PDB ID: 3G0Q). (C) Proposed mechanism of action of MutY based on the LRC. (D) Proposed mechanism based on the FLRC.*

al. later developed a crystal structure of MutY bound to 2′-fluoro-dA (FdA) containing DNA (denoted as the FLRC, Figure 14.B). The new structure contains direct contacts to FdA, and suggests that D144 is the general base rather than E43 (Figure 4.1D).

There is substantial support for an initial dA protonation step. First, kinetic isotope effects indicate that protonation of N7 occurs before deglycosylation.[38] Second, MutY is inactive towards a 7-deaza analogue.[35] Third, E43 is aligned for proton transfer to N7 (either directly[39,42] or indirectly through a bridging water molecule[39]). A recent study found that a carboxyl group is required in the E43 position since an E43D mutant maintains weak activity but an E43C mutant is inactive.[27] In addition, a pH profile indicates that E43 is initially neutral and that catalytic activity is hindered when the residue is initially anionic.[27] The non-enzymatic depurination of nucleosides and oligonucleotides is known to be acid catalyzed, with protonation of the nucleobase contributing up to 30 kJ mol^{-1}.[38] Therefore, this first step of the reaction may account for almost half of the catalytic activity of the enzyme.[44] There appears to be little leaving group stabilization after the proton transfer step. For example, N1 and N3-deaza-adenine substrates are both catalytically active (albeit at reduced rates),[35,37] which indicates that hydrogen bonding at these sites is not essential. In addition, MutY is active towards a modified substrate with the N6-amine group converted to a methyl group.[35] This activity is supported by KIE results that indicate a hydrogen bond to N6 in the reactant is broken before the depurination transition state.[38]

There is less definitive evidence regarding the hydrolysis step. Kinetic isotope effect experiments indicate that the hydrolysis step follows a $D_N*A_N^{\ddagger}$ mechanism.[38] In this mechanism, the glycosidic bond breaks in the first, rate-limiting, reversible step (D_N*), and a water molecule adds to the resulting oxacarbenium cation in the final irreversible step ($A_N^{\ddagger}$). Note that the KIE does not provide explicit evidence indicating which residue (E43 or D144) acts as the general base and activates the nucleophile. Other glycosylases contain a catalytically-essential aspartate or glutamate similarly located near the sugar moiety, ideally positioned to act as a general base

that activates the water nucleophile, such as D145 in hUNG2 (Chapter 3). Nevertheless, there is no evidence that the water nucleophile in MutY is deprotonated prior to attack on the anomeric carbon. Instead, a leading theory is that the anionic charge on D144 assists stabilization of the cationic intermediate.[27,38] Indeed, it has recently been shown that an anionic charge in this position is essential for MutY activity since a D144E mutant is catalytically active at wild-type levels and a D144C mutant is active at a pH where the cysteine residue is deprotonated.[27] Interestingly, computational studies on MutY,[45] as well as hUNG2 (Chapter 3), have determined that the aspartate residue is important, but did not observe full proton transfer from the nucleophile.

As discovered in Chapter 3 with hUNG2, computational studies can provide vital molecular level information regarding the role of active-site residues and aid experimental studies in revealing the mechanism employed by enzymes. However, previous computational studies on MutY have not considered the FLRC crystal structure or the associated alternate mechanism (D144 as general base).[45–46] Recent molecular dynamics calculations found that the FLRC geometry represents a more catalytically-competent reactant complex than the previous LRC.[47] Therefore, the present Chapter fills an important void in the literature by considering the mechanistic implications of the FLRC, with a particular emphasis placed on understanding the role of D144. For the first time, a rigorous analysis of the active site is carried out with QM/QM (ONIOM). Subsequently, the mechanism employed by MutY is critically analyzed using detailed reaction potential energy surface scans, which were successfully used in Chapter 3 to gain insight into the mechanism of action of hUNG2. New roles for active-site residues are identified, including the essential function of D144, which is consistent with experimental evidence and justifiably more involved than observed for other glycosylases.[13–14] Novel reaction PES carried out on a Y126F mutant, elucidates the catalytic importance of Y126, which has yet to be acknowledged in the literature. Most importantly, our analysis clarifies a unified role of active-

site Asp/Glu residues that are present in many enzymes in the DNA glycosylase family. These findings also have important implications for the mechanism of action of other enzymes that catalyze nucleoside or nucleotide deglycosylation reactions such as RNA hydrolases, phosphorylases and glycosidases.

4.2 Computational Details

4.2.1 Reactant Generation

In this study, the FLRC with MutY bound to an inhibitor (FdA)[42] was used as the starting point for all computational models. The enzyme-substrate complex was generated by first selecting a 10 Å sphere around the FdA residue (A5L18) in the 3G0Q crystal structure.[42] Second, additional residues were included to link small oligopeptides separated by 1–2 residue gaps. Third, residues with the functional group directed away from the bulk of the model were truncated to alanine (i.e., R-group truncated after C_β). A full list of residues included in the model is provided in Appendix C (Table C1). Truncation points were capped with hydrogen atoms constrained to the crystal structure orientation of the replaced atom. Specifically, the new C(N)–H bond lengths were allowed to relax, but the angles and dihedral angles were held fixed for the hydrogen relaxation step. The remaining hydrogen atoms were added manually to maximize hydrogen-bond contacts. All histidine residues were modeled in the Nε-tautomer, arginine residues were modeled as cationic, and glutamate/aspartate residues were modeled as anionic, with the exception of E43. The hydrogen atom locations were optimized with PM6 while fixing the heavy atom positions. Finally, the system was relaxed using ONIOM(M06-2X/ 6-31G(d):PM6) with the low-level region held fixed. M06-2X was used on the high-level region in Chapters 4 and 6 due to difficulties with SCF convergence problems with MPWB1K (see Section 2.2.1) and the excellent performance of M06-2X in Chapter 2. Furthermore, the low-level method was increased to PM6, which performs better for enzymatic systems.

The residues in the low-level region overlay well with crystal structures of the LRC (RMSD: 0.560 Å) and product complex (PDB ID: 1VRL, RMSD: 0.540 Å).[b,39] In addition, residues with increased B-values compared to the average backbone value were placed in the unconstrained DFT region (including E188). Therefore, the constraint placed on the low-level region throughout the study will have a minimal effect on the reactions studied herein. The DFT region contains all groups that directly interact with adenine or the proposed nucleophile, namely the FdA nucleoside, waters 28, 50 and 371, and the functional groups of R31, E43, Y126, D144, N146 and E188 (Figure 4.2 and Table C1 in Appendix C). The charge of the full system is –5 with 838 total atoms (424 heavy atoms) in the wild-type models. The corresponding DFT region contains 104 total atoms (54 heavy atoms) and a charge of –1.
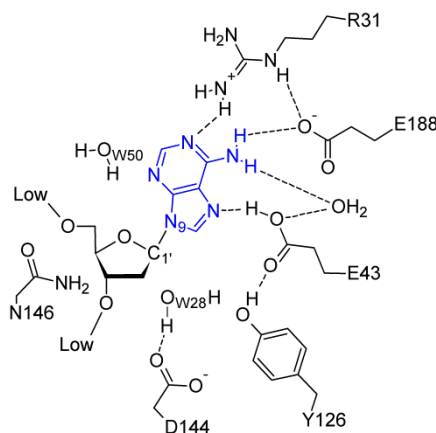
Figure 4.2. *Schematic of the residues included in the DFT region of the various ONIOM models.*

4.2.2 Conformational Search

Beyond the obvious differences in dA binding, the orientation of E188 is significantly altered between the LRC and FLRC (Figures 4.1A and 4.1B). Analysis of the electron density assigned to E188 in the FLRC indicates that the orientation of this residue is flexible.

---

[b] Overlays carried out with all atoms.

Specifically, no density was assigned to one of the carboxyl groups, and a solvent water molecule was placed in density that could instead be assigned to E188 (Figure C1 in Appendix C). Therefore, to address both the disparity in the density and deviations between the two crystal structures, a conformational search of the residues in the DFT region was carried out. The search was separated into two groups: (1) D144 and N146 and (2) R31 and E188. Wat376 was removed from the model to allow for alternate conformations of E188. E43 and Y126 were not included in the conformational search due to the catalytically required contact between E43 and N7 of adenine[27] and a strong contact between the hydroxyl of Y126 and E43, as evidenced by continuous electron density between the two groups (Figure C2 in Appendix C).[42]

Initially, each dihedral angle in the R-groups of the two residues of interest was modified in 60° increments and conformations with small interatomic distances were removed. Next, single-point energy calculations were carried out on each conformation with PM6. Structures within 100 kJ mol^{-1} of the most stable conformer were then relaxed with ONIOM(M06-2X/ 6-31G(d):PM6). At this point, the resulting ONIOM geometries for the D144/N146 set and the R31/E188 set were combined and reoptimized with ONIOM.

4.2.3 Reactions

Based on the above conformational search, three models were used in the present study (Table 4.1). The first uses the X-ray crystal structure coordinates as an initial guess (X-WT). The second uses the lowest energy conformation from the search, which involves a new orientation for E188 and the D144–Val147 helix-cap in place (CS-Cap). The third breaks the D144 helix-capping interaction in the CS-Cap model (CS-NoCap), but maintains the orientation of E188. In order to test how mutations affect the shape of the reaction PES, two mutants were also investigated. Since the focus of this Chapter (and indeed this Thesis) is on the role of D144, a D144N mutation was carried out starting from the X-WT reactant (X-D144N). Since significant

motion in Y126 was observed during the course of the study, a Y126F mutant was also investigated, based on the CS-Cap model (CS-Y126F).

Table 4.1. *Summary of the different models used in Chapter 4.*

Model	D144[a]	E188[b]	Mutation
X-WT	Helix cap	FLRC[c]	
X-D144N	Helix cap	FLRC[c]	D144N
CS-Cap	Helix cap	Alternate[d]	
CS-Y126F	Helix cap	Alternate[d]	Y126F
CS-NoCap	Broken cap	Alternate[d]	

[a] Orientation of D144. [b] Orientation of E188. [c] Conformation from FLRC crystal structure.[42] [d] Orientation from conformation search, see Computational Details.

The mechanism of action of MutY was studied using reaction PES. As illustrated in Chapter 3, this methodology provides detailed information regarding the shape of the surface and allows for a more thorough comparison between the different models and mechanisms than full transition state optimizations. In addition, full transition state optimizations of this model were prohibitively expensive. Therefore, surfaces of increasing resolution were utilized to obtain accurate transition state information.

The first step in the MutY reaction, transfer of a proton from E43 to N7, was modeled by scanning the $O\varepsilon,_{E43}$–H distance with a 0.100 Å increment starting from the optimized reactant. In the event of barrierless transfer, where a structure with E43 protonated could not be obtained, the scan started with an $O\varepsilon,_{E43}$–H length of 0.900 Å. The fully-relaxed activated reactant with the proton on adenine (RC*) was used as the initial point for investigating the deglycosylation mechanisms.

Three mechanisms were characterized for the hydrolysis step: mechanism A uses Wat28 as the nucleophile; mechanism B uses Wat50 as the nucleophile; and mechanism C involves partial attack on C1′ by D144 during deglycosylation, followed by nucleophilic attack by Wat28. No bias was explicitly introduced into the model with respect to which residue (E43 or D144) is

the general base. The hydrolysis step was modeled using a two-dimensional reaction PES with the glycosidic bond (C1′–N9) as one coordinate and the nucleophile attack distance (C1′–O$_{nuc}$) as the second coordinate. First, a surface spanning the entire reaction was generated using a step-size of 0.400 Å. Second, the regions around potential stationary points (reactant, TS, intermediate and product) were refined to a 0.200 Å grid. Third, minima for productive mechanisms were fully relaxed (constraints on the glycosidic bond and nucleophile distance removed) and the transition states were further refined to a 0.050 Å grid. The DFT regions were extracted from the stationary points and M06-2X/6-31G(d) frequency calculations were carried out to obtain estimates of the zero-point vibrational energy and thermal correction to Gibbs energy, as well as to verify the nature of stationary points. High-quality energetics for the refined stationary points were obtained with ONIOM(M06-2X/6-311+G(2df,2p):PM6).

All calculations were carried out with Gaussian 09 (versions A.02 and C.01).[48]

4.3 Results

4.3.1 Conformational Search

To explore other potentially catalytically competent conformations, and to investigate discrepancies in the location of E188 between different crystal structures, a conformational search was carried out on select active-site residues in the DFT region (Figure 4.2). The lowest 100 kJ mol^{-1} orientations of D144 and N146 corresponded to 13 conformations, which converged to two conformations after relaxation with ONIOM. The lowest energy conformation maintains a helix-capping interaction between D144 and the backbone amide of V147 observed in the X-ray crystal structure. The other orientation breaks this contact at a cost of 51.6 kJ mol^{-1}. Nine conformations of R31 and E188 were obtained after relaxation of 30 different orientations. 19 of the 30 conformations fell to the lowest energy structure, which contains E188 in a conformation that matches the experimental electron density of the FLRC. A structure that most closely resembles

the reported FLRC geometry was obtained with an energy of 66.1 kJ mol^{-1} relative to the minimum. When the two D144/N146 and nine R31/E188 conformations were combined and relaxed with ONIOM, the energetic differences observed in the separate optimizations were maintained.

A recent molecular dynamics study comparing the LRC and FLRC also identified different orientations of D144 and E188,[47] which are likely not due to overly tight binding of the inhibitor (MutY(D144N):dA and MutY:FdA have the same binding strengths).[21,31,35] Furthermore, an overlay of the active sites of the LRC, FLRC and a product complex (PDB ID: 1VRL) indicates that the FLRC bears a stronger resemblance to the product (RMSD = 0.593 Å) than the LRC does (RMSD = 0.920 Å). Consequently, a reactant based on the FLRC would require the least atomic motion to proceed through the reaction. As a result, alternate conformations of D144 and E188 were used to generate some of the models implemented in this study (Table 4.1).

4.3.2 Reactions

In this Chapter, the mechanism of action of MutY is characterized with models based on the FLRC structure that contains discrete interactions between adenine and the protein. In this section, proton transfer from E43 to N7 of adenine is presented first. Next, the resulting activated-reactant complexes (RC*) are used to model the hydrolysis reaction (Figure 4.1C) with three different mechanisms (A, B and C). The reaction PES for each mechanism will be discussed separately along with relaxed stationary points for the lowest energy mechanism for each wild-type model (X-WT, CS-Cap and CS-NoCap, Table 4.1).

4.3.2.1 Proton Transfer

As discussed in the Computational Details, the initial proton transfer step was modeled with 1D PES scans. Since a minimum for the reactant is only present for the X-WT model, the

proton transfer surfaces are plotted with respect to the RC* (Figure C3 in Appendix C). Based on the surfaces, proton transfer is estimated to be barrierless upon incorporation of ZPVE, and likely does not contribute to the total reaction barrier. Slight elongation of the glycosidic bond (by up to 0.021 Å) is observed, which is consistent with the effect of N7 protonation of nucleotides.[49–51] These results agree with the experimental evidence of an initial proton transfer step.[38] Although the previous large-model computational study observed proton transfer concomitant with depurination,[45] proton transfer was not explicitly modeled. Instead, elongation of the glycosidic bond was the first coordinate characterized, which forced proton transfer to occur during depurination.

4.3.2.2 Mechanism A – Wat28

The first hydrolysis mechanism investigated (A) most closely resembles the proposed mechanism based on the FLRC. Specifically, a water molecule (Wat28) below the plane of the sugar moiety acts as the nucleophile, which is activated by D144 through either hydrogen bonding or full proton transfer. In the calculated 2D reaction PES (Figure 4.3), the reactant well occurs in the bottom left corner, deglycosylation occurs along the horizontal axis and attack on the anomeric carbon occurs on the vertical axis.

In the reaction PES for this mechanism (Figure 4.3), only the CS-Cap model proceeds to products. The remaining models quickly reach relative energies over 220.0 kJ mol^{-1}, indicating that Mechanism A is unlikely. Nevertheless, analyzing the reaction will allow for a better understanding of how MutY functions. For example, the large barrier for nucleophilic attack at C1′ may arise in part since the proposed general base (D144) is involved in multiple hydrogen-bonding interactions with the backbone of V147 (X-WT, CS-Cap, CS-Y126F models), the R-group of N146 (CS-Cap, CS-NoCap, CS-Y126F) and/or the hydroxyl group of Y126 (X-WT).
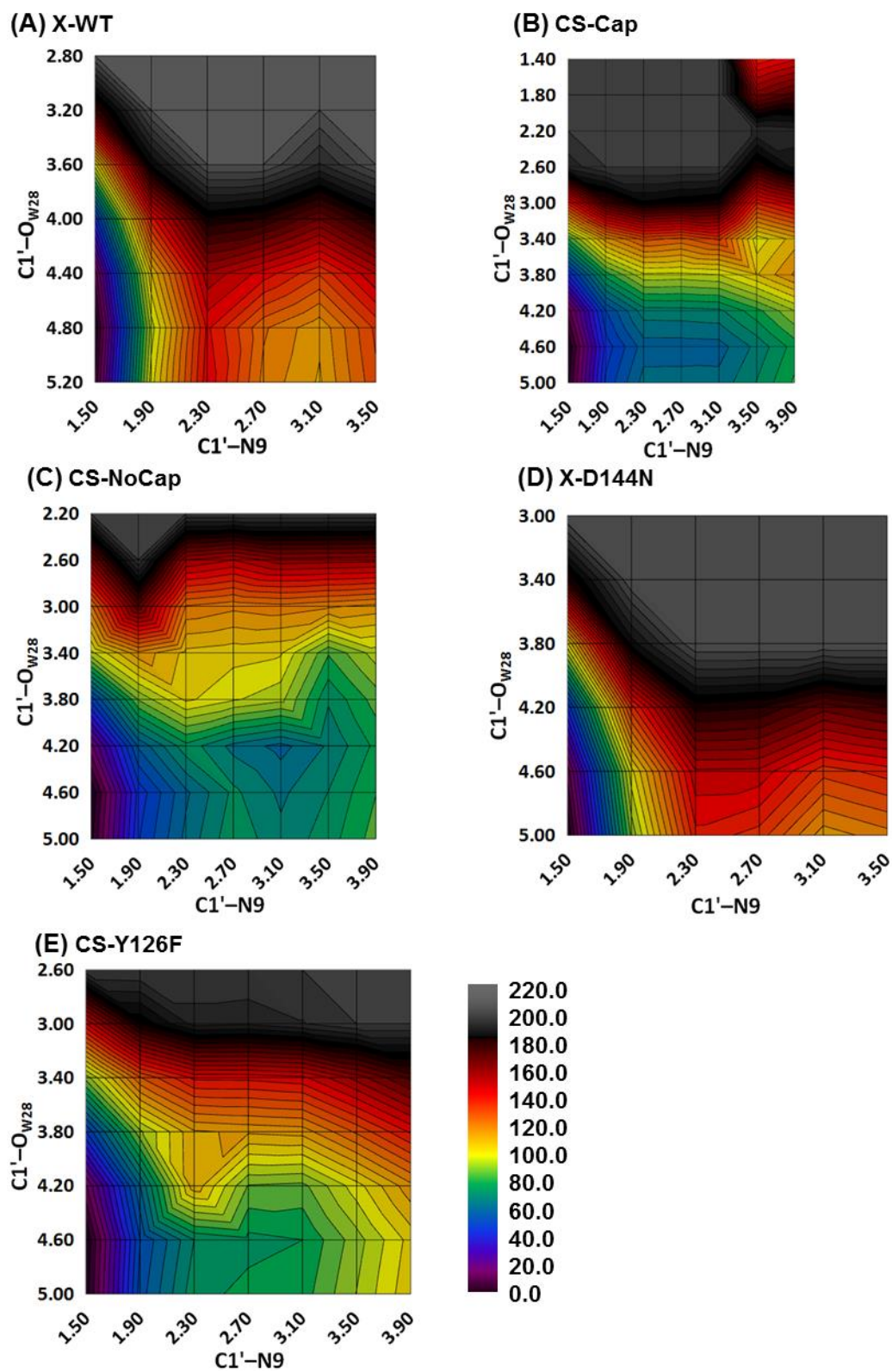
Figure 4.3. *ONIOM(M06-2X/6-31G(d):PM6) reaction PES (kJ mol^{-1}) for Mechanism A with various models and mutations. Each contour represents 5 kJ mol^{-1}.*

While the association step is very high in energy, the barrier for the deglycosylation step for the CS-Cap and CS-NoCap models is reasonable (63.8 kJ mol^{-1} and 64.0 kJ mol^{-1}, respectively). Comparing the surfaces for CS-Cap and CS-Y126F (Figures 4.3B and 4.3E), it can be seen that the Y126F mutation does not affect the mechanism (the shape of the surface is the same); however, the deglycosylation barrier is 15 kJ mol^{-1} larger (79.0 kJ mol^{-1} compared to 63.8 kJ mol^{-1}, TSD Table 4.2). This result indicates that the hydroxyl group on Y126 may contribute to catalysis in some way, most likely by stabilizing the E43 anion. In addition, as the hydrogen

Table 4.2. *Summary of reaction energetics (kJ mol^{-1}) estimated from reaction potential energy surfaces and relaxed stationary points.*[a]

Mechanism	Model	RC*	TSD	IC	TSA	PC
Reaction Potential Energy Surfaces[b]						
A – Wat28	X-WT	0.0	150.6	112.7	NR[c]	
	X-D144N	0.0	147.0	114.5	NR[c]	
	CS-Cap	0.0	63.8	60.5	201.0	129.2
	CS-Nocap	0.0	64.0	62.8	NR[c]	
	CS-Y126F	0.0	79.0	77.0	NR[c]	
B – Wat50	X-WT	0.0	–	–	180.0	162.2
	X-D144N	0.0	221.8	201.1	NR[c]	
	CS-Cap	0.0	32.7	27.1	NR[c]	
	CS-Nocap	0.0	25.4	18.1	NR[c]	
	CS-Y126F	0.0	35.6	32.0	NR[c]	
C – D144	CS-Cap	0.0	35.1	19.6	148.1	105.1
	CS-Nocap	0.0	30.5	14.3	97.5[d]	54.5[d]
Relaxed Stationary Points[e]						
B – Wat50	X-WT	0.0	–	–	222.8 (238.9)	216.0 (216.5)
C – D144	CS-Cap	0.0	30.9 (32.0)	7.8 (10.0)	156.7 (168.1)	104.4 (113.3)
C – D144	CS-NoCap	0.0	30.6 (31.1)	11.5 (17.7)	110.0[d] (115.8)	57.7[d] (61.0)

[a] ONIOM(M06-2X/6-31G(d):PM6) geometries. See Computational Details for model specifications. [b] Optimization level energies. [c] No reaction observed. [d] Geometry from CS-Cap surface. [e] ONIOM(M06-2X/6-311+G(2df,2p):PM6) single-point energies with ZPVE corrections included (Gibbs energies in parentheses).

bond between Y126 and E43 tightens, the anionic charge on E43 partially delocalizes onto Y126 and thereby brings the anionic charge closer to the cationic sugar. Support for a potential catalytic role of Y126 can be found by examining the distance between C1′ and the hydroxyl oxygen of Y126. In the CS-Cap model, d(C1′–O$_{Y126}$) decreases by 0.658 Å during the course of deglycosylation, while the CS-Y126F model shows only a 0.155 Å migration (Figure C4G in Appendix C).

In all models, the N6 amine of adenine hydrogen bonds with E188 and a water molecule (Wat371). Both interactions tighten near the transition state and then loosen again near the deglycosylated intermediate. The weakening of contacts to N6 after deglycosylation is supported by KIE data.[38] The only other hydrogen bond to the adenine nucleobase is a contact between N1 and R31. In all models, this interaction tightens to ~1.8 Å at the transition state and then weakens again (Figure C4B in Appendix C). While hydrogen-bonding interactions at N1 may not be necessary for MutY activity,[35,37] the leaving group stabilization provided by such contacts should be catalytic.[52]

4.3.2.3 Mechanism B – Wat50

The above results clearly indicate that a mechanism with Wat28 as the nucleophile and D144 as the general base does not lead to hydrolysis products. Analysis of the ONIOM optimized reactants shows that there is another water molecule equidistant from C1′, namely Wat50. This water molecule is initially involved in hydrogen bonds with N3 of adenine and an aspartate residue (D27) in the low-level region. The location of Wat50 leads to a mechanism where the water adds to the sugar upon deglycosylation with retention of stereochemistry at C1′, and possible proton transfer to the adenine leaving group, which resembles the reaction characterized by Brunk *et al.*[45]

Similar to Mechanism A, only one model (X-WT) leads to an AP-site product (Figure 4.4). However, the deglycosylation region of the reaction surfaces (bottom half of the surface) is much shallower than observed for Mechanism A, and no intermediate well is visible. This shape is similar to the reaction PES for the hydrolysis of free nucleosides,[53] and the TS region for S_N1 deglycosylation is known to be flat.[54–55] In addition, the very broad deglycosylation region concurs with KIE data that indicates low-barrier reversibility of the depurination step.[38] Based on the shape of the calculated surface, one could propose a mechanism whereby MutY catalyzes removal of the nucleobase, but only after partial release of the product does a water molecule add to the oxacarbenium cation intermediate. The difference in rate for adenine and DNA release provides support for a required conformational change prior to generating the AP-site product.[56]

In contrast to Mechanism A, the D144N mutation has a significant effect on the energetics of Mechanism B (Figure 4.4 and Table 4.2), possibly due to the lone pairs on Wat28 providing some stabilization to the deglycosylation step of Mechanism A. The X-D144N model contains weaker R31–N1 interactions than observed for the X-WT model (by up to 0.1 Å, Figure C5B in Appendix C), which may contribute to the increased deglycosylation barrier. Similar to Mechanism A, the interaction between Wat371 and the N6 amine of adenine weakens as the reaction proceeds, but is tighter for the D144N mutant than for X-WT. The interactions with adenine are very similar for the CS-Cap, CS-NoCap and CS-Y126F models (Figure C5 in Appendix C), which supports the observed minimal effect of the Y126F mutation on the energetics of Mechanism B.

Since Mechanism B does not involve D144 general base activity, the CS-NoCap surface is very similar to the CS-Cap surface. In fact, after the deglycosylation step, the CS-NoCap surface becomes very unstable and falls to one of two options, either reforming the helix-capping interaction with V147 or generating a covalent bond between C1′ and D144. There is some
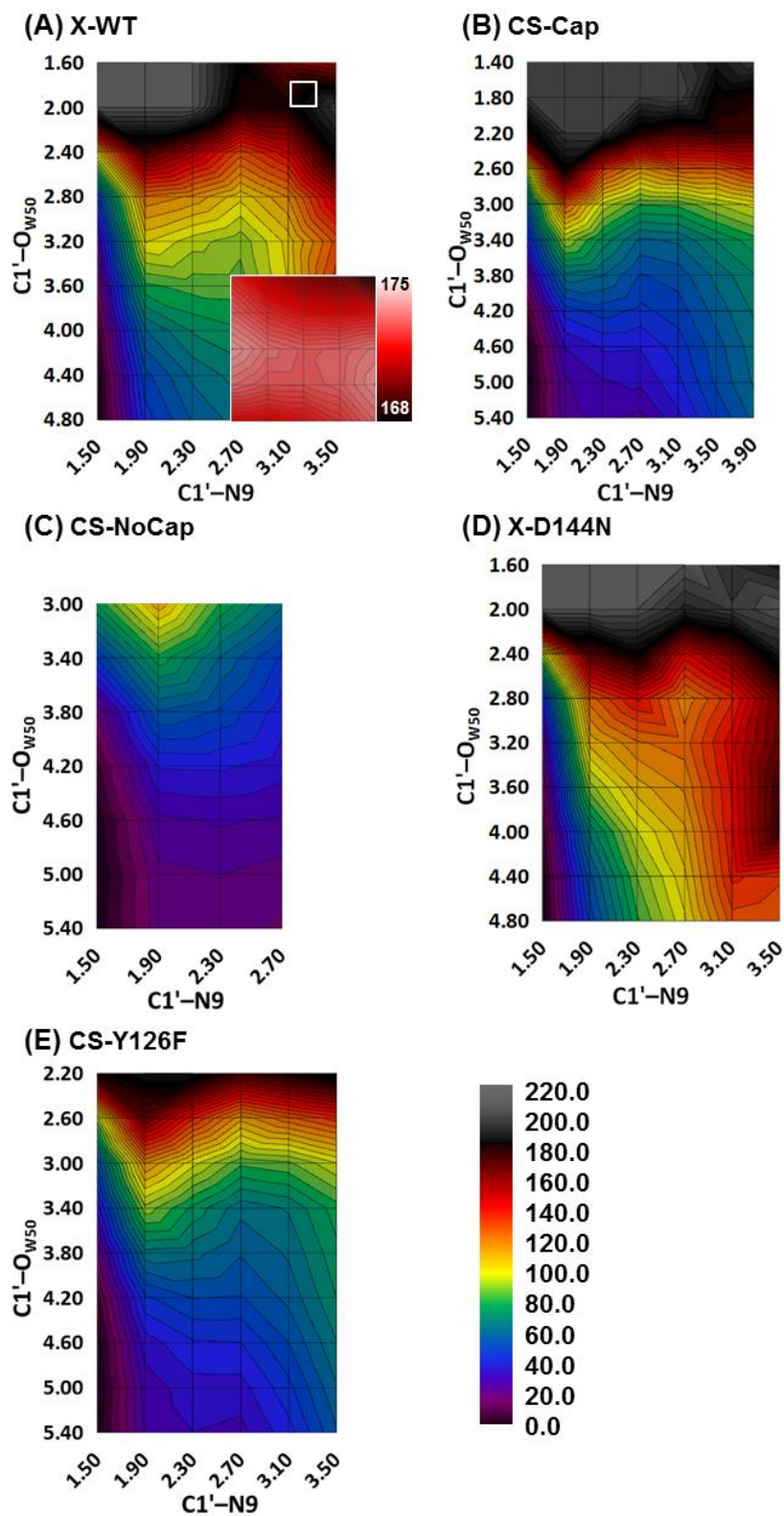
Figure 4.4*. ONIOM(M06-2X/6-31G(d):PM6) reaction PES (kJ mol^{-1}) for Mechanism B with various models and mutations. Each contour represents 5 kJ mol^{-1} on the 0.4 Å surfaces and 0.15 kJ mol^{-1} on the 0.05 Å inset surface.*

experimental support for the formation of a DNA–protein crosslink,[57–59] but this is not the major product of MutY activity. The instability of the CS-NoCap PES for Mechanism B indicates that the helix-cap does not need to be broken in the reactant in order to help stabilize the oxacarbenium cation. In addition, the CS-Cap helix-capping contact remains relatively stable over the course of the deglycosylation compared to the elongation observed in Mechanism A.

Mechanism B is the only mechanism that leads to products for the X-WT model, and therefore the stationary points identified from the reaction surface were relaxed (i.e., constraints on the reaction coordinates were removed from the minima, and the TS was further refined) to obtain better reaction energetics (Table 4.2). The refined structures are very similar to those from the reaction surface (Figure 4.5). In the TS, the water nucleophile (Wat50) hydrogen bonds to N3 of adenine as it approaches C1′. In the product complex, Wat50 is attached to the sugar moiety $d(\text{C1}'-\text{O}_{\text{Wat50}}) = 1.460$ Å and has partially transferred a proton to N9 of adenine. While this mechanism leads to products, the associated barrier is very large ($\Delta E^{\ddagger} = 222.8$ kJ mol^{-1}) and the product complex is highly endothermic ($\Delta E = 216.0$ kJ mol^{-1}). Therefore, it is unlikely that MutY follows such a mechanism.
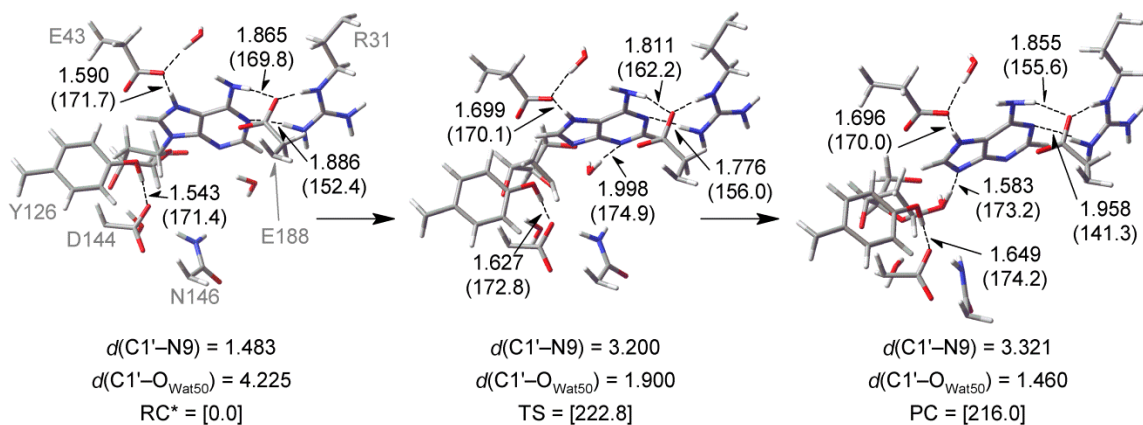
Figure 4.5. *DFT region of the refined stationary points for Mechanism B with the X-WT model. Selected ONIOM(M06-2X/6-31G(d):PM6) distances (Å) and angles (degrees, in parentheses) shown. ONIOM(M06-2X/6-311+G(2df,2p):PM6) relative energies (kJ mol^{-1}) in square brackets.*

4.3.2.4 Mechanism C – D144 Migration

In both of the previous mechanisms, a decrease in the distance between C1′ and a carboxyl group of D144 (by over 0.4 Å) was observed for the CS-Cap and CS-NoCap models, due to the migration of one or both groups. This spontaneous movement of D144 during depurination led to investigation of a new mechanism with these two models. Specifically, the effect of D144 motion on the deglycosylation step is explicitly modeled in Mechanism C. Since the dissociation and association steps involve different reaction coordinates, they are plotted on separate PES (Figure 4.6). In the first step, the glycosidic bond and C1′–Oδ_{D144} distances are the reaction coordinates, while the glycosidic bond and C1′–O$_{Wat28}$ distances were considered in the second step. Wat28 was selected due to the large migration of this group along the deglycosylation reaction PES (d(C1′–O$_{Wat28}$) reduces from ~4.1 Å to ~3.4 Å, Figure C6G in Appendix C). Previous studies on DNA glycosylases have not proposed such an explicit role for the active-site aspartate residue.[13–14,60–61] However, MutY excises a cationic nucleobase, resulting in a neutral leaving group. This is a crucial difference since a negative charge near the oxacarbenium intermediate that has been implicated in stabilization of the cation through an electrostatic sandwich has been removed. Specifically, the oxacarbenium cation intermediate in hUNG2 has been proposed to be stabilized by the uracilate anion, an active-site aspartate, and a nearby (–2) phosphate moiety.[60,62] Without the additional stabilization provided by the leaving group to the sugar, it is possible that D144 must play a larger role than observed for other glycosylases. Interestingly, a recent mutational study replaced D144 with glutamate and cysteine, and MutY retained activity as long as the pH maintains the anionic charge of the group.[27] Therefore, the charge of this residue is essential for catalysis. Similar results have been obtained for the helix-capping aspartate residue in hOgg1.[63]
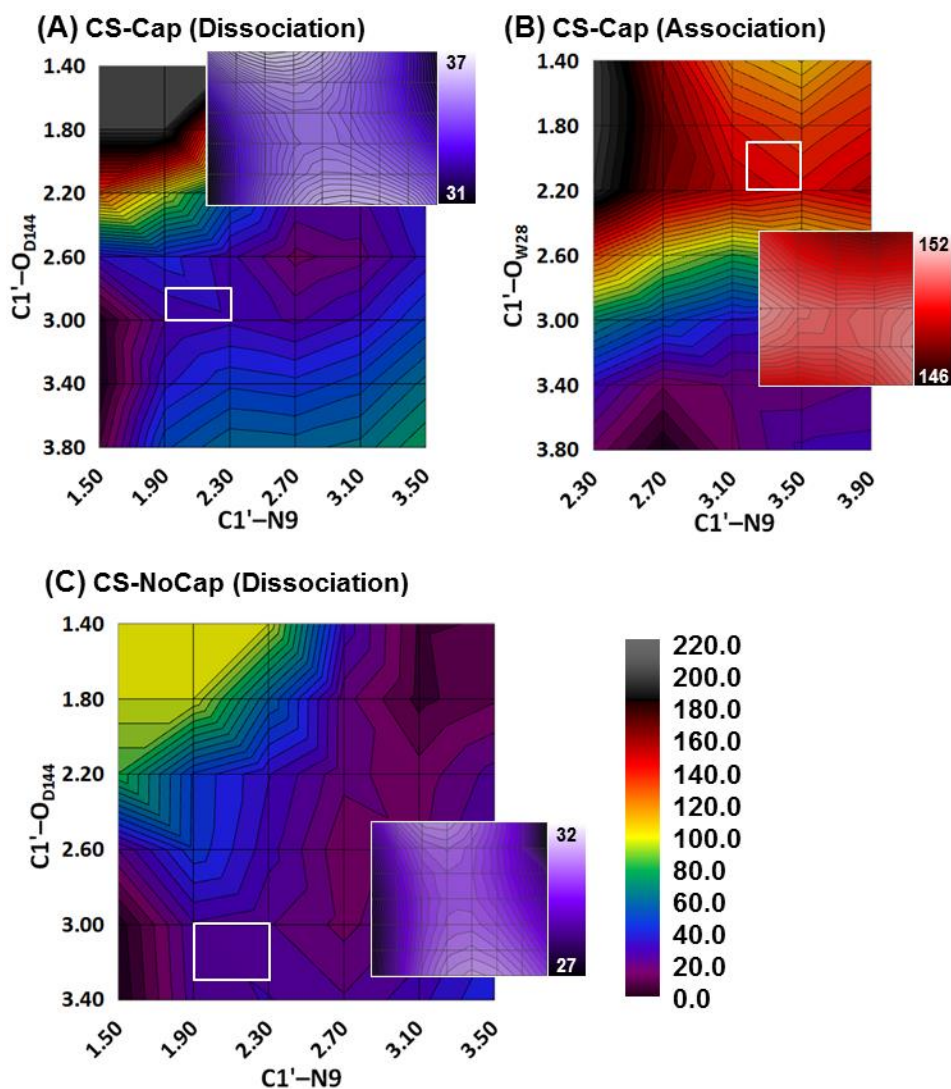
Figure 4.6. ONIOM(M06-2X/6-31G(d):PM6) reaction PES (kJ mol^{-1}) for the (A) CS-Cap dissociative step, (B) CS-Cap associative step and (C) CS-NoCap dissociative step of Mechanism C with refined regions near the TS inset. Each contour represents 5 kJ mol^{-1} on the 0.4 Å surfaces and 0.15 kJ mol^{-1} on the 0.05 Å inset surfaces.

In the first step of Mechanism C, the dA nucleotide is deglycosylated similarly to the other mechanisms with significant movement of D144 (i.e., CS-Cap and CS-NoCap). Specifically, the distance between C1′ and Oδ$_{D144}$ reduces from 3.400 Å to 2.600 Å between the RC* and intermediate complex on the CS-Cap surface (Figure 4.6A), which weakens the helix-capping interaction (d(N$_{V147}$–H···Oδ$_{D144}$) = 1.925 – 2.016 Å), Figure C6H in Appendix C.

Similar values for $d(C1'–O\delta_{D144})$ are obtained for the CS-NoCap model (3.400 Å in the reactant well and 2.400 Å in the intermediate, Figure 4.6C). The tight contact between the sugar moiety and D144 provides sufficient stabilization to the sugar, and therefore the $d(C1'–O_{Y126})$, which was observed to decrease in Mechanism A, actually increases in Mechanism C (Figure C6E, Appendix C). Based on this observation, the primary catalytic role of Y126 is stabilization of E43 in Mechanism C. These conclusions regarding the role of Y126 are supported by single-point calculations on a Y126F mutation of the Mechanism C stationary points that found the tyrosine residue contributes up to 10 kJ mol^{-1} to the barrier.[c]

Interestingly, a stable intermediate (Figure 4.7) is found for both models with a relative energy of 14.3 – 19.6 kJ mol^{-1}. Furthermore, the deglycosylation barrier for Mechanism C is the lowest thus far (30.5 – 35.1 kJ mol^{-1}), suggesting this is the most likely mechanism. Consistent with KIE data,[38] both interactions with the N6 amine (Wat371 and R31) weaken after the intermediate is formed (Figures C5B and C5D in Appendix C). Following the deglycosylation TS, D144 in the CS-NoCap model becomes unstable and either reforms the backbone interaction to V147 or covalently attaches to C1', as discussed for Mechanism B. Therefore, the water association step was only modeled with the CS-Cap model (Figure 4.6B, Figure 4.7) and the energies of the stationary points are reported relative to the reactants for the CS-Cap and CS-NoCap models (Table 4.2). From the reaction PES, the ΔE for addition of Wat28 to C1' is 97.5 kJ mol^{-1} relative to the CS-NoCap reactant and 148.1 kJ mol^{-1} relative to the CS-Cap reactant.

The intermediate well connecting the dissociation surface to the water association surface (Figure 4.6B) is quite broad. Indeed, if Wat28 is moved slightly further from the anomeric carbon (and the C1'–N9 distance is increased slightly), a second intermediate can be obtained that is

---

[c] ONIOM(M06-2X/6-311+G(2df,2p):PM6)//ONIOM(M06-2X/6-31G(d):PM6) calculations carried out by K. A. Wilson. Kellie, J. L.; Wilson, K. A.; Wetmore, S. D. *J. Am. Chem. Soc.* (Submitted July 2013).
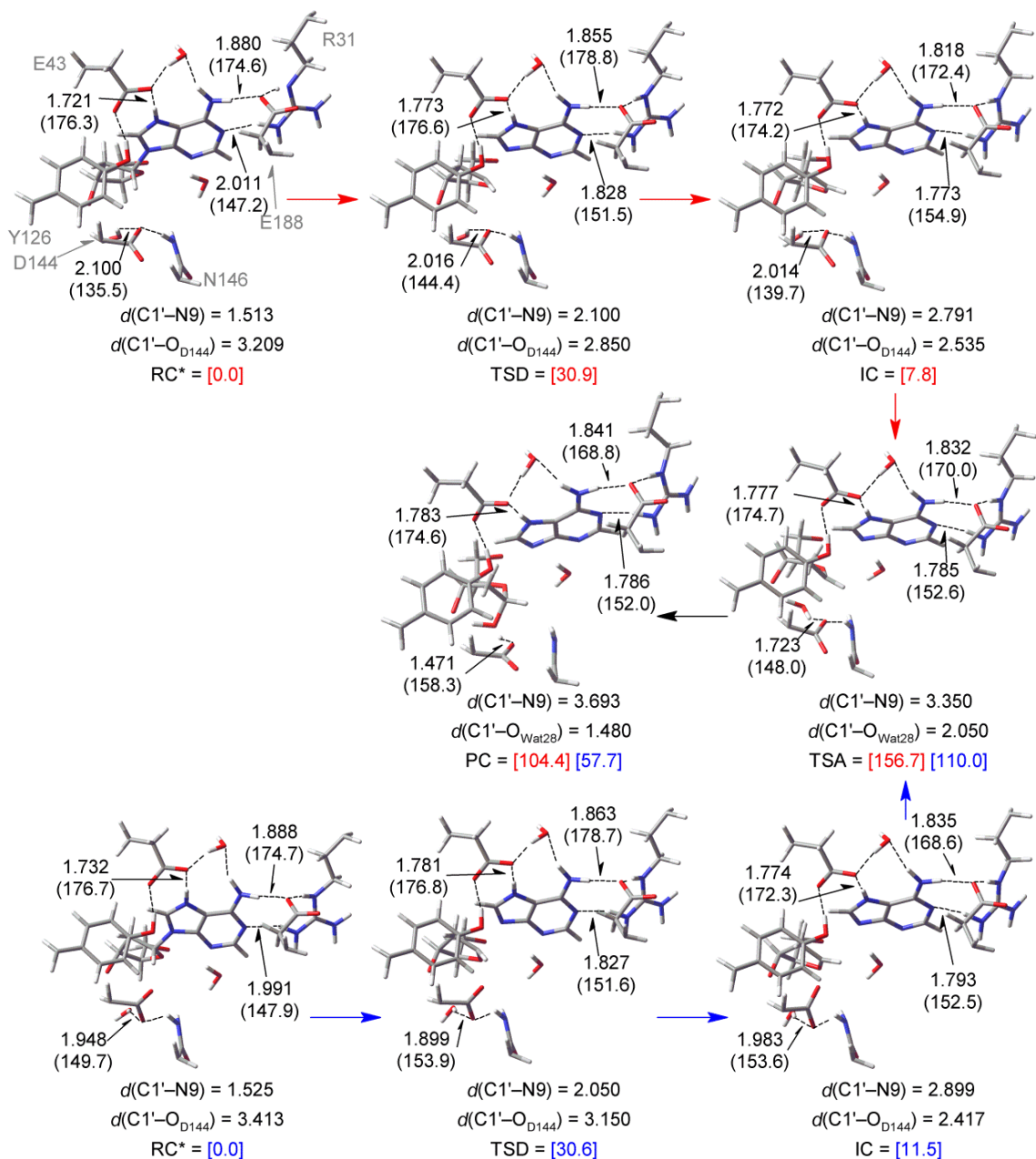
Figure 4.7. *DFT region of the refined stationary points for Mechanism C with the CS-Cap (upper, red arrows) and CS-NoCap (lower, blue arrows) models. Selected ONIOM(M06-2X/ 6-31G(d):PM6) distances (Å) and angles (degrees, in parentheses) shown. ONIOM(M06-2X/ 6-311+G(2df,2p):PM6) energies (kJ mol^{-1}) relative to the respective reactants (RC*) in square brackets.*

exothermic relative to RC*. Other deglycosylation reaction surfaces have demonstrated

stabilization of the system upon partial dissociation of the nucleophile from the active site, such

as hUNG2 (Chapter 3) and AAG.[61] This is an interesting result since an exothermic intermediate

is only obtained when the potential nucleophile begins to dissociate from the active site, indicating that the MutY active-site is ideally formed to stabilize the unstable oxacarbenium cation intermediate. Experimental evidence that adenine release is fast compared to DNA release supports the observed strong binding of MutY to the intermediate.[56]

4.4 Discussion

4.4.1 Proposed Mechanism of Action

In the present study, three mechanisms for depurination of dA by MutY were characterized. All three mechanisms begin with barrierless proton transfer from E43 to N7 of adenine, which is justified by experimental data and supported by the greater stability of the enzyme-substrate complex with protonated dA over neutral dA according to MD simulations. This finding suggests that the primary role of E43 is nucleobase activation. Subsequently, the lowest energy mechanism involves S_N1 depurination with significant involvement of D144 (Mechanism C) and models CS-Cap and CS-NoCap. Therefore, the stationary points for both were refined and compared to experiment to validate the results.

Experimental estimates $\Delta G^{\ddagger}$ for MutY are not known, but can be estimated by comparing several pieces of experimental data. Specifically, comparing the rate of MutY activity (0.2 s^{-1})[25,35] to the uncatalyzed hydrolysis of dA (6.8 $\times$ 10^{-10} s^{-1})[44] yields a rate enhancement of 2.9 $\times$ 10^8 at 37°C and a corresponding barrier reduction of ~50 kJ mol^{-1}. Combining the barrier reduction with the uncatalyzed hydrolysis barrier (~130 kJ mol^{-1})[44] leads to a predicted $\Delta G^{\ddagger}$ for MutY of ~80 kJ mol^{-1}. It must be acknowledged that the rate-limiting associative barrier calculated in the present work is likely overestimated since the proposed general base (D144) is involved in numerous hydrogen bonds that reduce its ability to accept a proton from the nucleophile, while release of the adenine nucleobase could increase the solvent accessibility of C1′ and thereby lower the barrier to water attack. With this in mind, the estimated experimental barrier reasonably compares

to the lowest energy associative barrier ($\Delta G^{\ddagger}$) for the D144-dependent pathway (98.5 kJ mol^{-1} relative to the relaxed intermediate or 115.8 kJ mol^{-1} relative to the reactant, Table 4.2). Combined with the low-barrier deglycosylation step ($\Delta G^{\ddagger} = 31.1 - 32.0$ kJ mol^{-1}), Mechanism C appears to be the most likely mechanism of action for MutY, which is consistent with a wealth of experimental data including the relative new, yet under studied, catalytically-competent FLRC structure.

4.4.2 Role of D144

In the literature, D144 is generally proposed to provide some electrostatic stabilization to the deglycosylation transition state, while the FLRC suggest that D144 (rather than E43 as suggested by the LRC) may act as a general base to activate the nucleophile.[13–14] These roles for D144 are primarily based on the observed catalytic contribution of active-site Asp/Glu residues in similar locations in other glycosylases, such as UDG (hUNG2, Chapter 3), hOgg1, NEIL1, AlkA and AAG.[13–14] This newly proposed mechanism provides the first computational support for these roles. In addition, we propose that D144 plays an even more explicit role than has been previously discussed for this (or similar) residue(s) in other glycosylases. Specifically, the distance between C1′ and the D144 functional group decreases substantially during deglycosylation in all mechanisms and models investigated. Previous studies on DNA glycosylases have proposed electrophile migration (rather than nucleophile migration) to catalyze the reaction.[13–14,60–61,64]

In contrast to other glycosylases (such as hUNG2), MutY excises a cationic nucleobase, which results in a neutral leaving group. This is a crucial difference from the reaction catalyzed by other glycosylases since the negatively charged nucleobase near the oxacarbenium intermediate has been removed, which has been implicated as an important part of the electrostatic sandwich that stabilizes the cation. For example, the oxacarbenium cation

intermediate associated with hUNG2 has been proposed to be stabilized by the uracilate anion, D145 and the –2 phosphate moiety (Chapter 3). The lack of additional stabilization of the cationic sugar by the leaving group explains the larger role for D144 observed in the present work compared to that discussed for other glycosylases. Interestingly, a recent mutational study replaced D144 with glutamate and cysteine, and MutY retains activity as long as the pH maintains the anionic charge of the group.[27] Therefore, the charge of this residue is essential for MutY catalysis. The importance of charge has also been displayed for the helix-capping aspartate residue in hOgg1 using alternative mutations and experimental conditions.[63] Definitive evidence of similar pH effects on Asp/Glu to cysteine mutations could verify the relative importance of the conserved residue across the glycosylases. It is also significant to note that the strong interaction between D144 and the oxacarbenium cation leads to a stable intermediate that can rearrange to an exothermic intermediate if the water nucleophile partially dissociates from the active site. This stabilizing effect suggests that addition of a water molecule to the anomeric carbon may not occur until after adenine release.

4.4.3 Role of Y126

For the first time, a potential catalytic role of Y126 has been identified. First, ONIOM calculations suggest that a Y126F mutant increases the reaction barrier for the preferred D144-dependent mechanism. Second, the distance between the anomeric carbon and the Y126 hydroxyl group substantially decreases over the course of the standard hydrolysis reaction (Mechanisms A and B). Third, molecular dynamics simulations showed significant variations in the interaction between Y126 and E43 with the dA substrate protonation state.[d] Together, these results lead to the proposal that Y126 may contribute to the efficiency of MutY. The primary role of Y126 is likely to stabilize the proton transfer step through a strong hydrogen bond to E43, which

---

[d] Molecular dynamics simulations carried out by K.A.W.. Kellie, J. L.; Wilson, K. A.; Wetmore, S. D. *Biochemistry* (Submitted September 2013).

alleviates the developing negative charge on this residue. A possible secondary role of Y126 may be to assist stabilization of charge developed in later reaction steps. For example, transition state stabilization by Y126 could occur in the deglycosylation step through hydrogen bonding with active-site anionic residues, such as E43, which draws the negative charge closer to the cationic sugar moiety. Interestingly, a glutamate–tyrosine dyad can also be found in AAG, and may have a similar function.[65–66] The role of Y126 in MutY, as well as similar residues in other enzymes, should be carefully considered in future experimental studies.

4.4.4 Effect of Model on Mechanism

Three different starting geometries were used to study potential MutY mechanisms in this Chapter. Interestingly, all three models produce reaction potential energy surfaces with similar shapes. In addition, the stationary points for the different mechanisms occur in the nearly the same location on the PES regardless of the model used. This result indicates that computational models of medium size (i.e., truncated enzyme–substrate complexes) can provide valuable information about the mechanism implemented by an enzyme, although the energetics obtained may not be suitably accurate. Mechanistic conclusions obtained with models of this size may be unaffected by the conformational flexibility of active-site residues. However, to properly investigate the mechanism, one should be careful not to introduce bias into the computational model. For example, too small of a model may remove critical residues and lead to very different results.[46,67–71] On the other hand, increasing to a large-scale model may only correct the problem if the high-level region is likewise increased in size to properly treat all bond formation/cleavage steps.[60–61,72] Furthermore, if a protein crystal structure is used to generate a reactant complex, care should be taken to identify any biases the structure may introduce (e.g., modifications to the substrate and/or key residues).

4.5 Conclusions

The present Chapter investigated the mechanism of action of MutY using a combination of three models, two mutations and three mechanisms. Potential energy surfaces were generated to determine the effect of various residues on the predicted mechanism and reaction energetics throughout the mechanism. This thorough investigation of the hydrolysis of dA by MutY yielded many interesting conclusions. From a model design perspective, considerable forethought should be put into generating medium-sized models. For example, rather than relaxing a protein crystal structure with molecular dynamics (MD) to generate a starting guess for the reactant, a conformational search of the active-site residues was carried out. A benefit to explicitly modeling all conformations in the above manner is that minima separated by very large barriers are guaranteed to be found, which may not occur during a standard (0.1 – 25 ns) MD equilibration that is often used to obtain enzyme reactant complexes (see, for example, references 45,73–80). Interestingly, both the X-WT model (based on crystal structure coordinates) and the CS-Cap model (result of the conformational search) lead to reaction PES with similar shapes. Therefore, valuable mechanistic information can be obtained from a variety of starting points, although the energetics can differ significantly.

The mechanism characterized in this Chapter is slightly different from previous proposals. In contrast to other glycosylases with an active-site Asp/Glu residue, D144 of MutY was found to directly catalyze the first (dissociation) step, with significant electrophile (sugar cation) migration towards the R-group during deglycosylation. The more standard role for a glycosylase active-site aspartate (i.e., acting as a general base) is then observed during the second (water attack) step. Protonation of the adenine leaving group before deglycosylation likely contributes to the enhanced role of D144 since the neutral adenine product does not provide enough stabilization to the sugar moiety when compared to other glycosylases such as hUNG2[60] and hOgg1.[81] Finally, for the first time, Y126 is identified as an important catalytic residue. By

hydrogen bonding to active-site anionic residues (for example, E43 or D144), Y126 draws negative charge closer to C1′, which stabilizes the buildup of cationic charge on the sugar moiety during deglycosylation. Future experimental studies should investigate the role of Y126.

4.6 References[e]

(1)   Cadet, J.; Douki, T.; Ravanat, J.-L., Oxidatively Generated Base Damage to Cellular DNA. *Free Radical Biol. Med.* **2010,** *49* (1), 9–21.

(2)   Tsuzuki, T.; Nakatsu, Y.; Nakabeppu, Y., Significance of Error-Avoiding Mechanisms for Oxidative DNA Damage in Carcinogenesis. *Cancer Sci.* **2007,** *98* (4), 465–470.

(3)   Paz-Elizur, T.; Sevilya, Z.; Leitner-Dagan, Y.; Elinger, D.; Roisman, L. C.; Livneh, Z., DNA Repair of Oxidative DNA Damage in Human Carcinogenesis: Potential Application for Cancer Risk Assessment and Prevention. *Cancer Lett.* **2008,** *266* (1), 60–72.

(4)   Kryston, T. B.; Georgiev, A. B.; Pissis, P.; Georgakilas, A. G., Role of Oxidative Stress and DNA Damage in Human Carcinogenesis. *Mutat. Res., Fundam. Mol. Mech. Mutagen.* **2011,** *711* (1-2), 193–201.

(5)   Ziech, D.; Franco, R.; Pappa, A.; Panayiotidis, M. I., Reactive Oxygen Species (ROS) – Induced Genetic and Epigenetic Alterations in Human Carcinogenesis. *Mutat. Res., Fundam. Mol. Mech. Mutagen.* **2011,** *711* (1-2), 167–173.

(6)   Evans, M. D.; Dizdaroglu, M.; Cooke, M. S., Oxidative DNA Damage and Disease: Induction, Repair and Significance. *Mutat. Res.* **2004,** *567* (1), 1–61.

(7)   Halliwell, B., Oxidative Stress and Neurodegeneration: Where Are We Now? *J. Neurochem.* **2006,** *97* (6), 1634–1658.

(8)   Tanrikulu, S.; Dogru-Abbasoglu, S.; Ozderya, A.; Ademoglu, E.; Karadag, B.; Erbil, Y.; Uysal, M., The 8-Oxoguanine DNA N-Glycosylase 1 (hOGG1) Ser326Cys Variant Affects the Susceptibility to Graves' Disease. *Cell Biochem. Funct.* **2011,** *29* (3), 244–248.

(9)   Markkanen, E.; Hubscher, U.; van Loon, B., Regulation of Oxidative DNA Damage Repair: The Adenine: 8-Oxo-guanine Problem. *Cell Cycle* **2012,** *11* (6), 1070–1075.

(10)   Michaels, M. L.; Miller, J. H., The GO System Protects Organisms from the Mutagenic Effect of the Spontaneous Lesion 8-Hydroxyguanine (7,8-Dihydro-8-oxoguanine). *J. Bacteriol.* **1992,** *174* (20), 6321–6325.

(11)   Lu, A. L.; Li, X.; Gu, Y.; Wright, P. M.; Chang, D.-Y., Repair of Oxidative DNA Damage: Mechanisms and Functions. *Cell Biochem. Biophys.* **2001,** *35* (2), 141–170.

---

[e] Bibliography and citations in ACS format.

(12)   Russo, M. T.; De Luca, G.; Degan, P.; Bignami, M., Different DNA Repair Strategies to Combat the Threat from 8-Oxoguanine. *Mutat. Res.* **2007,** *614* (1-2), 69–76.

(13)   Stivers, J. T.; Jiang, Y. L., A Mechanistic Perspective on the Chemistry of DNA Repair Glycosylases. *Chem. Rev. (Washington, DC, U. S.)* **2003,** *103* (7), 2729–2759.

(14)   Berti, P. J.; McCann, J. A. B., Toward a Detailed Understanding of Base Excision Repair Enzymes: Transition State and Mechanistic Analyses of N-glycoside Hydrolysis and N-glycoside Transfer. *Chem. Rev. (Washington, DC, U. S.)* **2006,** *106* (2), 506–555.

(15)   Sekiguchi, M.; Tsuzuki, T., Oxidative Nucleotide Damage: Consequences and Prevention. *Oncogene* **2002,** *21* (58), 8895–8904.

(16)   Arczewska, K. D.; Kusmierek, J. T., Bacterial DNA Repair Genes and Their Eukaryotic Homologues: 2. Role of Bacterial Mutator Gene Homologues in Human Disease. Overview of Nucleotide Pool Sanitization and Mismatch Repair Systems. *Acta Biochim. Pol.* **2007,** *54* (3), 435–457.

(17)   Lu, A. L.; Yuen, D. S.; Cillo, J., Catalytic Mechanism and DNA Substrate Recognition of *Escherichia coli* MutY Protein. *J. Biol. Chem.* **1996,** *271* (39), 24138–24143.

(18)   Pope, M. A.; Chmiel, N. H.; David, S. S., Insight into the Functional Consequences of hMYH Variants Associated with Colorectal Cancer: Distinct Differences in the Adenine Glycosylase Activity and the Response to AP Endonucleases of Y150C and G365D Murine MYH. *DNA repair* **2005,** *4* (3), 315–325.

(19)   Cheadle, J. P.; Sampson, J. R., MUTYH-Associated Polyposis- From Defect in Base Excision Repair to Clinical Genetic Testing. *DNA Repair* **2007,** *6* (3), 274–279.

(20)   Guan, Y.; Manuel, R. C.; Arvai, A. S.; Parikh, S. S.; Mol, C. D.; Miller, J. H.; Lloyd, S.; Tainer, J. A., MutY Catalytic Core, Mutant and Bound Adenine Structures Define Specificity for DNA Repair Enzyme Superfamily. *Nat. Struct. Biol.* **1998,** *5* (12), 1058–1064.

(21)   Wright, P. M.; Yu, J. A.; Cillo, J.; Lu, A. L., The Active Site of the *Escherichia coli* MutY DNA Adenine Glycosylase. *J. Biol. Chem.* **1999,** *274* (41), 29011–29018.

(22)   Williams, S. D.; David, S. S., A Single Engineered Point Mutation in the Adenine Glycosylase MutY Confers Bifunctional Glycosylase/AP Lyase Activity. *Biochemistry* **2000,** *39* (33), 10098–10109.

(23)   Zharkov, D. O.; Gilboa, R.; Yagil, I.; Kycia, J. H.; Gerchman, S. E.; Shoham, C.; Grollman, A. P., Role for Lysine 142 in the Excision of Adenine from A:G Mispairs by MutY DNA Glycosylase of *Escherichia coli*. *Biochemistry* **2000,** *39* (48), 14768–14778.

(24)   Chmiel, N. H.; Livingston, A. L.; David, S. S., Insight into the Functional Consequences of Inherited Variants of the hMYH Adenine Glycosylase Associated with Colorectal Cancer: Complementation Assays with hMYH Variants and Pre-steady-state Kinetics of the Corresponding Mutated *E. coli* Enzymes. *J. Mol. Biol.* **2003,** *327* (2), 431–443.

(25)   Chepanoske, C. L.; Lukianova, O. A.; Lombard, M.; Golinelli-Cohen, M. P.; David, S. S., A Residue in MutY Important for Catalysis Identified by Photocross-Linking and Mass Spectrometry. *Biochemistry* **2004,** *43* (3), 651–662.

(26)   Livingston, A. L.; Kundu, S.; Pozzi, M. H.; Anderson, D. W.; David, S. S., Insight into the Roles of Tyrosine 82 and Glycine 253 in the *Escherichia coli* Adenine Glycosylase MutY. *Biochemistry* **2005,** *44* (43), 14179–14190.

(27)   Brinkmeyer, M. K.; Pope, M. A.; David, S. S., Catalytic Contributions of Key Residues in the Adenine Glycosylase MutY Revealed by pH-dependent Kinetics and Cellular Repair Assays. *Chem. Biol.* **2012,** *19* (2), 276–286.

(28)   Lu, A. L.; Tsaiwu, J. J.; Cillo, J., DNA Determinants and Substrate Specificities of *Escherichia-coli* MutY. *J. Biol. Chem.* **1995,** *270* (40), 23582–23588.

(29)   Bulychev, N. V.; Varaprasad, C. V.; Dorman, G.; Miller, J. H.; Eisenberg, M.; Grollman, A. P.; Johnson, F., Substrate Specificity of *Escherichia coli* MutY Protein. *Biochemistry* **1996,** *35* (40), 13147–13156.

(30)   Porello, S. L.; Williams, S. D.; Kuhn, H.; Michaels, M. L.; David, S. S., Specific Recognition of Substrate Analogs by the DNA Mismatch Repair Enzyme MutY. *J. Am. Chem. Soc.* **1996,** *118* (44), 10684–10692.

(31)   Chepanoske, C. L.; Porello, S. L.; Fujiwara, T.; Sugiyama, H.; David, S. S., Substrate Recognition by *Escherichia coli* MutY Using Substrate Analogs. *Nucleic Acids Res.* **1999,** *27* (15), 3197–3204.

(32)   Chepanoske, C. L.; Langelier, C. R.; Chmiel, N. H.; David, S. S., Recognition of the Nonpolar Base 4-Methylindole in DNA by the DNA Repair Adenine Glycosylase MutY. *Org. Lett.* **2000,** *2* (9), 1341–1344.

(33)   Ohtsubo, T.; Nishioka, K.; Imaiso, Y.; Iwai, S.; Shimokawa, H.; Oda, H.; Fujiwara, T.; Nakabeppu, Y., Identification of Human MutY Homolog (hMYH) as a Repair Enzyme for 2-Hydroxyadenine in DNA and Detection of Multiple Forms of hMYH Located in Nuclei and Mitochondria. *Nucleic Acids Res.* **2000,** *28* (6), 1355–1364.

(34)   Chmiel, N. H.; Golinelli, M. P.; Francis, A. W.; David, S. S., Efficient Recognition of Substrates and Substrate Analogs by the Adenine Glycosylase MutY Requires the C-terminal Domain. *Nucleic Acids Res.* **2001,** *29* (2), 553–564.

(35)   Francis, A. W.; Helquist, S. A.; Kool, E. T.; David, S. S., Probing the Requirements for Recognition and Catalysis in FPG and MutY with Nonpolar Adenine Isosteres. *J. Am. Chem. Soc.* **2003,** *125* (52), 16235–16242.

(36)   Ushijima, Y.; Tominaga, Y.; Miura, T.; Tsuchimoto, D.; Sakumi, K.; Nakabeppu, Y., A Functional Analysis of the DNA Glycosylase Activity of Mouse MUTYH Protein Excising 2-Hydroxyadenine Opposite Guanine in DNA. *Nucleic Acids Res.* **2005,** *33* (2), 672–682.

(37)   Livingston, A. L.; O'Shea, V. L.; Kim, T.; Koo, E. T.; David, S. S., Unnatural Substrates Reveal the Importance of 8-Oxoguanine for *in vivo* Mismatch Repair by MutY. *Nat. Chem. Biol.* **2008,** *4* (1), 51–58.

(38)   McCann, J. A. B.; Berti, P. J., Transition-State Analysis of the DNA Repair Enzyme MutY. *J. Am. Chem. Soc.* **2008,** *130*, 5789–5797.

(39)   Fromme, J. C.; Banerjee, A.; Huang, S. J.; Verdine, G. L., Structural Basis for Removal of Adenine Mispaired with 8-Oxoguanine by MutY Adenine DNA Glycosylase. *Nature (London, U. K.)* **2004,** *427* (6975), 652–656.

(40)   Messick, T. E.; Chmiel, N. H.; Golinelli, M. P.; Langer, M. R.; Joshua-Tor, L.; David, S. S., Noncysteinyl Coordination to the 4Fe-4S (2+) Cluster of the DNA Repair Adenine Glycosylase MutY Introduced via Site-Directed Mutagenesis. Structural Characterization of an Unusual Histidinyl-Coordinated Cluster. *Biochemistry* **2002,** *41* (12), 3931–3942.

(41)   Manuel, R. C.; Hitomi, K.; Arvai, A. S.; House, P. G.; Kurtz, A. J.; Dodson, M. L.; McCullough, A. K.; Tainer, J. A.; Lloyd, R. S., Reaction Intermediates in the Catalytic Mechanism of *Escherichia coli* MutY DNA Glycosylase. *J. Biol. Chem.* **2004,** *279* (45), 46930–46939.

(42)   Lee, S.; Verdine, G. L., Atomic Substitution Reveals the Structural Basis for Substrate Adenine Recognition and Removal by Adenine DNA Glycosylase. *Proc. Nat. Acad. Sci. USA* **2009,** *106* (44), 18497–18502.

(43)   Luncsford, P. J.; Chang, D. Y.; Shi, G. L.; Bernstein, J.; Madabushi, A.; Patterson, D. N.; Lu, A. L.; Toth, E. A., A Structural Hinge in Eukaryotic MutY Homologues Mediates Catalytic Activity and Rad9-Rad1-Hus1 Checkpoint Complex Interactions. *J. Mol. Biol.* **2010,** *403* (3), 351–370.

(44)   Schroeder, G. K.; Wolfenden, R., Rates of Spontaneous Disintegration of DNA and the Rate Enhancements Produced by DNA Glycosylases and Deaminases. *Biochemistry* **2007,** *46* (47), 13638–13647.

(45)   Brunk, E.; Arey, J. S.; Rothlisberger, U., Role of Environment for Catalysis of the DNA Repair Enzyme MutY. *J. Am. Chem. Soc.* **2012,** *134* (20), 8608–8616.

(46)   Tiwari, S.; Agnihotri, N.; Mishra, P. C., Quantum Theoretical Study of Cleavage of the Glycosidic Bond of 2'-Deoxyadenosine: Base Excision-Repair Mechanism of DNA by MutY. *J. Phys. Chem. B* **2011,** *115* (12), 3200–3207.

(47)   Wilson, K. A. Computational Studies of DNA Repair: Dynamics of the MutY, hOgg1 and hUNG2 DNA Glycosylases. Honours, University of Lethbridge, Lethbridge, AB, 2013.

(48)   Frisch, M. J.; Trucks, G. W.; Schlegel, H. B.; Scuseria, G. E.; Robb, M. A.; Cheeseman, J. R.; Scalmani, G.; Barone, V.; Mennucci, B.; Petersson, G. A*., et al. Gaussian 09*, Revision A.02; Gaussian, Inc.: Wallingford CT, 2009.

(49)   Rios-Font, R.; Rodriguez-Santiago, L.; Bertran, J.; Sodupe, M., Influence of N7 Protonation on the Mechanism of the N-Glycosidic Bond Hydrolysis in 2 '-Deoxyguanosine. A Theoretical Study. *J. Phys. Chem. B* **2007,** *111* (21), 6071–6077.

(50)   Zheng, Y.; Xue, Y.; Yan, S. G., The Effects of Oxidation and Protonation on the N-glycosidic Bond Stability of 8-Oxo-2 '-deoxyguanosine: DFT Study. *THEOCHEM* **2008,** *860* (1-3), 52–57.

(51)   Zheng, Y.; Xue, Y.; Yan, G. S., The Influences of Oxidation and Cationization on the N-glycosidic Bond Stability of 8-Oxo-2 '-deoxyadenosine - A Theoretical Study. *J. Theor. Comput. Chem.* **2009,** *8* (6), 1253–1264.

(52)   McConnell, T. L.; Wheaton, C. A.; Hunter, K. C.; Wetmore, S. D., Effects of Hydrogen Bonding on the Acidity of Adenine, Guanine, and Their 8-Oxo Derivatives. *J. Phys. Chem. A* **2005,** *109* (28), 6351–6362.

(53)   Przybylski, J. L.; Wetmore, S. D., Modeling the Dissociative Hydrolysis of the Natural DNA Nucleosides. *J. Phys. Chem. B* **2010,** *114* (2), 1104–1113.

(54)   Baik, M. H.; Friesner, R. A.; Lippard, S. J., Theoretical Study on the Stability of N-Glycosyl Bonds: Why Does N7-Platination not Promote Depurination? *J. Am. Chem. Soc.* **2002,** *124* (16), 4495–4503.

(55)   Przybylski, J. L.; Wetmore, S. D., Designing an Appropriate Computational Model for DNA Nucleoside Hydrolysis: A Case Study of 2′-Deoxyuridine. *J. Phys. Chem. B* **2009,** *113* (18), 6533–6542.

(56)   McCann, J. A. B.; Berti, P. J., Adenine Release is Fast in MutY-Catalyzed Hydrolysis of G:A and 8-Oxo-G:A DNA Mismatches. *J. Biol. Chem.* **2003,** *278* (32), 29587–29592.

(57)   Tsai-wu, J. J.; Liu, H. F.; Lu, A. L., *Escherichia-coli* MutY Protein has Both N-Glycosylase and Apurinic/Apyrimidinic Endonuclease Activities on A·C and A·G Mispairs. *Proc. Nat. Acad. Sci. USA* **1992,** *89* (18), 8779–8783.

(58)   Williams, S. D.; David, S. S., Evidence that MutY is a Monofunctional Glycosylase Capable of Forming a Covalent Schiff Base Intermediate with Substrate DNA. *Nucleic Acids Res.* **1998,** *26* (22), 5123–5133.

(59)   Zharkov, D. O.; Grollman, A. P., MutY DNA Glycosylase: Base Release and Intermediate Complex Formation. *Biochemistry* **1998,** *37* (36), 12384–12394.

(60)   Dinner, A. R.; Blackburn, G. M.; Karplus, M., Uracil-DNA Glycosylase Acts by Substrate Autocatalysis. *Nature (London, U. K.)* **2001,** *413* (6857), 752–755.

(61)   Rutledge, L. R.; Wetmore, S. D., Modeling the Chemical Step Utilized by Human Alkyladenine DNA Glycosylase: A Concerted Mechanism Aids in Selectively Excising Damaged Purines. *J. Am. Chem. Soc.* **2011,** *133* (40), 16258–16269.

(62)   Parker, J. B.; Stivers, J. T., Uracil DNA Glycosylase: Revisiting Substrate-Assisted Catalysis by DNA Phosphate Anions. *Biochemistry* **2008,** *47* (33), 8614–8622.

(63)   Norman, D. P. G.; Chung, S. J.; Verdine, G. L., Structural and Biochemical Exploration of a Critical Amino Acid in Human 8-oxoguanine Glycosylase. *Biochemistry* **2003,** *42* (6), 1564–1572.

(64)   Bianchet, M. A.; Seiple, L. A.; Jiang, Y. L.; Ichikawa, Y.; Amzel, L. M.; Stivers, J. T., Electrostatic Guidance of Glycosyl Cation Migration Along the Reaction Coordinate of Uracil DNA Glycosylase. *Biochemistry* **2003,** *42* (43), 12455–12460.

(65)   Lau, A. Y.; Wyatt, M. D.; Glassner, B. J.; Samson, L. D.; Ellenberger, T., Molecular Basis for Discriminating Between Normal and Damaged Bases by the Human Alkyladenine Glycosylase, AAG. *Proc. Nat. Acad. Sci. USA* **2000,** *97* (25), 13573–13578.

(66)   Lingaraju, G. M.; Davis, C. A.; Setser, J. W.; Samson, L. D.; Drennan, C. L., Structural Basis for the Inhibition of Human Alkyladenine DNA Glycosylase (AAG) by 3,N4-Ethenocytosine-containing DNA. *J. Biol. Chem.* **2011,** *286* (15), 13205–13213.

(67)   Osakabe, T.; Fujii, Y.; Hata, M.; Tsuda, M.; Neya, S.; Hoshino, T., Quantum Chemical Study on Base Excision Mechanism of 8-Oxoguanine DNA Glycosylase: Substrate-Assisted Catalysis of the N-glycosidic Linkage Cleavage Reaction. *Chem-Bio Inf. J.* **2004,** *4* (3), 73–92.

(68)   Schyman, P.; Danielsson, J.; Pinak, M.; Laaksonen, A., Theoretical Study of the Human DNA Repair Protein hOGG1 Activity. *J. Phys. Chem. A* **2005,** *109* (8), 1713–1719.

(69)   Šebera, J.; Trantírek, L.; Tanaka, Y.; Sychrovský, V., Pyramidalization of the Glycosidic Nitrogen Provides the Way for Efficient Cleavage of the N-Glycosidic Bond of 8-OxoG with the hOGG1 DNA Repair Protein. *J. Phys. Chem. B* **2012,** *116* (41), 12535–12544.

(70)   Shim, E. J.; Przybylski, J. L.; Wetmore, S. D., Effects of Nucleophile, Oxidative Damage, and Nucleobase Orientation on the Glycosidic Bond Cleavage in Deoxyguanosine. *J. Phys. Chem. B* **2010,** *114* (6), 2319–2326.

(71)   Kellie, J. L.; Wetmore, S. D., Mechanistic and Conformational Flexibility of the Covalent Linkage Formed during β-Lyase Activity on an AP-Site: Application to hOgg1. *J. Phys. Chem. B* **2012,** *116* (35), 10786–10797.

(72)   Calvaresi, M.; Bottoni, A.; Garavelli, M., Computational Clues for a New Mechanism in the Glycosylase Activity of the Human DNA Repair Protein hOGG1. A Generalized Paradigm for Purine-Repairing Systems? *J. Phys. Chem. B* **2007,** *111* (23), 6557–6570.

(73)   Imhof, P.; Fischer, S.; Smith, J. C., Catalytic Mechanism of DNA Backbone Cleavage by the Restriction Enzyme EcoRV: A Quantum Mechanical/Molecular Mechanical Analysis. *Biochemistry* **2009,** *48* (38), 9061–9075.

(74)   Soliman, M. E. S.; Ruggiero, G. D.; Pernia, J. J. R.; Greiga, I. R.; Williams, I. H., Computational Mutagenesis Reveals the Role of Active-Site Tyrosine in Stabilising a Boat Conformation for the Substrate: QM/MM Molecular Dynamics Studies of Wild-Type and Mutant Xylanases. *Org. Biomol. Chem.* **2009,** *7* (3), 460–468.

(75)   Xu, D. G.; Guo, H., Quantum Mechanical/Molecular Mechanical and Density Functional Theory Studies of a Prototypical Zinc Peptidase (Carboxypeptidase A) Suggest a General Acid-General Base Mechanism. *J. Am. Chem. Soc.* **2009,** *131* (28), 9780–9788.

(76)   Brás, N. r. F.; Fernandes, P. A.; Ramos, M. J., QM/MM Studies on the β-Galactosidase Catalytic Mechanism: Hydrolysis and Transglycosylation Reactions. *J. Chem. Theory Comput.* **2010,** *6* (2), 421–433.

(77)   Carvalho, A. T. P.; Fernandes, P. A.; Ramos, M. J., The Catalytic Mechanism of RNA Polymerase II. *J. Chem. Theory Comput.* **2011,** *7* (4), 1177–1188.

(78)   Jana, G. A.; Alderete, J. B.; Delgado, E. J., On the Inhibition of AHAS by Chlorimuron Ethyl: A Theoretical Study. *Chem. Phys. Lett.* **2011,** *516* (4-6), 239–243.

(79)   Wu, R. B.; Gong, W. J.; Ting, L.; Zhang, Y. K.; Cao, Z. X., QM/MM Molecular Dynamics Study of Purine-Specific Nucleoside Hydrolase. *J. Phys. Chem. B* **2012,** *116* (6), 1984–1991.

(80)   Bushnell, E. A. C.; Gauld, J. W., An Assessment of Pure, Hybrid, Meta, and Hybrid-Meta GGA Density Functional Theory Methods for Open-Shell Systems: The Case of the Nonheme Iron Enzyme 8R-LOX. *J. Comput. Chem.* **2013,** *34* (2), 141–148.

(81)   Fromme, J. C.; Bruner, S. D.; Yang, W.; Karplus, M.; Verdine, G. L., Product-Assisted Catalysis in Base-Excision DNA Repair. *Nat. Struct. Biol.* **2003,** *10* (3), 204–211.

Chapter 5: Bifunctional Glycosylases Part 1:

Exploration of the Glycosylase/Lyase Mechanism[a]

5.1 Introduction

Cleavage of the DNA backbone (for example, β/δ-lyase activity) is an essential step in the repair of damaged nucleotides through the base and nucleotide excision repair pathways.[1–3] In the case of the glycosylases discussed in the previous two Chapters, the DNA backbone is nicked by an AP-endonuclease after removal of the damaged base. However, bifunctional glycosylases exhibit an additional lyase activity, and may nick the backbone. For example, human 8-oxoguanine–DNA glycosylase (hOgg1) catalyzes both deglycosylation and β-elimination of the 3′-phosphate of the 8-oxoguanine nucleotide (dOG) to yield an apurinic/apyrimidinic site (AP-site) with a nick on the 3′-side (Figure 5.1).[4–7] As mentioned in Chapters 1 and 3, hOgg1 activity is critical because of the high mutagenicity of the OG (nucleobase) lesion, which has a preference for Hoogsteen base pairing with adenine and thereby leads to G:C $\rightarrow$ T:A transversion mutations upon replication.[8–10] In addition, OG is a common product of attack on cellular DNA by reactive oxygen species and is formed 10^3 times per cell per day in normal cells.[11–13]

Shortly after the discovery of hOgg1, it was determined that K249 is responsible for catalysis and covalently binds to the AP-site.[14] Later studies of the various stages of the hOgg1 mechanism have focused on protein structure and lesion recognition. For example, Verdine *et al.* have successfully used a combination of protein–DNA cross-linking and borohydride trapping to obtain X-ray crystal structures of hOgg1 (with various mutations) at different stages in the

---
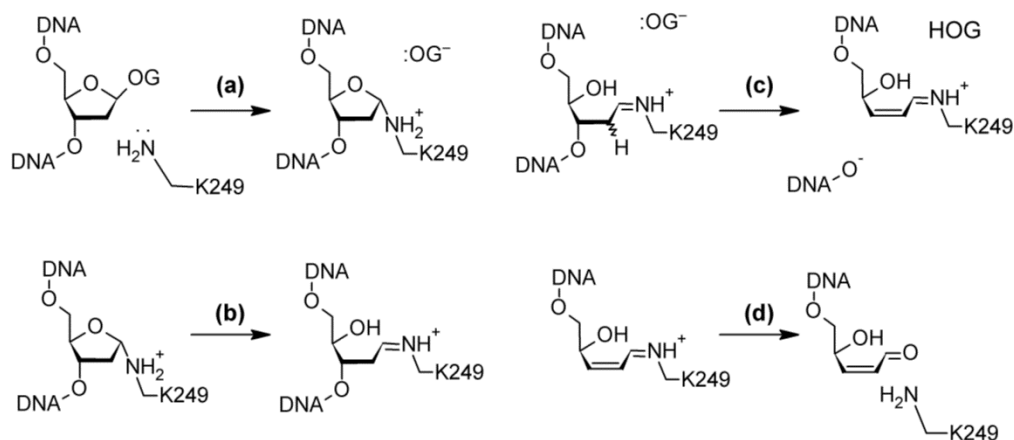
Figure 5.1. *General steps in the commonly accepted hOgg1 glycosylase/β-lyase mechanism,[1] including (**a**) deglycosylation via nucleophilic attack by K249; (**b**) ring opening through direct or base-assisted transfer of a proton from the amine group; (**c**) β-elimination of the 3'-phosphate with abstraction of a C2'-proton and (**d**) hydrolysis of the Schiff base to generate a nicked product and release the enzyme.*

binding and chemical steps.[1–2,15–23] In addition to providing support for the role of K249,[15] these studies have determined that D268 is catalytic in several steps, partially through the stabilization of multiple Schiff base intermediates (Figure 5.1).[2,23] Furthermore, the nucleobase generated upon deglycosylation has been found to behave as a cofactor for O3′-elimination, and displays a *pro–R:pro–S* preference for C2′–H abstraction depending on the C8-substituent.[1] Q315 has been identified to be weakly catalytic and important for substrate binding (and specificity) through hydrogen bonding with the OG nucleobase.[21,24] However, experimental studies show hOgg1 activity on substrates with reduced hydrogen-bonding capabilities,[25–26] which contradicts the proposed catalytic importance of hydrogen bonding and/or proton transfer to the OG nucleobase. Finally, recent evidence indicates that hOgg1 is in fact monofunctional *in vivo*, where D268 may play a more prominent role than in the bifunctional mechanism.[23]

Despite the abundance of experimental data and unanswered questions regarding the chemical step implemented by hOgg1, no computational study has examined the complete reaction mechanism of hOgg1 or any other bifunctional glycosylase. Indeed, previous computational analyses of hOgg1 have focused on the deglycosylation step,[27–31] with a select few

considering ring-opening (Figure 5.1a,b).[27,29] Furthermore, a thorough computational analysis of the β-elimination of a cross-linked AP-site has yet to be performed. Nevertheless, a few relevant examples can be found in the literature such as the α,β-elimination reactions of esters,[32] or the mechanism of action of phosphothreonine lyase (EC#: 4.2.3.–).[33] However, none of these examples involve a positively-charged imine linkage and thus they exhibit different electrostatics at the reaction center than the mechanism catalyzed by hOgg1 and other bifunctional glycosylases. The inherent flexibility of the bifunctional glycosylase reaction explains the absence of literature on the subject. For example, transfer of either proton from the K249 terminal amine to O4′ during ring opening yields different stereoisomers at the imine linkage (*E* and *Z* for *pro–S* and *pro–R* protons, respectively). In addition, abstraction of either C2′–H leads to different stereoisomers at the C2′–C3′ double bond in the lyase product (*Z* and *E* for *pro–S* and *pro–R* abstraction, respectively), and this isomeric information is lost upon crystallization of the intermediates due to reduction of the unsaturated bonds in the protein–DNA crosslink.[1] Therefore, there is a clear need for computer modeling of these flexible reactions, which will provide structural information that is difficult to obtain from experiments.

Since few lyases have been studied as extensively (and crystallized in as many different stages of the reaction) as hOgg1, this enzyme is an excellent candidate for investigating the complicated β-lyase reaction. This Chapter characterizes eight unique chemically-relevant pathways relevant to hOgg1 and other bifunctional glycosylases, which can use more than one mechanism (for example, lyase activity of hOgg1 has been shown to proceed with abstraction of either C2′–H proton).[1] The mechanisms consider the conformational and mechanistic flexibility of the different isomers of the imine linkage (Figure 5.1), the effect of transfer of either amino proton during the ring-opening step (**b**, Figure 5.1), and *pro–R* versus *pro–S* proton abstraction from C2′ during the β-lyase step (**c**, Figure 5.1). As a consequence of the complexity and number of reaction mechanisms considered, DFT and a small computational model are used.

Nevertheless, these results provide insight into the degree of movement required to form the different isomers of the covalent linkage throughout the mechanism. Indeed, small model studies are essential to understanding the mechanistic intricacies of the reaction before undertaking large-scale enzymatic modeling and help ensure that all sterically-relevant mechanisms are considered. To this end, this work will propose the most appropriate mechanisms for large-scale modeling of hOgg1 in Chapter 6. Furthermore, possible methods for catalysis of OG excision by hOgg1 will be identified by analyzing the barriers inherent to the glycosylase and β-lyase mechanisms. Finally, the results of this study will be discussed with respect to the possible monofunctional (glycosylase only) activity of hOgg1.[23] Although focus is placed on applying these results to one enzyme, the data within can be used for similar analyses of other systems with β-lyase activity, such as FPG,[34] EndoIII,[35] Endonuclease VIII,[36] and MutY which exhibits weak, uncoupled lyase ability),[37] as well as model peptides (for example, Lys-Trp-Lys).[38]

5.2 Computational Details

In this Chapter, the flexibility of the imine linkage formed during β-lyase activity was examined using the repair of dOG by hOgg1 as a representative system, a diverse collection of mechanisms, and a DFT model. First, the mechanisms investigated will be summarized, and the model implemented will be described. In the Results section, the DFT structures and energetics will be presented for all mechanisms, including detailed PES scans of the elimination phase for select mechanisms. The Discussion section will subsequently outline broad biochemical implications of the results, propose possible methods for catalysis of β-elimination and explain the potential monofunctional activity of hOgg1.

5.2.1 Mechanisms and Model

The main phases in the overall chemical reaction catalyzed by hOgg1 are outlined in Figure 5.1. In the first phase (a), S_N2 deglycosylation of the damaged nucleotide produces a free

OG^- nucleobase anion and an AP-site covalently bound to hOgg1 through the terminal amine of K249.[14] Although there has been some discussion of a possible S_N1 mechanism for hOgg1,[2,18,20,28,39] there is little experimental evidence to support such a statement. Indeed, these conclusions appear to be based on UDG, which shifts the pK_a of uracil by 3.4 units through a strong hydrogen bond with H268 to promote base departure.[40] No equivalent strong hydrogen bond with OG is observed in the hOgg1 active site.[15] In the second phase of the hOgg1 chemical step, the amine linkage rearranges to a Schiff base through transfer of a proton from Nζ to O4′ of the deoxyribose ring causing the ring to open (**b**).[1,41] The third phase (**c**) involves β-elimination of the 3′-phosphate group with abstraction of a proton from C2′. There is evidence that either the *pro–R* or *pro–S* proton (C2′–H_R and C2′–H_S) can be removed during hOgg1 activity.[1] The final phase (**d**) involves hydrolysis of the imine linkage to regenerate the enzyme and release the final product. In this Chapter, eight mechanisms were fully characterized for phases **a–c**. Consistent with Figure 5.1, the nomenclature for stationary points referring to deglycosylation will end in (a), those referring to the ring-opening step(s) will end in (b), and those corresponding to the elimination steps will end in (c); for example, the transition state for deglycosylation and succeeding intermediates are denoted as TS(a) and IC(a), respectively. Additional stationary points characterized for phases with more than one step are identified with a prime; for example, the intermediate between C2′–H abstraction and O3′-elimination is labelled IC(c′).

Table 5.1 summarizes the eight mechanisms considered. Deglycosylation (**a**) occurs via the same S_N2 pathway in all cases. Ring-opening (**b**) was modeled as either direct (D) or OG-assisted (A), and involves transfer of either the *pro–R* (N_R) or *pro–S* (N_S) proton on Nζ. A step-wise elimination (**c**) initiated by abstraction of either the *pro–R* (C_R) or the *pro–S* (C_S) proton on C2′ was characterized for all pathways. Thus, the nomenclature for each reaction pathway specifies the aspects of the phases (**b**) and (**c**) that differ across the mechanisms. For example, the

D-$N_R C_R$ mechanism denotes direct transfer of Nζ–H_R to O4′ in phase **(b)**, and abstraction of C2′–H_R in phase **(c)**.

Table 5.1. *Nomenclature for the glycosylase/β-lyase mechanisms investigated in Chapter 5.[a]*

Mechanism	Ring Opening	Nζ–H[b]	C2'–H[c]
D-$N_R C_R$	Direct	*Pro–R*	*Pro–R*
D-$N_R C_S$	Direct	*Pro–R*	*Pro–S*
D-$N_S C_R$	Direct	*Pro–S*	*Pro–R*
D-$N_S C_S$	Direct	*Pro–S*	*Pro–S*
A-$N_R C_R$	Assisted	*Pro–R*	*Pro–R*
A-$N_R C_S$	Assisted	*Pro–R*	*Pro–S*
A-$N_S C_R$	Assisted	*Pro–S*	*Pro–R*
A-$N_S C_S$	Assisted	*Pro–S*	*Pro–S*

[a] See Figure 5.2 for atom numbering. [b] Proton transferred from the amine to O4′ during ring opening. [c] Proton abstracted from C2′ during elimination step.

The smallest model capable of the reactions highlighted in phases **a–c** in Figure 5.1 was used. Specifically, for the glycosylase/β-lyase chemical steps catalyzed by hOgg1, this includes the OG nucleoside, 3′-phosphate and lysine nucleophile (Figure 5.2). Several previous computational investigations of OG deglycosylation have used models of similar size, but without the phosphate group.[27–28,30–31] Within this model, the OG nucleobase acts as the general base or general acid required at various stages in the mechanism, which eliminates the requirement of additional groups and model expansion. Although this approach allows the model to be consistent throughout the entire reaction pathway, the alignment of the OG nucleobase deviates from an orientation that would 'fit' in the hOgg1 active-site at some stages of the mechanisms. Nevertheless, the primary goal, and overall findings regarding the reactivity and flexibility of the imine linkage, are unaffected by limitation inherent to the model.
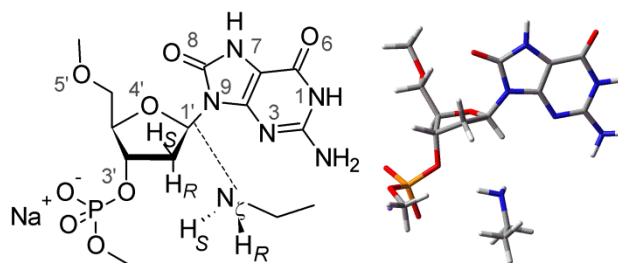
Figure 5.2. *2D (left) and 3D (right) representations of the computational model used in the present study, which contains 8-oxoguanosine 3'-monophosphate, ethyl amine (lysine) and a sodium counterion. Atomic numbering shown in grey, including pro–R and pro–S notation for hydrogen atoms involved in the abstraction steps.*

The truncation points of the DNA phosphate backbone (terminal oxygen atoms) were capped with methyl groups to prevent hydrogen-bonding interactions that are unfeasible in an extended system. The charge on the phosphate group was balanced with a sodium counterion since this method yields better nucleotide geometries than other (protonated or anionic) models.[42–43] The side chain of the nucleophilic lysine was modeled as ethyl amine since preliminary results show that the structure and energetics of the first (deglycosylation) barrier is unaffected by further extension of the amine. Although debates exist in the literature regarding the initial charge of the nucleophile and the potential mode of activation,[23,29] the lysine residue must be neutral to initiate repair. The neutral lysine used in this Thesis is supported by proposals that K249 may be activated during substrate binding,[17] and speculations from mutational studies that the pK_a of K249 in the hOgg1 active site may be shifted such that a significant percentage of the population is neutral.[2] Therefore, the nucleophile activation step (if required) would occur before the reactions investigated herein. Previous theoretical studies have activated the nucleophile by transferring a proton to the OG nucleobase,[27–29] which is consistent with the general observation that purine deglycosylation requires leaving group activation.[6,44] However, protonation of OG would diminish the ability of the nucleobase to act as a general base in later steps of the reaction, which is required by the model implemented.

5.2.2 Methodology

The initial geometry of the OG nucleotide was taken from the 1EBM crystal structure of hOgg1 bound to OG-containing DNA[10] to account for changes in the sugar-phosphate backbone upon flipping the nucleotide out of the helix and into the active site. Subsequently, a sodium counterion was added equidistant to the two phosphate oxygen atoms and a model lysine was positioned for S_N2 attack. Fully-optimized geometries were obtained using B3LYP/6-31G(d) in the presence of bulk solvent described by the IEF-PCM method implemented in Gaussian 09.[45] A dielectric constant of 4.24 (diethyl ether) was selected to represent the environment inside the active site.[46] Frequency calculations at the same level of theory were used to verify the nature of stationary points and obtain zero-point vibrational and Gibbs corrections. All stationary points were reoptimized with PCM-B3LYP/6-31+G(d) to determine the possible influence of diffuse functions on the reaction. The resulting structural changes are minor and the calculated reaction energetics are unchanged (see Appendix D).

Reaction potential energy surfaces were generated for select mechanisms (see Results) to assist characterization of the E2 and O3′-elimination transition states. The ring-opened intermediate (IC(b), Figure 5.1) was used as a starting point for these surfaces. The C2′–H and C3′–O3′ bonds defined the reaction coordinates and were altered in a step-wise manner by increments of 0.100 Å (C2′–H) or 0.200 Å (C3′–O3′) to generate the elimination surface. The stationary points identified from the surfaces were then relaxed to yield fully-optimized structures for the representative mechanisms and provide guesses for the remaining mechanisms.

The connection between intermediates and adjacent transition states for phases **(a)** and **(b)** were verified through Intrinsic Reaction Coordinate (IRC) calculations and through inspection. The connection between stationary points for phase **(c)** was verified by the reaction PES. Intermediates obtained through forward (from the preceding TS) and reverse (from the

succeeding TS) IRCs are related by low barrier rotations. Efforts were made to characterize the rotational transition states, but stable structures could not be found. Regardless, the motion is always associated with the nucleobase, which is a representative acid/base in the current model, and therefore the main conclusions of this study will be unaffected. Thus, the lowest energy minimum was selected to represent a given intermediate in each mechanism. Single-point calculations were carried out with M06-2X/6-311+G(2df,2p) since M06-2X performs well for S_N2 and E2/E1 reaction energetics.[47] The Gibbs energy was determined by combining the B3LYP Gibbs energy correction with the M06-2X/6-311+G(2df,2p) single-point energy calculated using the SMD solvation method, which includes the non-electrostatic component of the energy. This approach has recently been reported to yield reliable Gibbs energies.[48] All calculations were carried out with Gaussian 09 Revision A.02.[49]

5.3 Results

The energetics for the eight reaction mechanisms are presented in Table 5.2 and the SMD-M06-2X/6-311+G(2df,2p) Gibbs reaction surfaces are shown in Figure 5.3. Unless otherwise specified, all energies in the text refer to the Gibbs surface. Each aspect of the overall mechanism is discussed in detail below.
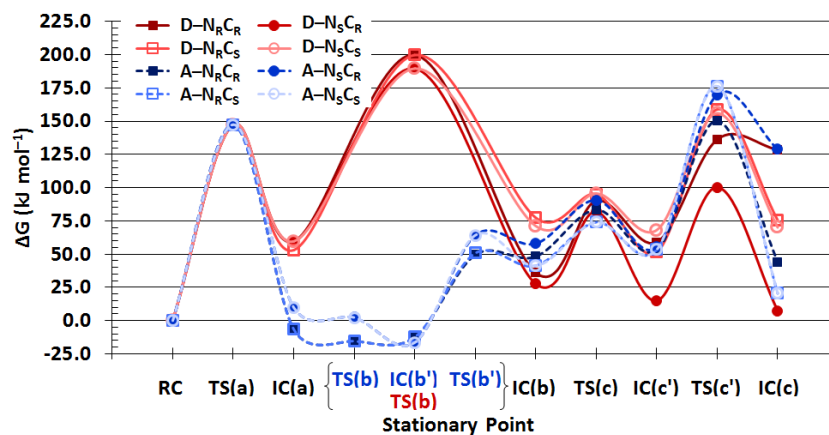
Figure 5.3. *SMD-M06-2X/6-311+G(2df,2p)//PCM-B3LYP/6-31G(d) Gibbs energies for all mechanisms, which involve direct (solid red) or assisted (dashed blue) ring opening, transfer of the Nε–$H_{R/S}$ (square/circle) proton and abstraction of the C2'–$H_{R/S}$ (filled/empty) proton.*

Table 5.2. *Relative energies (kJ mol^{-1}) for stationary points characterized along the eight glycosylase/β-lyase mechanisms.^{a}*

	D-N$_R$C$_R$	D-N$_S$C$_R$	D-N$_R$C$_S$	D-N$_S$C$_S$	A-N$_R$C$_R$	A-N$_S$C$_R$	A-N$_R$C$_S$	A-N$_S$C$_S$
				ΔE^{b}				
TS(a)	147.4	147.4	147.4	147.4	147.4	147.4	147.4	147.4
IC(a)	64.0	64.1	60.6	64.1	−5.6	5.8	−5.6	5.8
TS(b)	201.2	190.5	201.2	190.5	−15.8	−2.0	−15.8	−2.0
IC(b')					−10.0	−15.1	−10.0	−22.7
TS(b')					48.2	55.9	48.2	55.9
IC(b)	34.3	59.3	85.4	75.9	49.1	55.2	43.4	43.4
TS(c)	94.8	83.3	96.1	96.8	81.3	89.9	72.5	72.5
IC(c')	64.4	22.7	58.4	72.5	55.0	58.0	53.0	52.9
TS(c')	157.3	107.2	170.1	168.9	154.0	181.1	185.7	185.7
IC(c)	155.6	21.4	98.2	92.6	57.0	140.0	48.3	48.3
				ΔG^{c}				
TS(a)	147.4	147.4	147.4	147.4	147.4	147.4	147.4	147.4
IC(a)	59.6	59.6	53.0	59.8	−6.6	9.8	−6.6	9.8
TS(b)	199.8	189.6	199.8	189.6	−15.4	2.4	−15.4	2.3
IC(b')					−12.5	−12.9	−12.5	−22.2
TS(b')					49.5	64.2	50.7	64.2
IC(b)	36.0	27.6	77.4	71.1	48.1	57.8	41.2	41.2
TS(c)	90.2	81.9	95.1	95.7	83.3	90.6	74.1	74.1
IC(c')	59.0	15.0	51.6	68.1	53.2	55.4	53.3	53.3
TS(c')	136.2	100.3	158.9	156.0	150.3	170.0	176.3	176.3
IC(c)	128.6	7.4	75.5	70.1	44.2	128.7	20.5	20.5

^{a} Energies reported relative to a common reactant complex (Figure 5.2). ^{b} PCM-M06-2X/6-311+G(2df,2p)//PCM-B3LYP/6-31G(d) values including scaled (0.9806) zero-point vibrational energy correction. ^{c} SMD-M06-2X/6-311+G(2df,2p)//PCM-B3LYP/6-31G(d) values including unscaled correction to Gibbs energy.

5.3.1 Deglycosylation

All mechanisms share a common reactant (Figure 5.2) and concerted deglycosylation transition state (TS(a), Figure 5.4). In the reactant, the OG nucleotide is in an *anti* conformation about the glycosidic bond, and the deoxyribose ring adopts a C3′-*exo* pucker with a slight C2′-*endo* twist. The model lysine is positioned on the opposite side of the sugar moiety than the nucleobase, and is involved in a weak hydrogen bond to O3′. The transition state contains a glycosidic bond length of 2.441 Å and a C1′–Nζ distance of 2.381 Å, and therefore is slightly

earlier than the TS reported in a previous gas-phase study (d(C1′–N9) = 2.552 Å and d(C1′–Nζ) = 2.014 Å),[31] and other theoretical studies.[28–29] The barrier to deglycosylation is 147.4 kJ mol^{-1} on both the ΔE and the ΔG surfaces. Thus, the 3′-phosphate group lowers the calculated S_N2 barrier compared to a truncated (nucleoside) model with a neutral lysine nucleophile (186.2 kJ mol^{-1} as determined using B3LYP/6-31+G(d)).[28]
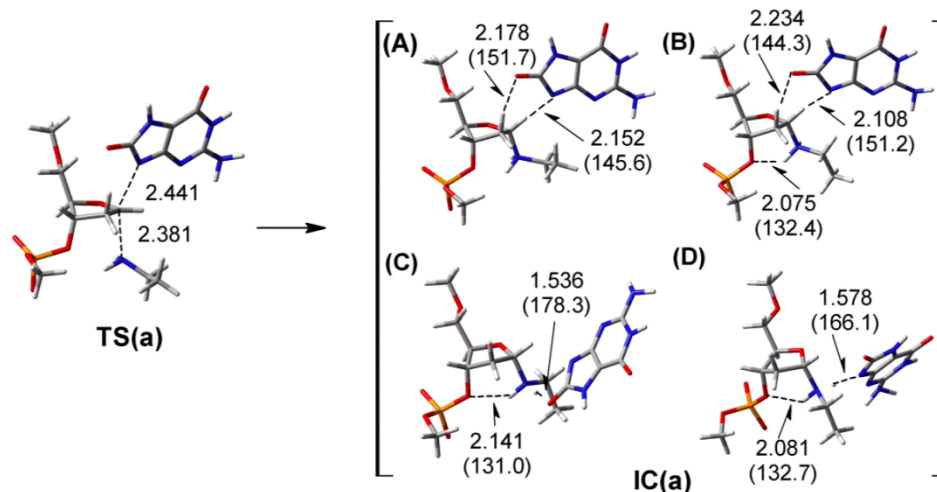
Figure 5.4. *Structures along the deglycosylation step for all mechanisms: (A) D-N_RC_R, D-N_SC_R and D-N_SC_S; (B) D-N_RC_S; (C) A-N_RC_R and A-N_RC_S; (D) A-N_SC_R and A-N_SC_S. Important PCM-B3LYP/6-31G(d) distances (Å) and angles (°, in parentheses) provided (sodium counterion omitted for clarity). Mechanism nomenclature and reaction energetics can be found in Tables 5.1 and 5.2, respectively.*

Following cleavage of the glycosidic bond, the PES divides into direct and base-assisted ring-opening mechanisms. Consequently, the deglycosylation TS falls to one of four deglycosylated intermediates (IC(a), Figure 5.4). The intermediates on the direct ring-opening surfaces contain a weak contact between O8 in OG and C2′–H_S (Figure 5.4A/B). In contrast, the assisted ring-opening intermediates contain strong hydrogen bonds between one of the amine hydrogen atoms and either O8 (Figure 5.4C, A-$N_RC_{R/S}$) or N9 (Figure 5.4D, A-$N_SC_{R/S}$) of the nucleobase. As a result, the assisted ring-opening intermediates are significantly more stable than those for direct transfer (by 43.2 – 66.4 kJ mol^{-1}, Table 5.2). Since the eight mechanisms diverge

after the deglycosylation step, the pathways involving direct ring-opening will first be discussed, followed by the base-assisted ring-opening mechanisms.

5.3.2 Direct Ring Opening: Nζ–H$_{R/S}$ Transfer

The structures for the mechanisms involving direct proton-transfer of Nζ–H$_R$ to O4′ are shown in Figure 5.5. Significant rotation about the crosslink is required to allow for transfer of the *pro–R* proton. The corresponding transition state (TS(b)) has a ΔG of 199.8 kJ mol^{-1} relative to the reactant (ΔG‡ = 140.2 kJ mol^{-1}). This common transition state falls to a distinct IC(b) geometry for each of the D-N$_R$C$_R$ and D-N$_R$C$_S$ mechanisms with relative Gibbs energies of 36.0 and 77.4 kJ mol^{-1}, respectively. In addition, D-N$_R$C$_R$ IC(b) (Figure 5.5, left) contains hydrogen-bonding interactions between the OG nucleobase and C1′–H and Nζ–H, while D-N$_R$C$_S$ IC(b) (Figure 5.5, right) contains a single C2′–H$_S$⋯O8 interaction.
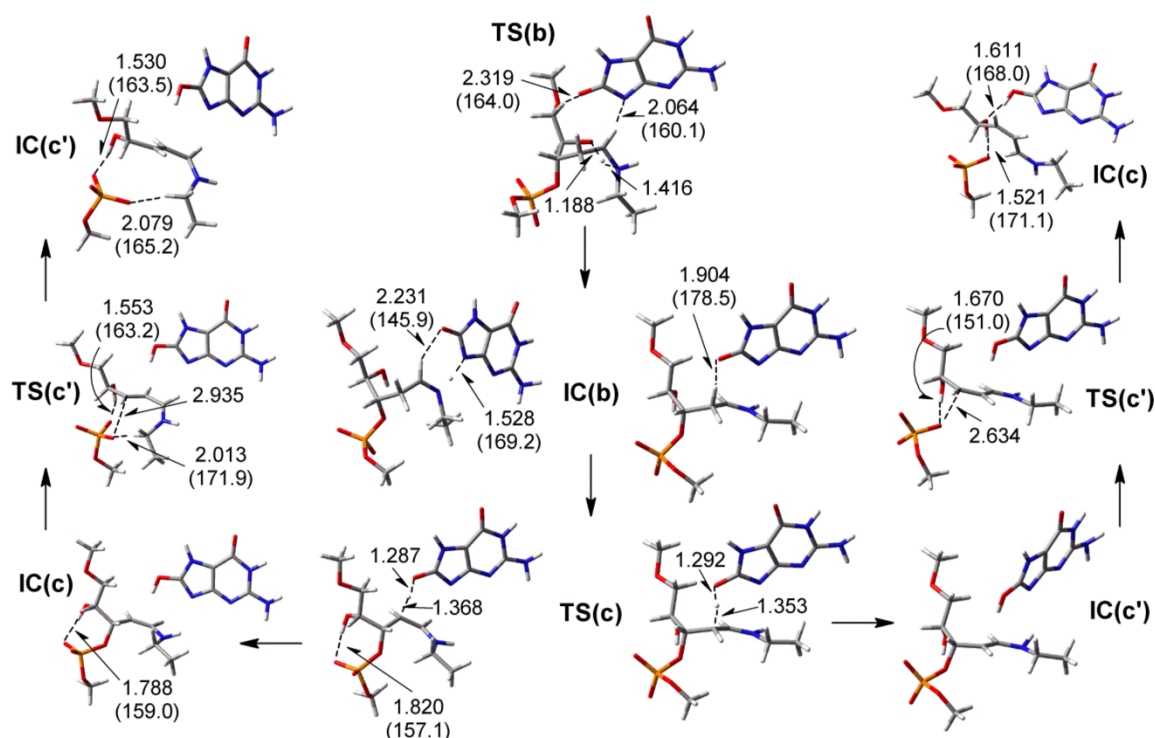
Figure 5.5. *Structures along the ring-opening and β-elimination steps of the D-N$_R$C$_R$ (left) and D-N$_R$C$_S$ (right) mechanisms. Important PCM-B3LYP/6-31G(d) distances (Å) and angles (°, in parentheses) provided (sodium counterion omitted for clarity). Mechanism nomenclature and reaction energetics can be found in Tables 5.1 and 5.2, respectively.*

In contrast to transfer of the *pro–R* proton, rotation of lysine is unnecessary for direct transfer of the *pro–S* Nζ–H (Figure 5.6). Ring opening occurs with a Gibbs energy of 189.6 kJ mol^{-1} relative to the reactant, which is only slightly lower (by 10.2 kJ mol^{-1}) than the *pro–R* proton transfer energy (Table 5.2). Proton transfer of the *pro–S* hydrogen leads to *E*-isomer intermediates (IC(b)) with similar structures to the *Z*-isomers characterized for D-N$_R$C$_{R/S}$. The largest difference in stability (6 kJ mol^{-1}) occurs for the D-N$_S$C$_R$ ring-opened intermediate since the hydrogen-bond acceptors are reversed compared to the corresponding D-N$_R$C$_R$ intermediate, and therefore D-N$_S$C$_R$ contains a strong (1.504 Å) Nζ–H···O8 hydrogen bond and a weak (2.291 Å) C2′–H$_R$···N9 contact. Attempts to characterize a structure similar to D-N$_R$C$_R$ IC(b) that is connected to an elimination product were unsuccessful.
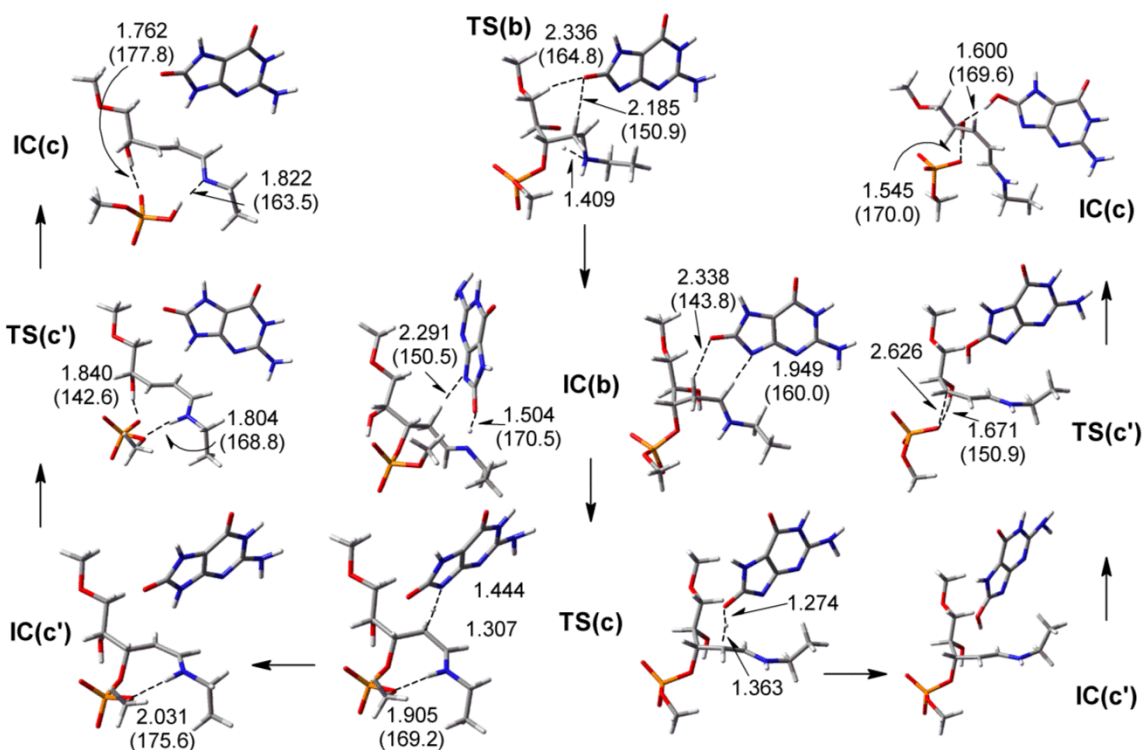
Figure 5.6. *Structures along the ring-opening and β-elimination steps of the D-N$_S$C$_R$ (left) and D-N$_S$C$_S$ (right) mechanisms. Important PCM-B3LYP/6-31G(d) distances (Å) and angles (°, in parentheses) provided (sodium counterion omitted for clarity). Mechanism nomenclature and reaction energetics can be found in Tables 5.1 and 5.2, respectively.*

5.3.3 Direct Ring Opening: β-Elimination

Subsequent to ring opening, abstraction of a proton from C2′ initiates elimination of O3′. The OG contact with C2′–H_S in the D-$N_R C_S$ ring-opened intermediate (Figure 5.5) reduces the barrier for abstraction to ~18 kJ mol^{-1} compared to a barrier of ~54 kJ mol^{-1} for *pro–R* abstraction (Table 5.2). The elimination intermediate IC(c′) is more stable for *pro–S* abstraction than for *pro–R* abstraction, which is in agreement with the lower TS(c) barrier. Following proton transfer, the O3′-elimination transition states (TS(c′)) and intermediates (IC(c)) are partially stabilized by a tight hydrogen bond (1.521 – 1.670 Å, Figure 5.5) between the new O4′-hydroxyl group and a phosphate oxygen atom. This additional stabilization is required since the positively charged imine is directed away from O3′ due to the *Z*-conformation about the C1′–Nζ linkage. As a result, a significant barrier (77.2 kJ mol^{-1} for D-$N_R C_R$ and 107.3 kJ mol^{-1} for D-$N_R C_S$) must be overcome to eliminate the phosphate. Furthermore, the elimination products (IC(c)) are endothermic (by 128.6 and 75.5 kJ mol^{-1} relative to the reactant for D-$N_R C_R$ and D-$N_R C_S$, respectively). Therefore, these reaction paths are improbable, especially in comparison to others examined in this Chapter (see below).

The structures and energetics characterized for the elimination pathways of the D-$N_S C_{R/S}$ mechanisms (Figure 5.6, Table 5.2) are similar to those for the respective D-$N_R C_{R/S}$ mechanisms. The only exception occurs for D-$N_S C_R$ O3′-elimination. Specifically, in the D-$N_S C_R$ mechanism, the *Z*-conformation about the C1′–C2′ double bond and the pseudo *Z*-conformation about C1′–Nζ in the intermediate (IC(c′)) place the imine hydrogen in close proximity to the terminal oxygen of the phosphate group (d(Nζ–H⋯O_{me}) = 2.031 Å). This additional stability, coupled with the O4′–H⋯O_P interaction observed in the other mechanisms, yields an O3′-elimination barrier of 85.3 kJ mol^{-1}, and produces the most stable IC(c) characterized for all mechanisms when the remaining Nζ–H is transferred to O3′ (ΔG = 7.4 kJ mol^{-1} relative to the reactant).

5.3.4 Assisted Ring Opening: Nζ–H$_{R/S}$ Transfer

From the summary of direct mechanisms in Figure 5.3 (red), it can be seen that catalysis of the high energy ring opening is necessary. Indeed, catalysis by a general base (modeled as the OG nucleobase anion, Figure 5.7) significantly changes the reaction energetics (Figure 5.3, blue). Along the base-assisted pathway, proton abstraction from lysine is barrierless (once zero-point vibrational and thermal corrections are included), and leads to exothermic IC(b′) intermediates (ΔG ranging from –22.2 to –12.5 kJ mol^{-1}, Table 5.2). The corresponding barriers for subsequent ring opening (TS(b′)) fall between 60 – 90 kJ mol^{-1}, and are significantly lower than the direct ring-opening barriers (>130 kJ mol^{-1}). The proton transfer in the A-N$_R$C$_{R/S}$ mechanisms is facilitated by O8 of OG (Figure 5.7A), while transfer involves N9 in the A-N$_S$C$_{R/S}$ mechanisms
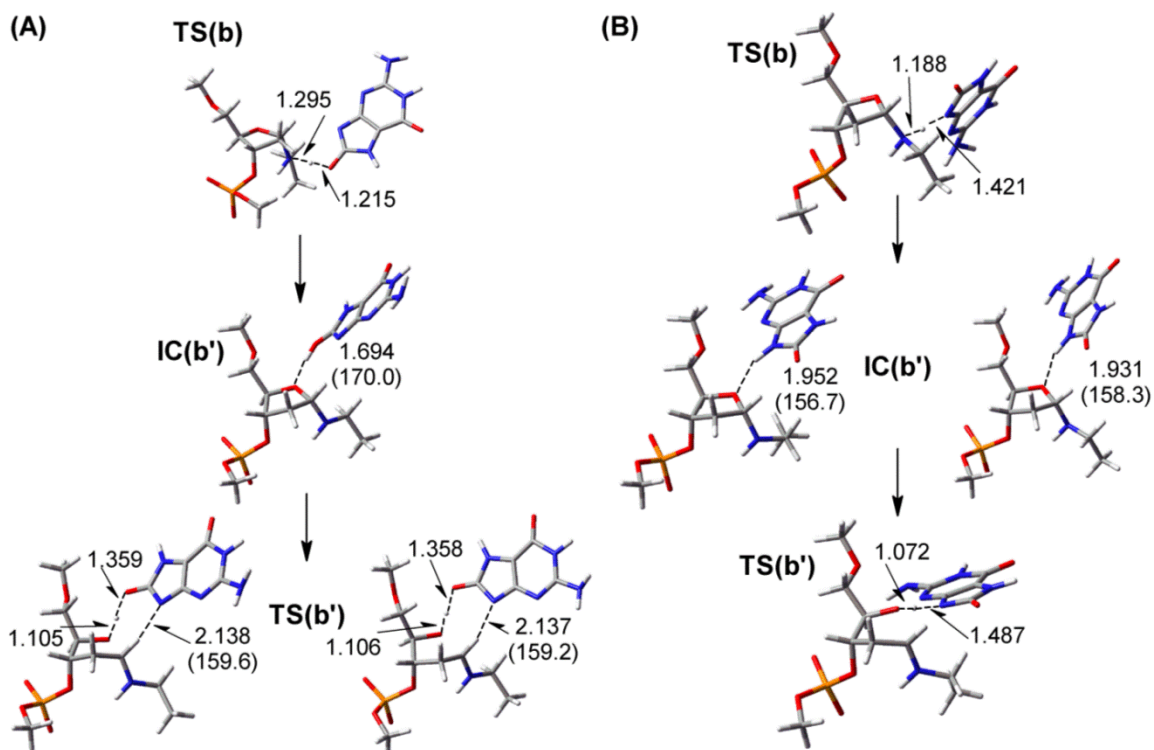
Figure 5.7. *Structures along the ring-opening step of the A-N$_R$C$_R$ (A, left), A-N$_R$C$_S$ (A, right), A-N$_S$C$_R$ (B, left) and A-N$_S$C$_S$ (B, right) mechanisms. Important PCM-B3LYP/6-31G(d) distances (Å) and angles (°, in parentheses) provided (sodium counterion omitted for clarity). Mechanism nomenclature and reaction energetics can be found in Tables 5.1 and 5.2, respectively.*

(Figure 5.7B). The location of the OG nucleobase in TS(b′) of the A-$N_RC_{R/S}$ mechanisms is stabilized by a weak (2.137 Å) C1′–H···N9 interaction (Figure 5.7A), but exhibits significant motion throughout the ring-opening step in A-$N_SC_{R/S}$ due to the involvement of N9 in the proton transfer (Figure 5.7B).

5.3.5 Assisted Ring Opening: β-Elimination

As observed for the direct mechanisms, the elimination phase corresponding to the assisted ring-opening mechanisms is a two-step process (Figure 5.8), involving C2′–H abstraction and then O3′-elimination. Throughout all four mechanisms, there is a strong O4′–H···N9 hydrogen bond ranging in length from 1.615 Å (A-N_SC_R IC(b)) to 1.967 Å (A-N_SC_R IC(c′)), with an average length of 1.87 Å. All four mechanisms have similar barriers for C2′–H abstraction ($\Delta G^{\ddagger} \approx 34$ kJ mol^{-1}) and similarly stable IC(c′) intermediates (53.2 – 55.4 kJ mol^{-1} relative to the reactant, Table 5.2). Since N9 forms a strong hydrogen bond with the 4′-hydroxyl, proton transfer occurs to O8 of OG. In addition, the O4′–H···O3′ interaction observed in the direct ring-opening mechanisms is impossible, which therefore increases the O3′-elimination barriers. The only exception occurs for the A-N_RC_R mechanism in which the imine linkage is oriented to promote an Nζ–H···O interaction that stabilizes the phosphate leaving group (Figure 5.8A). Since the A-N_RC_R mechanism contains additional leaving group stabilization compared to the remaining mechanisms, the O3′-elimination barrier ($\Delta G^{\ddagger} = 97.1$ kJ mol^{-1}) is lower than the barriers for the other assisted mechanisms (114.6 and 123.0 kJ mol^{-1} for the A-N_SC_R and A-$N_{R/S}C_S$ mechanisms, respectively (Table 5.2)). Despite the large barriers, the A-$N_{R/S}C_S$ mechanisms lead to the second most stable elimination product (IC(c)). This increased stability is due to a rotation about the C1′–C2′ bond, which allows proton transfer from Nζ to O3′ (d(O3′–H···Nζ) = 1.859 Å, Figure 5.8C). While a similar proton transfer occurs along the A-N_RC_R mechanism (IC(c), Figure 5.8A), the phosphate group adopts an inherently less stable orientation.
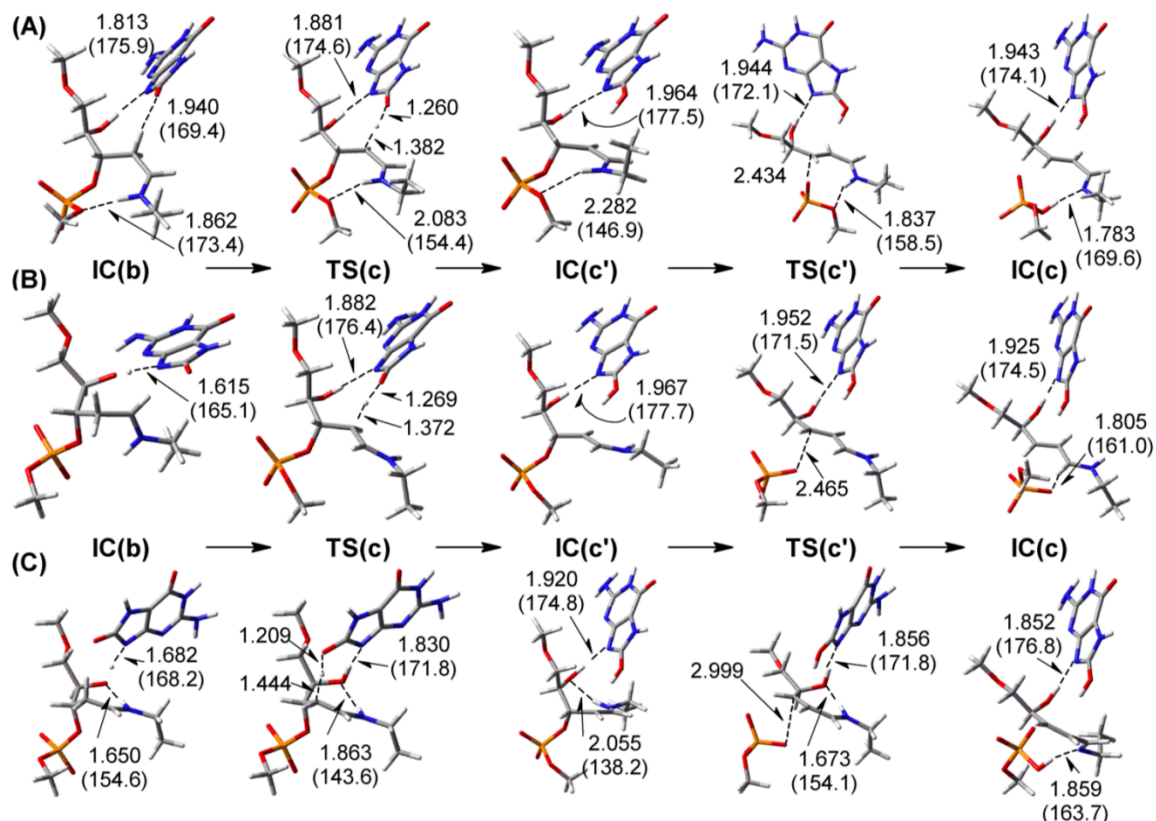
Figure 5.8. *Structures along the β-elimination step of the (A) A-N$_R$C$_R$, (B) A-N$_S$C$_R$, (C) A-N$_R$C$_S$ and A-N$_S$C$_S$ mechanisms. Important PCM-B3LYP/6-31G(d) distances (Å) and angles (°, in parentheses) provided (sodium counterion omitted for clarity). Mechanism nomenclature and reaction energetics can be found in Tables 5.1 and 5.2, respectively.*

5.3.6 β-Elimination: E1 versus E2 Pathway

In the mechanisms discussed above, the β-elimination step (Figure 5.1c) occurs through an E1 pathway with abstraction of a C2′–H by OG before dissociation of the 3′-phosphate group. Despite perfect alignment of the β-elimination angle (O3′–C3′–C2′–H$_{R/S}$), transition states corresponding to E2 mechanisms could not be characterized. To verify that the E1 mechanism is the lowest energy pathway, the reaction PES for the D-N$_S$C$_S$ and A-N$_R$C$_R$ mechanisms were characterized since these selections cover the three main points of variation among all reaction pathways (i.e., direct or assisted ring opening, Nζ–H$_{R/S}$ transfer, and C2′–H$_{R/S}$ abstraction).

The reaction PES (at the optimization level of theory) are shown in Figure 5.9, where IC(b) falls in the bottom left corner and IC(c) in the top right corner. Therefore, the possible IC(c′) for an E1 mechanism appears near the upper left corner of the surfaces. The surfaces reveal that abstraction of a proton occurs early (d(C2′···H) = 1.400 Å) in the E1 reaction and with a low barrier ($\Delta E^{\ddagger}$ = 16.1 and 19.3 kJ mol^{-1} for D-N$_S$C$_S$ and A-N$_R$C$_R$, respectively). A corresponding exothermic intermediate is found on both surfaces (ΔE = −12.8 and −7.8 kJ mol^{-1} compared to IC(b) for D-N$_S$C$_S$ and A-N$_R$C$_R$, respectively). A dissociative transition state is found at C3′–O3′ distances of 2.700 Å for the direct and 2.500 Å for the assisted ring-opening mechanisms. Consistent with TS(c′) characterized for the relaxed PES (Figure 5.6), the 4′-hydroxyl group stabilizes the phosphate group in the D-N$_S$C$_S$ mechanism, and thus lowers the barrier compared to A-N$_R$C$_R$. In contrast to the E1 pathway, an E2 transition state is ill-defined on both surfaces. Indeed, the synchronous regions of the potential energy surfaces (d(C2′···H) = 1.400, d(C3′···O3′) = 2.300 – 2.700 Å) are significantly higher in energy than the step-wise regions (> 130 kJ mol^{-1} relative to the IC(b) starting point). Since the starting structures were properly aligned for synchronous elimination (β-angle (O3′–C3′–C2′–H$_{R/S}$) ≈ 179°), the large energy difference between the two pathways (E1 versus E2) is likely due to stabilization of
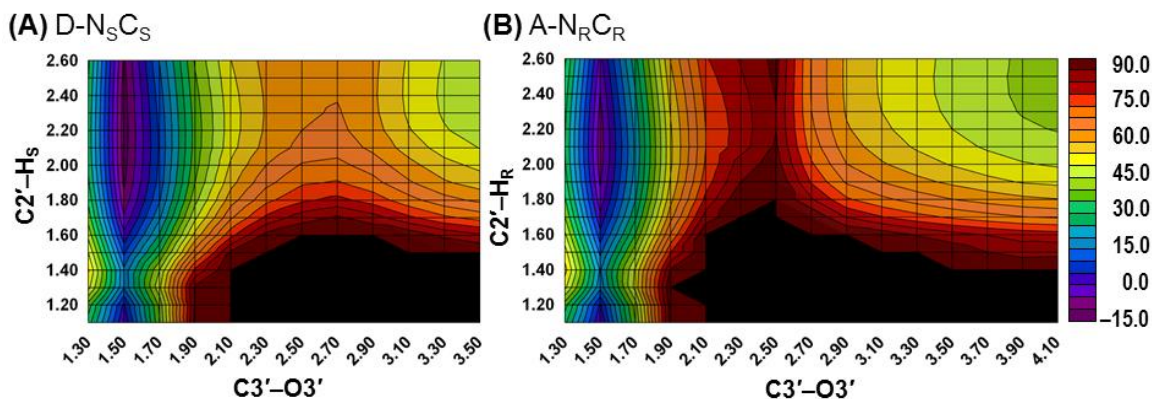
Figure 5.9. *PCM-B3LYP/6-31G(d) reaction potential energy surfaces for the elimination step of the D-N$_S$C$_S$ (A) and A-N$_R$C$_R$ (B) mechanisms (see Table 5.1 for nomenclature). The energies (ΔE, kJ mol^{-1}) are reported relative to the respective ring-opened intermediate (IC(b)) with constrained reaction coordinates.*

proton abstraction by the adjacent Schiff base moiety. Thus, the reaction surfaces clearly support the E1 mechanism reported in this Chapter. Nevertheless, an E2 pathway may be stabilized within the active site of an enzyme.

5.4 Discussion

Previous computational investigations of bifunctional glycosylases such as hOgg1 have focused on the deglycosylation step common to all glycosylases,[27–31] but have essentially neglected the lyase step. In fact, no computational study has been carried out on the β-elimination of a cross-linked AP-site. As the first step to understanding this challenging process, the core reaction catalyzed by hOgg1 was investigated with a DFT model. Although the present model uses the OG nucleobase in the place of possible active site acids/bases, the results can be extrapolated to other moieties acting in this capacity, and therefore to hOgg1 and other enzymes. In this Chapter, eight different reaction mechanisms were characterized that span the chemical step catalyzed by bifunctional glycosylases up to enzyme regeneration (Table 5.1 and Figure 5.1). This computational approach yields insight into the types of active-site residues that can contribute to the overall chemical reaction facilitated by hOgg1 and other β-lyases. To this end, each phase of the reaction (Figure 5.1) will be discussed separately, as well as the recently recognized monofunctional capability of hOgg1.[23]

5.4.1 Deglycosylation

The first chemical step facilitated by bifunctional glycosylases is cleavage of the glycosidic bond in the damaged nucleotide. Consistent with previous computational studies,[28–29,31] the barrier to deglycosylation of the OG nucleotide was found to be large ($\Delta G^{\ddagger} = 147.4$ kJ mol^{-1}), and rate-limiting if ring-opening is base catalyzed (Table 5.2). Since experiment has shown that the lyase step is rate-limiting,[25,50] hOgg1 must significantly reduce the deglycosylation barrier, which is consistent with the catalytic function of other glycosylases.[40,51]

Analysis of the hOgg1 active site (Figure 5.10) reveals different possible methods to reduce the depurination barrier for dOG lesions. First, the positive charge accumulating on Nζ throughout the deglycosylation reaction could be stabilized by the catalytically important D268.[2,23] This can result from electrostatic stabilization due to the proximity of the anionic (aspartate) and cationic (crosslink) charges.[2] Alternatively, D268 or a water molecule could partially or fully abstract a proton from K249 through a hydrogen bond with the terminal amine during the deglycosylation step to generate a neutral cross-linked intermediate.
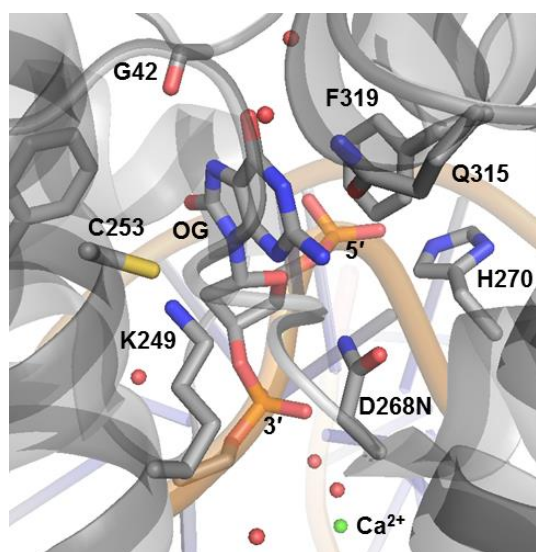
Figure 5.10*. Important hOgg1 active-site residues identified in the crystal structure of the D268N mutant (PDB ID: 1N3C).[2]*

Second, the OG leaving group could be stabilized through protonation by or hydrogen bonding with active-site residues. Previous computational investigations have protonated N3 or O8 of 8-oxoguanine through transfer from Lys prior to deglycosylation,[27,29–30] which lowers the deglycosylation barrier. Furthermore, water molecules present near O6 of OG in most crystal structures[1–2,15,18–19,21,23] could stabilize the departing base through hydrogen-bond donation. Indeed, a single water molecule bound to O6 can increase the N9 acidity of OG (a measure of leaving group ability) by 10.3 kJ mol^{-1}.[52] In addition, Q315, which is near O6/N1 of OG, has been shown to modestly affect catalysis and therefore may fulfill this role.[20,24] These hydrogen-

bonding interactions may be unnecessary, however, as a recent experimental study found nonpolar analogues of OG with little or no hydrogen-bonding accepting ability to be substrates of hOgg1.[25–26]

Third, the free nucleobase product could be stabilized by nonspecific interactions with active-site residues. For example, a cationic histidine residue (H270, Figure 5.10) is in close proximity to the 5′-phosphate, and one of the proposed roles of this amino acid is stabilization of the negative charge accumulating on the nucleobase.[24] Although a stacking interaction between OG and Phe319 could contribute to catalysis, recent work shows that stacking has little to no effect on the deglycosylation barrier of deoxyuridine,[53] and thus a catalytic contribution from the Phe319 residue is unlikely. From the above discussion, one can see that there are a multitude of possible catalytic approaches that hOgg1 can use to reduce the inherently large deglycosylation barrier.

5.4.2 Ring Opening

In this Chapter, two different ring-opening pathways were characterized that involve either direct or base (OG⁻) assisted proton transfer from Nζ to O4′. As expected, assisted transfer is significantly more favorable than direct transfer (by more than 70 kJ mol^{-1}, Table 5.2). However, direct transfer leads to a beneficial orientation of the 4′-hydroxyl group that lowers the subsequent elimination barriers. Therefore, the ideal enzymatic mechanism will use a general base positioned on the opposite side of the sugar plane opposite to the nucleobase. This location will allow interactions between the 4′-hydroxyl and 3′-phosphate groups without requiring rotation of the hydroxyl group by 180°, which would inevitably cleave strong hydrogen bonds between the 4′-hydroxyl and general base. Depending on the orientation of the sugar moiety and nearby water molecules in the active site, this role could be fulfilled by D268 in hOgg1. This new

proposal is consistent with evidence that this helix-capping residue is involved in multiple steps.[2,23]

A second point of mechanistic flexibility investigated in this manuscript is the effect of transferring the *pro–R* versus the *pro–S* Nζ proton. When the *pro–S* proton is transferred, the remaining N–H bond is directed towards the 3′-phosphate in the intermediate. In the subsequent elimination phase, the cationic Nζ–H···O_P hydrogen bond provides substantial stabilization to the leaving group. Furthermore, the *pro–S* hydrogen is aligned for transfer after nucleophilic attack by lysine at the anomeric carbon (IC(a), Figure 5.4), and therefore less rearrangement is required for transfer of Nζ–H_S to O4′ than transfer of Nζ–H_R. The reduced motion increases the probability that the ring-opening phase catalyzed by hOgg1 (or other bifunctional glycosylases) involves Nζ–H_S transfer since the peptide backbone constrains the orientation of the lysine sidechain (or other amine-containing nucleophile). Combined, these features indicate that transfer of Nζ–H_S is preferable to transfer of Nζ–H_R during enzyme-catalyzed ring opening.

5.4.3 β-Elimination

Eight mechanistic variations of the β-elimination of the 3′-phosphate group (with abstraction of a C2′–H) were characterized (Table 5.1). The mechanisms differ in the C2′-proton abstracted (C2′–H_S or C2′–H_R), the initial conformation of the imine linkage (*E* or *Z*) and the presence (or absence) of an O4′–H···N9 hydrogen bond. Reaction PES generated for two systems (D-N_SC_S and A-N_RC_R) clearly demonstrate a favored asynchronous (E1) mechanism (Figure 5.9). In general, *pro–S* abstraction is lower in energy than *pro–R* abstraction, consistent with the C2′–H_S hydrogen requiring less molecular motion/flexibility in order to interact with OG. The D/A-N_RC_R mechanisms are an exception and exhibit the lowest abstraction and O3′-dissociation barriers (Table 5.2). Despite large structural differences, all elimination mechanisms exhibit similar energetics. These results are consistent with experiments showing both *pro–R* and *pro–S*

proton abstraction.[1] Another noteworthy feature of the β-elimination step is that the O3′-dissociation barrier is larger than the C2′–H abstraction barrier is (by $20 - 90$ kJ mol^{-1}). Computational studies of similar reactions have conversely found that proton abstraction is rate-limiting,[32–33] likely due to the absence of cationic charge adjacent to the proton abstraction site in those systems.

Although the elimination barriers are lower than those for deglycosylation (and direct ring-opening), the barriers are quite large (up to 123.0 kJ mol^{-1}, Table 5.2). Therefore, it is useful to consider possible ways that enzymes might catalyze this reaction step. The most obvious mode of catalysis in hOgg1 involves stabilization of the phosphate leaving group. Examination of the hOgg1 active site (Figure 5.10) reveals a nearby calcium dication that could interact with the cleaved product upon displacement of a bound water molecule. Alternatively, since the phosphate group is accessible to solvent, proton transfer from solvent to the phosphate may distribute the charge. Finally, the proton transfer from Nζ observed in the D-N_SC_R, A-N_RC_R and A-$N_{R/S}C_S$ mechanisms (Figures 5.6 and 5.8) could reduce the charge on the 3′-phosphate moiety and prepare the protein–DNA linkage for hydrolysis and enzyme regeneration. A more subtle route for enzyme catalysis involves steric constraints that may promote rotation of the sugar–lysine linkage to better align a particular C2′–H for abstraction. In fact, modeling of crystal structures of the hOgg1-linked intermediate indicates rotation about C2′–C3′ leads to a lower energy geometry with C2′–H$_R$ in close proximity to the OG nucleobase,[1] which promotes *pro–R* proton abstraction by the base.

5.4.4 Monofunctional Activity

There is some debate in the literature regarding the relevance of the hOgg1 lyase activity *in vivo* since interactions with APE1 dissociate hOgg1 from the AP-site before elimination occurs.[23,25,54–56] The results in this Chapter (Figure 5.3) provide the first computational support for

the monofunctional activity of hOgg1. Specifically, the lowest energy point on the potential energy surface occurs during the ring-opening step, after the (Nζ) amine has been deprotonated, but before the deoxyribose ring has opened (Figure 5.3). If the protein–DNA crosslink is hydrolyzed at this point, the product would be an AP-site that can be processed by a more efficient AP-endonuclease (for example, APE1). Alternatively, a water molecule (potentially activated by a hydrogen bond to an active-site residue) could act as the nucleophile for the glycosylase step, and thus avoid the slow, multi-step enzyme regeneration pathway. Recent work indicates that an aspartate-activated water nucleophile lowers the deglycosylation barrier of the dOG nucleotide by ~20 kJ mol^{-1} compared to a lysine nucleophile (e.g., hOgg1) or ~10 kJ mol^{-1} compared to a proline nucleophile (e.g., FPG) in a protein environment ($\varepsilon = 4.2$).[31] This new proposal of a water nucleophile would additionally bypass the confusion surrounding the mechanism for K249 activation in hOgg1.[2,17,23,29]

Since the sugar moiety of the damaged nucleoside is solvent accessible in most (if not all) DNA glycosylases, it is reasonable to propose a mechanism of action for hOgg1 that is monofunctional in nature by either of the aforementioned mechanisms. Parallels can be drawn to MutY, which contains the same active-site motif as hOgg1 comprised of a helix-hairpin-helix element followed by a glycine/proline-rich loop ending in an invariant aspartate residue (HhH-GPD).[5–6] As discussed in Chapter 4, MutY uses a water nucleophile to catalyze deglycosylation of dA incorrectly incorporated opposite dOG.[57] A single mutation that incorporates lysine into the active site, equivalent to K249 in hOgg1, bestows bifunctional activity upon MutY.[37] Furthermore, some studies have even observed Schiff-base intermediates with wild-type protein, suggesting MutY exhibits weak, uncoupled lyase activity.[58–64] Thus, through comparison to the structurally similar MutY, one can envision a mechanism whereby the glycosylase and lyase activities of hOgg1 are uncoupled and the AP-site may be transferred to an AP-endonuclease for further processing. Indeed, there is evidence that hOgg1 glycosylase activity is increased and

lyase activity is uncoupled in the presence of human AP-endonuclease (HAP1).[55] A similar argument can be made for EndoIII since it contains the same active-site fold as hOgg1 and MutY,[65] and therefore may correspondingly exhibit uncoupled monofunctional activity that is not limited by slow lyase activity.

5.5 Conclusions

For the first time, the lyase step of a bifunctional glycosylase has been modeled. This emphasizes that small model computational approaches can provide several key conclusions regarding this complicated process through analysis of multiple reaction mechanisms. With respect to the first phase of the chemical step, the results clearly show that the protein must significantly lower the deglycosylation barrier. Catalysis will likely involve stabilization of both the nucleobase leaving group and the cationic charge developing on the protein–DNA crosslink. In the second phase, the most efficient rearrangement to a ring-opened Schiff base intermediate involves catalysis by a general base in the active site. Transfer of the *pro–S* proton on Nζ in the crosslink during ring opening requires less rotation about the C1′–Nζ bond, exhibits lower barriers, and leads to more stable intermediates during the elimination phase than *pro–R* transfer. Once the ring has opened, the crosslink is very flexible and can occupy many different conformations throughout the remainder of the mechanism. Therefore, as long as the phosphate leaving group is stabilized (for example, through active-site contacts), the similar energetics for the different elimination pathways suggest that there is no intrinsic preference for a given mechanism, and the preferred mechanism may instead be dictated by steric constraints within the active site. Perhaps most interestingly, the lowest energy structure along the various pathways occurs *before* the β-elimination phase, which implies that it may be possible to kinetically trap this (deglycosylated, ring-closed) intermediate. This finding provides the first computational support for the recent experimental observation that hOgg1 exhibits monofunctional activity *in vivo*,[23] and by analogy supports the uncoupled lyase behavior of MutY.[37] This intricate feature of

the reaction pathway underscores the complex mechanisms of action available to the DNA glycosylase family and will be further considered in Chapter 6.

Large model studies of hOgg1 lyase activity can be generated using the mechanistic insights outlined herein. Specifically, the present study indicates that mechanisms involving both *pro–S* and *pro–R* abstraction from C2′ during β-elimination must be considered since *pro–S* abstraction is slightly energetically favored, but *pro–R* abstraction leads to more facile O3′-elimination. Furthermore, most mechanisms characterized herein can likely be accommodated in the hOgg1 active site if the general acid/base role of OG in the small model is fulfilled by other residues (for example, an aspartate residue), and careful consideration of the active-site composition will aid identification of the subset of reactions that must be considered. Such large-scale modeling of hOgg1 may further clarify the roles of active-site residues proposed to be important for the catalytic activity of hOgg1 based on this small model study (for example, D268, H270, and Q315, Figure 5.10).[24] Although this Chapter is particularly interested in hOgg1, the results regarding the flexibility of the imine linkage may be applied equally well to other enzymes with β-lyase activity on an AP-site, such as EndoIII (hNTH in humans), Endonuclease VIII (hNEIL in humans), MutY (hMYH in humans) and FPG, as well as model peptides. Equivalent large model studies of these enzymes may reveal structural causes for the observed relative rates. Mechanisms that obey the steric constraints in the active site of a given enzyme can be selected for additional study by overlaying the DFT elimination products (with the OG nucleobase removed) onto the desired active site, and fulfilling the catalytic role(s) of OG in the small model by other groups as needed. Studies of such a diverse group of lyase-active enzymes will no doubt reveal additional mechanistic insights into this vital reaction.

5.6 References[b]

(1)   Fromme, J. C.; Bruner, S. D.; Yang, W.; Karplus, M.; Verdine, G. L., Product-Assisted Catalysis in Base-Excision DNA Repair. *Nat. Struct. Biol.* **2003,** *10* (3), 204–211.

(2)   Norman, D. P. G.; Chung, S. J.; Verdine, G. L., Structural and Biochemical Exploration of a Critical Amino Acid in Human 8-oxoguanine Glycosylase. *Biochemistry* **2003,** *42* (6), 1564–1572.

(3)   Hitomi, K.; Iwai, S.; Tainer, J. A., The Intricate Structural Chemistry of Base Excision Repair Machinery: Implications for DNA Damage Recognition, Removal, and Repair. *DNA Repair* **2007,** *6* (4), 410–428.

(4)   Sun, B.; Latham, K. A.; Dodson, M. L.; Lloyd, R. S., Studies on the Catalytic Mechanism of 5 DNA Glycosylases - Probing for Enzyme-DNA Imino Intermediates. *J. Biol. Chem.* **1995,** *270* (33), 19501–19508.

(5)   Stivers, J. T.; Jiang, Y. L., A Mechanistic Perspective on the Chemistry of DNA Repair Glycosylases. *Chem. Rev. (Washington, DC, U. S.)* **2003,** *103* (7), 2729–2759.

(6)   Berti, P. J.; McCann, J. A. B., Toward a Detailed Understanding of Base Excision Repair Enzymes: Transition State and Mechanistic Analyses of N-glycoside Hydrolysis and N-glycoside Transfer. *Chem. Rev. (Washington, DC, U. S.)* **2006,** *106* (2), 506–555.

(7)   Kuznetsov, N. A.; Koval, V. V.; Fedorova, O. S., Mechanism of Recognition and Repair of Damaged DNA by Human 8-Oxoguanine DNA Glycosylase hOGG1. *Biochemistry (Moscow)* **2011,** *76* (1), 118–130.

(8)   Sakai, A.; Nakanishi, M.; Yoshiyama, K.; Maki, H., Impact of Reactive Oxygen Species on Spontaneous Mutagenesis in *Escherichia coli*. *Genes Cells* **2006,** *11* (7), 767–778.

(9)   Fujimoto, H.; Pinak, M.; Nemoto, T.; Bunta, J. K., Structural Analysis of Base Mispairing in DNA Containing Oxidative Guanine Lesion. *Cent. Eur. J. Phys.* **2007,** *5* (1), 49–61.

(10)   McCulloch, S. D.; Kokoska, R. J.; Garg, P.; Burgers, P. M.; Kunkel, T. A., The Efficiency and Fidelity of 8-Oxo-guanine Bypass by DNA Polymerases δ and η. *Nucleic Acids Res.* **2009,** *37* (9), 2830–2840.

(11)   Cadet, J.; Douki, T.; Ravanat, J.-L., Oxidatively Generated Base Damage to Cellular DNA. *Free Radical Biol. Med.* **2010,** *49* (1), 9–21.

(12)   Kanvah, S.; Joseph, J.; Schuster, G. B.; Barnett, R. N.; Cleveland, C. L.; Landman, U., Oxidation of DNA: Damage to Nucleobases. *Acc. Chem. Res.* **2010,** *43* (2), 280–287.

(13)   van Loon, B.; Markkanen, E.; Hübscher, U., Oxygen as a Friend and Enemy: How to Combat the Mutational Potential of 8-Oxo-guanine. *DNA Repair* **2010,** *9* (6), 604–616.

---

[b] Bibliography and citations in ACS format.

(14)   Nash, H. M.; Lu, R. Z.; Lane, W. S.; Verdine, G. L., The Critical Active-Site Amine of the Human 8-Oxoguanine DNA Glycosylase, hOgg1: Direct Identification, Ablation and Chemical Reconstitution. *Chem. Biol.* **1997,** *4* (9), 693–702.

(15)   Bruner, S. D.; Norman, D. P. G.; Verdine, G. L., Structural Basis for Recognition and Repair of the Endogenous Mutagen 8-Oxoguanine in DNA. *Nature (London, U. K.)* **2000,** *403* (6772), 859–866.

(16)   Norman, D. P. G.; Bruner, S. D.; Verdine, G. L., Coupling of Substrate Recognition and Catalysis by a Human Base-Excision DNA Repair Protein. *J. Am. Chem. Soc.* **2001,** *123* (2), 359–360.

(17)   Bjørås, M.; Seeberg, E.; Luna, L.; Pearl, L. H.; Barrett, T. E., Reciprocal "Flipping" Underlies Substrate Recognition and Catalytic Activation by the Human 8-Oxo-guanine DNA Glycosylase. *J. Mol. Biol.* **2002,** *317* (2), 171–177.

(18)   Chung, S. J.; Verdine, G. L., Structures of End Products Resulting from Lesion Processing by a DNA Glycoylase/Lyase. *Chem. Biol.* **2004,** *11* (12), 1643–1649.

(19)   Banerjee, A.; Yang, W.; Karplus, M.; Verdine, G. L., Structure of a Repair Enzyme Interrogating Undamaged DNA Elucidates Recognition of Damaged DNA. *Nature (London, U. K.)* **2005,** *434* (7033), 612–618.

(20)   Banerjee, A.; Verdine, G. L., A Nucleobase Lesion Remodels the Interaction of Its Normal Neighbor in a DNA Glycosylase Complex. *Proc. Nat. Acad. Sci. USA* **2006,** *103* (41), 15020–15025.

(21)   Radom, C. T.; Banerjee, A.; Verdine, G. L., Structural Characterization of Human 8-Oxoguanine DNA Glycosylase Variants Bearing Active Site Mutations. *J. Biol. Chem.* **2007,** *282* (12), 9182–9194.

(22)   Lee, S.; Radom, C. T.; Verdine, G. L., Trapping and Structural Elucidation of a Very Advanced Intermediate in the Lesion-Extrusion Pathway of hOGG1. *J. Am. Chem. Soc.* **2008,** *130* (25), 7784–7785.

(23)   Dalhus, B.; Forsbring, M.; Helle, I. H.; Vik, E. S.; Forstrøm, R. J.; Backe, P. H.; Alseth, I.; Bjørås, M., Separation-of-Function Mutants Unravel the Dual-Reaction Mode of Human 8-Oxoguanine DNA Glycosylase. *Structure (Cambridge, MA, U. S.)* **2011,** *19* (1), 117–127.

(24)   van der Kemp, P. A.; Charbonnier, J. B.; Audebert, M.; Boiteux, S., Catalytic and DNA-Binding Properties of the Human Ogg1 DNA N-glycosylase/AP lyase: Biochemical Exploration of H270, Q315 and F319, Three Amino Acids of the 8-Oxoguanine-Binding Pocket. *Nucleic Acids Res.* **2004,** *32* (2), 570–578.

(25)   Zharkov, D. O.; Rosenquist, T. A.; Gerchman, S. E.; Grollman, A. P., Substrate Specificity and Reaction Mechanism of Murine 8-Oxoguanine-DNA Glycosylase. *J. Biol. Chem.* **2000,** *275* (37), 28607–28617.

(26)   McKibbin, P. L.; Kobori, A.; Taniguchi, Y.; Kool, E. T.; David, S. S., Surprising Repair Activities of Nonpolar Analogs of 8-oxoG Expose Features of Recognition and Catalysis by Base Excision Repair Glycosylases. *J. Am. Chem. Soc.* **2012,** *134* (3), 1653–1661.

(27)   Osakabe, T.; Fujii, Y.; Hata, M.; Tsuda, M.; Neya, S.; Hoshino, T., Quantum Chemical Study on Base Excision Mechanism of 8-Oxoguanine DNA Glycosylase: Substrate-Assisted Catalysis of the N-glycosidic Linkage Cleavage Reaction. *Chem-Bio Inf. J.* **2004,** *4* (3), 73–92.

(28)   Schyman, P.; Danielsson, J.; Pinak, M.; Laaksonen, A., Theoretical Study of the Human DNA Repair Protein hOGG1 Activity. *J. Phys. Chem. A* **2005,** *109* (8), 1713–1719.

(29)   Calvaresi, M.; Bottoni, A.; Garavelli, M., Computational Clues for a New Mechanism in the Glycosylase Activity of the Human DNA Repair Protein hOGG1. A Generalized Paradigm for Purine-Repairing Systems? *J. Phys. Chem. B* **2007,** *111* (23), 6557–6570.

(30)   Zheng, Y.; Xue, Y.; Yan, S. G., The Effects of Oxidation and Protonation on the N-glycosidic Bond Stability of 8-Oxo-2'-deoxyguanosine: DFT Study. *THEOCHEM* **2008,** *860* (1-3), 52–57.

(31)   Shim, E. J.; Przybylski, J. L.; Wetmore, S. D., Effects of Nucleophile, Oxidative Damage, and Nucleobase Orientation on the Glycosidic Bond Cleavage in Deoxyguanosine. *J. Phys. Chem. B* **2010,** *114* (6), 2319–2326.

(32)   Kim, Y.; Mohrig, J. R.; Truhlar, D. G., Free-Energy Surfaces for Liquid-Phase Reactions and Their Use to Study the Border Between Concerted and Nonconcerted α,β-Elimination Reactions of Esters and Thioesters. *J. Am. Chem. Soc.* **2010,** *132* (32), 11071–11082.

(33)   Pei, Q.; Christofferson, A.; Zhang, H.; Chai, J. J.; Huang, N., Computational Investigation of the Enzymatic Mechanisms of Phosphothreonine Lyase. *Biophys. Chem.* **2011,** *157* (1-3), 16–23.

(34)   de Jesus, K. P.; Serre, L.; Zelwer, C.; Castaing, B., Structural Insights into Abasic Site for FPG Specific Binding and Catalysis: Comparative High-Resolution Crystallographic Studies of FPG Bound to Various Models of Abasic Site Analogues-Containing DNA. *Nucleic Acids Res.* **2005,** *33* (18), 5936–5944.

(35)   Mazumder, A.; Gerlt, J. A.; Absalon, M. J.; Stubbe, J.; Cunningham, R. P.; Withka, J.; Bolton, P. H., Stereochemical Studies of the β-Elimination Reactions at Aldehydic Abasic Sites in DNA - Endonuclease III from *Escherichia-coli*, Sodium-Hydroxide, and Lys-Trp-Lys. *Biochemistry* **1991,** *30* (4), 1119–1126.

(36)   Zharkov, D. O.; Golan, G.; Gilboa, R.; Fernandes, A. S.; Gerchman, S. E.; Kycia, J. H.; Rieger, R. A.; Grollman, A. P.; Shoham, G., Structural Analysis of an *Escherichia coli* Endonuclease VIII Covalent Reaction Intermediate. *EMBO J.* **2002,** *21* (4), 789–800.

(37)   Williams, S. D.; David, S. S., Evidence that MutY is a Monofunctional Glycosylase Capable of Forming a Covalent Schiff Base Intermediate with Substrate DNA. *Nucleic Acids Res.* **1998,** *26* (22), 5123–5133.

(38)   Kurtz, A. J.; Dodson, M. L.; Lloyd, R. S., Evidence for Multiple Imino Intermediates and Identification of Reactive Nucleophiles in Peptide-Catalyzed β-Elimination at Abasic Sites. *Biochemistry* **2002,** *41* (22), 7054–7064.

(39)   Rogacheva, M. V.; Kuznetsova, S. A., Repair of 8-Oxoguanine in DNA. The Mechanisms of Enzymatic Catalysis. *Russ. Chem. Rev.* **2008,** *77* (9), 765–788.

(40)   Dong, J.; Drohat, A. C.; Stivers, J. T.; Pankiewicz, K. W.; Carey, P. R., Raman Spectroscopy of Uracil DNA Glycosylase-DNA Complexes: Insights into DNA Damage Recognition and Catalysis. *Biochemistry* **2000,** *39* (43), 13241–13250.

(41)   Scharer, O. D.; Jiricny, J., Recent Progress in the Biology, Chemistry and Structural Biology of DNA Glycosylases. *Bioessays* **2001,** *23* (3), 270–281.

(42)   Millen, A. L.; Manderville, R. A.; Wetmore, S. D., Conformational Flexibility of C8-Phenoxyl-2'-deoxyguanosine Nucleotide Adducts. *J. Phys. Chem. B* **2010,** *114* (12), 4373–4382.

(43)   Churchill, C. D. M.; Wetmore, S. D., Developing a Computational Model that Accurately Reproduces the Structural Features of a Dinucleoside Monophosphate Unit within B-DNA. *Phys. Chem. Chem. Phys.* **2011,** *13* (36), 16373–16383.

(44)   Schroeder, G. K.; Wolfenden, R., Rates of Spontaneous Disintegration of DNA and the Rate Enhancements Produced by DNA Glycosylases and Deaminases. *Biochemistry* **2007,** *46* (47), 13638–13647.

(45)   Scalmani, G.; Frisch, M. J., Continuous Surface Charge Polarizable Continuum Models of Solvation. I. General Formalism. *J. Chem. Phys.* **2010,** *132* (11), 114110.

(46)   Ng, J. A.; Vora, T.; Krishnamurthy, V.; Chung, S. H., Estimating the Dielectric Constant of the Channel Protein and Pore. *Eur. Biophys. J. Biophys. Lett.* **2008,** *37* (2), 213–222.

(47)   Zhao, Y.; Truhlar, D. G., Density Functional Calculations of E2 and S_N2 Reactions: Effects of the Choice of Density Functional, Basis Set, and Self-Consistent Iterations. *J. Chem. Theory Comput.* **2010,** *6* (4), 1104–1108.

(48)   Ribeiro, R. F.; Marenich, A. V.; Cramer, C. J.; Truhlar, D. G., Use of Solution-Phase Vibrational Frequencies in Continuum Models for the Free Energy of Solvation. *J. Phys. Chem. B* **2011,** *115* (49), 14556–14562.

(49)   Frisch, M. J.; Trucks, G. W.; Schlegel, H. B.; Scuseria, G. E.; Robb, M. A.; Cheeseman, J. R.; Scalmani, G.; Barone, V.; Mennucci, B.; Petersson, G. A*., et al. Gaussian 09*, Revision A.02; Gaussian, Inc.: Wallingford CT, 2009.

(50)   Bjørås, M.; Luna, L.; Johnson, B.; Hoff, E.; Haug, T.; Rognes, T.; Seeberg, E., Opposite Base-Dependent Reactions of a Human Base Excision Repair Enzyme on DNA Containing 7,8-Dihydro-8-oxoguanine and Abasic Sites. *EMBO J.* **1997,** *16* (20), 6314–6322.

(51)   Brinkmeyer, M. K.; Pope, M. A.; David, S. S., Catalytic Contributions of Key Residues in the Adenine Glycosylase MutY Revealed by pH-dependent Kinetics and Cellular Repair Assays. *Chem. Biol.* **2012,** *19* (2), 276–286.

(52)   McConnell, T. L.; Wheaton, C. A.; Hunter, K. C.; Wetmore, S. D., Effects of Hydrogen Bonding on the Acidity of Adenine, Guanine, and Their 8-Oxo Derivatives. *J. Phys. Chem. A* **2005,** *109* (28), 6351–6362.

(53)   Kellie, J. L.; Navarro-Whyte, L.; Carvey, M. T.; Wetmore, S. D., Combined Effects of π‑π Stacking and Hydrogen Bonding on the (N1) Acidity of Uracil and Hydrolysis of $2'$-Deoxyuridine. *J. Phys. Chem. B* **2012,** *116* (8), 2622‑2632.

(54)   Hill, J. W.; Hazra, T. K.; Izumi, T.; Mitra, S., Stimulation of Human 8-Oxoguanine-DNA Glycosylase by AP-endonuclease: Potential Coordination of the Initial Steps in Base Excision Repair. *Nucleic Acids Res.* **2001,** *29* (2), 430–438.

(55)   Vidal, A. E.; Hickson, I. D.; Boiteux, S.; Radicella, J. P., Mechanism of Stimulation of the DNA Glycosylase Activity of hOGG1 by the Major Human AP Endonuclease: Bypass of the AP Lyase Activity Step. *Nucleic Acids Res.* **2001,** *29* (6), 1285–1292.

(56)   Morland, I.; Luna, L.; Gustad, E.; Seeberg, E.; Bjørås, M., Product Inhibition and Magnesium Modulate the Dual Reaction Mode of hOgg1. *DNA Repair* **2005,** *4* (3), 381–387.

(57)   McCann, J. A. B.; Berti, P. J., Transition-State Analysis of the DNA Repair Enzyme MutY. *J. Am. Chem. Soc.* **2008,** *130* (17), 5789–5797.

(58)   Tsai-wu, J. J.; Liu, H. F.; Lu, A. L., *Escherichia-coli* MutY Protein has Both N-Glycosylase and Apurinic/Apyrimidinic Endonuclease Activities on A·C and A·G Mispairs. *Proc. Nat. Acad. Sci. USA* **1992,** *89* (18), 8779–8783.

(59)   Lu, A. L.; Tsaiwu, J. J.; Cillo, J., DNA Determinants and Substrate Specificities of *Escherichia-coli* MutY. *J. Biol. Chem.* **1995,** *270* (40), 23582–23588.

(60)   Gogos, A.; Cillo, J.; Clarke, N. D.; Lu, A. L., Specific Recognition of A/G and A/7,8-dihydro-8-oxoguanine (8-oxoG) Mismatches by *Escherichia coli* MutY: Removal of the C-terminal Domain Preferentially Affects A/8-oxoG Recognition. *Biochemistry* **1996,** *35* (51), 16665–16671.

(61)   Manuel, R. C.; Lloyd, R. S., Cloning, Overexpression, and Biochemical Characterization of the Catalytic Domain of MutY. *Biochemistry* **1997,** *36* (37), 11140–11152.

(62)   Guan, Y.; Manuel, R. C.; Arvai, A. S.; Parikh, S. S.; Mol, C. D.; Miller, J. H.; Lloyd, S.; Tainer, J. A., MutY Catalytic Core, Mutant and Bound Adenine Structures Define Specificity for DNA Repair Enzyme Superfamily. *Nat. Struct. Biol.* **1998,** *5* (12), 1058–1064.

(63)   Zharkov, D. O.; Grollman, A. P., MutY DNA Glycosylase: Base Release and Intermediate Complex Formation. *Biochemistry* **1998,** *37* (36), 12384–12394.

(64)   Williams, S. D.; David, S. S., Formation of a Schiff Base Intermediate is not Required for the Adenine Glycosylase Activity of *Escherichia coli* MutY. *Biochemistry* **1999,** *38* (47), 15417–15424.

(65)   Fromme, J. C.; Verdine, G. L., Structure of a Trapped Endonuclease III-DNA Covalent Intermediate. *EMBO J.* **2003,** *22* (13), 3461–3471.

Chapter 6: Bifunctional Glycosylases Part 2:

Human 8-Oxoguanine–DNA Glycosylase (hOgg1)[a]

6.1 Introduction

The previous Chapter used a small DFT model to investigate the bifunctional mechanism of action of hOgg1. Briefly, the proposed glycosylase/lyase mechanism involves four steps: (a) deglycosylation of the dOG nucleotide by an active-site lysine (K249), (b) rearrangement to a ring-opened Schiff-base intermediate, (c) β-elimination of the 3′-phosphate and (d) hydrolysis of the DNA–protein crosslink to regenerate the enzyme and release the product.[1–2] Among these steps, the β-lyase activity of hOgg1 is known to be significantly slower than the glycosylase activity.[3–7] Furthermore, there is evidence that hOgg1 behaves as a monofunctional glycosylase *in vivo,* similar to hUNG2 and MutY, and the AP-site product is processed by an AP-endonuclease.[4,7–8] Indeed, the results from Chapter 5 support kinetic trapping of the deglycosylated intermediate, and a possible monofunctional mechanism was proposed involving hydrolysis of the crosslink that occurs prior to β-elimination (Section 5.4.4). Therefore, the present Chapter examines the possible monofunctional activity of hOgg1.

In general, there are two pathways that could lead to monofunctional hOgg1 activity. First, K249 could act as the nucleophile as proposed for the bifunctional mechanism. The DNA–protein crosslink could then be hydrolyzed before β-elimination occurs. Second, a water molecule could act as the nucleophile, similar to the other monofunctional glycosylases. Since there have not been KIE experiments on monofunctional hOgg1 activity that parallel those for MutY[9] and hUNG2,[10] there is no experimental evidence indicating a preference for one of these pathways. Therefore, a computational study comparing the different mechanisms would be useful to

determine the most likely mechanism, as well as to propose experiments to aid elucidation of the monofunctional mechanism of hOgg1 action.

Although there has only been one computational study that specifically examined (uncatalyzed) dOG hydrolysis,[11] the many previous computational studies on dOG deglycosylation may contribute valuable information regarding a possible lysine nucleophile.[11–17] Nevertheless, the various works are difficult to compare due to the use of different models, methods and starting geometries (see Table E1 in Appendix E).[11–17] For example, three different crystal structures[18–20] have been used to obtain starting geometries of the dOG lesion and K249 nucleophile. Two of the crystal structures contain active-site mutations (K249Q and D268N in the 1EBM and 1N3C structures, respectively) and lead to an asynchronous mechanism.[12–13,17] The third structure (1FN7) does not contain an active-site mutation, but instead is bound to a tetrahydrofuran (THF) inhibitor (similar to an AP-site). The orientation of K249 in the 1FN7 structure supports an S_N2-type mechanism.[13–14] In addition to using a variety of starting geometries, most of the previous computational studies have been initiated with protonated K249.[12–14,17] While there is experimental evidence for a $K249^+$–$C253^-$ salt bridge in the reactant,[21] the computational models implemented have been too small to provide nucleophile activation, and therefore OG was biased to act as a general base prior to deglycosylation. Since different starting geometries for MutY models led to different energetics in Chapter 4, the variations in the mechanisms proposed from the previous computational literature on hOgg1 are likely due to the use of a range of model sizes and geometries used. Consequently, the present Chapter will investigate the deglycosylation of dOG by hOgg1 using a sufficiently sized model to account for nucleophile activation and leaving group stabilization.

As mentioned above, there are several crystal structures available for hOgg1 that could theoretically be used to generate a computational model. The hOgg1(K249Q):dOG (1EBM) and hOgg1(D268N):dOG (1N3C) structures are the most popular in the literature; however, both

contain mutations of key active-site residues. hOgg1 contains the same active-site fold as MutY (HhH-G/PD), where D268 in hOgg1 takes the place of the (D144) helix-capping residue in MutY. In Chapter 4, crystal structures of MutY with (LRC)[22] and without (FLRC)[23] a D144N mutation were compared, and the orientations of D144 and D144N were found to be significantly different. Therefore, it is likely that the D268N mutation in the 1N3C structure of hOgg1 contains a similarly large migration of the catalytically essential aspartate. Similarly, the K249Q mutation in the 1EBM structure may introduce structural changes to the active site that cannot be reversed easily in a computational model. Recently, a new structure has been deposited by the Verdine group (PDB ID: 3KTU) that is analogous to the MutY FLRC; specifically, the 3KTU structure does not contain any active-site mutations, but rather is co-crystallized with DNA containing the 2′-fluoro-dOG inhibitor (FdOG, Figure 6.1). Based on this discussion, 3KTU is used to generate an hOgg1 model in the present study.
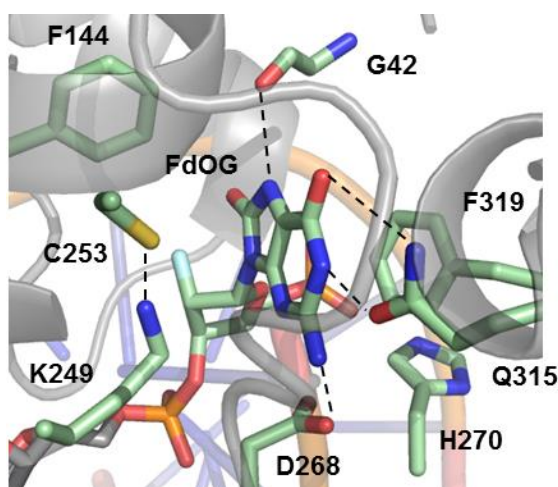
Figure 6.1. *Active site of hOgg1 bound to 2'-fluoro-dOG (FdOG, PDB ID: 3KTU).*

In this Chapter, the approach developed in Chapters 3 and 4 will be used to study the monofunctional mechanism of hOgg1 action. The first mechanism involves K249 as the nucleophile and the resulting DNA–protein crosslink is hydrolyzed to generate the AP-site. In the remaining two mechanisms, a water molecule acts as the nucleophile with either K249 or D268 acting as the general base that activates the nucleophile. A variety of mutations are carried out on

the three mechanisms to determine the catalytic effect of each active-site residue, which will validate the computational model and aid identification of the most likely mechanism. Based on these results, the proposed monofunctional mechanism involves K249 acting as a general base, rather than the nucleophile. Furthermore, this work reveals that the active-site aspartate (D268) stabilizes the charge buildup on the sugar moiety for the monofunctional mechanism, which is similar to the role proposed for the corresponding residues in other monofunctional glycosylases, such as hUNG2 (Chapter 3).

6.2 Computational Details

6.2.1 Model Generation

Initial heavy atom coordinates were taken from the hOgg1:FdOG crystal structure (PDB ID: 3KTU). Residues with heavy atoms within 10 Å of the FDG23 residue were included in the model. Additional residues were included to bridge small (1−2 amino acid) gaps in the backbone. Residues with R-groups directed away from the body of the resulting model were truncated to alanine. A calcium ion near the 3′ phosphate of FdOG was included with a coordinated water molecule (HOH55C) and two new water molecules were added to complete the coordination sphere. A full list of the model contents can be found in Table E2 (Appendix E). Cleaved bonds were capped with a hydrogen atom in the same orientation as the original atom. The remaining hydrogen atoms were added by hand to ensure optimal hydrogen-bond contacts are formed. The K249−C253 interaction was initially modeled as charge separated, D268 and D322 were anionic, and H270 and R324 were cationic. The total charge of the system is −3 and includes 1130 atoms (559 heavy atoms).

The unconstrained region of the model includes the high-level (DFT) region and a portion of the low-level (semi-empirical) region (Figure 6.2).[b] Specifically, the DFT region contains the FDG23 nucleoside, 3′-phosphate, the peptide bond between G42 and Q43 (including Cα of both residues), the R-groups of S147, K249, C253, D268, H270, Q315, F319, and three water molecules (HOH109C, HOH55C and HOH1A). The high-level region includes 121 atoms (63 heavy) and has a charge of −1. The unconstrained portion of the low-level region includes the 5′-phosphate, C5′ of DG24 (attached to the 3′-phosphate), the R-groups of F144 and M257, the Ca^{2+}, and the two coordinated water molecules (a total of 39 atoms, 18 heavy).
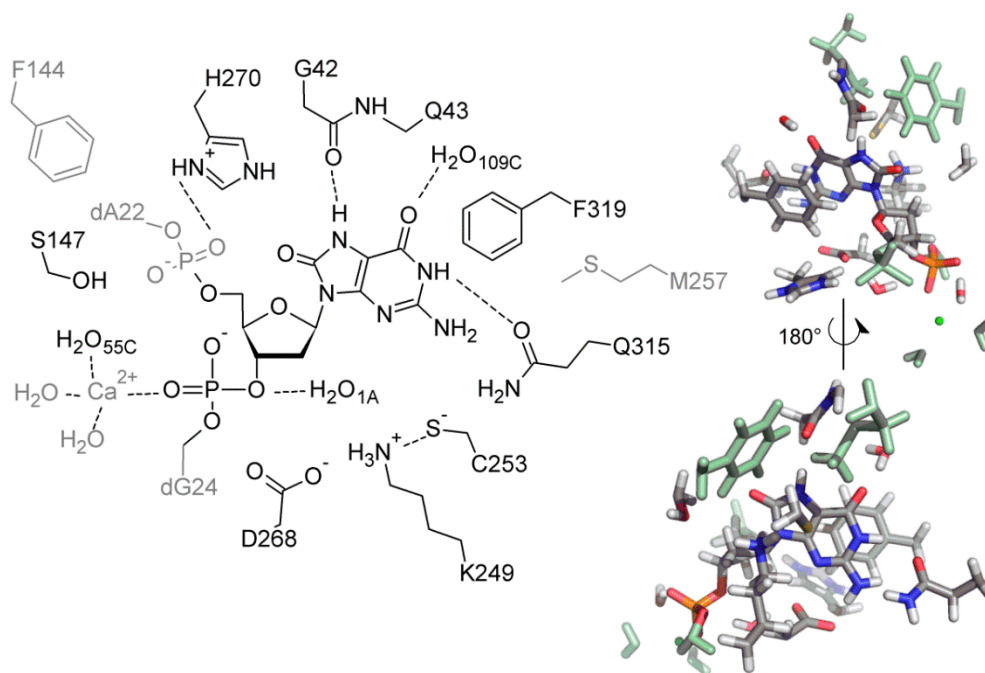
Figure 6.2. *Schematic (left) of the high (black) and unconstrained low-level (grey) regions of the ONIOM model. 3D model (right) of the high-level region of the hOgg1 reactant with unconstrained low-level atoms in green.*

6.2.2 Conformational Search

In Chapter 5, a conformational search of the MutY active-site provided a more catalytically-competent starting geometry than the X-ray coordinates. Therefore, a similar search

---

[b] Preliminary calculations with the entire low-level region constrained as in Chapters 3 and 4 indicated that the resulting active site is too tight to accommodate deglycosylation. Therefore, certain residues in the low-level region were allowed to relax in order to increase the flexibility of the system.

of the conformational space of the hOgg1 active site was carried out in the present Chapter. Prior to the conformational search of the active-site residues, the hydrogen atoms in the model were relaxed with PM6. The orientations of residues near the OG nucleobase, namely F144, K249, C253, D268, H270, Q315 and F319, were included in the search (K249 and C253 were modeled as neutral for the search due to a calculated barrierless proton transfer, see Section 6.3.2.1). First, the dihedral angles defining the conformation of the R-group were modified in 30° increments for all residues except K249 and Q315, which were rotated in 60° increments to reduce the number of conformers. In contrast to the MutY search, which simultaneously modified two residues, each group in the hOgg1 search was individually considered. This choice is justified since the only strong hydrogen bond occurs between K249 and C253, but this interaction must break during the reaction. Once the conformations were generated, PM6 single-point energy calculations were carried out. The conformers within 100 kJ mol^{-1} of the most stable geometry for each amino acid were optimized within the ONIOM model.

6.2.3 Mechanistic Overview

Previous computational studies of the mechanism of action of hOgg1 have focused on the bifunctional activity of the enzyme,[11–14,16–17] and therefore have investigated mechanisms with K249 as the nucleophile. A single study also examined the hydrolysis of a dOG nucleotide by an activated water molecule.[11] In the present Chapter, three mechanisms are characterized to specifically examine the monofunctional activity of hOgg1. All mechanisms begin with proton transfer from K249 to C253 (TS1–All, Figure 6.3), followed by a rearrangement step that orients K249 and/or D268 for the next step of the reaction (TS2, Figure 6.3). In the first mechanism (K249–Nuc), the deglycosylation step uses K249 as the nucleophile. After depurination, the DNA–protein crosslink is hydrolyzed to yield an AP-site and regenerate the enzyme. The other two mechanisms use a water molecule as the nucleophile and either K249 or D268 as the general base that activates the nucleophile (referred to as K249–GB and D268–GB, respectively).
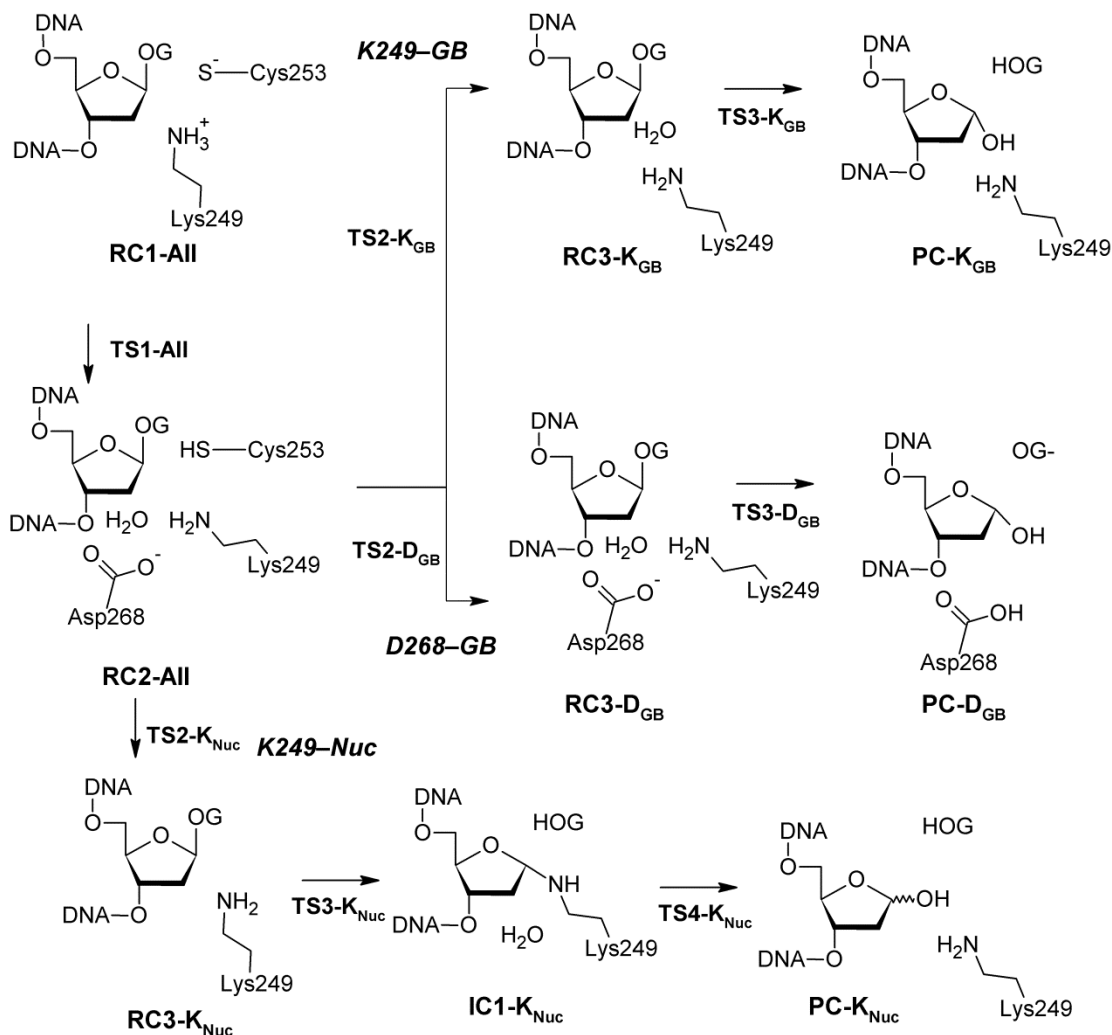
Figure 6.3. *Outline of the monofunctional mechanisms (K249–Nuc, K249–GB and D268–GB) characterized in the present work.*

6.2.4 Methodology

Optimizations were carried out with ONIOM, where the high-level region was treated with the M06-2X density functional method in conjunction with the 6-31G(d) basis set, and the low-level region was treated with the PM6 semi-empirical method. The DFT region was extracted from all stationary points and frequency calculations were carried out with M06-2X/6-31G(d) to obtain estimates of the zero-point vibrational correction and thermal correction to Gibbs energy. High-quality single-point energies were obtained with ONIOM(M06-2X/6-311+G(2df,2p):PM6). All calculations were carried out with Gaussian 09 (Rev. A.02 and C.01).[24]

Reactants, intermediates and products were fully optimized with ONIOM. However, transition state optimizations were prohibitively expensive. Therefore, reaction PES of increasing resolution were used to refine transition state geometries. This methodology was successfully used in Chapter 4 to study the mechanism of action of MutY. Each transition state is described by a different set of coordinates, and Table 6.1 summarizes the bond lengths and dihedral angles selected, as well as the associated step-size implemented. The initial guess for each transition state was generated by hand to connect the two adjacent stationary points, and then the reaction coordinates were altered to refine the portion of the surface around the TS.

Table 6.1. *Summary of reaction coordinates and increments used to refine transition states.*[a]

Mechanism	TS	Coordinates	Increments[b]
All	TS1	Nζ–H	0.025, 0.010
K249–Nuc	TS2	C253 Cα–Cβ–S–H	10.0, 5.0, 2.5
K249–Nuc	TS3	C1′–N9, C1′–Nζ	0.200, 0.100, 0.050
K249–GB	TS3	C1′–N9, C1′–O$_{Wat}$	0.400, 0.200, 0.050
D268–GB	TS3	C1′–N9, C1′–O$_{Wat}$	0.400, 0.200, 0.050

[a] See Section 6.2.3 for the definitions of the mechanisms and stationary points. [b] Step-sizes used to generated and refine reaction PES based on distances (Å) or dihedral angles (degrees).

6.2.5 Mutational Analysis

In order to validate the results of the mechanistic study, a mutational analysis was carried out on the Lys activation and deglycosylation steps. Specifically, the stationary points that characterize these reactions (RC1, TS1, and RC2 for Lys activation; and RC3, TS3 and IC1/PC for deglycosylation of all mechanisms) were modified with one of eleven mutations (F144A, K249A, K249Q, C253A, D268A, D268N, D268E, H270A, Q315A, F319A, K249C/C253K) or the G42–Q43 peptide bond was removed (G42-XX). The system was then relaxed with ONIOM(M06-2X/6-31G(d):PM6). In the case of the transition states, select distances were

constrained to the reported wild-type values to prevent the structure from collapsing (Nζ–H for Lys activation step; C1′–N9 and C1′–O$_{Wat}$(Nζ) for deglycosylation).

6.3 Results

6.3.1 Conformational Search

Prior to studying the potential monofunctional mechanism of hOgg1 action, the conformations of critical active-site residues (F144, K249, C253, D268, H270, Q315 and F319) were individually examined. Similar to MutY, two conformations of the helix-capping residue (D268) were identified (Table 6.2 and Table E2, Appendix E). One maintains the capping interaction, while the other breaks the hydrogen bond with the backbone (ΔE = 12.2 kJ mol^{-1}). The cost of breaking the helix cap is much smaller for hOgg1 than for MutY (ΔE = 51.6 kJ mol^{-1}) since the D268–backbone hydrogen bond is replaced with a D268–OG interaction with the exocyclic amine in hOgg1.

Table 6.2. *Relaxation of geometries in conformational search of hOgg1 active-site.*

Residue	Structures[a]	Residue	Structures[a]
F144	5 / 1	H270	11 / 2
K249	26 / 14	Q315	170 / 17
C253	7 / 3	F319	8 / 1
D268	9 / 2		

[a] Number of structures within 100 kJ mol^{-1} of the minimum after PM6 single-point energy calculation/ Number of unique structures after relaxation with ONIOM.

A large number of conformations were obtained for K249 and Q315, many of which are (slightly) more stable than the crystal structure geometry (Table E2, Appendix E). In addition, some of the alternate geometries place K249 in a better position for nucleophilic attack (d(C1′–Nζ) < 4 Å), or provide better (lone pair) alignment of the general bases (K249 and D268) with respect to the nucleophile. Therefore, one of these geometries was used as an initial guess for the RC3–K$_{Nuc}$ pathway, and another for the RC3–K$_{GB}$ and RC3–D$_{GB}$ mechanisms (Figure 6.3).

Three different conformations were obtained for C253, each with a different noncovalent interaction. The most stable conformation contains an S–H⋯O hydrogen bond to the K249 backbone carbonyl. The other two geometries contain a lone-pair–π or S–H⋯π interaction with F144. Since the conformational search was carried out on a system with K249 and C253 neutral (i.e., after Lys activation), these results indicate that the K249–C253 interaction is not stable after proton transfer. Therefore, after lysine is activated, there may be a preference for the hydrogen bond with C253 to break, which frees K249 to rearrange as required for subsequent steps in the mechanism.

6.3.2 Reaction Mechanism

In this section, the three mechanisms characterized in the present work (Figure 6.3) will be presented. First, the lysine activation step common to all pathways will be discussed, followed by the deglycosylation steps. A comparison of the reaction energetics for all mechanisms can be found in Table 6.3.

Table 6.3. *Reaction energetics (kJ mol^{-1}) for the three mechanisms investigated in the present work.*[a]

	K249–Nuc		K249–GB		D268–GB	
	ΔE^b	ΔG^c	ΔE^b	ΔG^c	ΔE^b	ΔG^c
RC1	0.0	0.0	0.0	0.0	0.0	0.0
TS1	–2.0	–2.3	–2.0	–2.3	–2.0	–2.3
RC2	–52.9	–58.5	–52.9	–58.5	–52.9	–58.5
TS2	–12.6	–7.0	NC^d	NC^d	NC^d	NC^d
RC3	7.9	–6.2	0.8	1.2	–36.8	–47.3
TS3	203.1	213.6	202.7	174.4	210.3	210.5
IC1	–14.8	–28.1	–	–	–	–
PC	–	–	19.0	17.1	131.4	123.9

[a] See Section 6.2.3 for the definitions of the mechanisms and stationary points. [b] ONIOM(M06-2X/6-311+G(2df,2p):PM6) single-point energies including scaled (0.958) ZPVE. [c] ONIOM(M06-2X/6-311+G(2df,2p): PM6) single-point energies including unscaled thermal correction to Gibbs energy. [d] Could not be characterized.

6.3.2.1 K249 Activation

Most of the previous computational investigations of the hOgg1 mechanism of action have used a cationically charged K249 residue as the nucleophile.[12–14,17] There is support that dOG substrate binding involves a K249$^+$–C253$^-$ contact.[21] Specifically, the dipole between the two residues is anti-aligned with the local dipole formed between O8 and N7H of OG (Figure 6.4). This dipole–dipole interaction has been proposed to assist the differentiation between undamaged guanine and OG.[21] However, protonated lysine cannot act as either a nucleophile or a general base. Therefore, the pathways studied in this Chapter all begin with proton transfer from K249 to C253 to activate K249.

The proton transfer step is barrierless after incorporation of the zero-point vibrational energy (TS1, Table 6.3), and the resulting activated reactant (RC2) is exothermic by 52.9 kJ mol^{-1} compared to RC1 (Table 6.3). This indicates that, although the salt bridge may be stable in the free enzyme, when the active site is solvent accessible, the environment shifts to be less polar after the substrate is bound, which catalyzes activation of the essential K249 residue. The neutral hydrogen bond is substantially longer than the charged interaction (by 0.192 Å, Figure 6.4), which decreases the strength of the contact, and therefore reduces the barrier to rearrangement of the K249 residue in preparation for the deglycosylation step.
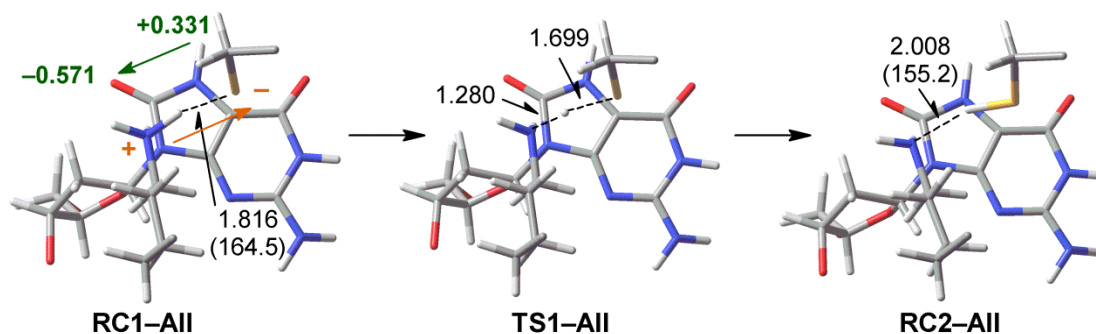
Figure 6.4. *Refined stationary points for the lysine activation step, including hydrogen-bond distances (Å) and angles (degrees, parentheses). ONIOM(M06-2X/6-311+G(2df,2p):PM6) Mulliken charges for NH7 and O8 shown (green). For clarity, only the dOG, K249 and C253 groups are included.*

6.3.2.2 K249 as Nucleophile

The first deglycosylation pathway examined in this Chapter (K249–Nuc) involves two phases: (1) S_N2 deglycosylation of dOG facilitated by K249, and (2) hydrolysis of the DNA–protein crosslink to yield the AP-site product. Before deglycosylation can occur, the K249 conformation must change to break the hydrogen bond with C253 and reorient Nζ below the sugar plane, which aligns the group for nucleophilic attack on the anomeric carbon. Rearrangement from RC2–All to RC3–K_{Nuc} costs 52.3 kJ mol^{-1} (ΔG, Table 6.3). Most of the rearrangement energy is associated with breaking the K249–C253 hydrogen bond, which has an estimated contribution of 51.5 kJ mol^{-1} (modeled by rotating the C253 Cβ–Oγ bond to remove the interaction). However, this step is also associated with other movement in the active site, including C253, the 3′-phosphate and Ca^{2+}.

After rearrangement, deglycosylation occurs with ΔG = 213.6 kJ mol^{-1} relative to RC1. Although the previously reported computational barriers are significantly smaller,[12–14,17] these studies used a cationic K249, which artificially catalyzes the reaction by protonating the leaving group during attack on the anomeric carbon. In the present work, the transition state occurs with glycosidic bond and nucleophilic distances of 2.350 and 2.300 Å, respectively (Figure 6.5). Pyramidalization of N7 occurs in the transition state as the negative charge accumulating on OG is delocalized to O8 and N7 (TS3–K_{Nuc}, Figure 6.5). The resulting intermediate is exothermic (ΔG = –28.1 kJ mol^{-1}) due to proton transfer from the crosslink to N9 of OG, and restoration of the D268–N2 hydrogen bond that breaks in the TS. Since the deglycosylated intermediate is exothermic with respect to RC1, it is possible that the DNA–protein crosslink persists for some time before proceeding to a ring-opening (bifunctional) or hydrolysis (monofunctional) step. The stability of the intermediate is consistent with the results from Chapter 5, as well as with the large hydrolysis barrier predicted with this model. Preliminary calculations on the hydrolysis of the DNA–protein crosslink (TS4–K_{Nuc}) indicate that the barrier is very large (> 300 kJ mol^{-1}), likely

due to active-site rearrangement (and possible OG release) that cannot be modeled with the current methodology (e.g., due to constraints on the low-level region), or due to the compression of the active-site in the crystal lattice (hOgg1 is in the same point group in all crystal structures, and therefore structural contributions from the lattice cannot be excluded). The large deglycosylation barrier and subsequent hydrolysis step make this monofunctional mechanism unlikely. Therefore the remaining two mechanisms are based on other monofunctional glycosylases that use a water molecule as the nucleophile.
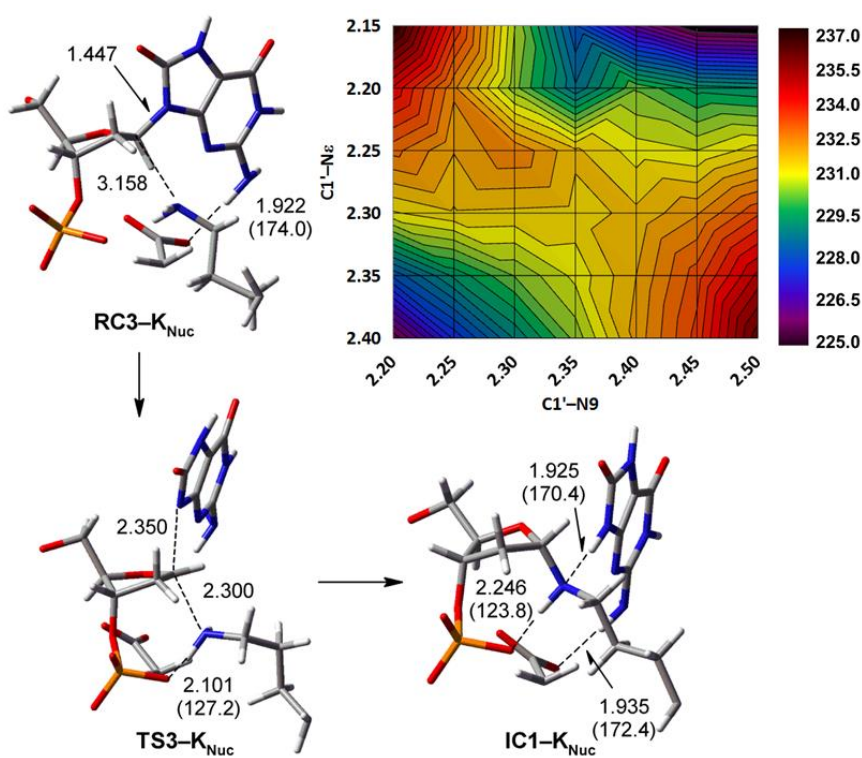
Figure 6.5. *Refined stationary points for the K249–Nuc deglycosylation step, including hydrogen-bond distances (Å) and angles (degrees, parentheses). For clarity, only the dOG, K249 and D268 groups are included. ONIOM(M06-2X/6-31G(d):PM6) reaction potential energy surface (ΔE relative to RC1–All, kJ mol^{-1}) near the transition state is presented, in which each contour corresponds to 0.30 kJ mol^{-1}.*

6.3.2.3 K249 as General Base

The first hydrolysis pathway explains the observed essential roles of both K249 and D268 in a monofunctional context. Specifically, K249 activates the water nucleophile and D268

electrostatically stabilizes the deglycosylation transition state (TS3–K$_{GB}$). The transition state for reorganization of the active site to place the water nucleophile and general base in position could not be characterized, but costs at least 59.7 kJ mol^{-1} (RC2 to RC3 energy difference, Table 6.3). RC3–K$_{GB}$ contains a hydrogen bond between the water nucleophile and D268 that aids orienting the nucleophile, and K249 is positioned such that the lone pair on Nζ is below the sugar plane in anticipation of proton transfer from the water molecule (Figure 6.6). The deglycosylation transition state occurs with a glycosidic bond length of 2.750 Å and a nucleophile distance of 2.250 Å, which is slightly dissociative, but still synchronous. In the transition state, the interaction between the water molecule and D268 is broken and proton transfer to K249 has
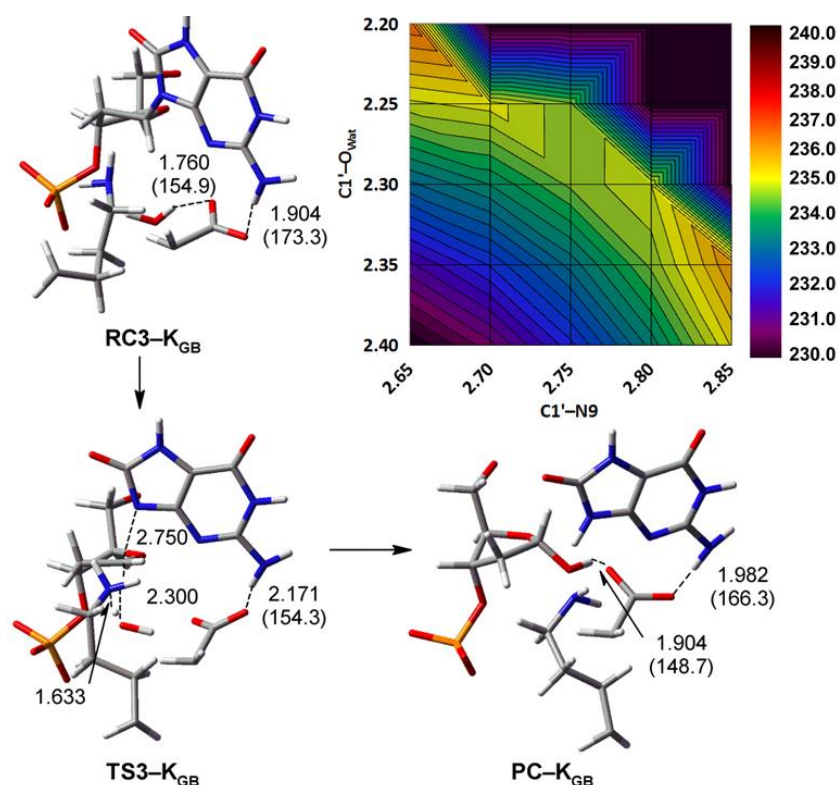
Figure 6.6. *Refined stationary points for the K249–GB deglycosylation step, including hydrogen-bond distances (Å) and angles (degrees, parentheses). For clarity, only the dOG, K249 and D268 groups are included. ONIOM(M06-2X/6-31G(d):PM6) reaction potential energy surface (ΔE relative to RC1–All, kJ mol^{-1}) near the transition state is presented, in which each contour corresponds to 0.25 kJ mol^{-1}.*

partially occurred. The barrier obtained for this reaction is the lowest of all pathways studied in this Chapter, especially on the Gibbs energy surface (ΔG = 174.4 kJ mol^{-1} relative to RC1). Immediately following the transition state, a proton on the water nucleophile is transferred to N9 of the OG anion in association with motion of the nucleobase that places N9 below the plane of the sugar. This motion occurs spontaneously, as can be observed by discontinuity in the upper right corner of the reaction PES, and leads to a stable product (ΔG = 17.1 kJ mol^{-1}). Similar proton transfer was observed in small model studies of dOG deglycosylation from the cationic Lys instead of a water nucleophile, as in the current mechanism.[13,17] In the product, D268 interacts with both the new 1′–hydroxyl and N2 of OG.

6.3.2.4 D268 as General Base

The final mechanism characterized in this Chapter uses a water nucleophile and D268 as the general base (D268–GB). This pathway was investigated since a commonly accepted role for the active-site aspartate in monofunctional glycosylases is activation of the nucleophile, as discussed for hUNG2 and MutY in Chapters 3 and 4.[25–26] As with the K249–GB mechanism, the rearrangement transition state (TS2) could not be characterized; however, the barrier must be at least 11.2 kJ mol^{-1} (Table 6.3). Similar to the K249–GB mechanism, the water nucleophile interacts with D268 (Figure 6.7), which assists activation of the nucleophile and orients the water for attack on the anomeric carbon. K249 stabilizes the OG nucleobase in the reactant and transition state through a hydrogen bond to N3 (d(Nζ–H···N3) = 2.082 – 2.099 Å, Figure 6.7). The deglycosylation transition state is later than observed for the K249–GB mechanism (d(C1′–O$_{Wat}$) = 2.000 Å and 2.250 Å for the D268–GB and K249–GB mechanisms, respectively), and exhibits a significant hydrolysis barrier ($\Delta G^{\ddagger}$ = 257.8 kJ mol^{-1}, relative to RC3–D$_{GB}$). Since the small model hydrolysis study with a formate–activated water molecule as the nucleophile characterized a smaller barrier (ΔE = 115.2 kJ mol^{-1}),[11] poor alignment of the Asp general base must significantly contribute to the large barrier obtained with the current model (PC–D$_{GB}$, Figure

6.7). Furthermore, proton transfer from the water molecule leads to an unstable conformer of neutral D268 (PC–D_{GB}, Figure 6.7), and thus a highly endothermic product (ΔG = 123.9 kJ mol^{-1}). Therefore, it is unlikely that D268 behaves as a general base in the mechanism of hOgg1 action, and instead the main role is likely stabilization of the sugar moiety similar to that proposed for other glycosylases.[25–26]
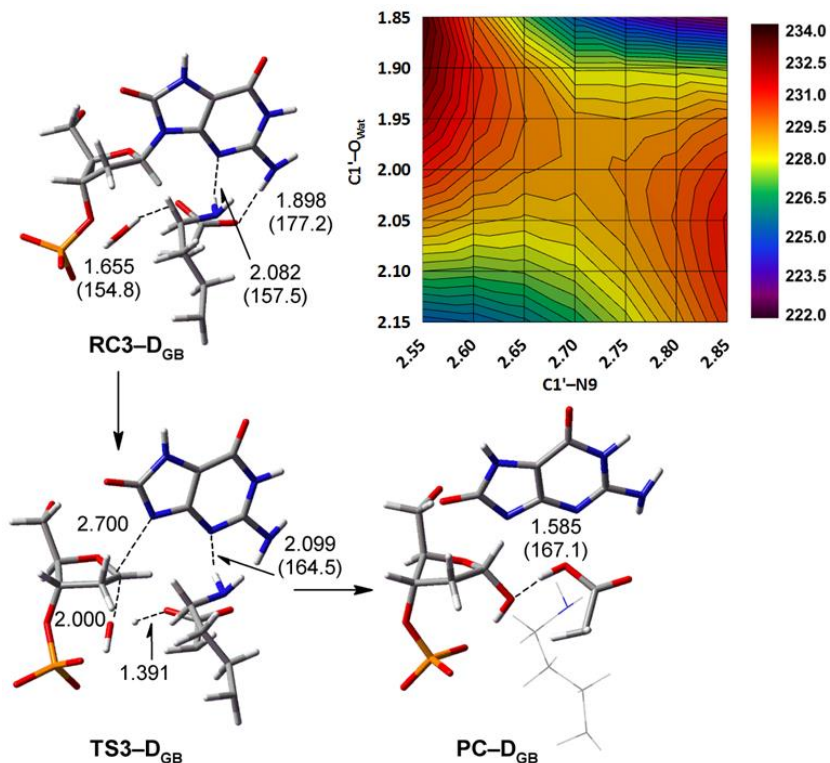
Figure 6.7. *Refined stationary points for the D268–GB deglycosylation step, including hydrogen-bond distances (Å) and angles (degrees, parentheses). For clarity, only the dOG, K249 and D268 groups are included. ONIOM(M06-2X/6-31G(d):PM6) reaction potential energy surface (ΔE relative to RC1–All, kJ mol^{-1}) near the transition state is presented, in which each contour corresponds to 0.30 kJ mol^{-1}.*

6.3.3 Mutational Analysis

To aid selection of the optimal mechanism and validate the present methodology, mutational analysis of the active site was carried out, similar to the study on hUNG2 in Chapter 3. All mutations considered in this Chapter have been studied experimentally,[7,20,27–28] with the exception of the G42-XX deletion. However, one cannot simply compare the rates obtained from

the experimental studies since these were carried out on substrates with different lengths.[5–7,29–30] Specifically, a preliminary comparison of hOgg1 activity indicates that the deglycosylation rate increases exponentially with substrate length (Figure 6.8). Thus, studies that used a 12-mer substrate cannot be directly compared to those carried out with a 30-mer substrate. Furthermore, the *in silico* mutations do not account for large changes in active-site geometry, since conformational searches were not carried out on the mutants. Therefore, the effects presented in this Section are purely an energetic contribution to the barriers. Furthermore, since the experimental values are measured based on OG release, the rates should correspond to the glycosylase activity; however, it is possible that OG release is delayed during the bifunctional mechanism, which may alter the results. To allow for a comparison of all data, the expected effect ($\Delta\Delta G$) of each modification has been evaluated within a given study and denoted in Table 6.4 as leading to either a large (++), a small (+/−) or no change (ø) (Table E5, Appendix E).
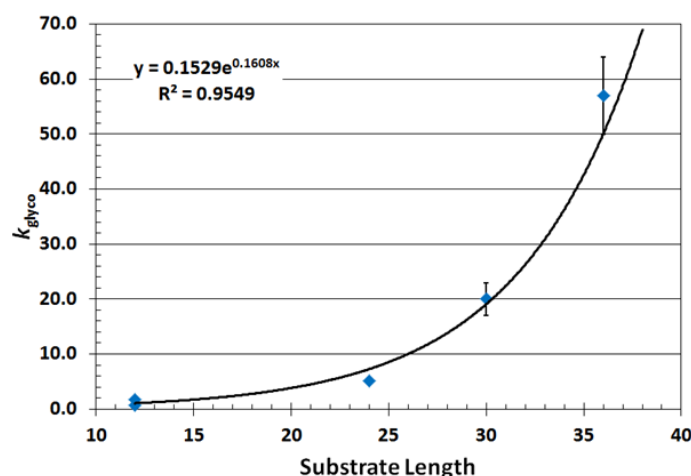
Figure 6.8. *Increasing substrate length (base pairs) exponentially increases the deglycosylation rate (min^{-1}) of hOgg1. Data from five experimental studies.*[5–7,29–30]

The largest contributor to the lysine activation step is D268, where removing the charge of this residue increases the barrier by 26.8 or 42.6 kJ mol^{-1} (D268N and D268A, respectively). The K249C/C253K double mutant increases the barrier by a similar amount, indicating that the proton transfer step is dependent on a local dipole. None of the other mutations appreciably affect

the barrier to proton transfer. However, all mutations substantially destabilize the activated reactant (RC2), except for the F319A modification (Table 6.4).

Table 6.4. *Effect of active-site mutations on the Gibbs reaction energetics (kJ mol⁻¹) of the lysine activation and deglycosylation steps of three different mechanisms.*[a,b]

Mutation (Effect)[c]	K249 Activation		Deglycosylation					
			K249–Nuc		K249–GB		D268–GB	
	TS1[d]	RC2[e]	TS3[d]	IC1[e]	TS3[d]	PC[e]	TS3[d]	PC[e]
F144A (ø)	3.1	37.6	−14.1	−18.8	−7.7	−10.5	−7.7	24.1
K249A (++)	–	–	–	–	85.3	51.1	6.1	33.1
K249Q (++)	–	–	–	–	73.6	47.6	−16.3	17.3
C253A (+)	–	–	−18.4	−5.8	26.2	−1.8	−17.9	51.9
D268A (++)	42.6	51.1	40.4	38.1	31.7	5.1	76.9	−95.8[g]
D268N (++)	26.8	58.2	48.0	5.7	−21.5	5.2	99.6	−129.4[g]
D268E (ø)	−2.6	37.1	−60.3	−51.8	6.0	13.6	−10.6	2.0
H270A (+)	2.0	48.6	−29.7	−4.2	−10.2	−3.7	−39.8	−18.3
Q315A (+)	−3.3	44.7	−7.2	−10.0	9.4	−8.1	20.6	33.4
F319A (+)	−2.0	7.3	−46.5	−36.5	19.4	−11.7	6.2	51.1
G42-XX (−)	−0.6	37.0	−36.8	−12.4	19.4	−22.8	−36.2	14.2
KCCK[f] (+)	29.6	58.5	–	–	20.3	22.3	6.5	−14.8

[a] See Section 6.2.3 for the definitions of the mechanisms and stationary points. [b] ONIOM(M06-2X/ 6-311+G(2df,2p):PM6) single-point energies including unscaled thermal correction to Gibbs energy. [c] Expected effect of mutation on barrier height (++, large increase; +, increase; ø, no effect; −, decrease). [d] A positive value indicates the mutant barrier is higher. [e] A positive values indicates the product is less stable in the mutant. [f] K249C/C253K double mutant. [g] Falls to PC–K_GB.

To assist interpretation of the data for the three deglycosylation pathways, the changes in Gibbs barrier heights (relative to the corresponding RC3) are summarized in Figure 6.9. Ranges were selected to represent a large change (> 30 kJ mol⁻¹), a small change (< 30 kJ mol⁻¹) and no change (< 10 kJ mol⁻¹) to the barrier height, and are shown as grey boxes. These ranges were selected based on inspection of the data and are qualitative, since truncated (and frozen) models are not expected to exactly reproduce experimental energetics (they should, however, correctly predict trends, as shown in Chapter 3 for hUNG2). Figure 6.9 clearly shows that the K249–GB mechanism matches the expected changes in all cases except for D268N (which arises since the

mutated group is involved in the Lys activation step) and H270A (which was not correctly predicted by any model).

In addition to yielding the lowest barrier ($\Delta G = 174.4$ kJ mol^{-1}, relative to RC1), the K249–GB mechanism reproduces the expected effect of 11 of 12 active-site mutations. Therefore, this is the most likely mechanism of hOgg1 monofunctional action. The least likely mechanism is K249–Nuc, where the standard bifunctional mechanism is redirected to a monofunctional product. Not only does this mechanism contain the largest barrier (indeed the final hydrolysis step could not be characterized), but very few mutational effects are reproduced with this pathway. This is an unexpected result based on the outcome of the small model study in Chapter 5, which indicated that the stability of the DNA–protein crosslink might stall the bifunctional reaction and allow for redirection to a monofunctional product.
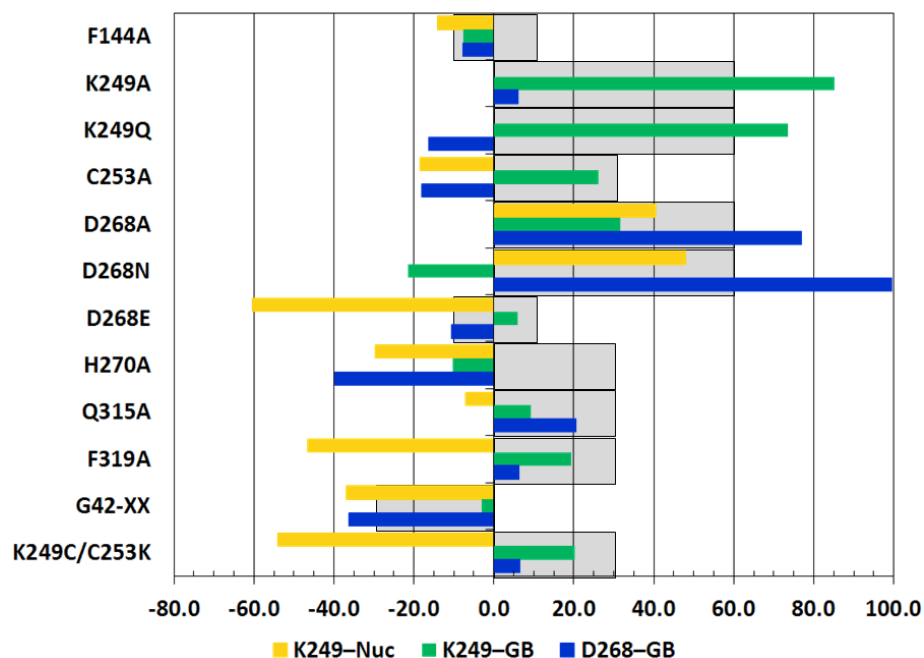
Figure 6.9. *Change in ONIOM(M06-2X/6-311+G(2df,2p):PM6) Gibbs barrier height (kJ mol^{-1}) due to various active-site mutations. A positive value indicates the mutant barrier is larger than the wild-type barrier. Grey boxes indicate the expected change (no, small or large change defined as less than 10, 30 or 60 kJ mol^{-1}, respectively).*

6.4 Discussion

Deglycosylation of dOG has been investigated computationally in numerous studies with mechanisms including S_N1 (and unimolecular dissociation),[13–15,17] S_N2,[11,13–14,16–17] A_N+D_N,[12] and σ-bond substitution[17] with K249 as the catalytic residue (i.e., the nucleophile). Hydrolysis of the dOG glycosidic bond by a fully- or partially-activated water molecule (OH^- and $HCOO^-\cdots H_2O$, respectively) has also been investigated.[11,c] In this Chapter, three mechanisms were investigated, one with K249 as the nucleophile, and two with a water nucleophile and either K249 or D268 as the general base. While most previous studies have included cationic K249, the mechanisms in this Chapter all begin with activation of K249 by C253. Therefore, for the purpose of comparing to previous work, K249 can be considered as neutral in all deglycosylation mechanisms.

6.4.1 Monofunctional Mechanism

This Thesis finds for the first time that the preferred mechanism of monofunctional hOgg1 action uses a water nucleophile, while K249 acts as the general base that shuttles a proton from the nucleophile to the OG^- leaving group (K249–GB, Figure 6.3). The lysine residue was initially modeled as cationic and is activated in the first reaction step by proton transfer to C253. This conclusion was made since the pathway exhibits the lowest deglycosylation barrier ($\Delta G =$ 174.4 kJ mol^{-1}, Table 6.3) and reproduces experimental effects of numerous active-site mutations (Figure 6.9). The barrier to deglycosylation is large ($\Delta G =$ 115.8 kJ mol^{-1} for MutY); however, the crystal structure contains hOgg1 bound to a small 13-mer substrate complex, which may affect the local structure. Based on the equation obtained from Figure 6.8, the expected rate of hOgg1 bound to a substrate of this size is approximately 1.2 min^{-1}, which is significantly slower than for MutY ($k_{glyco} =$ 12.2 min^{-1}).[31] Therefore, the truncated models implemented in this Thesis

---

[c] Unpublished work by J. L. Kellie, L. Navarro-Whyte and S. D. Wetmore on dOG deglycosylation in the presence of hydrogen-bonding and π–π interactions. All M06-2X structures and energies by JLK.

reasonably reproduce the relative barriers obtained for the two enzymes when compared with the experimental relative rates.

6.4.2 Role of D268

The helix-capping D268 residue participates in both the Lys activation and deglycosylation steps of the reaction. Indeed, the anionic charge on this residue is essential to both steps, as can be seen by the large negative effects of the D268A and D268N mutations compared to the minimal effect of the D268E mutation (Table 6.4).[30] The presence of the aspartate completely removes the barrier to Lys activation, which supports the use of a neutral K249 during the remainder of the mechanism. Most previous computational studies did not include D268 in the model, which partially explains why a cationic K249 nucleophile was typically used.[12–13,17] During the deglycosylation step, D268 performs the same function as characterized for the monofunctional glycosylase hUNG2 (Chapter 3). Specifically, the anionic charge stabilizes the cationic charge building on the sugar moiety in the transition state. However, D268 does not act as the general base that activates the nucleophile, as observed for MutY in Chapter 4.

6.4.3 Catalytic Role of Active-Site Residues

A large number of mutations were carried out on the hOgg1 active site to determine the catalytic contributions of various residues. A brief summary of the potential roles of these residues is presented here, with the exception of D268, which was discussed above. F144 and F319 are both involved in π–π interactions with OG. The T-shaped interaction with F144 is slightly anticatalytic (negative $\Delta\Delta G$ in Table 6.4), similar to the T-shaped interaction with an active-site His residue in AAG (with an ethenoadenine substrate).[32] In contrast, the stacking interaction with F319 reduces the deglycosylation barrier by 19.4 kJ mol^{-1}. It is interesting that the F319A mutation increases the barrier[28] since the parallel stacking interactions in hUNG2

(Section 3.4.2)[33–34] and AAG[32] were found to be anticatalytic. Nevertheless, a small model study carried out by the Wetmore group supports an F319 contribution to catalysis,[d] beyond the known structural role of the residue (i.e., orienting the substrate).[19] C253 reduces the depurination barrier by interacting with K249 through a very weak hydrogen bond ($d(N\zeta–H\cdots S)$ = 2.959 Å) that increases the proton affinity of the general base. Q315 participates in a weak $N\varepsilon–H\cdot\cdot N2$ hydrogen bond with OG that stabilizes the anionic leaving group, and thus catalyzes the reaction. The interaction between the G42 backbone carbonyl and N7 of OG is (slightly) anticatalytic since it destabilizes the OG anion. Thus, in combination with the significant effect of D268 (Section 6.4.2), the many small stabilizing interactions to the general base and leaving group form the bulk of the catalytic effect of hOgg1.

6.5 Conclusions

There has been some evidence in the literature that hOgg1 behaves as a monofunctional glycosylase (i.e., no lyase activity) *in vivo*.[4,7–8] In Chapter 5, potential glycosylase/lyase mechanisms were characterized with a small DFT model and support was found for diverting the DNA–protein cross-linked intermediate from β-elimination of the backbone to hydrolysis of the crosslink. The current Chapter used the methodology developed while studying hUNG2 (Chapter 3) and MutY (Chapter 4) to investigate possible monofunctional mechanisms for hOgg1. Specifically, all three enzymes in this Thesis, hUNG2, MutY and hOgg1, were studied with reaction potential energy surfaces and a large active-site model (treated entirely with QM) generated from crystal structures that do not contain active-site mutations. In addition, all three structures contain inhibitors with minimal modifications that should have a negligible effect on the geometry of the active site. This careful selection of starting geometries contributes to the systematic approach implemented in this Thesis to study enzymatic reaction mechanisms.

---

[d] Unpublished work by Jennifer L. Kellie, Lex Navarro-Whyte and Stacey D. Wetmore. $\Delta\Delta G^{\ddagger}$ = −1.9 kJ mol^{-1} at PCM-M06-2X/6-311+G(2d,p)//M06-2X/6-31+G(d,p) (ε = 4) using a nucleoside model and a formate-activated water nucleophile.

Interestingly, the most obvious monofunctional pathway (lysine as a nucleophile, followed by hydrolysis of the crosslink) is not the most likely mechanism. Instead, a mechanism whereby a water nucleophile is activated by K249 led to the lowest barrier ($\Delta G = 174.4$ kJ mol^{-1}) and reproduced a large number of known effects for active-site mutations. Therefore, for the first time, this Thesis presents atomic level evidence for a monofunctional hOgg1 mechanism of action that explains experimental observations. Furthermore, the trend in deglycosylation barriers obtained for various hOgg1 mutants are consistent with the experimental rates, which further validates the use of truncated enzyme models to study this kind of enzymatic reaction.

6.6 References[e]

(1) Banerjee, A.; Verdine, G. L., A Nucleobase Lesion Remodels the Interaction of Its Normal Neighbor in a DNA Glycosylase Complex. *Proc. Nat. Acad. Sci. USA* **2006,** *103* (41), 15020–15025.

(2) Fromme, J. C.; Bruner, S. D.; Yang, W.; Karplus, M.; Verdine, G. L., Product-Assisted Catalysis in Base-Excision DNA Repair. *Nat. Struct. Biol.* **2003,** *10* (3), 204–211.

(3) Zharkov, D. O.; Rosenquist, T. A.; Gerchman, S. E.; Grollman, A. P., Substrate Specificity and Reaction Mechanism of Murine 8-Oxoguanine-DNA Glycosylase. *J. Biol. Chem.* **2000,** *275* (37), 28607–28617.

(4) Hill, J. W.; Hazra, T. K.; Izumi, T.; Mitra, S., Stimulation of Human 8-Oxoguanine-DNA Glycosylase by AP-endonuclease: Potential Coordination of the Initial Steps in Base Excision Repair. *Nucleic Acids Res.* **2001,** *29* (2), 430–438.

(5) Kuznetsov, N. A.; Koval, V. V.; Zharkov, D. O.; Nevinsky, G. A.; Douglas, K. T.; Fedorova, O. S., Kinetics of Substrate Recognition and Cleavage by Human 8-Oxoguanine-DNA Glycosylase. *Nucleic Acids Res.* **2005,** *33* (12), 3919–3931.

(6) Krishnamurthy, N.; Haraguchi, K.; Greenberg, M. M.; David, S. S., Efficient Removal of Formamidopyrimidines by 8-Oxoguanine Glycosylases. *Biochemistry* **2008,** *47* (3), 1043–1050.

(7) Dalhus, B.; Forsbring, M.; Helle, I. H.; Vik, E. S.; Forstrøm, R. J.; Backe, P. H.; Alseth, I.; Bjørås, M., Separation-of-Function Mutants Unravel the Dual-Reaction Mode of Human 8-Oxoguanine DNA Glycosylase. *Structure (Cambridge, MA, U. S.)* **2011,** *19* (1), 117–127.

---

[e] Bibliography and citations in ACS format.

(8)   Morland, I.; Luna, L.; Gustad, E.; Seeberg, E.; Bjørås, M., Product Inhibition and Magnesium Modulate the Dual Reaction Mode of hOgg1. *DNA Repair* **2005,** *4* (3), 381–387.

(9)   McCann, J. A. B.; Berti, P. J., Transition-State Analysis of the DNA Repair Enzyme MutY. *J. Am. Chem. Soc.* **2008,** *130*, 5789–5797.

(10)   Werner, R. M.; Stivers, J. T., Kinetic Isotope Effect Studies of the Reaction Catalyzed by Uracil DNA Glycosylase: Evidence for an Oxocarbenium Ion-Uracil Anion Intermediate. *Biochemistry* **2000,** *39* (46), 14054–14064.

(11)   Shim, E. J.; Przybylski, J. L.; Wetmore, S. D., Effects of Nucleophile, Oxidative Damage, and Nucleobase Orientation on the Glycosidic Bond Cleavage in Deoxyguanosine. *J. Phys. Chem. B* **2010,** *114* (6), 2319–2326.

(12)   Osakabe, T.; Fujii, Y.; Hata, M.; Tsuda, M.; Neya, S.; Hoshino, T., Quantum Chemical Study on Base Excision Mechanism of 8-Oxoguanine DNA Glycosylase: Substrate-Assisted Catalysis of the N-glycosidic Linkage Cleavage Reaction. *Chem-Bio Inf. J.* **2004,** *4* (3), 73–92.

(13)   Schyman, P.; Danielsson, J.; Pinak, M.; Laaksonen, A., Theoretical Study of the Human DNA Repair Protein hOGG1 Activity. *J. Phys. Chem. A* **2005,** *109* (8), 1713–1719.

(14)   Calvaresi, M.; Bottoni, A.; Garavelli, M., Computational Clues for a New Mechanism in the Glycosylase Activity of the Human DNA Repair Protein hOGG1. A Generalized Paradigm for Purine-Repairing Systems? *J. Phys. Chem. B* **2007,** *111* (23), 6557–6570.

(15)   Zheng, Y.; Xue, Y.; Yan, S. G., The Effects of Oxidation and Protonation on the N-glycosidic Bond Stability of 8-Oxo-2'-deoxyguanosine: DFT Study. *THEOCHEM* **2008,** *860* (1-3), 52–57.

(16)   Kellie, J. L.; Wetmore, S. D., Mechanistic and Conformational Flexibility of the Covalent Linkage Formed during β-Lyase Activity on an AP-Site: Application to hOgg1. *J. Phys. Chem. B* **2012,** *116* (35), 10786–10797.

(17)   Šebera, J.; Trantírek, L.; Tanaka, Y.; Sychrovský, V., Pyramidalization of the Glycosidic Nitrogen Provides the Way for Efficient Cleavage of the N-Glycosidic Bond of 8-OxoG with the hOGG1 DNA Repair Protein. *J. Phys. Chem. B* **2012,** *116* (41), 12535–12544.

(18)   Bruner, S. D.; Norman, D. P. G.; Verdine, G. L., Structural Basis for Recognition and Repair of the Endogenous Mutagen 8-Oxoguanine in DNA. *Nature (London, U. K.)* **2000,** *403* (6772), 859–866.

(19)   Norman, D. P. G.; Bruner, S. D.; Verdine, G. L., Coupling of Substrate Recognition and Catalysis by a Human Base-Excision DNA Repair Protein. *J. Am. Chem. Soc.* **2001,** *123* (2), 359–360.

(20)   Norman, D. P. G.; Chung, S. J.; Verdine, G. L., Structural and Biochemical Exploration of a Critical Amino Acid in Human 8-oxoguanine Glycosylase. *Biochemistry* **2003,** *42* (6), 1564–1572.

(21) Banerjee, A.; Yang, W.; Karplus, M.; Verdine, G. L., Structure of a Repair Enzyme Interrogating Undamaged DNA Elucidates Recognition of Damaged DNA. *Nature (London, U. K.)* **2005,** *434* (7033), 612–618.

(22) Fromme, J. C.; Banerjee, A.; Huang, S. J.; Verdine, G. L., Structural Basis for Removal of Adenine Mispaired with 8-Oxoguanine by MutY Adenine DNA Glycosylase. *Nature (London, U. K.)* **2004,** *427* (6975), 652–656.

(23) Lee, S.; Verdine, G. L., Atomic Substitution Reveals the Structural Basis for Substrate Adenine Recognition and Removal by Adenine DNA Glycosylase. *Proc. Nat. Acad. Sci. USA* **2009,** *106* (44), 18497–18502.

(24) Frisch, M. J.; Trucks, G. W.; Schlegel, H. B.; Scuseria, G. E.; Robb, M. A.; Cheeseman, J. R.; Scalmani, G.; Barone, V.; Mennucci, B.; Petersson, G. A.*, et al. Gaussian 09*, Revision A.02; Gaussian, Inc.: Wallingford CT, 2009.

(25) Stivers, J. T.; Jiang, Y. L., A Mechanistic Perspective on the Chemistry of DNA Repair Glycosylases. *Chem. Rev. (Washington, DC, U. S.)* **2003,** *103* (7), 2729–2759.

(26) Berti, P. J.; McCann, J. A. B., Toward a Detailed Understanding of Base Excision Repair Enzymes: Transition State and Mechanistic Analyses of N-glycoside Hydrolysis and N-glycoside Transfer. *Chem. Rev. (Washington, DC, U. S.)* **2006,** *106* (2), 506–555.

(27) Nash, H. M.; Lu, R. Z.; Lane, W. S.; Verdine, G. L., The Critical Active-Site Amine of the Human 8-Oxoguanine DNA Glycosylase, hOgg1: Direct Identification, Ablation and Chemical Reconstitution. *Chem. Biol.* **1997,** *4* (9), 693–702.

(28) van der Kemp, P. A.; Charbonnier, J. B.; Audebert, M.; Boiteux, S., Catalytic and DNA-Binding Properties of the Human Ogg1 DNA N-glycosylase/AP lyase: Biochemical Exploration of H270, Q315 and F319, Three Amino Acids of the 8-Oxoguanine-Binding Pocket. *Nucleic Acids Res.* **2004,** *32* (2), 570–578.

(29) Kuznetsov, N. A.; Koval, V. V.; Nevinsky, G. A.; Douglas, K. T.; Zharkov, D. O.; Fedorova, O. S., Kinetic Conformational Analysis of Human 8-Oxoguanine-DNA Glycosylase. *J. Biol. Chem.* **2007,** *282* (2), 1029–1038.

(30) McKibbin, P. L.; Kobori, A.; Taniguchi, Y.; Kool, E. T.; David, S. S., Surprising Repair Activities of Nonpolar Analogs of 8-oxoG Expose Features of Recognition and Catalysis by Base Excision Repair Glycosylases. *J. Am. Chem. Soc.* **2012,** *134* (3), 1653–1661.

(31) Francis, A. W.; Helquist, S. A.; Kool, E. T.; David, S. S., Probing the Requirements for Recognition and Catalysis in FPG and MutY with Nonpolar Adenine Isosteres. *J. Am. Chem. Soc.* **2003,** *125* (52), 16235–16242.

(32) Rutledge, L. R.; Wetmore, S. D., Modeling the Chemical Step Utilized by Human Alkyladenine DNA Glycosylase: A Concerted Mechanism Aids in Selectively Excising Damaged Purines. *J. Am. Chem. Soc.* **2011,** *133* (40), 16258–16269.

(33) Shaw, R. W.; Feller, J. A.; Bloom, L. B., Contribution of a Conserved Phenylalanine Residue to the Activity of *Escherichia coli* Uracil DNA Glycosylase. *DNA Repair* **2004,** *3* (10), 1273–1283.

(34)   Kellie, J. L.; Navarro-Whyte, L.; Carvey, M. T.; Wetmore, S. D., Combined Effects of π–π Stacking and Hydrogen Bonding on the (N1) Acidity of Uracil and Hydrolysis of 2′-Deoxyuridine. *J. Phys. Chem. B* **2012,** *116* (8), 2622–2632.

Chapter 7: Predicting Binding Energies of

DNA–Protein Stacking Contacts

7.1 Introduction

The previous four Chapters of this Thesis have studied the reaction mechanism catalyzed by various DNA glycosylases, and π–π stacking interactions between active-site residues and the substrate nucleobase were observed in both hUNG2 and hOgg1. These contacts have also been found in other glycosylases,[1] such as AAG.[2] While the mechanistic role of hydrogen-bonding interactions can be relatively simple to infer (e.g., increasing N1/N9 acidity), the same is not true for stacking interactions since very little is known about these systems, especially their effect on reaction mechanisms and barriers when the charge of one moiety changes over time.

In Chapter 3, the impact of the dU:F158 stacking interaction on the hUNG2 deglycosylation barrier height was determined by mutating phenylalanine to glycine (i.e., removing the functional group). Additionally, the effect of stacking on S_N2 deglycosylation barriers was recently studied by the Wetmore group using full optimizations and truncated models (methyl-capped dU nucleoside hydrolyzed by OH^- or $HCOO^- \cdots H_2O$) that explicitly include stacking (benzene) and hydrogen-bonding (H_2O, HF or NH_3) contacts with the nucleobase.[3] However, these previously employed methodologies require the system to be optimized both in the presence and absence of the noncovalent interaction, which can be computationally demanding. Furthermore, Gly or Ala mutations can mask the effect of the contact by replacing it with a C–H$\cdots\pi$ interaction. Therefore, it would be beneficial to be able to gauge the contribution of active-site π–π contacts to binding and catalysis without carrying out additional expensive calculations (particularly TS optimizations).

This Chapter approaches the problem of calculating the binding strength of active-site π–π contacts by developing and testing approaches for predicting the interaction energy of DNA–protein π–π stacking contacts in natural contexts using our understanding of the PES of the corresponding (highly studied) truncated systems. The following section outlines the frequency of DNA–protein π–π contacts to demonstrate the wide applicability of such a predictive tool.

7.1.1 Frequency of DNA–Protein π–π Contacts[a]

A few researchers have mined the protein data bank (PDB) in search of different noncovalent interactions between amino acids and nucleotides in hopes to determine the types of contacts governing DNA–protein binding.[4–5] While hydrogen-bond contacts are easily defined in search routines, the other subcategories of van der Waals interactions (such as π–π and C–H···π contacts) are more difficult to express in easily scripted terms. For example, an early study defined all amino acid–nucleobase pairs with a separation of < 3.9 Å to be a van der Waals contact, as long as the pair was not also defined as a hydrogen bond.[4] A later study increased the maximum separation to 7.5 Å, but did not discriminate from hydrogen bonds.[5] These studies concluded that van der Waals contacts occur significantly more often than hydrogen bonding.[4–5]

Unfortunately, not all of the interactions identified with the above criteria will correspond to a π–π contact. For example, many interactions could be classified as C/N–H···π or simple van der Waals dispersion systems. In fact, it can be very difficult to categorize π–π contacts without resorting to visual inspection. For example, each system in Figure 7.1 was characterized as a π–π interactions by Baker *et al.*;[5] however, these would more correctly be defined as a hydrogen-bonding, C–H···π or van der Waals (dispersion) contact. To this end, the Wetmore group carried out an analysis of DNA–protein systems in the PDB, specifically searching for stacking and T-shaped contacts between a number of π-delocalized amino acids (Phe, His, Trp, Tyr, Arg, Asp

---

[a] Unpublished results of a study carried out in the Wetmore group by Katie Wilson and Cidney Stinnissen, and co-supervised by Jenifer Kellie. Results analyzed by Jennifer Kellie.

and Glu) and the DNA nucleobases.[b] Potential π–π contacts were identified by searching for amino acid sidechain–nucleobase pairs with heavy atom–heavy atom distances within 5 Å. These contacts were then visually inspected to remove hydrogen-bonding and C–H···π systems, as well as to ensure the relative orientations correspond to π–π contacts (i.e., some overlap was observed between the π-systems of the two groups). The π–π heterodimers were then categorized as stacked or T-shaped based on the tilt angle between the planes of the two groups (Section 7.2.1).
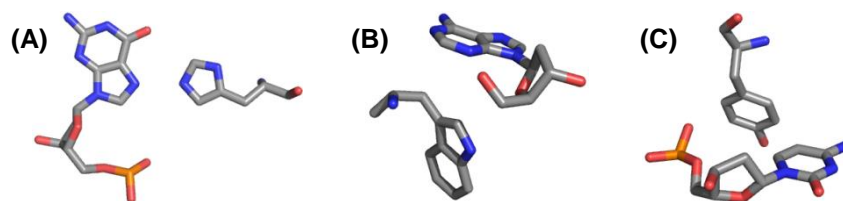
Figure 7.1. *Example systems found during a search of the PDB for π–π contacts that are not true stacking or T-shaped interactions.[5] (A) Hydrogen bond: H149:G6 from PDB 1A1I;[6] (B) C–H···π: W117:A14 from PDB 1SXQ;[7] and (C) van der Waals: Y55:C512 from PDB 1A3Q.[8]*

The search carried out by the Wetmore group identified 250 X-ray crystal structures with a total of 599 π–π contacts (24% of mined structures contained contacts). Interactions with Trp, His, Phe and Tyr (WHFY set) occurred in 175 structures with a total of 344 interactions, while contacts involving Arg, Glu and Asp (RED set) were found in 92 structures (255 interactions, Table 7.1). Approximately half of the crystal structures with DNA–protein π–π contacts contained more than one interaction, with the average number of contacts being three in the case of the WHFY set and four for the RED set. Stacking interactions account for 73% of the WHFY contacts and 76% of the RED contacts found (Table 7.1).

---

[b] A search of the PDB carried out on May 24, 2011 identified 1065 structures with DNA and protein, a resolution of 2.5 Å or better, and any systems with greater than 90% homology were removed.

Table 7.1. *Natural occurrence of DNA–protein π–π contacts found in a search of the PDB.*[a]

	Total		Stacking		T-Shaped	
	Structures	Contacts	Structures	Contacts	Structures	Contacts
WHFY	175	344	134	251	63	93
RED	92	255	75	195	36	60
Total	250	599	200	446	97	153

[a] A search of the PDB found 1065 X-ray crystal structures with resolutions greater than 2.5 Å on May 24, 2011. Contacts involving F, H, W and Y were identified in structures deposited from 1991 onward. Contacts involving R, E and D were identified in structures deposited from 2010 onward.

The largest number of stacking and T-shaped contacts involves hydrolases and transferases (Table 7.2). Systems containing the cyclic WHFY residues were also frequently found in lyases, while the acyclic RED residues were frequently found in transcription and DNA-binding proteins. Interactions with charged residues (such as Arg) arose in proteins that often exhibit low DNA-sequence specificity, which indicates that combination systems (where the same group is involved in both π–π and hydrogen-bonding interactions) may be important (for example, intercalation into the DNA helix). Interestingly, very few (three) π–π DNA–protein contacts were found in replication proteins, such as polymerases, despite recent evidence that stacking interactions play an important role in their activity.[9]

Table 7.2. *Natural DNA–protein π–π contacts by protein classification.*[a]

	Count[b]				Percent by Content[c]			
	WHFY		RED		WHFY		RED	
Classification	S[d]	T[e]	S[d]	T[e]	S[d]	T[e]	S[d]	T[e]
DNA-Binding Protein	9	5	12	6	6%	8%	15%	17%
Hydrolase	27	24	16	8	19%	37%	20%	22%
Isomerase	1	1	4	1	1%	2%	5%	3%
Lyase	15	10	4	0	10%	15%	5%	0%
Oxidoreductase	5	4	8	3	3%	6%	10%	8%
Transcription	11	4	15	4	8%	6%	19%	11%
Transferase	61	11	12	11	42%	17%	15%	31%
Transport Protein	7	1	0	0	5%	2%	0%	0%
Other[f]	9	5	8	3	6%	8%	10%	8%

[a] A search of the PDB found 1065 X-ray crystal structures with resolutions greater than 2.5 Å on May 24, 2011. Contacts involving F, H, W and Y were identified in structures deposited from 1991 onward. Contacts involving R, E and D were identified in structures deposited from 2010 onward. [b] Number of π–π contacts. [c] Percentage of contacts by system content and shape. [d] Stacking geometry. [e] T-shaped geometry. [f] All other protein classifications contained four contacts or fewer each.

By comparing the frequency of involvement of each nucleobase in DNA–protein contacts, one can infer binding preferences. For example, T occurs in significantly more systems than the other nucleobases (especially pairs involving Arg), which implies a preference for stacking interactions when binding to T-containing DNA sequences (Table 7.3). In the WHFY set, Phe and Tyr are involved in the largest number of contacts. Although these results are similar to those reported by Baker *et al.*,[5] the previous study reported a large number of His contacts. In the present analysis, His contacts account for only 11% of the WHFY set. In contrast, Phe accounts for 44% of the contacts. The discrepancy between the two studies is likely due to the stricter contact definition used by the Wetmore group (for example, Figure 7.1A).

Table 7.3. *Composition of π–π contacts found in a search of the PDB.*[a]

	Stacking				T-Shaped			
	A	C	G	T	A	C	G	T
Phe	21	19	25	34	9	16	8	20
His	7	14	1	11	4	0	0	0
Trp	8	11	6	17	0	2	0	1
Tyr	15	15	20	38	0	10	7	5
Arg	23	53	25	92	9	4	18	13
Glu	0	0	1	1	0	2	0	6
Asp	0	0	0	0	1	5	2	2
Total	74	112	78	193	23	39	35	47

[a] A search of the PDB found 1065 X-ray crystal structures with resolutions greater than 2.5 Å on May 24, 2011. Contacts involving F, H, W and Y identified in structures deposited from 1991 on. Contacts involving R, E and D identified in structures deposited from 2010 on.

In addition to determining the frequency of DNA–protein π–π interactions, the binding energy (BE) was calculated to predict the possible contribution of these contacts to DNA–protein binding.[c] The average BE for the combined WHFY and RED sets is –14.5 kJ mol^{-1}, which is half the interaction energy of a hydrogen-bonded water dimer at the same level of theory. However,

[c] Binding energies determined without counterpoise correction at the M06-2X/6-31+G(d,p) level of theory. Model heterodimers generated by overlaying MP2/6-31G(d,p) C_S-symmetric monomers onto the crystal structure geometry.

the strongest interactions are -47.8 kJ mol^{-1} for the WHFY set and -134.3 kJ mol^{-1} for the RED set, which is on par with the strength of the natural (A:T and G:C) base pairs that each contain two strong hydrogen bonds. Combined with the large observed frequency of π–π contacts, it is clear that these noncovalent interactions are important for DNA–protein binding.

Due to the demonstrated importance of amino acid–nucleobase π–π interactions, it would be useful to generate a method for predicting the corresponding BE based on a minimal number of measurements in the experimental (or computational) geometry and the known shape of the PES for a model heterodimer. A simple predictive tool is especially helpful for these interactions since the proper treatment of dispersion driven complexes (such as π–π contacts) is computationally expensive, generally requiring a basis set of at least 6-31+G(d,p) quality, if not larger to obtain interaction energies.[10–11] Therefore, various novel approaches for predicting the binding energy of naturally occurring stacked amino acid–nucleobase heterodimers are developed in the present Chapter using the previously studied PES for truncated stacking systems.[12–14] A focus is placed on stacking systems since stacking interactions occur more frequently than T-shaped interactions in DNA–protein complexes (Table 7.1). The previous work examined ideal contacts (tilt $= 0°$), and therefore, potential energy surfaces for the dependence of BE on deviating from a parallel geometry are characterized for the truncated systems in the present Chapter. Finally, the newly-developed methods are applied to a large test set of experimental structures.

7.2 Computational Details

7.2.1 Stacking Characteristics

The geometry of a π–π stacked system can be defined by a small set of variables (Figure 7.2). In an ideal system, the planes of the two π–systems are parallel ($\omega = 0°$); however, this orientation is rarely observed in natural DNA–protein contacts.[5,15] In the present work, the tilt angle (ω, Figure 7.2) between the two monomers is calculated as the angle between the planes

defined by intracyclic atoms for all ring systems, or the central sp^2 carbon and its substituents for the acyclic amino acids (i.e., Arg, Asp and Glu). A stacking interaction is defined by a tilt angle of less than 45°. The vertical separation (R_1) between the two systems is defined as the distance between the center of the amino acid functional group (ring centroid or central sp^2 carbon for cyclic and acyclic groups, respectively) and the plane of the nucleobase. The relative orientation of the groups (α) is measured as the improper dihedral angle formed by the glycosidic bond of the nucleobase and the Cγ–Cβ bond for Phe, His, Trp, Tyr and Asp, the Cδ–Cγ bond for Glu, or the Cζ–Nε bond for Arg.[d] The position of the amino acid centroid with respect to the center of mass of the nucleobase (R_2) is measured to a 0.5 Å grid with the Y-axis parallel to the glycosidic bond and the WC face in the direction of the positive X-axis.
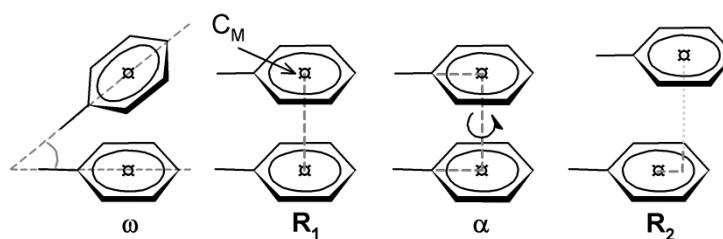
Figure 7.2. *Schematic of the variables that describe π–π contacts: tilt angle (ω) between the planes of the groups; vertical displacement (R_1) between the centers of mass; improper dihedral (α) between the backbone truncations; and the horizontal displacement (R_2) of the two groups.*

7.2.2 Prediction Methods

The binding energy of individual DNA–protein stacking contacts can be predicted in a number of ways. The first method investigated here has been previously presented by the Wetmore lab,[16] herein referred to as the summation method (BE_{Sum}). This approach takes advantage of the methodology implemented to optimize small stacking heterodimers. Specifically, the PES for these systems have been explicitly determined as a function of R_1, α and

---

[d] It should be noted that α is measured about an axis formed by the two centers of mass and perpendicular to the two monomer planes in previous publications on truncated models.[13–14,17–28] However, this is not a simple measurement in crystal structures; therefore, the present α deviates slightly from the previous definition.

R_2, and therefore the effect of each variable on the binding energy is known.[12–14] In the BE_{Sum} prediction method, the values for R_1, α and R_2 are first measured from the desired structure and rounded to the closest increment used to scan the PES (0.1 Å for R_1, 30° for α, and 0.5 Å for R_2). The energetic effect of deviation in each of the three variables from the optimum value is then determined and added to the optimum binding energy of the model system (BE_{Best}) (Equation 7.1).

$$BE_{Sum} = BE_{Best} + \Delta E(R_1) + \Delta E(\alpha) + \Delta E(R_2) \qquad [7.1]$$

The summation method has been shown to predict binding energies reasonably well for systems with ω near zero.[17] It is known, however, that ideal T-shaped π–π contacts ($\omega = 90°$) can have binding energies similar to stacked contacts, but exhibit substantially longer R_1 distances.[16,18] Therefore, for systems with $\omega > 10°$, the effect of R_1 ($\Delta E(R_1)$) may be overestimated and this method will predict binding energies that are too weak. To account for this potential error, a second prediction method was developed, which will be referred to as the distance-dependent method (BE_{R1}, Equation 7.2).

$$BE_{R1} = BE_{Best} + \Delta E(\alpha) + \Delta E(R_2) + \Delta E(R_1, \omega) \qquad [7.2]$$

In the distance-dependent method, first the optimum vertical separation ($R_{1,eq}$) for a given ω is determined. A relationship between ω and $R_{1,eq}$ for each combination of amino acid and nucleobase can be obtained by fitting data at various ω (10 – 40°) using a linear regression (Equation 7.3, see Section 7.2.3 for calculation methodology). The effect of deviating from the optimum separation on the binding energy ($\Delta E(R_1,\omega)$) was then fit to a Morse potential (Equation 7.4) using at least 50 data points for systems spanning $0 \leq \omega \leq 40°$ and $R_1 - R_{1,eq} \geq -0.40$ Å.

$$R_{1,eq} = a_1 * \omega + a_2 \qquad [7.3]$$

$$\Delta E(R_1; \omega) = b_1 * \left[1 - e^{\left(-b_2 * (R_1 - R_{1,eq}) \right)} \right] \qquad [7.4]$$

In the final prediction method (the tilt-dependent method, BE_{Tilt}), an additional term is introduced into Equation 7.2 to account for the different binding strengths of T-shaped and stacking orientations (Equation 7.5). For example, if the T-shaped orientation is substantially stronger than the stacking orientation, then increasing ω should increase the BE. The energetic effect of tilt ($\Delta E(\omega)$) is determined by fitting the optimum binding energy at various ω ($10 - 40°$) to a second-order polynomial (Equation 7.6).

$$BE_{Tilt} = BE_{Best} + \Delta E(\alpha) + \Delta E(R_2) + \Delta E(R_1, \omega) + \Delta E(\omega) \qquad [7.5]$$

$$\Delta E(\omega) = c_1 * \omega^2 + c_2 * \omega + c_3 \qquad [7.6]$$

7.2.3 Using the Database

In order to use the methods developed in this Thesis to predict the binding energy of a system of interest, the user should first find the heterodimer image that most closely resembles the system of interest in the Table of Contents sheet of Appendix F and click the associated hyperlink, which will open the corresponding interaction page. Second, the values for R_1, α, R_2 and ω must be measured and inserted into the highlighted cells. To assist in determining R_2, a figure of an 8✕8 Å grid overlaid onto the natural nucleobases is provided on each sheet. From this information, the spreadsheet will output the nearest point on the previously calculated R_1 and α PES to assist in the next step. Third, the corresponding $\Delta E(R_1)$, $\Delta E(\alpha)$ and $\Delta E(R_2)$ must be copied from the summaries provided into the appropriate cells near the measured values. Finally, the different binding energies (BE_{Sum}, BE_{R1} and BE_{Tilt}) will be automatically calculated. A sample completed spreadsheet for an adenine–phenylalanine contact is provided in Appendix F along with additional instructions on the use of the document.

7.2.4 Additional Calculations

The previous studies that characterized the PES of stacking contacts did not investigate the effect of tilt on BE. Therefore, in order to determine the effect of ω on $R_{1,eq}$ and BE, additional calculations were required. Heterodimers consisting of all possible combinations of nucleobases and amino acids were generated, including multiple orientations and charges of the amino acids. The truncated monomers used to study the PES in the previous and current studies are shown in Figure 7.3. For each system, the monomers were oriented at the pre-determined optimum α rotation, and R_2 was set to [0.0 Å, 0.0 Å].[13,19] To alter ω, the amino acid was rotated in 10°
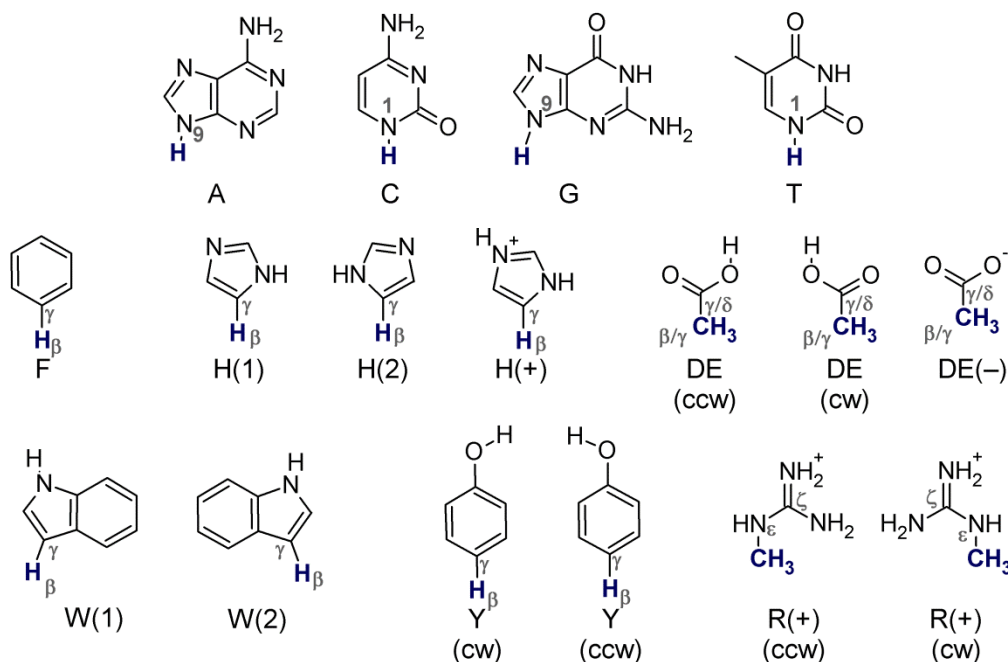
Figure 7.3. *Truncated monomers and orientations used to study the potential energy surface of nucleobase–amino acid stacking contacts. Important atomic labels included.*

increments about an axis that goes through the plane and center of mass of the amino acid, is perpendicular to the truncation point, and parallel to the plane of the nucleobase. Therefore, as ω increases, the truncation point is moved away from the plane of the nucleobase. For each ω, R_1 was varied in 0.1 Å increments for at least seven points to ensure the minimum was defined.

Single-point calculations were carried out with the same method used to determine the PES for the R_1, α and R_2 variables. Specifically, in the case of the cyclic amino acids (Phe, His, Trp and Tyr) counterpoise-corrected MP2/6-31G*(0.25) was implemented. M06-2X/6-31+G(d,p) (without counterpoise correction) was used for the acyclic amino acids (Arg, Asp and Glu).[e] All calculations were carried out with Gaussian 09 (Rev. A.02 and C.01).[20]

7.3 Results

As outlined in Section 7.2, three methods for predicting the binding energy of DNA–protein π–π stacking contacts using the PES of truncated systems were developed. First, the summation method uses the PES of an ideal system ($\omega = 0°$) to define the optimum R_1. Second, the distance-dependent method calculates the optimum R_1 with respect to ω and uses the new R_1 value to determine the deviation in R_1 and the corresponding effect on BE. Third, the tilt-dependent method adds an additional correction for deviations from parallel orientations. The three methods were tested with a set of 192 DNA–protein contacts obtained from the PDB (135 with Phe, His, Trp and Tyr; 56 with Arg and Glu). A full list of the contacts (with measurements and predicted binding energies) included in the test set can be found in Appendix G (Table G1). In this section, the deviations obtained for the cyclic and acyclic residues will be discussed separately for each method. In addition, the fitting of the equations used to determine the new terms introduced in this study will be presented.

7.3.1 Summation Method

The summation method is the simplest formula considered herein (Equation 7.1). The optimum geometry obtained from a previous study of the PES of a truncated system is used to define the best possible BE, R_1, α and R_2.[13,19] The binding energy of the system of interest is then determined by adding the effect of the R_1, α and R_2 measured in the crystal structure compared

---

[e] Calculations for Arg, Asp and Glu were carried out by R. A. Wells.

with the optimum value to the BE_{Best} to the BE. The MUD from the calculated BE for the complete test set with this method is 4.0 kJ mol^{-1} for the cyclic residues (4.8 kJ mol^{-1} overall, Table 7.4). Since the binding energies in the test set cover a large range, the mean unsigned percent deviation (MUPD) may be a more accurate measure of performance, which is 24% for the cyclic amino acids (41% overall). The large deviations (> 80%) observed for the acyclic systems (Arg and Glu) compared to the cyclic systems (Phe, His, Tyr, Trp) may be due to contacts with Arg and Glu involving a large electrostatic component, which could cause, for example, a

Table 7.4. *Deviations in stacking interaction energies determined with the three different prediction methods based on tilt angle.*

	Summation[a]		Distance Dependent[b]		Tilt Dependent[c]	
	MUD[d]	MUPD[e]	MUD[d]	MUPD[e]	MUD[d]	MUPD[e]
Phe, His, Trp and Tyr						
$\omega < 10°$	4.1	22%	4.0	21%	4.0	21%
$\omega > 10°$	4.0	26%	4.0	30%	4.2	25%
All	4.0	24%	4.0	26%	4.1	23%
Arg and Glu						
$\omega < 10°$	5.4	81%	7.3	90%	7.3	90%
$\omega > 10°$	7.9	81%	7.3	90%	12.8	112%
All	6.6	81%	7.3	90%	9.8	100%
Total						
$\omega < 10°$	4.6	41%	5.1	43%	5.0	43%
$\omega > 10°$	5.0	41%	4.9	46%	6.5	49%
All	4.8	41%	5.0	45%	5.8	46%

[a] See Section 2.2.1 for definition. [b] See Section 2.2.2 for definition. [c] See Section 2.2.3 for definition. [d] Mean unsigned deviation of predicted binding energy. [e] Mean unsigned percent deviation of predicted binding energy.

decrease in the independence of R_1, α and R_2. However, this error is still small enough to determine a trend in the binding energies and compare the calculated strengths to hydrogen-bonding contacts. The summation method assumes that ω has no effect on the interaction energy. However, the BE deviations for systems with $\omega > 10°$ are generally slightly larger than for

contacts closer to the ideal stacked orientation ($\omega = 0°$), especially for Arg and Glu (Table 7.4). Therefore, it may be possible to reduce the error by accounting for the effect of ω on the BE.

7.3.2 Distance-Dependent Method

One of the most obvious effects of increasing the tilt angle between the two π-systems is that sterics will push the two groups further apart. Therefore, the optimum R_1 obtained from a PES scan of a parallel heterodimer will be too small, and the $\Delta E(R_1)$ value will over correct at longer R_1. In this section, the dependence of R_1 on ω, and subsequently how deviations from the optimum R_1 affect the BE, will be determined. As an example, the results for the adenine–Phe (A:F) heterodimer will be presented (parameters for all combinations can be found in Appendix G). Finally, deviations in the predicted BE from the calculated values for the test set will be discussed.

7.3.2.1 Dependence of R_1 on Tilt

A linear dependence between ω and R_1 was observed for all combinations. In some heterodimers, the optimum R_1 for $\omega = 0°$ and $\omega = 10°$ were the same, and therefore the value for $\omega = 0°$ was removed from the fitting set since ω has a negligible effect for these small values. In the example of A:F, the optimum R_1 ($R_{1,eq}$) can be obtained from Equation 7.7 with a correlation of 0.971. The average correlation constant for all combinations was 0.971, with a minimum value of 0.833 for the G:DE(CCW) system.

$$R_{1,eq} = \left(2.00 \times 10^{-2}\ \tfrac{\text{Å}}{deg}\right) * \omega + 3.34\ \text{Å} \qquad [7.7]$$

7.3.2.2 Dependence of BE on R_1

The effect of deviating from $R_{1,eq}$ on the BE was fit to a Morse potential (Equation 7.4) using a least-squares approach. A minimum of 50 data points was used for the fitting, and the R_1–

$R_{1,eq}$ deviations ranged from -0.400 Å to over 0.600 Å. The results for A:F are shown in Figure 7.4. Coefficient values of $b_1 = 37.1$ kJ mol^{-1} and $b_2 = 1.08$ Å^{-1} were obtained for the A:F system with a correlation of 0.966 (the average correlation constant was 0.962, with a minimum value of 0.912 for the T:R(CW) heterodimer). The Morse potential is similar in form to the Lennard-Jones potential used to describe the dissociation of dispersion-driven complexes, where compression of the complex leads to a steep increase in the energy and expansion is associated with a much smaller energetic cost.[21] The Lennard-Jones potential has been successfully used to predict the binding energy of simple van der Waals complexes (see, for example, references 22–24).
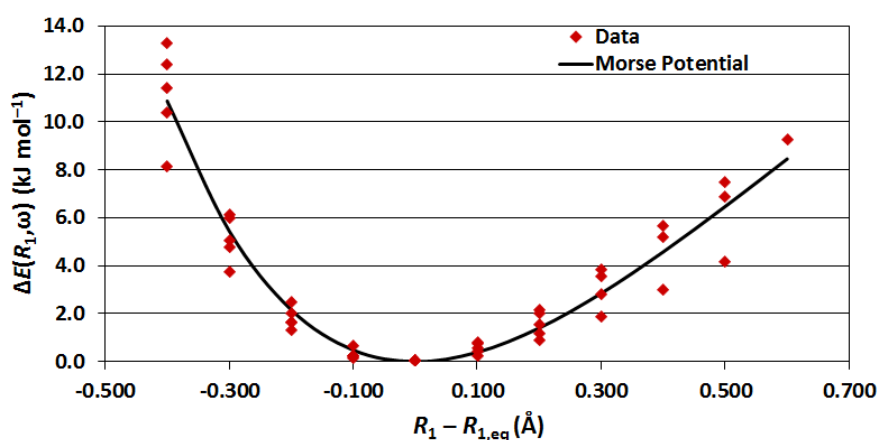
Figure 7.4. *Example of fitting deviation in vertical separation (R_1–$R_{1,eq}$, Å) to deviation in binding energy ($\Delta E(R_1,\omega)$, kJ mol^{-1}) for the adenine–phenylalanine system using a Morse potential.*

7.3.2.3 Deviations

Roughly half of the contacts in the test set contain $\omega > 10°$ (98 with $\omega > 10°$; 19 with $\omega > 20°$), which indicates that the MUD should improve when the R_1 correction is implemented. Interestingly, there is no improvement in the overall MUD for the cyclic amino acids (Table 7.4) and only a slight improvement for the acyclic residues with $\omega > 10°$ (MUD = 7.3 kJ mol^{-1}). The overall MUD actually increases from 4.8 kJ mol^{-1} to 5.0 kJ mol^{-1} upon inclusion of the $\Delta E(R_1,\omega)$

correction. However, the results show significant improvement when broken down by nucleobase and are discussed in detail in Section 7.4.1.

7.3.3 Tilt Dependent Method

The ω of a system connects the stacking orientation ($\omega = 0°$) with a T-shaped geometry ($\omega = 90°$). These two ideal forms are governed by different forces, where stacking is dispersion driven (with a large quadrapole moment contribution) and T-shaped interactions are more closely related to a special type of hydrogen bond (for example, C/N–H$\cdots\pi$).[25–26] The relative strength of the stacking and T-shaped orientations is system dependent,[16] and therefore difficult to predict. In addition, the strength of T-shaped interactions changes with the edge directed to the π-face.[16] In this study, only one edge was directed towards the nucleobase face, specifically the edge opposite the truncation point. Therefore, the tilt-dependent method does not account for all possible edge–face combinations, which can affect the predicted energies.

7.3.3.1 Dependence of BE on Tilt

A portion of the PES connecting the stacking and T-shaped geometries was fit to a second order polynomial (Equation 7.6). In the event that the binding energy for $\omega = 0$ and 10° are the same, $\omega = 0°$ was removed from the fitting set since ω had little to no effect for these small values. The average correlation constant for the fitting procedure was 0.988, with a median value of 0.997. The example system (A:F) was fit to a second order polynomial with coefficients $c_1 = -1.64\times10^{-3}$ kJ mol^{-1} deg^{-2}, $c_2 = 0.307$ kJ mol^{-1} deg^{-1} and $c_3 = -0.261$ kJ mol^{-1}, and a correlation of 0.971.

7.3.3.2 Deviations

Introducing a correction for ω to the distance-dependent method slightly improves the performance for the cyclic amino acids (MUPD, Table 7.4). However, the tilt correction

decreases the performance for the acyclic residues (MUPD increases from 81% to 100%), likely due to a significant dependence on edge. The tilt-dependent method yields an MUD of 5.8 kJ mol^{-1} for the complete test set (MUPD = 46%), which indicates that future studies should investigate the effect of the edge and potentially include an additional term.

7.4 Discussion

Many DNA–protein interfaces contain van der Waals contacts such as π–π stacking interactions.[27] Due to the computational difficulties associated with the accurate calculation of stacking interaction energies, it would be beneficial to develop a means to predict binding strengths observed in nature or simulations. There have been a number of predictive methods developed based on substituted benzene dimers that correlate the binding energy to chemical features such as the Hammett constant of the substituent.[28–30] However, a parallel method has not been proposed for biological contacts, such as DNA–protein interactions. In the present study, three different methods were developed and tested. The optimal method (for ω > 10°) introduces a correction for the vertical separation between the nucleobase and amino acid that is dependent on the tilt angle between the two planes. Since a difference in behaviour for all three methods was observed for the cyclic amino acids (Phe, His, Trp and Tyr) and the acyclic amino acids (Arg and Glu), the different groups will be discussed separately below. Additionally, a few examples from the test set will be presented to demonstrate how these methods can be used to predict binding energies using experimental crystal structures.

7.4.1 Cyclic Amino Acids

A breakdown of the performance of the prediction methods with respect to the individual nucleobases and cyclic amino acids is provided in Table 7.5. The best binding energies (smallest MUD) are obtained for contacts with adenine. The tilt-dependent method performs better than the summation and distance-dependent methods for all nucleobases except thymine. Since the tilt

calculations were carried out with $R_2 = [0.0$ Å, 0.0 Å$]$, the methyl group on thymine may introduce steric conflicts not present in natural systems, where the R_2 deviates from this value. Therefore, the tilt-dependent method may behave differently for systems containing thymine than the other nucleobases. Comparable performances are obtained for cytosine and guanine contacts, which may be explained by their structural similarities (i.e., both contain a carboxyl group and exocyclic amine).

Table 7.5. *Deviations in stacking interaction energies for the cyclic amino acids determined with the three different prediction methods averaged over the nucleobases and amino acid.*

	Summation[a]		Distance Dependent[b]		Tilt Dependent[c]	
	MUD[d]	MUPD[e]	MUD[d]	MUPD[e]	MUD[d]	MUPD[e]
A	3.2	18%	2.9	19%	2.9	16%
C	4.4	28%	4.4	29%	4.2	28%
G	4.1	23%	4.3	27%	3.7	18%
T	3.5	19%	3.4	19%	4.5	24%
Phe	2.6	22%	2.7	27%	2.8	19%
His	5.1	34%	5.0	35%	4.7	30%
Trp	3.1	13%	3.0	14%	4.0	18%
Tyr	5.3	27%	5.3	28%	5.0	25%
His(+)	2.4	13%	2.4	13%	2.3	13%

[a] See Section 2.2.1 for definition. [b] See Section 2.2.2 for definition. [c] See Section 2.2.3 for definition. [d] Mean unsigned deviation of predicted binding energy. [e] Mean unsigned percent deviation of predicted binding energy.

When the results are separated based on the amino acid, the best binding energies are predicted for dimers with phenylalanine and cationic histidine (Table 7.5). Interestingly, while the tilt-dependent method has the largest MUD for Phe-containing systems, it yields the smallest MUPD, which indicates that the deviations are more consistent for these weak systems. When considering the MUD and MUPD, the tilt-dependent method yields the best results for all cyclic amino acids except tryptophan. This result is expected since Trp is larger than the other amino acids, which increases the edge-dependence of ω, as well as the dipole moment. Based on the

above analyses, the tilt-dependent method performs the best for DNA–protein contacts involving the planar, cyclic amino acids.

7.4.2 Acyclic Amino Acids

The PDB search carried out by the Wetmore group only identified two contacts involving glutamate,[f] which is not enough to generate an MUD for the residue. Therefore, only arginine contacts are discussed here. The MUD (MUPD) for arginine systems were 6.5 (68%), 6.7 (72%) and 9.8 (84%) kJ mol^{-1} for the summation, distance-dependent and tilt-dependent methods, respectively. It is clear that the predicted BE for the cyclic amino acids are significantly more reliable than those involving arginine. Therefore, it is recommended that BE prediction of π–π contacts involving acyclic amino acids be carried out explicitly by extracting the isolated contact from the structure of interest.

7.4.3 Example Applications

To demonstrate how the prediction methods work in practice, two examples with $\omega > 10°$ were selected from the test set. The first example is an adenine–tryptophan contact (A:W) and the second example is a cytosine–tyrosine contact (C:Y, Figure 7.5). The A:W interaction from the 2GB7 crystal structure contains a significantly elongated R_1 (R_1–$R_{1,eq}$ = 0.455 Å, Table 7.6),
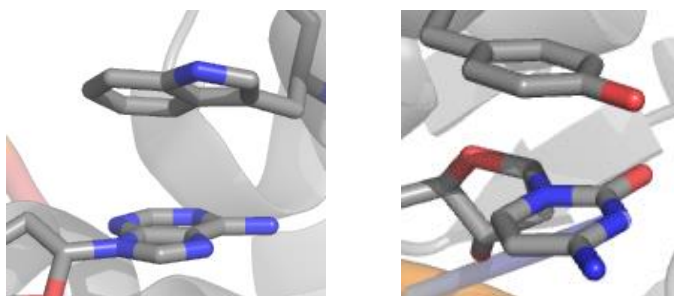
Figure 7.5. *Example DNA–protein interactions: adenine–tryptophan (PDB ID: 2GB7, left) and cytosine–tyrosine (PDB ID: 2HHV, right).*

---

[f] Note that the PDB search for arginine, glutamate and aspartate contacts was limited to those structures deposited from 2009 to May 24, 2011.

Table 7.6. *Prediction of DNA–Protein contacts with example systems.*[a]

Characteristics[b]	Measured					PES	
PDB	BE_{Calc}[c]	ω	R_1	α	R_2	R_1	α
2GB7 (A0:W61)	−14.0	20.0	4.294	163.3	[−1.0, 0.0]	4.300	150.0
2HHV (C6:Y714)	−18.5	13.3	3.543	321.8	[0.0, 0.0]	3.500	330.0
Energetic Contributions[d]							
PDB	$\Delta E(R_1)$	$\Delta E(\alpha)$	$\Delta E(R_2)$	$R_{1,eq}$	$R_1 - R_{1,eq}$	$\Delta E(R_1,\omega)$	$\Delta E(\omega)$	BE_{Best}
2GB7	4.2	4.5	2.8	3.839	0.455	6.3	6.7	−32.0
2HHV	0.1	7.3	1.0	3.491	0.052	0.1	−1.7	−22.7
Binding Energies and Deviations								
	Summation			Distance-Dependent			Tilt-Dependent		
PDB	BE_{Sum}	UD[e]	UPD[f]	BE_{R1}	UD[e]	UPD[f]	BE_{Tilt}	UD[e]	UPD[f]
2GB7	−20.5	6.5	47%	−18.5	4.5	32%	−11.8	2.2	16%
2HHV	−14.3	4.1	23%	−14.3	4.1	22%	−16.0	2.4	13%

[a] Energies in kJ mol^{−1}; distances in Å, angles in degrees. [b] Definition of variables in Section 7.2.1. [c] M06-2X/6-31+G(d,p) single-point energy on MP2/6-31G(d,p) C_S-symmetric monomers overlayed onto the crystal structure geometry. [d] Definitions in Section 7.2.2. [e] Unsigned deviation from the calculated value (BE_{Calc}). [f] Unsigned percent deviation from the calculated value (BE_{Calc}).

which changes the R_1 energy correction by 2.1 kJ mol^{−1} (compare $\Delta E(R_1)$ and $\Delta E(R_1,\omega)$), and increases the accuracy of the prediction (deviation reduced from 6.5 to 4.5 kJ mol^{−1}). Incorporating the correction for ω further decreases the deviation from the calculated BE. In addition, the C:Y contact exhibits a minimal deviation in R_1 ($\Delta E(R_1) = \Delta E(R_1,\omega)$), leading to no difference between the BE predicted with the summation and distance-dependent methods; however, the tilt correction reduces the deviation from 4.1 to 2.4 kJ mol^{−1}. These two examples demonstrate that DNA–protein π–π interactions can contribute to the strength of substrate binding. In addition, the binding energies of the systems were predicted with very good accuracy (error < 2.5 kJ mol^{−1}), which supports the use of the methods developed in this Chapter for estimating the strength of similar DNA–protein contacts.

An important application of predicting binding energies is the characterization of DNA–protein binding interfaces, such as the contacts in the active site of a DNA polymerase.[9] In addition, it is useful to predict the binding strength of active-site contacts in reactants and

products to determine whether stacking interactions contribute to catalysis or are strictly involved in binding. As an example, an interaction between the active-site histidine residue in AAG and the substrate may be catalytic.[2] In the case of an initially neutral substrate, such as ethenoadenine, the product is anionic. A recent study by the Wetmore group has found that anionic π–π interactions can be significantly stronger than neutral contacts,[14] which would indicate that this interaction should be catalytic. In contrast, for cationic substrates (for example, 3-methyladenine), the product is neutral, which indicates that the binding interaction weakens over the course of the reaction and is thus anticatalytic. Indeed, the mutational analysis carried out on AAG by Rutledge and Wetmore found the π–π interactions to be catalytic for ethenoadenine and anticatalytic for 3-methyladenine.[2] To what degree these contacts are catalytic or anticatalytic can be determined by comparing the predicted binding energies of these contacts in the reactant and product complexes. The methods presented in this Thesis could be used in this way, but further calculations are required on DNA–protein complexes containing charged nucleobases (for example, N9 deprotonated adenine) and other products to generate the required PES and fit equations analogous to Equations 7.3, 7.4 and 7.6.

7.5 Conclusions

In this Chapter, three methods for predicting DNA–protein stacking interactions were developed. The first method uses previously reported PES on ideal parallel systems to determine the energetic effect of deviations from the optimum R_1, α and R_2 values with no accommodation for non-parallel monomers. The second method corrects the effect of R_1 for a dependence of the optimum R_1 on ω. Indeed, a linear relationship between optimum R_1 and ω was found for all nucleobase–amino acid pairs. Furthermore, the energetic effect of deviations in R_1 can be fit to a Morse potential with high correlation. The final method also corrects for the effect of ω on the binding energy. All three approaches perform similarly, however, the tilt-corrected method slightly outperforms the others in the case of the planar, cyclic amino acids (Phe, His, Trp and

Tyr). It is therefore recommended that either the distance (for acyclic amino acids) or tilt-dependent (for cyclic amino acids) methods be used to predict DNA–protein stacking binding energies (for example, in experimentally or computationally determined complexes).

7.6 References[g]

(1)   Berti, P. J.; McCann, J. A. B., Toward a Detailed Understanding of Base Excision Repair Enzymes: Transition State and Mechanistic Analyses of N-glycoside Hydrolysis and N-glycoside Transfer. *Chem. Rev. (Washington, DC, U. S.)* **2006,** *106* (2), 506–555.

(2)   Rutledge, L. R.; Wetmore, S. D., Modeling the Chemical Step Utilized by Human Alkyladenine DNA Glycosylase: A Concerted Mechanism Aids in Selectively Excising Damaged Purines. *J. Am. Chem. Soc.* **2011,** *133* (40), 16258–16269.

(3)   Kellie, J. L.; Navarro-Whyte, L.; Carvey, M. T.; Wetmore, S. D., Combined Effects of π–π Stacking and Hydrogen Bonding on the (N1) Acidity of Uracil and Hydrolysis of 2′-Deoxyuridine. *J. Phys. Chem. B* **2012,** *116* (8), 2622–2632.

(4)   Luscombe, N. M.; Laskowski, R. A.; Thornton, J. M., Amino Acid-Base Interactions: A Three-Dimensional Analysis of Protein-DNA Interactions at an Atomic Level. *Nucleic Acids Res.* **2001,** *29* (13), 2860–2874.

(5)   Baker, C. M.; Grant, G. H., Role of Aromatic Amino Acids in Protein-Nucleic Acid Recognition. *Biopolymers* **2007,** *85* (5-6), 456–470.

(6)   Elrod-Erickson, M.; Benson, T. E.; Pabo, C. O., High-Resolution Structures of Variant Zif268-DNA Complexes: Implications for Understanding Zinc Finger DNA Recognition. *Struct. Fold. Des.* **1998,** *6* (4), 451–464.

(7)   Lariviere, L.; Morera, S., Structural Evidence of a Passive Base-Flipping Mechanism for β-Glucosyltransferase. *J. Biol. Chem.* **2004,** *279* (33), 34715–34720.

(8)   Cramer, P.; Larson, C. J.; Verdine, G. L.; Muller, C. W., Structure of the Human NF-κ B p52 Homodimer-DNA Complex at 2.1 Å Resolution. *EMBO J.* **1997,** *16* (23), 7078–7090.

(9)   Xia, S. L.; Vashishtha, A.; Bulkley, D.; Eom, S. H.; Wang, J. M.; Konigsberg, W. H., Contribution of Partial Charge Interactions and Base Stacking to the Efficiency of Primer Extension at and beyond Abasic Sites in DNA. *Biochemistry* **2012,** *51* (24), 4922–4931.

(10)   Rezac, J.; Riley, K. E.; Hobza, P., Evaluation of the Performance of Post-Hartree-Fock Methods in Terms of Intermolecular Distance in Noncovalent Complexes. *J. Comput. Chem.* **2012,** *33* (6), 691–694.

---

[g] Bibliography and citations in ACS format.

(11)   Riley, K. E.; Platts, J. A.; Rezac, J.; Hobza, P.; Hill, J. G., Assessment of the Performance of MP2 and MP2 Variants for the Treatment of Noncovalent Interactions. *J. Phys. Chem. A* **2012,** *116* (16), 4159–4169.

(12)   Rutledge, L. R.; Campbell-Verduyn, L. S.; Hunter, K. C.; Wetmore, S. D., Characterization of Nucleobase-Amino Acid Stacking Interactions Utilized by a DNA Repair Enzyme. *J. Phys. Chem. B* **2006,** *110* (39), 19652–19663.

(13)   Churchill, C. D. M.; Wetmore, S. D., Noncovalent Interactions Involving Histidine: The Effect of Charge on π-π Stacking and T-Shaped Interactions with the DNA Nucleobases. *J. Phys. Chem. B* **2009,** *113* (49), 16046–16058.

(14)   Wells, R. A.; Kellie, J. L.; Wetmore, S. D., Surprising Strength of Charged DNA–Protein π–π Interactions: A Preliminary Study of Cytosine. *J. Phys. Chem. B (Submitted July 2013).*

(15)   Unpublished work by Wilson, K. A.; Stinnissen, C.; Kellie, J. L. and Wetmore, S. D.

(16)   Rutledge, L. R.; Durst, H. F.; Wetmore, S. D., Evidence for Stabilization of DNA/RNA-Protein Complexes Arising from Nucleobase-Amino Acid Stacking and T-Shaped Interactions. *J. Chem. Theory Comput.* **2009,** *5* (5), 1400–1410.

(17)   Rutledge, L. R.; Durst, H. F.; Wetmore, S. D., Computational Comparison of the Stacking Interactions Between the Aromatic Amino Acids and the Natural or (Cationic) Methylated Nucleobases. *Phys. Chem. Chem. Phys.* **2008,** *10* (19), 2801–2812.

(18)   Rutledge, L. R.; Wetmore, S. D., Remarkably Strong T-Shaped Interactions between Aromatic Amino Acids and Adenine: Their Increase upon Nucleobase Methylation and a Comparison to Stacking. *J. Chem. Theory Comput.* **2008,** *4* (10), 1768–1780.

(19)   Rutledge, L. R.; Campbell-Verduyn, L. S.; Wetmore, S. D., Characterization of the Stacking Interactions Between DNA or RNA Nucleobases and the Aromatic Amino Acids. *Chem. Phys. Lett.* **2007,** *444* (1-3), 167–175.

(20)   Frisch, M. J.; Trucks, G. W.; Schlegel, H. B.; Scuseria, G. E.; Robb, M. A.; Cheeseman, J. R.; Scalmani, G.; Barone, V.; Mennucci, B.; Petersson, G. A.*, et al. Gaussian 09*, Revision A.02; Gaussian, Inc.: Wallingford CT, 2009.

(21)   Lim, T. C., Long Range Relationship Between Morse and Lennard-Jones Potential Energy Functions. *Mol. Phys.* **2007,** *105* (8), 1013–1018.

(22)   Kalugina, Y. N.; Cherepanov, V. N.; Buldakov, M. A.; Zvereva-Loete, N.; Boudon, V., Theoretical Investigation of the Potential Energy Surface of the van der Waals Complex CH_4-N_2. *J. Chem. Phys.* **2009,** *131* (13), 134304.

(23)   Pakhira, S.; Dasa, A. K., Spectroscopic Properties, Potential Energy Surfaces and Interaction Energies of RgClF (Rg = Kr and Xe) van der Waals Complexes. *Eur. Phys. J. D* **2012,** *66* (5), 144.

(24) Vacek, J.; Konvicka, K.; Hobza, P., A Molecular-Dynamics Study of the Benzene···Ar$_2$ Complex - Application of the Nonempirical *ab-initio* and Empirical Lennard-Jones 6-12 Potentials. *Chem. Phys. Lett.* **1994,** *220* (1-2), 85–92.

(25) Williams, J. H., The Molecular Electric Quadrupole-Moment and Solid-State Architecture. *Acc. Chem. Res.* **1993,** *26* (11), 593–598.

(26) Hobza, P.; Müller-Dethlefs, K., Characteristics of Non-covalent Complexes and Their Determination by Experimental and Theoretical Techniques. In *Non-Covalent Interactions: Theory and Experiment*, Hirst, J., Ed. Royal Society of Chemistry: Cambridge, UK, 2009; pp 21–69.

(27) Privalov, P. L.; Dragan, A. I.; Crane-Robinson, C., Interpreting protein/DNA interactions: distinguishing specific from non-specific and electrostatic from non-electrostatic components. *Nucleic Acids Res.* **2011,** *39* (7), 2483–2491.

(28) Sanders, J. M., Optimal π-Stacking Interaction Energies in Parallel-Displaced Aryl/Aryl Dimers are Predicted by the Dimer Heavy Atom Count. *J. Phys. Chem. A* **2010,** *114* (34), 9205–9211.

(29) Sayyed, F. B.; Suresh, C. H., Accurate Prediction of Cation-π Interaction Energy Using Substituent Effects. *J. Phys. Chem. A* **2012,** *116* (23), 5723–5732.

(30) Wheeler, S. E.; Houk, K. N., Substituent Effects in the Benzene Dimer are due to Direct Interactions of the Substituents with the Unsubstituted Benzene. *J. Am. Chem. Soc.* **2008,** *130* (33), 10854–10855.

Chapter 8: Conclusions

8.1 Conclusions
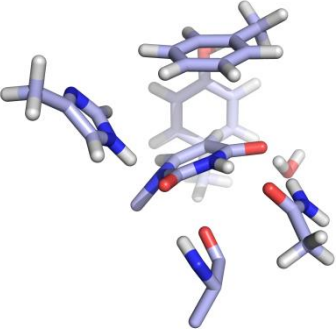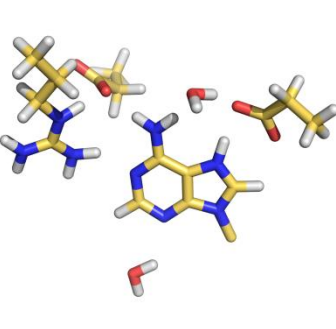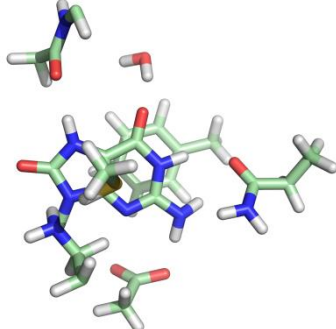
This Thesis set out to elucidate the monofunctional mechanism of action of select DNA glycosylases using an entirely quantum mechanical model (ONIOM(DFT:SE)) and reaction potential energy surfaces. To ensure that the DFT method used in the high-level region was capable of optimizing both noncovalent interactions and transition states, method testing was initially carried out. After selecting an appropriate DFT method, the mechanisms of action of three glycosylases were characterized, namely hUNG2, MutY and hOgg1. In addition, a preliminary study of the β-lyase activity of hOgg1 was carried out with a small model and numerous mechanisms. A simple method for predicting the binding strength of nucleobase–amino acid π–π stacking interactions was also developed to permit researchers to quickly compare the effects of these interactions in glycosylase active sites. In this chapter, the major conclusions regarding monofunctional glycosylases will be summarized, and the usefulness of the methodology applied in this Thesis will be discussed. Finally, possible future directions for investigating the DNA glycosylases will be outlined.

8.1.1 Monofunctional Glycosylase Mechanism

A general mechanism for the monofunctional activity of DNA glycosylases can be developed by analyzing the results of this Thesis. As discussed in Chapter 3 with respect to hUNG2, and in the literature,[1–6] leaving group stabilization is essential. Table 8.1 summarizes all contacts with the nucleobase leaving group in example reactant complexes of hUNG2, MutY and hOgg1. The two enzymes that utilize an S_N1 mechanism (hUNG2 and MutY) contain many contacts involving hydrogen bond (and proton) donation to the nucleobase. In contrast, the hOgg1 active site contains only one stabilizing interaction, and instead contains many contacts that are either weakly stabilizing (e.g., an N–H···π interaction with K249) or weakly destabilizing (e.g., a

hydrogen bond between N1 and Q315). These comparisons suggest that one may be able to estimate how dissociative a mechanism will be based on the number and type of interactions with the nucleobase leaving group. This conclusion is supported by a recent study of AAG which found an S_N2 mechanism when removing both neutral (e.g., ethenoadenine, εA) and cationic (e.g., 3-methyladenine, meA) lesions.[7] The active-site of AAG contains few (εA) or no (meA) stabilizing hydrogen bonds to the substrate, and instead forms two stacking and one T-shaped interaction with the lesion. The mechanisms characterized in the previous study are consistent with the proposed little leaving group stabilization resulting in an S_N2 mechanism.

Table 8.1 *Comparison of contacts with the nucleobase leaving group in the ONIOM(DFT:SE) optimized reactant complexes of hUNG2, MutY and hOgg1.*

hUNG2[a]	MutY[b]	hOgg1[c]
Nucleobase as Hydrogen Bond Acceptor (Stabilizing)[d]		
H268–O2 (1.965, 159.5)	R31–N1 (2.011, 147.2)	Wat–O6 (1.894, 167.8)
D144(BB)–O2 (2.216,155.7)	Wat–N3 (2.234, 128.1)	
N204–O4 (1.993, 164.3)		
Wat–O4 (1.967, 170.2)		
Nucleobase as Hydrogen Bond Donor (Destabilizing)[d]		
N3–N204 (2.015, 158.7)	N7–E43 (1.721, 176.3)	N7–G42 (1.977, 179.3)
	N6–E188 (1.880, 174.6)	N1–Q315 (2.211, 153.4)
	N6–Wat (2.012, 153.6)	N2–D268 (1.899, 174.0)
Other Factors		
U:F158 (π–π) (3.98)[e]	Cationic Nucleobase	OG:K249 (π–π) (3.14)[f]
U:Y126 (π–π) (4.46)[g]		OG:F319 (π–π) (3.15)[e]
U:D144(BB) (lp–π) (2.48)[h]		K249–C253 (Dipole–Dipole)

[a] Reactant complex for the wat_{Asp}^{His} model of hUNG2 from Chapter 3. [b] Activated reactant complex for the CS-Cap model of MutY from Chapter 4. [c] Reactant complex of hOgg1 after K249 activation from Chapter 6. [d] Hydrogen bond distance (Å) and angle (degrees) provided. [e] Distance (Å) between the centroid of the amino acid ring and the plane of the nucleobase. [f] Distance (Å) between the terminal NH_2 group and the plane of OG. [g] Distance (Å) between the centroid of the uracil ring and the plane of the tyrosine ring. [h] Distance (Å) between the backbone carbonyl and the plane of uracil.

Another important feature that has been widely discussed in the literature for the glycosylases is electrostatic stabilization of the sugar moiety by an active-site aspartate/glutamate residue.[4–5,8–11] All three enzymes considered in this Thesis contain an aspartate residue on the side of the sugar opposite the nucleobase (Figure 8.1). For the two enzymes studied here that did not involve significant aspartate migration (hUNG2 and hOgg1), the distance between the sugar and aspartate is ~3.6 Å (d(C1′–O$_{Asp}$) = 3.624–3.687 Å) in the reactant. This distance is greatly reduced in the case of MutY (by > 0.4 Å). In addition, only the MutY reactant places the aspartate directly below the sugar ring, while the hUNG2 and hOgg1 active sites place the aspartate closer to C2′ and O4′, respectively. This is consistent with the observed MutY mechanism involving partial attack of the aspartate on the anomeric carbon. In contrast to some proposals in the literature,[4–5,12–13] it was found that the aspartate residue is a very poor general base. In the case of hUNG2, another general base (histidine) may activate the nucleophile. However, neither hOgg1 nor MutY contain a second general base in the vicinity of the nucleophile. Shuttling a proton to N9 of the OG$^-$ leaving group partially makes up for the lack of a general base in hOgg1. A similar proton transfer is not possible during the mechanism of action of MutY since the adenine moiety is already neutral and hydrogen bonded to a cationic (arginine) residue, which makes it a very
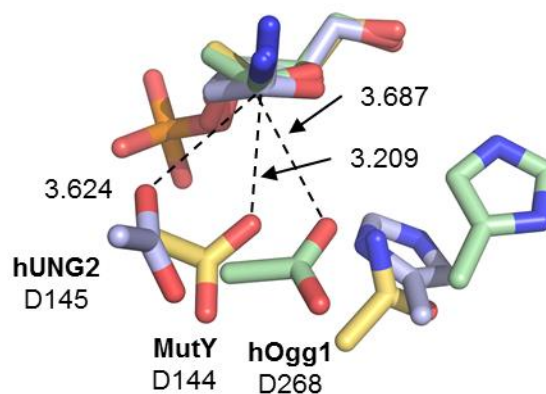
Figure 8.1 *Overlay of the hUNG2 (light blue), MutY (yellow) and hOgg1 (green) ONIOM(DFT:SE) sugar moiety in the reactant complexes (C1′–O$_{Asp}$ distance (Å) provided).*

poor base. Thus, the barrier for addition of the water nucleophile to the sugar is larger than anticipated for MutY and hOgg1, which is consistent with hUNG2 being significantly faster (k_{deglyco} = 540 min^{-1})[14] than MutY and hOgg1 (k_{deglyco} = 12±2[3] and 20±3 min^{-1},[15] respectively). From this discussion, the trend in deglycosylation rate is related to the d(C1′–O) and orientation of the functional group. Further support for this conclusion is obtained by considering AAG, where the catalytic glutamate residue is 4.258 Å from the anomeric carbon (for εA)[7] and the rate of εA removal is only 0.048 min^{-1}.[16]

Together, these results suggest that there are three essential components in the mechanism of action of the DNA glycosylases. First, leaving group stabilization is important and dictates to what extent the mechanism is dissociative. Second, the sugar moiety requires significant electrostatic stabilization, often from a combination of the phosphate backbone, nucleobase leaving group and an active site aspartate/glutamate residue. Third, the water nucleophile must be activated, either by the protein or through contact with solvent. Therefore, to properly characterize these reactions using computer simulations, all three components must be included in the computational model.

8.1.2 Effectiveness of Current Methodology

One of the unique features of this Thesis is the use of an entirely quantum mechanical description of the enzyme model with ONIOM(DFT:SE). A number of benefits to this approach became evident during the course of this study. First, while these models are small enough to be treated entirely with QM, they are large enough to include the effects of the protein environment (such as sterics and electrostatics). The importance of the protein environment can easily be seen by comparing the hUNG2 barrier height predicted with the total ONIOM energy (ΔE = 34.8 kJ mol^{-1}) to that calculated with just the high-level region (ΔE = 87.8 kJ mol^{-1}). This has been discussed in a number of recent computational enzymology reviews.[17–20] Second, since both the

high and low levels of the model were treated with QM, the model (high-level) region is polarized by the low-level region in all calculations, including optimizations,[21] a feature that can be prohibitively expensive for QM/MM calculations.[22] In addition, using a SE method to describe the low-level region allows for proton transfer to occur anywhere in the system (although this was not observed in any model in this Thesis),[23] which is not permitted with an MM treatment.

In addition to using the ONIOM technique, reaction PES for all mechanisms of interest were generated in this Thesis. This methodology provides a large amount of information that may be difficult (or impossible) to obtain using standard stationary point optimizations. The most obvious benefit to a reaction PES is that one does not need to develop a guess for the TS beyond an understanding of which bonds break and/or form during the reaction. This removes a significant amount of user-generated bias. In addition, multiple pathways can be plotted on the same surface (e.g., E1 and E2 as shown in Chapter 5), which allows for a detailed comparison. A second benefit to this method results when a TS region is flat (plateaued). Transition states with a flat PES are very difficult to optimize with standard Berny algorithms. A reaction PES can be used to refine a TS structure when optimizations are exhibiting slow convergence. In addition, the computational cost of a frequency calculation (required for Berny optimization of a TS) scales significantly faster than the energy or gradient.[24] Therefore, refining a reaction PES may be the only way to reach and verify a TS. Finally, contacts in the active-site can be observed for non-stationary points and thus provide significant insight into the interplay between different interactions as the reaction proceeds, as discussed for leaving group stabilization in hUNG2 in Chapter 3.

8.1.3 Role of π–π Contacts

Both the hUNG2 and hOgg1 active-sites contain π–π contacts with the nucleobase leaving group. Determining the role of these contacts is computationally very difficult. In Chapter

3, the catalytic effect of a stacking interaction between uracil and a phenylalanine was estimated by mutating the residue to glycine. Similarly, other studies have mutated the stacking residues to alanine.[7] However, a mutation like this replaces the π–π contact with a possible C–H···π contact, which can complicate interpretation of the results. Furthermore, mutations require the model to be relaxed, which can also obscure the effect of the mutated residue. Therefore, in Chapter 7, a method for predicting the binding energy of nucleobase–amino acid π–π stacked systems was developed to aid the understanding of the strength of these contacts. Combined with studies on the difference between neutral, cationic and anionic π–π systems,[25–27] these predictions may be used to determine whether an active-site contact will be catalytic or anti-catalytic.

Based on small model studies of nucleobase–amino acid stacking interactions,[25,27] these weak contacts observed in many DNA glycosylases are likely playing multiple roles depending on the substrate. Since charged contacts are stronger than neutral contacts,[27–31] stacking interactions can stabilize an anionic leaving group (like OG), catalyze proton transfer (for example protonation of A in MutY), or assist in specifically binding cationic damage (such as 3-methyladenine by AAG).[7] Stacking interactions can be very strong (especially for cationic π-systems), which may offset the loss of hydrogen-bonding interactions in enzymes with broad substrate specificity, although the increased binding to a cationic substrate comes at the cost of these interactions being anti-catalytic.[7]

8.2 Future Work

8.2.1 Molecular Dynamics

The analysis of the enzyme-substrate complexes in this Thesis has identified a number of interactions in the reactants that are essential for catalysis. For example, the catalytic aspartate in MutY is a helix-capping residue. If this contact breaks for a short period of time, the barrier to deglycosylation could be reduced. The methodology used to study the reaction mechanism in this

Thesis cannot account for protein dynamics. A recent study carried out a molecular dynamics (MD) analysis of the MutY reactant complexes to determine the flexibility of these (and other) important interactions.[32] The MD results validated the alternate geometries of active-site residues obtained with the conformational search in Chapter 4. Therefore, similar MD investigations could be carried out on other enzyme systems (such as human thymine–DNA glycosylase (hTDG), EC # 3.2.2.29) in conjunction with truncated enzyme models to ensure a catalytically-competent reactant complex is used.

There are, however, a number of difficulties associated with molecular dynamics. Chief among them is the use of MM to treat the system. The results in Chapters 3, 4 and 6 clearly indicate that the reactant complexes contain numerous features with subtle electronic effects. MM force fields may not properly treat these effects and therefore introduce error into the most important component of the system. One way to increase the accuracy is to treat the active site with a QM method. Introducing QM into the model significantly increases the computational cost, which may be slightly mitigated by using a semi-empirical method, such as PM6, which is cheaper than DFT. Any results obtained with MD therefore require significant analysis of both the results and the methodology implemented.

8.2.2 Lyase Mechanism

In Chapter 6, the mechanism of action of hOgg1 was investigated from a monofunctional perspective. While this study provided interesting results with respect to deglycosylation of dOG, the possible lyase activity was not addressed. Future studies could model the complicated β-lyase activity of hOgg1 using a similarly sized model. A comparison of the barriers obtained in the two studies may elucidate why hOgg1 is only monofunctional in the presence of AP-endonuclease.[10,33–34] In addition, the mechanism obtained from a large model examination of the

β-lyase activity could be applied to studies of other bifunctional glycosylases such as FPG[35] and EndoIII[36].

8.2.3 Other Glycosylases

As mentioned above, the methodology developed in this Thesis could be applied to other DNA glycosylases. By using the same method (ONIOM(DFT:SE)) for a number of active sites, the role of various residues can be more easily compared. Once enough examples have been compiled, the structure/function relationship of active-site residues in new glycosylases can be predicted. The use of reaction PES to study the mechanism could assist in answering some of the remaining questions regarding the glycosylases. Most prominent among these is hTDG, which is interesting for a number of reasons. First, hTDG does not contain an active-site aspartate or glutamate residue, nor is there an obvious general base to activate the water nucleophile.[37–38] Second, TDG repairs deaminated 5-methylcytosine lesions that are currently under investigation due to their use in epigenetics.[39–40]

Comparing the active sites of hUNG2[41] and hTDG[37] (Figure 8.2, overlay based on substrate location), it can be seen that there are a number of similarities and dissimilarities. For example, the stacking interaction with the nucleobase is still present, although this involves a tyrosine in hTDG instead of a phenylalanine. The T-shaped interaction with Y126 is absent in hTDG, which sterically permits the 5-methyl group to bind in the active site. Interestingly, hTDG does not contain a residue analogous to H268 in hUNG2, which removes the catalytically essential H268–O2 interaction.[2] A histidine residue can be found near O4, and in the presence of substrate may occupy an alternate position that introduces a His–O4 contact. Both enzymes contain an asparagine residue near N3/O4 of the substrate, as well as a proline residue directly below the nucleobase, where a backbone carbonyl can aid stabilization of the substrate through a lone-pair–
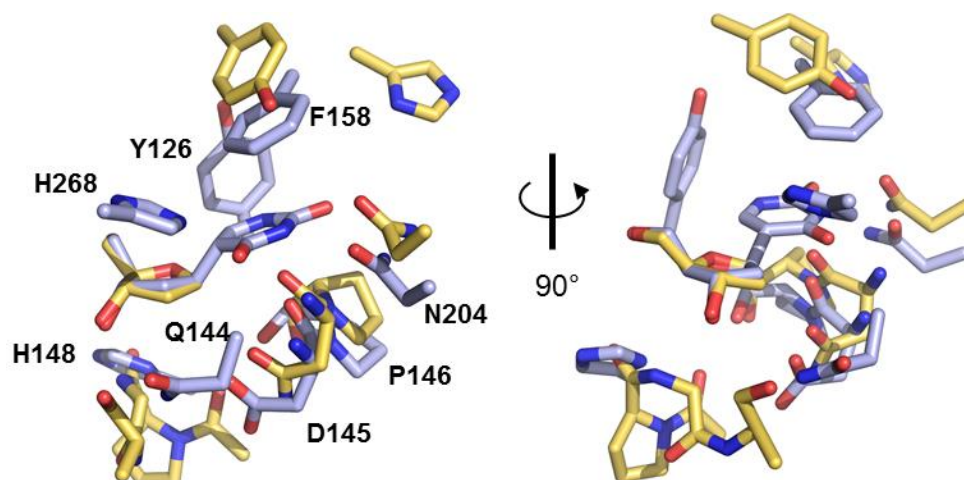
Figure 8.2 *Overlay of the hUNG2:ψU (light blue, PDB ID: 1EMH) and hTDG:AP-site (yellow, PDB ID: 2RBA) active sites with hUNG2 residues labeled.*

π contact. More importantly, hTDG does not appear to contain the two stabilizing residues D145 and H148. In their place are an asparagine and another proline residue. Neither of these residues are good activators, which makes the mechanism of this enzyme difficult to predict. Nevertheless, there is a serine residue nearby that may be able to interact with the nucleophile and provide additional stabilization.

hTDG has many (potential) stabilizing contacts to the nucleobase, which should push the reaction towards an S_N1 mechanism, but there is very little stabilization of the sugar moiety and nucleophile, which should reduce the overall rate. Based on the discussion in Section 8.1.1, hTDG should therefore be slightly slower than MutY, and in fact the rate of hTDG ($k_{deglyco}$ = 0.91 min^{-1})[42] is approximately 13-fold slower than MutY ($k_{deglyco}$ = 12.2 min^{-1}).[3] Together, the features of the hTDG active site make this enzyme an interesting candidate for a future ONIOM study and can be used as a further test case for the methodology developed in this Thesis.

8.3 Final Thoughts

In conclusion, the research in this Thesis used a large-scale ONIOM(DFT:SE) approach in combination with reaction PES to investigate the mechanism of action of select DNA

glycosylases, with a specific focus on the chemical step in the glycosylase activity. From these results, a general mechanism was proposed that specifies characteristics of the active site that can be used to predict the S_N1/S_N2 character of the hydrolysis reaction. In addition, the hOgg1 β-lyase mechanism was elucidated for the first time using a small DFT model. These results are invaluable for designing a large model study of the reaction that can determine the catalytic effect of various active-site residues in this enzyme. Finally, a method of predicting the binding energy of nucleobase–amino acid π–π contacts was rationally developed that can be used to assist both computational and experimental researchers analyze active-site complexes.

8.4 References[a]

(1)   Drohat, A. C.; Xiao, G. Y.; Tordova, M.; Jagadeesh, J.; Pankiewicz, K. W.; Watanabe, K. A.; Gilliland, G. L.; Stivers, J. T., Heteronuclear NMR and Crystallographic Studies of Wild-Type and H187Q *Escherichia coli* Uracil DNA Glycosylase: Electrophilic Catalysis of Uracil Expulsion by a Neutral Histidine 187. *Biochemistry* **1999,** *38* (37), 11876–11886.

(2)   Drohat, A. C.; Stivers, J. T., *Escherichia coli* Uracil DNA Glycosylase: NMR Characterization of the Short Hydrogen Bond from His187 to Uracil O2. *Biochemistry* **2000,** *39* (39), 11865–11875.

(3)   Francis, A. W.; Helquist, S. A.; Kool, E. T.; David, S. S., Probing the Requirements for Recognition and Catalysis in FPG and MutY with Nonpolar Adenine Isosteres. *J. Am. Chem. Soc.* **2003,** *125* (52), 16235–16242.

(4)   Stivers, J. T.; Jiang, Y. L., A Mechanistic Perspective on the Chemistry of DNA Repair Glycosylases. *Chem. Rev. (Washington, DC, U. S.)* **2003,** *103* (7), 2729–2759.

(5)   Berti, P. J.; McCann, J. A. B., Toward a Detailed Understanding of Base Excision Repair Enzymes: Transition State and Mechanistic Analyses of N-glycoside Hydrolysis and N-glycoside Transfer. *Chem. Rev. (Washington, DC, U. S.)* **2006,** *106* (2), 506–555.

(6)   McCann, J. A. B.; Berti, P. J., Transition-State Analysis of the DNA Repair Enzyme MutY. *J. Am. Chem. Soc.* **2008,** *130*, 5789–5797.

(7)   Rutledge, L. R.; Wetmore, S. D., Modeling the Chemical Step Utilized by Human Alkyladenine DNA Glycosylase: A Concerted Mechanism Aids in Selectively Excising Damaged Purines. *J. Am. Chem. Soc.* **2011,** *133* (40), 16258–16269.

(8)   Krokan, H. E.; Standal, R.; Slupphaug, G., DNA Glycosylases in the Base Excision Repair of DNA. *Biochem. J.* **1997,** *325*, 1–16.

[a] Bibliography and citations in ACS format.

(9)   Bianchet, M. A.; Seiple, L. A.; Jiang, Y. L.; Ichikawa, Y.; Amzel, L. M.; Stivers, J. T., Electrostatic Guidance of Glycosyl Cation Migration Along the Reaction Coordinate of Uracil DNA Glycosylase. *Biochemistry* **2003,** *42* (43), 12455–12460.

(10)   Dalhus, B.; Forsbring, M.; Helle, I. H.; Vik, E. S.; Forstrøm, R. J.; Backe, P. H.; Alseth, I.; Bjørås, M., Separation-of-Function Mutants Unravel the Dual-Reaction Mode of Human 8-Oxoguanine DNA Glycosylase. *Structure (Cambridge, MA, U. S.)* **2011,** *19* (1), 117–127.

(11)   Brinkmeyer, M. K.; Pope, M. A.; David, S. S., Catalytic Contributions of Key Residues in the Adenine Glycosylase MutY Revealed by pH-dependent Kinetics and Cellular Repair Assays. *Chem. Biol.* **2012,** *19* (2), 276–286.

(12)   Dinner, A. R.; Blackburn, G. M.; Karplus, M., Uracil-DNA Glycosylase Acts by Substrate Autocatalysis. *Nature (London, U. K.)* **2001,** *413* (6857), 752–755.

(13)   Fromme, J. C.; Bruner, S. D.; Yang, W.; Karplus, M.; Verdine, G. L., Product-Assisted Catalysis in Base-Excision DNA Repair. *Nat. Struct. Biol.* **2003,** *10* (3), 204–211.

(14)   Slupphaug, G.; Eftedal, I.; Kavli, B.; Bharati, S.; Helle, N. M.; Haug, T.; Levine, D. W.; Krokan, H. E., Properties of a Recombinant Human Uracil-DNA Glycosylase from the *Ung* Gene and Evidence That *Ung* Encodes the Major Uracil-DNA Glycosylase. *Biochemistry* **1995,** *34* (1), 128–138.

(15)   McKibbin, P. L.; Kobori, A.; Taniguchi, Y.; Kool, E. T.; David, S. S., Surprising Repair Activities of Nonpolar Analogs of 8-oxoG Expose Features of Recognition and Catalysis by Base Excision Repair Glycosylases. *J. Am. Chem. Soc.* **2012,** *134* (3), 1653–1661.

(16)   Hendershot, J. M.; Wolfe, A. E.; O'Brien, P. J., Substitution of Active Site Tyrosines with Tryptophan Alters the Free Energy for Nucleotide Flipping by Human Alkyladenine DNA Glycosylase. *Biochemistry* **2011,** *50* (11), 1864–1874.

(17)   Ramos, M. J.; Fernandes, P. A., Computational Enzymatic Catalysis. *Acc. Chem. Res.* **2008,** *41* (6), 689–698.

(18)   Lonsdale, R.; Ranaghan, K. E.; Mulholland, A. J., Computational Enzymology. *Chem. Commun.* **2010,** *46* (14), 2354–2372.

(19)   Siegbahn, P. E. M.; Himo, F., The Quantum Chemical Cluster Approach for Modeling Enzyme Reactions. *Wiley Interdiscip. Rev.-Comput. Mol. Sci.* **2011,** *1* (3), 323–336.

(20)   Lonsdale, R.; Harvey, J. N.; Mulholland, A. J., A Practical Guide to Modelling Enzyme-Catalysed Reactions. *Chem. Soc. Rev.* **2012,** *41* (8), 3025–3038.

(21)   Humbel, S.; Sieber, S.; Morokuma, K., The IMOMO Method: Integration of Different Levels of Molecular Orbital Approximations for Geometry Optimization of Large Systems: Test for n-Butane Conformation and S_N2 Reaction: RCl+Cl. *J. Chem. Phys.* **1996,** *105* (5), 1959–1967.

(22)   Vreven, T.; Byun, K. S.; Komaromi, I.; Dapprich, S.; Montgomery, J. A.; Morokuma, K.; Frisch, M. J., Combining Quantum Mechanics Methods with Molecular Mechanics Methods in ONIOM. *J. Chem. Theory Comput.* **2006,** *2* (3), 815–826.

(23)   Lundberg, M., Understanding Cross-Boundary Events in ONIOM QM:QM' Calculations. *J. Comput. Chem.* **2012,** *33* (4), 406–415.

(24)   Mallikarjun Sharada, S.; Zimmerman, P. M.; Bell, A. T.; Head-Gordon, M., Automated Transition State Searches without Evaluating the Hessian. *J. Chem. Theory Comput.* **2012,** *8* (12), 5166–5174.

(25)   Rutledge, L. R.; Campbell-Verduyn, L. S.; Wetmore, S. D., Characterization of the Stacking Interactions Between DNA or RNA Nucleobases and the Aromatic Amino Acids. *Chem. Phys. Lett.* **2007,** *444* (1-3), 167–175.

(26)   Ballester, P., Anions and π-Aromatic Systems. Do They Interact Attractively? In *Recognition of Anions*, Vilar, R., Ed. Springer-Verlag Berlin: Berlin, 2008; Vol. 129, pp 127–174.

(27)   Churchill, C. D. M.; Wetmore, S. D., Noncovalent Interactions Involving Histidine: The Effect of Charge on π-π Stacking and T-Shaped Interactions with the DNA Nucleobases. *J. Phys. Chem. B* **2009,** *113* (49), 16046–16058.

(28)   Rutledge, L. R.; Campbell-Verduyn, L. S.; Hunter, K. C.; Wetmore, S. D., Characterization of Nucleobase-Amino Acid Stacking Interactions Utilized by a DNA Repair Enzyme. *J. Phys. Chem. B* **2006,** *110* (39), 19652–19663.

(29)   Rutledge, L. R.; Durst, H. F.; Wetmore, S. D., Computational Comparison of the Stacking Interactions Between the Aromatic Amino Acids and the Natural or (Cationic) Methylated Nucleobases. *Phys. Chem. Chem. Phys.* **2008,** *10* (19), 2801–2812.

(30)   Rutledge, L. R.; Wetmore, S. D., Remarkably Strong T-Shaped Interactions between Aromatic Amino Acids and Adenine: Their Increase upon Nucleobase Methylation and a Comparison to Stacking. *J. Chem. Theory Comput.* **2008,** *4* (10), 1768–1780.

(31)   Rutledge, L. R.; Churchill, C. D. M.; Wetmore, S. D., A Preliminary Investigation of the Additivity of π−π or π+−π Stacking and T-Shaped Interactions between Natural or Damaged DNA Nucleobases and Histidine. *J. Phys. Chem. B* **2010,** *114* (9), 3355–3367.

(32)   Wilson, K. A. Computational Studies of DNA Repair: Dynamics of the MutY, hOgg1 and hUNG2 DNA Glycosylases. Honours, University of Lethbridge, Lethbridge, AB, 2013.

(33)   Hill, J. W.; Hazra, T. K.; Izumi, T.; Mitra, S., Stimulation of Human 8-Oxoguanine-DNA Glycosylase by AP-endonuclease: Potential Coordination of the Initial Steps in Base Excision Repair. *Nucleic Acids Res.* **2001,** *29* (2), 430–438.

(34)   Vidal, A. E.; Hickson, I. D.; Boiteux, S.; Radicella, J. P., Mechanism of Stimulation of the DNA Glycosylase Activity of hOGG1 by the Major Human AP Endonuclease: Bypass of the AP Lyase Activity Step. *Nucleic Acids Res.* **2001,** *29* (6), 1285–1292.

(35)   Boiteux, S.; Oconnor, T. R.; Lederer, F.; Gouyette, A.; Laval, J., Homogeneous *Escherichia-coli* FPG Protein - A DNA Glycosylase which Excises Imidazole Ring-Opened Purines and Nicks DNA at Apurinic Apyrimidinic Sites. *J. Biol. Chem.* **1990,** *265* (7), 3916–3922.

(36)   Kow, Y. W.; Wallace, S. S., Mechanism of Action of *Escherichia-coli* Endonuclease-III. *Biochemistry* **1987,** *26* (25), 8200–8206.

(37)   Maiti, A.; Morgan, M. T.; Pozharski, E.; Drohat, A. C., Crystal Structure of Human Thymine DNA Glycosylase Bound to DNA Elucidates Sequence-Specific Mismatch Recognition. *Proc. Nat. Acad. Sci. USA* **2008,** *105* (26), 8890–8895.

(38)   Maiti, A.; Morgan, M. T.; Drohat, A. C., Role of Two Strictly Conserved Residues in Nucleotide Flipping and N-Glycosylic Bond Cleavage by Human Thymine DNA Glycosylase. *J. Biol. Chem.* **2009,** *284* (52), 36680–36688.

(39)   Abu, M.; Waters, T. R., The Main Role of Human Thymine-DNA Glycosylase is Removal of Thymine Produced by Deamination of 5-Methylcytosine and not Removal of Ethenocytosine. *J. Biol. Chem.* **2003,** *278* (10), 8739–8744.

(40)   Cortellino, S.; Xu, J. F.; Sannai, M.; Moore, R.; Caretti, E.; Cigliano, A.; Le Coz, M.; Devarajan, K.; Wessels, A.; Soprano, D.*, et al.* , Thymine DNA Glycosylase Is Essential for Active DNA Demethylation by Linked Deamination-Base Excision Repair. *Cell* **2011,** *146* (1), 67–79.

(41)   Parikh, S. S.; Walcher, G.; Jones, G. D.; Slupphaug, G.; Krokan, H. E.; Blackburn, G. M.; Tainer, J. A., Uracil-DNA Glycosylase-DNA Substrate and Product Structures: Conformational Strain Promotes Catalytic Efficiency by Coupled Stereoelectronic Effects. *Proc. Nat. Acad. Sci. USA* **2000,** *97* (10), 5083–5088.

(42)   Waters, T. R.; Swann, P. F., Kinetics of the Action of Thymine DNA Glycosylase. *J. Biol. Chem.* **1998,** *273* (32), 20007–20014.

Appendix A: Supplemental Information for

Chapter 2: DFT Method Testing

Table of Contents

Appendix B: Supplemental Information for Chapter 3:

Monofunctional Glycosylases Part 1:

Human Uracil–DNA Glycosylase (hUNG2)

Table of Contents

Appendix C: Supplemental Information for Chapter 4:

Monofunctional Glycosylases Part 2:

Adenine–DNA Glycosylase (MutY)

Table of Contents

Appendix D: Supplemental Information for

Chapter 5: Bifunctional Glycosylases Part 1:

Exploration of the Glycosylase/Lyase Mechanism

Table of Contents

Appendix E: Supplemental Information for Chapter 6:

Bifunctional Glycosylases Part 2:

Human 8-Oxoguanine–DNA Glycosylase (hOgg1)

Table of Contents

Appendix F: Excel Document for Prediction of

DNA–Protein Stacking Contacts

Appendix G: Supplemental Information for Chapter 7

Predicting Binding Energies of DNA–Protein Stacking Contacts

Table of Contents

Appendix A: Supplemental Information for

Chapter 2: DFT Method Testing

Table of Contents

Table A1. *Compilation of benchmark results (kcal mol^{-1}) for various DFT functionals with a double-ζ quality basis set.*[a,b]

Method	Interactions					BH	MMUE[d]
	HB	CT	DI	WI	Total[c]		
GGA							
HCTH	1.47	2.04	0.44	0.43	1.10	5.40	3.25
BLYP	1.04	2.48	0.70	0.75	1.24	8.30	4.77
OLYP	2.67	1.77	2.14	0.94	1.88	6.00	3.94
mPWPW91	0.85	3.02	0.58	0.54	1.25	8.60	4.92
BP86	0.74	2.80	0.68	0.84	1.27	9.40	5.33
G96LYP	2.24	1.59	2.25	1.78	1.97	6.90	4.43
PBE	1.09	3.76	0.68	0.30	1.46	9.50	5.48
PW91						9.80	
Meta-GGA							
VSXC	0.70	3.61	1.21	1.62	1.79	5.10	3.44
BB95	1.24	2.26	0.90	0.79	1.30	8.30	4.80
BB25						3.70	
Hybrid-GGA							
MPW1K	1.05	0.94	0.43	0.25	0.67	1.41	1.04
B97-2	0.70	1.12	0.58	0.32	0.68	3.11	1.89
mPW1PW91	0.87	1.38	0.50	0.30	0.76	3.92	2.34
B98	0.95	1.66	0.41	0.22	0.81	4.12	2.46
B3PW91	0.78	1.29	0.69	0.77	0.88	4.40	2.64
PBE1PBE	1.34	1.80	0.47	0.21	0.96	4.61	2.78
X3LYP	1.14	1.73	0.42	0.22	0.88	5.18	3.03
MPW3LYP	1.46	2.16	0.36	0.26	1.06	5.56	3.31
B97-1	1.18	1.95	0.48	2.26	1.47	4.22	2.84
O3LYP	1.86	1.33	1.73	0.79	1.43	4.70	3.06
B3LYP	1.42	1.45	0.52	3.51	1.72	5.02	3.37
OPW91						5.40	
Hybrid-Meta-GGA							
XB1K	0.66			0.04	0.35	1.35	0.85
BB1K	0.61	0.75	0.69	0.28	0.58	1.42	1.00
MPWB1K	1.18	0.84	0.36	1.42	0.95	1.49	1.22
B1B95	0.68	1.00	0.80	0.35	0.71	3.22	1.96
X1B95	0.51			0.04	0.28	3.26	1.77
MPW1B95	1.25	1.20	0.41	1.63	1.12	3.59	2.36

[a] Top ten functionals in bold, functionals tested in the present study highlighted in red. [b] From Zhao, Y.; Pu, J. Z.; Lynch, B. J.; Truhlar, D. G. *Phys. Chem. Chem. Phys.* **2004**, *6*, 673–676; Zhao, Y.; Truhlar, D. G. *J. Phys. Chem. A* **2004**, *108*, 6908–6918; Zhao, Y.; Truhlar, D. G. *J. Chem. Theory Comput.* **2005**, *1*, 415–432; and Zhao, Y.; Truhlar, D. G. *Phys. Chem. Chem. Phys.* **2005**, *7*, 2701–2705. [c] Average of the four MUEs reported for interaction energies. [d] Average of the MUEs for interactions and barrier heights.

Table A2. *Compilation of benchmark results (kcal mol^{-1}) for various DFT functionals with a triple-ζ quality basis set.*[a,b]

	Weak Interactions						Barrier Heights					
	HB	CT	DI	WI	SS	Total	HA transfer	Nuc. Sub.	Unimol. Assoc.	Other	Total	MMUE
LSDA and GGA												
SPWL	4.64	6.78	2.93	0.37	0.35	3.01	23.48	8.50	5.90	17.72	13.90	7.85
HCTH	1.68	1.31	0.55	0.39		0.98				5.20	5.20	1.83
OLYP	3.60	1.57	2.35	0.88		2.10				5.90	5.90	2.86
G96LYP	2.95	1.20	2.57	1.86		2.15				6.60	6.60	3.04
PBE	0.45	2.95	0.46	0.17	2.05	1.22	14.93	6.97	3.35	9.31	8.64	4.52
mPWLYP	0.65	2.70	0.38	0.39		1.03	15.76	8.14	3.79		9.23	4.54
mPWPW91	0.57	2.25	0.56	0.49		0.97	14.10	7.45	3.10	8.50	8.29	4.63
BLYP	1.18	1.67	1.00	0.56	3.92	1.67	14.66	8.40	3.51	7.66	8.56	4.73
BP86	0.72	2.03	0.66	0.90		1.08	15.51	6.91	3.87	9.30	8.90	4.99
Meta-GGA												
VSXC	0.45	2.84	1.10	1.30	6.97	2.53	7.44	5.30	2.40	5.00	5.04	3.64
mPWKCIS	0.97	1.85	0.57	0.48		0.97	13.65	6.66	3.07		7.79	3.89
TPSSKCIS	0.55	2.17	0.49	0.39		0.90	13.37	7.64	2.98		8.00	3.94
TPSS	0.45	2.20	0.52	0.31	2.53	1.20	14.65	7.75	4.04	7.71	8.54	4.46
BB95	1.83	1.48	1.18	0.82		1.33	13.88	6.36	3.40	8.00	7.91	4.62
Hybrid-GGA												
BHandHLYP	0.42	0.42	0.75	0.35		0.49	3.04	1.39	1.98		2.14	***1.19***
MPW1K	0.40	0.44	0.52	0.21	2.25	0.76	1.89	1.28	2.42	1.38	1.74	1.20
B97-3	1.16	0.48	0.82	0.49	3.09	1.21	2.41	0.80	1.42		1.54	1.33
B3PW91	1.03	0.64	0.97	0.80		0.86				4.40	4.40	1.57
B97-2	1.07	0.56	0.87	0.26	2.73	1.10	3.52	1.47	1.91	3.20	2.52	1.73
B97-1	0.50	1.17	0.28	0.13	1.57	0.73	5.18	3.21	1.83	4.22	3.61	2.01
B98	0.44	0.91	0.34	0.14	2.15	0.79	5.18	2.96	1.97	4.06	3.54	2.02
mPW1PW91	0.40	0.65	0.53	0.45	2.43	0.89	5.99	1.94	2.00	3.76	3.42	2.02
PBE1PBE	0.59	1.04	0.35	0.14	1.84	0.79	6.62	2.05	2.16	4.43	3.82	2.14
X3LYP	0.53	0.96	0.45	0.19	2.49	0.92	8.48	2.90	2.06	4.43	4.47	2.50
B3LYP	0.55	0.71	0.78	0.31	3.15	1.10	8.49	3.25	2.02	4.49	4.56	2.64
MPW3LYP	0.72	1.39	0.31	0.21	2.11	0.95	9.29	4.29	2.21	4.93	5.18	2.83
O3LYP	2.77	1.20	1.97	0.74		1.67	8.27	4.42	2.27	4.40	4.84	3.26
Hybrid-Meta-GGA												
XB1K	0.45			0.04		0.25				1.23	1.23	***0.57***
M06-2X	0.45	0.36	0.25	0.17	0.34	0.31	1.61	1.22	0.92		1.25	***0.67***
PWB6K	0.44	0.25	0.24	0.15	0.79	0.37	1.61	1.10	1.53	1.28	1.38	***0.82***
M05-2X	0.40	0.46	0.27	0.09	0.62	0.37	2.00	1.48	1.77		1.75	***0.89***
MPWB1K	0.41	0.24	0.50	0.10	1.32	0.51	1.69	1.19	1.61	1.34	1.46	***0.93***
BMK	0.68	0.41	0.78	0.76	2.49	1.02	1.49	0.91	1.58		1.33	***1.14***
BB1K	0.85	0.68	1.02	0.31	2.03	0.98	1.58	1.30	1.44	1.15	1.37	***1.15***
M06	0.26	1.11	0.26	0.20	0.56	0.48	3.38	1.78	1.69		2.28	***1.15***
X1B95	0.49			0.04		0.27				3.01	3.01	***1.18***
M06-HF	0.66	0.37	0.59	0.22	0.51	0.47	4.39	1.61	1.45		2.48	1.23
M05	0.58	0.68	0.23	0.14	1.48	0.62	3.79	0.80	2.24		2.28	1.24
MPWKCIS1K	0.59	0.52	0.75	0.28	2.56	0.94	1.97	1.17	2.05	1.71	1.73	1.29
MPW1B95	0.46	0.47	0.50	0.13	1.46	0.60	4.62	1.21	1.31	3.18	2.58	1.48
PW6B95	0.53	0.69	0.40	0.11	1.21	0.59	5.36	2.05	1.43	3.14	3.00	1.66
B1B95	1.13	0.53	1.11	0.37	2.34	1.10	4.73	1.08	1.21	2.96	2.50	1.72
M06-L	0.21	1.80	0.32	0.19	0.47	0.60	5.93	3.58	1.86		3.79	1.80
PBEh	0.40	1.04	0.35	0.12	2.01	0.78	6.62	2.05	2.16		3.61	1.84
PBE1KCIS	0.49	0.89	0.32	0.19	1.92	0.76	7.07	2.41	1.91	3.72	3.78	2.10
MPW1KCIS	0.87	0.85	0.66	0.32	2.65	1.07	8.64	3.55	1.96	4.41	4.64	2.66
TPSS1KCIS	0.49	1.22	0.46	0.27	2.39	0.97	9.26	4.88	2.12	4.69	5.24	2.86
TPSSh	0.41	1.44	0.49	0.25	2.64	1.05	11.51	5.78	3.23	5.97	6.62	3.53
TPSSKCIS	0.55	2.17	0.49	0.18	2.48	1.17	13.37	7.64	2.98	7.01	7.75	4.10

[a] Top ten functionals in bold, functionals tested in the present study highlighted in red. [b] From Zhao, Y.; Pu, J. Z.; Lynch, B. J.; Truhlar, D. G. *Phys. Chem. Chem. Phys.* **2004**, *6*, 673; Zhao, Y.; Truhlar, D. G. *J. Phys. Chem. A* **2004**, *108*, 6908; Zhao, Y.; Truhlar, D. G. *J. Chem. Theory Comput.* **2005**, *1*, 415; and Zhao, Y.; Truhlar, D. G. *Phys. Chem. Chem. Phys.* **2005**, *7*, 2701; Zhao, Y.; Gonzalez-Garcia, N.; Truhlar, D. G. *J. Phys. Chem. A* **2005**, *109*, 2012; Zhao, Y.; Truhlar, D. G. *J. Phys. Chem. A* **2005**, *109*, 5656; Zhao, Y.; Truhlar, D. G. *Theor. Chem. Account* **2008**, *120*, 215. [c] Average of the four MUEs reported for interaction energies. [d] Average of the MUEs reported for barrier heights [e] Average of all MUEs.

Table A3. *Compilation of benchmark results (kcal mol^{-1}) for various DFT-D functionals.*[a,b]

Method	Interactions	Barriers	Total[c]
	GGA		
BLYP-D3	1.1	7.1	2.3
PBE-D3	2.2	6.8	3.7
PBE	2.3	7.2	3.9
TPSS	2.8	6.9	4.2
BLYP	2.9	8.8	4.3
	Meta GGA		
TPSS-D3	1.3	6.1	2.5
	Hybrid GGA		
ωB97X-D	0.5	3.6	2.0
PW6B95-D3	0.5	3.3	2.2
PW6B95	0.7	3.8	2.3
B3PW91-D3	0.7	3.7	2.7
B3LYP-D3	1.4	4.8	2.9
PBE1PBE-D3	1.2	4.5	3.4
PBE38-D3	1.0	5.3	3.9
B3LYP	3.0	6.4	4.1
	Hybrid-Meta GGA		
M06-2X-D3	0.8	2.7	2.1
M05-2X-D3	0.7	3.2	2.4
B1B95-D3	0.9	3.2	2.4
MPW1B95-D3	0.6	3.4	2.5
BMK-D3	1.2	3.2	2.5
M06-D3	1.0	3.3	2.5
MPWB1K-D3	0.6	4.2	3.0
revPBE0-D3	0.7	4.4	3.1
PWB6K-D3	0.7	4.5	3.2
M05-D3	1.3	4.6	3.5
TPSS0-D3	0.8	5.0	3.6
revPBE38-D3	0.8	5.2	3.7
TPSSh-D3	1.0	5.1	3.7
M06-HF-D3	1.4	5.5	4.1
BHLYP-D3	1.2	6.8	4.9
	Long Range		
CAM-B3LYP-D3	1.4	4.4	3.4
LC-ωPBE-D3	0.4	4.9	3.4

[a] Top ten functionals in bold, functionals tested in the present study highlighted in red. [b] Antony, J.; Grimme, S.; Liakos, D. G.; Neese, F. *J. Phys. Chem. A* **2011**, *115*, 11210; Goerigk, L.; Grimme, S. *Phys. Chem. Chem. Phys.* **2011**, *13*, 6670; Grimme, S. *Wiley Interdisciplinary Reviews: Computational Molecular Science* **2011**, *1*, 211; Hujo, W.; Grimme, S. *Phys. Chem. Chem. Phys.* **2011**, *13*, 13942–13950. [c] Average of the MUEs for interactions and barrier heights.

Table A4. *Reference Energetics for the HB, PP, PT, SN2 and UNI Test Sets in the Present Work*

	ΔE_I			ΔE_a	ΔE_R		ΔE_{Gas}	ΔE_{PCM}
HB[a]		**PT**[d]				**UNI**[e]		
A:T	−64.6	C(O2Ha)			−4.8	1.400	0.8	2.2
C:G	−120.5	C(O2Hb)			−2.0	1.500	0.0	0.0
		C(N3H)			29.2	1.600	19.5	17.8
PP		TS (N1H → O2Ha)		138.9		1.700	43.1	44.5
A:T[b]	−51.2	TS (O2Hb → N3H)		154.4		1.800	71.6	66.5
U:U[b]	−42.3	C(O2Ha) + H_2O			1.9	1.900	101.3	93.2
F:W (S)[b]	−21.8	C(O2Hb) + H_2O			8.8	2.000	129.6	117.8
F:W (T)[b]	−24.0	C(N3H) + H_2O			25.4	2.100	140.2	139.2
U:F (S)[c]	−21.7	TS (N1H → O2Ha) + H_2O		48.4		2.200	156.0	149.7
U:F (T)[c]	−11.7	TS (O2Hb → N3H) + H_2O		55.7		2.300	167.5	163.1
						2.400	175.9	173.7
		SN2[e]				2.500	182.2	180.0
		OH^-		81.0	−125.2	2.600	187.0	185.4
		$HCOO^-\cdots H_2O$		155.1	47.2	2.700	190.9	185.1
						2.800	193.9	187.0
						2.900	85.1	188.6

[a] CCSD(T)/CBS(D,T)//MP2/cc-pVTZ from reference XX. [b] CCSD(T)/CBS(D,T)//CP-MP2/cc-pVTZ from reference XX. [c] CCSD(T)/CBS(D,T)//CP-MP2/6-31G*(0.25) from reference XX. [d] CCSD(T)/CBS(D,T)//MP2/6-31+G(d,p). [e] (PCM-)MP2/6-311+G(2df,p)//B3LYP/6-311+G(2d,p).
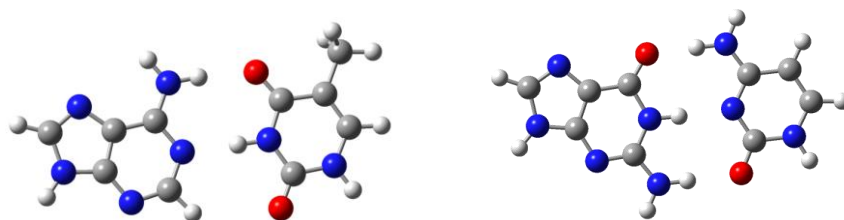
Figure A1. *Structure of HB test set systems: adenine–thymine base pair (left) and guanine–cytosine base pair (right).*

U:U Stack   **U:F Stack**   **F:W Stack**

A:T Stack   **U:F T-shape**   **F:W T-shape**
(Left: PP$_E$ test, Right: PP$_O$ test)
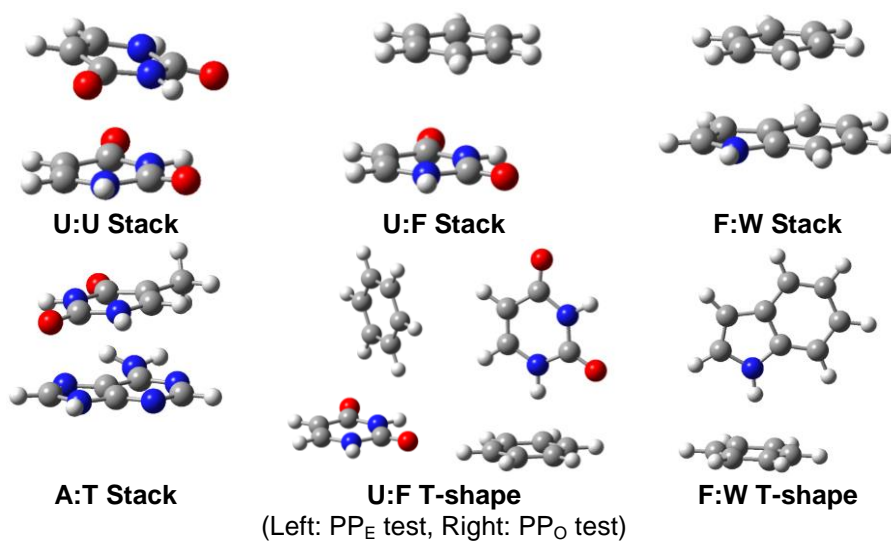
Figure A2. *Structure of the PP test set systems.*

C(N1H)   **C(O2H(N1))**   **C(O2H(N3)**   **C(N3H)**   **TS–N1O2**   **TS–O2N3**

C(N1H):H$_2$O   **C(O2H(N1)):H$_2$O**   **C(O2H(N3):H$_2$O**   **C(N3H):H$_2$O**   **TS–N1O2:H$_2$O**   **TS–O2N3:H$_2$O**
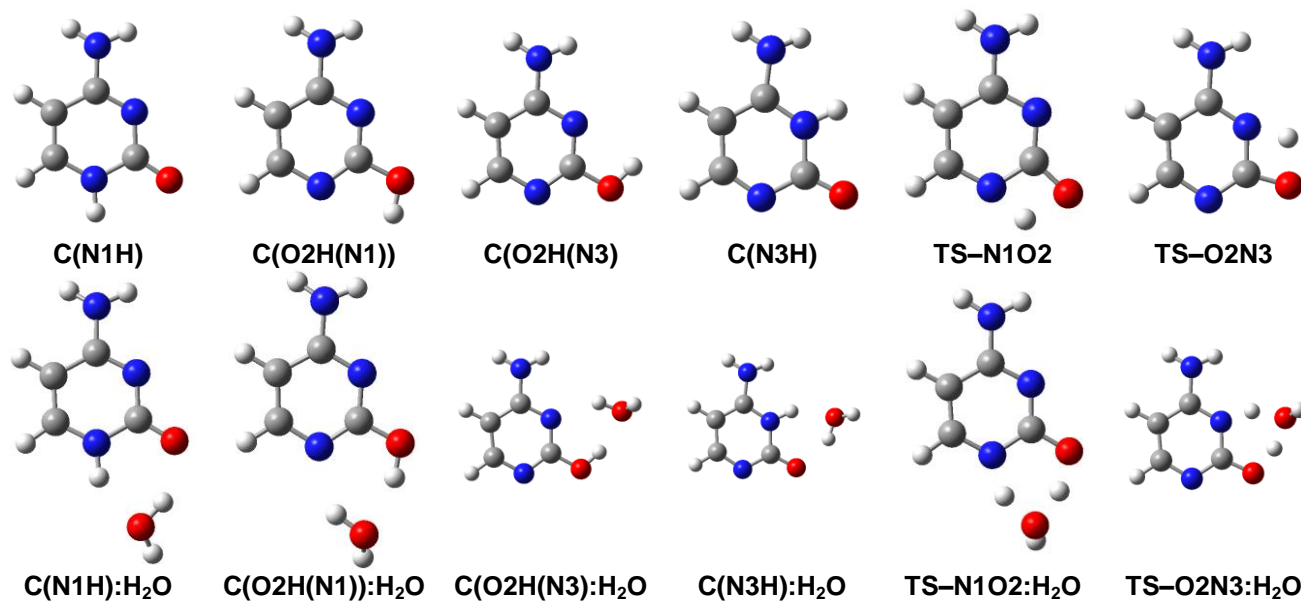
Figure A3. *Structure of the PT test set systems.*

SN2 – OH⁻   **SN2 – HCOO⁻···H₂O**   **UNI**
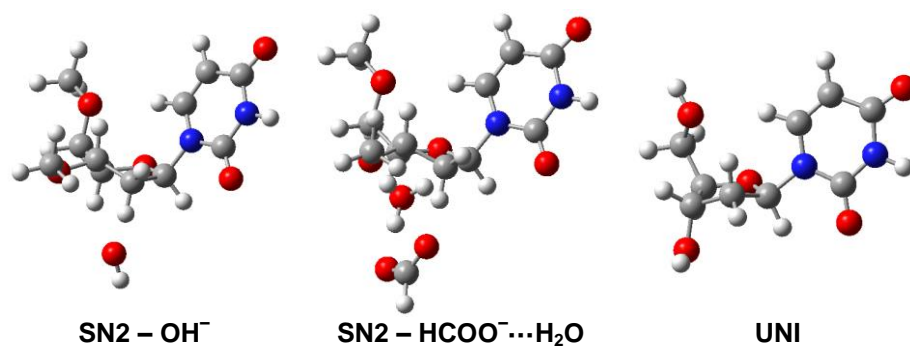
Figure A4. *Reactant structures for the SN2 and UNI test sets.*
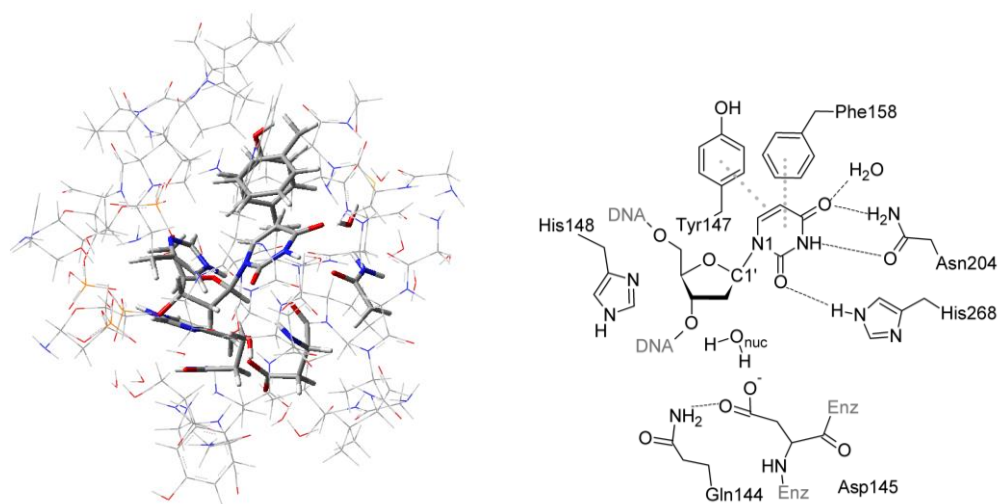
Figure A5. *hUNG2 reactant (left) and schematic of DFT region (right).*

Table A5. *Mean unsigned errors of binding energies (ΔE$_I$), barrier heights (ΔE$_a$), reaction energies (ΔE$_R$) and total MUE for energies (kJ mol^{-1}).*[a]

Method	Basis Set	ΔE$_I$			ΔE$_a$		ΔE$_R$		MMUE[d]
		HB	PP$_E$[b]	PP$_O$[c]	PT	SN2	PT	SN2	
B3LYP	6-31G(d)	**1.4**	*20.0*		5.8	*39.3*	*6.1*	50.7	20.5
B3LYP	6-31G(d,p)	**0.4**	19.9		*9.6*	*39.2*	3.5	55.3	*21.3*
B97-2	6-31G(d)	*9.5*	*20.5*		5.4	*33.3*	*6.0*	57.6	22.1
B97-2	6-31G(d,p)	8.1	*20.4*		*9.1*	32.9	3.2	*60.0*	22.3
MPW1K	6-31G(d)	1.7	17.8		5.9	**16.8**	3.6	*57.3*	17.2
MPW1K	6-31G(d,p)	1.8	17.8		5.1	**16.3**	**0.8**	54.4	16.0
MPWB1K	6-31G(d)	1.5	11.0	15.8	5.6	20.1	2.9	42.5	14.2
MPWB1K	6-31G(d,p)	**0.8**	11.1	15.5	**1.3**	**18.7**	**0.7**	**39.4**	**12.5**
BB1K	6-31G(d)	7.8	15.2	*21.0*	5.1	20.3	3.1	47.9	17.2
BB1K	6-31G(d,p)	6.9	15.1	20.2	**1.8**	20.0	**0.8**	45.8	15.8
B1B95	6-31G(d)	8.3	15.8	*23.0*	**4.6**	29.8	4.4	46.9	19.0
B1B95	6-31G(d,p)	7.2	15.6	*22.8*	*10.1*	29.3	1.7	52.4	19.9
M06-2X	6-31G(d)	5.2	**0.6**	2.7	5.2	25.6	1.4	50.5	13.0
M06-2X	6-31G(d,p)	6.3	**0.5**	**2.3**	7.5	25.4	2.9	48.8	13.4
ωB97X-D	6-31G(d)	*10.1*	**3.3**	**1.3**	5.3	22.1	*5.7*	**40.7**	**12.6**
ωB97X-D	6-31G(d,p)	*11.8*	3.7	**2.1**	4.8	22.4	3.0	**38.9**	**12.4**

[a] Lowest three values in bold and highest three values in italics for each measurement. [b] Binding energies calculated with database geometries. [c] Binding energies calculated on optimized geometries including scaled zero-point vibrational energy corrections. [d] Average of the seven MUE in energies reported.

Table A6. Summary of Enzyme–Substrate Contacts and Nucleotide Conformation in the hUNG2 Active Site Optimized using ONIOM with Various Density Functionals in the High Level Region.

Method	Basis Set	Gly[a] (Å)	P[b] (°)	dOG–F319 Sep[c] (Å)	Tilt[d] (°)	F319–H270 Sep[e] (Å)	Tilt[f] (°)	G42⋯N7 Y⋯H (Å)	X–H⋯Y (°)	Owat⋯O6 Y⋯H (Å)	X–H⋯Y (°)	D268⋯Owat Y⋯H (Å)	X–H⋯Y (°)
B3LYP	6-31G(d)	1.460	175.3	3.41	5.7	4.57	59.8	1.820	171.0	1.902	163.5	1.780	161.7
B3LYP	6-31G(d,p)	1.459	175.4	3.41	5.8	4.57	59.5	1.805	170.6	1.909	163.6	1.768	162.4
M06-2X	6-31G(d)	1.448	154.1	3.19	6.7	4.33	62.0	1.870	175.9	1.861	168.0	1.659	161.0
M06-2X	6-31G(d,p)	1.444	147.4	3.16	5.0	4.43	67.4	1.856	179.0	1.861	172.7	1.612	164.5
ωB97X-D	6-31G(d)	1.440	169.9	3.28	6.0	4.39	58.2	1.770	171.4	1.820	174.1	1.736	171.9
ωB97X-D	6-31G(d,p)	1.438	157.3	3.25	4.6	4.55	64.7	1.770	170.7	1.805	176.3	1.711	173.1
Average		1.448	163.2	3.28	5.6	4.47	61.9	1.815	173.1	1.859	169.7	1.711	165.8

[a] Glycosidic bond length. [b] Pseudorotational angle. [c] Separation between the plane of the 8-oxoguanine nucleobase and center of the phenylalanine ring. [d] Interplanar angle between uracil and phenylalanine ring. [e] Separation between the plane of the histidine ring and the center of the phenylalanine ring. [f] Interplanar angle between the histidine and phenylalanine rings.
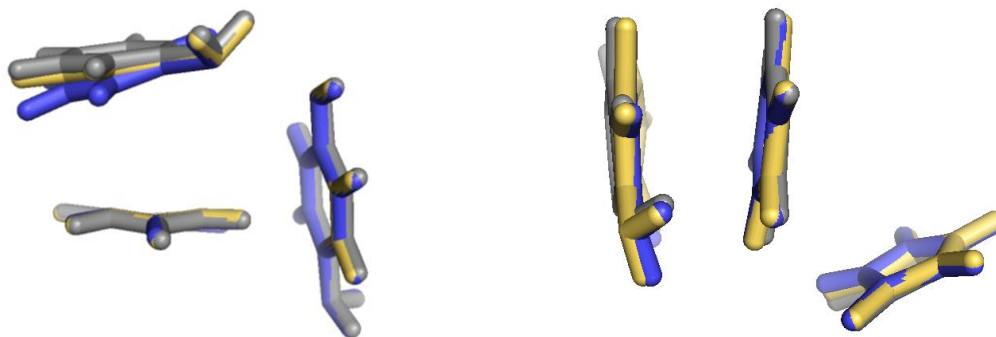
Figure A6. Overlay of the π–π interactions in the hUNG2 (left) and hOgg1 (right) active sites optimized with B3LYP (grey), M06-2X (blue) and ωB97X-D (yellow) methods with the 6-31G(d) basis set.

Full citation for reference 85.

Frisch, M. J.; Trucks, G. W.; Schlegel, H. B.; Scuseria, G. E.; Robb, M. A.; Cheeseman, J. R.; Scalmani, G.; Barone, V.; Mennucci, B.; Petersson, G. A.; Nakatsuji, H.; Caricato, M.; Li, X.; Hratchian, H. P.; Izmaylov, A. F.; Bloino, J.; Zheng, G.; Sonnenberg, J. L.; Hada, M.; Ehara, M.; Toyota, K.; Fukuda, R.; Hasegawa, J.; Ishida, M.; Nakajima, T.; Honda, Y.; Kitao, O.; Nakai, H.; Vreven, T.; Montgomery, J., J. A; Peralta, J. E.; Ogliaro, F.; Bearpark, M.; Heyd, J. J.; Brothers, E.; Kudin, K. N.; Staroverov, V. N.; Kobayashi, R.; Normand, J.; Raghavachari, K.; Rendell, A.; Burant, J. C.; Iyengar, S. S.; Tomasi, J.; Cossi, M.; Rega, N.; Millam, N. J.; Klene, M.; Knox, J. E.; Cross, J. B.; Bakken, V.; Adamo, C.; Jaramillo, J.; Gomperts, R.; Stratmann, R. E.; Yazyev, O.; Austin, A. J.; Cammi, R.; Pomelli, C.; Ochterski, J. W.; Martin, R. L.; Morokuma, K.; Zakrzewski, V. G.; Voth, G. A.; Salvador, P.; Dannenberg, J. J.; Dapprich, S.; Daniels, A. D.; Farkas, Ö.; Foresman, J. B.; Ortiz, J. V.; Cioslowski, J.; Fox, D. J.; Revision A.02 (C.01); Gaussian, Inc.: Wallingford CT, **2009**.

Reference Geometries

Hydrogen Bonding (HB)

Adenine$\cdots$Thymine BE$_{(CCSD(T)/CBS(D,T)//MP2/cc-pVTZ)}$ = -64.6 kJ mol^{-1}

0 1

N	-4.1463095	0.0276066	0.4989510
C	-4.1783269	0.0241149	1.8693855
C	-3.0503934	0.0075345	2.6143561
C	-1.7764463	-0.0075165	1.9134149
N	-1.8409343	-0.0044729	0.5342848
C	-2.9776615	0.0158134	-0.2412098
C	-3.0337782	0.0039661	4.1067561
O	-0.6903188	-0.0223257	2.4988523
O	-2.9710806	0.0231200	-1.4594154
N	0.6342733	-0.0396251	-0.8445604
C	1.8085815	-0.0725030	-0.1925510
C	2.9816390	-0.0450617	-0.9713088
C	2.8096988	0.0150597	-2.3538115
N	1.6523629	0.0464189	-3.0268028
C	0.6173449	0.0155645	-2.1932329
N	4.3110053	-0.0631092	-0.6210230
C	4.9362856	-0.0138224	-1.7844380
N	4.0874208	0.0345553	-2.8553711
N	1.8292763	-0.1390909	1.1445440
H	-0.3707005	0.0368460	-2.6349270
H	6.0061912	-0.0105896	-1.9082208
H	4.3375082	0.0791089	-3.8297046
H	0.9607282	-0.0976204	1.6743842
H	2.7192948	-0.1141775	1.6075837
H	-4.9945252	0.0435817	-0.0428232
H	-0.9349425	-0.0189830	0.0123682
H	-5.1632478	0.0355348	2.3150232
H	-2.5162678	-0.8784794	4.4795452
H	-2.4928573	0.8705738	4.4831417
H	-4.0449522	0.0166200	4.5078085

Guanine$\cdots$Cytosine (BE$_{(CCSD(T)/CBS(D,T)//MP2/cc-pVTZ)}$ = -120.5 kJ mol^{-1})

0 1

C	-0.0229712	-0.0480749	-0.0719441
N	0.0000759	-0.0168921	1.3245438
C	1.1503206	0.0040801	2.0405389
C	2.3452042	0.0087522	1.4043050
C	2.3170717	-0.0031116	-0.0306151
N	1.1736034	-0.0283191	-0.7146207
O	-1.1130393	-0.0913005	-0.6441911
N	3.4540655	0.0098553	-0.7230323
H	-0.9005733	-0.0257697	1.7762054
H	1.0534904	0.0163290	3.1157164
H	3.2717111	0.0246724	1.9546693
H	4.3302399	0.0321232	-0.2356398
H	3.4359148	0.0053872	-1.7559696
O	3.3972002	0.0109043	-3.4726734
C	2.3875616	0.0130651	-4.1871260

N	1.1145854	0.0310366	-3.6139350
C	-0.0775444	0.0323402	-4.2884331
N	-0.1732898	0.0033938	-5.6012194
C	1.0402621	-0.0098012	-6.1913149
C	2.3078207	-0.0029108	-5.6122031
N	3.2996130	-0.0154881	-6.5657346
C	2.6406835	-0.0296497	-7.7063072
N	1.2780162	-0.0285733	-7.5379087
N	-1.1921460	0.1041805	-3.5275378
H	1.0971133	0.0303654	-2.5816916
H	3.0901188	-0.0410594	-8.6845665
H	0.5712941	-0.0311152	-8.2541952
H	-2.0566625	-0.0497999	-4.0129402
H	-1.1578384	-0.0296823	-2.5196712

π–π Interactions (PP)

Adenine:Thymine, stacked $BE_{(CCSD(T)/CBS(D,T)//CP-MP2/cc-pVTZ)} = -51.2$ kJ mol^{-1}

0 1

N	0.2793014	2.4068393	-0.6057517
C	-1.0848570	2.4457461	-0.5511608
H	-1.6594403	3.0230294	-1.2560905
N	-1.5977117	1.7179877	0.4287543
C	-0.4897255	1.1714358	1.0301910
C	-0.3461366	0.2914710	2.1172343
N	-1.4187090	-0.1677767	2.8101441
H	-1.2388750	-0.9594802	3.4047578
H	-2.2918734	-0.1788223	2.3073619
N	0.8857630	-0.0700763	2.4919494
C	1.9352348	0.4072878	1.7968022
H	2.9060330	0.0788414	2.1458181
N	1.9409775	1.2242019	0.7402202
C	0.6952186	1.5779858	0.4063984
H	0.8610073	2.8298045	-1.3104502
N	1.2754606	-0.6478993	-1.9779104
C	1.4130533	-1.5536850	-0.9550667
H	2.4258769	-1.8670780	-0.7468778
C	0.3575976	-2.0239499	-0.2530575
C	0.4821292	-3.0179494	0.8521221
H	0.1757705	-2.5756065	1.7986281
H	-0.1601691	-3.8770412	0.6639498
H	1.5112443	-3.3572767	0.9513659
C	-0.9684711	-1.5298112	-0.5939792
O	-2.0029280	-1.8396957	-0.0199453
N	-0.9956916	-0.6383870	-1.6720420
H	-1.9014057	-0.2501720	-1.8985760
C	0.0684702	-0.1191762	-2.3763759
O	-0.0397875	0.7227006	-3.2531083
H	2.0853289	-0.2760176	-2.4454577

Uracil:Uracil, stacked $BE_{(CCSD(T)/CBS(D,T)//CP-MP2/cc-pVTZ)} = -42.3$ kJ mol^{-1}

0 1

N	2.0113587	-1.2132073	-0.0980673
C	2.0257076	-0.6971797	-1.3644029
H	2.2975208	-1.3910592	-2.1456459
C	1.7145226	0.5919651	-1.6124892
H	1.7272873	0.9908466	-2.6120050
C	1.3089605	1.4575340	-0.5205890
O	0.9205926	2.6110864	-0.6260457
N	1.3768885	0.8397454	0.7346356
H	1.0518040	1.3862229	1.5233710
C	1.6459909	-0.4852113	1.0187267
O	1.5611090	-0.9718061	2.1298059
H	2.1294635	-2.2015046	0.0568134
N	-2.0113587	1.2132073	-0.0980673
C	-2.0257076	0.6971797	-1.3644029
H	-2.2975208	1.3910592	-2.1456459
C	-1.7145226	-0.5919651	-1.6124892
H	-1.7272873	-0.9908466	-2.6120050

```
C   -1.3089605   -1.4575340   -0.5205890
O   -0.9205926   -2.6110864   -0.6260457
N   -1.3768885   -0.8397454    0.7346356
H   -1.0518040   -1.3862229    1.5233710
C   -1.6459909    0.4852113    1.0187267
O   -1.5611090    0.9718061    2.1298059
H   -2.1294635    2.2015046    0.0568134
```

Phenylalanine:Tryptophan, stacked BE$_{\text{(CCSD(T)/CBS(D,T)//CP-MP2/cc-pVTZ)}}$ = −21.8 kJ mol^{-1}

```
0 1
C   -0.0210742    1.5318615   -1.3639345
C   -1.2746794    0.9741030   -1.6074097
C   -1.3783055   -0.2256981   -2.3084154
C   -0.2289426   -0.8664053   -2.7687944
C    1.0247882   -0.3035171   -2.5312410
C    1.1289996    0.8966787   -1.8299830
H    0.0600740    2.4565627   -0.8093957
H   -2.1651002    1.4654521   -1.2405676
H   -2.3509735   -0.6616122   -2.4926698
H   -0.3103419   -1.7955762   -3.3172704
H    1.9165847   -0.7940845   -2.8993942
H    2.1000347    1.3326757   -1.6400420
H   -2.9417647    0.8953834    2.2239054
C   -2.0220674    0.4258540    1.9013549
C   -0.8149418    1.0740453    2.1066982
H   -0.7851529    2.0443812    2.5856086
C    0.3704286    0.4492852    1.6847458
C    1.7508619    0.8038935    1.7194004
H    2.1870108    1.6998281    2.1275903
C    2.4451359   -0.2310742    1.1353313
N    1.5646462   -1.2137812    0.7555384
C    0.2861214   -0.8269486    1.0618752
C   -0.9284667   -1.4853121    0.8606937
H   -0.9729200   -2.4554847    0.3834013
C   -2.0792848   -0.8417668    1.2876443
H   -3.0389974   -1.3203846    1.1468400
H    1.8075741   -2.0366963    0.2333038
H    3.5028794   -0.3485344    0.9695233
```

Phenylalanine:Tryptophan, T-shaped BE$_{\text{(CCSD(T)/CBS(D,T)//CP-MP2/cc-pVTZ)}}$ = −24.0 kJ mol^{-1}

```
0 1
C    2.5118997    1.6250148    0.0000000
C    2.7130094    0.9578537   -1.2082918
C    3.1177821   -0.3767436   -1.2083647
C    3.3213848   -1.0437307    0.0000000
C    3.1177821   -0.3767436    1.2083647
C    2.7130094    0.9578537    1.2082918
H    2.2024038    2.6611358    0.0000000
H    2.5511760    1.4736908   -2.1445900
H    3.2702999   -0.8951406   -2.1448379
H    3.6368139   -2.0781521    0.0000000
H    3.2702999   -0.8951406    2.1448379
H    2.5511760    1.4736908    2.1445900
H    0.8065245   -0.4358866    0.0000000
```

```
N   -0.1442408   -0.7686927   0.0000000
C   -0.5161122   -2.0893220   0.0000000
C   -1.8898755   -2.1814495   0.0000000
C   -2.3932317   -0.8470830   0.0000000
C   -1.2640653    0.0195887   0.0000000
C   -1.3896004    1.4117668   0.0000000
C   -2.6726501    1.9366450   0.0000000
C   -3.8054511    1.0974790   0.0000000
C   -3.6798167   -0.2817209   0.0000000
H    0.2310024   -2.8653173   0.0000000
H   -2.4585759   -3.0956052   0.0000000
H   -0.5188733    2.0539520   0.0000000
H   -2.8077570    3.0097859   0.0000000
H   -4.7905991    1.5439372   0.0000000
H   -4.5580187   -0.9142916   0.0000000
```

Uracil:Phenylalanine, stacked $BE_{(CCSD(T)/CBS(D,T)//CP\text{-}MP2/6\text{-}31G^*(0.25))} = -21.7$ kJ mol^{-1}

0 1
```
C     0.42826000    1.81481000    1.02864000
C     1.62555000    1.81481000    0.30924000
C     1.60117000    1.81481000   -1.08734000
C     0.37951000    1.81481000   -1.76452000
C    -0.81779000    1.81481000   -1.04512000
C    -0.79341000    1.81481000    0.35147000
N    -0.44615000   -1.68519000    1.64873000
C    -1.63550000   -1.68519000    0.95472000
C    -1.67041000   -1.68519000   -0.39640000
C    -0.42635000   -1.68519000   -1.15558000
O    -0.32400000   -1.68519000   -2.37879000
N     0.72095000   -1.68519000   -0.34078000
C     0.80382000   -1.68519000    1.04262000
O     1.85406000   -1.68519000    1.67094000
H     0.36053000    1.81481000   -2.85179000
H     2.53329000    1.81481000   -1.64741000
H     2.57664000    1.81481000    0.83645000
H     0.44724000    1.81481000    2.11591000
H    -1.72551000    1.81481000    0.91153000
H    -1.76888000    1.81481000   -1.57232000
H    -2.53081000   -1.68519000    1.56807000
H    -2.60548000   -1.68519000   -0.94061000
H     1.61330000   -1.68519000   -0.82847000
H    -0.42892000   -1.68519000    2.66168000
```

Uracil:Phenylalanine, T-shaped (Phe edge) $BE_{(CCSD(T)/CBS(D,T)//CP\text{-}MP2/6\text{-}31G^*(0.25))} = -11.7$ kJ mol^{-1}

0 1
```
N    -1.65913   -2.45000   -0.60872
C    -0.94705   -2.45000   -1.78710
C     0.40459   -2.45000   -1.80132
C     1.14446   -2.45000   -0.54608
O     2.36579   -2.45000   -0.42388
N     0.31181   -2.45000    0.58921
C    -1.07208   -2.45000    0.65094
O    -1.71721   -2.45000    1.69099
C    -0.25241    1.24029    1.11508
```

```
C      0.95613   1.24037   0.41451
C      1.56030   2.45001   0.06429
C      0.95600   3.65975   0.41460
C     -0.25239   3.65966   1.11507
C     -0.85662   2.44990   1.46533
H     -1.54567  -2.45000  -2.69235
H      0.96328  -2.45000  -2.72781
H      0.78698  -2.45000   1.48845
H     -2.67214  -2.45000  -0.60736
H     -0.72243   0.29902   1.38755
H      1.42619   0.29912   0.14203
H      2.50055   2.45021  -0.48075
H      1.42623   4.60088   0.14201
H     -0.72262   4.60080   1.38766
H     -1.79688   2.44998   2.01038
```

Uracil:Phenylalanine, T-shaped (Ura edge) $BE_{(CCSD(T)/CBS(D,T)//CP-MP2/6-31G*(0.25))} = -27.6$ kJ mol^{-1}

```
0 1
N        0.58855600    0.04729700   -0.00828400
C        1.02880800   -1.25401600   -0.00695900
C        2.34343400   -1.56853400   -0.00143600
C        3.34705400   -0.50681800    0.00399000
O        4.57730200   -0.65753900    0.00953900
N        2.78358700    0.79294100    0.00243900
C        1.44143800    1.15199900   -0.00302300
O        1.03205500    2.32255200   -0.00339700
C       -3.24464100   -1.44337600    0.04864100
C       -3.09662300   -0.80296100   -1.18492000
C       -2.79048800    0.55993300   -1.23270100
C       -2.63190600    1.28423400   -0.04620900
C       -2.78118800    0.64190000    1.18777500
C       -3.08742600   -0.72092200    1.23482300
H        0.24204700   -2.00073200   -0.01091600
H        2.68669700   -2.59405100   -0.00072300
H        3.44210800    1.56350700    0.00636200
H       -0.40226500    0.26384500   -0.01046900
H       -3.48705100   -2.50228100    0.08541200
H       -3.22168100   -1.36394400   -2.10725900
H       -2.67300400    1.05819300   -2.19114800
H       -2.37660700    2.33934700   -0.08250500
H       -2.65594300    1.20393100    2.10920800
H       -3.20492300   -1.21822600    2.19393000
```

Proton Transfer (PT)

Cytosine (N1H tautomer) $E_{(CCSD(T)/CBS(D,T)//MP2/6-31+G(d,p))} = -394.459935$ Hartree (without ZPVE)
0 1

N	1.27656800	0.89655800	0.00255700
C	0.19326300	1.71737800	0.00101600
H	0.38713200	2.78141300	-0.00199700
C	-1.05794100	1.18145800	-0.00071300
H	-1.93761000	1.80680800	-0.01748600
C	-1.13133800	-0.25372700	0.00303500
N	-2.36339200	-0.84993800	-0.06422500
H	-2.36928200	-1.84235100	0.12294000
H	-3.16575000	-0.33207600	0.25617600
N	-0.08070400	-1.05392000	0.00702800
C	1.19215600	-0.51748100	0.00058300
O	2.23312500	-1.17472400	-0.00021900
H	2.21637300	1.26932900	0.00107500

Cytosine (O2H(N1) tautomer) $E_{(CCSD(T)/CBS(D,T)//MP2/6-31+G(d,p))} = -394.462124$ Hartree (without ZPVE)
0 1

N	1.30139500	0.98991600	0.00229000
C	0.16709400	1.72212100	0.00302500
H	0.29816500	2.79768600	0.00406600
C	-1.09629000	1.15935200	-0.00225400
H	-1.98804700	1.77042800	-0.01334800
C	-1.15608400	-0.24805500	0.00095200
N	-2.35073800	-0.92532900	-0.06851300
H	-2.29313500	-1.90703800	0.16094000
H	-3.17398600	-0.45172100	0.26863800
N	-0.04671600	-1.00263000	0.00241500
C	1.10916700	-0.33334500	0.00017800
O	2.21436400	-1.11683900	0.00171800
H	2.97118900	-0.50878400	0.00121600

Cytosine (O2H(N3) tautomer) $E_{(CCSD(T)/CBS(D,T)//MP2/6-31+G(d,p))} = -394.461038$ Hartree (without ZPVE)
0 1

N	1.29453500	1.04773500	0.00382400
C	0.13710700	1.73942500	0.00339100
H	0.23576700	2.81867500	0.00565900
C	-1.11513100	1.14619500	-0.00378700
H	-2.02113500	1.73599100	-0.01461900
C	-1.14261600	-0.25868900	0.00038400
N	-2.31808800	-0.97173300	-0.06987900
H	-2.23747000	-1.94680500	0.17938300
H	-3.15232200	-0.51522000	0.26470800
N	-0.00695800	-0.97615800	0.00292300
C	1.13664000	-0.27551600	0.00091400
O	2.28419000	-0.99628900	0.00094300
H	2.01920700	-1.92972500	-0.00616900

Cytosine (N3H tautomer) $E_{(CCSD(T)/CBS(D,T)//MP2/6-31+G(d,p))} = -394.448478$ Hartree (without ZPVE)
0 1

N	1.39615700	1.00303800	0.00782200
C	0.27726400	1.70693800	0.00148900

H	0.41089100	2.78486200	0.00231900
C	-1.03966600	1.19732800	0.00133500
H	-1.90233300	1.84588600	0.00734500
C	-1.16819600	-0.17520600	0.00318500
N	-2.36151400	-0.86320800	-0.07853000
H	-2.39010500	-1.76877100	0.36868700
H	-3.18177900	-0.30850600	0.11741400
N	-0.02693600	-0.91227300	0.00755800
C	1.29299000	-0.37810600	0.00307800
O	2.23715000	-1.16616400	-0.00586000
H	-0.06217600	-1.92278700	-0.06135500

Cytosine (N1H→O2H(N1) transition state) $E_{(CCSD(T)/CBS(D,T)//MP2/6-31+G(d,p))} = -394.402213$ Hartree (without ZPVE)

0 1

N	1.31236100	0.82882600	-0.00435200
C	0.28593800	1.69436300	0.00251100
H	0.50966800	2.75288400	0.00309400
C	-1.00132300	1.19410100	0.00239000
H	-1.85515000	1.85547700	-0.00583200
C	-1.16066800	-0.21900600	0.00224400
N	-2.40971700	-0.77080900	-0.05996800
H	-2.45850900	-1.76021000	0.13372300
H	-3.19944600	-0.21666700	0.22836600
N	-0.13743000	-1.09183900	0.00107900
C	1.07557600	-0.52435800	-0.00146400
O	2.24844900	-1.06949000	0.00565500
H	2.46220700	0.29059700	0.00401100

Cytosine (N3H→O2H(N3) transition state) $E_{(CCSD(T)/CBS(D,T)//MP2/6-31+G(d,p))} = -394.396913$ Hartree (without ZPVE)

0 1

N	1.42001500	1.04173900	0.00358900
C	0.26236900	1.73551000	0.00313400
H	0.37476800	2.81414800	0.00474300
C	-1.02188100	1.19471000	-0.00200200
H	-1.89407200	1.83198500	-0.00806500
C	-1.14554200	-0.20601700	0.00204600
N	-2.33687500	-0.87533500	-0.06468000
H	-2.32357200	-1.85101600	0.19168200
H	-3.16104400	-0.37000500	0.22010400
N	-0.00352500	-0.90232800	-0.00195600
C	1.23390100	-0.28404600	0.00062800
O	2.08189600	-1.25847600	0.00141600
H	0.81836300	-1.84678500	-0.00130100

Cytosine···H₂O (N1H tautomer) $E_{(CCSD(T)/CBS(D,T)//MP2/6-31+G(d,p))} = -470.848401$ Hartree (without ZPVE)

0 1

N	0.76332700	0.70319700	0.03502800
C	-0.21179500	1.64558100	0.01227800
H	0.11393800	2.67688200	0.01159600
C	-1.52266600	1.27214800	-0.00867400
H	-2.31628900	2.00307700	-0.04215900
C	-1.77453200	-0.13801500	-0.00102700
N	-3.06657700	-0.58554300	-0.07456100
H	-3.19267200	-1.56932300	0.11479000

H	-3.80654900	0.02667000	0.22878900
N	-0.82567700	-1.06115100	0.01493300
C	0.49323500	-0.67755300	0.01466100
O	1.44220400	-1.48100500	0.00761800
H	1.75151300	0.95974800	0.04273900
O	3.56244700	0.26927500	-0.09456400
H	3.07521800	-0.58112300	-0.06369600
H	4.33467500	0.16941400	0.47228500

Cytosine···H$_2$O (O2H(N1) tautomer) E$_{(CCSD(T)/CBS(D,T)//MP2/6-31+G(d,p))}$ = −470.847930 Hartree (without ZPVE)

0 1

N	0.82622100	0.72628200	0.00619900
C	-0.17819800	1.62953500	0.00071100
H	0.12188500	2.67084000	-0.00148300
C	-1.51313900	1.27676100	-0.00670900
H	-2.29602700	2.02193800	-0.02376000
C	-1.79178500	-0.10518800	0.00338000
N	-3.07779000	-0.58390300	-0.06123200
H	-3.17721400	-1.56322800	0.16382600
H	-3.81794100	0.01517300	0.26841100
N	-0.81782300	-1.02486600	0.00771700
C	0.43900900	-0.56285900	0.00217200
O	1.38408600	-1.51539800	0.00032500
H	2.26873300	-1.08613000	-0.01621800
O	3.57465200	0.19867800	-0.08473500
H	2.80806600	0.80282500	-0.01926800
H	4.17301800	0.42026300	0.63766400

Cytosine···H$_2$O (O2H(N3) tautomer) E$_{(CCSD(T)/CBS(D,T)//MP2/6-31+G(d,p))}$ = −470.845239 Hartree (without ZPVE)

0 1

N	-0.71643400	-1.78998800	0.01889300
C	-1.91610900	-1.18360400	0.06427400
H	-2.77401000	-1.84450700	0.11178100
C	-2.08910400	0.19224000	0.05320900
H	-3.07103000	0.64247400	0.09355500
C	-0.92064300	0.96422900	-0.01587000
N	-0.94898500	2.34349200	0.02191300
H	-0.11962300	2.79486300	-0.33605900
H	-1.81020600	2.78051000	-0.26949300
N	0.29384900	0.38971200	-0.05374500
C	0.32973800	-0.95982600	-0.03831400
O	1.53126300	-1.55577500	-0.08720900
H	2.23398900	-0.86997900	-0.10194300
O	3.09191800	0.76626100	0.00349400
H	3.56104600	1.04957200	0.79679000
H	2.17207500	1.08243000	0.08585200

Cytosine···H$_2$O (N3H tautomer) E$_{(CCSD(T)/CBS(D,T)//MP2/6-31+G(d,p))}$ = −470.838487 Hartree (without ZPVE)

0 1

N	-0.73451400	-1.82590300	0.00690100
C	-1.89681900	-1.18672100	-0.01063300
H	-2.77392200	-1.82682500	-0.01867700
C	-2.08391600	0.20699800	-0.02036100
H	-3.06684400	0.65182600	-0.05151500

C	-0.93782400	0.98045500	0.00300300
N	-0.91366800	2.35424800	0.07493900
H	-0.08319900	2.81316300	-0.27190600
H	-1.76936900	2.81647100	-0.19267600
N	0.25502700	0.34030600	0.04759400
C	0.41059400	-1.06392000	0.01143500
O	1.56349100	-1.52847100	-0.00628900
H	1.13395800	0.86426300	0.08685300
O	3.02744200	0.80273800	-0.08922900
H	3.78695500	0.94679700	0.48573800
H	2.84481800	-0.16126600	-0.08036100

Cytosine···H$_2$O (N1H→O2H(N1) transition state) E$_{(CCSD(T)/CBS(D,T)//MP2/6-31+G(d,p))}$ = −470.824116 Hartree (without ZPVE)

0 1

N	0.84604100	0.72431100	0.00550700
C	-0.14361900	1.63964900	-0.00347500
H	0.16146400	2.67838600	-0.00955900
C	-1.46385800	1.26113700	-0.00718600
H	-2.26027500	1.99066400	-0.02774400
C	-1.71677800	-0.13583400	0.00586900
N	-2.99837100	-0.61176600	-0.04992700
H	-3.10473200	-1.59543100	0.15045000
H	-3.74948100	-0.01019900	0.24701000
N	-0.74705600	-1.05417200	0.01049000
C	0.52738400	-0.61287900	-0.00128800
O	1.51114700	-1.45477000	-0.01222700
H	2.50256700	-0.78196600	-0.02933500
O	3.19647700	0.23646800	-0.08009800
H	2.07967900	0.80367300	0.00428400
H	3.78669900	0.34024700	0.67748200

Cytosine···H$_2$O (N3H→O2H(N3) transition state) E$_{(CCSD(T)/CBS(D,T)//MP2/6-31+G(d,p))}$ = −470.817899 Hartree (without ZPVE)

0 1

N	-0.40620900	-1.86557800	0.00818000
C	-1.66496200	-1.40866000	0.01939500
H	-2.43414100	-2.17346100	0.03314100
C	-2.03729200	-0.06565600	0.01376000
H	-3.07388400	0.23818600	0.01799100
C	-0.99930300	0.86671100	-0.00413400
N	-1.19368000	2.22671100	0.05172800
H	-0.43071500	2.80026700	-0.27789400
H	-2.10523600	2.55647300	-0.22635500
N	0.27064500	0.42759600	-0.00029400
C	0.55986200	-0.92407900	-0.01056800
O	1.81132200	-1.24476700	-0.03684000
H	2.42252300	-0.19373300	-0.04098000
O	2.60615500	1.00758400	-0.05940700
H	3.09688700	1.31635200	0.71366000
H	1.33961700	1.02238000	0.02240100

S_N2 Hydrolysis (SN2)

S_N2 Hydrolysis (SN2)

dU:OH⁻ Nucleophile, Reactant E$_{(MP2/6-311+G(2df,p)//B3LYP/6-311+G(2d,p))}$ = −988.416423 (without ZPVE)

-1 1

O	-1.79137900	2.42686000	-0.12557600
C	-2.60856200	1.44535600	-0.77131000
H	-2.72813300	1.71244800	-1.83005300
H	-3.60252100	1.42667300	-0.30493000
C	-2.01533200	0.06941300	-0.66373800
O	-0.73200000	0.04678400	-1.34051100
C	0.05188800	-0.98343300	-0.79838400
H	0.28854500	-1.73264800	-1.54906600
N	1.37350500	-0.35614100	-0.39108800
C	1.47487400	0.98240800	-0.14621600
H	0.55129900	1.52690900	-0.29084200
C	2.62539400	1.59124300	0.23021500
H	2.66189700	2.65430700	0.41168200
C	3.83241500	0.82039200	0.38533000
O	4.93900300	1.23251800	0.71574600
N	3.64353100	-0.54041100	0.11019200
H	4.45228000	-1.13948100	0.20492900
C	2.47415000	-1.19003500	-0.26390400
O	2.44388000	-2.39193300	-0.45505500
C	-1.67770100	-0.43692600	0.73713800
C	-0.72199400	-1.58199000	0.37924500
H	-0.06158000	-1.90871000	1.18276200
H	-1.31906000	-2.40611100	-0.04398300
H	-1.16700100	0.34627400	1.31906500
H	-2.65755400	-0.69073300	-1.14807800
O	-2.51857500	-2.61037300	-1.63911000
H	-2.72936400	-3.17768600	-2.38832000
C	-2.33413900	3.72098500	-0.21382200
H	-2.44003500	4.04528500	-1.25934400
H	-3.32200700	3.77881900	0.26605300
H	-1.65263900	4.40142600	0.29928800
O	-2.87119500	-0.78542300	1.41815600
C	-2.65347600	-1.34305900	2.69146100
H	-3.63241500	-1.48154600	3.15319200
H	-2.15296200	-2.31652400	2.63026000
H	-2.05097500	-0.67641500	3.32836400

dU:OH⁻ Nucleophile, Transition State E$_{(MP2/6-311+G(2df,p)//B3LYP/6-311+G(2d,p))}$ = −988.383992 (without ZPVE)

-1 1

O	-1.60273200	2.43774600	0.04409800
C	-2.53936300	1.63430500	-0.66030800
H	-2.62276100	1.98315700	-1.69924500
H	-3.53069200	1.71511700	-0.19214700
C	-2.14143200	0.18286400	-0.65482800
O	-0.92934100	-0.01057700	-1.42286600
C	-0.36083300	-1.15505200	-1.01311200
H	0.16905400	-1.75389000	-1.72405100
N	1.36590600	-0.38749400	-0.32460300
C	1.59843400	0.93682800	-0.38507200
H	0.73910100	1.52436100	-0.69251500

C	2.78580600	1.54554500	-0.08609100
H	2.90990200	2.61665900	-0.14665300
C	3.90193400	0.73947700	0.32183200
O	5.03349600	1.12464400	0.62538600
N	3.59517400	-0.62512300	0.35434700
H	4.34002900	-1.25137100	0.62785500
C	2.37485800	-1.23396700	0.04304600
O	2.26185500	-2.45603200	0.11490800
C	-1.82702800	-0.46577000	0.69423000
C	-0.96648800	-1.66722700	0.26606700
H	-0.20256700	-1.96030000	0.98117500
H	-1.60145100	-2.51327500	0.00258400
H	-1.25108100	0.22631700	1.32057100
H	-2.90978000	-0.42158400	-1.14998200
O	-2.00133600	-2.42978900	-2.05865100
H	-1.92875100	-2.40934400	-3.02087300
C	-1.94439500	3.80318600	0.03670600
H	-1.98229200	4.20415400	-0.98618800
H	-2.91980900	3.97800200	0.51347500
H	-1.17517100	4.33497100	0.59721600
O	-3.05045200	-0.77107000	1.34816900
C	-2.87095900	-1.31494100	2.63742200
H	-3.86331400	-1.45117100	3.06945300
H	-2.36302500	-2.28588100	2.60271200
H	-2.29008600	-0.63845900	3.28070100

dU:OH⁻ Nucleophile, Product $E_{(MP2/6\text{-}311+G(2df,p)//B3LYP/6\text{-}311+G(2d,p))} = -988.465783$ (without ZPVE)

-1 1

O	3.65601100	-1.31362500	-1.34665500
C	4.18885500	-0.59140500	-0.25102700
H	5.10007200	-0.05896600	-0.56233300
H	4.45666900	-1.28161400	0.56211200
C	3.18827500	0.40214400	0.29439900
O	2.91063100	1.41442800	-0.67458300
C	1.68046300	2.05128100	-0.32544500
H	1.16659100	2.24474600	-1.27009900
N	-2.26427000	0.12599200	-0.49239100
C	-2.99640800	0.24679500	-1.61013200
H	-2.42315200	0.51323000	-2.49924600
C	-4.35590500	0.07279200	-1.74161100
H	-4.86423500	0.19144300	-2.68803400
C	-5.11643500	-0.27539900	-0.58083800
O	-6.33797900	-0.46963100	-0.50426700
N	-4.31749100	-0.39162300	0.55811000
H	-4.78907100	-0.63536500	1.41804100
C	-2.92812600	-0.20724000	0.64806600
O	-2.39043400	-0.35840800	1.75516400
C	1.81135100	-0.14677100	0.67281400
C	0.92470600	1.11070900	0.61100300
H	-0.08798700	0.90069100	0.26400100
H	0.87075200	1.56172100	1.60349400
H	1.48998200	-0.87804700	-0.07690600
H	3.63680600	0.84791800	1.19465300
O	1.92256600	3.28312700	0.34086800

H	2.39850400	3.85364900	-0.27392600
C	4.55662500	-2.26619100	-1.85601200
H	5.47858100	-1.79383900	-2.22593000
H	4.83084200	-3.01151400	-1.09535600
H	4.06124200	-2.77241000	-2.68486300
O	1.89608600	-0.76806900	1.94106300
C	0.73750800	-1.54062400	2.25980100
H	0.88081500	-1.90746100	3.27691700
H	-0.18536600	-0.95661100	2.19999200
H	0.65077900	-2.39728600	1.57862600

dU:HCOO$^-\cdots$H$_2$O Nucleophile, Reactant E$_{(MP2/6-311+G(2df,p)//B3LYP/6-311+G(2d,p))}$ = -1177.964089 (without ZPVE)

-1 1

C	-1.70321400	2.09541100	-0.41519300
H	-2.05640400	2.03205400	-1.45022400
H	-2.49302700	2.55298800	0.19583800
C	-1.46172800	0.69936600	0.09571200
O	-0.50451600	0.03278300	-0.76159700
C	0.21007700	-0.93286700	-0.03427500
H	0.06678600	-1.92168000	-0.46114200
N	1.67703000	-0.61505400	-0.18434000
C	2.10754400	0.63454300	-0.53615400
H	1.31277900	1.34963100	-0.70265900
C	3.41386200	0.95754100	-0.67647800
H	3.71533700	1.95438400	-0.95860700
C	4.43468100	-0.03871900	-0.46205900
O	5.64579300	0.11172200	-0.55413800
N	3.90661700	-1.29046900	-0.11247100
H	4.57202700	-2.03251700	0.05777300
C	2.57729900	-1.64343900	0.05782300
O	2.24427400	-2.76399400	0.39796300
C	-0.86788200	0.55345800	1.49591100
C	-0.27094800	-0.85796700	1.41838900
H	0.53312700	-1.05886000	2.12478300
H	-1.07377600	-1.58734300	1.53918000
H	-0.08584800	1.30787700	1.65801300
H	-2.40020100	0.13924100	0.05546900
O	-2.87076200	-0.04815100	-2.83693400
H	-2.00371100	-0.31321500	-2.50713400
H	-3.48158900	-0.65373400	-2.33725000
O	-4.43733200	-1.77046700	-1.39880000
C	-3.84159200	-2.41254800	-0.49834300
O	-2.68595500	-2.24433700	-0.04876500
H	-4.43349200	-3.24652500	-0.03805800
O	-0.51115400	2.88075300	-0.33498000
O	-1.89005200	0.73922000	2.45870800
C	-0.68395100	4.16981100	-0.87936500
H	0.26796500	4.69492500	-0.78902900
H	-0.97033800	4.12309900	-1.93814100
H	-1.45483000	4.73465900	-0.33644200
C	-1.42598500	0.71336400	3.79046200
H	-2.27825300	0.94334300	4.43042000
H	-1.03292500	-0.27224100	4.06776000
H	-0.64050100	1.46461800	3.95686800

dU:HCOO⁻···H₂O Nucleophile, Transition State $E_{(MP2/6-311+G(2df,p)//B3LYP/6-311+G(2d,p))} = -1177.901164$ (without ZPVE)

-1 1

C	-0.98716100	2.71470900	-0.16137000
H	-1.15276800	3.21546100	-1.12676700
H	-1.63169900	3.20240800	0.58480700
C	-1.42833400	1.27874900	-0.26035700
O	-0.73171600	0.62065600	-1.38352500
C	-0.64129600	-0.64833400	-1.14084000
H	-0.05687300	-1.23725100	-1.82089900
N	1.92395100	-0.61770800	-0.49094100
C	2.75101900	0.28177500	-1.05086400
H	2.25659700	1.01312700	-1.68918600
C	4.11167300	0.35872000	-0.88776900
H	4.70933200	1.11500600	-1.37591500
C	4.75865900	-0.59594800	-0.03598400
O	5.96351400	-0.67634600	0.22668500
N	3.85707300	-1.50410700	0.52658400
H	4.24471500	-2.20246300	1.14607600
C	2.47022700	-1.54958600	0.33822700
O	1.81641600	-2.41954600	0.93021300
C	-1.14246400	0.34616000	0.91912200
C	-1.06316000	-1.03560400	0.22588900
H	-0.32254200	-1.71414800	0.65315000
H	-2.05248400	-1.50917000	0.20435600
H	-0.17355300	0.58467500	1.37013900
H	-2.49680500	1.23922100	-0.49175600
O	-2.29737700	-1.40870100	-2.28446900
H	-2.25238100	-0.97376300	-3.14402000
H	-3.16603400	-1.02612600	-1.82963200
O	-4.34040800	-0.36115500	-1.24785900
C	-4.80653000	-0.92372000	-0.19966400
O	-4.30107900	-1.83883900	0.45700300
H	-5.78598700	-0.51177400	0.13800200
O	0.36896100	2.80036300	0.21397400
O	-2.17851400	0.52976100	1.85759000
C	0.83149900	4.12822600	0.31659300
H	1.88230400	4.07982400	0.59911600
H	0.74125900	4.66004300	-0.64085200
H	0.27661500	4.68924100	1.08163700
C	-2.11272900	-0.35686900	2.96375100
H	-2.87454500	-0.02992900	3.67095500
H	-2.33199800	-1.38373600	2.65906800
H	-1.12710700	-0.31714000	3.44490800

dU:HCOO⁻···H₂O Nucleophile, Product $E_{(MP2/6-311+G(2df,p)//B3LYP/6-311+G(2d,p))} = -1177.946398$ (without ZPVE)

-1 1

C	-1.91243700	2.76388600	-0.17477800
H	-2.83435800	2.94993900	-0.74601300
H	-1.90871600	3.43708500	0.69545400
C	-1.92155600	1.33990700	0.33624800
O	-2.10042200	0.42506800	-0.75259600
C	-1.46722800	-0.81645800	-0.45299400
H	-0.77812000	-1.04328200	-1.26740000

N	2.35796900	-0.48757300	-0.53282800
C	3.11950600	-0.14832800	-1.58558200
H	2.57083400	0.30456300	-2.41192900
C	4.47996000	-0.30986900	-1.71659500
H	5.01415900	-0.00548700	-2.60547400
C	5.20766700	-0.90106000	-0.63557500
O	6.42421300	-1.12431300	-0.57190800
N	4.37860800	-1.23723600	0.43732700
H	4.82559600	-1.66125100	1.23846100
C	2.99166900	-1.05237500	0.52911600
O	2.42143700	-1.41150700	1.57320700
C	-0.65439200	0.85280500	1.04024300
C	-0.77968600	-0.66760500	0.89236800
H	0.18193500	-1.17695900	0.93428200
H	-1.43841900	-1.04954400	1.67836700
H	0.23202600	1.20311400	0.50299600
H	-2.76296800	1.25881800	1.04100200
O	-2.44512000	-1.86346300	-0.39087500
H	-2.78474000	-2.03738400	-1.28135000
H	-3.93883500	-1.71120600	0.33480000
O	-4.91086100	-1.72977900	0.58883800
C	-5.61595700	-2.14891000	-0.44811200
O	-5.17938500	-2.47604500	-1.52723100
H	-6.68938300	-2.16818100	-0.20634000
O	-0.78139700	3.00636000	-0.98695400
O	-0.64511600	1.32749400	2.37517300
C	-0.73664100	4.32205800	-1.48250600
H	0.16636200	4.41045400	-2.08648000
H	-1.61104900	4.54707100	-2.11057100
H	-0.69522900	5.06033100	-0.66842000
C	0.64140600	1.23907200	2.98405300
H	0.51010000	1.51499100	4.03123300
H	1.06274800	0.23299500	2.90860000
H	1.34137600	1.93833700	2.51074100

Unimolecular Cleavage (UNI)

Coordinates available from author upon request.

MP2/6-311+G(2df,p) Energetics and B3LYP/6-311+G(2d,p) Geometric Information for UNI Reference Geometries Optimized in the Gas Phase.

C1'–N1 (Å)	E (Hartree)	ΔE (kJ/mol)	P (°)	χ (°)	O5'–H···N1		C2'–H···O2		O2–H···O5'	
					H···Y (Å)	X–H···Y (°)	H···Y (Å)	X–H···Y (°)	H···Y (Å)	X–H···Y (°)
1.400	−834.29176	0.8	161.0	234.9						
1.500	−834.29205	0.0	161.8	228.2						
1.600	−834.28462	19.5	164.7	220.2						
1.700	−834.27564	43.1	195.1	188.0						
1.800	−834.26478	71.6	204.1	184.9						
1.900	−834.25347	101.3	209.4	182.8						
2.000	−834.24269	129.6	213.0	178.8						
2.100	−834.23864	140.2	244.1	167.0	2.017	162.7	2.172	136.6		
2.200	−834.23265	156.0	244.1	163.6	1.965	165.5	2.092	144.0		
2.300	−834.22827	167.5	239.2	162.6	1.923	167.8	2.039	148.4		
2.400	−834.22505	175.9	233.8	162.3	1.889	169.6	1.984	152.3		
2.500	−834.22267	182.2	227.2	161.7	1.869	170.7	1.921	156.1		
2.600	−834.22084	187.0	221.4	161.1	1.847	171.6	1.853	159.9		
2.700	−834.21933	190.9	216.2	160.5	1.828	172.3	1.786	163.7		
2.800	−834.21820	193.9	209.8	159.5	1.815	172.5	1.699	167.9		
2.900	−834.25965	85.1	235.2	131.2	1.999	137.1	0.995		1.717	160.5

MP2/6-311+G(2df,p) Energetics and B3LYP/6-311+G(2d,p) Geometric Information for UNI Reference Geometries Optimized in Water Solvent.

C1'–N1 (Å)	E (Hartree)	ΔE (kJ/mol)	P (°)	χ (°)	C6–H···O5'		C1'–H···O2	
					H···Y (Å)	X–H···Y (°)	H···Y (Å)	X–H···Y (°)
1.400	−834.31273	2.2	167.2	239.2	2.349	162.1		
1.500	−834.31357	0.0	168.3	233.1	2.309	163.4		
1.600	−834.30677	17.8	171.3	228.3	2.271	161.7		
1.700	−834.29661	44.5	179.1	214.6	2.356	144.4		
1.800	−834.28824	66.5	206.7	188.3				
1.900	−834.27806	93.2	209.3	187.0				
2.000	−834.26869	117.8	210.3	186.6				
2.100	−834.26054	139.2	211.8	186.6				
2.200	−834.25653	149.7	5.7	186.8	2.452	133.4		
2.300	−834.25145	163.1	7.2	199.4	2.375	148.9		
2.400	−834.24740	173.7	3.4	235.5	2.541	137.2		
2.500	−834.24501	180.0	176.9	238.5				
2.600	−834.24297	185.4	4.7	239.7				
2.700	−834.24305	185.1	203.3	242.5			2.050	153.8
2.800	−834.24232	187.0	200.2	249.2			1.978	160.1
2.900	−834.24172	188.6	200.9	249.7			1.951	163.0

Active Site (AS) (DFT Region Only)

ONIOM(MPWB1K/6-31G(d,p):PM3) hUNG2 reactant complex (DFT region only)

```
0 1
C        -4.50290000   -2.29760000    0.70360000
C        -3.69230000   -3.54850000    1.05670000
C        -4.21430000   -1.83770000   -0.73430000
C        -4.29910000   -2.96080000   -1.76860000
C        -3.97560000   -2.42450000   -3.14690000
O        -4.78460000   -1.72300000   -3.75920000
N        -2.78840000   -2.74940000   -3.64490000
N        -2.32140000   -3.53650000    0.86860000
C        -1.45360000   -4.64220000    1.13570000
C        -0.12530000   -4.00280000    1.45040000
O         0.09760000   -2.81780000    1.27530000
C        -1.36580000   -5.71060000    0.03820000
C        -0.78570000   -5.21310000   -1.28830000
O        -0.04270000   -6.04350000   -1.88270000
O        -1.08350000   -4.07170000   -1.64800000
N         0.88410000   -4.74520000    2.06750000
C         4.93610000   -2.21970000    0.66920000
C         5.99590000   -1.31760000    1.29050000
C         5.50810000    0.03060000    1.75090000
C         5.03100000    0.97810000    0.84790000
C         5.59600000    0.39960000    3.08140000
C         4.63970000    2.23580000    1.26060000
C         5.22630000    1.66540000    3.50720000
C         4.74300000    2.59280000    2.59990000
O         4.36950000    3.84210000    2.94620000
C         6.42700000   -4.55120000   -1.94140000
C         5.51880000   -4.93830000   -3.12040000
C         5.27180000   -3.81290000   -4.07100000
N         4.06340000   -3.17610000   -4.13340000
C         6.12450000   -3.25900000   -4.97760000
C         4.20540000   -2.25430000   -5.05550000
N         5.43400000   -2.26600000   -5.59410000
C         2.25370000    2.86100000    5.45350000
C         1.28060000    4.04610000    5.40210000
C         0.16790000    3.83040000    4.40330000
C        -1.05510000    3.29310000    4.78160000
C         0.34370000    4.20780000    3.07880000
C        -2.07460000    3.13200000    3.85970000
C        -0.68370000    4.07780000    2.16290000
C        -1.89760000    3.53460000    2.54810000
C        -3.91660000   -3.55920000    5.62250000
C        -2.61360000   -3.90420000    4.91800000
C        -1.71490000   -2.69580000    4.73520000
O        -2.13600000   -1.68370000    4.19520000
N        -0.45580000   -2.82640000    5.15280000
C        -5.62790000    5.39500000   -1.68660000
C        -5.18130000    4.10710000   -2.37490000
C        -4.15530000    3.32050000   -1.62580000
N        -2.83100000    3.65990000   -1.61500000
```

C	-4.33570000	2.14270000	-0.96590000
C	-2.23450000	2.70820000	-0.95680000
N	-3.09910000	1.76570000	-0.53890000
C	1.93980000	0.24700000	2.21610000
C	0.90130000	-0.18560000	3.06870000
N	-0.31680000	-0.29500000	2.48760000
C	-0.56040000	-0.31360000	1.14230000
N	0.53570000	-0.16980000	0.33640000
C	1.72390000	0.16250000	0.88920000
O	1.04450000	-0.47450000	4.27750000
O	-1.70350000	-0.46670000	0.73380000
C	0.61040000	-0.90510000	-1.00660000
C	-0.49430000	-0.62870000	-1.98830000
C	0.13670000	0.20010000	-3.10470000
C	1.63890000	0.12050000	-2.81800000
O	-0.18110000	-0.27290000	-4.34660000
O	1.80190000	-0.55610000	-1.58930000
C	2.23660000	1.50230000	-2.79600000
O	3.61100000	1.49150000	-2.70690000
P	4.53940000	2.97730000	-2.80110000
P	-0.46510000	0.75210000	-5.75170000
O	2.50980000	-4.38410000	-1.78100000
O	3.51550000	-1.91190000	4.81200000
H	-4.15162573	-1.51798258	1.34679754
H	-5.53255794	-2.58765701	0.72750531
H	-3.82021919	-3.66553547	2.11255955
H	-4.05134137	-4.30225343	0.38748773
H	-3.19480979	-1.51285620	-0.73832725
H	-4.99569913	-1.15068250	-0.98394446
H	-3.52852280	-3.66165550	-1.52383002
H	-5.32104711	-3.27677158	-1.79479307
H	-2.00566376	-2.83417104	1.50660052
H	-1.84073293	-5.22614871	1.94442244
H	-0.67348945	-6.44148815	0.40070326
H	-2.37640483	-5.99027217	-0.17478204
H	0.57443558	-5.68747475	2.19488230
H	1.09837408	-4.34161644	2.95699813
H	4.57385196	-2.84495612	1.45833316
H	4.26200691	-1.57446957	0.14558163
H	6.31753399	-1.82316007	2.17698778
H	6.69511352	-1.11593953	0.50606803
H	4.96638751	0.72498966	-0.18972247
H	5.95755887	-0.30829708	3.79767991
H	4.25643297	2.93667737	0.54871708
H	5.31466934	1.92701942	4.54095342
H	6.61955562	-5.46706678	-1.42273790
H	7.23580003	-4.00337488	-2.37801213
H	4.56724736	-5.17620104	-2.69278958
H	6.05639353	-5.67889231	-3.67485128
H	7.13704873	-3.54893438	-5.16623491
H	3.43235721	-1.57315259	-5.34419196
H	5.77567174	-1.65953372	-6.31205478
H	2.78116851	2.88188638	6.38422054
H	1.73962312	1.97311767	5.14970743

H	0.81355267	4.09026313	6.36377375
H	1.84587371	4.88063190	5.04304271
H	-1.21137971	2.99988156	5.79870353
H	1.28605558	4.60419183	2.76298441
H	-3.00296272	2.69452742	4.16245469
H	-0.54015561	4.39830044	1.15217032
H	-2.69102027	3.42726381	1.83826677
H	-3.93326859	-2.51372853	5.84968176
H	-3.99185035	-4.12244726	6.52913659
H	-4.74137824	-3.79870700	4.98431723
H	-2.08884316	-4.56863897	5.57225615
H	-2.88383754	-4.22526056	3.93372779
H	-0.13585104	-3.70407504	5.50961815
H	-5.10544548	5.50339608	-0.75913487
H	-6.68069684	5.35316969	-1.50013544
H	-5.41048826	6.23085990	-2.31824101
H	-6.05055106	3.48435370	-2.41349573
H	-4.70329141	4.41528474	-3.28122773
H	-2.40959037	4.46835574	-2.02586890
H	-5.25798854	1.62177972	-0.81448698
H	-1.18130037	2.67893804	-0.77021415
H	2.86047722	0.62637276	2.60767344
H	2.54266367	0.37107813	0.23267794
H	0.51371950	-1.94589232	-0.77789884
H	-1.21579510	-0.01051458	-1.49617034
H	-0.79189388	-1.56553507	-2.41100312
H	-0.22226342	1.20803950	-3.11486036
H	2.15416799	-0.41896833	-3.58505463
H	1.88571427	1.96173019	-1.89560947
H	2.00542499	1.93939212	-3.74489862
H	3.62320264	-2.02182634	5.75958448

Table A7. *Summary of Important Contacts and Nucleoside Characteristics of the hUNG2 Enzyme–Substrate Complex Optimized with Various DFT Functionals and Basis Sets.*

Method		Gly[a] (Å)	χ[b] (°)	N1[c] (°)	P[d] (°)	Ow–O4 Y···H (Å)	Ow–O4 X–H···Y (°)	N204–O4 Y···H (Å)	N204–O4 X–H···Y (°)	N204–N3 Y···H (Å)	N204–N3 X–H···Y (°)	H268–O2 Y···H (Å)	H268–O2 X–H···Y (°)	On–H148 Y···H (Å)	On–H148 X–H···Y (°)	On–D145 Y···H (Å)	On–D145 X–H···Y (°)	Q144–D145 Y···H (Å)	Q144–D145 X–H···Y (°)	dU–F58 Sep[e] (Å)	dU–F58 Tilt[f] (°)	dU–Y126 Sep[g] (Å)	dU–Y126 Tilt[f] (°)
B3LYP	d[h]	1.591	167.7	16.1	-24.1	1.917	169.0	1.884	168.0	1.954	160.6	1.890	167.2	2.120	155.7	2.051	160.6	1.821	164.2	4.01	15.2	4.46	80.7
	d,p[i]	1.592	167.4	16.0	-23.8	1.922	168.7	1.880	168.2	1.951	160.3	1.886	167.2	2.123	155.8	2.059	160.1	1.814	164.1	4.00	15.3	4.46	80.6
B97-2	d[h]	1.573	168.1	15.7	-24.1	1.939	168.9	1.912	167.8	1.993	160.2	1.901	167.0	2.145	155.2	2.069	161.1	1.830	164.6	4.01	15.2	4.47	81.3
	d,p[i]	1.574	167.8	15.6	-23.8	1.947	168.7	1.911	168.0	1.995	159.8	1.899	166.8	2.147	155.3	2.079	160.6	1.823	164.4	4.00	15.4	4.47	81.2
MPW1K	d[h]	1.546	169.2	15.1	-20.7	1.930	171.4	1.977	164.9	1.987	159.7	1.946	164.8	2.147	155.9	2.110	159.4	1.894	165.6	4.05	16.3	4.60	85.8
	d,p[i]	1.547	168.9	15.0	-20.5	1.936	171.2	1.979	165.1	1.990	159.4	1.946	164.7	2.144	156.1	2.125	158.9	1.889	165.5	4.04	16.5	4.60	85.9
MPWB1K	d[h]	1.532	179.2	15.1	-10.7	1.941	172.4	1.928	165.7	1.869	162.1	1.960	158.8	2.185	151.5	2.112	160.0	1.958	163.7	4.07	14.0	4.50	83.0
	d,p[i]	1.533	179.2	15.1	-26.7	1.950	172.2	1.928	166.0	1.866	162.2	1.962	158.6	2.187	151.8	2.122	159.6	1.958	163.4	4.06	13.9	4.51	83.3
BB1K	d[h]	1.534	179.3	15.1	-26.6	1.948	172.8	1.929	165.7	1.872	162.2	1.957	159.3	2.192	151.6	2.112	160.4	1.959	163.8	4.07	14.0	4.52	83.2
	d,p[i]	1.535	179.2	15.1	-25.0	1.956	172.7	1.928	165.8	1.867	162.2	1.957	159.0	2.192	151.8	2.122	159.9	1.960	163.5	4.07	13.9	4.52	83.3
B1B95	d[h]	1.560	168.6	15.5	-26.4	1.947	167.9	1.938	167.3	1.977	160.9	1.935	160.0	2.150	154.8	2.084	160.6	1.872	164.4	3.94	17.3	4.43	81.4
	d,p[i]	1.560	167.8	15.2	-26.0	1.945	168.0	1.934	167.9	1.973	160.7	1.944	159.8	2.148	155.8	2.089	160.8	1.865	164.1	4.02	16.3	4.42	81.2
M06-2X	d[h]	1.558	165.7	15.8	-27.7	1.971	165.4	1.926	164.4	1.996	156.7	2.049	142.6	2.086	157.2	2.097	156.9	1.882	163.6	3.63	28.3	4.39	79.3
	d,p[i]	1.556	164.6	15.5	-28.1	1.987	165.6	1.936	164.6	2.015	155.0	2.119	134.1	2.091	157.0	2.102	156.8	1.878	163.3	3.88	18.3	4.38	78.4
ωB97X-D	d[h]	1.561	168.6	16.0	-27.6	1.941	167.6	1.897	167.0	1.955	159.9	1.889	163.6	2.076	156.1	2.095	157.8	1.848	164.6	3.77	11.0	4.42	80.5
	d,p[i]	1.562	168.4	15.8	-27.1	1.949	167.4	1.892	167.3	1.948	159.8	1.887	164.0	2.072	156.5	2.108	157.4	1.844	164.5	3.76	11.0	4.42	80.5

[a] Glycosidic bond length of dU. [b] Dihedral angle about the glycosidic bond. [c] Out-of-plane angle about N1 of dU. [d] Pseudorotational angle of the dU deoxyribose sugar moiety. [e] Distance between the plane of uracil and the center of the phenylalanine ring. [f] Interplanar angle between the two ring systems. [g] Distance between the plane of the tyrosine ring and the center of the uracil ring. [h] 6-31G(d) basis set. [i] 6-31G(d,p) basis set.

Appendix B: Supplemental Information for Chapter 3:

Monofunctional Glycosylases Part 1:

Human Uracil–DNA Glycosylase (hUNG2)

Table of Contents

Table B1. *Full list of residues and water molecules in the hUNG2 ONIOM model.*

Residue	Backbone	Sidechain	Group	Backbone	Nucleobase
Leu142[a]	Low	--	dG3 – O3'	Low	--
Gly143	Low		dT4	Low	--
Gln144	Low	**High**	P2U5	**High**	**High**
Asp145	**High**	**High**	dA6	Low	--
Pro146	Low	Low	dT7 – PO3	Low	--
Tyr147	Low	**High**			
His148	Low	**High**	W600	**High**	
Gly149	Low		W602	Low	
Gln152	Low	Low	W606	Low	
Ala153	Low	Low	W607	Low	
Leu156	Low	--	W615	Low	
Cys157	Low	Low	W617	Low	
Phe158	Low	**High**	W624	Low	
Ser159	Low	--	W655	Low	
Pro167	Low	Low	W702	Low	
Pro168	Low	Low	W722	Low	
Ser169	Low	Low	W723	Low	
Leu170	Low	Low	W724	Low	
Ile173	--	Low	W725	Low	
Leu203	Low	--	W726	Low	
Asn204	Low	**High**	W727	**High**	
Ala205	Low	Low	W728	Low	
Val206	Low	Low	W748	Low	
Thr208	Low	--	W757	Low	
Val209	Low	Low			
Gln213	Low	--			
Ala214	Low	Low			
Asn215	Low	Low			
Trp245	Low	Low			
Gly246	Low				
Tyr248	Low	Low			
Ala249	Low	Low			
His268	Low	**High**			
Pro269	Low	Low			
Ser270	Low	Low			
Ser273	Low	Low			

[a] Residue numbering from 1EMH crystal structure.
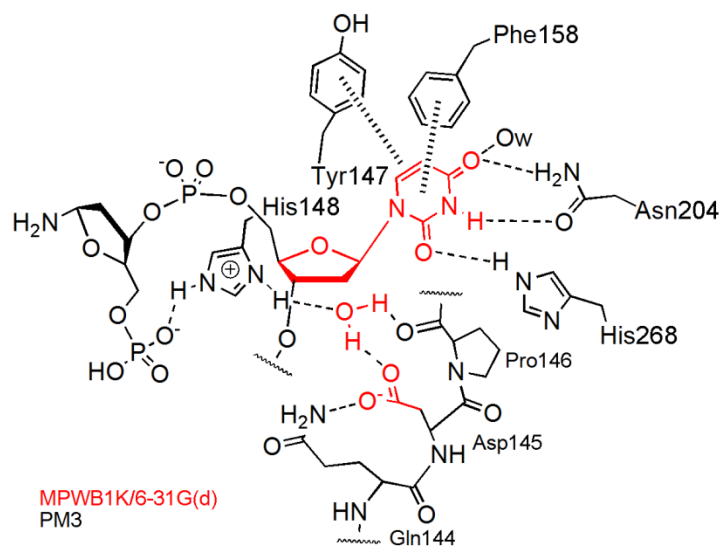
Figure B1. *Definition of reduced high-level region used on the* $wat_{Asp}^{Pro}(+)$ *geometries to reproduce previous work.*

Table B2. ONIOM(MPWB1K/6-31G(d):PM3) Optimization Energies (kJ mol^{-1}) for the **wat$_{Asp}^{Pro}$** PES.

Nucleophile-C1' Distance (Å)	Glycosidic Bond Length (Å)											
	1.30	1.50	1.70	1.90	2.10	2.30	2.50	2.70	2.90	3.10	3.30	3.50
1.20									99.8	90.0	86.9	90.0
1.40						81.0	28.6	–1.1	–16.7	–23.6	**–24.7**	–23.2
1.60						53.8	16.0	–3.4	–12.1	–14.5	–12.8	–9.1
1.80					86.7	43.4	15.9	2.1	–3.6	–4.0	–1.5	2.8
2.00			88.1	94.9	62.4	33.6	14.6	5.0	2.1	3.3	6.5	
2.20		41.8	33.9	58.9	42.9	25.0	12.3	5.8	4.9	6.9	10.1	
2.40	86.7	32.6	31.9	36.6	30.6	19.7	11.3	7.3	7.2	10.0	14.0	
2.60	86.7	10.0	15.1	26.1	**25.4**	18.5	12.8	10.6	11.4	14.7	18.4	
2.80	73.8	2.0	9.8	23.4	25.4	20.8	16.4	15.3	16.6	20.1	23.9	
3.00	68.1	**0.0**	9.0	24.2	27.7	24.4	20.8	20.6	22.6	27.0	30.9	
3.20	67.7	1.5	10.6	26.7	30.6	28.1	25.7	25.8	26.6	27.6	31.3	
3.40	70.0	3.3	12.5	29.3	34.7	33.2	31.4	26.6	25.9	28.4	32.0	

Table B3. ONIOM(MPWB1K/6-31G(d):PM3) Optimization Energies (kJ mol^{-1}) for the **wat$_{Asp}^{His}$** PES.

Nucleophile-C1' Distance (Å)	Glycosidic Bond Length (Å)													
	1.30	1.50	1.70	1.90	2.10	2.30	2.50	2.70	2.90	3.10	3.30	3.50	3.70	3.90
1.20										85.2	*80.0*	*73.0*	67.0	61.0
1.40							54.9	4.3	–18.9	–34.0	–42.6	–49.5	–53.2	**–56.1**
1.60						80.0	44.3	22.0	6.4	–2.9	–22.6	–27.3	–28.9	–30.4
1.80						65.2	36.3	19.4	9.0	3.9	2.8	2.5	5.2	7.5
2.00					74.6	47.2	26.3	15.2	8.6	6.5	7.2	8.1	11.6	13.6
2.20		70.9	62.9	62.4	*60.0*	46.8	31.2	22.7	19.3	4.7	5.7	8.5	11.7	15.5
2.40		61.0	54.7	56.9	48.6	35.2	25.6	21.3	19.7	21.0			14.2	15.2
2.60		28.5	29.3	39.5	39.1	30.4	23.8	20.4	20.2	22.6				15.8
2.80	94.2	12.8	17.6	31.4	34.0	28.6	24.2	22.2	22.8	25.6	29.2	29.8		
3.00	85.5	5.9	12.3	28.3	32.9	29.2	26.2	25.2	26.6	30.2	34.1	38.7		
3.20	81.7	2.6	9.8	26.2	**32.8**	30.3	28.5	29.2	31.6	36.2				
3.40	79.6	0.8	8.0	26.3	33.6	32.9	32.1	33.8	37.3	43.1				
3.60	78.2	**0.0**	9.2	28.5	36.3	37.7	38.2	40.2	44.5	50.4				
3.80	77.9	0.5	11.1	30.6	39.6	41.7	42.5	45.4	50.2	55.1				
4.00	75.7	1.2	12.8	33.5	43.3	45.9	47.0	50.2	56.1	61.1				

Table B4. ONIOM(MPWB1K/6-31G(d):PM3) Optimization Energies (kJ mol⁻¹) for the **wat**$_{Asp}^{Pro}$**(+)** PES.

Nucleophile-C1' Distance (Å)	\ Glycosidic Bond Length (Å)											
	1.30	1.50	1.70	1.90	2.10	2.30	2.50	2.70	2.90	3.10	3.30	3.50
1.20												
1.40									68.7	61.0	59.2	**59.0**
1.60									72.2	66.9	66.3	68.1
1.80									**97.0**	97.6	101.6	106.9
2.00								95.5	92.7	94.1	97.8	103.4
2.20							90.8	85.2	84.2	86.4	90.5	96.4
2.40		80.6	81.3	91.6	91.7	85.4	79.5	76.9	77.5	80.6	85.3	91.1
2.60		46.3	53.9	70.2	75.8	74.5	72.3	71.8	73.8	77.3	82.3	87.4
2.80		26.4	37.7	57.7	67.2	68.8	68.7	69.3	72.3	76.1	80.8	85.2
3.00	88.8	15.7	28.6	50.8	62.2	65.5	66.8	68.7	72.2	75.8	80.5	83.9
3.20	82.5	9.2	23.1	47.3	60.3	64.6	66.4	68.8	72.8	76.6	81.6	84.7
3.40	76.5	5.1	20.5	45.5	59.3	64.4	66.8	69.6	73.6	77.9	82.8	
3.60	73.9	1.7	18.5	45.2	60.0	65.8	68.5	71.3	75.2		84.1	
3.80	71.3	**0.0**	17.7	45.9	60.8	66.9	69.5	72.5	76.7		85.4	
4.00	70.8	0.2	18.1	46.6	62.4	68.7	71.3	74.2	78.2			

Table B5. ONIOM(MPWB1K/6-31G(d):PM3) Single-Point Energies (kJ mol⁻¹) with a Small Model Region for the **wat**$_{Asp}^{Pro}$**(+)** PES.

Nucleophile-C1' Distance (Å)	\ Glycosidic Bond Length (Å)											
	1.30	1.50	1.70	1.90	2.10	2.30	2.50	2.70	2.90	3.10	3.30	3.50
1.20												
1.40										10.9	**9.5**	11.1
1.60									28.3	20.6	20.3	21.0
1.80								*55.0*	52.0	**51.2**	54.9	63.0
2.00							*55.0*	53.0	49.7	50.3	53.1	60.8
2.20						*48.0*	46.6	38.7	38.0	39.9	42.1	50.3
2.40		62.9	54.3	57.9	50.3	39.7	30.6	25.6	27.2	30.2	33.5	42.3
2.60		25.0	27.2	37.3	34.3	27.6	22.9	**20.9**	24.4	27.4	33.4	42.0
2.80	84.2	6.1	18.9	27.3	**29.2**	25.4	21.8	25.8	31.3	30.7	35.3	43.0
3.00	72.6	0.7	19.2	32.9	32.3	30.1	27.4	28.3	31.6	34.4	41.2	50.6
3.20	*73.7*	4.4	19.1	32.8	37.4	36.2	34.3	37.7	38.1	38.4	50.2	55.9
3.40	74.8	2.5	16.1	32.7	38.5	39.2	37.4	39.7	41.2	44.1	54.3	
3.60	78.9	1.8	13.5	32.5	38.0	38.6	40.6	43.6	42.9		59.0	
3.80	76.5	**0.0**	10.1	33.5	38.9	40.6	42.4	44.0	45.4			
4.00	73.2	-0.7	12.2	34.9	39.5	41.5	44.0	50.2	51.2			

Table B6. *Comparison of Glycosidic and Nucleophilic Distances (Å) and Barrier Heights (kJ mol^{-1}) for Stationary Points from the PES and Relaxed Geometries.*

Model	Reactant		Transition State		Product		$\Delta E^{\ddagger}$
	C1'–N1	C1'–O$_{nuc}$	C1'–N1	C1'–O$_{nuc}$	C1'–N1	C1'–O$_{nuc}$	
			wat$_{Asp}^{Pro}$				
Constrained	1.50	3.00	2.10	2.60	3.30	1.40	25.4
Relaxed	1.537	2.984	1.975	2.727	3.283	1.436	26.7
			wat$_{Asp}^{His}$				
Constrained	1.50	3.50	2.10	3.20	3.90	1.40	32.8
Relaxed	1.545	3.579	2.096	3.088	4.261	1.419	34.8
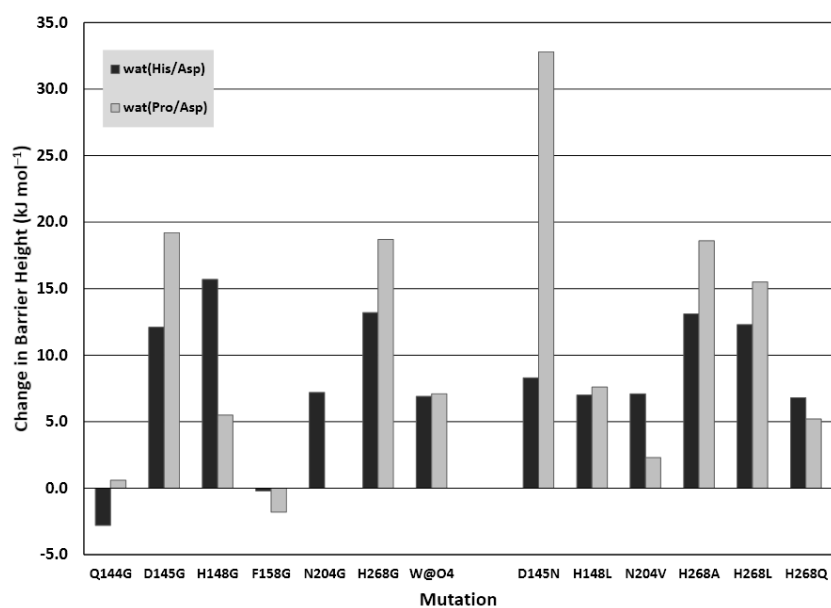
Figure B2. *Comparison of the changes in barrier height determined for the* **wat$_{Asp}^{Pro}$** *(grey bars) and* **wat$_{Asp}^{His}$** *(black bars) models due to point mutations, where a positive value is an increase in barrier.*

Table B7. *Changes in important distances across the reaction potential energy surfaces*

A. Asn204 Hydrogen Bond with O4 of Uracil

wat$_{Asp}^{Pro}$ Surface

Glycosidic Bond Length (Å)

Nucleophile-C1' Distance (Å)	1.30	1.50	1.70	1.90	2.10	2.30	2.50	2.70	2.90	3.10	3.30
1.20									1.933		1.925
1.40						1.926	1.930	1.935	1.927	1.924	**1.917**
1.60					1.936	1.924	1.936	1.928	1.920	1.920	1.920
1.80					1.917	1.914	1.929	1.922	1.923	1.918	1.921
2.00			1.904	1.906	1.907	1.905	1.919	1.919	1.920	1.918	1.923
2.20	1.948	1.915	1.899	1.896	1.895	1.901	1.915	1.921	1.924	1.927	
2.40	1.940	1.903	1.908	1.901	1.898	1.902	1.903	1.913	1.923		
2.60	1.892	1.893	1.916	1.903	**1.899**	1.902	1.904	1.911	1.926	1.930	1.929
2.80	1.868	1.914	1.914	1.911	1.900	1.902	1.905	1.916	1.918	1.932	1.931
3.00	1.824	**1.911**	1.919	1.911	1.901	1.903	1.905	1.915	1.930	1.932	1.934
3.20	1.824	1.913	1.925	1.918	1.902	1.907	1.905	1.925	1.929	1.927	1.923
3.40	1.825	1.917	1.926	1.913	1.901	1.906	1.906	1.916	1.922	1.930	

wat$_{Asp}^{His}$ Surface

Glycosidic Bond Length (Å)

Nucleophile-C1' Distance (Å)	1.30	1.50	1.70	1.90	2.10	2.30	2.50	2.70	2.90	3.10	3.30	3.50	3.70	3.90
1.20									1.878	1.894				
1.40							1.875	1.904	1.884	1.905	1.907	1.905	1.902	**1.913**
1.60						1.875	1.871	1.913	1.915	1.915	1.913	1.908	1.911	1.914
1.80						1.878	1.886	1.906	1.912	1.918	1.918	1.924	1.914	1.916
2.00				1.889	1.889	1.891	1.891	1.899	1.913	1.922	1.921	1.926	1.921	1.933
2.20		1.914	1.900	1.892		1.905	1.913	1.917	1.924	1.914	1.917	1.916	1.926	1.929
2.40		2.029	1.987	1.947	1.912	1.901	1.905	1.912	1.920	1.927			1.932	1.937
2.60		2.023	2.008	1.948	1.915	1.902	1.904	1.910	1.922	1.933				1.925
2.80	2.021	2.009	1.981	1.945	1.914	1.902	1.902	1.910	1.926	1.934		1.925		
3.00	2.026	2.012	1.981	1.947	1.917	1.900	1.903	1.912	1.923	1.935		1.923		
3.20	2.023	2.014	1.982	1.956	**1.915**	1.900	1.902	1.906	1.924	1.936				
3.40	2.028	2.018	1.985	1.945	1.908	1.898	1.904	1.919	1.926	1.936				
3.60	2.023	**2.000**	1.968	1.916	1.898	1.900	1.915	1.928	1.929					
3.80	2.002	1.980	1.949	1.909	1.895	1.898	1.926	1.927	1.928					

B. His268 Hydrogen Bond with O2 of Uracil

wat$_{Asp}^{Pro}$ Surface

Glycosidic Bond Length (Å)

Nucleophile-C1' Distance (Å)	1.30	1.50	1.70	1.90	2.10	2.30	2.50	2.70	2.90	3.10	3.30
1.20									1.843		1.910
1.40						1.837	1.836	1.837	1.844	1.909	**1.909**
1.60					1.834	1.827	1.827	1.830	1.814	1.888	1.890
1.80					1.841	1.827	1.828	1.827	1.819	1.877	1.891
2.00			1.945	1.864	1.845	1.829	1.827	1.831	1.823	1.879	1.888
2.20	2.024	1.974	1.943	1.880	1.852	1.830	1.817	1.827	1.837	1.882	
2.40	2.026	1.938	1.918	1.889	1.868	1.840	1.835	1.829	1.837		
2.60	1.968	1.946	1.921	1.891	**1.872**	1.848	1.838	1.836	1.846	1.849	1.850
2.80	1.968	1.950	1.927	1.895	1.874	1.857	1.842	1.838	1.840	1.851	1.849
3.00	1.916	1.956	1.927	1.894	1.875	1.861	1.844	1.837	1.847	1.847	1.850
3.20	1.918	**1.960**	1.931	1.896	1.875	1.851	1.841	1.842	1.850	1.839	1.842
3.40	1.923	1.958	1.930	1.894	1.874	1.851	1.844	1.853	1.838	1.844	

wat$_{Asp}^{His}$ Surface

Glycosidic Bond Length (Å)

Nucleophile-C1' Distance (Å)	1.30	1.50	1.70	1.90	2.10	2.30	2.50	2.70	2.90	3.10	3.30	3.50	3.70	3.90
1.20									1.811	1.805				
1.40							1.855	1.829	1.822	1.820	1.804	1.852	1.867	**1.875**
1.60						1.865	1.864	1.855	1.854	1.850	1.812	1.857	1.864	1.879
1.80						1.871	1.864	1.855	1.851	1.834	1.835	1.864	1.880	1.888
2.00				1.906	1.878	1.868	1.860	1.850	1.832	1.829	1.852	1.887	1.901	1.894
2.20		1.972	1.942	1.907		1.855	1.846	1.831	1.832	1.843	1.887	1.880	1.868	1.865
2.40		1.955	1.937	1.893	1.865	1.857	1.846	1.838	1.836	1.834			1.893	1.895
2.60		1.966	1.943	1.901	1.871	1.861	1.851	1.837	1.835	1.844				1.878
2.80	1.960	1.966	1.949	1.904	1.874	1.862	1.850	1.838	1.832	1.844		1.841		
3.00	1.957	1.967	1.950	1.908	1.876	1.863	1.850	1.838	1.831	1.842		1.866		
3.20	1.958	1.968	1.953	1.914	**1.877**	1.863	1.848	1.829	1.830	1.839				
3.40	1.959	1.970	1.954	1.907	1.874	1.859	1.836	1.827	1.835	1.862				
3.60	1.960	**1.968**	1.943	1.892	1.869	1.848	1.821	1.822	1.832					
3.80	1.976	1.967	1.938	1.888	1.865	1.834	1.823	1.826	1.843					

C. Water Hydrogen Bond with O4 of Uracil

$\text{wat}_{\text{Asp}}^{\text{Pro}}$ Surface

Glycosidic Bond Length (Å)

Nucleophile-C1' Distance (Å)	1.30	1.50	1.70	1.90	2.10	2.30	2.50	2.70	2.90	3.10	3.30
1.20									1.887		1.887
1.40						1.899	1.895	1.892	1.887	1.894	**1.888**
1.60					1.915	1.901	1.894	1.886	1.878	1.893	1.891
1.80					1.912	1.899	1.895	1.887	1.887	1.866	1.897
2.00			1.934	1.928	1.913	1.900	1.901	1.895	1.890	1.898	1.899
2.20	1.965	1.952	1.935	1.928	1.915	1.904	1.900	1.902	1.902	1.905	
2.40	1.959	1.954	1.942	1.926	1.918	1.905	1.900	1.897	1.903		
2.60	1.959	1.950	1.944	1.926	**1.921**	1.909	1.902	1.897	1.906	1.902	1.899
2.80	1.964	1.953	1.941	1.934	1.921	1.910	1.905	1.899	1.895	1.903	1.899
3.00	1.955	**1.952**	1.946	1.935	1.925	1.913	1.906	1.898	1.904	1.902	1.899
3.20	1.955	1.950	1.948	1.942	1.924	1.913	1.904	1.908	1.904	1.891	1.889
3.40	1.957	1.954	1.950	1.936	1.925	1.914	1.907	1.905	1.898	1.892	

$\text{wat}_{\text{Asp}}^{\text{His}}$ Surface

Glycosidic Bond Length (Å)

Nucleophile-C1' Distance (Å)	1.30	1.50	1.70	1.90	2.10	2.30	2.50	2.70	2.90	3.10	3.30	3.50	3.70	3.90
1.20									1.871	1.873				
1.40							1.873	1.897	1.879	1.883	1.874	1.877	1.877	**1.889**
1.60						1.887	1.884	1.915	1.908	1.900	1.883	1.882	1.883	1.894
1.80						1.895	1.896	1.908	1.905	1.900	1.897	1.910	1.899	1.902
2.00			1.916	1.914		1.908	1.904	1.906	1.900	1.899	1.905	1.912	1.908	1.915
2.20		1.961	1.935	1.921		1.927	1.919	1.912	1.913	1.901	1.908	1.900	1.907	1.906
2.40		1.987	1.967	1.953	1.939	1.925	1.916	1.911	1.908	1.900			1.915	1.910
2.60		1.976	1.961	1.946	1.939	1.922	1.915	1.909	1.908	1.909				1.895
2.80	2.006	1.979	1.962	1.943	1.937	1.921	1.914	1.910	1.906	1.909		1.900		
3.00	2.007	1.978	1.961	1.942	1.937	1.921	1.913	1.911	1.906	1.909		1.899		
3.20	2.009	1.979	1.961	1.945	**1.937**	1.922	1.912	1.904	1.904	1.910				
3.40	2.006	1.978	1.960	1.940	1.933	1.922	1.913	1.912	1.914	1.916				
3.60	2.006	**1.971**	1.955	1.941	1.927	1.921	1.914	1.914	1.913					
3.80	1.977	1.957	1.943	1.936	1.927	1.916	1.925	1.916	1.915					

D. Asp145 Hydrogen Bond with the Water Nucleophile

wat_{Asp}^{Pro} Surface

Glycosidic Bond Length (Å)

Nucleophile-C1' Distance (Å)	1.30	1.50	1.70	1.90	2.10	2.30	2.50	2.70	2.90	3.10	3.30
1.20									0.991		0.990
1.40						1.036	1.029	1.024	1.021	1.019	**1.020**
1.60					1.594	1.571	1.559	1.545	1.531	1.526	1.526
1.80					1.727	1.710	1.700	1.696	1.728	1.729	1.737
2.00			1.868	1.850	1.830	1.835	1.832	1.839	1.853	1.863	1.881
2.20	1.916	1.916	1.949	1.990	1.967	1.990	1.974	1.990	2.075	2.136	
2.40	1.913	2.002	2.219	2.255	2.263	2.230	2.242	2.225	2.226		
2.60	1.968	2.032	2.321	2.285	**2.178**	2.167	2.098	2.053	2.022	1.963	1.939
2.80	1.971	2.265	2.236	2.127	2.094	2.075	2.005	1.985	1.915	1.892	1.871
3.00	1.981	**2.285**	2.169	2.108	2.028	1.989	1.960	1.935	1.893	1.863	1.830
3.20	2.005	2.258	2.079	2.022	1.986	1.963	1.925	1.894	1.869	1.764	1.771
3.40	2.043	2.172	2.061	2.000	1.979	1.956	1.881	1.790	1.776	1.765	

wat_{Asp}^{His} Surface

Glycosidic Bond Length (Å)

Nucleophile-C1' Distance (Å)	1.30	1.50	1.70	1.90	2.10	2.30	2.50	2.70	2.90	3.10	3.30	3.50	3.70	3.90
1.20									1.860	1.856				
1.40								2.026	2.051	2.036	2.037		2.047	**2.039**
1.60						1.568	1.624	2.144	2.281			2.044	2.187	2.194
1.80						1.842	2.016	2.267	2.295					
2.00				1.896	2.023	2.206	2.297	2.334	2.367					
2.20		1.918	1.951	2.061		2.323	2.337	2.373	2.378					
2.40		2.525	2.453	2.436	2.422	2.377	2.365	2.265	2.246	2.202			2.103	2.088
2.60		2.401	2.358	2.330	2.276	2.225	2.192	2.151	2.134	2.110				2.025
2.80	2.356	2.311	2.275	2.251	2.196	2.155	2.127	2.093	2.076	2.061				
3.00	2.292	2.241	2.211	2.194	2.136	2.124	2.099	2.068	2.056	2.043		2.051		
3.20	2.211	2.177	2.152	2.123	**2.113**	2.111	2.097	2.074	2.057	2.041		2.032		
3.40	2.150	2.140	2.111	2.116	2.115	2.091	2.068	2.050	2.031	2.015				
3.60	2.132	**2.129**	2.110	2.127	2.108	2.073	2.073	2.055	2.000					
3.80	2.130	2.107	2.089	2.095	2.095	2.055	2.046	2.021	1.954					

E. His148 Hydrogen Bond with the Water Nucleophile

$\text{wat}^{\text{His}}_{\text{Asp}}$ Surface

Nucleophile-C1' Distance (Å)	Glycosidic Bond Length (Å)													
	1.30	1.50	1.70	1.90	2.10	2.30	2.50	2.70	2.90	3.10	3.30	3.50	3.70	3.90
1.20									1.032	1.032				
1.40								1.047	1.048	1.047	1.048	1.046	1.046	**1.045**
1.60						2.598	2.349	1.739	1.620	1.523	1.071	1.069	1.067	1.066
1.80						2.217	1.981	1.796	1.766	1.718	1.688	1.674	1.657	1.638
2.00				2.420	2.170	1.999	1.922	1.857	1.826	1.795	1.792	1.781	1.780	1.772
2.20		2.515	2.394	2.188		2.144	2.118	2.078	2.066	1.884	1.883	1.881	1.891	1.887
2.40		2.229	2.181	2.166	2.156	2.136	2.111	2.141	2.124	2.097			1.977	1.916
2.60		2.189	2.160	2.132	2.201	2.199	2.192	2.175	2.166	2.147				1.942
2.80	2.172	2.153	2.134	2.122	2.186	2.190	2.185	2.162	2.155	2.151		2.132		
3.00	2.128	2.137	2.120	2.106	2.168	2.156	2.158	2.164	2.165	2.165		2.162		
3.20	2.125	2.135	2.121	2.166	**2.167**	2.151	2.149	2.156	2.163	2.171				
3.40	2.136	2.145	2.192	2.173	2.164	2.166	2.174	2.181	2.195	2.205				
3.60	2.145	**2.142**	2.160	2.137	2.144	2.169	2.160	2.170	2.224					
3.80	2.165	2.185	2.199	2.175	2.168	2.200	2.195	2.216	2.303					

F. Closest Contact Distance between Uracil and Phe158

wat_{Asp}^{Pro} Surface

Glycosidic Bond Length (Å)

Nucleophile-C1' Distance (Å)	1.30	1.50	1.70	1.90	2.10	2.30	2.50	2.70	2.90	3.10	3.30
1.20									3.9		3.5
1.40						4	3.9	3.9	3.9	3.7	3.6
1.60					4	4	3.9	4	3.8	3.6	3.6
1.80					4	4	3.9	3.9	3.8	3.6	3.6
2.00			4.1	4	4	4	3.9	3.9	3.8	3.6	3.6
2.20	4.1	4.1	4.1	4	4	4	4	3.9	3.8	3.8	
2.40	4.1	4.1	4.1	4.1	4.1	4	4	3.9	3.9		
2.60	4.1	4.1	4.1	4.1	4.1	4	4	3.9	3.9	3.9	3.8
2.80	4.1	4.1	4	4.1	4.1	4	4	3.9	3.9	3.9	3.8
3.00	4.2	4.1	4	4	4.1	4	4	3.9	3.9	3.9	3.8
3.20	4.2	4	4	4.1	4.1	4	4	3.9	3.9	4	3.9
3.40	4.2	4	4.1	4.1	4.1	4	4	4	4	3.9	

wat_{Asp}^{His} Surface

Glycosidic Bond Length (Å)

Nucleophile-C1' Distance (Å)	1.30	1.50	1.70	1.90	2.10	2.30	2.50	2.70	2.90	3.10	3.30	3.50	3.70	3.90
1.20									4.2	4.1				
1.40							4	4.1	4.2	4.1	3.9	3.8	3.7	3.7
1.60						4.1	4.1	4.1	4.1	4.1	4	3.8	3.7	3.6
1.80						4.1	4.1	4.1	4	4	4	3.9	3.7	3.6
2.00				4.1	4.1	4.1	4.1	4	4	3.9	3.9	3.8	3.6	3.5
2.20		4.1	4.1	4.1		4.1	4	4	4	4	3.8	3.6	3.6	3.4
2.40		4.1	4.1	4.1	4.1	4.1	4	4	3.9	3.9			3.6	3.6
2.60		4.1	4.1	4.1	4.1	4.1	4	4	3.9	3.9				3.7
2.80	4.1	4.1	4.1	4.1	4.1	4.1	4	4	3.9	3.9		3.7		
3.00	4.1	4.1	4.1	4.1	4.1	4.1	4	4	3.9	3.9		3.6		
3.20	4.1	4.1	4.1	4.1	4.1	4.1	4	4	3.9	3.9				
3.40	4.2	4.1	4.1	4.1	4.1	4.1	4	3.9	3.9	3.8				
3.60	4.1	4.1	4.1	4.1	4.1	4	4	4	3.8					
3.80	4.1	4.1	4	4	4.1	4	4	4	4					

Coordinates for the DFT region relaxed stationary points characterized for the $\text{wat}^{\text{Pro}}_{\text{Asp}}$ model.

$\text{wat}^{\text{Pro}}_{\text{Asp}}$ Reactant Complex

C	-4.215765	-1.829547	-0.721593	H
C	-4.320547	-2.957529	-1.748875	H
C	-3.993284	-2.427514	-3.129111	H
O	-4.804640	-1.728112	-3.740176	H
N	-2.805792	-2.749453	-3.625304	H
N	-2.327961	-3.525851	0.900366	H
C	-1.471289	-4.635906	1.179033	H
C	-0.136425	-3.998454	1.468594	H
O	0.101057	-2.821585	1.268168	H
C	-1.412919	-5.734743	0.105265	H
C	-0.864655	-5.263390	-1.244058	H
O	-0.070822	-6.054030	-1.821076	H
O	-1.220951	-4.147620	-1.633387	H
C	5.991104	-1.331706	1.302730	H
C	5.501218	0.019140	1.755776	H
C	5.026792	0.962195	0.846646	H
C	5.598833	0.397629	3.082665	H
C	4.653728	2.228527	1.250201	H
C	5.245803	1.671353	3.499436	H
C	4.769649	2.596500	2.585907	H
O	4.411584	3.852960	2.923002	H
C	5.533105	-5.009451	-3.095982	H
C	5.320582	-3.934394	-4.106060	H
N	4.061441	-3.659412	-4.530905	H
C	6.214520	-3.138170	-4.760919	H
C	4.196038	-2.712317	-5.421620	H
N	5.478869	-2.359809	-5.594345	H
C	1.303369	4.072490	5.386440	H
C	0.185791	3.861711	4.392004	H
C	-1.039733	3.333750	4.774848	H
C	0.360426	4.234964	3.066326	H
C	-2.062057	3.174261	3.855437	H
C	-0.667832	4.103299	2.151555	H
C	-1.884484	3.568957	2.541398	H
C	-2.621951	-3.875053	4.946797	H
C	-1.720782	-2.670935	4.756178	H
O	-2.142938	-1.659063	4.217425	H
N	-0.459139	-2.805113	5.165336	H
C	-5.163156	4.112283	-2.400217	H
C	-4.145563	3.315905	-1.650188	H
N	-2.824362	3.665558	-1.597366	H
C	-4.330781	2.114694	-1.035674	H
C	-2.235184	2.696423	-0.958280	H
N	-3.101134	1.733679	-0.593378	H
C	1.894371	0.355332	2.259331	H
C	0.881830	-0.148351	3.102561	H
N	-0.337956	-0.272992	2.527568	H
C	-0.592868	-0.261662	1.182476	H
N	0.491993	-0.059657	0.376585	H

C	1.665438	0.317841	0.932251	H
O	1.050321	-0.473487	4.300087	H
O	-1.732210	-0.443559	0.776568	H
C	0.623396	-0.814498	-0.956192	H
C	-0.466492	-0.645293	-1.976142	H
C	0.153710	0.171492	-3.106694	H
C	1.656745	0.082250	-2.824884	H
O	-0.185715	-0.306216	-4.340604	H
O	1.805030	-0.400061	-1.507923	H
C	2.281235	1.444205	-2.965976	H
O	3.643420	1.440737	-2.749973	H
O	1.564709	-3.337440	-2.241559	H
O	3.533380	-1.906969	4.801716	H
H	-4.923728	-1.042964	-1.035990	H
H	-3.204925	-1.411666	-0.794906	H
H	-3.643054	-3.767777	-1.489050	H
H	-5.344803	-3.341866	-1.791174	H
H	-2.156023	-3.306203	-3.088048	H
H	-2.532793	-2.391723	-4.551351	H
H	-1.884359	-2.677442	0.598864	H
H	-1.777571	-5.128018	2.113595	H
H	-0.807142	-6.578181	0.448768	H
H	-2.439072	-6.119806	-0.000379	H
H	6.483462	-1.836716	2.151225	H
H	6.786498	-1.169696	0.554369	H
H	4.947933	0.701815	-0.205416	H
H	4.275799	2.955681	0.537650	H
H	5.952762	-0.315904	3.815235	H
H	5.349836	1.944273	4.542145	H
H	4.480528	3.998245	3.883106	H
H	5.960039	-5.905781	-3.575666	H
H	4.532082	-5.308310	-2.745440	H
H	7.286485	-3.052100	-4.714975	H
H	5.872960	-1.636677	-6.231600	H
H	3.371802	-2.238831	-5.944201	H
H	0.880157	4.267463	6.382513	H
H	1.847893	4.990835	5.105184	H
H	-1.203264	3.044817	5.814811	H
H	-3.007652	2.750508	4.167104	H
H	-2.693392	3.486360	1.828388	H
H	-0.528115	4.478577	1.132435	H
H	1.311417	4.645743	2.744524	H
H	-2.093972	-4.700335	5.447410	H
H	-2.853626	-4.212612	3.926438	H
H	-0.121523	-3.625307	5.668100	H
H	0.172590	-2.029836	4.979850	H
H	-6.041547	3.464855	-2.566160	H
H	-4.755294	4.324051	-3.408067	H
H	-1.181063	2.629817	-0.745936	H
H	-2.854156	0.882760	-0.110120	H
H	-5.211671	1.510021	-0.900655	H
H	1.766267	2.110907	-2.259803	H
H	2.037079	1.790281	-3.981569	H
H	2.112044	-0.646940	-3.493027	H

H	-0.161802	1.218778	-3.004268	H
H	-1.369823	-0.200149	-1.589078	H
H	-0.699390	-1.633191	-2.358489	H
H	0.706285	-1.845687	-0.638866	H
H	2.439342	0.524096	0.211863	H
H	2.863389	0.598995	2.656274	H
H	-1.098002	-0.623513	3.114412	H
H	4.068516	-1.416643	5.445937	H
H	2.756371	-1.355767	4.628460	H
H	0.932534	-4.048417	-2.404580	H
H	2.103623	-3.665842	-1.512993	H

$\text{wat}_{\text{Asp}}^{\text{Pro}}$ Transition State Complex

C	-4.225360	-1.823594	-0.716337	H
C	-4.319404	-2.951833	-1.743315	H
C	-3.993795	-2.423306	-3.123281	H
O	-4.802032	-1.724319	-3.738253	H
N	-2.804960	-2.745024	-3.617974	H
N	-2.327545	-3.513916	0.916269	H
C	-1.470810	-4.626876	1.184479	H
C	-0.134621	-3.991839	1.470682	H
O	0.099945	-2.813777	1.270032	H
C	-1.417597	-5.728652	0.111680	H
C	-0.875028	-5.267973	-1.242592	H
O	-0.065631	-6.053336	-1.810641	H
O	-1.245834	-4.165272	-1.649824	H
C	5.989317	-1.327501	1.305596	H
C	5.500226	0.023943	1.756975	H
C	5.018444	0.963805	0.848950	H
C	5.605755	0.405694	3.082347	H
C	4.648871	2.231107	1.251621	H
C	5.253976	1.679724	3.498285	H
C	4.771176	2.602091	2.585693	H
O	4.415003	3.859472	2.920116	H
C	5.533934	-5.003574	-3.093374	H
C	5.312553	-3.920262	-4.093445	H
N	4.048027	-3.615836	-4.482777	H
C	6.205460	-3.146498	-4.776083	H
C	4.179874	-2.677041	-5.383384	H
N	5.465657	-2.355138	-5.593308	H
C	1.297410	4.078230	5.381168	H
C	0.181714	3.866077	4.384272	H
C	-1.045229	3.341380	4.767570	H
C	0.357996	4.233389	3.057217	H
C	-2.066082	3.178188	3.847058	H
C	-0.667022	4.092728	2.139966	H
C	-1.884741	3.561356	2.530044	H
C	-2.618259	-3.870368	4.960380	H
C	-1.720835	-2.662143	4.772410	H
O	-2.154391	-1.647628	4.249215	H
N	-0.452126	-2.794142	5.161298	H
C	-5.173147	4.100368	-2.388168	H

C	-4.084843	3.351495	-1.686344	H
N	-2.771637	3.720190	-1.765990	H
C	-4.191164	2.171276	-1.011901	H
C	-2.109518	2.782820	-1.148724	H
N	-2.919436	1.820248	-0.674990	H
C	1.885029	0.376556	2.256482	H
C	0.888435	-0.138773	3.103707	H
N	-0.339322	-0.266304	2.547490	H
C	-0.619160	-0.165178	1.205360	H
N	0.410733	0.140227	0.384901	H
C	1.591877	0.445717	0.932919	H
O	1.077423	-0.481055	4.302435	H
O	-1.773613	-0.363480	0.817415	H
C	0.804038	-1.081436	-1.115852	H
C	-0.302669	-1.016148	-2.074459	H
C	0.172289	0.005732	-3.103269	H
C	1.691924	0.032020	-2.863975	H
O	-0.150700	-0.351431	-4.375436	H
O	1.906559	-0.610864	-1.602059	H
C	2.242596	1.431048	-2.845127	H
O	3.614974	1.449248	-2.744300	H
O	1.577057	-3.472655	-2.174794	H
O	3.543567	-1.905677	4.794976	H
H	-4.943114	-1.045093	-1.027666	H
H	-3.222383	-1.386768	-0.780307	H
H	-3.637885	-3.758102	-1.481868	H
H	-5.341270	-3.342644	-1.786178	H
H	-2.164501	-3.317295	-3.086472	H
H	-2.543939	-2.402814	-4.552190	H
H	-1.888254	-2.649726	0.650757	H
H	-1.772093	-5.121783	2.119387	H
H	-0.811631	-6.570855	0.457772	H
H	-2.444391	-6.113631	0.011903	H
H	6.479495	-1.832309	2.155391	H
H	6.786318	-1.166407	0.558408	H
H	4.930943	0.699604	-0.201196	H
H	4.264453	2.956785	0.541273	H
H	5.962459	-0.306576	3.814796	H
H	5.361066	1.954288	4.540163	H
H	4.470771	4.004864	3.881186	H
H	5.968217	-5.890762	-3.582773	H
H	4.536829	-5.317375	-2.745004	H
H	7.279653	-3.081603	-4.757495	H
H	5.863577	-1.640017	-6.239191	H
H	3.352580	-2.198040	-5.896419	H
H	0.869569	4.271356	6.375637	H
H	1.841570	4.998015	5.103414	H
H	-1.210716	3.057578	5.808784	H
H	-3.011848	2.755041	4.159075	H
H	-2.689656	3.467843	1.813810	H
H	-0.524796	4.457560	1.117958	H
H	1.310157	4.641364	2.735338	H
H	-2.091265	-4.692962	5.466940	H
H	-2.842312	-4.211072	3.939409	H

H	-0.103087	-3.614048	5.656140	H
H	0.175411	-2.014800	4.965922	H
H	-6.042086	3.425822	-2.474795	H
H	-4.839564	4.288945	-3.427808	H
H	-1.038683	2.736533	-1.034237	H
H	-2.619451	0.992779	-0.172521	H
H	-5.044575	1.559281	-0.775490	H
H	1.757275	1.962671	-2.014965	H
H	1.896143	1.898305	-3.778069	H
H	2.198017	-0.589439	-3.599864	H
H	-0.244258	0.987335	-2.847389	H
H	-1.260608	-0.808751	-1.622624	H
H	-0.331417	-2.002105	-2.533981	H
H	0.906250	-1.882789	-0.410597	H
H	2.367503	0.701381	0.224055	H
H	2.872512	0.568191	2.635666	H
H	-1.087073	-0.630314	3.138696	H
H	4.062527	-1.407831	5.446409	H
H	2.762146	-1.361605	4.608303	H
H	0.999851	-4.231009	-2.338050	H
H	2.252116	-3.810204	-1.576228	H

wat_{Asp}^{Pro} Product Complex

C	-4.211356	-1.832060	-0.730182	H
C	-4.287009	-2.961029	-1.757274	H
C	-3.985653	-2.445691	-3.145564	H
O	-4.798208	-1.750397	-3.748804	H
N	-2.810445	-2.795830	-3.669180	H
N	-2.324905	-3.518489	0.917789	H
C	-1.477792	-4.638285	1.169544	H
C	-0.147171	-4.003776	1.486493	H
O	0.075645	-2.822604	1.308101	H
C	-1.422001	-5.682357	0.043775	H
C	-0.634682	-5.250070	-1.164290	H
O	0.013866	-6.045397	-1.818080	H
O	-0.698783	-3.972961	-1.397579	H
C	5.975471	-1.341326	1.299370	H
C	5.476293	0.006639	1.753737	H
C	5.001811	0.954287	0.849252	H
C	5.578917	0.377395	3.082301	H
C	4.660087	2.227165	1.258728	H
C	5.242084	1.652281	3.505455	H
C	4.779717	2.587363	2.595895	H
O	4.435622	3.845642	2.941244	H
C	5.534344	-4.994278	-3.123792	H
C	5.299813	-3.896716	-4.105992	H
N	4.029843	-3.552107	-4.449386	H
C	6.189732	-3.146262	-4.817105	H
C	4.159783	-2.612601	-5.352127	H
N	5.447294	-2.328997	-5.605866	H
C	1.288562	4.028988	5.416522	H
C	0.167421	3.831641	4.423860	H

C	-1.064211	3.321142	4.807977	H
C	0.347956	4.196448	3.096551	H
C	-2.085359	3.164315	3.886204	H
C	-0.678033	4.066397	2.179928	H
C	-1.899384	3.542525	2.569213	H
C	-2.615955	-3.929027	4.947122	H
C	-1.725546	-2.714229	4.754931	H
O	-2.176026	-1.711158	4.228508	H
N	-0.452502	-2.832818	5.136448	H
C	-5.165158	4.099219	-2.368918	H
C	-3.926679	3.508502	-1.780283	H
N	-2.695072	4.066830	-1.976015	H
C	-3.802024	2.351991	-1.070120	H
C	-1.853515	3.256383	-1.385116	H
N	-2.471674	2.203479	-0.835209	H
C	1.768451	0.642636	2.296251	H
C	0.867234	-0.036592	3.116363	H
N	-0.397802	-0.131508	2.634283	H
C	-0.808058	0.322432	1.401144	H
N	0.055879	1.025326	0.654088	H
C	1.291537	1.147029	1.106282	H
O	1.143125	-0.537654	4.256369	H
O	-1.961864	0.071131	1.015450	H
C	1.006472	-1.409607	-1.332942	H
C	-0.249742	-0.964159	-2.041629	H
C	0.228526	0.021625	-3.114249	H
C	1.750581	0.034221	-2.905389	H
O	-0.146848	-0.352935	-4.383194	H
O	1.985683	-0.489464	-1.617668	H
C	2.293070	1.430031	-2.964478	H
O	3.663438	1.438716	-2.809193	H
O	1.378552	-2.697990	-1.847860	H
O	3.551677	-1.980237	4.774436	H
H	-4.938724	-1.063643	-1.042061	H
H	-3.219933	-1.362626	-0.776674	H
H	-3.597531	-3.762438	-1.490776	H
H	-5.299166	-3.377018	-1.788688	H
H	-2.150440	-3.312780	-3.117678	H
H	-2.523758	-2.414004	-4.585990	H
H	-1.875579	-2.636861	0.727739	H
H	-1.801829	-5.173009	2.073525	H
H	-0.987898	-6.626731	0.382821	H
H	-2.455896	-5.903093	-0.241886	H
H	6.467343	-1.844691	2.149365	H
H	6.772741	-1.173938	0.554015	H
H	4.895959	0.695075	-0.200233	H
H	4.286897	2.961898	0.551490	H
H	5.925025	-0.343931	3.811025	H
H	5.343580	1.917182	4.550437	H
H	4.462020	3.968168	3.906667	H
H	5.976004	-5.868363	-3.629494	H
H	4.542771	-5.324159	-2.774544	H
H	7.265125	-3.107086	-4.828795	H
H	5.853529	-1.611872	-6.249827	H

H	3.330447	-2.108676	-5.837263	H
H	0.868250	4.214434	6.416044	H
H	1.832625	4.950454	5.143724	H
H	-1.230693	3.037002	5.848769	H
H	-3.033308	2.744274	4.196157	H
H	-2.699995	3.440852	1.849485	H
H	-0.530705	4.422103	1.156075	H
H	1.305751	4.592951	2.775315	H
H	-2.090017	-4.745022	5.466388	H
H	-2.829376	-4.279312	3.927315	H
H	-0.098473	-3.643870	5.640876	H
H	0.176922	-2.057906	4.912714	H
H	-5.972104	3.350245	-2.311140	H
H	-4.983202	4.271376	-3.448783	H
H	-0.780624	3.377876	-1.342748	H
H	-2.049707	1.459096	-0.291999	H
H	-4.526643	1.630962	-0.739823	H
H	1.790592	2.004522	-2.176518	H
H	1.992390	1.855767	-3.932869	H
H	2.223844	-0.602507	-3.655285	H
H	-0.169483	1.012097	-2.873876	H
H	-0.922292	-0.497338	-1.334488	H
H	-0.762707	-1.781774	-2.527457	H
H	0.918769	-1.477990	-0.257473	H
H	1.973495	1.689777	0.461214	H
H	2.797812	0.731034	2.593950	H
H	-1.083460	-0.635144	3.191633	H
H	4.053874	-1.471036	5.430231	H
H	2.787432	-1.423258	4.540793	H
H	0.167667	-3.577591	-1.781918	H
H	2.098057	-3.053748	-1.295371	H

wat$_{\text{Asp}}^{\text{His}}$ Reactant Complex.

C	-4.229429	-1.831311	-0.721636	H
C	-4.298486	-2.955439	-1.756227	H
C	-3.976261	-2.410197	-3.132178	H
O	-4.801992	-1.734302	-3.751328	H
N	-2.772912	-2.694384	-3.613662	H
N	-2.327257	-3.536391	0.872378	H
C	-1.462342	-4.644972	1.146508	H
C	-0.128166	-4.007855	1.444565	H
O	0.104082	-2.833481	1.228358	H
C	-1.379082	-5.722554	0.055760	H
C	-0.794054	-5.231676	-1.271837	H
O	-0.031463	-6.052143	-1.855822	H
O	-1.104001	-4.098089	-1.642207	H
C	5.999840	-1.315493	1.300490	H
C	5.529320	0.040229	1.756179	H
C	5.098277	1.002011	0.845100	H
C	5.580349	0.398449	3.091771	H
C	4.705379	2.259627	1.255428	H
C	5.210836	1.665153	3.515686	H

C	4.766415	2.604348	2.600411	H
O	4.393219	3.855223	2.942698	H
C	5.515553	-4.945960	-3.097703	H
C	5.269285	-3.828640	-4.057836	H
N	4.045698	-3.227850	-4.158865	H
C	6.131825	-3.254129	-4.941988	H
C	4.187028	-2.307564	-5.082615	H
N	5.430308	-2.285781	-5.584695	H
C	1.266442	4.063807	5.394975	H
C	0.157958	3.837330	4.392217	H
C	-1.057958	3.278632	4.762695	H
C	0.331994	4.224373	3.070355	H
C	-2.069367	3.101445	3.834354	H
C	-0.687997	4.078382	2.148129	H
C	-1.893141	3.510245	2.524372	H
C	-2.616514	-3.877633	4.935832	H
C	-1.719654	-2.666483	4.724104	H
O	-2.131548	-1.670098	4.153466	H
N	-0.458808	-2.789444	5.151204	H
C	-5.196453	4.100769	-2.378680	H
C	-4.137179	3.318793	-1.669177	H
N	-2.829359	3.715852	-1.624990	H
C	-4.260672	2.078102	-1.118825	H
C	-2.188116	2.735914	-1.055775	H
N	-3.005906	1.720587	-0.727641	H
C	2.032182	0.202044	2.130271	H
C	0.939137	-0.157555	2.952997	H
N	-0.244279	-0.277993	2.302813	H
C	-0.407740	-0.371995	0.940307	H
N	0.733473	-0.308506	0.193200	H
C	1.891280	0.040597	0.799620	H
O	1.008577	-0.379733	4.181149	H
O	-1.525940	-0.506366	0.474883	H
C	0.923893	-1.144810	-1.092340	H
C	-0.173136	-1.132613	-2.110452	H
C	0.198313	-0.015190	-3.074330	H
C	1.721189	0.055833	-2.895038	H
O	-0.182195	-0.314796	-4.354329	H
O	2.043878	-0.669571	-1.721656	H
C	2.230974	1.466670	-2.798729	H
O	3.609365	1.484901	-2.737709	H
O	2.470162	-4.297804	-1.780779	H
O	3.449807	-1.850037	4.843636	H
H	-4.958915	-1.063745	-1.033959	H
H	-3.231438	-1.383420	-0.788564	H
H	-3.601232	-3.748888	-1.496686	H
H	-5.311397	-3.367391	-1.805783	H
H	-2.116375	-3.238242	-3.071356	H
H	-2.502769	-2.336071	-4.541335	H
H	-1.879471	-2.692154	0.559544	H
H	-1.776629	-5.152658	2.069317	H
H	-0.782593	-6.572087	0.400140	H
H	-2.400933	-6.104615	-0.085978	H
H	6.489700	-1.826290	2.146938	H

H	6.794472	-1.162357	0.549250	H
H	5.061124	0.760381	-0.214089	H
H	4.353296	2.998982	0.541982	H
H	5.901349	-0.328692	3.826022	H
H	5.274531	1.920401	4.566057	H
H	4.445214	3.992357	3.904821	H
H	5.950397	-5.806162	-3.629937	H
H	4.538386	-5.267851	-2.706881	H
H	7.172813	-3.425252	-5.148005	H
H	5.846455	-1.609465	-6.262885	H
H	3.417903	-1.629110	-5.433877	H
H	0.834011	4.254509	6.387957	H
H	1.802722	4.987852	5.117162	H
H	-1.223011	2.979668	5.799850	H
H	-3.006445	2.652695	4.136874	H
H	-2.693099	3.411462	1.803210	H
H	-0.552476	4.466191	1.133190	H
H	1.276091	4.658101	2.758188	H
H	-2.074730	-4.693125	5.437934	H
H	-2.847676	-4.226165	3.918759	H
H	-0.115785	-3.600719	5.666676	H
H	0.170963	-2.020906	4.940581	H
H	-6.069416	3.438048	-2.507857	H
H	-4.830263	4.310521	-3.403308	H
H	-1.126395	2.695198	-0.876432	H
H	-2.710717	0.850361	-0.310932	H
H	-5.113682	1.431852	-1.001979	H
H	1.775254	1.929289	-1.912315	H
H	1.856034	2.005412	-3.679994	H
H	2.204214	-0.454601	-3.726513	H
H	-0.251714	0.927376	-2.736460	H
H	-1.173566	-1.078901	-1.716352	H
H	-0.074966	-2.073360	-2.643928	H
H	1.124336	-2.138798	-0.710227	H
H	2.720080	0.134746	0.115287	H
H	2.984609	0.432973	2.570777	H
H	-1.045062	-0.570144	2.860782	H
H	4.000727	-1.368541	5.481186	H
H	2.701379	-1.270764	4.640402	H
H	2.727960	-3.833878	-2.588152	H
H	1.753774	-4.903123	-2.032620	H

wat$_{Asp}^{His}$ Transition State Complex

C	-4.229940	-1.826258	-0.725206	H
C	-4.305168	-2.950428	-1.758649	H
C	-3.977645	-2.412801	-3.134636	H
O	-4.788781	-1.723401	-3.757141	H
N	-2.778645	-2.719058	-3.617839	H
N	-2.327317	-3.526131	0.885224	H
C	-1.463634	-4.636544	1.151652	H
C	-0.128144	-4.000871	1.444817	H
O	0.104611	-2.826431	1.225798	H

C	-1.388440	-5.718219	0.062826	H
C	-0.811556	-5.237220	-1.270711	H
O	-0.037947	-6.051862	-1.850033	H
O	-1.132338	-4.110818	-1.654921	H
C	5.990613	-1.317705	1.305026	H
C	5.505861	0.033295	1.761296	H
C	5.030579	0.978306	0.855506	H
C	5.601540	0.408244	3.089325	H
C	4.651662	2.241240	1.262658	H
C	5.243150	1.678799	3.509883	H
C	4.762841	2.604416	2.599511	H
O	4.401775	3.859465	2.939501	H
C	5.505657	-4.951629	-3.089634	H
C	5.263234	-3.834900	-4.052431	H
N	4.038834	-3.237731	-4.168312	H
C	6.131752	-3.262934	-4.932067	H
C	4.186106	-2.323159	-5.097705	H
N	5.433872	-2.300512	-5.586800	H
C	1.273613	4.064929	5.395523	H
C	0.161773	3.847250	4.395062	H
C	-1.063441	3.313656	4.771269	H
C	0.341525	4.219746	3.069887	H
C	-2.078938	3.146436	3.845443	H
C	-0.681953	4.084843	2.150253	H
C	-1.896773	3.541397	2.532108	H
C	-2.620934	-3.890145	4.944103	H
C	-1.727540	-2.679090	4.744114	H
O	-2.159735	-1.678141	4.195720	H
N	-0.463858	-2.798549	5.154674	H
C	-5.187675	4.096599	-2.378355	H
C	-4.085194	3.357053	-1.688485	H
N	-2.787802	3.784670	-1.708822	H
C	-4.157867	2.138592	-1.080080	H
C	-2.103496	2.845534	-1.118704	H
N	-2.882036	1.824834	-0.722039	H
C	1.896526	0.326589	2.221529	H
C	0.874245	-0.148562	3.059283	H
N	-0.339332	-0.280167	2.472118	H
C	-0.580190	-0.221675	1.117818	H
N	0.477679	0.016551	0.313118	H
C	1.642454	0.329491	0.885775	H
O	1.022938	-0.451294	4.275078	H
O	-1.734890	-0.394439	0.713483	H
C	1.004666	-1.296734	-1.232618	H
C	-0.116786	-1.276179	-2.169206	H
C	0.217219	-0.109887	-3.095712	H
C	1.739484	0.012646	-2.904368	H
O	-0.129638	-0.354074	-4.387736	H
O	2.050090	-0.726589	-1.711308	H
C	2.230804	1.426803	-2.771845	H
O	3.604909	1.471741	-2.743530	H
O	2.283140	-4.051800	-1.789836	H
O	3.476385	-1.888849	4.836239	H
H	-4.958946	-1.056941	-1.034286	H

H	-3.234299	-1.372354	-0.785512	H
H	-3.613948	-3.748926	-1.497379	H
H	-5.320805	-3.356216	-1.807898	H
H	-2.136772	-3.285182	-3.080417	H
H	-2.514632	-2.376231	-4.551548	H
H	-1.886349	-2.666446	0.605303	H
H	-1.772685	-5.144069	2.076602	H
H	-0.792277	-6.567877	0.407339	H
H	-2.412227	-6.098802	-0.070440	H
H	6.482294	-1.825251	2.152313	H
H	6.786659	-1.155710	0.556911	H
H	4.952972	0.719280	-0.196713	H
H	4.267793	2.969491	0.554752	H
H	5.956872	-0.306722	3.819738	H
H	5.342680	1.948025	4.553934	H
H	4.449121	3.994417	3.902398	H
H	5.929209	-5.817096	-3.621760	H
H	4.527284	-5.269194	-2.696653	H
H	7.174735	-3.432882	-5.128095	H
H	5.855300	-1.627276	-6.266710	H
H	3.417557	-1.651595	-5.465249	H
H	0.843638	4.254426	6.389846	H
H	1.812523	4.988078	5.119365	H
H	-1.230829	3.022776	5.810293	H
H	-3.022394	2.713799	4.151359	H
H	-2.698553	3.448725	1.812134	H
H	-0.541505	4.463226	1.132987	H
H	1.292500	4.634623	2.753409	H
H	-2.088303	-4.707883	5.452723	H
H	-2.846446	-4.237328	3.925495	H
H	-0.120566	-3.611555	5.664959	H
H	0.162230	-2.019793	4.954262	H
H	-6.051749	3.414595	-2.453790	H
H	-4.869758	4.289244	-3.422600	H
H	-1.036521	2.846256	-0.965770	H
H	-2.560809	0.985984	-0.250952	H
H	-4.989469	1.479945	-0.899902	H
H	1.775911	1.854628	-1.868993	H
H	1.817927	1.969463	-3.633430	H
H	2.260957	-0.499219	-3.710058	H
H	-0.264270	0.793038	-2.705115	H
H	-1.086524	-1.252854	-1.697493	H
H	-0.032570	-2.215625	-2.717408	H
H	1.172091	-2.063458	-0.496050	H
H	2.444921	0.546409	0.192369	H
H	2.876013	0.522051	2.618507	H
H	-1.102543	-0.621614	3.054988	H
H	4.013922	-1.386771	5.468833	H
H	2.703060	-1.335393	4.643803	H
H	2.676635	-3.748949	-2.619221	H
H	1.639775	-4.736247	-2.031866	H

wat$_{Asp}^{His}$ Product Complex

C	-4.222181	-1.816234	-0.714571	H
C	-4.284643	-2.946155	-1.741600	H
C	-3.967722	-2.432773	-3.127699	H
O	-4.772012	-1.733730	-3.749859	H
N	-2.786719	-2.787355	-3.623915	H
N	-2.343300	-3.516008	0.905688	H
C	-1.471245	-4.632561	1.125334	H
C	-0.136545	-4.001004	1.432180	H
O	0.117711	-2.836399	1.201462	H
C	-1.386786	-5.673834	0.000271	H
C	-0.706330	-5.241225	-1.296754	H
O	0.019964	-6.106764	-1.851703	H
O	-0.915080	-4.091487	-1.718876	H
C	5.971098	-1.354979	1.332321	H
C	5.483384	-0.000431	1.779118	H
C	5.016640	0.944715	0.869363	H
C	5.585752	0.377806	3.105616	H
C	4.676901	2.220596	1.270324	H
C	5.253979	1.656685	3.520315	H
C	4.793201	2.587695	2.605665	H
O	4.449579	3.847967	2.941911	H
C	5.442522	-4.903895	-3.070930	H
C	5.184151	-3.718430	-3.972386	H
N	3.993450	-3.038113	-4.150909	H
C	6.054540	-3.138079	-4.833751	H
C	4.145566	-2.092258	-5.067474	H
N	5.395306	-2.146331	-5.489253	H
C	1.284168	4.061462	5.411258	H
C	0.164348	3.866900	4.417288	H
C	-1.070317	3.363163	4.800212	H
C	0.350758	4.226108	3.089413	H
C	-2.089750	3.207336	3.876359	H
C	-0.672895	4.095030	2.170509	H
C	-1.897838	3.579127	2.558561	H
C	-2.646950	-3.888895	4.967860	H
C	-1.746378	-2.682871	4.776176	H
O	-2.188806	-1.662506	4.274966	H
N	-0.468163	-2.827666	5.130062	H
C	-5.152442	4.099742	-2.394428	H
C	-3.920909	3.500065	-1.798746	H
N	-2.682669	4.052871	-1.972682	H
C	-3.811539	2.330148	-1.107961	H
C	-1.854458	3.224584	-1.385666	H
N	-2.485927	2.167043	-0.860389	H
C	1.763813	0.671150	2.353864	H
C	0.858498	-0.025797	3.154300	H
N	-0.400451	-0.124391	2.660919	H
C	-0.804941	0.335525	1.425572	H
N	0.072903	1.037261	0.684656	H
C	1.295649	1.172211	1.161043	H
O	1.132480	-0.527112	4.295033	H
O	-1.959663	0.108295	1.042502	H

C	1.386259	-1.956150	-2.048016	H
C	0.082799	-1.208352	-2.132124	H
C	0.325625	-0.123170	-3.174443	H
C	1.854697	-0.006903	-3.170173	H
O	-0.162371	-0.445337	-4.422387	H
O	2.383212	-1.037945	-2.358700	H
C	2.334034	1.322553	-2.673671	H
O	3.710406	1.392300	-2.792391	H
O	1.502976	-3.001140	-3.000121	H
O	3.557798	-1.956623	4.793983	H
H	-4.951182	-1.049763	-1.029840	H
H	-3.230914	-1.344925	-0.756720	H
H	-3.586394	-3.736555	-1.470431	H
H	-5.295512	-3.365714	-1.780107	H
H	-2.136797	-3.332134	-3.072172	H
H	-2.504906	-2.423998	-4.544885	H
H	-1.898789	-2.649869	0.652499	H
H	-1.777064	-5.179508	2.028456	H
H	-0.876838	-6.571981	0.360188	H
H	-2.417875	-5.973620	-0.220156	H
H	6.453734	-1.858121	2.187571	H
H	6.775451	-1.196619	0.591674	H
H	4.916551	0.679495	-0.178931	H
H	4.304747	2.952582	0.559956	H
H	5.924397	-0.341138	3.839713	H
H	5.351674	1.926165	4.564374	H
H	4.459366	3.973731	3.907385	H
H	5.852801	-5.707595	-3.698563	H
H	4.480116	-5.285048	-2.692148	H
H	7.094281	-3.332868	-5.018643	H
H	5.853736	-1.505609	-6.190868	H
H	3.413793	-1.367515	-5.487642	H
H	0.863060	4.250137	6.409889	H
H	1.832022	4.980716	5.137906	H
H	-1.240139	3.081832	5.841283	H
H	-3.039343	2.789753	4.184385	H
H	-2.694804	3.474716	1.835429	H
H	-0.522572	4.441363	1.144233	H
H	1.312391	4.616117	2.770436	H
H	-2.124295	-4.709942	5.482405	H
H	-2.862071	-4.234572	3.946177	H
H	-0.119045	-3.651590	5.616527	H
H	0.168586	-2.059139	4.911001	H
H	-5.962783	3.354199	-2.339381	H
H	-4.965378	4.267519	-3.474227	H
H	-0.781485	3.336322	-1.328904	H
H	-2.078057	1.406622	-0.324404	H
H	-4.544471	1.607008	-0.801150	H
H	1.998959	1.447927	-1.642450	H
H	1.843899	2.098738	-3.273847	H
H	2.210843	-0.134692	-4.196795	H
H	-0.120176	0.810892	-2.822588	H
H	-0.114635	-0.751579	-1.168940	H
H	-0.749200	-1.841745	-2.394001	H

H	1.586909	-2.352409	-1.055728	H
H	1.979512	1.739659	0.537096	H
H	2.787880	0.769442	2.666340	H
H	-1.092419	-0.625805	3.215421	H
H	4.023821	-1.435789	5.466206	H
H	2.776300	-1.426443	4.553577	H
H	3.089049	-3.167368	-3.642662	H
H	0.807296	-3.651826	-2.801197	H

Appendix C: Supplemental Information for Chapter 4:

Monofunctional Glycosylases Part 2:

Adenine–DNA Glycosylase (MutY)

Table of Contents

Table C1. *Model contents, layer division and residue charges.*

Residue Name	#	Backbone	R-Group	Charge	Residue Name	#	Backbone	R-Group	Charge
PHE	21	Low	Low	0	LEU	132	Low	CUT	0
ARG	25	Low	Low	1	SER	133	Low	Low	0
ARG	26	Low	Low	1	LEU	134	Low	Low	0
ASP	27	Low	Low	-1	ALA	142	Low	Low	0
LEU	28	Low	Low	0	VAL	143	Low	Low	0
PRO	29	Low	Low	0	**ASP**	**144**	**Low**	**High**	**-1**
TRP	30	Low	Low	0	GLY	145	Low	Low	0
ARG	**31**	**Low**	**High**	**1**	**ASN**	**146**	**Low**	**High**	**0**
LYS	32	Low	CUT	0	VAL	147	Low	Low	0
ASP	33	Low	CUT	0	MET	148	Low	CUT	0
LYS	38	Low	CUT	0	ARG	149	Low	Low	1
VAL	39	Low	Low	0	GLY	184	Low	Low	0
TRP	40	Low	CUT	0	ALA	185	Low	Low	0
VAL	41	Low	CUT	0	PHE	186	Low	CUT	0
SER	42	Low	Low	0	ASN	187	Low	Low	0
GLU	**43**	**Low**	**High**	**0**	**GLU**	**188**	**Low**	**High**	**-1**
VAL	44	Low	CUT	0	ALA	189	Low	Low	0
MET	45	Low	CUT	0	LEU	190	Low	Low	0
LEU	46	Low	Low	0	ILE	191	Low	Low	0
GLN	47	Low	Low	0	GLU	192	Low	Low	-1
GLN	48	Low	Low	0	LEU	193	Low	CUT	0
THR	49	Low	Low	0	GLY	194	Low	Low	0
ARG	50	Low	CUT	0	ALA	195	Low	Low	0
VAL	51	Low	Low	0	LEU	196	Low	Low	0
GLU	52	Low	Low	-1	dC	17	Low	CUT	-1
THR	53	Low	Low	0	**A5L**	**18**	**Phos - Low**	**High**	**-1**
VAL	54	Low	Low	0	dG	19	Low	CUT	-1
ILE	55	Low	Low	0	dT	20	Low	CUT	-1
PHE	58	Low	Low	0	HOH	7		Low	
TYR	**126**	**Low**	**High**	**0**	**HOH**	**371**		**High**	
THR	127	Low	Low	0	HOH	376*		Low	
VAL	128	Low	CUT	0	HOH	26		Low	
GLY	129	Low	Low	0	**HOH**	**28**		**High**	
ALA	130	Low	Low	0	**HOH**	**50**		**High**	
VAL	131	Low	Low	0					

*Only in X-WT and X-D144N models.
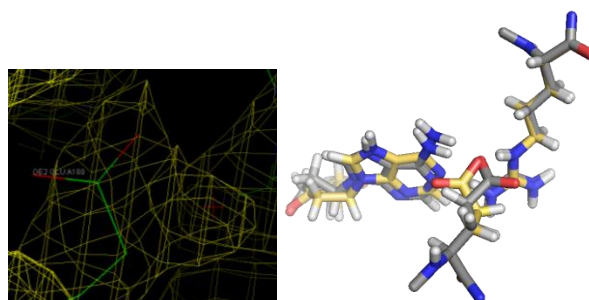
Figure C1. *Electron density and position of E188 in the 3G0Q crystal structure (left). Overlay of the position of E188 in the X-WT (yellow) and CS-Cap (grey) models (right).*
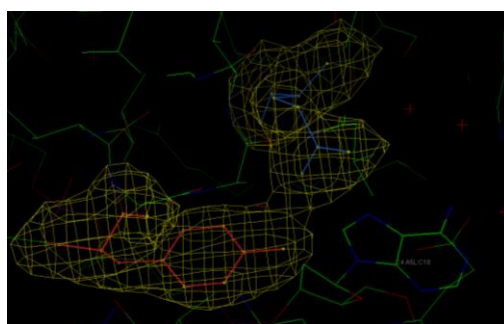
Figure C2. *Electron density assigned to Y126 (red) and E43 (blue) in the 3G0Q crystal structure.*
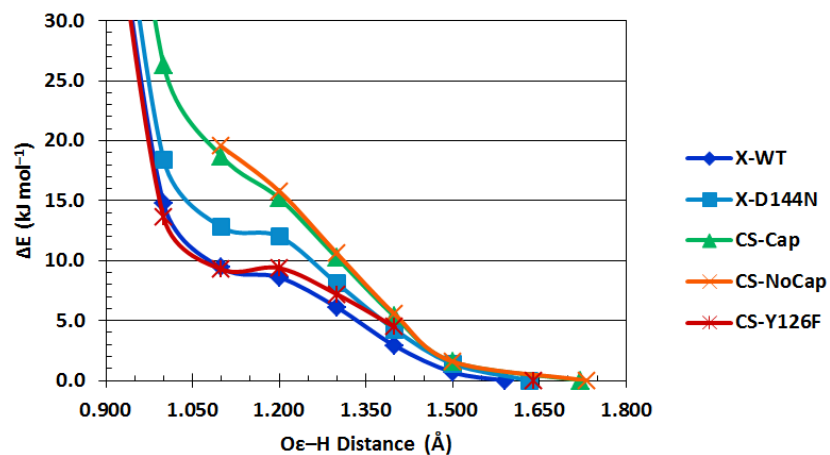
Figure C3. *ONIOM(M06-2X/6-31G(d):PM6) reaction potential energy surface for proton transfer from E43 to N7 of adenine with all models studied. Energies (kJ mol^{-1}) are plotted relative to the corresponding activated reactant complexes.*
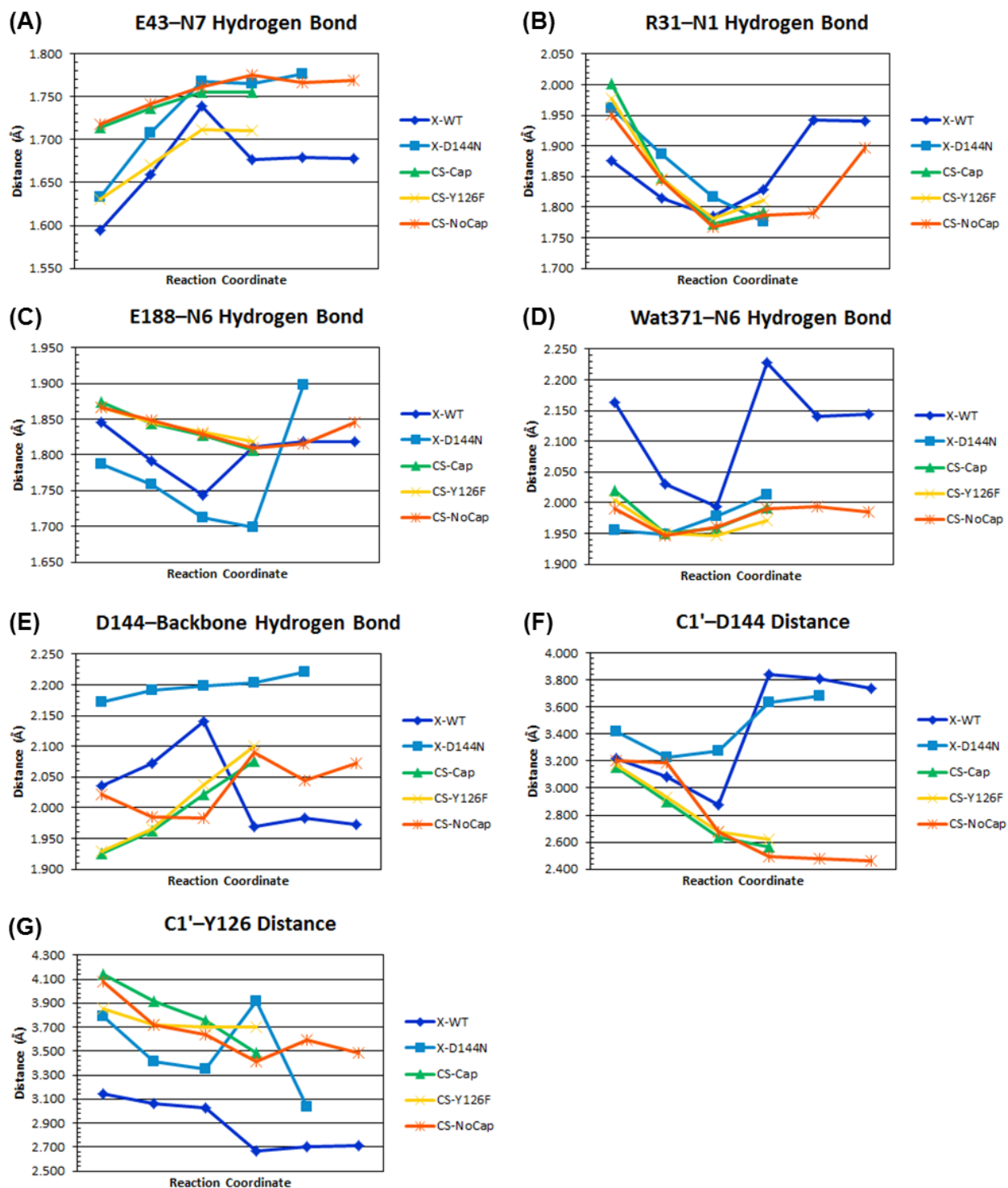
Figure C4. *Select ONIOM(M06-2X/6-31G(d):PM6) distances (Å) along the low energy pathway for the deglycosylation step of Mechanism A with various models. In (E) the CS-NoCap model refers to an interaction with the backbone amine of N146 and all other models refer to the standard helix-capping interaction with V147.*
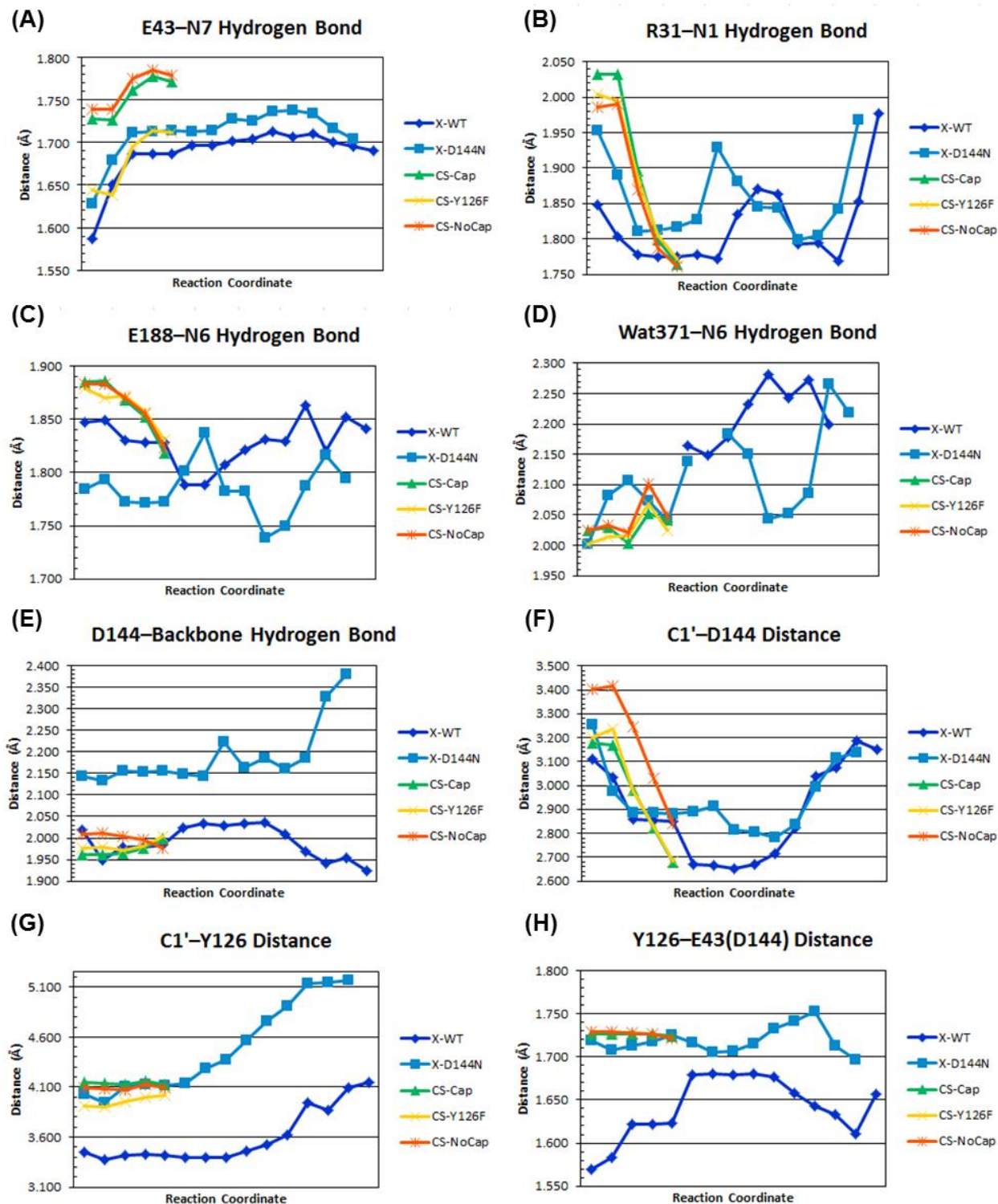
Figure C5. *Select ONIOM(M06-2X/6-31G(d):PM6) distances (Å) along the low energy pathway for Mechanism B with various models. In (E) the CS-NoCap model refers to an interaction with the backbone amine of N146 and all other models refer to the standard helix-capping interaction with V147.*
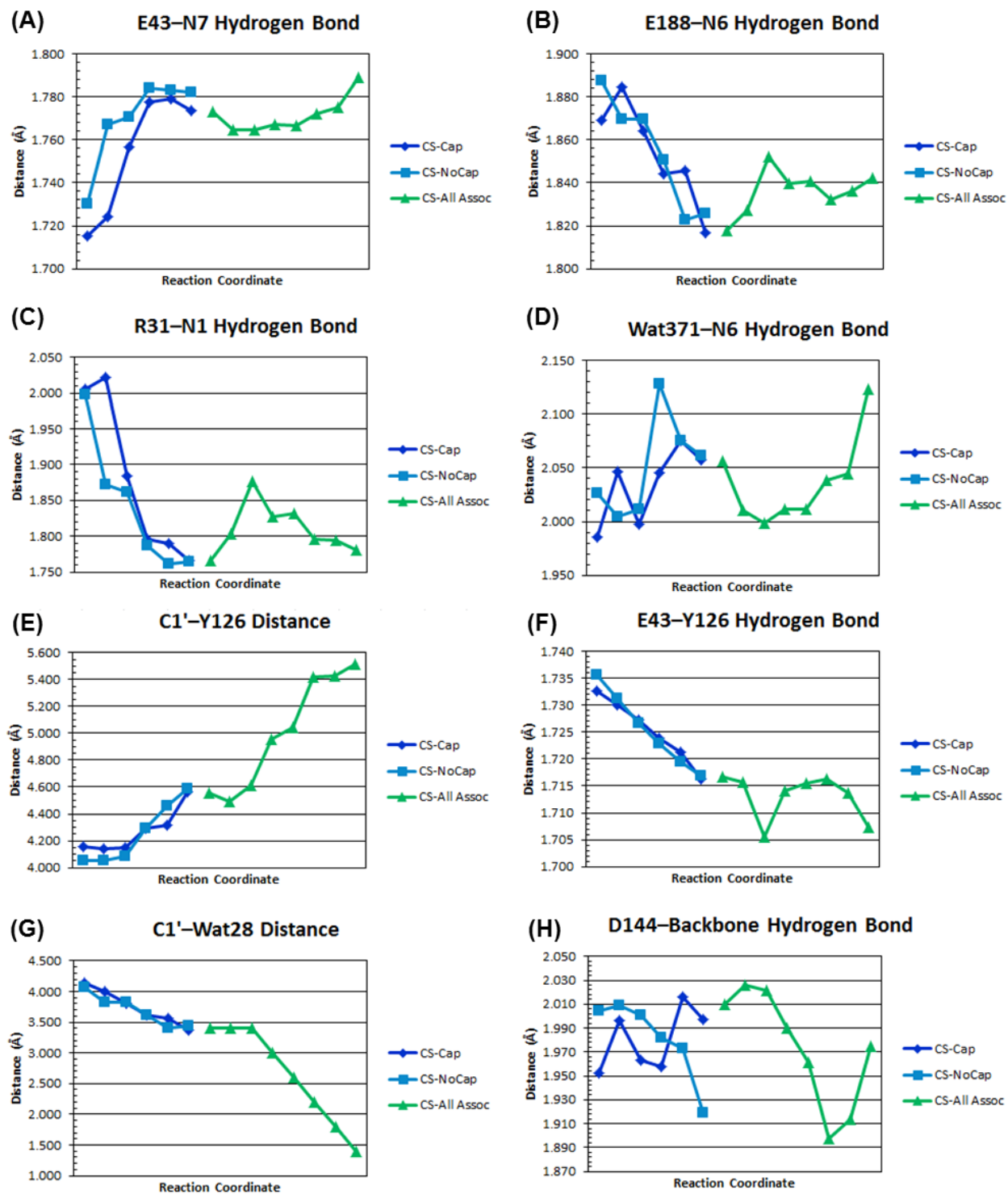
Figure C6. *Select ONIOM(M06-2X/6-31G(d):PM6) distances (Å) along the low energy pathway for Mechanism C with various models. In (H) the CS-NoCap model refers to an interaction with the backbone amine of N146 and all other models refer to the standard helix-capping interaction with V147.*

Full citation for reference 53

Frisch, M. J.; Trucks, G. W.; Schlegel, H. B.; Scuseria, G. E.; Robb, M. A.; Cheeseman, J. R.; Scalmani, G.; Barone, V.; Mennucci, B.; Petersson, G. A.; Nakatsuji, H.; Caricato, M.; Li, X.; Hratchian, H. P.; Izmaylov, A. F.; Bloino, J.; Zheng, G.; Sonnenberg, J. L.; Hada, M.; Ehara, M.; Toyota, K.; Fukuda, R.; Hasegawa, J.; Ishida, M.; Nakajima, T.; Honda, Y.; Kitao, O.; Nakai, H.; Vreven, T.; Montgomery, J., J. A; Peralta, J. E.; Ogliaro, F.; Bearpark, M.; Heyd, J. J.; Brothers, E.; Kudin, K. N.; Staroverov, V. N.; Kobayashi, R.; Normand, J.; Raghavachari, K.; Rendell, A.; Burant, J. C.; Iyengar, S. S.; Tomasi, J.; Cossi, M.; Rega, N.; Millam, N. J.; Klene, M.; Knox, J. E.; Cross, J. B.; Bakken, V.; Adamo, C.; Jaramillo, J.; Gomperts, R.; Stratmann, R. E.; Yazyev, O.; Austin, A. J.; Cammi, R.; Pomelli, C.; Ochterski, J. W.; Martin, R. L.; Morokuma, K.; Zakrzewski, V. G.; Voth, G. A.; Salvador, P.; Dannenberg, J. J.; Dapprich, S.; Daniels, A. D.; Farkas, Ö.; Foresman, J. B.; Ortiz, J. V.; Cioslowski, J.; Fox, D. J.; Revision A.02 and C.01; Gaussian, Inc.: Wallingford CT, **2009**.

Coordinates for the DFT region of the X-WT activated reactant (RC*) (*truncation points capped with H)*
ONIOM(M06-2X/6-31G(d):PM6) E = -2768.07119 Hartrees

```
-1 1
C        7.90678200  -4.26095900  -2.13389800
C        6.42612000  -3.88888800  -1.93214700
C        5.63611400  -3.98076400  -3.23680300
N        4.24361200  -3.62658300  -3.01416100
C        3.40162700  -3.28425500  -3.99636400
N        3.78050900  -3.32075300  -5.27871600
N        2.16670300  -2.91360900  -3.65941900
C        1.53020300   1.43480700   6.36763100
C        1.80876200   0.00275400   5.91365300
C        0.95683800  -0.34536800   4.69748100
O        1.42133000  -1.22531500   3.89284200
O       -0.12843200   0.22978200   4.55891600
C       -6.13835900   0.98819900   7.04317300
C       -5.28426400   0.64132500   5.84434600
C       -5.74928600  -0.23867300   4.87155900
C       -4.00652200   1.18048400   5.68277100
C       -4.99409100  -0.55696800   3.75086000
C       -3.23571100   0.87935200   4.56777000
C       -3.74541000   0.04582100   3.56513200
O       -3.04324200  -0.15352900   2.42674900
C       -6.48398600   1.40734100   1.59875200
C       -5.95573600   0.34612500   0.60699500
O       -6.78456300  -0.30469200  -0.06095800
O       -4.69404600   0.24315300   0.51244700
C       -6.84261400   0.35213300  -3.33956700
C       -6.07052000   1.34542900  -4.22803600
O       -6.31144500   1.37492600  -5.43588500
N       -5.13382300   2.08274500  -3.62805800
C        0.21180300  -6.93094900  -0.85879700
C        1.02383200  -5.84523100  -1.60283400
C        1.53983900  -4.73774300  -0.66969300
O        2.78120000  -4.39681000  -0.83374400
O        0.77170100  -4.30660400   0.18212200
N        1.30672800  -1.20924800  -1.54685700
C        0.38147600  -0.42405800  -2.14620500
N       -0.43566300   0.45793600  -1.60812500
C       -0.33586500   0.48015800  -0.27255000
C        0.53438800  -0.31736700   0.46128800
C        1.44441700  -1.14948700  -0.21445400
N        2.46895400  -1.79990700   0.38838000
N        0.31402300  -0.05611800   1.79234500
C       -0.64266300   0.85530300   1.87254400
N       -1.05381200   1.22771600   0.65635400
C       -2.15944100   2.17994200   0.39384700
C       -2.54711200   3.03377900   1.59870000
C       -3.20279100   4.26168000   0.90722100
O       -4.62296500   4.12495200   0.97087100
C       -2.66002500   4.14733300  -0.56806900
O       -1.68641700   3.09205100  -0.54045100
C       -1.95616800   5.37678600  -1.13330400
O       -1.30599200   5.11234200  -2.35973300
O        3.97129400  -1.73447000   3.23036300
O       -5.60823500   3.84092800  -1.39445300
O       -1.13973300   1.97243400  -4.97539900
H        8.35162000  -3.60575100  -2.91484400
H        7.98917100  -5.28891600  -2.52753300
H        6.33782800  -2.86346100  -1.55433600
H        5.95296300  -4.53206900  -1.18493100
```

H	6.06182000	-3.28146400	-3.97622100
H	5.72411900	-4.98765500	-3.67279100
H	3.75765100	-3.91902400	-2.13338500
H	4.67235500	-3.72558300	-5.56840800
H	3.11311500	-3.10213100	-6.02019300
H	1.51883000	-2.58883900	-4.37546900
H	1.97753200	-2.53117400	-2.71254200
H	2.01918300	1.62938900	7.34212100
H	0.43979900	1.53902600	6.50583200
H	2.86214200	-0.16846400	5.65274300
H	1.56567800	-0.69663300	6.72343900
H	0.70653100	-0.59984000	2.61812500
H	-5.76725700	1.93003800	7.48301900
H	-7.18159400	1.18730000	6.72597100
H	-6.74954900	-0.64766500	4.98561000
H	-3.61692200	1.87285900	6.43138900
H	-5.38998600	-1.21151100	2.97760200
H	-2.24749300	1.31660100	4.45824400
H	-3.70490000	-0.08652500	1.65034500
H	-5.79533100	1.49802400	2.45691600
H	-6.37393400	2.38385600	1.07084900
H	-6.75475000	-0.60845700	-3.87833300
H	-6.38927100	0.21797400	-2.34556600
H	-4.61971300	2.75496400	-4.20791100
H	-5.13812100	2.29769300	-2.63357900
H	0.59160600	-7.03332400	0.17188100
H	0.35385000	-7.90988700	-1.35673900
H	1.87815400	-6.29219100	-2.13577000
H	0.40472200	-5.35578100	-2.37560900
H	-1.16540500	5.70364700	-0.43813800
H	-2.67807900	6.21538000	-1.17505900
H	-3.48289200	3.84898300	-1.22842600
H	-2.86990600	5.21062700	1.36354600
H	-1.64727500	3.36696600	2.12611700
H	-3.24537800	2.56371500	2.28705500
H	-3.01305300	1.59600100	0.03001700
H	-1.02815500	1.22486500	2.80690400
H	0.31466800	-0.52819600	-3.23034000
H	2.69559800	-2.72051000	-0.02086900
H	2.47927500	-1.81966200	1.40678300
H	4.27210700	-0.85273500	2.95042000
H	3.07164500	-1.56773600	3.59974900
H	-5.29948100	4.04599700	-0.49218000
H	-5.99086900	4.64793600	-1.78137300
H	-1.75861900	2.66157900	-5.28599200
H	-1.27375800	1.98625100	-4.01284300
H	8.47901219	-4.17978618	-1.23341836
H	-0.82844589	-6.68101839	-0.84099397
H	1.84873105	2.17457465	5.66322792
H	-1.83045597	5.19490729	-3.15955830
H	-5.19997207	4.74107476	1.42809697
H	-7.49248422	1.27254831	1.92990494
H	-7.86834809	0.64938304	-3.27314414
H	-6.14417999	0.21442952	7.78219053

Coordinates for the DFT region of the X-D144N activated reactant (RC*) (*truncation points capped with H)*
ONIOM(M06-2X/6-31G(d):PM6) E = -2748.87638 Hartrees

0 1
C	7.91269400	-4.26213200	-2.13804100
C	6.42899700	-3.89803000	-1.94526200
C	5.64757700	-3.99081200	-3.25513300
N	4.24965900	-3.64841700	-3.03693200
C	3.40827300	-3.30005900	-4.01552800
N	3.78881500	-3.31568700	-5.29645900
N	2.16645100	-2.94161500	-3.68089000
C	1.51699500	1.47248200	6.36321200
C	1.83965500	0.02675900	5.97742200
C	1.08649200	-0.36858900	4.72461200
O	1.68914900	-1.04463900	3.83962600
O	-0.10133800	0.01124700	4.62707800
C	-6.19275800	0.97412700	7.00718000
C	-5.21064400	0.68024900	5.89135000
C	-5.50502100	-0.24011300	4.88523000
C	-3.93646900	1.25150000	5.90026800
C	-4.54405500	-0.65241900	3.96641600
C	-2.96096400	0.85534100	4.99446200
C	-3.25153700	-0.13158300	4.04406100
O	-2.30236400	-0.62513200	3.20195400
C	-6.48763200	1.41581700	1.64721600
C	-6.09228700	0.67604900	0.37251700
N	-5.04206900	1.23741800	-0.26893600
O	-6.61438400	-0.37237800	0.00271400
C	-6.86194700	0.31546300	-3.35918100
C	-6.07411000	1.30579000	-4.23865900
O	-6.28731700	1.32117400	-5.44442900
N	-5.13691400	2.04859500	-3.62635700
C	0.21445200	-6.94084200	-0.83343400
C	1.01911100	-5.86591700	-1.59765600
C	1.49935100	-4.71509900	-0.70079100
O	2.73375500	-4.35472600	-0.86855200
O	0.71329400	-4.26049700	0.12300800
N	1.15248400	-1.20829500	-1.56324500
C	0.19563800	-0.41376800	-2.09306900
N	-0.53807500	0.50856200	-1.49726000
C	-0.28781200	0.56355200	-0.18490300
C	0.63499400	-0.21931900	0.48648200
C	1.44457000	-1.10720200	-0.25728800
N	2.50194200	-1.76497100	0.24862300
N	0.55397300	0.09685700	1.82555100
C	-0.37291200	1.03548600	1.96372700
N	-0.89851900	1.35963600	0.78018800
C	-2.01458600	2.27965100	0.51995300
C	-2.48170900	3.14585200	1.68855200
C	-3.19271000	4.31134900	0.93380700
O	-4.61118400	4.11921400	0.95195900
C	-2.62152300	4.17003600	-0.52380300
O	-1.58417000	3.18352100	-0.43784100
C	-1.98853900	5.40510300	-1.15766700
O	-1.34870100	5.07610300	-2.36849400
O	4.12809900	-1.45186200	2.74839700
O	-5.62228300	3.82226200	-1.40672900
O	-1.31511500	1.96722000	-4.19909800
H	8.35723100	-3.60540900	-2.91756600
H	8.00135300	-5.28961000	-2.53029000
H	6.33237400	-2.87391200	-1.56491500
H	5.95568000	-4.54656300	-1.20259800

H	6.06987700	-3.28420500	-3.98884600
H	5.74246700	-4.99390600	-3.69588800
H	3.76785700	-3.93018000	-2.15500700
H	4.68399900	-3.71392000	-5.59034600
H	3.11448100	-3.11462100	-6.03678200
H	1.53168300	-2.58203300	-4.39191000
H	1.95673600	-2.60894000	-2.72845800
H	1.97109500	1.70195000	7.34453900
H	0.42162300	1.55925100	6.47357600
H	2.90860700	-0.13550800	5.79787800
H	1.53424300	-0.63999900	6.79221100
H	1.03548900	-0.44310300	2.63095500
H	-5.97899900	1.96947500	7.43186000
H	-7.22505700	1.02994300	6.61032200
H	-6.50923000	-0.65165300	4.82799400
H	-3.69497200	2.00793900	6.64991700
H	-4.77824800	-1.37660900	3.18944200
H	-1.96347200	1.28357500	5.04040500
H	-1.42468800	-0.49930600	3.63314400
H	-5.78657400	1.10105800	2.44168300
H	-6.29296800	2.50136000	1.50394400
H	-4.72087700	0.81877700	-1.13499900
H	-4.87104200	2.23364000	-0.14151700
H	-6.78115500	-0.64191000	-3.90244800
H	-6.40393900	0.16429800	-2.37107600
H	-4.61662400	2.70553600	-4.22155300
H	-5.21864000	2.34261600	-2.65627400
H	0.59828900	-7.02674400	0.19725300
H	0.35607700	-7.92595700	-1.31711700
H	1.88902500	-6.31311700	-2.10303100
H	0.40432900	-5.41332600	-2.39635900
H	-1.20971100	5.80694600	-0.48736500
H	-2.75072600	6.20301600	-1.23731000
H	-3.41089200	3.78361200	-1.18330900
H	-2.91821900	5.29278700	1.35915200
H	-1.61644100	3.55635100	2.21887300
H	-3.15816600	2.66339300	2.39255100
H	-2.82434300	1.64730700	0.14714900
H	-0.67035600	1.46865200	2.90881100
H	0.01381100	-0.53650800	-3.16118700
H	2.68506300	-2.70358800	-0.15213700
H	2.71492900	-1.69256500	1.24455800
H	4.49751600	-0.56719400	2.57458800
H	3.37841900	-1.28952600	3.35551600
H	-5.26574500	4.26433400	-0.61705800
H	-5.93216700	4.52107900	-2.01550800
H	-2.08400800	2.53101400	-4.43300000
H	-1.24387900	2.07355400	-3.23740800
H	1.84352201	2.20002126	5.64979296
H	-6.15652589	0.22665068	7.77194557
H	-7.50375930	1.26869859	1.94844928
H	-7.88504756	0.61739338	-3.27549529
H	8.48026380	-4.17686580	-1.23499383
H	-0.82582243	-6.69099264	-0.81598684
H	-5.19587930	4.73029173	1.40617856
H	-1.85985878	5.16564557	-3.17614483

Coordinates for the DFT region of the CS-Cap activated reactant (RC*) (*truncation points capped with H*)
ONIOM(M06-2X/6-31G(d):PM6) E = -2767.98217 Hartrees

```
-1 1
C      7.94543100   -4.30860400   -2.11689900
C      6.47688200   -3.88856800   -1.98001700
C      5.72878300   -3.93941700   -3.31065900
N      4.36413700   -3.49927900   -3.07604200
C      3.48074600   -3.27092700   -4.04913500
N      3.81824400   -3.38128100   -5.33619900
N      2.23075200   -2.93470200   -3.71020600
C      1.50822000    1.41415700    6.33003500
C      1.82229400   -0.00813300    5.85665800
C      1.02857200   -0.38017400    4.61225200
O      1.53434600   -1.18762300    3.78413800
O     -0.10863200    0.12912800    4.49190100
C     -6.21153500    0.98242900    6.98894400
C     -5.23473700    0.66772600    5.87744700
C     -5.54476400   -0.25382600    4.87802700
C     -3.95045000    1.21255100    5.88934100
C     -4.58809600   -0.70152500    3.97385600
C     -2.97667200    0.78029100    4.99907800
C     -3.28395900   -0.21548900    4.06334300
O     -2.33613300   -0.75389400    3.24699700
C     -6.49071600    1.38522200    1.55882300
C     -6.15069600    0.65465400    0.22916100
O     -6.80861500   -0.37506200   -0.05285500
O     -5.20826600    1.15164800   -0.44302900
C     -6.84281300    0.30331400   -3.37518400
C     -6.01126500    1.40965700   -4.05975200
O     -6.33064900    1.80109400   -5.18081200
N     -4.94042400    1.81033900   -3.36969900
C      0.23948100   -6.87568000   -0.80189900
C      0.99408800   -5.53221400   -0.83667700
C      2.48729900   -5.51922200   -1.19986200
O      3.05437800   -4.39502000   -0.97118600
O      3.03342900   -6.51093600   -1.71497000
N      1.03351300   -1.15426000   -1.71861300
C      0.12097500   -0.31905900   -2.27463900
N     -0.63141100    0.58621200   -1.68482400
C     -0.45835500    0.61171400   -0.36053100
C      0.44708000   -0.18662500    0.32652100
C      1.25085700   -1.09430800   -0.39868900
N      2.20782400   -1.85848700    0.16013500
N      0.30641900    0.09564500    1.66761200
C     -0.64661000    1.01893500    1.78753400
N     -1.13174800    1.36616200    0.59813000
C     -2.32656100    2.27537500    0.40999200
C     -2.41651000    3.31225100    1.52122300
C     -3.24798500    4.41054300    0.82441200
O     -4.61456900    4.09226000    1.01507900
C     -2.79650300    4.26640000   -0.66099300
O     -2.11944700    2.97887800   -0.75570100
C     -1.82375000    5.33380300   -1.15483600
O     -1.24924600    5.03282500   -2.40680100
O      3.89811100   -1.42280200    2.55202900
O     -5.59692000    3.82539000   -1.42285700
O     -1.28486100    1.95560800   -4.19778100
H      8.43944500   -3.68403900   -2.89466800
H      8.01211900   -5.34696900   -2.48355000
H      6.40810000   -2.86157000   -1.59999600
H      5.93933400   -4.51728700   -1.26414800
H      6.20642400   -3.27000400   -4.04765000
```

H	5.74944200	-4.95304500	-3.73619500
H	3.92653900	-3.82705300	-2.16622000
H	4.72992300	-3.74854700	-5.61799800
H	3.12234800	-3.24457300	-6.07231900
H	1.58143900	-2.61205500	-4.42544600
H	2.01528300	-2.54930300	-2.78284500
H	1.97192200	1.59015900	7.31849200
H	0.41469800	1.50455800	6.45034800
H	2.88745000	-0.15681900	5.63647100
H	1.55807500	-0.72191000	6.64606000
H	0.75404000	-0.42489800	2.45266200
H	-5.98487600	1.97558500	7.41322500
H	-7.24521200	1.04730300	6.59542900
H	-6.56182700	-0.63077800	4.81057600
H	-3.69892600	1.97590000	6.62941200
H	-4.84058800	-1.41101400	3.18992600
H	-1.97285300	1.19212300	5.04253200
H	-1.45442500	-0.53177500	3.62701600
H	-5.76966000	1.05802200	2.33175100
H	-6.26559900	2.46494400	1.42410100
H	-6.76855100	-0.57095500	-4.05071700
H	-6.42944800	0.01582200	-2.39624300
H	-4.46397300	2.66281000	-3.69049600
H	-4.88655600	1.61802200	-2.36986800
H	0.52832500	-7.45563100	0.09428500
H	0.53507900	-7.48145900	-1.67453400
H	0.53182400	-4.86270700	-1.58510200
H	0.89084900	-4.99391600	0.11449000
H	-0.97906200	5.42520400	-0.45318800
H	-2.33315000	6.31719300	-1.12882900
H	-3.68388800	4.22126400	-1.29748800
H	-2.98764500	5.41656500	1.20622300
H	-1.41636800	3.71166600	1.73454000
H	-2.90787200	2.98397800	2.43614100
H	-3.20639600	1.62705900	0.35078400
H	-0.97829100	1.42938900	2.73088600
H	-0.00528000	-0.39772500	-3.35385800
H	2.48168400	-2.73758600	-0.29477000
H	2.51272800	-1.72692800	1.12558000
H	4.25394100	-0.51779900	2.50363200
H	3.16466400	-1.36154100	3.20148400
H	-5.41916100	3.22773100	-0.67829200
H	-6.06375500	4.59161900	-1.05358300
H	-2.05899600	2.48056700	-4.49571000
H	-1.33706200	2.03641400	-3.23091300
H	-6.17972293	0.23495978	7.75391312
H	1.83746763	2.17005881	5.64804640
H	8.48817315	-4.22095846	-1.19893973
H	-0.81267054	-6.68106745	-0.80365824
H	-7.86168967	0.62102741	-3.29870831
H	-7.49715237	1.26831381	1.90279729
H	-5.19753842	4.73096819	1.43197048
H	-1.79195059	5.14150907	-3.19118579

Coordinates for the DFT region of the CS-Y126F activated reactant (RC*) (*truncation points capped with H*)
ONIOM(M06-2X/6-31G(d):PM6) E = -2692.77442 Hartrees

-1 1

C	7.94211600	-4.30566100	-2.11541500
C	6.47409700	-3.88483400	-1.97614400
C	5.72320100	-3.93574700	-3.30516100
N	4.35670200	-3.50377800	-3.06530200
C	3.46964500	-3.27350000	-4.03518700
N	3.80477600	-3.37920200	-5.32340000
N	2.22151300	-2.93852000	-3.68978200
C	1.52002600	1.44011800	6.34268600
C	1.79915300	0.01325600	5.86708900
C	0.95058100	-0.33897600	4.64905100
O	1.40113600	-1.22599600	3.84956000
O	-0.13617800	0.23741800	4.50712700
C	-6.18879700	0.99407900	7.00654000
C	-5.22613200	0.66890100	5.88155700
C	-5.56320600	-0.25744300	4.89521600
C	-3.95310500	1.23839600	5.85762500
C	-4.63808800	-0.65107000	3.93293800
C	-3.01648700	0.84785300	4.90657300
C	-3.35157600	-0.11773700	3.95669500
H	-2.61061300	-0.44328600	3.23306700
C	-6.49533600	1.39220100	1.56878300
C	-6.14723500	0.64524900	0.25013800
O	-6.79907300	-0.39177700	-0.02020300
O	-5.20629500	1.13816800	-0.42700400
C	-6.85358800	0.28677900	-3.35965400
C	-6.02624100	1.39021800	-4.05362600
O	-6.34135400	1.76407500	-5.18161700
N	-4.96530300	1.81094300	-3.36049900
C	0.23986000	-6.88452100	-0.77920400
C	1.00515300	-5.54728100	-0.80873900
C	2.49809300	-5.54983600	-1.17618200
O	3.07847600	-4.43198800	-0.95091200
O	3.03161100	-6.54870600	-1.69050000
N	1.06357800	-1.20791600	-1.64175900
C	0.18238600	-0.34734200	-2.21144900
N	-0.57651000	0.55886900	-1.63281500
C	-0.45305500	0.55041200	-0.30048000
C	0.40456300	-0.28467600	0.40475600
C	1.22759300	-1.18560400	-0.31142300
N	2.13709900	-1.98172700	0.27151900
N	0.20117800	-0.04933900	1.74508700
C	-0.72952100	0.89490600	1.85179000
N	-1.15382800	1.28792900	0.64923200
C	-2.28287700	2.25095400	0.42299400
C	-2.45587400	3.23368200	1.57358300
C	-3.23946100	4.36462000	0.85991900
O	-4.62166600	4.09175800	1.01014300
C	-2.75601100	4.21789800	-0.62483300
O	-1.92537200	3.02581700	-0.66223400
C	-1.89954000	5.35978600	-1.16316000
O	-1.28516600	5.05268100	-2.39601700
O	3.77549100	-1.52284600	2.69529400
O	-5.60671900	3.81675100	-1.41683200
O	-1.29785000	1.94428100	-4.19491300
H	8.43482200	-3.68328300	-2.89578200
H	8.00767800	-5.34501700	-2.47933500
H	6.40670300	-2.85755500	-1.59657500
H	5.93748800	-4.51284400	-1.25893900
H	6.19485800	-3.26158700	-4.04148600

H	5.74855800	-4.94801700	-3.73397000
H	3.92479400	-3.84080900	-2.15739300
H	4.71421500	-3.75014700	-5.60775800
H	3.10801800	-3.23977200	-6.05813400
H	1.56236200	-2.63106900	-4.40261100
H	2.00893300	-2.55715700	-2.75821600
H	2.00718700	1.61678500	7.32042500
H	0.43015500	1.54618400	6.48339200
H	2.85469900	-0.14823600	5.60846000
H	1.56040100	-0.69739200	6.66756300
H	0.62656200	-0.58104800	2.55522000
H	-5.94085800	1.98388200	7.42596600
H	-7.22233300	1.07663300	6.61642600
H	-6.57558300	-0.65065000	4.87245300
H	-3.69148200	1.99435000	6.60121700
H	-4.93549700	-1.34915100	3.15357100
H	-2.01561000	1.26771200	4.92671200
H	-5.76749100	1.09231100	2.34604500
H	-6.28541900	2.47262400	1.41477200
H	-6.78181300	-0.59110300	-4.03049900
H	-6.43596500	0.00524300	-2.38075800
H	-4.49771200	2.66719100	-3.68486900
H	-4.91862300	1.62920700	-2.35849600
H	0.52569500	-7.47001900	0.11448400
H	0.53251600	-7.48879800	-1.65386500
H	0.54750300	-4.86923900	-1.55220100
H	0.91024700	-5.01311600	0.14580600
H	-1.07542400	5.57095500	-0.46251300
H	-2.51105100	6.28266800	-1.18640200
H	-3.63046500	4.05456100	-1.26140400
H	-2.95943700	5.35875900	1.25705100
H	-1.47455200	3.61435500	1.88149600
H	-3.01810900	2.86891500	2.43216300
H	-3.18689900	1.65872600	0.23668000
H	-1.08624000	1.27761000	2.79794700
H	0.09287800	-0.40586600	-3.29571100
H	2.47386600	-2.81757400	-0.22049500
H	2.45164100	-1.84407500	1.23435800
H	4.13033900	-0.62044400	2.61400700
H	3.00456200	-1.42793900	3.30308700
H	-5.42668200	3.25148200	-0.64900600
H	-6.00231400	4.63108700	-1.06792100
H	-2.09336500	2.45233700	-4.46526700
H	-1.30206500	2.04442000	-3.22861400
H	8.48641246	-4.21560044	-1.19861052
H	-0.81155472	-6.68596182	-0.78036032
H	1.84342747	2.18804827	5.64920795
H	-1.81729644	5.14408157	-3.18979476
H	-5.20302582	4.72945438	1.43081399
H	-7.49939056	1.26875520	1.91740252
H	-7.87211567	0.60512947	-3.28120430
H	-6.16502404	0.24691933	7.77210337

Coordinates for the DFT region of the CS-NoCap activated reactant (RC*) (*truncation points capped with H*)
ONIOM(M06-2X/6-31G(d):PM6) E = -2767.96301 Hartrees

-1 1

C	7.95359300	-4.29477500	-2.10491700
C	6.48427100	-3.87725000	-1.96873100
C	5.73674200	-3.93244500	-3.29937300
N	4.37095400	-3.49517200	-3.06651600
C	3.48825300	-3.27097700	-4.04129000
N	3.82781600	-3.38577100	-5.32761000
N	2.23759700	-2.93558800	-3.70517300
C	1.50105800	1.42699400	6.32713000
C	1.82381700	0.00545300	5.85668900
C	1.04091800	-0.36612400	4.60480600
O	1.55095800	-1.17730100	3.78246200
O	-0.09072000	0.15032000	4.47423300
C	-6.21501000	0.97711000	6.97915400
C	-5.22853800	0.66979000	5.87381600
C	-5.53929200	-0.21618000	4.84118000
C	-3.93970100	1.20152300	5.91122800
C	-4.58760800	-0.63384200	3.91884900
C	-2.96438300	0.78563500	5.01438200
C	-3.27856400	-0.16755700	4.03757300
O	-2.32973700	-0.68993800	3.21344300
C	-6.46599200	1.47784400	1.72260900
C	-5.79839700	0.79392300	0.50038900
O	-6.21066500	1.15850100	-0.64261700
O	-4.89812900	-0.02927800	0.74009600
C	-6.85720400	0.25925200	-3.43452700
C	-6.01742500	1.37896200	-4.08785500
O	-6.30335700	1.77002800	-5.21762500
N	-4.98123000	1.78651000	-3.35152700
C	0.25341200	-6.87900300	-0.79066600
C	1.00731500	-5.53530200	-0.82599300
C	2.50099600	-5.52305900	-1.18835400
O	3.06849300	-4.39980600	-0.95915000
O	3.04630600	-6.51583500	-1.70325200
N	1.05035200	-1.15632800	-1.72603900
C	0.13181100	-0.32978500	-2.28488200
N	-0.62349200	0.57481700	-1.69881900
C	-0.44930200	0.61035700	-0.37457900
C	0.46337000	-0.18046000	0.31400900
C	1.27031500	-1.08631000	-0.40728600
N	2.23930000	-1.83905800	0.15134500
N	0.32844200	0.11144400	1.65332600
C	-0.62945800	1.03085200	1.76932900
N	-1.11962900	1.37062900	0.58016400
C	-2.36570000	2.23574400	0.42078000
C	-2.41428400	3.30461000	1.50408000
C	-3.27567100	4.38719700	0.82075600
O	-4.62486700	4.05222700	1.05715200
C	-2.85485600	4.23186300	-0.66893900
O	-2.28332700	2.88985100	-0.78482700
C	-1.82246100	5.25088500	-1.14985700
O	-1.26865200	4.97567700	-2.41902800
O	3.91909300	-1.42155700	2.56457200
O	-5.60763400	3.80833400	-1.43524400
O	-1.28935800	1.94378700	-4.20383500
H	8.44643700	-3.67084200	-2.88396700
H	8.02235900	-5.33379200	-2.46940700
H	6.41346500	-2.84960200	-1.59089000
H	5.94770400	-4.50535100	-1.25161700
H	6.21308800	-3.26334900	-4.03751400

H	5.76024000	-4.94694200	-3.72286300
H	3.93374100	-3.82354500	-2.15689000
H	4.74020000	-3.75271700	-5.60708500
H	3.13379300	-3.24864500	-6.06515300
H	1.58898000	-2.61947000	-4.42389100
H	2.02034100	-2.53838100	-2.78193600
H	1.96265400	1.60783800	7.31589500
H	0.40699800	1.51184800	6.44541000
H	2.89092800	-0.14035700	5.64433000
H	1.55555800	-0.70937600	6.64374500
H	0.77362500	-0.40571800	2.44069000
H	-5.99801300	1.97254600	7.40390800
H	-7.24610900	1.03595800	6.57810100
H	-6.56164200	-0.57642600	4.75351600
H	-3.68613300	1.94157500	6.67407600
H	-4.84423900	-1.25920700	3.06931400
H	-1.95789100	1.18894200	5.07374600
H	-1.45149800	-0.48832700	3.60784800
H	-5.84643000	1.26973900	2.60964700
H	-6.36584500	2.57204800	1.53777800
H	-6.81025800	-0.58584100	-4.14809500
H	-6.41933800	-0.04805500	-2.47751400
H	-4.48519900	2.63823500	-3.64328600
H	-5.00490500	1.61332900	-2.34844500
H	0.54196000	-7.45796700	0.10631300
H	0.55052700	-7.48548000	-1.66238700
H	0.54550600	-4.86627300	-1.57509200
H	0.90339200	-4.99628000	0.12459300
H	-0.96676500	5.27129900	-0.45540100
H	-2.27386100	6.26039400	-1.08238100
H	-3.75269400	4.24527000	-1.28828400
H	-3.00766100	5.39821400	1.18533500
H	-1.40685700	3.70886000	1.66830300
H	-2.86710400	2.99355300	2.44438200
H	-3.19202200	1.51842900	0.46724700
H	-0.96239100	1.44287800	2.71127300
H	0.00387500	-0.41621000	-3.36343000
H	2.50085100	-2.72772500	-0.29150000
H	2.52751300	-1.71333100	1.12250000
H	4.26671500	-0.51374500	2.50929500
H	3.17833400	-1.35788700	3.20603800
H	-5.87847100	3.06421200	-0.86980900
H	-6.34638200	4.44013100	-1.43620000
H	-2.04970700	2.49032900	-4.49969500
H	-1.34980400	2.00833800	-3.23620800
H	8.49606599	-4.20413874	-1.18708906
H	-0.79902163	-6.68593512	-0.79353761
H	1.82685414	2.18319537	5.64381721
H	-1.80684260	5.10891462	-3.20273625
H	-5.21138034	4.70736392	1.44237626
H	-7.49449538	1.28529115	1.94622517
H	-6.18610359	0.23267805	7.74719403
H	-7.86880104	0.58944166	-3.32251706

Coordinates for the DFT region of the X-WT Mechanism B TS (*truncation points capped with H*)
ONIOM(M06-2X/6-31G(d):PM6) E = -2768.00223 Hartrees

```
-1 1
C        7.98627300  -4.17998400  -2.13213600
C        6.48517400  -3.92153100  -1.94802500
C        5.73485000  -4.07439000  -3.26699600
N        4.31889000  -3.85473800  -3.05655900
C        3.45844000  -3.51099200  -4.01485600
N        3.81725200  -3.50115500  -5.30196600
N        2.21774700  -3.20416700  -3.62848700
C        1.50371800   1.50699800   6.35297900
C        1.85985800   0.07418400   5.96887900
C        1.02202700  -0.42083300   4.79088200
O        1.49893600  -1.41478900   4.14081200
O       -0.05824700   0.13254600   4.56577400
C       -6.14099100   0.95922800   7.03919000
C       -5.26966500   0.64272100   5.84282900
C       -5.70497900  -0.23870800   4.85806600
C       -4.01575600   1.24065100   5.67883400
C       -4.95266300  -0.49261000   3.71783500
C       -3.25132700   1.00758600   4.54503900
C       -3.74604100   0.18789000   3.52338100
O       -3.05003100   0.08477200   2.37355600
C       -6.51233600   1.34326800   1.57172800
C       -5.99947400   0.30416400   0.54919900
O       -6.83978800  -0.39387100  -0.05545600
O       -4.74588800   0.26415500   0.37262400
C       -6.85120700   0.24293900  -3.33561500
C       -6.08696700   1.22990200  -4.23915900
O       -6.35451100   1.26167300  -5.44238000
N       -5.12715200   1.95217300  -3.66266800
C        0.29592900  -6.93730000  -0.81552300
C        1.09174100  -5.85211300  -1.57839400
C        1.66826500  -4.77992500  -0.64362700
O        2.94421400  -4.55075000  -0.79242100
O        0.93007400  -4.28874400   0.19813500
N        1.85999700  -1.46043800  -1.50952700
C        0.95339900  -0.69536800  -2.15367100
N        0.08417600   0.14617700  -1.64644500
C        0.08877100   0.14952600  -0.29599000
C        0.95856000  -0.63330400   0.47524400
C        1.92319700  -1.41464700  -0.16211300
N        2.95794800  -2.03791000   0.46593700
N        0.63369200  -0.35377600   1.77690500
C       -0.38456000   0.53837100   1.72601700
N       -0.73685700   0.87630000   0.49971600
C       -3.13798100   2.78367300  -0.41491100
C       -2.46847100   3.24254900   0.84505900
C       -3.24703200   4.56559200   0.92895900
O       -4.58776200   4.09292100   1.11779700
C       -3.15581500   5.03635700  -0.53733100
O       -3.46523700   3.79359400  -1.16333500
C       -1.82673500   5.56454400  -1.14076600
O       -1.44607100   4.90957900  -2.34800500
O        4.00465700  -1.67608400   3.31717300
O       -5.66106200   3.76042500  -1.41862100
O       -2.07947100   2.17362700  -1.86964600
H        8.39584900  -3.48170600  -2.89519300
H        8.14504000  -5.19190200  -2.54662600
H        6.30855700  -2.90872600  -1.56788800
H        6.05036800  -4.60382200  -1.21240700
```

H	6.10745600	-3.33519200	-3.99752600
H	5.92164300	-5.06580800	-3.70708200
H	3.86270200	-4.10387200	-2.14615100
H	4.72974600	-3.84066400	-5.61247800
H	3.13903100	-3.26185400	-6.02709500
H	1.55857800	-2.84232600	-4.31316900
H	2.13123200	-2.77092000	-2.67716000
H	1.93970700	1.75577200	7.34134300
H	0.40400600	1.56754200	6.43851100
H	2.91714100	-0.05102200	5.69695900
H	1.68062400	-0.59528500	6.82181000
H	0.93827100	-0.85813400	2.63640200
H	-5.79830500	1.91122000	7.48021200
H	-7.18575400	1.13377300	6.71200400
H	-6.68372600	-0.69754800	4.97229700
H	-3.64927600	1.93318200	6.43914900
H	-5.33086900	-1.14455500	2.93404500
H	-2.29003700	1.49729700	4.40714400
H	-3.68538100	0.07840400	1.59185100
H	-5.80283300	1.44131200	2.40958400
H	-6.42977300	2.33021800	1.05514100
H	-6.75207600	-0.72450200	-3.86006800
H	-6.39545200	0.12357800	-2.34026900
H	-4.60336600	2.61673800	-4.24246300
H	-5.08051400	2.13346300	-2.66532300
H	0.68008500	-7.02335100	0.21514500
H	0.44498400	-7.92210900	-1.29994900
H	1.92237800	-6.30350100	-2.14339200
H	0.45232200	-5.34116100	-2.31917000
H	-0.99198700	5.40501100	-0.44933900
H	-1.91564400	6.65350300	-1.27247300
H	-3.99367200	5.69953300	-0.78623300
H	-2.91256100	5.27884000	1.69470700
H	-1.40000800	3.40573000	0.68193800
H	-2.65094700	2.56769000	1.67251800
H	-3.73657200	1.88541600	-0.46236000
H	-0.84371500	0.89072300	2.63626600
H	0.96237800	-0.78551500	-3.24311100
H	3.14536900	-2.97202300	0.07241600
H	2.93531400	-2.04158700	1.48602400
H	4.22520000	-0.78194900	3.00329700
H	3.10997200	-1.57152800	3.73499600
H	-5.46253000	3.81016100	-0.47244400
H	-6.53640100	4.17009900	-1.53282500
H	-1.78395400	3.04486000	-2.22747600
H	-1.32863000	1.55010000	-1.80013800
H	8.53897215	-4.07874628	-1.22154576
H	-0.74645760	-6.69639834	-0.79830165
H	1.82055383	2.24133036	5.64215480
H	-7.88085443	0.52694193	-3.27183020
H	-7.51288883	1.19276324	1.91978311
H	-6.13884660	0.19056285	7.78353488
H	-5.23271921	4.70424205	1.48100048
H	-1.92585106	5.07398008	-3.16310216

Coordinates for the DFT region of the X-WT Mechanism B product (*truncation points capped with H*)
ONIOM(M06-2X/6-31G(d):PM6) E = -2768.01318 Hartrees

-1 1

C	8.03728300	-4.14689800	-2.09755800
C	6.52080200	-4.00811700	-1.93324100
C	5.81672300	-4.21846900	-3.26873400
N	4.38063700	-4.18671600	-3.07824600
C	3.50648300	-3.81812600	-4.01166000
N	3.84353000	-3.74545500	-5.29838300
N	2.25273300	-3.58357500	-3.59933900
C	1.43937300	1.44646400	6.23844200
C	1.69100000	0.07012500	5.61691700
C	0.92918300	-0.14145200	4.29629100
O	1.26630400	-1.18274200	3.62721000
O	0.05524800	0.66482300	3.96930400
C	-6.13731600	0.93871100	7.02480300
C	-5.27248400	0.60131900	5.82330000
C	-5.72273900	-0.28803500	4.85148100
C	-4.02144800	1.19816000	5.62811400
C	-4.99118800	-0.54866800	3.69846500
C	-3.27607000	0.95940200	4.47944200
C	-3.79038100	0.13193100	3.47510500
O	-3.11918500	0.01693400	2.30420900
C	-6.52599200	1.31726100	1.54945900
C	-6.01312900	0.31312600	0.49045900
O	-6.84045200	-0.43175500	-0.07808700
O	-4.76698400	0.33897300	0.24827500
C	-6.85000200	0.18146500	-3.34856300
C	-6.03252400	1.29479300	-4.03589700
O	-6.42376100	1.79043200	-5.08727300
N	-4.85384800	1.57397300	-3.45626000
C	0.33363200	-6.95063500	-0.77529300
C	1.13199500	-5.85589000	-1.51655000
C	1.70476800	-4.79862300	-0.56060800
O	2.96795700	-4.52637300	-0.73248400
O	0.97311300	-4.34913500	0.31091600
N	2.24580300	-1.51372800	-1.65894100
C	1.49050600	-0.78848100	-2.51804500
N	0.50759500	0.04360500	-2.27261600
C	0.23222300	0.11820700	-0.95416700
C	0.93035200	-0.58508000	0.03030600
C	1.99935300	-1.40663400	-0.34025400
N	2.83939900	-2.00867800	0.54193000
N	0.35454600	-0.24451100	1.22529400
C	-0.63349100	0.61768600	0.94639700
N	-0.74636300	0.86316600	-0.35744800
C	-3.27950200	2.98577500	-0.68355100
C	-2.52421400	3.28553600	0.60379000
C	-3.24029900	4.60265500	0.89557500
O	-4.55175900	4.11880700	1.14341300
C	-3.16690500	5.25430700	-0.51329100
O	-3.54474800	4.16953800	-1.31499000
C	-1.83711400	5.73318600	-1.19795100
O	-1.46319400	4.92996400	-2.34024800
O	3.89011500	-1.71384500	3.48905600
O	-5.67764800	3.72268100	-1.42995300
O	-2.43417000	2.36426000	-1.69944600
H	8.40608700	-3.40086600	-2.83567900
H	8.27003400	-5.13247800	-2.54228300
H	6.25436200	-3.01610100	-1.55138400
H	6.13282300	-4.72983500	-1.20937000

H	6.11053700	-3.42368100	-3.97749400
H	6.12767900	-5.16850400	-3.72626700
H	3.95503000	-4.31565600	-2.13187800
H	4.78564200	-3.97346100	-5.62707600
H	3.15671900	-3.46787700	-6.00395900
H	1.60820100	-3.12081500	-4.23559700
H	2.20521000	-3.20756100	-2.64012700
H	1.91934400	1.51603400	7.23329800
H	0.34968500	1.57331800	6.37758100
H	2.75782800	-0.10870400	5.41577600
H	1.38176600	-0.71917000	6.31040300
H	0.59555400	-0.62137400	2.17403300
H	-5.77742200	1.88831000	7.45818500
H	-7.17824000	1.13028900	6.69537700
H	-6.70042000	-0.74393600	4.98378600
H	-3.64221700	1.90082900	6.37269200
H	-5.38705500	-1.20479300	2.92623100
H	-2.31928900	1.44955000	4.31031500
H	-3.76173900	0.07805100	1.52894600
H	-5.81031300	1.38834300	2.38427800
H	-6.43595500	2.32335300	1.06841600
H	-6.73735200	-0.69733500	-4.01268800
H	-6.44249700	-0.09726800	-2.36355400
H	-4.31218300	2.36729500	-3.82341800
H	-4.69610000	1.33728300	-2.48477300
H	0.70798800	-7.04898900	0.25786900
H	0.48664100	-7.92915700	-1.27091500
H	1.96200600	-6.29493400	-2.09309800
H	0.49364400	-5.33616000	-2.25185300
H	-0.97447700	5.70471100	-0.52446500
H	-1.98102700	6.77662300	-1.50651600
H	-3.94128000	6.03455400	-0.59231400
H	-2.82399700	5.19799000	1.71885000
H	-1.45386500	3.44477100	0.42542500
H	-2.71527300	2.54736800	1.37304100
H	-4.14265400	2.34875200	-0.56010900
H	-1.26385900	1.01203800	1.73258600
H	1.75608800	-0.91916700	-3.57084600
H	3.13311400	-2.93807000	0.21240400
H	2.52050800	-2.02906600	1.50806100
H	4.16683100	-0.87975300	3.07365900
H	2.92068900	-1.57722100	3.64089800
H	-5.24910600	4.20999200	-2.14999800
H	-6.62056800	3.93810900	-1.51410900
H	-1.97582000	3.15867900	-2.12333600
H	-1.74058700	1.73391900	-1.22946200
H	8.57184461	-4.03734678	-1.17715460
H	-0.70834485	-6.70755015	-0.76559797
H	1.78259255	2.24294331	5.61176741
H	-1.94215166	5.06828303	-3.16065485
H	-5.23605147	4.70015603	1.48308508
H	-6.15157058	0.17721257	7.77634604
H	-7.52263658	1.15781299	1.90467147
H	-7.87856657	0.46892953	-3.28284328

Coordinates for the DFT region of the CS-Cap Mechanism C dissociative TS (*truncation points capped with H)*
ONIOM(M06-2X/6-31G(d):PM6) E = -2767.96885 Hartrees

```
-1 1
C        7.98481000  -4.26859000  -2.11406500
C        6.50570400  -3.89927100  -1.99128100
C        5.78849700  -3.96102900  -3.33587000
N        4.39223500  -3.65004900  -3.10408200
C        3.49686100  -3.43390900  -4.06533400
N        3.83983900  -3.45763400  -5.35410600
N        2.22916300  -3.21279700  -3.69967800
C        1.49946500   1.45368500   6.32739300
C        1.78985100   0.03332300   5.84157100
C        0.98167000  -0.33417100   4.60218300
O        1.38294600  -1.30309300   3.89624600
O       -0.05027000   0.33178100   4.36982600
C       -6.20790200   0.97911000   6.98794100
C       -5.21313800   0.67989700   5.88632600
C       -5.49663900  -0.24713300   4.88339000
C       -3.94367800   1.26099700   5.89778600
C       -4.53109000  -0.65298300   3.96909900
C       -2.96219700   0.87317000   4.99515600
C       -3.24467400  -0.11615000   4.04368500
O       -2.29818000  -0.59402600   3.19625400
C       -6.50011200   1.36974000   1.56794400
C       -6.14936300   0.64286000   0.24171100
O       -6.79386800  -0.38864800  -0.05078400
O       -5.20337900   1.15104500  -0.42406000
C       -6.85007800   0.26639500  -3.37364400
C       -6.02643900   1.38075200  -4.05391300
O       -6.36050100   1.79215400  -5.16236200
N       -4.94328600   1.76840700  -3.37398900
C        0.26185400  -6.91573400  -0.77014300
C        1.08212400  -5.61393600  -0.80153600
C        2.58139200  -5.71440000  -1.13318800
O        3.23306200  -4.63467400  -0.91935600
O        3.05898200  -6.75804900  -1.61371500
N        1.28875000  -1.53036000  -1.68876300
C        0.44000700  -0.69794600  -2.33980500
N       -0.27204200   0.29116900  -1.85253300
C       -0.15166000   0.40283600  -0.51816000
C        0.66681300  -0.41683200   0.26000400
C        1.45946500  -1.39754200  -0.36541700
N        2.37275000  -2.15402000   0.26972200
N        0.47956100  -0.02631500   1.56473300
C       -0.41497700   0.98183300   1.53435700
N       -0.80595000   1.28646200   0.31042300
C       -2.64918000   2.27927400   0.14662800
C       -2.51074500   3.20036500   1.32664900
C       -3.30087500   4.41326800   0.80682700
O       -4.64872300   4.07731900   1.01915700
C       -2.95034600   4.39344000  -0.69844000
O       -2.78391900   2.93178200  -0.94991600
C       -1.72276800   5.18505800  -1.13648600
O       -1.27051600   4.91105100  -2.43552100
O        3.81849600  -1.62974800   2.84609100
O       -5.62071100   3.80007600  -1.43058600
O       -1.30070700   1.94352300  -4.20123100
H        8.46900200  -3.62212100  -2.88061600
H        8.08731400  -5.30068900  -2.49150900
H        6.39433900  -2.88061600  -1.59919000
H        5.97689600  -4.55474400  -1.29324900
```

```
H      6.21640600   -3.22638100   -4.04026900
H      5.90430400   -4.95098700   -3.80169500
H      3.98632200   -3.99320000   -2.19357900
H      4.76870600   -3.76654200   -5.65230100
H      3.13341100   -3.32563700   -6.08160000
H      1.58073200   -2.85882000   -4.39912200
H      2.03330900   -2.80830500   -2.76237600
H      1.98080600    1.62054300    7.30955600
H      0.40893400    1.55862000    6.46565600
H      2.85179700   -0.12509000    5.60658600
H      1.53895600   -0.68952000    6.62696400
H      0.80415100   -0.53110900    2.40865300
H     -6.00250700    1.97741600    7.41106000
H     -7.23691200    1.02824800    6.58009400
H     -6.50068500   -0.65831700    4.81603000
H     -3.71306000    2.02611400    6.64295500
H     -4.76444900   -1.36294500    3.17989800
H     -1.97473200    1.32587600    5.02158700
H     -1.41472800   -0.32182000    3.54102600
H     -5.77885700    1.04750400    2.34238600
H     -6.28222500    2.45093200    1.43337900
H     -6.77029100   -0.60585200   -4.05087100
H     -6.43429100   -0.02289400   -2.39604900
H     -4.47198600    2.62368900   -3.69361500
H     -4.88146300    1.56776500   -2.37699500
H      0.52839500   -7.50750600    0.12628700
H      0.54282400   -7.53446700   -1.63868100
H      0.67459600   -4.92615400   -1.56456600
H      0.99417700   -5.06122100    0.14330100
H     -0.87313100    4.96529900   -0.47218000
H     -1.95030900    6.25875300   -0.96546500
H     -3.83741100    4.62607900   -1.29313300
H     -2.98334900    5.36495100    1.27443000
H     -1.45944700    3.47656500    1.45341700
H     -2.93182000    2.81472200    2.25164300
H     -3.07634100    1.29167600    0.15929900
H     -0.75923300    1.46385800    2.44033500
H      0.34610600   -0.86967000   -3.41352800
H      2.68025700   -3.03200300   -0.16687200
H      2.61720400   -1.99917800    1.24856500
H      4.13555400   -0.71757500    2.72881100
H      3.00761500   -1.53858600    3.39758300
H     -5.45815000    3.12477400   -0.74888000
H     -6.26428800    4.42149200   -1.05356300
H     -2.09328500    2.51582500   -4.30750700
H     -1.24466500    1.79743000   -3.24690600
H      8.51291006   -4.17336094   -1.18835351
H     -0.78486615   -6.69383707   -0.77636290
H      1.82523939    2.20791648    5.64189616
H     -1.81644516    5.07842027   -3.20723914
H     -5.23239260    4.71981658    1.42918952
H     -6.17781689    0.23652578    7.75772250
H     -7.87052675    0.57855957   -3.29530099
H     -7.50714740    1.24595293    1.90773285
```

Coordinates for the DFT region of the CS-Cap Mechanism C intermediate (*truncation points capped with H*)
ONIOM(M06-2X/6-31G(d):PM6) E = -2767.97490 Hartrees

-1 1

C	8.07325100	-4.17929300	-2.12026000
C	6.57025100	-3.97667700	-2.01696600
C	5.88799800	-4.20079700	-3.35922300
N	4.47022000	-4.22022600	-3.10233800
C	3.50482000	-4.11463900	-4.00127400
N	3.75948200	-4.17048400	-5.31311000
N	2.26008200	-4.04429700	-3.51278500
C	1.48163600	1.52841500	6.30609100
C	1.77066600	0.11124800	5.81400700
C	0.96213400	-0.27036300	4.57756600
O	1.26715300	-1.35850300	4.00343700
O	0.03772000	0.48958400	4.22346300
C	-6.19817700	0.97818900	6.98982700
C	-5.18603600	0.68280600	5.90102100
C	-5.44685200	-0.25765800	4.90377700
C	-3.92416800	1.28272600	5.91600000
C	-4.46893900	-0.65208600	3.99764700
C	-2.93031000	0.90644700	5.02131500
C	-3.19219200	-0.08981000	4.07093500
O	-2.24129700	-0.55067700	3.22450200
C	-6.50996900	1.34024700	1.59441800
C	-6.12659600	0.64282700	0.26489100
O	-6.74831300	-0.38842700	-0.06274600
O	-5.17771600	1.17507100	-0.38973800
C	-6.86560300	0.18412800	-3.36522800
C	-6.05626900	1.27840800	-4.08988000
O	-6.37195000	1.61819800	-5.22691900
N	-5.00188200	1.73813800	-3.40872900
C	0.30965200	-6.98858000	-0.71794300
C	1.24515600	-5.77819100	-0.59055900
C	2.72091300	-6.01918900	-0.96543200
O	3.49548000	-5.02312000	-0.74892700
O	3.08011400	-7.09254300	-1.48172900
N	1.66752300	-2.15278100	-1.59372400
C	0.89735900	-1.35138200	-2.37237300
N	0.17622100	-0.31441300	-2.02721900
C	0.18802300	-0.09949100	-0.69381900
C	0.92213900	-0.87343600	0.20876200
C	1.73133000	-1.91992700	-0.27065000
N	2.54852800	-2.65488700	0.49979300
N	0.63645600	-0.37195900	1.45614600
C	-0.23519100	0.64625500	1.25081800
N	-0.52213600	0.85673500	-0.01626700
C	-2.89867700	2.28391000	-0.34040700
C	-2.66302300	2.93035300	0.97591800
C	-3.36125400	4.28934500	0.74913000
O	-4.70625700	4.02099800	1.03470500
C	-3.11716700	4.51304700	-0.75856400
O	-3.06356900	3.10593100	-1.27462800
C	-1.81913300	5.21904600	-1.15905600
O	-1.35495200	4.91841200	-2.44663600
O	3.75634200	-1.77394300	3.14110400
O	-5.66853100	3.75076600	-1.44500900
O	-1.33350300	1.92185100	-4.21021200
H	8.50767300	-3.46553400	-2.85645000
H	8.28110600	-5.18353900	-2.53334200
H	6.33022800	-2.96412400	-1.67066200
H	6.12313900	-4.66068500	-1.29014800

H	6.13699800	-3.39488900	-4.07398000
H	6.22304500	-5.14077600	-3.82119900
H	4.15067400	-4.48477600	-2.13466100
H	4.72664700	-4.19265400	-5.64848000
H	3.05328700	-3.86735400	-5.99064200
H	1.48773100	-3.88405400	-4.15528600
H	2.15204100	-3.52278900	-2.60894900
H	1.96639800	1.69071500	7.28767400
H	0.39144900	1.63454900	6.45162900
H	2.83319600	-0.04195800	5.57248400
H	1.53541600	-0.61877900	6.59696100
H	0.86424300	-0.79743800	2.37145800
H	-6.01021700	1.98246800	7.40698400
H	-7.22273000	1.01148100	6.56930100
H	-6.44300400	-0.68807700	4.83291300
H	-3.71066700	2.05683800	6.65706500
H	-4.68449300	-1.37113200	3.21159300
H	-1.95284200	1.38233600	5.03800600
H	-1.36264400	-0.20721100	3.51663300
H	-5.79633600	1.01278900	2.37326600
H	-6.30239600	2.42552400	1.48298300
H	-6.78571700	-0.70855000	-4.01429500
H	-6.43711400	-0.07127400	-2.38338600
H	-4.54550500	2.58544400	-3.76798200
H	-4.97267300	1.60965200	-2.39966000
H	0.51357700	-7.69879700	0.10817300
H	0.57881300	-7.53079400	-1.64037100
H	0.90872700	-4.95706800	-1.24681100
H	1.22424200	-5.34720100	0.41970700
H	-1.00841500	4.92591000	-0.47577400
H	-1.96935900	6.30479900	-0.98123800
H	-4.00298100	4.91009100	-1.25316300
H	-2.91428600	5.10777100	1.34180000
H	-1.57884400	3.04842900	1.06865400
H	-3.07537100	2.38773400	1.82000200
H	-2.88584000	1.23973800	-0.57936700
H	-0.62655400	1.21157000	2.08820200
H	0.89321600	-1.61121600	-3.43534400
H	2.96281200	-3.50425600	0.09653500
H	2.76357800	-2.39714000	1.46306500
H	4.03368600	-0.86781200	2.92399900
H	2.88980200	-1.65937000	3.60133700
H	-5.58182300	3.12266200	-0.70842300
H	-6.41167500	4.33826500	-1.22764600
H	-2.14072900	2.48401900	-4.21389000
H	-1.18688300	1.71199100	-3.28055500
H	8.56673615	-4.06986937	-1.17718054
H	-0.72473990	-6.71498591	-0.72686859
H	-7.88758194	0.49081994	-3.28523369
H	-7.51967640	1.20193767	1.92039576
H	-6.16876954	0.24292832	7.76663260
H	-5.28937676	4.67796098	1.42196588
H	-1.89152865	5.06530538	-3.22900920
H	1.80311506	2.28521937	5.62140249

Coordinates for the DFT region of the CS-Cap Mechanism C associative TS (*truncation points capped with H)*
ONIOM(M06-2X/6-31G(d):PM6) E = -2767.92531 Hartrees

```
-1 1
C         8.07317800   -4.17680500   -2.13830200
C         6.56258700   -4.04153500   -2.04165700
C         5.90534700   -4.29012000   -3.39319700
N         4.49318500   -4.44678500   -3.14899800
C         3.51713300   -4.26829500   -4.02394000
N         3.75264100   -4.24240400   -5.33958300
N         2.27866900   -4.21504300   -3.51276900
C         1.47676900    1.48672400    6.28745900
C         1.73934300    0.08507100    5.73594400
C         0.92818100   -0.23977900    4.48170600
O         1.17793700   -1.34598200    3.91337100
O         0.06049500    0.57529100    4.10826700
C        -6.19074700    0.96329500    7.00668500
C        -5.17585800    0.67467100    5.91827200
C        -5.43757000   -0.25346200    4.90985200
C        -3.91169900    1.27081400    5.94182600
C        -4.46029500   -0.63631400    3.99777800
C        -2.91865100    0.90546700    5.04214000
C        -3.18361200   -0.07368800    4.07524400
O        -2.23739800   -0.51817700    3.21742000
C        -6.52416700    1.29251300    1.54019700
C        -6.26929600    0.49788400    0.22802100
O        -6.92393700   -0.54608200    0.05045000
O        -5.39168400    0.95219700   -0.56597800
C        -6.89025600    0.16502100   -3.38569000
C        -6.06020200    1.22828000   -4.12642800
O        -6.41481600    1.66624600   -5.21202200
N        -4.92129100    1.55528000   -3.49898900
C         0.29468400   -7.00011100   -0.73669900
C         1.25266300   -5.81478700   -0.56042800
C         2.71963000   -6.07789200   -0.95513100
O         3.51458900   -5.09577300   -0.74856300
O         3.05422800   -7.15429400   -1.48176900
N         1.75602700   -2.26108800   -1.63772300
C         1.02601700   -1.47283100   -2.46601500
N         0.28304700   -0.43547900   -2.17469100
C         0.22058700   -0.20414600   -0.84487700
C         0.91580200   -0.95739400    0.10707300
C         1.75181800   -2.00681400   -0.31626300
N         2.53120900   -2.73282900    0.50186100
N         0.56016700   -0.43663400    1.32852000
C        -0.30999300    0.56807900    1.05850800
N        -0.53653500    0.75221800   -0.22552600
C        -3.15227500    2.67048000   -1.06258900
C        -2.87614200    2.80042000    0.39792200
C        -3.21184000    4.28443500    0.60181700
O        -4.59863900    4.17910000    0.97119700
C        -2.91847200    4.85379000   -0.83832800
O        -2.72186600    3.68020100   -1.71059900
C        -1.67796500    5.67198600   -1.18266700
O        -1.23370300    5.37108700   -2.48763800
O         3.69934900   -1.83647300    3.19316000
O        -5.04073800    3.43577000   -1.28727500
O        -1.33736400    1.93995000   -4.19408500
H         8.48198800   -3.43103000   -2.85726800
H         8.32097200   -5.16209700   -2.57621400
H         6.27261300   -3.04483000   -1.68835000
H         6.14448400   -4.75062000   -1.32222000
```

H	6.08601300	-3.44854200	-4.08720400
H	6.32522400	-5.18339900	-3.87738100
H	4.18152900	-4.67380100	-2.16799300
H	4.71498800	-4.25949200	-5.68968400
H	3.04136700	-3.89061500	-5.98744300
H	1.50168500	-4.02330300	-4.14223700
H	2.19528400	-3.69392600	-2.60673900
H	1.97089700	1.60344400	7.27053800
H	0.38942700	1.60608100	6.44581000
H	2.80091600	-0.07533300	5.49259600
H	1.49127400	-0.67290400	6.48665700
H	0.76394900	-0.82557300	2.26602600
H	-6.00523800	1.96601500	7.42882000
H	-7.21433000	0.99728600	6.58376800
H	-6.43366300	-0.68368700	4.83422100
H	-3.69698300	2.03506900	6.69287100
H	-4.67701600	-1.34588800	3.20351200
H	-1.94244700	1.38451900	5.05870700
H	-1.36333600	-0.13708200	3.47755300
H	-5.78325500	0.96691300	2.29423100
H	-6.28659800	2.36482300	1.36399200
H	-6.85506000	-0.72940000	-4.03783000
H	-6.44560200	-0.10852800	-2.41738000
H	-4.40041200	2.37582900	-3.82941900
H	-4.84355500	1.27815100	-2.52798000
H	0.48414000	-7.74548200	0.06165300
H	0.56177600	-7.51153400	-1.67729900
H	0.93194300	-4.95768600	-1.17700900
H	1.24667800	-5.42800000	0.46779300
H	-0.84785900	5.43033100	-0.50914400
H	-1.91920100	6.73808900	-1.02668300
H	-3.82494400	5.33494500	-1.21868900
H	-2.62704300	4.80774100	1.36677900
H	-1.80504600	2.60812300	0.45845000
H	-3.45348100	2.14528200	1.03425300
H	-3.22189400	1.72846800	-1.58278900
H	-0.75226400	1.14265400	1.86488000
H	1.07880600	-1.74727100	-3.52467100
H	2.97898200	-3.57348300	0.11802700
H	2.71150600	-2.46051600	1.46729800
H	3.98631200	-0.93884400	2.95530000
H	2.80528200	-1.70435300	3.59373600
H	-5.48977000	2.57200600	-1.14358600
H	-5.15689000	3.85963600	-0.40191300
H	-2.07638200	2.58856900	-4.17495500
H	-1.11452100	1.76298100	-3.27263400
H	8.56113389	-4.07233822	-1.19178959
H	-0.73640985	-6.71424508	-0.74181347
H	1.80541572	2.26064262	5.62568767
H	-1.83609095	5.27515496	-3.22893807
H	-5.23682053	4.74660209	1.40967814
H	-6.16335771	0.22535199	7.78101693
H	-7.90033542	0.50152398	-3.27889437
H	-7.52075210	1.19056720	1.91612943

Coordinates for the DFT region of the CS-Cap Mechanism C product (*truncation points capped with H*)
ONIOM(M06-2X/6-31G(d):PM6) E = -2767.94541 Hartrees

```
-1 1
C        8.08351500  -4.14945100  -2.15508100
C        6.57067400  -4.04395400  -2.05632100
C        5.91951900  -4.29437500  -3.41061200
N        4.51170300  -4.49553000  -3.17020100
C        3.53099900  -4.29281700  -4.03533600
N        3.76092100  -4.23467500  -5.35073800
N        2.29473500  -4.24966900  -3.51722200
C        1.47524900   1.46807900   6.28768400
C        1.73585900   0.07082100   5.72381700
C        0.92021300  -0.24760400   4.46996800
O        1.16115400  -1.35722900   3.90405500
O        0.05961200   0.57418200   4.09541600
C       -6.18768800   0.92560900   7.01562500
C       -5.17330500   0.64607500   5.92395100
C       -5.43533700  -0.27239800   4.90662800
C       -3.91006800   1.24442800   5.94982100
C       -4.46011800  -0.64247800   3.98694100
C       -2.91892700   0.89175700   5.04297500
C       -3.18434500  -0.07655300   4.06507100
O       -2.24149600  -0.50655900   3.19767700
C       -6.53304100   1.28295000   1.53564600
C       -6.33667100   0.51655200   0.19927200
O       -6.84218300  -0.61288300   0.11662400
O       -5.66487800   1.06157900  -0.73343700
C       -6.88050500   0.22059600  -3.42394000
C       -6.12644700   1.38373100  -4.10005000
O       -6.68433500   2.12528000  -4.89991400
N       -4.82062200   1.45560900  -3.79896000
C        0.31084900  -7.00477000  -0.75790600
C        1.27409800  -5.82749200  -0.56111100
C        2.73833800  -6.09380000  -0.96459600
O        3.53860100  -5.11619900  -0.75806100
O        3.06563600  -7.16897600  -1.49876800
N        1.78571700  -2.30254500  -1.63293900
C        1.07430100  -1.51160000  -2.47468400
N        0.33248900  -0.46973700  -2.19960800
C        0.24996000  -0.23210000  -0.87159200
C        0.92552500  -0.98685600   0.09449300
C        1.76015800  -2.04388600  -0.31214400
N        2.51525700  -2.77880100   0.52171900
N        0.55591600  -0.45562100   1.30740100
C       -0.30132300   0.55661900   1.01758800
N       -0.50780000   0.73395800  -0.26991800
C       -3.44408800   2.79617100  -1.14538000
C       -2.93824000   2.78131400   0.30003700
C       -3.16317000   4.26934800   0.58908700
O       -4.60846400   4.22082600   0.89506100
C       -2.87447300   4.89609700  -0.83027800
O       -2.71888500   3.77761000  -1.72283500
C       -1.62672500   5.69733700  -1.16781100
O       -1.22182500   5.45512300  -2.50138100
O        3.68814000  -1.84718700   3.20344100
O       -4.82324600   3.32426700  -1.24293400
O       -1.34498300   1.94815000  -4.18569200
H        8.47787900  -3.38891900  -2.86663800
H        8.34850200  -5.12516500  -2.60478800
H        6.26120900  -3.05632500  -1.69436800
H        6.16698400  -4.76672300  -1.34246500
```

H	6.07665800	-3.43950100	-4.09402200
H	6.36484300	-5.16872100	-3.90631800
H	4.20384800	-4.71726700	-2.18634900
H	4.72143100	-4.24804700	-5.70607400
H	3.04716100	-3.86942600	-5.98793200
H	1.51616700	-4.04591100	-4.14120200
H	2.21718800	-3.73806800	-2.60469600
H	1.97157800	1.57637000	7.27064200
H	0.38829600	1.58677700	6.44967000
H	2.79680100	-0.08657000	5.47532100
H	1.49209800	-0.69315900	6.46971300
H	0.74688600	-0.83832300	2.24930000
H	-6.00487500	1.92720600	7.44151900
H	-7.21171600	0.95848100	6.59371500
H	-6.43020200	-0.70553600	4.82977200
H	-3.69463500	2.00128300	6.70806700
H	-4.67871300	-1.34363400	3.18540600
H	-1.94406000	1.37339500	5.06104300
H	-1.36705700	-0.12340500	3.45543600
H	-5.78380400	0.91542300	2.25983500
H	-6.29872800	2.36078200	1.39418700
H	-6.81189000	-0.63402700	-4.12678300
H	-6.39885600	-0.07749400	-2.48269000
H	-4.28415200	2.26726700	-4.12415800
H	-4.44773500	0.89371700	-3.04760300
H	0.49670000	-7.76448400	0.02776200
H	0.57788500	-7.50156600	-1.70640400
H	0.95679800	-4.95688300	-1.16006000
H	1.27255500	-5.45984100	0.47413000
H	-0.78734300	5.40444100	-0.52829500
H	-1.84973600	6.75733300	-0.95816300
H	-3.77125200	5.46687700	-1.11301100
H	-2.61157700	4.73743800	1.40756500
H	-1.88537300	2.52818500	0.22579300
H	-3.47538100	2.14167900	0.98949000
H	-3.39126400	1.86713900	-1.69076300
H	-0.75085000	1.14363900	1.81115200
H	1.14432300	-1.78827400	-3.53187200
H	2.98740300	-3.60402500	0.13496100
H	2.70599900	-2.48981800	1.48030300
H	3.97020300	-0.94983600	2.95886600
H	2.78880100	-1.71719700	3.59376600
H	-5.38343600	2.46428400	-1.07696900
H	-4.97377300	3.85045900	-0.32815000
H	-2.01717900	2.66713800	-4.18750700
H	-1.09087500	1.85247900	-3.25920100
H	1.80279622	2.24695402	5.63120360
H	8.57115589	-4.04695556	-1.20819080
H	-0.71968542	-6.71685795	-0.76024374
H	-7.90106828	0.50996269	-3.28387750
H	-7.52431636	1.16837835	1.92184089
H	-6.15837529	0.18524165	7.78756862
H	-5.24329307	4.74933031	1.38421869
H	-1.83873274	5.31498416	-3.22345160

Coordinates for the DFT region of the CS-NoCap Mechanism C dissociative TS (*truncation points capped with H*)
ONIOM(M06-2X/6-31G(d):PM6) E = -2767.95126 Hartrees

```
-1 1
C        7.99019900   -4.25739300   -2.10366500
C        6.51093100   -3.88741800   -1.98078200
C        5.79280000   -3.95017100   -3.32493000
N        4.39750600   -3.63288700   -3.09439500
C        3.50367000   -3.41924600   -4.05795300
N        3.84861000   -3.45149200   -5.34630000
N        2.23620000   -3.19151700   -3.69635800
C        1.49459000    1.46418300    6.32714300
C        1.79374400    0.04357300    5.84647300
C        0.99602000   -0.32307200    4.60016400
O        1.40034500   -1.29171700    3.89514600
O       -0.03059200    0.34739700    4.36166300
C       -6.21338700    0.97380400    6.97904400
C       -5.21055600    0.68047100    5.88347400
C       -5.49699500   -0.21313300    4.84982500
C       -3.93418600    1.24357800    5.92214400
C       -4.53522500   -0.59902700    3.92443200
C       -2.94957200    0.86248000    5.01968600
C       -3.24026700   -0.08915700    4.03304400
O       -2.28920500   -0.56432900    3.19067300
C       -6.47494600    1.46204900    1.73013900
C       -5.78003700    0.81265200    0.50386200
O       -6.20624300    1.15701700   -0.64099000
O       -4.83378500    0.04115800    0.74059900
C       -6.86389400    0.22386400   -3.43086900
C       -6.03341600    1.34400300   -4.09329100
O       -6.32770700    1.73263200   -5.22122000
N       -4.99570900    1.76153000   -3.36478200
C        0.27412200   -6.91541700   -0.76263300
C        1.08779400   -5.60944900   -0.79701800
C        2.58759900   -5.70155700   -1.12881100
O        3.23256500   -4.61841300   -0.91448400
O        3.07068600   -6.74283800   -1.60974300
N        1.28357300   -1.50374500   -1.69495800
C        0.42302300   -0.68012500   -2.34128400
N       -0.30012400    0.29844600   -1.84875000
C       -0.17796400    0.40796800   -0.51507300
C        0.65492800   -0.40224500    0.25844500
C        1.45724100   -1.37054100   -0.37212300
N        2.38683600   -2.11535500    0.25658200
N        0.47186300   -0.01399400    1.56462600
C       -0.43523500    0.98154300    1.54217800
N       -0.83687900    1.28191100    0.32036300
C       -2.64508000    2.23930700    0.19268400
C       -2.50138600    3.19063100    1.35030900
C       -3.31333600    4.38536700    0.81711200
O       -4.65004700    4.04257100    1.05913900
C       -2.97582200    4.33891000   -0.69203600
O       -2.80986500    2.87269800   -0.91854900
C       -1.75498000    5.13943800   -1.13895100
O       -1.29393700    4.88504800   -2.44156300
O        3.83373000   -1.61905400    2.84272900
O       -5.62977200    3.78520400   -1.44179400
O       -1.30416700    1.93294500   -4.20702700
H        8.47386500   -3.61266800   -2.87203200
H        8.09256100   -5.29037700   -2.47866100
H        6.40021300   -2.86824200   -1.58987000
H        5.98208000   -4.54174500   -1.28172500
```

H	6.22348300	-3.21906700	-4.03132100
H	5.90479600	-4.94192200	-3.78795600
H	3.98952000	-3.97554000	-2.18419500
H	4.77695800	-3.76457000	-5.64133200
H	3.14378000	-3.32138900	-6.07539600
H	1.58922200	-2.84271700	-4.39985100
H	2.03702600	-2.78071400	-2.76216400
H	1.97476700	1.63756200	7.30895200
H	0.40356600	1.56330400	6.46438600
H	2.85769000	-0.11244500	5.61922900
H	1.53835300	-0.67907100	6.63060300
H	0.80380900	-0.51620800	2.40705500
H	-6.01635800	1.97373800	7.40296800
H	-7.24028000	1.01746000	6.56535100
H	-6.50870500	-0.60276100	4.76046600
H	-3.70014100	1.98745900	6.68763400
H	-4.77583900	-1.22975500	3.07424000
H	-1.95671400	1.30145100	5.06608200
H	-1.40993900	-0.30289300	3.54852800
H	-5.85663200	1.24963000	2.61646200
H	-6.38239500	2.55918100	1.55687500
H	-6.81339300	-0.62624300	-4.13781500
H	-6.42137300	-0.07536900	-2.47327200
H	-4.50470800	2.61129400	-3.66874100
H	-5.01123100	1.59582300	-2.36062900
H	0.54273100	-7.50371300	0.13542000
H	0.55778800	-7.53501700	-1.62973200
H	0.67650600	-4.92534900	-1.56137700
H	0.99692000	-5.05517900	0.14653300
H	-0.90080300	4.92527200	-0.47846000
H	-1.99187900	6.20980100	-0.96065700
H	-3.86763500	4.56133000	-1.27938400
H	-2.99284000	5.34740900	1.26192900
H	-1.45272900	3.48220000	1.46326600
H	-2.91196400	2.81703800	2.28523300
H	-3.09433700	1.25479900	0.25743800
H	-0.78319600	1.45873200	2.44839800
H	0.32847000	-0.84902900	-3.41534600
H	2.68456600	-2.99937900	-0.17375600
H	2.61837600	-1.97039400	1.23994700
H	4.14735500	-0.70586200	2.72393000
H	3.02252800	-1.52855900	3.39420600
H	-5.92240800	3.01354600	-0.92368800
H	-6.42263000	4.32028600	-1.61487700
H	-2.09088900	2.51265800	-4.31808000
H	-1.25333600	1.79290200	-3.25115400
H	8.51895297	-4.15989381	-1.17856330
H	-0.77346617	-6.69767708	-0.76958591
H	1.81602816	2.21779323	5.63892128
H	-1.83271923	5.06048954	-3.21650427
H	-5.24018356	4.69780215	1.43862678
H	-7.50314261	1.26375491	1.95011895
H	-7.87683491	0.54985113	-3.31869453
H	-6.18493715	0.23324972	7.75084058

Coordinates for the DFT region of the CS-NoCap Mechanism C intermediate (*truncation points capped with H)*
ONIOM(M06-2X/6-31G(d):PM6) E = -2767.95738 Hartrees

-1 1

C	8.11143700	-4.11428000	-2.10511000
C	6.59641300	-4.03175100	-2.00997800
C	5.95254400	-4.29287100	-3.36615300
N	4.54477000	-4.50713400	-3.13286400
C	3.56506400	-4.28620500	-3.99649400
N	3.79787800	-4.21587100	-5.30968800
N	2.32888900	-4.23453500	-3.47862000
C	1.45181600	1.55668100	6.29548400
C	1.75094100	0.14238400	5.80099800
C	0.95189500	-0.24371100	4.55901600
O	1.22536700	-1.36450900	4.03020200
O	0.07087200	0.54212500	4.15786400
C	-6.20869400	0.94479100	6.97157800
C	-5.18427600	0.64491100	5.89422300
C	-5.41570800	-0.33267200	4.92472700
C	-3.93897100	1.27893800	5.89056900
C	-4.42838400	-0.72241700	4.02808700
C	-2.93456700	0.90470800	5.00587700
C	-3.16831600	-0.12152100	4.08070400
O	-2.20510800	-0.58811000	3.25610100
C	-6.48501300	1.35925000	1.79220200
C	-5.74576800	1.05851800	0.46433200
O	-6.38171400	1.10376100	-0.62437800
O	-4.52116300	0.85077100	0.59711000
C	-6.88066200	0.10406000	-3.42927400
C	-6.06719500	1.24483500	-4.07630000
O	-6.35044700	1.62561500	-5.20862500
N	-5.05897000	1.69387100	-3.32251700
C	0.35374800	-7.01723200	-0.70511000
C	1.31972800	-5.84116400	-0.51566200
C	2.78427300	-6.12051700	-0.91086700
O	3.59059200	-5.14530600	-0.71619800
O	3.10700700	-7.20530800	-1.42781000
N	1.86031400	-2.30921400	-1.54992900
C	1.15601700	-1.49418800	-2.37536000
N	0.43416600	-0.44390600	-2.08142000
C	0.36189300	-0.22506400	-0.75028300
C	1.02756900	-1.00569200	0.20074400
C	1.84437200	-2.06946400	-0.22575300
N	2.58522700	-2.82757900	0.59949000
N	0.66498800	-0.49536900	1.42499600
C	-0.18021100	0.53220500	1.15810000
N	-0.37927000	0.74121000	-0.12560400
C	-2.81483300	2.30266900	-0.30901400
C	-2.60892100	2.98939300	0.99110200
C	-3.40242400	4.29669600	0.75291000
O	-4.72773400	3.97182800	1.06284000
C	-3.18796400	4.50125200	-0.75958200
O	-3.09831900	3.09045100	-1.25035900
C	-1.89946600	5.22072900	-1.17828100
O	-1.41581700	4.89226900	-2.45608900
O	3.72442000	-1.78384200	3.20388100
O	-5.70737500	3.77570000	-1.48139000
O	-1.35005200	1.90080300	-4.21956200
H	8.49483400	-3.35125700	-2.81992300
H	8.39204600	-5.08775500	-2.55040600
H	6.27108800	-3.04837700	-1.65030900
H	6.20129300	-4.75938800	-1.29634800

H	6.10403200	-3.43835300	-4.05101200
H	6.40889600	-5.16375600	-3.85785400
H	4.23639100	-4.73235200	-2.15063400
H	4.75706300	-4.24866100	-5.66686700
H	3.08393800	-3.85808900	-5.95099500
H	1.55050700	-4.02080900	-4.09981700
H	2.25786600	-3.73686400	-2.55847800
H	1.93303600	1.71932900	7.27892000
H	0.36054900	1.65616000	6.43930800
H	2.81600700	-0.00291900	5.56368000
H	1.51900100	-0.59207200	6.58042500
H	0.84836700	-0.89707400	2.36078900
H	-6.02773900	1.95263500	7.38328600
H	-7.22996600	0.97150900	6.54248800
H	-6.40040200	-0.79138800	4.86603300
H	-3.74594700	2.07814100	6.61034200
H	-4.62292600	-1.45683700	3.25129500
H	-1.97129500	1.41002200	5.00675400
H	-1.33998300	-0.18868900	3.51382700
H	-5.87615700	0.93547100	2.60393900
H	-6.32701700	2.45832900	1.89047500
H	-6.81517600	-0.73761700	-4.14380100
H	-6.43573300	-0.20141900	-2.47496700
H	-4.58026500	2.55434300	-3.61597900
H	-5.10905800	1.53866000	-2.31731000
H	0.53780500	-7.77084200	0.08703000
H	0.62300700	-7.52285800	-1.64829900
H	1.00821400	-4.97466000	-1.12323300
H	1.31599700	-5.46422600	0.51626400
H	-1.08557300	4.96358400	-0.48489500
H	-2.06717500	6.30793300	-1.03419600
H	-4.08119200	4.88509800	-1.24532400
H	-2.98829600	5.14983700	1.32152300
H	-1.53406400	3.18930900	1.08357400
H	-2.98769000	2.41782800	1.83054600
H	-2.63050200	1.27542100	-0.54417900
H	-0.62588400	1.10434300	1.96334500
H	1.21492000	-1.75707600	-3.43611900
H	3.05664700	-3.64535900	0.19663800
H	2.81149300	-2.52399100	1.54723100
H	3.98265500	-0.88054200	2.95463000
H	2.84602700	-1.67114900	3.64413600
H	-6.08157100	3.03144100	-0.98146000
H	-6.46712200	4.25221900	-1.86020300
H	-2.17005600	2.43690200	-4.30617900
H	-1.14418400	1.94581500	-3.27819800
H	8.59701018	-3.99977761	-1.15853307
H	-0.67719744	-6.73088414	-0.71262009
H	1.76957721	2.31696692	5.61292036
H	-1.94317499	5.03811539	-3.24489974
H	-5.32625099	4.63204453	1.41989959
H	-7.89834346	0.41417371	-3.31502015
H	-7.52286997	1.16778572	1.96853790
H	-6.18347046	0.21509275	7.75375716

Appendix D: Supplemental Information for

Chapter 5: Bifunctional Glycosylases Part 1:

Exploration of the Glycosylase/Lyase Mechanism

Table of Contents

Table D1. *Reaction energetics (kJ mol^{-1}) for eight possible glycosylase/lyase mechanisms optimized with IEF-PCM-B3LYP/6-31+G(d).*[a]

	D-N$_R$C$_R$	D-N$_S$C$_R$	D-N$_R$C$_S$	D-N$_S$C$_S$	A-N$_R$C$_R$	A-N$_S$C$_R$	A-N$_R$C$_S$	A-N$_S$C$_S$
				ΔE^{b}				
TS(a)	145.2	145.2	145.2	145.2	145.2	145.2	145.2	145.2
IC(a)	67.0	67.1	67.1	67.1	–2.7	5.9	–2.7	5.9
TS(b)	199.3	190.3	199.3	190.3	–16.4	–5.0	–16.4	–5.0
IC(b')					–10.5	–14.6	–10.5	–22.3
TS(b')					45.2	51.5	45.2	51.5
IC(b)	38.3	32.3	87.9	75.7	49.3	56.6	30.0	30.0
TS(c)	93.5	79.6	93.9	93.8	79.6	87.8	70.4	70.4
IC(c')	60.6	22.2	60.5	71.3	54.8	56.5	52.0	52.0
TS(c')	ND[d]	ND	174.2	ND	ND	ND	185.8	ND
IC(c)	157.8	25.3	105.8	96.9	57.6	141.2	48.9	48.9
				ΔG^{c}				
TS(a)	142.9	142.9	142.9	142.9	142.9	142.9	142.9	142.9
IC(a)	65.5	65.7	65.7	65.7	–2.9	6.7	–2.9	6.7
TS(b)	198.4	190.9	198.4	190.9	–12.7	–1.2	–12.7	–1.2
IC(b')					–9.7	–14.4	–9.7	–18.3
TS(b')					49.4	64.9	49.5	64.8
IC(b)	40.9	28.1	81.4	73.6	50.2	60.6	33.5	33.6
TS(c)	94.2	82.9	91.6	95.1	86.1	91.4	76.9	76.9
IC(c')	59.7	22.0	54.8	62.4	54.6	54.9	53.1	53.1
TS(c')	ND	ND	160.3	ND	ND	ND	184.2	ND
IC(c)	134.4	8.4	94.7	78.3	46.7	130.4	27.1	27.1

[a] Energies reported relative to a common reactant complex (Figure 1). [b] PCM-M06-2X/6-311+G(2df,2p)//PCM-B3LYP/6-31+G(d) values including scaled (0.9806) zero-point vibrational energy correction. [c] SMD-M06-2X/6-311+G(2df,2p)//PCM-B3LYP/6-31+G(d) values including unscaled correction to Gibbs energy. [d] Could not be optimized at PCM-B3LYP/6-31+G(d).

Full citation for reference 49.

Frisch, M. J. T., G. W.; Schlegel, H. B. Scuseria, G. E.; Robb, M. A.; Cheeseman, J. R.; Scalmani, G.; Barone, V.; Mennucci, B.; Petersson, G. A.; Nakatsuji, H.; Caricato, M.; Li, X.; Hratchian, H. P.; Izmaylov, A. F.; Bloino, J.; Zheng, G.; Sonnenberg, J. L.; Hada, M.; Ehara, M.; Toyota, K.; Fukuda, R.; Hasegawa, J.; Ishida, M.; Nakajima, T.; Honda, Y.; Kitao, O.; Nakai, H.; Vreven, T.; Montgomery, Jr., J. A.; Peralta, J. E.; Ogliaro, F.; Bearpark, M.; Heyd, J. J.; Brothers, E.; Kudin, K. N.; Staroverov, V. N.; Kobayashi, R.; Normand, J.; Raghavachari, K.; Rendell, A.; Burant, J. C.; Iyengar, S. S.; Tomasi, J.; Cossi, M.; Rega, N.; Millam, N. J.; Klene, M.; Knox, J. E.; Cross, J. B.; Bakken, V.; Adamo, C.; Jaramillo, J.; Gomperts, R.; Stratmann, R. E.; Yazyev, O.; Austin, A. J.; Cammi, R.; Pomelli, C.; Ochterski, J. W.; Martin, R. L.; Morokuma, K.; Zakrzewski, V. G.; Voth, G. A.; Salvador, P.; Dannenberg, J. J.; Dapprich, S.; Daniels, A. D.; Farkas, Ö.; Foresman, J. B.; Ortiz, J. V.; Cioslowski, J.; Fox, D. J.; Revision A.1 .; Gaussian, Inc.: Wallingford CT, **2009**.

IEF-PCM-M06-2X/6-311+G(2df,2p)//IEF-PCM-B3LYP/6-31G(d) Energies and Structures.

RC (all mechanisms)   -1982.08947322

O	0.48738800	-3.63325900	-1.61067900
C	0.81738600	-3.11561400	-0.33087000
C	1.00158200	-1.60922500	-0.46691700
O	-0.24102000	-0.96028800	-0.79802200
C	1.49987800	-0.92735000	0.82057200
O	2.29049400	0.23842700	0.50185600
C	0.20805300	-0.46144200	1.48794100
C	-0.72460800	-0.18010100	0.29691600
N	-2.12885600	-0.48570300	0.55024700
C	-2.63360700	-1.69247300	1.09157700
N	-4.00462400	-1.57324200	1.02263400
C	-4.35978800	-0.35863800	0.43916000
C	-5.62350000	0.21648300	0.14716000
O	-6.75510300	-0.22772700	0.34163300
N	-5.43988200	1.49365900	-0.46159000
C	-4.23237300	2.08514600	-0.72915500
N	-4.24822800	3.28884500	-1.37846800
N	-3.07518400	1.52301100	-0.43770100
C	-3.18800700	0.30692100	0.13611300
O	-1.98944000	-2.63555800	1.54051900
P	3.90233100	0.07818500	0.21031800
O	4.34366300	1.36886900	-0.45038200
O	4.20426400	-1.20048100	-0.54418100
O	4.52831600	-0.09545000	1.70898700
C	4.46197600	1.00838100	2.62377500
C	0.20563500	-5.01805300	-1.57294100
N	0.88721000	2.78085500	-0.83826600
C	1.53424100	4.10045500	-0.83573500
C	1.84171200	4.54217500	0.59353700
Na	5.18314400	0.07478400	-2.23640300
H	1.75904000	-3.56432300	0.02888200
H	0.02027000	-3.33673100	0.39278800
H	1.70449900	-1.42048700	-1.28206500
H	2.08241900	-1.59995400	1.45643200
H	-0.19805000	-1.26417300	2.10533300
H	0.36470500	0.42629400	2.10423800
H	-0.70674100	0.87575900	0.01145600
H	-4.63549400	-2.29314200	1.34211700
H	-6.30189400	1.95301000	-0.73546600
H	-5.04968500	3.89389600	-1.25488500
H	-3.35682400	3.76841800	-1.37485300
H	4.99103000	1.87796700	2.22151400
H	3.42105100	1.27960100	2.83154200
H	-0.03652000	-5.32751900	-2.59345600
H	1.07144400	-5.60101900	-1.21915600
H	-0.65094300	-5.24047900	-0.91798500
H	4.94272000	0.67988400	3.54770100
H	1.54434000	2.08263300	-0.48798700
H	0.67622400	2.50575300	-1.79710800
H	2.46603900	4.13251600	-1.42803400
H	0.84405800	4.81693700	-1.30046300
H	2.28999100	5.54239300	0.60855300
H	0.92712300	4.55873500	1.19649000
H	2.54860900	3.85041100	1.06742200

TS(a) (all mechanisms)   -1982.03103674

O	0.28110100	-2.79055900	-1.89247900
C	0.70712200	-2.35958200	-0.61423600

```
C         1.26335100   -0.95536700   -0.75439300
O         0.18337000   -0.04268700   -1.20935400
C         1.75730200   -0.32879600    0.56090000
O         2.87301200    0.54809900    0.32955500
C         0.54793300    0.49402300    1.02612800
C        -0.18014000    0.75224800   -0.25470200
N        -2.26293100   -0.31743600    0.43455900
C        -2.37858800   -1.23085100    1.45981100
N        -3.73312500   -1.43409600    1.72363900
C        -4.47345100   -0.62167500    0.86863300
C        -5.85851500   -0.42466000    0.70471100
O        -6.82458200   -0.93614500    1.28876500
N        -6.08566300    0.54023000   -0.32836400
C        -5.10907600    1.18283400   -1.04384100
N        -5.54052500    2.03998800   -2.04281100
N        -3.82460700    0.98367300   -0.86787600
C        -3.52116200    0.05389200    0.09347800
O        -1.44272500   -1.79138000    2.07126200
P         4.38785100   -0.11687200    0.25619000
O         5.30527700    0.95879400   -0.28229900
O         4.35485900   -1.42457100   -0.50744500
O         4.69286700   -0.47541100    1.81655300
C         4.89021700    0.59692500    2.75248800
C        -0.33464300   -4.06614700   -1.85197600
C         0.74136000    4.02760100   -0.77920900
C         0.68345200    4.39702900    0.70063800
N         1.12013500    2.61585800   -0.96523000
Na        6.00419800   -0.58286700   -1.93728100
H         1.52245500   -2.99840900   -0.23571100
H        -0.11178700   -2.37719000    0.11984200
H         2.02427200   -0.92108400   -1.53230600
H         2.03147900   -1.09163200    1.29338200
H        -0.09095000   -0.13870700    1.65716400
H         0.82144800    1.40224900    1.56212000
H        -0.98382200    1.43569700   -0.45392800
H        -4.09204600   -2.04358400    2.44270700
H        -7.06232800    0.69490500   -0.55089200
H        -6.37813300    2.57462000   -1.84172100
H        -4.78798100    2.62291500   -2.38980200
H         5.74018400    1.21802200    2.45433500
H         3.99146300    1.21880300    2.82601800
H        -0.63116400   -4.31073800   -2.87508300
H         0.35875800   -4.83872700   -1.48450200
H        -1.22694000   -4.06301400   -1.20917300
H         5.09106000    0.13373500    3.72036800
H         2.04388200    2.42265900   -0.57744600
H         1.16597500    2.38855500   -1.95795900
H         1.43590600    4.70413200   -1.30089600
H        -0.24403900    4.16884300   -1.23865600
H         0.41072200    5.45096000    0.81912500
H        -0.05878600    3.79214700    1.23237500
H         1.65703500    4.24797500    1.18342600
```

IC(a) (D-N$_R$C$_R$, D-N$_S$C$_R$ and D-N$_S$C$_S$)   -1982.06707993

```
O        -1.66327500    3.60279700   -1.24635000
C        -1.62724700    2.78124700   -0.09229700
C        -2.01638300    1.37176500   -0.51664200
O        -0.95374300    0.79539600   -1.33306300
C        -2.17696300    0.38624000    0.64613600
O        -2.98098800   -0.74638200    0.21947300
C        -0.75539500   -0.13284500    0.82317700
C        -0.26646200   -0.19291100   -0.62012600
```

N	2.69595300	-0.00265300	0.32650600
C	2.68401300	1.17826300	1.04381300
N	4.00383100	1.59231200	1.24948900
C	4.85343300	0.67379500	0.64104100
C	6.25371700	0.60730500	0.52323600
O	7.14268300	1.36816200	0.93750100
N	6.61663800	-0.56377800	-0.21738700
C	5.73577100	-1.47854400	-0.73265100
N	6.29023300	-2.50936200	-1.48093800
N	4.43456300	-1.39562600	-0.60475200
C	3.99683000	-0.29057800	0.08647100
O	1.68934700	1.80877300	1.46431500
P	-4.63112600	-0.67279700	0.34309200
O	-5.17278300	-1.79249100	-0.51920400
O	-5.13015500	0.72264100	0.03812400
O	-4.87719600	-0.93512300	1.93251800
C	-4.58331500	-2.22806300	2.48389900
H	-2.34376200	3.14688000	0.66280400
H	-0.62157700	2.77728300	0.35548900
H	-2.92094100	1.41275100	-1.12535700
H	-2.60463300	0.83561300	1.54464700
H	-0.11047500	0.58780700	1.34163900
H	-0.71796800	-1.08569300	1.35280900
H	0.81840800	-0.09948500	-0.72010300
H	4.26888200	2.43881100	1.72912000
H	7.60904600	-0.65464900	-0.40181500
H	7.17200600	-2.87454800	-1.13734100
H	5.61698800	-3.24898900	-1.64513200
H	-5.15533300	-3.00689200	1.97063900
H	-3.51300500	-2.44907500	2.40665900
C	-1.21463000	4.91987000	-0.98400600
H	-1.27472600	5.47347500	-1.92472300
H	-1.84504500	5.42109600	-0.23252500
H	-0.17408000	4.92901700	-0.62667600
H	-4.86984500	-2.19205100	3.53663000
Na	-6.53105100	-0.16696300	-1.60464700
N	-0.64786600	-1.53960300	-1.29403900
H	-1.54173100	-1.84722700	-0.88446500
H	-0.85415100	-1.29762600	-2.26881700
C	0.39953600	-2.62807900	-1.27006400
H	-0.00745400	-3.44623100	-1.86956700
H	1.27332000	-2.21735800	-1.78055300
C	0.76612700	-3.08306800	0.13432700
H	1.45680200	-3.92749100	0.04707400
H	1.27883800	-2.28728600	0.68123500
H	-0.10989500	-3.42516800	0.69650700

IC(a) (D-N$_R$C$_S$)   -1982.06821827

O	-1.78426800	3.58047100	-1.51291800
C	-1.72380100	2.88190300	-0.28245600
C	-2.07033100	1.42464200	-0.55900700
O	-0.99312200	0.80318100	-1.31994800
C	-2.19103300	0.55764900	0.69933000
O	-2.93690100	-0.65056800	0.39219200
C	-0.74694600	0.12136800	0.92459400
C	-0.25800100	-0.06578100	-0.50690800
N	2.77193200	0.13318600	0.16963800
C	2.77510800	1.34118900	0.84048200
N	4.09927400	1.69179700	1.12619200
C	4.93607000	0.70231400	0.61939700
C	6.33417100	0.54837000	0.61598600
O	7.23475900	1.27300700	1.06867400

```
N          6.67972800   -0.67428600   -0.04622600
C          5.78634600   -1.56036800   -0.58900400
N          6.33157300   -2.65549400   -1.24689500
N          4.48659900   -1.39668800   -0.56621700
C          4.06663700   -0.23637700    0.04047600
O          1.78948700    2.03840000    1.16505900
P         -4.59254400   -0.65616200    0.45840700
O         -5.02473800   -1.95912500   -0.17913000
O         -5.16828400    0.61121800   -0.13406700
O         -4.88010800   -0.61491300    2.06112400
C         -4.54310100   -1.75757200    2.86400000
H         -2.44865500    3.30208800    0.43565000
H         -0.71715200    2.95394700    0.15756700
H         -2.97914800    1.37392800   -1.16058400
H         -2.64341200    1.07392700    1.54881500
H         -0.13051600    0.91404300    1.36269800
H         -0.66652400   -0.77034100    1.55009500
H          0.82156700    0.05829300   -0.62697900
H          4.37795300    2.54098900    1.59326400
H          7.67585900   -0.83197000   -0.14615700
H          7.16204600   -3.05350100   -0.82184100
H          5.62933900   -3.36218000   -1.43289300
H         -5.06127500   -2.65062200    2.50214000
H         -3.46176500   -1.93283700    2.85504000
C         -1.37503000    4.93005900   -1.38639300
H         -1.45154200    5.38345900   -2.37812300
H         -2.02018000    5.48585900   -0.68764100
H         -0.33507300    5.00600400   -1.03518700
H         -4.86475400   -1.53004200    3.88198900
Na        -6.40522800   -0.71222600   -1.62833500
N         -0.57708800   -1.49193700   -1.01497100
H         -1.55899300   -1.68466300   -0.76399900
H         -0.53523200   -1.44439700   -2.03844200
C          0.34661100   -2.57266700   -0.51551000
H          1.36483900   -2.20869900   -0.67106400
H          0.17883700   -2.65347800    0.56004200
C          0.07975100   -3.89442100   -1.22215000
H          0.76501800   -4.65166600   -0.83000700
H         -0.94378900   -4.24610100   -1.05285000
H          0.25079200   -3.81637900   -2.30149400
```

IC(a) (A-N$_R$C$_R$ and A-N$_R$C$_S$)   -1982.09274104

```
O          2.87699500    3.97893600   -0.02699400
C          2.67775700    2.91547300   -0.93690400
C          2.39047200    1.65254900   -0.13855700
O          1.13531400    1.79789500    0.58136100
C          2.22664500    0.38898300   -1.00294100
O          2.65973300   -0.77352800   -0.26066000
C          0.70885300    0.29098300   -1.16914500
C          0.21062900    0.82179000    0.17399600
N         -2.92363700   -0.10602900    0.39065200
C         -2.69866200   -1.42674400    0.13700500
N         -3.85809600   -2.03972200   -0.29996000
C         -4.86140700   -1.07532600   -0.32382700
C         -6.22343600   -1.13287600   -0.68466500
O         -6.91282100   -2.07971600   -1.08750400
N         -6.80983100    0.16012900   -0.52896400
C         -6.15022100    1.28328600   -0.09517400
N         -6.88499200    2.45716600   -0.08100200
N         -4.88337400    1.30601300    0.23898900
C         -4.23863300    0.10344100    0.10831200
O         -1.59503800   -2.04742300    0.27035600
```

```
P      4.25306000   -1.22221400   -0.34412700
O      4.48554800   -2.20486200    0.78191500
O      5.14625800   -0.00001800   -0.37333600
O      4.34207600   -1.92131300   -1.81337600
C      3.65207400   -3.16234200   -2.03829100
H      3.58143300    2.75257800   -1.54731700
H      1.84102400    3.13817100   -1.61977400
H      3.19192500    1.51014300    0.58964000
H      2.76114000    0.44639400   -1.95392100
H      0.37275400    0.96206700   -1.96518800
H      0.36170000   -0.71976600   -1.39306400
H     -0.79864700    1.23429000    0.16098200
H     -3.94318200   -3.01464000   -0.54484900
H     -7.77847700    0.22213400   -0.82117000
H     -7.85985700    2.37090300    0.18343200
H     -6.41148100    3.19038500    0.43382600
H      4.00707300   -3.93236600   -1.34699900
H      2.57146300   -3.03221600   -1.91666100
C      3.11875200    5.21208500   -0.67907800
H      3.26610800    5.96429400    0.09993400
H      4.01982700    5.16729500   -1.31060400
H      2.26675900    5.51046000   -1.30917700
H      3.86976700   -3.45872900   -3.06615700
Na     6.26721500   -0.82992500    1.50484900
N      0.16174000   -0.30905100    1.17894700
H     -0.55938600   -1.04775700    0.80732600
H      1.08609900   -0.75845700    1.19087800
C     -0.24790100    0.10864700    2.55536700
H      0.41909900    0.91327700    2.87249200
H     -1.26226400    0.50152800    2.45335900
C     -0.20706100   -1.08074300    3.50754700
H     -0.55399100   -0.76950000    4.49769600
H     -0.85797000   -1.88577100    3.15215500
H      0.80946600   -1.47686200    3.61512900
```

IC(a) (A-N$_S$C$_R$ and A-N$_S$C$_S$)   -1982.08796656

```
O     -1.08898700    2.61905100   -2.86002900
C     -2.07994700    2.56868500   -1.85452800
C     -1.73358100    1.43323300   -0.90192100
O     -0.48844900    1.72296100   -0.21484200
C     -2.77407200    1.21896700    0.21126400
O     -2.78020300   -0.15739300    0.64987900
C     -2.18746700    2.03715500    1.36569300
C     -0.68551000    1.80825000    1.17186800
N      2.31780000    0.23560000    1.03043200
C      2.97254800    1.39209300    1.41837300
N      4.25558400    1.36276200    0.87818900
C      4.39654800    0.19704500    0.12900100
C      5.46718400   -0.31737400   -0.62967100
O      6.59773600    0.13933400   -0.84575500
N      5.08676100   -1.57120000   -1.20610300
C      3.87207100   -2.18270900   -1.04347300
N      3.67877500   -3.36921000   -1.73287100
N      2.89222500   -1.68186400   -0.32862300
C      3.17369100   -0.47217800    0.24902600
O      2.51031400    2.30633500    2.12731200
P     -3.53551000   -1.34077900   -0.23440700
O     -2.96578300   -2.64767300    0.27090000
O     -3.40696300   -1.07026700   -1.71749800
O     -5.10125100   -1.13775000    0.16363800
C     -5.53427000   -1.46043600    1.49506900
H     -3.07203100    2.37450000   -2.29595900
```

H	-2.13223200	3.52729300	-1.31136100
H	-1.60320300	0.51930400	-1.48274100
H	-3.78375400	1.52533700	-0.07456600
H	-2.40838600	3.10005400	1.22859700
H	-2.57688700	1.72703600	2.33734200
H	-0.02433800	2.57397300	1.57988300
H	4.93327800	2.10316100	0.97646300
H	5.78917500	-1.98527700	-1.80850600
H	4.49603300	-3.96002700	-1.83831500
H	2.88287700	-3.88499000	-1.37610300
H	-5.32096600	-2.50783500	1.72777600
H	-5.04192600	-0.81512500	2.23081300
C	-1.30278000	3.67356000	-3.77973200
H	-0.49445700	3.62875500	-4.51368000
H	-2.26774000	3.56866200	-4.30019500
H	-1.28086900	4.65527300	-3.28172200
H	-6.61171900	-1.28694600	1.52361600
Na	-2.17309100	-3.05526900	-1.92310100
N	-0.22535500	0.50710300	1.79734900
H	-0.88972700	-0.22511200	1.51812000
H	0.78005000	0.28144200	1.38081800
C	-0.06836800	0.54662600	3.28556300
H	0.75077900	1.24617800	3.47070100
H	-0.98696400	0.94350600	3.72737200
C	0.24542300	-0.84273100	3.82838100
H	0.38756600	-0.78706200	4.91218100
H	-0.57189400	-1.54595100	3.63061800
H	1.16333700	-1.23674800	3.38216700

TS(b) (D- N_RC_R and D- N_RC_S)   -1982.00861242

O	0.63138500	-2.64505500	-2.06780800
C	0.88291500	-2.25658100	-0.72961800
C	1.61535200	-0.92874600	-0.76599100
O	0.68968300	0.10783600	-1.29208300
C	2.04550600	-0.37900400	0.59984100
O	3.15821500	0.52040900	0.44105600
C	0.82614000	0.41410000	1.08997500
C	0.13811800	0.95488400	-0.15457600
N	-2.83079900	0.16232000	0.37499800
C	-2.70528600	-1.03372100	1.04791200
N	-3.97692800	-1.56788100	1.26425000
C	-4.91532200	-0.70161900	0.71399000
C	-6.31928200	-0.75136000	0.63365100
O	-7.12689700	-1.60042900	1.04242600
N	-6.80001600	0.40815900	-0.05339100
C	-6.01328400	1.41283100	-0.55482800
N	-6.67293100	2.41677800	-1.25164500
N	-4.70698600	1.43801500	-0.46058400
C	-4.15808300	0.35074900	0.17561200
O	-1.64857400	-1.59221000	1.42632800
P	4.68705200	-0.11294300	0.38578400
O	5.61128200	1.02114100	0.00268200
O	4.72121700	-1.34259500	-0.49835800
O	4.91665500	-0.61568500	1.91936400
C	5.07100300	0.36461300	2.95874800
H	1.53652800	-2.98884700	-0.22583600
H	-0.04919100	-2.17140600	-0.14994200
H	2.45210600	-0.97233900	-1.46126100
H	2.31012200	-1.17993500	1.29540100
H	0.10716000	-0.26751100	1.56026900
H	1.10606900	1.19149300	1.80353000
H	-0.95432300	0.84867800	-0.14152200

```
H      -4.15989800   -2.44155400    1.73332300
H      -7.80107500    0.42008900   -0.21060800
H      -7.57330100    2.69403700   -0.87589000
H      -6.06886900    3.21522600   -1.40916800
H       5.92898300    1.01155200    2.75383300
H       4.16719000    0.97624200    3.05417700
C      -0.15531200   -3.82175300   -2.14590400
H      -0.30643700   -4.03537400   -3.20706700
H       0.35133300   -4.67906200   -1.67599400
H      -1.13303500   -3.68554100   -1.66155300
H       5.23519700   -0.18685500    3.88639800
Na      6.44313900   -0.34654300   -1.73796600
N       0.60097100    2.22040600   -0.76720500
H       1.10867200    1.18072600   -1.58284100
H      -0.19018500    2.69038400   -1.20946700
C       1.41143500    3.20561100   -0.00667700
H       0.83873700    3.55495400    0.86105500
H       2.30369600    2.69069600    0.34900500
C       1.78361200    4.37600400   -0.91032900
H       2.38822500    5.09501900   -0.34932000
H       2.36625600    4.03647100   -1.77306200
H       0.89374400    4.90105300   -1.27722200
```

TS(b) (D- N$_S$C$_R$ and D- N$_S$C$_S$)   -1982.01251693

```
O      -1.16903200    3.07491900   -1.76481600
C      -1.26960000    2.49900300   -0.47471500
C      -1.88972800    1.12394000   -0.63728500
O      -0.90358500    0.24260700   -1.31935600
C      -2.19644900    0.37584600    0.66614700
O      -3.14397400   -0.68117200    0.40772400
C      -0.86479200   -0.28397100    1.02884500
C      -0.26894300   -0.70685700   -0.30195900
N       2.69105200   -0.01346500    0.30884000
C       2.58797700    1.19252200    0.96894800
N       3.87114200    1.68610500    1.21293700
C       4.79395800    0.78195400    0.69796300
C       6.20078700    0.77888200    0.66165500
O       7.02623800    1.60227400    1.08687200
N       6.65968200   -0.40580300    0.00300100
C       5.85257500   -1.38815000   -0.51012500
N       6.49534900   -2.42564400   -1.17269900
N       4.54404800   -1.36388800   -0.45647600
C       4.01605500   -0.24968600    0.14964300
O       1.54200700    1.78712000    1.31993200
P      -4.76466800   -0.34002100    0.41463100
O      -5.46094800   -1.57377600   -0.11423000
O      -5.04084000    0.95945000   -0.31264500
O      -5.06341800   -0.07903100    1.99510300
C      -5.01912800   -1.18702900    2.90911900
H      -1.93074800    3.10078900    0.17193400
H      -0.28424100    2.42579000    0.01023500
H      -2.76259000    1.17212100   -1.28688100
H      -2.56930100    1.04090000    1.44919100
H      -0.17444100    0.44388800    1.47278900
H      -0.99737500   -1.12712400    1.71130200
H       0.82245700   -0.61511200   -0.36413200
H       4.07112800    2.55519900    1.68371400
H       7.66413900   -0.45632200   -0.12151900
H       7.37198200   -2.73165700   -0.76452300
H       5.86624300   -3.20275500   -1.33891200
H      -5.74015100   -1.95656300    2.61801800
H      -4.01449600   -1.62235200    2.94461300
```

```
C      -0.47476500    4.31090100   -1.74799900
H      -0.43031500    4.66638200   -2.78054100
H      -0.99716000    5.06012600   -1.13301400
H       0.54773300    4.19275300   -1.36115800
H      -5.27701200   -0.79044200    3.89287700
Na     -6.55946500   -0.18017300   -1.68831400
N      -0.81026700   -1.91016600   -0.95731100
H      -1.55905600   -2.33359000   -0.40775700
H      -1.28507400   -0.81422000   -1.70475900
C       0.14902300   -2.91462800   -1.47841400
H      -0.43426800   -3.60237800   -2.09771200
H       0.84373300   -2.38448000   -2.13608800
C       0.90557700   -3.66421100   -0.38430200
H       1.55358000   -4.42131700   -0.83840000
H       1.53954200   -2.98349200    0.19252700
H       0.21593100   -4.17412000    0.29835200
```

TS(b) (A- N$_R$C$_R$ and A- N$_R$C$_S$)   -1982.09247548

```
O       3.06045600    3.92499400   -0.01157100
C       2.82368400    2.86254400   -0.91481800
C       2.45345200    1.62292600   -0.11348800
O       1.20178600    1.84096800    0.58070300
C       2.24434000    0.36694000   -0.98278800
O       2.66897700   -0.81371900   -0.26446000
C       0.72301400    0.30699500   -1.12951500
C       0.24251500    0.86423400    0.21205400
N      -3.01252900    0.04722900    0.39790500
C      -2.75012700   -1.26652800    0.25773500
N      -3.85863400   -1.97108300   -0.13611400
C      -4.89925200   -1.05512400   -0.25586900
C      -6.25467900   -1.20284800   -0.62920800
O      -6.89130700   -2.21040600   -0.95637700
N      -6.89317300    0.07117500   -0.59321800
C      -6.28674900    1.25625800   -0.25032800
N      -7.06631100    2.39257500   -0.34917800
N      -5.02712200    1.36038600    0.09766200
C      -4.33576800    0.18024300    0.08053300
O      -1.61174200   -1.85293700    0.45483400
P       4.24989400   -1.28317900   -0.38186700
O       4.49627900   -2.27613300    0.73314000
O       5.16361900   -0.07577500   -0.42517600
O       4.30415200   -1.97878400   -1.85656900
C       3.58757900   -3.20483600   -2.07412200
H       3.72982000    2.64761500   -1.50500800
H       2.01225500    3.12125100   -1.61560500
H       3.23943700    1.43932500    0.62344800
H       2.76342200    0.42217600   -1.94291000
H       0.40140500    0.97594200   -1.93360700
H       0.35452300   -0.69865400   -1.34206400
H      -0.74194300    1.33331000    0.17565700
H      -3.89660700   -2.96646300   -0.29818400
H      -7.85959500    0.06749600   -0.90008600
H      -8.04659200    2.29328200   -0.11244500
H      -6.63584400    3.19204000    0.10023200
H       3.94125000   -3.98592600   -1.39435300
H       2.51197200   -3.05606600   -1.93038000
C       3.37493300    5.13665500   -0.67131600
H       3.54901200    5.88911700    0.10212300
H       4.28192800    5.03982800   -1.28869600
H       2.54926700    5.47208500   -1.31794700
H       3.77896600   -3.50017100   -3.10768000
Na      6.29018300   -0.91231100    1.43872700
```

N	0.13950700	-0.22700700	1.22020100
H	-0.77143500	-1.05560700	0.82040800
H	1.03233300	-0.73038100	1.23867200
C	-0.21259700	0.24208100	2.58681200
H	0.48566400	1.02901600	2.88834900
H	-1.21313900	0.67866400	2.51369300
C	-0.19845200	-0.92051400	3.57438200
H	-0.50056300	-0.57084300	4.56677900
H	-0.89069300	-1.70876100	3.26150300
H	0.80344900	-1.35790600	3.66272500

TS(b) (A- N_SC_R and A- N_SC_S)   -1982.08779258

O	1.09721800	-2.51260900	-2.95397700
C	2.08745200	-2.47262800	-1.94685000
C	1.70141000	-1.39840600	-0.93955100
O	0.46795600	-1.76211900	-0.27213300
C	2.73782100	-1.20818100	0.18253500
O	2.71683300	0.14843300	0.67860700
C	2.17433600	-2.09319300	1.29779500
C	0.66424100	-1.90308200	1.11415500
N	-2.30552400	-0.39551700	0.99730900
C	-3.02393100	-1.55492400	1.24867800
N	-4.27764800	-1.40512600	0.66397600
C	-4.33521300	-0.16413400	0.03351900
C	-5.35393100	0.47812900	-0.70083600
O	-6.49401200	0.10050500	-0.99805500
N	-4.89683700	1.76515100	-1.12869900
C	-3.66394600	2.29873900	-0.86411300
N	-3.39323800	3.53996900	-1.41421900
N	-2.73348500	1.67833900	-0.17587600
C	-3.09293500	0.43321800	0.26072800
O	-2.62982100	-2.54762000	1.88236600
P	3.46622600	1.36799200	-0.15680900
O	2.87374000	2.65477500	0.37376300
O	3.36613200	1.13722700	-1.64924400
O	5.03023200	1.17682000	0.25825700
C	5.43759000	1.46561800	1.60507300
H	3.07033700	-2.22012100	-2.37907100
H	2.17698900	-3.45347300	-1.44994400
H	1.54267900	-0.46143600	-1.47513100
H	3.75335000	-1.47945600	-0.11829700
H	2.43125300	-3.14085400	1.11252600
H	2.55275200	-1.81410900	2.28333100
H	0.03985300	-2.72214300	1.47567100
H	-4.99662700	-2.11233900	0.67051900
H	-5.56039100	2.27602300	-1.69995800
H	-4.18151900	4.17176800	-1.50016900
H	-2.59690600	3.98391700	-0.97202800
H	5.20793200	2.50331500	1.86452800
H	4.94145800	0.79368100	2.31402200
C	1.35307000	-3.50792500	-3.92684500
H	0.54241200	-3.45889800	-4.65811700
H	2.31202900	-3.33630000	-4.44088600
H	1.37303700	-4.51444600	-3.48084600
H	6.51656500	1.30415200	1.64675700
Na	2.11897300	3.10796100	-1.83272100
N	0.14924100	-0.66595100	1.79925800
H	0.78744700	0.10630400	1.57764500
H	-0.93238800	-0.44107400	1.36153700
C	-0.01984000	-0.80469100	3.27539700
H	-0.82636600	-1.53023800	3.41443500
H	0.89798900	-1.21296800	3.71164300

C	-0.36755300	0.53880100	3.90695500
H	-0.52163500	0.41038800	4.98300500
H	0.43892400	1.26792100	3.76626300
H	-1.28648900	0.94753000	3.47587800

IC(b') (A- N$_R$C$_R$ and A- N$_R$C$_S$)   -1982.09327228

O	0.55610300	3.04526400	-0.11207700
C	1.23603100	2.18807700	-1.00925700
C	1.66432800	0.94796100	-0.23732100
O	0.50416400	0.25768900	0.26818500
C	2.41563300	-0.07664300	-1.10736300
O	3.40593100	-0.78205400	-0.32812100
C	1.32036100	-1.07001300	-1.49650200
C	0.40945500	-1.12353400	-0.26630600
N	-2.85652900	-0.01106900	-0.20357600
C	-2.78536200	0.86905300	0.79096300
N	-4.00146000	1.23428800	1.28091200
C	-4.94367300	0.52692500	0.54083400
C	-6.35924800	0.48461600	0.59897700
O	-7.14437600	1.08113500	1.33966200
N	-6.83876600	-0.42003900	-0.38912300
C	-6.05529300	-1.13817700	-1.26367600
N	-6.71586100	-2.01018200	-2.10110000
N	-4.74527000	-1.07310900	-1.29460500
C	-4.20256500	-0.23318800	-0.36604300
O	-1.69217000	1.39027500	1.31821900
P	4.91528600	-0.13981400	-0.17635400
O	5.63890100	-0.97324700	0.85991900
O	4.85536900	1.35201700	0.08482100
O	5.54189900	-0.33522300	-1.67281700
C	5.83845700	-1.66365400	-2.12961100
H	2.12806500	2.68613000	-1.42338500
H	0.57942900	1.90804600	-1.84988100
H	2.29145100	1.25607400	0.60344500
H	2.89572900	0.38436900	-1.97568800
H	0.76245600	-0.67650800	-2.35221600
H	1.72440900	-2.04876900	-1.76156000
H	-0.64898900	-1.24399900	-0.50448700
H	-4.17280700	1.88572400	2.03335700
H	-7.84391400	-0.55525000	-0.38387900
H	-7.63353500	-1.73231700	-2.42785800
H	-6.12184000	-2.36453400	-2.84099300
H	6.55432000	-2.15148300	-1.46121700
H	4.92689100	-2.26857500	-2.18893600
C	0.01356000	4.18702600	-0.74826300
H	-0.48782800	4.77717600	0.02283600
H	0.79839200	4.80065300	-1.21726200
H	-0.71947200	3.90904900	-1.52106100
H	6.27276300	-1.56335400	-3.12655400
Na	6.06638000	1.00473300	2.05007000
N	0.79663700	-2.12935600	0.66911200
H	-0.88082600	1.04250400	0.84599200
H	1.78873800	-2.04145300	0.88665100
C	-0.00298900	-2.18603100	1.89662600
H	0.05021000	-1.24661200	2.47135200
H	-1.05207300	-2.31142600	1.59951200
C	0.43323100	-3.35602200	2.77514200
H	-0.18186800	-3.41011800	3.68015500
H	0.34244300	-4.30419300	2.23440000
H	1.47899300	-3.24495300	3.08894400

IC(b') (A- N$_S$C$_R$)   -1982.09574549

O	0.68894100	-1.96251800	-0.91770000
C	-0.44035200	-1.38035300	-1.54146400
C	-1.16005700	-0.53169000	-0.50276600
O	-0.26624600	0.47602500	0.00791100
C	-2.37664600	0.22194700	-1.07416500
O	-3.42288300	0.33446400	-0.08357700
C	-1.81351700	1.61880100	-1.33209500
C	-0.79297000	1.80788400	-0.19239500
N	2.62667900	0.54605600	-0.28732300
C	3.00383900	1.72751500	-0.93797800
N	4.38599100	1.73653000	-0.88393200
C	4.84899500	0.60211100	-0.21776800
C	6.15830600	0.15766200	0.09239800
O	7.24922000	0.67393100	-0.15630800
N	6.08901900	-1.08301700	0.79471900
C	4.93913000	-1.75091300	1.12614900
N	5.07638700	-2.96458800	1.75031000
N	3.73344300	-1.31010800	0.82512400
C	3.73544700	-0.13762000	0.14917900
O	2.26614300	2.56824100	-1.44563300
P	-4.48770400	-0.90792100	0.10659900
O	-5.22294000	-0.65384700	1.40606300
O	-3.79205000	-2.24840000	-0.02227000
O	-5.46263400	-0.75139600	-1.19529300
C	-6.31784200	0.39784000	-1.28532200
H	-1.12693300	-2.15854900	-1.91235600
H	-0.12949200	-0.76020700	-2.39929900
H	-1.47278200	-1.17779900	0.32152700
H	-2.77713900	-0.25118600	-1.97592500
H	-1.29955800	1.63053900	-2.29978000
H	-2.59342300	2.38470500	-1.34609500
H	0.04990500	2.43485400	-0.49448000
H	4.95120400	2.47834400	-1.26827600
H	6.99228700	-1.48693000	1.01767200
H	5.88423300	-3.10261300	2.34485000
H	4.21262900	-3.31293100	2.14744600
H	-6.99426000	0.44601100	-0.42647600
H	-5.72718300	1.31923400	-1.33479500
C	1.48358700	-2.72180900	-1.80967700
H	2.33961900	-3.08648400	-1.23777200
H	0.92516400	-3.57714500	-2.22080400
H	1.84716600	-2.10792800	-2.64811600
H	-6.89666800	0.28793500	-2.20482000
Na	-4.47795200	-2.75533900	2.15467700
N	-1.31117900	2.32103100	1.06069000
H	-2.21464100	1.88715100	1.25099700
H	1.64581400	0.27107800	-0.16955700
C	-1.44706000	3.77886300	1.10322200
H	-0.45838500	4.21213900	0.90357000
H	-2.12323900	4.17435800	0.32164000
C	-1.94461000	4.23567900	2.47325200
H	-2.01937000	5.32803500	2.51416900
H	-2.93908300	3.82464500	2.68742300
H	-1.26313500	3.90145400	3.26274800

IC(b') (A- N$_S$C$_S$)   -1982.09852619

O	-0.51911200	1.74487100	-1.26778000
C	0.67814000	1.17989700	-1.76681200
C	1.28642800	0.31979100	-0.66630100
O	0.35104200	-0.69541600	-0.26830100

C	2.55694000	-0.41980200	-1.12733500
O	3.49429100	-0.56444200	-0.03637000
C	2.02773900	-1.80612200	-1.49224900
C	0.90208500	-2.05383200	-0.47920500
N	-2.57053500	-0.64334000	-0.31861400
C	-3.03441800	-1.93930000	-0.58059800
N	-4.40413500	-1.86929100	-0.40424700
C	-4.77648700	-0.57747500	-0.03480000
C	-6.04062500	-0.00864500	0.26081200
O	-7.15940600	-0.52487600	0.26135200
N	-5.88015900	1.37024300	0.59182700
C	-4.69064600	2.04964000	0.62578200
N	-4.74159000	3.39060300	0.90800300
N	-3.52899400	1.49083300	0.34900000
C	-3.61797400	0.18222200	0.01560400
O	-2.36901300	-2.92236700	-0.89726200
P	4.56440700	0.64999100	0.26172700
O	5.21066300	0.34649100	1.59744200
O	3.90520200	2.00863300	0.12916800
O	5.62048600	0.51438000	-0.97871500
C	6.46001300	-0.64796600	-1.04725400
H	1.39341700	1.96905800	-2.05157300
H	0.47051100	0.56921800	-2.66199700
H	1.51624200	0.95758000	0.19178200
H	3.05188700	0.07884500	-1.96627400
H	1.61270600	-1.77644400	-2.50509100
H	2.80450100	-2.57198100	-1.45506200
H	0.06114000	-2.62023000	-0.88266100
H	-5.01907200	-2.66047200	-0.52053200
H	-6.74924700	1.85927300	0.77804900
H	-5.48858400	3.72213100	1.50527200
H	-3.83740500	3.79324900	1.12076600
H	7.08187700	-0.73040700	-0.15057000
H	5.85816300	-1.55683400	-1.15634400
C	-1.21029100	2.51582800	-2.23261300
H	-2.12883700	2.86489600	-1.75673000
H	-0.61321100	3.38050300	-2.56233300
H	-1.46927500	1.91522900	-3.11859200
H	7.09563000	-0.52544800	-1.92682200
Na	4.52124200	2.47279500	2.33046800
N	1.36722600	-2.71361700	0.69706700
H	2.17895000	-2.23992900	1.08882700
H	-1.57547600	-0.39710500	-0.36201300
C	0.38042900	-3.05622300	1.72442700
H	-0.51677100	-3.41132900	1.20412700
H	0.77282100	-3.90861500	2.29606500
C	0.00833600	-1.93027700	2.70000000
H	-0.69926200	-2.29347000	3.45615100
H	0.89931800	-1.56474200	3.22745400
H	-0.44372900	-1.08621700	2.17276600

TS(b') (A- $N_R C_R$)   -1982.06740881

O	1.00454600	3.42256600	0.28805300
C	1.23500500	2.46923900	-0.73193900
C	1.65722000	1.16936600	-0.05478700
O	0.55672100	0.51114500	0.59736700
C	2.25422300	0.13247300	-1.02744500
O	3.18609600	-0.72995300	-0.33858200
C	1.08479000	-0.74271300	-1.48023400
C	0.28001300	-1.13094900	-0.26028500
N	-2.73559000	-0.14511500	0.00157300
C	-2.61951200	1.15230300	0.38399100

N	-3.86131300	1.74483500	0.48273400
C	-4.81175200	0.78304500	0.15624900
C	-6.22187200	0.82223900	0.09992900
O	-7.01163300	1.74552700	0.33416900
N	-6.71460200	-0.45810200	-0.29411600
C	-5.93857800	-1.55466800	-0.57948200
N	-6.61763600	-2.72141700	-0.88370700
N	-4.62905700	-1.56011400	-0.52244700
C	-4.07359700	-0.36978900	-0.13497900
O	-1.54444100	1.79784400	0.63105200
P	4.76722600	-0.26598300	-0.20121100
O	5.38628900	-1.15694500	0.85365600
O	4.86727400	1.22766000	0.02560300
O	5.35864400	-0.56765900	-1.69201100
C	5.49149000	-1.93109700	-2.12227800
H	2.03621800	2.81401700	-1.40604600
H	0.32557900	2.31302000	-1.33176700
H	2.41411200	1.41423200	0.69493200
H	2.75366700	0.60628500	-1.87773000
H	0.44647600	-0.17253300	-2.16157500
H	1.44459500	-1.62965800	-2.00917000
H	-0.80519200	-1.01841300	-0.28422100
H	-4.02915300	2.69708800	0.77075100
H	-7.72529200	-0.53802600	-0.29997700
H	-7.47058600	-2.61616000	-1.42137300
H	-6.00217300	-3.42624800	-1.27245100
H	6.14643400	-2.48843100	-1.44586900
H	4.51279100	-2.42165200	-2.16746700
C	0.30600600	4.56410800	-0.17307900
H	0.20936800	5.24428100	0.67725200
H	0.85225200	5.07778300	-0.97995000
H	-0.69632100	4.29405500	-0.53301000
H	5.92969900	-1.90344600	-3.12196600
Na	5.96342700	0.80518300	2.04748500
N	0.73258400	-2.11603900	0.51851200
H	-0.38472700	1.08894500	0.60373400
H	1.74208300	-2.23872300	0.53880900
C	0.00050800	-2.57098500	1.70396800
H	0.29461800	-1.96271500	2.56989500
H	-1.06077400	-2.38063100	1.52031200
C	0.25126200	-4.05106600	1.97944700
H	-0.29328000	-4.36205300	2.87690900
H	-0.08283900	-4.66876600	1.13951100
H	1.31646000	-4.24836500	2.14952000

TS(b') (A- $N_R C_S$)   -1982.06749472

O	0.94430600	3.41786500	0.21599000
C	1.17369100	2.43904700	-0.77923400
C	1.64207400	1.16930000	-0.07531500
O	0.57003100	0.49563400	0.60610200
C	2.24968500	0.12623000	-1.03284400
O	3.18979900	-0.71796400	-0.33319400
C	1.08861500	-0.76626300	-1.47355600
C	0.28929800	-1.14976600	-0.24826400
N	-2.71785400	-0.14956800	0.02767500
C	-2.60753700	1.12976200	0.46862900
N	-3.85120200	1.71574900	0.58171300
C	-4.79684600	0.76842400	0.20292600
C	-6.20608200	0.80988200	0.13034200
O	-6.99935600	1.72238400	0.39329900
N	-6.69302900	-0.45244100	-0.32452200
C	-5.91290700	-1.53622200	-0.64545700

N	-6.58670000	-2.69062400	-1.00252100
N	-4.60395100	-1.54300400	-0.57465700
C	-4.05415100	-0.36960300	-0.13165100
O	-1.53590700	1.76524600	0.75432200
P	4.76560600	-0.23644700	-0.19811000
O	5.39909900	-1.13124500	0.84491100
O	4.85128400	1.25583700	0.04364300
O	5.35395800	-0.51537700	-1.69470800
C	5.50425200	-1.87242300	-2.13898500
H	1.94866200	2.78289100	-1.48409700
H	0.25406800	2.24322100	-1.35168600
H	2.40349100	1.45200400	0.65644700
H	2.74431200	0.59359100	-1.88955200
H	0.44409000	-0.21078500	-2.16118600
H	1.45689600	-1.65564800	-1.99243600
H	-0.79581400	-1.03617900	-0.26762600
H	-4.02329100	2.65507100	0.90725500
H	-7.70353100	-0.53062000	-0.34985900
H	-7.43925200	-2.56677500	-1.53658700
H	-5.96797700	-3.37784900	-1.41662500
H	6.16852400	-2.42743200	-1.46978800
H	4.53224200	-2.37591500	-2.18676500
C	0.19162400	4.51832600	-0.25955700
H	0.09753300	5.22332700	0.57059600
H	0.69369400	5.02276200	-1.10023300
H	-0.81129100	4.20165000	-0.57715700
H	5.93950300	-1.82874300	-3.13945000
Na	5.96602700	0.82363200	2.05241400
N	0.74583100	-2.13225500	0.53114600
H	-0.37540600	1.06739200	0.65917700
H	1.75538900	-2.25472700	0.54754600
C	0.01858600	-2.58817700	1.71908800
H	0.31952000	-1.98364900	2.58524300
H	-1.04296700	-2.39351100	1.54162100
C	0.26537600	-4.07012100	1.98845000
H	-0.27550200	-4.38215800	2.88776200
H	-0.07548200	-4.68371000	1.14821600
H	1.33073500	-4.27187900	2.15209400

TS(b') (A- N_SC_R and A- N_SC_S)   -1982.06525635

O	-0.25247100	-1.57957600	2.70428000
C	1.02858900	-0.98352500	2.65461900
C	1.09572400	-0.09901100	1.41380200
O	0.17829300	0.98067900	1.52245800
C	2.50540500	0.52251600	1.22641700
O	2.91941100	0.48764700	-0.15749700
C	2.40593300	2.00243100	1.62201300
C	1.22833500	2.63107600	0.92179900
N	-2.00540800	0.88482000	0.20811500
C	-2.73678500	2.05252000	0.36256400
N	-4.05926200	1.77542300	0.02540100
C	-4.16314000	0.42913700	-0.31234200
C	-5.26134000	-0.36675800	-0.69801500
O	-6.45573700	-0.07567600	-0.84554200
N	-4.82322700	-1.70899000	-0.92346700
C	-3.53408100	-2.15499000	-0.79298000
N	-3.33253100	-3.50972300	-0.99024800
N	-2.52746900	-1.38795600	-0.44471800
C	-2.87087400	-0.08877400	-0.18357400
O	-2.31144700	3.16352300	0.72751500
P	3.57307000	-0.90017000	-0.77967400
O	3.42190400	-0.80686000	-2.28265200

O	2.96902700	-2.11367800	-0.10680300
O	5.13062900	-0.80738800	-0.30576700
C	5.97574100	0.19874000	-0.88455600
H	1.81402000	-1.75399600	2.59425700
H	1.20935100	-0.37591700	3.55834800
H	0.86358800	-0.71673800	0.54104100
H	3.25969600	0.01826100	1.83878800
H	2.25715600	2.07932800	2.70127500
H	3.33244500	2.52351000	1.36037000
H	0.50760800	3.22912400	1.46644600
H	-4.81176400	2.44485700	0.07766300
H	-5.56758500	-2.36478000	-1.13219100
H	-3.88161200	-3.94585300	-1.72214000
H	-2.34967200	-3.74719500	-1.04624500
H	6.01538100	0.09201900	-1.97267400
H	5.61597100	1.20183500	-0.62946700
C	-0.44101300	-2.36818700	3.86239200
H	-1.45044800	-2.78375900	3.80865000
H	0.28538700	-3.19495700	3.91554800
H	-0.34931800	-1.76775000	4.78124600
H	6.97185300	0.05280300	-0.46207300
Na	2.12395100	-2.78237800	-2.18371200
N	1.27214300	2.81174500	-0.37728200
H	1.97735000	2.27738000	-0.88226800
H	-0.70999800	0.85047200	0.93749500
C	0.27021400	3.53164700	-1.17939700
H	-0.59604500	3.71249000	-0.53704700
H	0.70634400	4.49224800	-1.47990900
C	-0.13491400	2.72063000	-2.40848400
H	-0.84970800	3.29599400	-3.00563000
H	0.72872900	2.49476100	-3.04601600
H	-0.61159100	1.78325900	-2.10762100

IC(b) (D- N$_R$C$_R$)   -1982.07328951

O	2.66101000	4.01837200	0.97770200
C	2.47652000	3.18051400	-0.14654700
C	2.51641600	1.73483300	0.32383500
O	1.29389800	1.44915100	0.99902900
C	2.73489800	0.72142400	-0.80988600
O	2.70424900	-0.59792800	-0.22553300
C	1.66182200	0.75048400	-1.92246500
C	0.24317500	0.64470000	-1.44214000
N	-2.88966200	0.28769100	-0.58993600
C	-3.12400500	1.64813800	-0.70002900
N	-4.43287800	1.88943600	-0.28906100
C	-5.01033200	0.68251300	0.09913900
C	-6.28645400	0.35862500	0.60317800
O	-7.26481900	1.07736600	0.84700800
N	-6.36249300	-1.05010800	0.84511100
C	-5.35452000	-1.95068700	0.62067400
N	-5.60232300	-3.26056400	0.98768800
N	-4.17729400	-1.62191800	0.14101700
C	-4.02154100	-0.28487300	-0.10448100
O	-2.32295600	2.51516000	-1.09263000
P	4.11720800	-1.30011900	0.28338200
O	3.71749500	-2.48724700	1.13144000
O	5.02303300	-0.27417200	0.92937400
O	4.82688400	-1.74927800	-1.11584600
C	4.32735200	-2.88679200	-1.83353200
H	3.27353100	3.35393900	-0.89049100
H	1.51012300	3.39406300	-0.63037700
H	3.36829900	1.62377800	1.00668500

H	3.70746400	0.89983100	-1.28058500
H	1.75503100	1.70046500	-2.46019800
H	1.89559100	-0.04857400	-2.63092900
H	-0.31270100	1.55434300	-1.20477800
H	-4.85291000	2.80468300	-0.23553500
H	-7.23382300	-1.35744600	1.26223300
H	-6.55174800	-3.59223900	0.86271100
H	-4.91474900	-3.90047600	0.60825500
H	4.25170200	-3.75820100	-1.17707300
H	3.34461700	-2.67391300	-2.26969200
C	2.56094900	5.39194700	0.65035400
H	2.71973500	5.95453800	1.57372800
H	3.32339000	5.69010900	-0.08682500
H	1.56839000	5.64041200	0.24477700
H	5.03929700	-3.08805100	-2.63663200
Na	5.04666900	-1.61179900	2.87703000
N	-0.46222600	-0.42336100	-1.34394100
H	1.34529600	0.51643500	1.27076300
H	-1.51999700	-0.24018500	-1.01261800
C	-0.06678200	-1.81117900	-1.59481600
H	-0.69411200	-2.16954700	-2.41917900
H	0.97675100	-1.85433600	-1.90717300
C	-0.29782000	-2.66622200	-0.34651900
H	-0.06889100	-3.71173900	-0.57685900
H	0.35781600	-2.34210000	0.46683000
H	-1.33988300	-2.60439200	-0.01619400

IC(b) (D-N$_R$C$_S$)   -1982.05491453

O	-1.48134100	3.85867300	-0.93532900
C	-1.12952000	2.62910300	-0.32488400
C	-2.21351300	1.61599800	-0.65210000
O	-2.11097000	1.26519300	-2.03693100
C	-2.18270200	0.35470500	0.23389900
O	-3.16760300	-0.55636100	-0.31974600
C	-0.85656600	-0.41056700	0.33283400
C	-0.31444100	-0.86965500	-0.95781200
N	2.54745200	-0.24189700	0.45040500
C	2.34493800	0.91228700	1.17101000
N	3.56446900	1.56278000	1.35442500
C	4.55520700	0.80857500	0.73342300
C	5.94371600	0.99369400	0.59824000
O	6.68596800	1.90130200	1.00317200
N	6.50020800	-0.09351100	-0.14901400
C	5.79159800	-1.15274400	-0.65306400
N	6.51051000	-2.06758200	-1.40910700
N	4.49769100	-1.30295200	-0.50744000
C	3.87652200	-0.29364500	0.19031900
O	1.25218800	1.35113800	1.60760900
P	-4.67737100	-0.64580500	0.34663300
O	-5.56178300	-1.31473400	-0.68439900
O	-5.12862800	0.70809700	0.85080400
O	-4.43909400	-1.59157300	1.65559000
C	-4.14754800	-2.98338500	1.46683300
H	-1.04080300	2.74565000	0.76645900
H	-0.15116600	2.28085500	-0.68796100
H	-3.18642100	2.09073200	-0.46592400
H	-2.47079700	0.64427700	1.24872600
H	-0.06827600	0.24992200	0.78924400
H	-0.97846800	-1.24718700	1.02781000
H	-0.49269100	-0.26197900	-1.84180400
H	3.68309400	2.43685100	1.84326400
H	7.49138600	-0.00804000	-0.34214300

```
H      7.45514200   -2.25635200   -1.09217800
H      5.98564400   -2.92098800   -1.56116400
H     -4.95123500   -3.47654200    0.91179400
H     -3.20142500   -3.11417700    0.92894700
C     -0.51148100    4.86464500   -0.71065000
H     -0.86640700    5.77115700   -1.20823500
H     -0.38131400    5.07126600    0.36309800
H      0.46778800    4.58536900   -1.12910800
H     -4.06101600   -3.42385300    2.46218500
Na    -7.04142100    0.51402900   -0.49367600
N      0.38044100   -1.94414500   -1.12454400
H     -2.80023300    0.59274100   -2.18148200
H      0.74901100   -2.11749100   -2.05662300
C      0.81196500   -2.88990600   -0.07077600
H      1.28168900   -2.27906900    0.70389200
H     -0.08263600   -3.38311800    0.32390900
C      1.80782800   -3.89112700   -0.64076700
H      2.07002900   -4.61489400    0.13640600
H      1.38985200   -4.44650100   -1.48861100
H      2.72415000   -3.37647700   -0.94783200
```

IC(b) (D- N$_S$C$_R$)   -1982.07563383

```
O      0.64677700    3.76498300    0.04405400
C      0.41970500    2.46614600   -0.47597700
C     -1.07876800    2.21001000   -0.49820600
O     -1.66010900    2.98255700   -1.54579200
C     -1.43441100    0.72309400   -0.68084800
O     -2.87618900    0.63101300   -0.78253000
C     -0.84147800    0.12097100   -1.96747100
C     -1.44258700   -1.20911400   -2.28678100
N      2.00336000   -0.87725400   -0.64379500
C      1.61783100   -1.78670600    0.29145500
N      2.61785600   -1.97614200    1.22602200
C      3.68276600   -1.15259900    0.87491000
C      4.94456900   -0.92908000    1.46557600
O      5.45864300   -1.41960700    2.47931200
N      5.66241800    0.03655100    0.69694800
C      5.19620100    0.65473200   -0.43710700
N      6.02133500    1.61737100   -0.99279300
N      4.01932200    0.42406800   -0.96601400
C      3.25922700   -0.48982200   -0.28409200
O      0.50262000   -2.40329400    0.34562700
P     -3.77394500    0.28440100    0.55938200
O     -5.21629100    0.31119400    0.10512300
O     -3.42571400    1.21097300    1.71159500
O     -3.31083700   -1.24569700    0.88263200
C     -2.57777200   -1.59745900    2.07322800
H      0.91975100    1.70648800    0.14522300
H      0.83094200    2.38157200   -1.49414100
H     -1.49503000    2.51091400    0.47316700
H     -1.07865600    0.14649000    0.17876200
H     -1.03371000    0.80542600   -2.79783400
H      0.24023600   -0.00326800   -1.81701500
H     -2.21382700   -1.28077100   -3.05379800
H      2.56587900   -2.60414900    2.01384600
H      6.56214900    0.29858400    1.08349800
H      7.01734400    1.43402400   -0.94820800
H      5.72002300    1.88016400   -1.92392500
H     -2.56861000   -0.76509400    2.77985300
H     -3.07475100   -2.46120600    2.52416000
C      2.02174900    4.09819400    0.06265600
H      2.10568100    5.09769000    0.49785000
```

H	2.60417900	3.38932600	0.67156400
H	2.45078400	4.11044800	-0.95141600
H	-1.55502900	-1.86732400	1.79339000
Na	-5.66600000	1.87718600	1.78710700
N	-1.09414600	-2.29147900	-1.69797900
H	-2.59446100	2.71282200	-1.57891000
H	-0.35497700	-2.27075800	-0.88282200
C	-1.66524900	-3.61282600	-1.99254000
H	-2.39771400	-3.50241700	-2.79792000
H	-0.84324800	-4.23638000	-2.36054700
C	-2.28759200	-4.23154700	-0.74111400
H	-2.68183000	-5.22277900	-0.98579600
H	-1.53613700	-4.34122500	0.04656700
H	-3.10116300	-3.60640500	-0.36350100

IC(b) (D- N$_S$C$_S$)   -1982.0589202

O	-1.15803500	3.66131200	-1.23785100
C	-1.13388500	2.75282000	-0.14828900
C	-1.91943900	1.51569900	-0.55418200
O	-1.13898600	0.77860700	-1.49988500
C	-2.27791100	0.60341800	0.62542500
O	-3.06470100	-0.49984500	0.11190900
C	-1.04177100	-0.01199800	1.30900900
C	-0.19986100	-0.84102300	0.39382000
N	2.70173000	-0.00497200	0.30759300
C	2.70279400	1.16044800	1.04575400
N	4.02385400	1.58024700	1.21817400
C	4.86089900	0.67296500	0.57564300
C	6.25898600	0.61008000	0.42693700
O	7.15440900	1.36773500	0.83176800
N	6.60741700	-0.55118400	-0.33501300
C	5.71774900	-1.46486800	-0.83743900
N	6.25672100	-2.48726800	-1.60618200
N	4.41951000	-1.38714800	-0.67734400
C	3.99626000	-0.28918300	0.03112900
O	1.71186300	1.76895800	1.50715700
P	-4.71920400	-0.42390000	0.17709400
O	-5.23037300	-1.51669500	-0.73574600
O	-5.20092600	0.98215900	-0.10284700
O	-5.03071200	-0.73324500	1.74805800
C	-4.84327900	-2.06200100	2.25551200
H	-1.60552200	3.20893400	0.74000200
H	-0.10191400	2.48449100	0.12149600
H	-2.86420200	1.83888500	-1.00918500
H	-2.85139900	1.15803000	1.37405200
H	-0.39271300	0.77180400	1.71182400
H	-1.39566000	-0.63826400	2.13661100
H	0.82915600	-0.52423800	0.15638600
H	4.29892800	2.41832200	1.70682600
H	7.59524700	-0.63639600	-0.54519900
H	7.14697700	-2.85477200	-1.28835100
H	5.58067900	-3.22452900	-1.76902000
H	-5.43293800	-2.78323800	1.68209400
H	-3.78524200	-2.34736600	2.22251000
C	-0.34270100	4.79469000	-1.00574000
H	-0.40548900	5.42459300	-1.89728200
H	-0.68862600	5.37354000	-0.13426400
H	0.70657500	4.51058500	-0.83722900
H	-5.17906500	-2.05147400	3.29422300
Na	-6.55154800	0.14139900	-1.81933700
N	-0.57623300	-2.00088900	-0.03514100
H	-1.52794500	-2.30494800	0.17361600

H	-1.72066100	0.08552000	-1.85528300
C	0.23930800	-2.88376100	-0.88924500
H	-0.23271400	-2.91300300	-1.87710700
H	1.22031000	-2.41379800	-0.98846300
C	0.34337900	-4.28512100	-0.29322100
H	0.93269600	-4.91817400	-0.96336200
H	0.83801500	-4.26154900	0.68242500
H	-0.64388700	-4.74623000	-0.17681000

IC(b) (A- N$_R$C$_R$)   -1982.06970684

O	-0.56401600	-2.36637800	2.18315400
C	0.08660300	-1.14180400	1.88658100
C	0.65164100	-1.23417700	0.46485200
O	-0.33417200	-1.41141800	-0.52413900
C	1.57508400	-0.02622400	0.15631400
O	2.50403200	-0.37280200	-0.90922200
C	0.78812100	1.17824400	-0.33698800
C	1.52922500	2.40229100	-0.67395800
N	-2.54967300	0.24016900	-0.00662400
C	-2.58535700	1.35326700	0.80274500
N	-3.90096700	1.79777500	0.90404000
C	-4.71078900	0.93982900	0.16651200
C	-6.10068200	0.91008400	-0.06093500
O	-7.00320600	1.65509000	0.34965400
N	-6.42240900	-0.19621900	-0.90661100
C	-5.51582400	-1.08768000	-1.42232200
N	-6.03914300	-2.13315100	-2.16699500
N	-4.22562600	-1.02980100	-1.20165200
C	-3.83296200	-0.00492300	-0.38132400
O	-1.61894600	1.91412300	1.37541300
P	3.96628300	-0.98729100	-0.54588300
O	4.60827600	-1.46546200	-1.82771200
O	3.92563900	-1.99574600	0.58568200
O	4.64012300	0.43230200	-0.00785000
C	5.87044200	0.37129900	0.73333000
H	0.91357800	-0.97256200	2.59915400
H	-0.61171900	-0.29710000	1.97569100
H	1.30565800	-2.11338100	0.43338900
H	2.14948300	0.22977200	1.05514900
H	0.20794700	0.89025000	-1.22649700
H	-0.00886400	1.47501900	0.38596100
H	0.94429900	3.25946100	-1.00707600
H	-4.19935100	2.57386200	1.47467200
H	-7.41407800	-0.33202000	-1.06580300
H	-6.82563600	-1.90380900	-2.76460400
H	-5.31336600	-2.63368700	-2.66684500
H	5.75104000	-0.25953800	1.61820500
H	6.67562100	-0.01999300	0.10268800
C	-1.20942000	-2.33922700	3.43961400
H	-1.68430900	-3.31410200	3.58133600
H	-0.49606100	-2.16733900	4.26271300
H	-1.98138100	-1.55565400	3.48302900
H	6.11297000	1.39212900	1.03515200
Na	4.61805700	-3.65528800	-0.92271400
N	2.80386200	2.58544000	-0.60382600
H	-1.13463900	-0.85279700	-0.30662300
H	3.41900900	1.80148600	-0.32807900
C	3.49208600	3.84856500	-0.92553400
H	4.24341100	3.61434600	-1.68547000
H	2.75554200	4.52252400	-1.36920600
C	4.13822300	4.46728200	0.31288100
H	4.65895100	5.38524200	0.02401600

H	3.38502900	4.71722000	1.06597400
H	4.87148500	3.79006600	0.76238700

IC(b) (A- N$_S$C$_R$)   -1982.06666792

O	0.07902500	-2.08601300	2.53925400
C	1.27835700	-1.33739500	2.53473800
C	1.20112300	-0.31758500	1.40217000
O	0.18308100	0.63441000	1.65785800
C	2.54133500	0.45725500	1.25013800
O	2.94385900	0.55925000	-0.13434400
C	2.33173700	1.89467500	1.75478300
C	1.16222800	2.53766500	1.06305100
N	-2.06143300	0.70414600	0.30284900
C	-2.66193700	1.90791200	0.63073200
N	-4.01996700	1.81277900	0.33636400
C	-4.27892200	0.53989400	-0.16175800
C	-5.46807100	-0.08270900	-0.59111800
O	-6.62995700	0.34447500	-0.64245900
N	-5.18349700	-1.42021500	-1.00783900
C	-3.94395700	-2.00531300	-1.00044200
N	-3.89343300	-3.33529200	-1.38356100
N	-2.85050500	-1.39759300	-0.60576200
C	-3.04151400	-0.11444300	-0.16392900
O	-2.11326500	2.92614900	1.10049300
P	3.69272100	-0.71743700	-0.87807600
O	3.47642500	-0.52730200	-2.36360500
O	3.22192300	-2.02436400	-0.27927400
O	5.25265200	-0.51974900	-0.44677300
C	5.99049100	0.59146200	-0.97715700
H	2.14651400	-1.99600100	2.37475700
H	1.41253800	-0.81387700	3.49745500
H	1.00829100	-0.85794200	0.47061700
H	3.34848200	-0.01375700	1.82079800
H	2.13767200	1.87441100	2.82873700
H	3.24153300	2.47836700	1.57664800
H	0.33959300	2.98370600	1.61026200
H	-4.69216400	2.54589800	0.50308100
H	-5.99905500	-1.96380800	-1.26615800
H	-4.51472700	-3.60881000	-2.13657200
H	-2.94286100	-3.65157200	-1.53319100
H	5.99779600	0.56570600	-2.07089700
H	5.56156300	1.54091100	-0.63725600
C	0.02196600	-3.01532400	3.60302400
H	-0.93082800	-3.54437900	3.51915400
H	0.84455000	-3.74652700	3.55052900
H	0.06734600	-2.51376100	4.58258700
H	7.01052800	0.49964900	-0.59882300
Na	2.36109900	-2.62254800	-2.37564000
N	1.21399400	2.77400900	-0.21583700
H	1.97769900	2.32851900	-0.72598700
H	-0.65745600	0.51132100	1.07762000
C	0.19758600	3.48169700	-1.01260300
H	-0.64962400	3.67701100	-0.35120000
H	0.64077200	4.43148000	-1.33416900
C	-0.23233800	2.64845400	-2.21835700
H	-0.94987400	3.22080100	-2.81512400
H	0.61902500	2.40073600	-2.86385500
H	-0.71478600	1.72434900	-1.88815700

IC(b) (A- N$_R$C$_S$ and A- N$_S$C$_S$)   -1982.07133542

O	-0.10490600	3.01409100	1.11821600

C	0.50454600	2.47074100	-0.04124700
C	1.15402400	1.14253800	0.34851700
O	0.20631500	0.20407900	0.85732000
C	2.00184100	0.56027300	-0.80525300
O	2.92329800	-0.42296600	-0.27990700
C	1.22830800	-0.12326900	-1.95406200
C	0.78568600	-1.52783600	-1.73024100
N	-2.18225200	0.26586100	-0.37982900
C	-2.42090700	0.75053300	-1.64968200
N	-3.79107300	0.70509900	-1.89133600
C	-4.42377100	0.20392100	-0.75746700
C	-5.77886100	-0.04303800	-0.45782700
O	-6.80075000	0.13332000	-1.13575100
N	-5.88653600	-0.57470900	0.86519600
C	-4.83347500	-0.81891900	1.70915700
N	-5.15305900	-1.27464100	2.97639200
N	-3.57963200	-0.59288900	1.39755300
C	-3.39228600	-0.05793100	0.15093200
O	-1.57923400	1.16520800	-2.47800700
P	4.42111700	0.04050800	0.22473800
O	4.96875900	-1.10192000	1.05442100
O	4.37960800	1.39950200	0.89247200
O	5.23812900	0.22586600	-1.17902900
C	5.56338800	-0.93878700	-1.94998400
H	1.28491800	3.15422000	-0.41819500
H	-0.23688300	2.32830500	-0.84080500
H	1.86424100	1.34749800	1.15550700
H	2.56968600	1.38412700	-1.25119200
H	0.30569300	0.44374900	-2.20665900
H	1.85053500	-0.12493600	-2.85475800
H	0.73748500	-2.19916200	-2.58741200
H	-4.23209200	1.04094100	-2.73389800
H	-6.83780400	-0.71531800	1.18602500
H	-5.93612400	-1.91499700	3.04106700
H	-4.33715400	-1.60905900	3.47530800
H	6.18230700	-1.62877300	-1.36843700
H	4.65491000	-1.45661100	-2.27853600
C	-0.83331500	4.19353600	0.83909500
H	-1.27067400	4.53324000	1.78189400
H	-0.18405000	4.98937700	0.43939600
H	-1.64142200	4.00932700	0.11510900
H	6.11803500	-0.59276200	-2.82480100
Na	5.18632000	0.40882600	2.84642800
N	0.41036400	-1.99664200	-0.59784800
H	-0.71326000	0.34841200	0.43599000
H	0.40451100	-1.29433300	0.19465900
C	-0.08592300	-3.35494300	-0.34685100
H	-1.10258100	-3.24723600	0.04429700
H	-0.14080700	-3.87938800	-1.30485600
C	0.80596700	-4.09423400	0.64978700
H	0.38708500	-5.08728400	0.83936400
H	1.82055200	-4.21190300	0.25773600
H	0.86084400	-3.55966200	1.60341300

TS(c) (D- $N_R C_R$)   -1982.04730426

O	-2.21627900	3.88293000	0.18753200
C	-1.44341000	2.69490400	0.09087800
C	-2.39044700	1.54710500	-0.23402300
O	-2.76764000	1.63148900	-1.59501200
C	-1.79695200	0.16255900	0.12169800
O	-2.74751900	-0.90768900	-0.18082100
C	-0.53222600	-0.14578100	-0.65679500

```
C         0.11770800    -1.40399700    -0.62369600
N         2.89571200    -0.34759800    -0.21711500
C         2.57753000     0.90912300     0.15902000
N         3.70164400     1.67032600     0.38180100
C         4.80164400     0.85708700     0.12997400
C         6.19301700     1.09492700     0.19405500
O         6.82074400     2.11667300     0.49504700
N         6.89112400    -0.09394200    -0.17147200
C         6.30414900    -1.28582600    -0.52218900
N         7.16199100    -2.29949100    -0.90729800
N         5.00828900    -1.47987900    -0.56229400
C         4.26044300    -0.37892600    -0.24003000
O         1.39318300     1.39970000     0.31349100
P        -4.37197200    -0.84453900    -0.01698300
O        -4.96734500     0.04362500    -1.11557400
O        -4.82748800    -0.48937300     1.38164200
O        -4.71134500    -2.40799200    -0.28987000
C        -4.47502300    -2.96393000    -1.59304500
H        -0.91365700     2.50615500     1.03745800
H        -0.68267400     2.79070100    -0.69662200
H        -3.26575200     1.68488600     0.41901400
H        -1.62758100     0.13948900     1.20391600
H        -0.59864700     0.22306100    -1.68262100
H         0.49366800     0.60775100    -0.15652800
H         0.79879400    -1.60705200    -1.44396500
H         3.70792800     2.64201600     0.65402400
H         7.89934100     0.00487800    -0.21083100
H         8.04733800    -2.35363800    -0.41696100
H         6.69276300    -3.19581400    -0.96036700
H        -4.97182200    -2.36810600    -2.36452100
H        -3.40103200    -3.01053100    -1.79976500
C        -1.41426800     5.02717500     0.40707600
H        -2.08683100     5.88671400     0.47329100
H        -0.84014200     4.94850700     1.34400900
H        -0.70500900     5.19025100    -0.41906200
H        -4.89023500    -3.97372200    -1.58234100
Na       -6.26944200     1.13612200     0.48611400
N         0.14400300    -2.34215900     0.30325600
H        -3.58166200     1.08207700    -1.67663200
H         0.83668900    -3.06969100     0.16628800
C        -0.53895800    -2.36897800     1.60617800
H        -0.12136500    -1.57608900     2.23811600
H        -1.59735400    -2.15952000     1.44137200
C        -0.35373200    -3.73034100     2.26854300
H        -0.85895900    -3.73747100     3.23855600
H        -0.78342800    -4.52988800     1.65562900
H         0.70640700    -3.95052000     2.44054400
```

TS(c) (D- $N_R C_S$)   -1982.04658614

```
O         3.81672400    -2.61391400     0.92883400
C         2.63386000    -2.40548500     1.69497300
C         2.00812200    -1.06178300     1.32541200
O         1.48621400    -1.13321400     0.00117200
C         0.96337200    -0.67109500     2.35275000
O         2.06228700     1.12609200    -1.03531800
C         0.11603700     0.38217100     2.29930500
C         0.15368800     1.34473300     1.23320300
N        -2.09210100    -0.55130100    -0.07812800
C        -1.85470700    -1.75213200    -0.60385200
N        -2.97373600    -2.35799100    -1.08988200
C        -4.02248100    -1.47304700    -0.86838800
C        -5.40677200    -1.54856000    -1.16328300
```

O	-6.05790400	-2.43986000	-1.71093500
N	-6.04402000	-0.35458100	-0.71920600
C	-5.42263000	0.69920400	-0.09273000
N	-6.21244300	1.78620800	0.20513100
N	-4.13667800	0.73312600	0.17330000
C	-3.44267000	-0.36986100	-0.24081300
O	-0.70055400	-2.38311500	-0.68346100
P	3.62274800	1.22233200	-0.99016400
O	4.30377500	0.34637300	-2.05564800
O	4.19020400	0.94947000	0.42005800
O	3.99527800	2.81442300	-1.28505600
C	3.73990400	3.31214300	-2.59443700
H	2.88657200	-2.41966200	2.76680900
H	1.91786900	-3.21860800	1.49955600
H	2.80602900	-0.29594600	1.33043200
H	0.88642700	-1.30654000	3.23461000
H	0.06997300	-1.80941200	-0.36395500
H	-0.61069500	0.50494500	3.09555800
H	0.93436000	1.29820000	0.46155200
H	-3.01215100	-3.25302700	-1.55631900
H	-7.03184000	-0.29822900	-0.94210900
H	-7.18143400	1.60856900	0.43995600
H	-5.76464100	2.44473200	0.82994300
H	4.28847500	2.73667400	-3.34948300
H	2.66865400	3.27587100	-2.83323400
C	4.37762800	-3.90453000	1.14618800
H	5.28009500	-3.97288600	0.53365200
H	4.64659600	-4.04722300	2.20218000
H	3.67626700	-4.69415700	0.84501900
H	4.07429700	4.35419800	-2.62129700
Na	5.02470000	-1.04768100	-0.39469500
N	-0.65553400	2.35688800	1.11512900
H	1.71467200	-0.25705500	-0.50585800
H	-0.49805100	2.94877000	0.30258400
C	-1.84263200	2.69793800	1.91736000
H	-2.68901600	2.14884900	1.48516200
H	-1.68134000	2.34354400	2.93729300
C	-2.08297300	4.20461600	1.89866000
H	-2.97627100	4.43564800	2.48648700
H	-1.23850700	4.75192800	2.32930000
H	-2.25234200	4.56796900	0.87859700

TS(c) (D- N$_S$C$_R$)   -1982.05105626

O	-0.23556000	4.06136700	-0.64844500
C	-0.01176400	2.66183900	-0.54770900
C	-1.29929800	1.94903900	-0.92239900
O	-1.52732100	2.11305000	-2.32192300
C	-1.30900900	0.45599500	-0.54939600
O	-2.64465300	-0.03552300	-0.92584000
C	-0.25983300	-0.35603800	-1.29156400
C	-0.35073100	-1.77549300	-1.32541500
N	1.98900100	-0.04287000	0.25588500
C	1.82667700	0.23661200	1.60474100
N	3.09134300	0.20463900	2.18908200
C	4.03828400	-0.07349800	1.20565900
C	5.44154800	-0.21307700	1.25260800
O	6.22895500	-0.11230200	2.20202600
N	5.93747500	-0.51111300	-0.05544900
C	5.17127300	-0.65291700	-1.18282500
N	5.84696600	-0.87365700	-2.36678600
N	3.86310800	-0.53280800	-1.19493600
C	3.31714200	-0.22679000	0.01932700

O	0.76400500	0.47699400	2.19800500
P	-3.82726500	-0.10396700	0.19589800
O	-5.13241100	-0.37009700	-0.52286900
O	-3.83341400	1.08756500	1.13476700
O	-3.28464200	-1.44363000	1.00346600
C	-3.65136800	-1.61687300	2.38316200
H	0.26916900	2.38573400	0.47957200
H	0.80531000	2.35552700	-1.21872000
H	-2.11488900	2.41040400	-0.34873600
H	-1.17532600	0.35357900	0.53265200
H	0.00233900	0.05123800	-2.27079400
H	0.84946400	-0.21704500	-0.61391300
H	0.31118500	-2.30547800	-2.00980900
H	3.27284900	0.41884400	3.15792400
H	6.94775200	-0.56931700	-0.11754500
H	6.69128400	-1.43108500	-2.31311900
H	5.23005300	-1.16649100	-3.11480500
H	-3.33181500	-0.75649200	2.97569100
H	-4.73421000	-1.75341200	2.47820300
C	0.91783400	4.80918600	-0.32011600
H	0.65659900	5.86689400	-0.41523500
H	1.25082900	4.61366700	0.71161600
H	1.75570700	4.58582400	-0.99962400
H	-3.14470600	-2.51866500	2.73192500
Na	-6.01847500	1.57089400	0.49840400
N	-1.06407400	-2.54387100	-0.53997400
H	-2.31397400	1.57706400	-2.52253800
H	-1.75751500	-2.11388600	0.08283300
C	-1.01242600	-4.00967000	-0.52320200
H	-0.20713400	-4.32258100	-1.19384300
H	-0.73804000	-4.32388800	0.49010400
C	-2.34940200	-4.62612200	-0.93393000
H	-2.29366300	-5.71668100	-0.85533600
H	-3.15755600	-4.27611800	-0.28337800
H	-2.60147800	-4.36276400	-1.96594600

TS(c) (D- N$_S$C$_S$)   -1982.04621183

O	0.46601600	-2.85246700	-1.73883500
C	0.44860700	-1.77152500	-0.81911300
C	1.77781200	-1.04386400	-0.92368700
O	1.82305600	-0.34170800	-2.17066300
C	2.08090100	-0.09049300	0.25167800
O	3.34310500	0.56832500	-0.10027600
C	1.06012500	0.98582600	0.58093400
C	0.50848300	1.76109900	-0.46625000
N	-2.43488600	0.44896400	0.30675000
C	-2.01919800	-0.27111100	1.36859400
N	-3.04449400	-1.00298800	1.91979900
C	-4.18444700	-0.73611700	1.16831600
C	-5.51637100	-1.19795800	1.26579800
O	-6.03662500	-1.98782800	2.06177100
N	-6.29780300	-0.60230500	0.23187600
C	-5.83301500	0.29000500	-0.70409800
N	-6.74358800	0.70729900	-1.65661000
N	-4.59062400	0.70441900	-0.76525600
C	-3.76455900	0.16359800	0.18293800
O	-0.82486500	-0.31768800	1.85971900
P	4.78004700	-0.05438900	0.41077600
O	5.84809500	0.50905100	-0.50605500
O	4.72248200	-1.56519500	0.51791700
O	4.91437500	0.52516800	1.93207100
C	5.09277200	1.93513700	2.12351100

H	0.30980900	-2.14199800	0.20882300
H	-0.38722800	-1.09121100	-1.04041500
H	2.57259500	-1.80135800	-0.90075400
H	2.24024000	-0.69862600	1.14712100
H	0.00233000	0.33352800	1.14165300
H	1.36409000	1.57412900	1.45437800
H	0.41997400	1.32698300	-1.45882500
H	-2.96484500	-1.61863100	2.71548800
H	-7.25737000	-0.92683500	0.18928700
H	-7.69969400	0.83354500	-1.34457400
H	-6.40164100	1.49804400	-2.18964500
H	5.99386800	2.28578200	1.61076200
H	4.22399300	2.49056100	1.75270200
C	-0.75116800	-3.57272400	-1.73926700
H	-0.64806800	-4.38197700	-2.46733100
H	-0.96777700	-4.00644300	-0.74993200
H	-1.60108100	-2.93557600	-2.02915800
H	5.19428300	2.09669800	3.19885100
Na	6.45499100	-1.70559700	-1.02661600
N	0.03177800	2.98143400	-0.33862800
H	0.09474100	3.42335800	0.57471400
H	2.63259600	0.19828100	-2.12333800
C	-0.70107900	3.72175900	-1.37270900
H	-0.20914200	4.69265500	-1.49974100
H	-0.58342300	3.16662700	-2.30714400
C	-2.17870500	3.90009900	-1.02560200
H	-2.67008800	4.48010100	-1.81444900
H	-2.67450800	2.93046400	-0.93068000
H	-2.29800300	4.44788200	-0.08360700

TS(c) (A- N$_R$C$_R$)   -1982.05265601

O	-0.54985400	-2.79053000	1.61992300
C	0.11180200	-1.54494700	1.48652100
C	0.69024400	-1.44671100	0.07057900
O	-0.27933400	-1.58950800	-0.94345500
C	1.55141800	-0.15991900	-0.08010900
O	2.66799800	-0.43833800	-0.99261600
C	0.77917000	1.02112300	-0.61624200
C	1.40575900	2.27939300	-0.72707400
N	-2.49149200	0.11583000	-0.29150700
C	-2.34759000	1.18569900	0.51771700
N	-3.56305600	1.71811500	0.86301600
C	-4.54091600	0.94580300	0.24351500
C	-5.95378800	1.01926000	0.25047200
O	-6.71045300	1.80834900	0.82550300
N	-6.48230500	-0.02702800	-0.55907900
C	-5.73808200	-0.95998400	-1.24200300
N	-6.44615000	-1.93101800	-1.91930100
N	-4.42706300	-0.99938600	-1.23111000
C	-3.84139500	-0.03414300	-0.46404900
O	-1.23826900	1.68822600	0.95194800
P	4.10493500	-0.89040200	-0.36379900
O	4.90073700	-1.60854100	-1.43180500
O	3.92358900	-1.62351700	0.95099100
O	4.79654100	0.57623400	-0.01127700
C	5.61955500	1.19979500	-1.01318800
H	0.93733000	-1.47213100	2.21476300
H	-0.58287600	-0.71548700	1.68639800
H	1.38491900	-2.28536100	-0.04612400
H	1.97730200	0.08352700	0.90039700
H	0.13823800	0.78851000	-1.46910800
H	-0.25745000	1.34768500	0.23761700

H	0.84916600	3.08494500	-1.20565600
H	-3.70294400	2.51994700	1.45978300
H	-7.49465400	-0.08428800	-0.56654300
H	-7.32144800	-1.64700500	-2.34335200
H	-5.85964900	-2.46698100	-2.54781200
H	6.42557400	0.52905000	-1.31923000
H	5.02895000	1.47673700	-1.89364200
C	-1.16590500	-2.93761100	2.88262000
H	-1.65290900	-3.91668600	2.89431600
H	-0.43204600	-2.89380300	3.70421900
H	-1.92522400	-2.15923000	3.05763800
H	6.03983900	2.09907600	-0.55620400
Na	5.03868900	-3.45909600	0.01818300
N	2.57688900	2.63848500	-0.23642200
H	-1.07713500	-1.05081000	-0.71097100
H	3.20604900	1.91541600	0.12023200
C	3.07769500	4.01584900	-0.18962500
H	4.05757600	4.03747700	-0.67891400
H	2.39878400	4.63383000	-0.78427500
C	3.18125400	4.54266200	1.24220200
H	3.57987300	5.56256900	1.23365100
H	2.19916300	4.55656500	1.72519000
H	3.85323700	3.92096000	1.84371700

TS(c) (A- N$_S$C$_R$)		-1982.04899848	
O	-0.39977600	-3.09564400	1.40610600
C	0.20677500	-1.81930800	1.52072700
C	0.88206200	-1.48014900	0.18802900
O	-0.00875400	-1.46281700	-0.90796800
C	1.71950700	-0.17909300	0.29720700
O	2.78558200	-0.22436500	-0.70130400
C	0.92465500	1.08453300	0.03393200
C	1.54658800	2.29917400	0.38436000
N	-2.32737100	0.05822200	-0.16637200
C	-2.30196100	0.93130600	0.86140300
N	-3.56648000	1.33474100	1.20639000
C	-4.45307000	0.67452400	0.36044800
C	-5.86452800	0.69138900	0.26453500
O	-6.70347700	1.31183500	0.92569100
N	-6.27439700	-0.17984200	-0.78560700
C	-5.43216700	-0.91800300	-1.58338300
N	-6.03373300	-1.75261500	-2.50148900
N	-4.12498000	-0.90627500	-1.47390900
C	-3.65095500	-0.10421900	-0.47654400
O	-1.25709600	1.36398800	1.48714700
P	4.22993400	-0.89538200	-0.32601400
O	4.91601000	-1.25119000	-1.63084400
O	4.07845500	-2.02249900	0.67799800
O	5.01836400	0.31886000	0.44825600
C	5.47440400	1.43908400	-0.31862000
C	-1.09413000	-3.46646900	2.57889400
N	1.27017800	3.48388100	-0.12702200
C	1.79112300	4.76978600	0.34873300
C	2.58883100	5.49705200	-0.73248500
Na	4.96993700	-3.47918900	-0.92072800
H	0.96909100	-1.83222800	2.31870600
H	-0.54212400	-1.06058100	1.79101000
H	1.60272000	-2.27946400	-0.00914000
H	2.17966100	-0.13130500	1.29173700
H	0.42791600	1.07799800	-0.94002400
H	-0.18697100	1.16154800	0.83492300
H	2.26605400	2.31534300	1.20305800

H	-3.79423000	1.96960900	1.95721500
H	-7.27875500	-0.27433200	-0.88810300
H	-6.89615900	-1.42785200	-2.92219600
H	-5.37670900	-2.12061700	-3.17897600
H	6.13990900	1.11539000	-1.12480300
H	4.62999800	1.99027900	-0.75053500
H	-1.53175400	-4.45248600	2.39937400
H	-0.42237800	-3.52759000	3.45090000
H	-1.90147600	-2.75557800	2.81575800
H	6.01892700	2.09252100	0.36745400
H	0.62411900	3.51883900	-0.91096900
H	-0.83063500	-0.97279000	-0.65593100
H	0.94436300	5.38080800	0.68145400
H	2.41173500	4.56381400	1.22502800
H	2.93728600	6.46108100	-0.34822600
H	3.45924200	4.90906800	-1.04039700
H	1.97208000	5.69055300	-1.61712000

TS(c) (A- N_RC_S and A- N_SC_S)   -1982.05592105

O	0.05647800	-3.08922300	0.87376400
C	-0.47376200	-2.34284800	-0.20759600
C	-1.14697400	-1.08861400	0.35241200
O	-0.25512300	-0.28202500	1.11804600
C	-1.88188500	-0.29436000	-0.75504500
O	-2.95381800	0.47482500	-0.12080200
C	-1.06020400	0.67049100	-1.60742500
C	-0.67982900	1.94204700	-1.11641300
N	2.16782300	-0.00432100	-0.29775600
C	2.24355900	-0.17449600	-1.63260500
N	3.54304700	-0.22223400	-2.05865300
C	4.34926700	-0.07860700	-0.93320400
C	5.75534300	-0.06348100	-0.76704600
O	6.65865500	-0.17725900	-1.60016400
N	6.06297500	0.11161100	0.61301000
C	5.14192100	0.24660700	1.62508900
N	5.64516800	0.33835000	2.90429100
N	3.84300100	0.23564600	1.43688200
C	3.46571600	0.05634300	0.13820300
O	1.25396900	-0.29099200	-2.46135600
P	-4.44183300	-0.18418200	0.04963700
O	-5.20984400	0.70083400	1.01313000
O	-4.37276300	-1.65573100	0.41403300
O	-5.06070100	-0.11223000	-1.46567000
C	-5.31889900	1.17356500	-2.04348900
C	0.73496200	-4.25126700	0.44147200
N	-0.49133200	2.28787400	0.13809700
C	0.03920700	3.57197000	0.59164000
C	-0.89924300	4.25785000	1.58438500
Na	-5.57055100	-1.18426200	2.35038900
H	-1.22776400	-2.93855300	-0.74896100
H	0.31906400	-2.08344500	-0.92402300
H	-1.92539500	-1.42541400	1.04230600
H	-2.33946100	-1.02029300	-1.43572500
H	0.22125500	0.12734600	-1.99196700
H	-1.46122400	0.76212300	-2.61997900
H	-0.45441700	2.71995200	-1.84629000
H	3.84145200	-0.34419600	-3.01530600
H	7.05283100	0.07611700	0.83093400
H	6.52861200	0.81986800	3.02045100
H	4.94538100	0.62128800	3.57955200
H	-6.02623600	1.74145800	-1.43044000
H	-4.39050000	1.74586800	-2.14978300

```
H          1.11036000   -4.75830500    1.33454100
H          0.06564700   -4.93625100   -0.10389000
H          1.58538200   -4.00560000   -0.21376800
H         -5.75005700    0.99586500   -3.03141300
H          0.63269400   -0.25470300    0.66695000
H         -0.59080400    1.52652800    0.82509200
H          1.01903500    3.39571100    1.05180700
H          0.19764500    4.19891000   -0.29136800
H         -0.45815400    5.20175900    1.92191400
H         -1.86947000    4.46982000    1.12419500
H         -1.06699000    3.62848200    2.46514500
```

IC(c') (D- N$_R$C$_R$)   -1982.06344742

```
O         -2.36394500    3.70601700    0.47101900
C         -1.66488600    2.51653400    0.13870300
C         -2.68867400    1.42318400   -0.14064300
O         -3.26133100    1.65784800   -1.41392900
C         -2.06563800    0.01397800   -0.01358200
O         -3.07097300   -1.04588100   -0.19280500
C         -0.98569700   -0.22020700   -1.02707800
C          0.05715100   -1.09597400   -0.99211800
N          3.12491400   -0.29866600   -0.36929200
C          2.86043700    1.00009700   -0.30372100
N          3.96117300    1.77496100   -0.12658000
C          5.04109900    0.89882600   -0.07618600
C          6.43426800    1.11565600    0.08581900
O          7.06348900    2.16521600    0.22625800
N          7.10494900   -0.13832700    0.06109800
C          6.50261600   -1.36709800   -0.09066400
N          7.33955600   -2.45524000   -0.15583700
N          5.20726200   -1.53365200   -0.22895600
C          4.49191600   -0.37381800   -0.22978100
O          1.66800700    1.58345400   -0.39132700
P         -4.66661800   -0.94208200    0.12275900
O         -5.34038100   -0.04894400   -0.93009200
O         -4.99094500   -0.55039400    1.54940300
O         -5.07822500   -2.49644800   -0.09012000
C         -4.92877200   -3.09650400   -1.38659900
C         -1.49469100    4.80329900    0.67441200
N          0.48504900   -1.99870700   -0.05673500
C         -0.06813400   -2.14132500    1.28615100
C          0.52750300   -3.36753600    1.97499900
Na        -6.37132600    1.18158000    0.74503700
H         -1.00199500    2.22169900    0.96917200
H         -1.03822400    2.67398100   -0.75201900
H         -3.44884300    1.50386000    0.65179700
H         -1.70100100   -0.09006400    1.01154700
H         -1.15633800    0.26854200   -1.98259900
H          0.96957100    0.90482100   -0.56532500
H          0.69429700   -1.11819400   -1.87507400
H          3.98278100    2.78314100   -0.06592700
H          8.11569400   -0.07521800    0.11877900
H          8.20185600   -2.41892900    0.37332600
H          6.85124900   -3.33845700   -0.07440900
H         -5.45753000   -2.51300900   -2.14656400
H         -3.86982400   -3.17318900   -1.65195300
H         -2.11604700    5.66604300    0.92880900
H         -0.78827800    4.61529000    1.49862100
H         -0.91440200    5.03461000   -0.23221600
H         -5.36441700   -4.09559100   -1.32053600
H         -4.05035200    1.06673800   -1.46746900
H          1.49197100   -2.12902400   -0.10153900
```

H	0.12517800	-1.24398500	1.89671200
H	-1.15340600	-2.25131900	1.19872800
H	0.11065700	-3.47676700	2.98141100
H	0.30790800	-4.27814300	1.40777500
H	1.61646300	-3.27717100	2.07074600

IC(c') (D- N$_R$C$_S$)   -1982.06502530

O	0.83589800	-3.50110000	-0.66376000
C	0.75400700	-2.14972700	-0.24221000
C	2.02817300	-1.43776600	-0.67015100
O	1.98113500	-1.21512100	-2.07915600
C	2.30960200	-0.13087100	0.09676400
O	3.54604800	0.39806300	-0.51099900
C	1.27628400	0.96065000	0.08556000
C	0.41486100	1.20232800	-0.94100100
N	-2.73325700	0.33129700	-0.08769100
C	-2.42230800	-0.04629700	1.14518000
N	-3.48367100	-0.48093400	1.87197800
C	-4.58891400	-0.37348400	1.03328400
C	-5.96141800	-0.67725400	1.22731200
O	-6.54302900	-1.12886500	2.21491900
N	-6.67519500	-0.38005800	0.03375200
C	-6.12690300	0.12628200	-1.12329400
N	-6.98475500	0.28605500	-2.18600400
N	-4.85135300	0.40157700	-1.26833100
C	-4.09217400	0.12987600	-0.16921700
O	-1.21607000	-0.03036100	1.70738600
P	4.98626800	0.19984000	0.25164900
O	6.07073300	0.40845000	-0.78822200
O	5.04146100	-1.10910900	1.01581200
O	4.98115800	1.39612200	1.36773400
C	4.99909600	2.75760200	0.91655000
C	-0.33239600	-4.23386400	-0.35169600
N	-0.40296400	2.28918700	-1.08990600
C	-0.55567300	3.27600700	-0.02658900
C	-1.53990900	4.36639800	-0.43874900
Na	6.94393500	-1.67986400	-0.21086700
H	0.64766400	-2.09814500	0.85467400
H	-0.12681600	-1.66339800	-0.68725500
H	2.86809200	-2.10577900	-0.42835600
H	2.53408400	-0.40332300	1.13241900
H	-0.53974400	0.26387900	1.04477500
H	1.39137300	1.69866500	0.87716100
H	0.34710800	0.48814200	-1.75644700
H	-3.46464700	-0.81166600	2.82635300
H	-7.66089900	-0.61730400	0.06225700
H	-7.94564100	0.52956200	-1.97905500
H	-6.58437100	0.83080400	-2.93982700
H	5.88041600	2.95000000	0.29634000
H	4.09426700	2.98807500	0.34330700
H	-0.17690000	-5.25644400	-0.70582500
H	-0.52137200	-4.25617800	0.73367000
H	-1.22118100	-3.81429900	-0.84839300
H	5.03390500	3.38559800	1.80965100
H	2.73769500	-0.63089000	-2.26655800
H	-1.27086400	2.06777900	-1.56686000
H	-0.88980700	2.79792900	0.90904600
H	0.42967200	3.71307300	0.17558800
H	-1.63179500	5.11498100	0.35456900
H	-1.20577200	4.86982800	-1.35211900
H	-2.53605300	3.94626000	-0.62105600

IC(c') (D- N$_S$C$_R$)   -1982.07849520

O	-0.87550700	4.10071900	-0.79112900
C	-0.52728800	2.72489400	-0.72897800
C	-1.77580200	1.89921400	-0.99228500
O	-2.13130800	2.02971400	-2.36821000
C	-1.60481400	0.41635600	-0.62684800
O	-2.91843800	-0.21636400	-0.91320300
C	-0.55516900	-0.29575000	-1.42119200
C	-0.19332200	-1.58879000	-1.19944500
N	2.26434300	0.21919500	0.29911300
C	2.15571300	0.80240300	1.56932800
N	3.45338600	0.84207900	2.04671100
C	4.33184600	0.29983400	1.10673200
C	5.73721000	0.11186100	1.11911600
O	6.56540000	0.39119700	1.98655600
N	6.14954300	-0.49644200	-0.10564800
C	5.32599600	-0.85462200	-1.14076400
N	5.91597100	-1.36958900	-2.26268400
N	4.01840400	-0.67506500	-1.11907200
C	3.57306200	-0.09002600	0.01554800
O	1.13099400	1.19164200	2.11987800
P	-4.02182200	-0.41129200	0.26410900
O	-5.28973700	-0.94128600	-0.37701500
O	-4.21716400	0.82532800	1.12730500
O	-3.23641100	-1.57357900	1.13423900
C	-3.62674400	-1.78938800	2.49782000
C	0.23475400	4.94299300	-0.55852600
N	-0.63107800	-2.41171700	-0.20457900
C	-0.33393900	-3.83857400	-0.19150000
C	-1.34952500	-4.68992600	-0.96248300
Na	-6.45360700	0.87263800	0.49953000
H	-0.12176700	2.47520800	0.26417200
H	0.24384300	2.49393900	-1.48119500
H	-2.57962200	2.29137200	-0.35390400
H	-1.42127200	0.32745400	0.45051500
H	-0.17469600	0.19172300	-2.31220400
H	1.45285300	0.02491200	-0.29203900
H	0.55812500	-2.04074000	-1.84681200
H	3.70097100	1.22389400	2.94715100
H	7.15186100	-0.62812300	-0.18875900
H	6.79334800	-1.86335300	-2.16283600
H	5.26793300	-1.79497600	-2.91313300
H	-3.56321300	-0.85950100	3.06955000
H	-4.64751400	-2.18592600	2.54976600
H	-0.12300200	5.97483700	-0.61555300
H	0.67608300	4.77158300	0.43632900
H	1.02315500	4.79694300	-1.31448400
H	-2.93576100	-2.52673300	2.91163700
H	-2.83374800	1.37245900	-2.51458900
H	-1.47781800	-2.13599700	0.28907200
H	0.67125300	-3.97655700	-0.60628700
H	-0.28924100	-4.16789900	0.85366400
H	-1.09334400	-5.75401800	-0.89379500
H	-2.35772200	-4.55397000	-0.55533500
H	-1.37218100	-4.40725700	-2.02078400

IC(c') (D- N$_S$C$_S$)   -1982.05943408

O	0.45656600	-2.54841300	-1.96463300
C	0.49300200	-1.45173200	-1.06486900
C	1.89185900	-0.85966300	-1.09287900

O	2.08243900	-0.17508000	-2.33363200
C	2.21326300	0.05719100	0.10414600
O	3.59170900	0.53680700	-0.14933200
C	1.34210900	1.25355100	0.35483100
C	0.76462400	2.00209600	-0.63331400
N	-2.62883600	0.31309900	0.11162000
C	-2.20698000	-0.05740800	1.31315300
N	-3.17854900	-0.60066600	2.09309800
C	-4.33865600	-0.58166000	1.32497500
C	-5.66328700	-1.01122000	1.59512300
O	-6.14037100	-1.52965000	2.60622100
N	-6.47444800	-0.76070700	0.45399700
C	-6.04728300	-0.18676900	-0.72233200
N	-6.97994100	-0.09006700	-1.72954600
N	-4.81391500	0.20738500	-0.93761400
C	-3.96532500	-0.01158800	0.10711900
O	-0.97430200	0.04925300	1.79561000
P	4.87213700	-0.24165300	0.52120800
O	6.11079100	0.24572700	-0.20623800
O	4.67016300	-1.74485600	0.54833200
O	4.84265400	0.26465100	2.07727700
C	5.08904200	1.65017100	2.35300300
C	-0.82127800	-3.15157400	-2.02173000
N	0.20915600	3.22871300	-0.49107200
C	-0.64042100	3.86319000	-1.49476200
C	-2.13675100	3.74869400	-1.19121900
Na	6.60994100	-1.98404900	-0.72234100
H	0.26009200	-1.79133100	-0.04115900
H	-0.25971100	-0.70071000	-1.34449200
H	2.60226500	-1.69455100	-1.02137600
H	2.23815800	-0.56690800	1.00289700
H	-0.37103900	0.46288000	1.11739600
H	1.44505600	1.69720000	1.34721200
H	0.74700700	1.61768800	-1.64994100
H	-3.06889200	-0.95101600	3.03417100
H	-7.43126800	-1.08617700	0.53890900
H	-7.94347600	0.06744800	-1.46022200
H	-6.67506900	0.50304800	-2.49167300
H	6.07298700	1.95193600	1.98001100
H	4.31885800	2.28039200	1.89456900
H	-0.76007000	-3.97175100	-2.74224500
H	-1.12335400	-3.55767400	-1.04276700
H	-1.59353100	-2.43976000	-2.35158800
H	5.05577700	1.76701500	3.43860800
H	0.17465700	3.62118300	0.44306200
H	2.92570300	0.30079100	-2.22693300
H	-0.34960700	4.91787400	-1.57815200
H	-0.40953400	3.39252200	-2.45590400
H	-2.72099700	4.22836700	-1.98541900
H	-2.43778200	2.69983000	-1.11024100
H	-2.38260700	4.24954600	-0.24676900

IC(c') (A- N$_R$C$_R$)   -1982.06681569

O	-0.53770700	-2.25115500	2.07193400
C	0.17570800	-1.09031900	1.68811200
C	0.77651700	-1.31686200	0.29726600
O	-0.19383600	-1.62718300	-0.68315800
C	1.69262200	-0.13204500	-0.10517700
O	2.73331600	-0.64627300	-1.01475900
C	0.97965500	1.00097000	-0.77363800
C	1.47866700	2.27252000	-0.82145500
N	-2.47503800	0.21167300	-0.36588500

```
C     -2.50546000    1.39771200    0.23365100
N     -3.76152300    1.84267200    0.48637300
C     -4.62327600    0.86023900    0.00648500
C     -6.03930400    0.76038300   -0.00085100
O     -6.89092700    1.54083000    0.42652500
N     -6.41468400   -0.46672100   -0.61262700
C     -5.54718300   -1.40838800   -1.11974200
N     -6.11292500   -2.55702900   -1.61701100
N     -4.23994100   -1.28311400   -1.09835300
C     -3.79981200   -0.13570100   -0.51503700
O     -1.46284700    2.13349700    0.59637700
P      4.19572100   -1.00038300   -0.38580100
O      4.94637400   -1.85909500   -1.38376600
O      4.07644000   -1.56157500    1.01973700
O      4.90053800    0.48649700   -0.23823400
C      5.42922500    1.09773700   -1.42756100
C     -1.15442100   -2.10970700    3.33526500
N      2.64115900    2.72587700   -0.28891000
C      2.91224900    4.13706800   -0.04208000
C      2.45286000    4.62245700    1.33693800
Na     5.13870400   -3.49944600    0.27790000
H      0.98796000   -0.88677800    2.40596100
H     -0.49252000   -0.21378300    1.69140100
H      1.43006200   -2.19210400    0.37237800
H      2.19749900    0.22494400    0.80021600
H      0.17984400    0.74749900   -1.46347100
H     -0.62186900    1.73413400    0.23042100
H      0.91386200    3.04172000   -1.34893500
H     -4.01005900    2.71878700    0.92370500
H     -7.41259100   -0.64819900   -0.61430600
H     -7.02315600   -2.48208200   -2.05419600
H     -5.45878000   -3.12852500   -2.13751200
H      6.16910600    0.44380900   -1.89673000
H      4.62908100    1.31708900   -2.14243200
H     -1.67625300   -3.04659100    3.54847200
H     -0.41655600   -1.92165400    4.13208400
H     -1.88491000   -1.28511500    3.34100200
H      5.90397900    2.03155100   -1.11700700
H     -0.97032200   -1.03498200   -0.56565400
H      3.27861400    2.05076700    0.12194200
H      3.98943400    4.29961800   -0.15925600
H      2.41500700    4.71497200   -0.83003000
H      2.69083300    5.68454300    1.46783800
H      1.37085600    4.49518700    1.45374300
H      2.95087600    4.06059900    2.13507100
```

IC(c') (A- N$_S$C$_R$)   -1982.06551516

```
O     -0.13998600   -2.45497000    2.19256700
C      0.46859000   -1.20830000    1.91064600
C      1.11818000   -1.27934100    0.52677300
O      0.19643500   -1.57237900   -0.50661500
C      1.95616600   -0.01010800    0.23267700
O      2.90296500   -0.34041700   -0.83555300
C      1.16331900    1.17519400   -0.22939400
C      1.44147200    2.43681400    0.19399900
N     -2.28403500   -0.01640600   -0.15189200
C     -2.48011600    1.12399200    0.49863600
N     -3.78698200    1.45889600    0.62702800
C     -4.50638000    0.44271100    0.00345200
C     -5.89982600    0.24152600   -0.18027900
O     -6.85358400    0.93416400    0.17612900
N     -6.10365200   -0.97309100   -0.88988000
```

C	-5.11144900	-1.82057500	-1.33071400
N	-5.52097000	-2.98184500	-1.93654000
N	-3.82904500	-1.59858400	-1.15135300
C	-3.55160300	-0.45618800	-0.46806400
O	-1.54357900	1.91405900	1.01299400
P	4.39924300	-0.87248300	-0.45468300
O	5.00316600	-1.45136800	-1.72055200
O	4.38331000	-1.79519100	0.75153000
O	5.18047900	0.48946700	0.01919800
C	5.40630000	1.51972700	-0.95155300
C	-0.77553900	-2.47135300	3.45418400
N	0.96087900	3.60477500	-0.33043600
C	0.82200500	4.81535200	0.47829100
C	0.81251400	6.06691500	-0.39539700
Na	5.23846900	-3.48161500	-0.59225000
H	1.23938900	-0.97873100	2.66616400
H	-0.28212400	-0.40199600	1.95639800
H	1.83075300	-2.10959900	0.55175200
H	2.52568300	0.25409400	1.13202000
H	0.52255800	1.01671900	-1.09603500
H	-0.64606800	1.57190500	0.75700600
H	2.12728200	2.58445400	1.02854300
H	-4.15443900	2.28120300	1.08477400
H	-7.07754900	-1.22192700	-1.02619300
H	-6.38886100	-2.96529700	-2.45702000
H	-4.77145200	-3.47504600	-2.40568700
H	5.98416800	1.13576000	-1.79846100
H	4.45593400	1.92607600	-1.31521600
H	-1.21455900	-3.46436800	3.58322000
H	-0.06241600	-2.28616900	4.27379100
H	-1.57587800	-1.71672600	3.51678100
H	5.97128800	2.30936300	-0.45031200
H	0.26966100	3.50463300	-1.06677400
H	-0.63027800	-1.06097200	-0.36271600
H	-0.09238500	4.77572800	1.09098100
H	1.67003600	4.84402900	1.17162700
H	0.70190000	6.96181900	0.22589700
H	1.74177300	6.15093800	-0.96802700
H	-0.02501400	6.04778700	-1.10313400

IC(c') (A- N_RC_S and A- N_SC_S)   -1982.06783248

O	0.21341900	-3.09821600	0.08957700
C	-0.45891700	-2.20918800	-0.78310100
C	-1.20332300	-1.16807800	0.05323900
O	-0.34592300	-0.44424700	0.92677500
C	-2.06775900	-0.24281700	-0.83735100
O	-3.03751500	0.41177100	0.04289500
C	-1.35568100	0.82224300	-1.64241700
C	-0.83163300	1.98288300	-1.13664700
N	2.19566000	0.12557100	-0.35700500
C	2.41729300	0.25946800	-1.66143500
N	3.73335400	0.25265900	-1.98702100
C	4.42784200	0.10225200	-0.78947800
C	5.81532200	0.02272400	-0.49951800
O	6.78659600	0.06612800	-1.25520100
N	5.98822800	-0.13359400	0.90324300
C	4.97548400	-0.19428300	1.83429800
N	5.35163800	-0.41195500	3.13661000
N	3.69969600	-0.11088100	1.53164300
C	3.45114600	0.02642900	0.20140400
O	1.50210600	0.38107900	-2.61258600
P	-4.53815100	-0.21432300	0.19807400

O	-5.18834200	0.47364900	1.38377700
O	-4.51811600	-1.73169900	0.24532400
O	-5.26799500	0.19273100	-1.21205200
C	-5.46594900	1.58185000	-1.50608000
C	0.95485200	-4.07903800	-0.60734600
N	-0.67346200	2.32985000	0.16212400
C	0.23063200	3.39609000	0.58114600
C	-0.24667500	4.05780900	1.87257400
Na	-5.55246000	-1.62707700	2.32944600
H	-1.18428200	-2.75728700	-1.40797300
H	0.26044500	-1.72878100	-1.46509600
H	-1.91065900	-1.70839800	0.69103900
H	-2.61507200	-0.88534400	-1.53554000
H	0.59872800	0.48993100	-2.19321300
H	-1.55908000	0.82762200	-2.71087100
H	-0.50783600	2.74789500	-1.84288300
H	4.12050900	0.34500600	-2.91564200
H	6.95216300	-0.24948400	1.19750000
H	6.24131800	-0.03703300	3.44101900
H	4.59963200	-0.26684600	3.79882600
H	-6.06606200	2.06325000	-0.72688900
H	-4.50501100	2.10000600	-1.59648000
H	1.44265500	-4.70874100	0.14150000
H	0.30744400	-4.70920600	-1.23822800
H	1.72621500	-3.62522900	-1.24958200
H	-5.99689300	1.63085300	-2.45976700
H	0.53008500	-0.30820200	0.49359700
H	-0.79165600	1.55864100	0.81918300
H	1.25058900	3.00456400	0.71527100
H	0.27354200	4.13445500	-0.22778900
H	0.45014600	4.84704200	2.17567800
H	-1.24039000	4.49831400	1.74139700
H	-0.30263100	3.32848500	2.68898000

TS(c') (D- N$_R$C$_R$)   -1982.02601706

O	-2.78133900	3.69258400	0.59509200
C	-1.75577800	2.76984400	0.91446000
C	-2.17189700	1.41004500	0.35082500
O	-2.13031600	1.45894400	-1.05939700
C	-1.36546000	0.27319700	0.91382800
O	-3.70238000	-1.46221800	0.53753300
C	-0.40412000	-0.37118100	0.20773000
C	0.36559700	-1.49908300	0.64866400
N	3.16770200	-0.06697700	0.11791500
C	3.12885500	1.23487800	0.35697800
N	4.32556500	1.85626500	0.23650800
C	5.23246900	0.86122500	-0.12015100
C	6.62698800	0.89851500	-0.38831100
O	7.41100500	1.84675900	-0.37530900
N	7.07127800	-0.41268400	-0.71332100
C	6.28279700	-1.54070000	-0.75648900
N	6.89444200	-2.70188900	-1.15588600
N	4.99485000	-1.54161300	-0.49272000
C	4.48886000	-0.31568500	-0.18576000
O	2.04762900	1.94061600	0.69799700
P	-4.58863500	-0.75434100	-0.48521200
O	-3.81051400	-0.32944800	-1.78777400
O	-5.39199400	0.45275900	0.04150600
O	-5.76424700	-1.81958600	-1.00305600
C	-5.32921500	-3.01823000	-1.62873000
C	-2.48182100	5.01167700	1.01782300
N	0.00129800	-2.43926000	1.47539000

C	-1.31578100	-2.67785400	2.10502700
C	-1.56397000	-4.17809400	2.22726900
Na	-4.60635400	1.89040300	-1.50372200
H	-1.61971800	2.70989800	2.00656200
H	-0.79840700	3.07953400	0.46412900
H	-3.20116800	1.22748600	0.70402700
H	-1.57655500	0.00440900	1.94424000
H	-0.17118200	-0.01614000	-0.79428700
H	1.28440400	1.33071100	0.70792300
H	1.37670300	-1.58358800	0.25317600
H	4.51007900	2.84214400	0.35961300
H	8.05099500	-0.47079700	-0.97031700
H	7.87571400	-2.82362800	-0.93993300
H	6.33385800	-3.52952100	-0.99681100
H	-4.81595100	-2.80960300	-2.57672200
H	-4.64912400	-3.58441500	-0.97881400
H	-3.32980500	5.64004200	0.73536400
H	-2.34479800	5.06340500	2.10855300
H	-1.57164600	5.39359700	0.53116200
H	-6.21585600	-3.62845100	-1.83150300
H	-2.66078000	0.63770500	-1.39324400
H	0.70937500	-3.14047500	1.68206100
H	-1.30139500	-2.20800000	3.09566200
H	-2.09211800	-2.20042600	1.49319900
H	-2.52989100	-4.33650400	2.71475700
H	-1.60115200	-4.65215000	1.24155800
H	-0.79597800	-4.67603600	2.83185300

TS(c') (D- $N_R C_S$)   -1982.02179669

O	-1.78111000	3.41196700	-1.08150400
C	-1.13755200	2.32934100	-0.44228000
C	-2.13333900	1.17232200	-0.32433500
O	-2.36489000	0.59981100	-1.59779400
C	-1.64033000	0.15632100	0.68241000
O	-3.79702900	-1.06384300	-0.20940300
C	-0.74352900	-0.86470100	0.50324100
C	-0.27081100	-1.23794200	-0.78581000
N	2.94630400	-0.21573000	0.48720500
C	2.77045600	0.87992000	1.20819700
N	3.89851600	1.60285900	1.40751300
C	4.90973500	0.90893500	0.74777900
C	6.29682400	1.17257500	0.59310500
O	6.97754500	2.10667900	1.01510100
N	6.88114300	0.13741300	-0.18827000
C	6.21496700	-0.94803800	-0.71026200
N	6.95252100	-1.80232100	-1.49119800
N	4.92902900	-1.16377400	-0.54399800
C	4.29085200	-0.20805400	0.18828700
O	1.61319800	1.29866500	1.72616300
P	-5.18443300	-0.52369300	0.23042800
O	-6.27361400	-0.66188500	-0.85509800
O	-5.16108500	0.90457100	0.81759800
O	-5.64200300	-1.46705700	1.53490400
C	-5.81035700	-2.85708300	1.29750500
C	-0.92972300	4.53197100	-1.23391000
N	0.56892100	-2.21095600	-1.02510500
C	1.22142300	-3.07998900	-0.02817200
C	2.34409100	-3.88134700	-0.67558000
Na	-6.75648200	1.53592100	-0.65335500
H	-0.78018300	2.63203600	0.55705400
H	-0.25936400	1.99767100	-1.02245800
H	-3.07293900	1.56578700	0.08642400

H	-1.97676100	0.33278400	1.70192900
H	0.92144500	0.66772500	1.44446000
H	-0.47858700	-1.48331400	1.35622100
H	-0.66205100	-0.69675500	-1.64353000
H	3.98121800	2.46731900	1.92431700
H	7.86679500	0.26830800	-0.38991700
H	7.93623700	-1.90854600	-1.27757900
H	6.48186900	-2.67680600	-1.68719500
H	-6.61146300	-3.04257700	0.57010300
H	-4.88430400	-3.31288400	0.92234300
H	-1.51214900	5.31423200	-1.72705800
H	-0.57518100	4.90786600	-0.26109300
H	-0.05205300	4.29366800	-1.85482800
H	-6.07845500	-3.32822000	2.24951400
H	-3.02384900	-0.12111000	-1.35029100
H	0.80091300	-2.38964900	-1.99726400
H	1.62251500	-2.43238600	0.75453400
H	0.45751600	-3.73730100	0.40235100
H	2.76624900	-4.56912600	0.06305200
H	1.97712600	-4.48053900	-1.51696400
H	3.14386600	-3.21702400	-1.01746200

TS(c') (D- N_SC_R)   -1982.04500717

O	-1.07229300	4.30759800	-0.70004100
C	-0.53819800	3.00145000	-0.58889000
C	-1.67971400	1.99830100	-0.75471700
O	-2.10529600	1.99580400	-2.10722100
C	-1.25902300	0.60175100	-0.35061300
O	-3.27029400	-0.23848700	-1.16526800
C	-0.31146200	-0.12427800	-1.02783000
C	-0.02577200	-1.48271200	-0.73570700
N	2.62927000	0.70479500	0.52095700
C	3.09375000	1.83611200	1.21292100
N	4.46334200	1.65798800	1.27781300
C	4.83150700	0.47119900	0.64062700
C	6.09456600	-0.14066700	0.43009000
O	7.21841100	0.23090100	0.76457000
N	5.92048500	-1.36322400	-0.29017400
C	4.72691100	-1.88124400	-0.71850000
N	4.76764900	-3.03845700	-1.44453000
N	3.56504000	-1.28794700	-0.50430000
C	3.67304300	-0.11784900	0.16647600
O	2.42024600	2.75874500	1.65348400
P	-4.24956700	-0.46026900	0.00938900
O	-5.65161200	-0.95981900	-0.37164200
O	-4.32261000	0.68883100	1.03410500
O	-3.45072200	-1.74103700	0.80599800
C	-3.96679700	-2.13775000	2.07336100
C	-0.06714600	5.30234900	-0.65085400
N	-0.80681300	-2.27975100	-0.04786400
C	-0.50537500	-3.68188800	0.25470500
C	-1.47333500	-4.62639100	-0.46121300
Na	-6.58011000	0.74708400	0.82660100
H	-0.03855400	2.87135400	0.38519900
H	0.21382300	2.82210600	-1.37599000
H	-2.49880200	2.29386000	-0.08670200
H	-1.60806300	0.25294800	0.61735400
H	0.17473400	0.29441300	-1.90502200
H	1.65487100	0.56701400	0.27488100
H	0.89755300	-1.92133600	-1.11337900
H	5.08672000	2.31866100	1.71783400
H	6.78720500	-1.84218900	-0.51245500

```
H          5.53815800   -3.67725900   -1.29938700
H          3.87013800   -3.48646300   -1.57377000
H         -3.86312500   -1.33310800    2.81006900
H         -5.02547500   -2.40931200    1.98536700
H         -0.56862900    6.27219300   -0.71893900
H          0.50672800    5.25594400    0.28796000
H          0.63893800    5.20631600   -1.49160000
H         -3.40351400   -3.01402000    2.40801600
H         -2.75201400    1.25152000   -2.11143000
H         -1.75188700   -1.95815800    0.23922100
H          0.53254800   -3.87449200   -0.03243100
H         -0.57814700   -3.81166200    1.34065600
H         -1.27824700   -5.65943800   -0.15411800
H         -2.51020600   -4.38029900   -0.21157400
H         -1.35722100   -4.55688500   -1.54752400
```

TS(c') (D- N$_S$C$_S$)   -1982.02171870
```
O          0.97085400   -2.83584000   -1.51842300
C          0.62303000   -1.85566100   -0.56228300
C          1.82321100   -0.92788900   -0.35974600
O          2.01130000   -0.12181400   -1.50751800
C          1.64404800   -0.10056500    0.89585100
O          3.86486800    0.94689200   -0.03416300
C          0.91737900    1.04786200    1.05789100
C          0.35560700    1.75868500   -0.03996200
N         -2.74959000    0.23202000    0.62069200
C         -2.60753900   -0.72972700    1.51856900
N         -3.73048400   -1.45308100    1.74563700
C         -4.70185100   -0.90762400    0.91045000
C         -6.06621800   -1.23917000    0.69841600
O         -6.75669000   -2.12008800    1.21020100
N         -6.61142500   -0.35742600   -0.27535900
C         -5.93274000    0.65968200   -0.90760600
N         -6.62867300    1.36192800   -1.86001800
N         -4.66865500    0.94168500   -0.68417900
C         -4.06604600    0.12991900    0.22939800
O         -1.48710900   -1.02057300    2.18468100
P          5.16050400    0.11350100    0.15298900
O          6.13906600    0.20941200   -1.03789300
O          4.92519600   -1.35696600    0.56248500
O          5.92467000    0.76570100    1.49229800
C          6.32061900    2.12732000    1.41070400
C         -0.09393300   -3.72896700   -1.78494500
N         -0.28273100    2.89043500    0.08066500
C         -0.84470700    3.68278700   -1.02322700
C         -2.34213800    3.92239500   -0.84143000
Na         6.23703000   -2.04006900   -1.14908300
H          0.34453000   -2.33315600    0.39295400
H         -0.24409600   -1.26499600   -0.90339100
H          2.71185300   -1.54681400   -0.18082700
H          2.07461400   -0.53774700    1.79365700
H         -0.79123500   -0.41021800    1.86734000
H          0.86882600    1.51105000    2.04245800
H          0.50002800    1.36255900   -1.04207700
H         -3.83290000   -2.22913700    2.38469100
H         -7.57401700   -0.55439500   -0.52769700
H         -7.62652900    1.47457100   -1.73149900
H         -6.15862100    2.20722100   -2.15875600
H          7.04459300    2.28562200    0.60021600
H          5.45733700    2.78458200    1.24018400
H          0.26544800   -4.44623200   -2.52713900
H         -0.40301800   -4.27446100   -0.87914900
```

H	-0.97245900	-3.20336800	-2.19032700
H	6.78971200	2.39617200	2.36354400
H	-0.41289800	3.27157200	1.01615200
H	2.81551200	0.41190900	-1.21973900
H	-0.29753900	4.63138900	-1.05627900
H	-0.63355000	3.14040200	-1.94765000
H	-2.70408400	4.54627400	-1.66516300
H	-2.90048500	2.98186600	-0.83844400
H	-2.54457800	4.45657500	0.09413500

TS(c') (A- N_RC_R)   -1982.02765616

O	-0.41526800	-3.30407200	-0.23386500
C	0.07599700	-2.03848300	0.16563000
C	0.39904300	-1.22146500	-1.09003400
O	-0.72272700	-0.97287200	-1.91208300
C	1.17327200	0.02583100	-0.71749300
O	3.33759800	-0.94065700	-1.26992500
C	0.97599500	1.21502400	-1.37391800
C	1.72038400	2.40312000	-1.12947800
N	-2.71542500	0.45699100	-0.32223000
C	-2.56081000	1.61834800	0.29931400
N	-3.70448400	2.10943200	0.83083800
C	-4.69652100	1.18026700	0.52701300
C	-6.08646600	1.14590900	0.81800600
O	-6.78568600	1.95064000	1.43317900
N	-6.64513500	-0.04153200	0.27202500
C	-5.95489500	-1.00433600	-0.43060000
N	-6.66721400	-2.10938600	-0.82118100
N	-4.66748800	-0.93762300	-0.68689400
C	-4.05747700	0.16837400	-0.18567000
O	-1.42412800	2.29789900	0.43305400
P	4.17304600	-0.97398900	0.01873400
O	5.33717300	-1.97622700	0.05232400
O	3.34630400	-1.01026700	1.32664300
O	4.87382600	0.59253200	0.11644900
C	5.93867800	0.85594100	-0.79834600
C	-0.77759900	-4.11090100	0.86700800
N	2.87079100	2.49071100	-0.51535100
C	3.55649700	3.75471800	-0.22196700
C	3.76353300	3.93800900	1.28193300
Na	4.65294300	-2.72754600	2.07287100
H	0.99607500	-2.14002300	0.76233400
H	-0.67554400	-1.51191300	0.77948000
H	1.10135400	-1.81488300	-1.68719800
H	1.75970600	-0.02131300	0.19533500
H	0.25416800	1.25724100	-2.18527400
H	-0.70913700	1.80132900	-0.02198100
H	1.32035700	3.34505700	-1.50419000
H	-3.80665800	2.97262100	1.34617100
H	-7.63104700	-0.17198300	0.47218400
H	-7.65051200	-1.99240400	-1.03107900
H	-6.17270200	-2.69089900	-1.48642200
H	6.74518600	0.12843600	-0.66205000
H	5.59221200	0.80774200	-1.83900700
H	-1.14116600	-5.06135500	0.46712000
H	0.08053500	-4.30792800	1.53062000
H	-1.57694700	-3.64658200	1.46646500
H	6.32062300	1.86128500	-0.59090600
H	-1.43248900	-0.57114500	-1.35994200
H	3.41147800	1.64218200	-0.25135700
H	4.52123200	3.73544700	-0.74005100
H	2.96286300	4.56973100	-0.64535000

H	4.31654300	4.86484200	1.46514100
H	2.80456100	3.99475900	1.80638200
H	4.33940300	3.10450500	1.69592500

TS(c') (A- N_SC_R)   -1982.0168470

O	0.20870200	-3.10954800	-0.46235200
C	-0.13500600	-1.83078100	-0.95985500
C	-0.64544500	-0.98241300	0.21483100
O	0.29123800	-0.83330000	1.25969500
C	-1.22673100	0.31432700	-0.26252300
O	-3.65753800	0.30740900	0.14800900
C	-0.94730800	1.52068300	0.33365200
C	-1.70635900	2.64885700	-0.04194200
N	2.64841500	0.41147900	0.04418400
C	2.73316000	1.41976200	-0.81379500
N	4.00073200	1.71639900	-1.18344500
C	4.81760600	0.81484800	-0.50548300
C	6.22654300	0.63241700	-0.49449900
O	7.10740900	1.24321500	-1.09895600
N	6.54755900	-0.44517400	0.37496800
C	5.64240500	-1.19337500	1.09478600
N	6.14962500	-2.23538000	1.82663900
N	4.34362400	-0.99128800	1.06690200
C	3.95604000	0.01918600	0.24539500
O	1.71898200	2.12469400	-1.31227400
P	-4.40144800	-1.03503200	0.00085800
O	-5.24534600	-1.44809900	1.23006800
O	-3.50655500	-2.20816500	-0.46986400
O	-5.47422000	-0.85346500	-1.28398500
C	-6.51285800	0.09807700	-1.12205300
C	0.70028100	-3.96293800	-1.47728600
N	-1.65133400	3.82324500	0.54201200
C	-2.49437100	4.98066200	0.21406900
C	-3.43401300	5.34364800	1.36315800
Na	-4.26628500	-3.47799800	1.22795600
H	-0.93740500	-1.90907600	-1.70730100
H	0.74275200	-1.35677100	-1.43164800
H	-1.51546300	-1.53156300	0.60477400
H	-1.85181600	0.28035700	-1.14341600
H	-0.31709800	1.55281200	1.21919100
H	0.88311200	1.78988200	-0.92096200
H	-2.43002600	2.54845100	-0.84607300
H	4.28566600	2.43880200	-1.83001100
H	7.53448700	-0.67753500	0.40827600
H	7.08711000	-2.14961600	2.19810600
H	5.48367100	-2.63557700	2.47562500
H	-7.16712200	-0.16333600	-0.27948000
H	-6.11121100	1.10670300	-0.94915300
H	0.94329500	-4.91882000	-1.00565600
H	-0.04936500	-4.13226000	-2.26605700
H	1.61021700	-3.55452000	-1.94501400
H	-7.10694100	0.10891300	-2.04305000
H	-1.01747400	3.93489900	1.32993200
H	1.13194400	-0.49544100	0.87373300
H	-1.83092500	5.81803700	-0.02746500
H	-3.05474200	4.72546400	-0.68864000
H	-4.02718300	6.21990900	1.08303300
H	-4.11513000	4.51742300	1.58666500
H	-2.87486500	5.59166800	2.27193100

TS(c') (A- N_RC_S and A- N_SC_S)   -1982.01528264

O	-0.72815100	-2.62008200	1.00987400
C	-0.62334800	-1.83738600	-0.16812200
C	-0.92276600	-0.37989700	0.19342900
O	0.09695900	0.16915500	1.03116900
C	-1.24634700	0.42917900	-1.02971500
O	-3.78292900	0.71721900	0.54490700
C	-1.13327500	1.76787200	-1.27277500
C	-0.83139300	2.84915500	-0.36861700
N	2.46146700	0.30944900	-0.54043300
C	2.68257900	0.68892800	-1.79395800
N	3.97678100	0.58351300	-2.17054900
C	4.66131900	0.08774700	-1.06348200
C	6.03091000	-0.23162500	-0.85646000
O	6.98623900	-0.14820100	-1.62623600
N	6.19869600	-0.71230500	0.47097300
C	5.20073600	-0.84437600	1.41071200
N	5.55843600	-1.38703900	2.61515100
N	3.94278600	-0.53018700	1.18689100
C	3.70158800	-0.07431400	-0.06932100
O	1.77931100	1.14185500	-2.65958000
P	-4.54617100	-0.41475600	-0.14090300
O	-5.49758200	-1.22655700	0.77898600
O	-3.66363100	-1.38916700	-0.97841300
O	-5.51714200	0.28138500	-1.33583000
C	-6.50235800	1.19738600	-0.89167200
C	-0.29531300	-3.95171500	0.80723200
N	-0.45032700	2.76230200	0.86729400
C	-0.24734100	3.89974500	1.77052500
C	-1.21120000	3.84099000	2.95638600
Na	-4.47602200	-3.12103000	0.21431400
H	-1.35462400	-2.17131800	-0.91407400
H	0.39215500	-1.91942600	-0.59048500
H	-1.86907700	-0.34509800	0.75669200
H	-1.71837400	-0.15283000	-1.81639800
H	0.90227800	1.15825000	-2.22299800
H	-1.49360500	2.11826400	-2.23616200
H	-0.97829900	3.85679400	-0.75397800
H	4.35803300	0.81173200	-3.07838300
H	7.14292800	-1.00925000	0.69370200
H	6.50526600	-1.25085600	2.94460900
H	4.84963100	-1.29926200	3.33226300
H	-7.23934600	0.70798600	-0.23980600
H	-6.05334300	2.03376300	-0.33771600
H	-0.41614800	-4.47961200	1.75670000
H	-0.89176000	-4.46233300	0.03344100
H	0.76344600	-3.99206100	0.50758300
H	-7.01962400	1.59414700	-1.77352500
H	-0.25706700	1.79368300	1.21721800
H	0.95589200	0.14842800	0.53250100
H	0.79196300	3.86151900	2.11440000
H	-0.38099700	4.81838400	1.19248500
H	-1.01919600	4.69116600	3.61842300
H	-2.25018500	3.88489600	2.61804300
H	-1.07334700	2.92061800	3.53227700

IC(c) (D- $N_R C_R$)   -1982.02689538

O	-3.33046900	3.34648800	0.66089000
C	-2.13266800	2.69063300	1.06668700
C	-2.17475400	1.29523900	0.44585600
O	-2.08029200	1.40538600	-0.95271600
C	-1.21317600	0.30520800	1.02695300
O	-3.61779600	-1.80099700	0.21917900

C	-0.27975100	-0.33198300	0.28721200
C	0.54407200	-1.41723500	0.74845600
N	3.27166100	0.09569800	0.11207800
C	3.22286800	1.41899300	0.13150000
N	4.41632000	2.01964400	-0.08690100
C	5.33113000	0.98564400	-0.27013400
C	6.72624500	0.98752600	-0.53760600
O	7.50388800	1.93012000	-0.68092400
N	7.18011600	-0.35645700	-0.63830100
C	6.39980100	-1.48146600	-0.49304000
N	7.02198800	-2.68850400	-0.68798700
N	5.11056500	-1.44745700	-0.23736600
C	4.59568100	-0.19087100	-0.14148500
O	2.13661400	2.16487600	0.34481400
P	-4.55742400	-0.88269800	-0.55325200
O	-3.87653100	-0.18505100	-1.79299100
O	-5.29667200	0.19023500	0.27684800
O	-5.79499600	-1.79822600	-1.20283000
C	-5.42625700	-2.86332700	-2.06739500
C	-3.41146300	4.68827900	1.11940600
N	0.16178800	-2.38720900	1.52727200
C	-1.19698300	-2.70437400	2.02678400
C	-1.38611800	-4.21728300	2.07085400
Na	-4.63592000	1.94328900	-0.99326200
H	-2.08552600	2.63480200	2.16477600
H	-1.25274900	3.24346800	0.70370700
H	-3.15760700	0.87379000	0.73907700
H	-1.34322700	0.06798900	2.08058500
H	-0.12330300	-0.01763800	-0.74339500
H	1.37611800	1.56286200	0.45611600
H	1.58106300	-1.44151800	0.41312500
H	4.59482700	3.01351800	-0.12692300
H	8.16111600	-0.45029000	-0.87910700
H	8.00318200	-2.76340500	-0.45095600
H	6.46711400	-3.48178500	-0.39246800
H	-4.94309000	-2.48993000	-2.98047700
H	-4.73979300	-3.56092300	-1.56986500
H	-4.36173700	5.09322800	0.76429200
H	-3.38859200	4.73472900	2.21728100
H	-2.58625700	5.29503000	0.72007300
H	-6.34040500	-3.39971800	-2.34399900
H	-2.67739700	0.65679900	-1.35360300
H	0.87978500	-3.06491100	1.77576500
H	-1.29359600	-2.27336000	3.02960100
H	-1.93810500	-2.23882200	1.36288200
H	-2.38753300	-4.43271700	2.45339000
H	-1.30698900	-4.65240900	1.06995200
H	-0.65960700	-4.70704500	2.73082100

IC(c) (D- $N_R C_S$)   -1982.04915706

O	3.81672400	-2.61391400	0.92883400
C	2.63386000	-2.40548500	1.69497300
C	2.00812200	-1.06178300	1.32541200
O	1.48621400	-1.13321400	0.00117200
C	0.96337200	-0.67109500	2.35275000
O	2.06228700	1.12609200	-1.03531800
C	0.11603700	0.38217100	2.29930500
C	0.15368800	1.34473300	1.23320300
N	-2.09210100	-0.55130100	-0.07812800
C	-1.85470700	-1.75213200	-0.60385200
N	-2.97373600	-2.35799100	-1.08988200
C	-4.02248100	-1.47304700	-0.86838800

```
C     -5.40677200   -1.54856000   -1.16328300
O     -6.05790400   -2.43986000   -1.71093500
N     -6.04402000   -0.35458100   -0.71920600
C     -5.42263000    0.69920400   -0.09273000
N     -6.21244300    1.78620800    0.20513100
N     -4.13667800    0.73312600    0.17330000
C     -3.44267000   -0.36986100   -0.24081300
O     -0.70055400   -2.38311500   -0.68346100
P      3.62274800    1.22233200   -0.99016400
O      4.30377500    0.34637300   -2.05564800
O      4.19020400    0.94947000    0.42005800
O      3.99527800    2.81442300   -1.28505600
C      3.73990400    3.31214300   -2.59443700
C      4.37762800   -3.90453000    1.14618800
N     -0.65553400    2.35688800    1.11512900
C     -1.84263200    2.69793800    1.91736000
C     -2.08297300    4.20461600    1.89866000
Na     5.02470000   -1.04768100   -0.39469500
H      2.88657200   -2.41966200    2.76680900
H      1.91786900   -3.21860800    1.49955600
H      2.80602900   -0.29594600    1.33043200
H      0.88642700   -1.30654000    3.23461000
H      0.06997300   -1.80941200   -0.36395500
H     -0.61069500    0.50494500    3.09555800
H      0.93436000    1.29820000    0.46155200
H     -3.01215100   -3.25302700   -1.55631900
H     -7.03184000   -0.29822900   -0.94210900
H     -7.18143400    1.60856900    0.43995600
H     -5.76464100    2.44473200    0.82994300
H      4.28847500    2.73667400   -3.34948300
H      2.66865400    3.27587100   -2.83323400
H      5.28009500   -3.97288600    0.53365200
H      4.64659600   -4.04722300    2.20218000
H      3.67626700   -4.69415700    0.84501900
H      4.07429700    4.35419800   -2.62129700
H      1.71467200   -0.25705500   -0.50585800
H     -0.49805100    2.94877000    0.30258400
H     -2.68901600    2.14884900    1.48516200
H     -1.68134000    2.34354400    2.93729300
H     -2.97627100    4.43564800    2.48648700
H     -1.23850700    4.75192800    2.32930000
H     -2.25234200    4.56796900    0.87859700
```

IC(c) (D- N$_S$C$_R$)   -1982.07582791

```
O      0.95284400    4.29933600    0.47076700
C      0.36760600    3.01797300    0.32314000
C      1.47521800    1.97714700    0.17015000
O      2.15412600    1.85140100    1.40623900
C      0.91981500    0.65092900   -0.30730200
O      3.62190600   -1.96775300   -0.89897100
C      0.48490600   -0.31343100    0.51982100
C      0.10897400   -1.65543500    0.05300300
N     -2.78940600    0.73975300   -0.35701600
C     -3.36635100    1.84725400   -1.00047500
N     -4.72571900    1.59941900   -0.95628800
C     -4.97934000    0.38790100   -0.31062600
C     -6.18744000   -0.29474500   -0.01495000
O     -7.35189600    0.01853300   -0.25919900
N     -5.89422200   -1.51232100    0.67233500
C     -4.64493700   -1.96907300    1.00001900
N     -4.56622800   -3.13249900    1.71305100
N     -3.53714700   -1.31181100    0.70540000
```

C	-3.75736500	-0.14332800	0.06232600
O	-2.78090300	2.80719000	-1.48625100
P	4.46800600	-0.76250700	-0.26166300
O	5.92550400	-1.17106200	-0.14809200
O	3.89133700	-0.25570900	1.06923900
O	4.25658500	0.38879300	-1.41005200
C	4.94310000	1.63279300	-1.22779800
C	-0.02037800	5.31398900	0.62592600
N	0.84777700	-2.30055400	-0.76813700
C	0.40518700	-3.61553300	-1.22703900
C	1.40852500	-4.70373600	-0.83502100
Na	5.94435500	-0.63988800	2.08839300
H	-0.30164200	2.99982300	-0.55144700
H	-0.23469800	2.75943200	1.21089000
H	2.15577100	2.34635100	-0.61388300
H	0.92350600	0.46931600	-1.38108000
H	0.43724700	-0.12640500	1.59182600
H	-1.78914000	0.63632100	-0.22454900
H	-0.82546400	-2.08511700	0.44192300
H	-5.41503500	2.22681500	-1.34274700
H	-6.71525200	-2.03884500	0.95166500
H	-5.30778400	-3.81353500	1.61460300
H	-3.63682100	-3.52869200	1.76494600
H	4.59801300	2.13941500	-0.31887600
H	6.02588800	1.47333400	-1.17122300
H	0.51280000	6.26584900	0.69899600
H	-0.70955600	5.35114000	-0.23205000
H	-0.61738800	5.16808700	1.54030600
H	4.71440300	2.25382700	-2.09667700
H	2.79590900	1.10464400	1.29838900
H	2.62319300	-1.90057200	-0.86089500
H	-0.59700100	-3.85650700	-0.83928200
H	0.33129800	-3.56765100	-2.32109700
H	1.09917200	-5.66877100	-1.25064700
H	2.40749300	-4.46601400	-1.21280000
H	1.47055000	-4.80185000	0.25443600

IC(c) (D- N_SC_S)   -1982.05090655

O	3.84473700	-2.75377400	0.29433100
C	2.69065300	-2.78165100	1.12861200
C	1.97926900	-1.43281500	1.06829700
O	1.38268900	-1.26794300	-0.21825400
C	0.96309800	-1.32324600	2.19280100
O	1.86933700	1.18920500	-0.78966900
C	0.18192500	-0.25323400	2.46052900
C	0.25070600	0.95640700	1.68745100
N	-2.10654900	-0.50698100	-0.14575800
C	-1.98671100	-1.76663600	-0.56059800
N	-3.17675100	-2.34517700	-0.88411200
C	-4.14911000	-1.37367300	-0.67643400
C	-5.55501500	-1.38633100	-0.85347800
O	-6.30105000	-2.28591000	-1.24610700
N	-6.08098200	-0.11215000	-0.49816600
C	-5.34541100	0.95918100	-0.04784000
N	-6.04084400	2.12574500	0.17740500
N	-4.04326300	0.93323400	0.11778000
C	-3.45367600	-0.25198700	-0.22115200
O	-0.87938400	-2.47302700	-0.67434100
P	3.42423900	1.35327800	-0.73168800
O	4.14416000	0.69616500	-1.92120100
O	4.01813300	0.89203200	0.61779200
O	3.70923100	2.99080000	-0.76963400

```
C        3.37276100    3.67941400   -1.97000900
C        4.44205600   -4.03920200    0.15729700
N       -0.41617200    2.02677300    1.99609800
C       -0.36205800    3.28501900    1.22858400
C       -1.76421200    3.76667900    0.86612700
Na       5.04360700   -0.84679800   -0.51293400
H        2.99157500   -3.00153300    2.16535000
H        2.00902900   -3.57792200    0.79273100
H        2.73160700   -0.63548900    1.19606000
H        0.86418000   -2.18037300    2.85827600
H       -0.05858900   -1.90904900   -0.48499200
H       -0.51455000   -0.28948200    3.29567300
H        0.90768100    1.04482200    0.80891000
H       -3.30561900   -3.27452900   -1.25777600
H       -7.07824200   -0.01126200   -0.65224600
H       -6.99618800    2.04463700    0.50333800
H       -5.50198000    2.81800800    0.68239200
H        3.95120400    3.29929300   -2.82091600
H        2.30372700    3.57974800   -2.19859800
H        5.30617200   -3.92749500   -0.50232800
H        4.77603900   -4.42838900    1.12945200
H        3.73802900   -4.75239500   -0.29139600
H        3.60829900    4.73789500   -1.81916100
H       -1.04204200    2.00813800    2.80097100
H        1.55530300   -0.30438900   -0.55014700
H        0.16232000    4.02370100    1.84482400
H        0.24640600    3.08005800    0.34503400
H       -1.68343800    4.66297600    0.24335500
H       -2.31557000    2.99730400    0.31800800
H       -2.33517300    4.03329800    1.76362300
```

IC(c) (A- $N_R C_R$)   -1982.06264119

```
O       -0.49314700    3.49205900    0.21875400
C       -0.12017000    2.14858500   -0.03291700
C        0.08268900    1.43289200    1.31188200
O       -1.11616400    1.25406200    2.03323800
C        0.88923500    0.16807800    1.12421000
O        4.50172300   -0.22715500    1.07121900
C        0.59085100   -1.00762000    1.71000600
C        1.39989400   -2.22976500    1.59532100
N       -2.82403600   -0.35112900    0.28289300
C       -2.49386000   -1.33032800   -0.55048900
N       -3.54492600   -1.84030600   -1.23390100
C       -4.66211400   -1.12666300   -0.80750300
C       -6.03419500   -1.20660000   -1.16635800
O       -6.59998100   -1.94723400   -1.97005400
N       -6.76395700   -0.23674700   -0.42631600
C       -6.23188400    0.63918600    0.49351300
N       -7.09902500    1.54178000    1.05449100
N       -4.95586600    0.68245800    0.80607400
C       -4.18770000   -0.21192100    0.12947600
O       -1.27394200   -1.81886600   -0.75658200
P        4.70901600    0.58424700   -0.31239200
O        5.69530300    1.71224800   -0.05846700
O        3.38442700    1.01751800   -0.92998200
O        5.34569200   -0.53089700   -1.34110000
C        6.67299900   -1.00379300   -1.08234900
C       -0.82897500    4.18878600   -0.96464600
N        2.61215100   -2.25667900    1.18806800
C        3.28185000   -3.54719200    1.05895400
C        3.59090800   -3.84538900   -0.41229400
Na       4.15041800    3.21910800   -0.87771400
```

H	0.81273000	2.10846600	-0.61822900
H	-0.90315400	1.63351800	-0.61282100
H	0.70602600	2.10619400	1.92279400
H	1.77716600	0.26557100	0.49835000
H	-0.30205200	-1.07790500	2.32805900
H	-0.64586600	-1.35875700	-0.15784600
H	0.89645900	-3.16196600	1.88920400
H	-3.51342600	-2.58514000	-1.91616000
H	-7.75169300	-0.19230300	-0.65296000
H	-8.06446600	1.26242100	1.17512000
H	-6.71077500	2.03118500	1.85121600
H	7.39021400	-0.17677200	-1.09892600
H	6.72672900	-1.50822000	-0.11059400
H	-1.09560300	5.20885900	-0.67581600
H	0.01679800	4.22612100	-1.67136700
H	-1.68572000	3.72659200	-1.47888200
H	6.91657100	-1.71708800	-1.87347300
H	-1.74355900	0.75289100	1.46174800
H	3.76387800	-0.90580600	1.02691900
H	4.22096100	-3.48823200	1.62332900
H	2.67820200	-4.35728600	1.49677800
H	4.17347900	-4.76942600	-0.49546400
H	2.66516600	-3.96843100	-0.98502700
H	4.16325700	-3.02742100	-0.86142600

IC(c) (A- $N_S C_R$)   -1982.03319784

O	0.98569000	3.83347700	-0.89302200
C	0.28807600	2.69138100	-0.44117100
C	0.04872800	1.76602600	-1.64721800
O	1.23220000	1.24146600	-2.20152800
C	-0.99185100	0.73136000	-1.32383700
O	-4.35017700	-1.11815700	0.21336000
C	-0.88076700	-0.57551000	-1.67206800
C	-1.97373100	-1.45325900	-1.37247600
N	2.55166000	-0.26974100	-0.09516600
C	2.11866700	-1.08120200	0.86104900
N	3.10961600	-1.63493300	1.59645700
C	4.29942000	-1.13352000	1.07457200
C	5.65859700	-1.34958700	1.42888300
O	6.14219600	-2.05236700	2.31520900
N	6.48954700	-0.58539200	0.56500400
C	6.05354000	0.22876700	-0.45661000
N	7.01479500	0.93119800	-1.13548400
N	4.78625300	0.39794400	-0.76356700
C	3.92617300	-0.29187900	0.03037100
O	0.85055700	-1.38167700	1.13621400
P	-4.51494300	0.28684500	0.81275200
O	-5.96862100	0.80565600	0.87730100
O	-3.58665600	1.36589100	0.18590400
O	-3.94663300	0.21268500	2.39392600
C	-4.62457100	-0.66626900	3.27802800
C	1.31371900	4.71685100	0.16279200
N	-2.00140300	-2.70891400	-1.71895300
C	-3.12117900	-3.62091700	-1.41638900
C	-3.79330500	-4.12135500	-2.69360300
Na	-5.36475800	2.74917400	-0.04489700
H	-0.67921100	2.97361900	0.00626100
H	0.86920200	2.15900100	0.32931900
H	-0.40076900	2.40482200	-2.42653900
H	-1.90358500	1.06051300	-0.80165600
H	-0.00638800	-0.93817800	-2.21029700
H	0.27227800	-0.88709500	0.52448100

H	-2.85797700	-1.10211000	-0.80145500
H	2.99697200	-2.26151100	2.38151300
H	7.47982000	-0.64062000	0.77830900
H	7.93543000	0.52025000	-1.22402500
H	6.67439300	1.36843500	-1.98271600
H	-5.67152100	-0.36509600	3.41873000
H	-4.60691700	-1.69997000	2.90661800
H	1.84308500	5.56447000	-0.27995600
H	0.41350200	5.08567500	0.67949900
H	1.96695100	4.23489500	0.90646800
H	-4.11284000	-0.62933500	4.24631000
H	-1.21858600	-3.10013700	-2.24192000
H	1.72506500	0.77260000	-1.48720400
H	-2.70879900	-4.45689900	-0.84105100
H	-3.81042500	-3.05890700	-0.78133000
H	-4.59648600	-4.81583600	-2.42823300
H	-4.22944500	-3.29081800	-3.25715500
H	-3.08809700	-4.65361400	-3.34226500

IC(c) (A- N$_R$C$_S$ and A- N$_S$C$_S$)   -1982.06711354

O	0.38025500	-1.68030100	2.46131900
C	0.15437000	-0.31537900	2.78713300
C	0.88444200	0.54726200	1.74594900
O	0.49874200	0.17213500	0.43050900
C	0.70699900	2.01787200	2.05233500
O	4.24640200	0.76027000	-0.35551900
C	0.79842500	3.08146500	1.22734700
C	1.14479300	3.16214200	-0.20514200
N	-2.28707500	0.69075400	0.22200600
C	-2.98717300	1.75074800	0.60718300
N	-4.30885400	1.65193300	0.33773200
C	-4.48404200	0.41520300	-0.27939300
C	-5.64042400	-0.24250000	-0.77967000
O	-6.81424100	0.12323800	-0.79282700
N	-5.26003700	-1.50338500	-1.31648400
C	-3.98138600	-2.01163700	-1.35015900
N	-3.83526300	-3.27421300	-1.86119400
N	-2.93229100	-1.37460100	-0.87536200
C	-3.21762100	-0.15901200	-0.33759100
O	-2.50995900	2.83640000	1.20959800
P	4.01927300	-0.84564300	-0.20386900
O	3.12266200	-1.37952500	-1.31460900
O	3.57776800	-1.21598500	1.20182300
O	5.56035800	-1.36347400	-0.37933400
C	6.19853700	-1.20808300	-1.65032200
C	-0.21129600	-2.57817300	3.38911600
N	2.02908600	2.45797900	-0.79433100
C	2.24773000	2.68601800	-2.22195500
C	1.80914000	1.46113500	-3.03269800
Na	1.49429300	-1.93638200	0.31156400
H	0.54253100	-0.09600800	3.79373500
H	-0.92662500	-0.10322900	2.78172600
H	1.95353000	0.30081400	1.81460900
H	0.48903400	2.24197300	3.09747100
H	-1.54028100	2.73282000	1.32137200
H	0.59146500	4.05897300	1.66627300
H	0.61199200	3.95313300	-0.75535700
H	-5.01788700	2.34181900	0.54497900
H	-6.03312400	-2.06293500	-1.66087700
H	-4.49126800	-3.58123900	-2.56819700
H	-2.87451300	-3.52649700	-2.05671300
H	5.61062200	-1.67905500	-2.44548800

```
H          6.34218100   -0.14761400   -1.88681000
H          0.01543900   -3.59035600    3.04647700
H          0.20396800   -2.43740600    4.39671600
H         -1.30182500   -2.44478200    3.43067300
H          7.17335900   -1.69749000   -1.57961600
H          3.38555200    1.25716900   -0.37821500
H         -0.47020600    0.34660900    0.32208200
H          1.72313300    3.59019900   -2.56907100
H          3.32377400    2.84616300   -2.36189200
H          2.06086300    1.60627700   -4.08933000
H          2.30621600    0.55665000   -2.66783200
H          0.72592000    1.31516500   -2.95292300
```

Appendix E: Supplemental Information for Chapter 6:

Bifunctional Glycosylases Part 2:

Human 8-Oxoguanine–DNA Glycosylase (hOgg1)

Table of Contents

Table E1. *Summary of model, mechanism and method used in previous computational studies of dOG deglycosylation.*

Mechanism	Model				Starting Geometry	Method	Ref
	OG	Sugar	Nucleophile	Other			
A_N+D_N	Oxo-imidazole	furane	methyl amine (cationic)	χ constrained	1EBM (K249Q)	B3LYP/6-31G(d,p)	1
S_N1 S_N2	Oxo-imidazole	2′,5′-dideoxyribose	lysine (cationic)		1N3C (D268N), 1EBM (K249Q) 1FN7 (WT:THF)	B3LYP/6-31+G(d,p)// B3LYP/6-31G(d)	2
S_N2, S_N1	OG	3′,5′-diphosphate	lysine (cationic)	Functional groups: D268, H270, Q315, F319, I152 Backbone: M271, V269, N151, G42	1EBM (K249Q)	(CPCM-)B3LYP/DZVP (with 3-21G and STO-3G)	3
Dissociation	OG	nucleoside	None			(PCM-)B3LYP/6-31++G(d,p)	4
S_N2	OG	2′,3′,5′-trideoxyribose	OH⁻, HCOO⁻···H₂O, methyl amine, pyrrolidine (proline)			(PCM-)B3LYP/6-311+G(2d,p)// B3LYP/6-31G(d)	5
S_N2	OG	nucleoside (methyl capped)	OH⁻, HCOO⁻···H₂O	benzene, H₂O, NH₃, HF		(PCM-)M06-2X/6-311+G(2d,p)// M06-2X/6-31+G(d,p)	6
S_N2	OG	3′-monophosphate	Ethyl amine (neutral)		1EBM (dOG nucleotide only)	(PCM-)M06-2X/6-311+G(2d,p)// B3LYP/6-31G(d)	7
S_N2, S_N1, σ-bond sub., Dissociation	OG	furane	lysine (cationic and neutral)	Lys backbone constrained, C3′ and C4′ constrained	1N3C (D268N)	(CPCM-)B3LYP/6-31G(d,p)	8

(1) Osakabe, T.; Fujii, Y.; Hata, M.; Tsuda, M.; Neya, S.; Hoshino, T. *Chem-Bio Inf. J.* **2004**, *4*, 73–92; (2) Schyman, P.; Danielsson, J.; Pinak, M.; Laaksonen, A. *J. Phys. Chem. A* **2005**, *109*, 1713–1719; (3) Calvaresi, M.; Bottoni, A.; Garavelli, M. *J. Phys. Chem. B* **2007**, *111*, 6557–6570; (4) Zheng, Y.; Xue, Y.; Yan, S. G. *THEOCHEM* **2008**, *860*, 52–57; (5) Shim, E. J.; Przybylski, J. L.; Wetmore, S. D. *J. Phys. Chem. B* **2010**, *114*, 2319–2326; (6) Unpublished work by Jennifer Kellie and Lex Navarro-Whyte. All M06-2X values by JK. Initial geometries from MPWB1K optimizations run by LNW (7) Kellie, J. L.; Wetmore, S. D. *J. Phys. Chem. B* **2012**, *116*, 10786–10797; (8) Šebera, J.; Trantírek, L.; Tanaka, Y.; Sychrovský, V. *J. Phys. Chem. B* **2012**, *116*, 12535–12544.

Table E2. *List of model contents, layer divisions and charges.*

Residue	PM6–Freeze	PM6–Move	DFT	Truncations	Charge DFT/PM6
DC21	O3′			Remaining backbone and nucleobase	0/0
DA22	Sugar, phosphate, N9	O3′		Nucleobase truncated to N9.	0/−1
FDG23		P, OP1, OP2	**Sugar, nucleobase**		0/−1
DG24	C1′, C2′, C3′, C4′,O4′, O3′, N9	C5′	**P, OP1, OP2, O5′**	Nucleobase truncated to N9.	−1/−1
DT25	P, OP1, OP2, O5′			Sugar and nucleobase removed.	0/−1
L37	BB, Cβ			R-Group truncated to Cβ	0/0
V38	All				0/0
L39	BB, Cβ			R-Group truncated to Cβ	0/0
P40	All				0/0
S41	All				0/0
G42	N		**Cα, C, O**		0/0
Q43	C, O, R-Group		**N, Cα**		0/0
S44	All				0/0
F45	All				0/0
V130	All				0/0
R131	BB, Cβ			R-Group truncated to Cβ	0/0
L133	All				0/0
R134	BB, Cβ			R-Group truncated to Cβ	0/0
Q135	All				0/0
C140	All				0/0
L141	BB, Cβ			R-Group truncated to Cβ	0/0
F142	BB, Cβ			R-Group truncated to Cβ	0/0
S143	All				0/0
F144	BB	R-Group			0/0
I145	All				0/0
C146	All				0/0
S147	BB		**R-Group**		0/0
S148	All				0/0
C149	All				0/0
N150	All				0/0
N151	All				0/0
I152	All				0/0
A153	All				0/0
R154	BB, Cβ			R-Group truncated to Cβ	0/0
I155	All				0/0
T156	All				0/0
G157	All				0/0

Table E2. *List of model contents, layer divisions and charges.*

Residue	PM6–Freeze	PM6–Move	DFT	Truncations	Charge DFT/PM6
M158	BB, Cβ			R-Group truncated to Cβ	0/0
V159	All				0/0
T248	All				0/0
K249	BB		**R-Group**		1/1
V250	All				0/0
A251	All				0/0
D252	All				0/−1
C253	BB		**R-Group**		−1/−1
I254	All				0/0
C255	BB, Cβ			R-Group truncated to Cβ	0/0
L256	All				0/0
M257	BB	R-Group			0/0
A264	All				0/0
V265	All				0/0
P266	All				0/0
V267	All				0/0
D268	BB		**R-Group**		−1/−1
V269	All				0/0
H270	BB		**R-Group**		1/1
M271	All				0/0
W272	BB, Cβ			R-Group truncated to Cβ	0/0
H273	BB, Cβ			R-Group truncated to Cβ	0/0
I274	All				0/0
A311	All				0/0
G312	All				0/0
W313	All				0/0
A314	All				0/0
Q315	BB		**R-Group**		0/0
A316	All				0/0
V317	All				0/0
L318	All				0/0
F319	BB		**R-Group**		0/0
S320	All				0/0
A321	All				0/0
D322	All				0/−1
L323	All				0/0
R324	All				0/1
Q325	BB, Cβ			R-Group truncated to Cβ	0/0
Calcium		CA1(C)			0/2
Waters	4(A), 326(A), 328(A), 336(A), 352(A), 364(A), 369(A), 374(A), 389(A)	2 added water molecules to solvate Ca²⁺	**109(C), 55(C), 1(A)**		0/0

Notes: BB – backbone atoms (N, C, O, Cα).

Table E3. *Summary of the alternate geometries (°) obtained from a conformational search of the hOgg1 active site with ONIOM(M06-2X/6-31G(d):PM6).*

Residue Altered	Count[a]	ΔE[b]	F144 αβ[c]	F144 βγ[d]	K249 αβ[c]	K249 βγ[d]	K249 γδ[e]	K249 δε[f]	C253 αβ[c]	D268 αβ[c]	D268 βγ[d]	H270 αβ[c]	H270 βγ[d]	Q315 αβ[c]	Q315 βγ[d]	Q315 γδ[e]	F319 αβ[c]	F319 βγ[d]
Any	53	0.0	151.1	89.4	55.4	−168.8	165.3	−62.7	173.1	−44.2	128.5	150.0	−80.7	44.6	−83.3	156.9	59.2	88.3
		Std. Dev.[g]	0.01	0.05	0.04	0.02	0.04	0.01	0.01	0.01	0.03	0.02	0.01	0.01	0.03	0.04	0.02	0.02
K249	1	−20.5	150.5	90.2	64.4	**−87.6**	**−170.3**	−48.2	177.1	−43.5	126.5	151.5	−81.3	42.5	−84.4	157.2	56.5	85.5
K249	1	−9.7	151.6	91.6	57.7	**−76.1**	**−164.9**	**−176.4**	**149.9**	−44.7	128.9	149.7	−80.5	44.5	−83.2	156.5	59.7	88.8
Q315	8	−6.0	151.2	91.7	58.0	−167.7	163.4	−62.8	173.5	−44.8	130.8	149.1	−81.5	**74.3**	**−122.4**	**66.9**	57.0	83.6
K249	1	−5.2	150.5	90.0	**99.2**	**−75.1**	**−55.6**	**−45.8**	176.9	−44.6	128.0	151.0	−80.3	44.3	−84.1	158.3	60.1	89.3
C253	4	0.0	151.1	89.3	55.3	−168.8	165.3	−62.7	**−137.2**	−44.2	128.5	150.1	−80.7	44.6	−83.3	157.0	59.2	88.3
Q315	2	0.8	149.2	89.6	59.7	−166.5	163.2	−63.5	172.9	−44.4	133.0	150.2	−80.0	**−37.0**	**75.2**	**47.3**	60.0	95.1
K249	1	0.9	150.4	92.2	**98.9**	**−76.9**	**−55.3**	**−153.6**	176.9	−45.8	128.9	151.2	−80.4	43.7	−82.4	154.5	59.3	88.0
Q315	24	1.6	150.0	88.7	56.2	−169.7	163.9	−64.3	175.1	−45.8	129.3	151.9	−79.7	**−23.4**	**89.4**	172.6	61.0	88.8
Q315	13	4.8	149.3	88.7	55.1	−170.7	162.8	−65.4	174.6	−44.8	130.9	151.8	−79.9	54.4	**−107.6**	**−98.7**	60.4	97.1
K249	2	5.8	149.6	91.6	**71.7**	**−139.4**	**55.8**	**154.4**	176.2	−44.9	127.3	152.0	−80.6	43.6	−85.1	159.5	59.8	89.1
Q315	2	6.2	151.2	92.3	58.9	−167.6	162.6	−62.9	173.5	−44.8	131.9	148.7	−81.9	**−21.2**	**94.3**	**−103.6**	55.2	82.0
Q315	4	7.7	149.3	89.7	56.4	−168.8	163.7	−63.8	173.8	−43.8	132.7	149.9	−79.5	39.1	**−100.5**	**−54.8**	60.5	91.6
K249	1	8.1	151.1	91.6	45.9	−178.4	176.7	**53.4**	177.3	−44.7	130.1	149.9	−81.7	43.2	−82.3	153.7	55.2	84.4
K249	1	8.5	151.2	91.5	**98.6**	**−68.9**	**−75.1**	**69.2**	175.6	−44.6	128.8	150.1	−80.5	44.8	−82.7	156.1	59.8	88.7
K249	2	9.1	150.1	91.1	**79.5**	**−153.4**	**87.5**	**90.0**	178.0	−43.7	127.4	152.1	−81.0	43.8	−83.9	157.4	59.8	88.6
H270	4	9.5	150.6	87.4	53.2	−170.2	167.2	−64.4	173.4	−44.3	131.5	**166.6**	**106.2**	43.7	−86.7	162.6	62.5	90.9
Q315	6	10.4	150.1	86.3	51.5	−171.1	166.7	−64.4	174.2	−45.0	126.9	151.0	−80.0	**59.8**	−82.9	**−9.8**	61.1	87.2
K249	1	11.3	148.9	91.6	**40.2**	**−116.3**	153.7	**58.2**	173.4	−45.9	128.5	152.4	−80.5	43.4	−84.3	158.0	59.7	88.9
D268	1	12.2	151.6	91.4	57.9	−166.8	164.5	−62.6	172.3	**−29.0**	**103.3**	149.6	−81.8	48.6	−82.4	157.7	58.2	86.6
Q315	35	13.4	149.9	89.8	56.7	−168.5	164.2	−63.3	173.4	−44.4	130.9	149.7	−80.1	**154.7**	**76.2**	**5.4**	60.1	89.5
K249	1	14.5	150.8	89.8	**97.2**	**−103.3**	**−68.8**	**−170.4**	176.9	−44.4	126.7	151.3	−81.1	44.1	−81.1	158.1	57.8	87.2
Q315	3	14.7	151.5	84.8	50.3	−171.8	169.0	−64.3	174.2	−46.1	120.8	149.7	−81.0	50.1	**−179.6**	**−0.6**	61.8	91.6
K249	3	18.8	150.6	93.0	**107.9**	**−123.2**	**59.7**	**179.2**	176.2	−46.6	132.6	150.9	−81.9	43.8	−81.3	152.4	56.8	85.3
K249	1	26.3	150.7	91.6	**−6.8**	**158.9**	**−102.2**	**63.2**	177.1	−44.3	128.6	150.5	−80.3	45.0	−83.4	157.6	60.4	89.5
C253	1	26.5	151.0	92.0	54.4	−168.0	167.1	−64.9	**24.3**	−44.5	128.9	149.9	−80.7	44.2	−83.4	157.0	58.4	87.1
Q315	1	29.2	150.0	88.8	55.0	−168.7	166.2	−63.2	172.9	−44.3	129.0	149.7	−79.5	**−11.1**	**75.0**	**36.1**	62.7	92.3
C253	1	30.0	151.2	90.2	54.6	−167.6	167.4	−64.5	**−36.3**	−44.4	128.8	149.9	−80.7	44.6	−83.2	157.0	59.2	88.3
Q315	9	31.2	149.8	89.8	56.8	−168.5	164.1	−63.3	173.3	−44.4	131.1	149.7	−80.0	**−158.5**	**−41.5**	**108.8**	60.2	89.5
Q315	2	31.5	150.0	89.1	55.5	−169.1	165.6	−63.5	173.5	−44.2	130.2	150.0	−79.5	**0.6**	**89.1**	**45.4**	62.0	88.7
Q315	1	35.3	149.9	89.5	58.2	−168.2	163.0	−63.7	173.5	−45.2	130.9	150.9	−79.7	**−19.0**	**103.5**	**90.5**	57.7	90.8
Q315	18	36.7	149.9	89.9	56.9	−168.2	164.5	−63.1	173.2	−44.4	130.9	149.4	−80.0	**−171.6**	**−54.2**	**9.7**	60.1	89.4
Q315	5	49.1	149.9	89.9	56.8	−168.3	164.4	−63.2	173.2	−44.4	131.0	149.5	−80.0	**153.8**	**51.7**	**−78.9**	60.1	89.4
Q315	10	62.7	149.9	89.7	57.0	−168.3	164.4	−63.3	173.2	−44.4	131.1	149.9	−79.8	**−170.4**	**−62.8**	**−92.0**	60.2	89.9

[a] Number of structures that relax to the this geometry. [b] Energy (kJ mol⁻¹) relative to the geometry closest to the 3KTU crystal structure. [c] Dihedral angle about the Cα–Cβ bond. [d] Dihedral angle about the Cβ–Cγ bond. [e] Dihedral angle about the Cγ–Cδ bond. [f] Dihedral angle about the Cδ–Cε bond. [g] Standard deviation in measured angles for the structures closest to the 3KTU crystal structure.
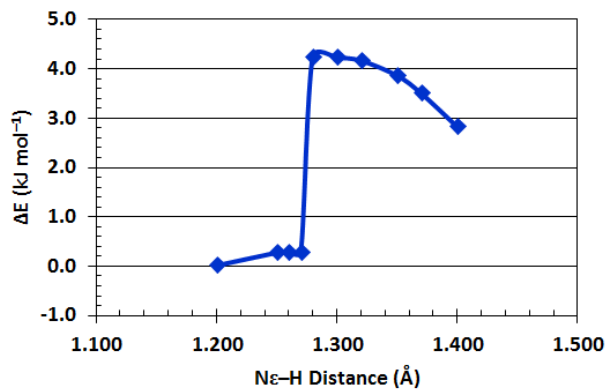
Figure E1. *ONIOM(M06-2X/6-31G(d):PM6) reaction potential energy surface for proton transfer from K249 to C253.*

Table E4. *Effect of active-site mutations on the reaction energetics (kJ mol^{-1}) of the lysine activation and deglycosylation steps of three different mechanisms.*[a]

Mutation (Effect)[b]	K249 Activation		Deglycosylation					
			K249–Nuc		K249–GB		D268–GB	
	TS1[c]	RC2[d]	TS3[c]	IC1[d]	TS3[c]	PC[d]	TS3[c]	PC[d]
					$\Delta\Delta E$[e]			
F144A (ø)	–4.8	30.8	–2.9	–7.5	–33.1	–0.6	2.5	24.0
K249A (++)	–	–	–	–	61.0	34.6	8.2	22.2
K249Q (++)	–	–	–	–	48.3	34.0	–6.0	26.2
C253A (+)	–	–	–1.4	3.1	2.0	4.0	–27.8	25.7
D268A (++)	34.0	53.7	49.3	44.6	–6.1	7.8	94.6	–69.0[f]
D268N (++)	30.4	52.8	69.5	9.6	–37.6	0.3	97.8	–130.5[f]
D268E (ø)	–3.6	27.5	–31.8	–38.6	–7.3	26.2	–4.4	–2.2
H270A (+)	–2.9	33.6	–32.1	2.4	–34.6	0.4	–22.8	–5.3
Q315A (+)	–3.6	28.2	10.1	–1.6	2.1	1.5	6.9	15.3
F319A (+)	–3.3	1.7	–13.9	–14.4	–9.9	–4.3	–3.2	32.4
G42-XX (–)	–3.0	28.7	–12.9	–10.7	–39.2	–7.3	–2.1	9.9
KCCK[f] (+)	29.2	52.9	–	–	6.2	30.4	3.8	14.7
					$\Delta\Delta G$[g]			
F144A (ø)	3.1	37.6	–14.1	–18.8	–7.7	–10.5	–7.7	24.1
K249A (++)	–	–	–	–	85.3	51.1	6.1	33.1
K249Q (++)	–	–	–	–	73.6	47.6	–16.3	17.3
C253A (+)	–	–	–18.4	–5.8	26.2	–1.8	–17.9	51.9
D268A (++)	42.6	51.1	40.4	38.1	31.7	5.1	76.9	–95.8[f]
D268N (++)	26.8	58.2	48.0	5.7	–21.5	5.2	99.6	–129.4[f]
D268E (ø)	–2.6	37.1	–60.3	–51.8	6.0	13.6	–10.6	2.0
H270A (+)	2.0	48.6	–29.7	–4.2	–10.2	–3.7	–39.8	–18.3
Q315A (+)	–3.3	44.7	–7.2	–10.0	9.4	–8.1	20.6	33.4
F319A (+)	–2.0	7.3	–46.5	–36.5	19.4	–11.7	6.2	51.1
G42-XX (–)	–0.6	37.0	–36.8	–12.4	19.4	–22.8	–36.2	14.2
KCCK[f] (+)	29.6	58.5	–	–	20.3	22.3	6.5	–14.8

[a] See Section 6.2.3 for the definitions of the mechanisms and stationary points. [b] Expected effect of mutation on barrier height (++, large increase; +, increase; ø, no effect; –, decrease). [c] A positive value indicates the mutant barrier is higher. [d] A positive values indicates the product is less stable in the mutant. [e] ONIOM(M06-2X/6-311+G(2df,2p):PM6) single-point energies including scaled (0.958) zero-point vibrational energy. [f] K249C/C253K double mutant. [f] Falls to PC–K$_{GB}$. g ONIOM(M06-2X/6-311+G(2df,2p):PM6) single-point energies including unscaled thermal correction to Gibb's energy.

Table E5. *Summary of experimental hOgg1 mutational kinetics data.*

Mutation	Rate (min^{-1})	Substrate Length	Reference
K249C	No Activity	25	1
K249Q	No Activity	25	1
WT	100 %	34	2
H270A	0.60 %	34	2
H270R	29.10 %	34	2
H270L	< 0.1 %	34	2
Q315A	62.00 %	34	2
F319A	0.50 %	34	2
K249Q	< 0.1 %	34	2
WT	5.2 ± 0.5	24	3
K249C/C253K	0.46 ± 0.09	24	3
C253A	0.45 ± 0.03	24	3
C253W		24	3
WT	0.106 ± 0.018	25	4
D268N	0.0016 ± 0.00027	25	4
D268E		25	4
D268Q		25	4

(1) Nash, H. M.; Lu, R. Z.; Lane, W. S.; Verdine, G. L. *Chem. Biol.* **1997**, *4*, 693–702.
(2) van der Kemp, P. A.; Charbonnier, J. B.; Audebert, M.; Boiteux, S. *Nucleic Acids Res.* **2004**, *32*, 570–578
(3) Dalhus, B.; Forsbring, M.; Helle, I. H.; Vik, E. S.; Forstrøm, R. J.; Backe, P. H.; Alseth, I.; Bjørås, M. *Structure (Cambridge, MA, U. S.)* **2011**, *19*, 117–127
(4) Norman, D. P. G.; Chung, S. J.; Verdine, G. L. *Biochemistry* **2003**, *42*, 1564–1572

Full citation for reference 24.

Frisch, M. J. T., G. W.; Schlegel, H. B. Scuseria, G. E.; Robb, M. A.; Cheeseman, J. R.; Scalmani, G.; Barone, V.; Mennucci, B.; Petersson, G. A.; Nakatsuji, H.; Caricato, M.; Li, X.; Hratchian, H. P.; Izmaylov, A. F.; Bloino, J.; Zheng, G.; Sonnenberg, J. L.; Hada, M.; Ehara, M.; Toyota, K.; Fukuda, R.; Hasegawa, J.; Ishida, M.; Nakajima, T.; Honda, Y.; Kitao, O.; Nakai, H.; Vreven, T.; Montgomery, Jr., J. A.; Peralta, J. E.; Ogliaro, F.; Bearpark, M.; Heyd, J. J.; Brothers, E.; Kudin, K. N.; Staroverov, V. N.; Kobayashi, R.; Normand, J.; Raghavachari, K.; Rendell, A.; Burant, J. C.; Iyengar, S. S.; Tomasi, J.; Cossi, M.; Rega, N.; Millam, N. J.; Klene, M.; Knox, J. E.; Cross, J. B.; Bakken, V.; Adamo, C.; Jaramillo, J.; Gomperts, R.; Stratmann, R. E.; Yazyev, O.; Austin, A. J.; Cammi, R.; Pomelli, C.; Ochterski, J. W.; Martin, R. L.; Morokuma, K.; Zakrzewski, V. G.; Voth, G. A.; Salvador, P.; Dannenberg, J. J.; Dapprich, S.; Daniels, A. D.; Farkas, Ö.; Foresman, J. B.; Ortiz, J. V.; Cioslowski, J.; Fox, D. J.; Revision A.02 (C.01) .; Gaussian, Inc.: Wallingford CT, **2009**.

ONIOM(M06-2X/6-311+G(2df,2p):PM6)//ONIOM(M06-2X/6-31G(d):PM6) energetics and coordinates. (DFT region only, truncation points capped with a hydrogen atom).

Lys Activation: RC1–All   E = −3875.584519 a.u.

O	-0.97626300	-6.05723900	-2.30171300
C	-2.10903000	-5.58898800	-1.58949700
C	-1.65570800	-5.34766200	-0.16474900
O	-0.92153400	-4.12698700	-0.10926900
C	-2.79180800	-5.23629400	0.87245300
O	-2.41693500	-6.14540000	1.92775900
C	-2.71874800	-3.79182100	1.33949300
C	-1.24323800	-3.44831500	1.08925400
N	-0.95024300	-2.03864400	0.90257100
C	-1.55567900	-1.23231100	-0.10747200
N	-0.66840900	-0.21986600	-0.35394000
C	0.47350000	-0.37517200	0.43270000
C	1.73196700	0.29062200	0.40987700
O	2.07477300	1.26585600	-0.25447200
N	2.62837000	-0.33830900	1.29347300
C	2.38034800	-1.49174000	1.98512300
N	3.40320900	-1.98857800	2.72884300
N	1.21395800	-2.10747500	1.98137800
C	0.31946600	-1.52133900	1.17091800
O	-2.66687000	-1.38991400	-0.58758700
P	-3.47523500	-6.81683000	2.93338500
O	-2.85506900	-8.17307500	3.34846200
O	-4.84738600	-6.91799600	2.32485800
O	-3.37467900	-5.74293600	4.12257700
C	-1.15179000	1.28469400	-4.32300900
C	-1.03338200	2.37788000	-3.22793000
O	-1.34760600	2.11367200	-2.07566000
N	-0.64681400	3.61390900	-3.62325300
C	-0.76610200	4.77655200	-2.76441800
C	-6.42959700	-1.69237900	0.97647600
O	-6.01894300	-1.60125400	2.31960400
C	-2.05522600	-2.60947800	8.19507500
C	-1.37408900	-2.51213100	6.81603900
C	-2.11060400	-1.62761100	5.80526100
C	-1.64312800	-1.85475900	4.37565100
N	-2.36755100	-0.92695700	3.46562500
C	-2.01731400	2.91079300	4.80925400
S	-0.95636500	1.64062700	4.00894500
C	0.94658800	-5.42506600	4.27565600
C	1.97205800	-5.28782900	3.08459700
O	3.11197400	-4.83443200	3.35295400
O	1.56299400	-5.66484900	1.95592800
C	4.32950100	-6.48979600	0.48253700
C	3.71149500	-6.83934100	-0.84455800
N	4.43090000	-7.24452500	-1.96274500
C	2.39987600	-6.82273200	-1.22062900
C	3.59031800	-7.47427500	-2.96714900
N	2.35212500	-7.22415200	-2.54075400
C	8.21791300	1.42281700	3.55650000
C	7.55799400	0.02299000	3.58209200
C	6.05639800	-0.03579100	3.33615500
O	5.57664700	0.21072700	2.22681300
N	5.30594400	-0.38230400	4.39389800
C	6.33508900	-1.20750200	-0.76247400
C	4.90048600	-1.69112100	-0.94759900
C	4.42201200	-2.81114000	-0.25937400
C	4.02254500	-1.00124800	-1.78899500

C	3.10293900	-3.24341600	-0.40999300
C	2.71497400	-1.44850300	-1.96994700
C	2.24905600	-2.56786800	-1.28277900
O	3.01287700	2.17865800	-2.79101100
O	-4.85114700	-9.14371000	1.11524700
O	-0.01456200	-7.83231700	2.18579500
H	-2.93336900	-6.32717700	-1.57806000
H	-2.49266300	-4.64275100	-2.00203700
H	-1.01691200	-6.18296100	0.14345000
H	-3.78350500	-5.51904100	0.49470700
H	-3.32971100	-3.16146000	0.68556100
H	-3.04688500	-3.68007200	2.37463200
H	-0.59086500	-3.79092800	1.89973600
H	-0.89602300	0.58202000	-0.94249700
H	3.56705300	0.06444900	1.35380600
H	3.27867600	-2.96771500	3.01840500
H	4.32760800	-1.75693900	2.37498000
H	-2.23590700	1.15449000	-4.52956800
H	-0.77452800	0.34137600	-3.87235100
H	-0.45801000	3.77320500	-4.61295100
H	-0.67785800	4.43348000	-1.71526500
H	-5.60699400	-2.19029400	0.44194300
H	-6.55500400	-0.68731400	0.52382200
H	-6.72382600	-1.20217500	2.86703300
H	-1.58489900	-3.44396300	8.75399100
H	-3.11383800	-2.89288600	8.04717500
H	-1.31285100	-3.53173400	6.41783600
H	-0.33834700	-2.16608300	6.92631700
H	-3.19047800	-1.83360700	5.86638900
H	-1.96016500	-0.56094800	6.03712400
H	-1.80894400	-2.88902800	4.06183900
H	-0.57915900	-1.61894500	4.26745900
H	-2.12353400	-1.11633700	2.48742100
H	-3.38454300	-1.01056800	3.55479100
H	-2.77374000	2.45386400	5.48288000
H	-2.58167300	3.47565600	4.04441200
H	-1.98205500	0.17356900	3.70146200
H	0.04006500	-5.94297900	3.94118700
H	0.65214900	-4.38070800	4.52420400
H	3.66309700	-5.80193300	1.01574600
H	5.27410800	-5.95528600	0.24716200
H	5.47847800	-7.32274300	-2.04280300
H	1.52071100	-6.54021700	-0.67494100
H	3.87373900	-7.81410400	-3.95458200
H	1.47733300	-7.29818500	-3.09716000
H	8.62284400	1.65123100	4.55461300
H	7.46667200	2.20476900	3.32978600
H	7.96549500	-0.60669300	2.77583700
H	7.79302300	-0.48730300	4.52326300
H	5.71432700	-0.72858200	5.25291200
H	4.33248100	-0.66280000	4.24980500
H	6.63396500	-1.33705900	0.29569100
H	6.39109000	-0.12287100	-0.95528400
H	5.08758600	-3.34586900	0.41969700
H	4.34663600	-0.09735900	-2.29849500
H	2.71114900	-4.06493700	0.18737500
H	2.04575300	-0.88893300	-2.62426400
H	1.22124500	-2.90760800	-1.39502500
H	2.41183700	1.61815700	-3.31758900
H	2.81259500	1.91370100	-1.87260200
H	-4.93571600	-9.19226100	0.13196000
H	-4.96440800	-8.16592900	1.36727200
H	0.35964000	-6.94514200	1.96874000

H	-0.95909900	-7.68404100	2.33614000
H	-0.03124790	5.51084550	-3.02074300
H	-1.73535828	5.20554747	-2.91072301
H	-0.63271366	1.52211734	-5.22804486
H	-1.38501646	3.57214130	5.36397758
H	-7.32751717	-2.25249068	0.81863342
H	9.00023939	1.43340718	2.82660051
H	7.02578394	-1.73018305	-1.39068178
H	4.54352288	-7.35895381	1.06876165
H	1.36742228	-5.88566574	5.14493524
H	-3.54975945	-6.15570403	4.97144059
H	-1.20037326	-6.49730855	-3.12494649
H	-1.99158020	-1.72726524	8.79719613

Lys Activation: TS1–All   E = -3875.582959 a.u.   (348.65i cm^{-1})

O	-0.97444800	-6.06002700	-2.29995900
C	-2.10655100	-5.58977700	-1.58742600
C	-1.65243900	-5.34897400	-0.16296300
O	-0.91410200	-4.13114600	-0.10852200
C	-2.78807000	-5.23311200	0.87421100
O	-2.41454600	-6.14227000	1.93024200
C	-2.71205800	-3.78788100	1.33865500
C	-1.23627600	-3.44761800	1.08784400
N	-0.93988500	-2.04025100	0.89510500
C	-1.54695300	-1.23233000	-0.11054700
N	-0.66199100	-0.21577300	-0.35221000
C	0.47948400	-0.37119600	0.43471500
C	1.73749600	0.29459900	0.41302600
O	2.07995400	1.27240800	-0.24846300
N	2.63466200	-0.33619500	1.29469200
C	2.38725100	-1.49206100	1.98263400
N	3.41031100	-1.99017300	2.72604600
N	1.22196700	-2.10894700	1.97658000
C	0.32632900	-1.52126000	1.16830600
O	-2.65653300	-1.39037300	-0.59439000
P	-3.47340600	-6.81544600	2.93356700
O	-2.85311700	-8.17216200	3.34786700
O	-4.84510800	-6.91759700	2.32372200
O	-3.37479100	-5.74324600	4.12384300
C	-1.15229100	1.28405900	-4.32300900
C	-1.03447300	2.37781600	-3.22854000
O	-1.34923500	2.11431600	-2.07630000
N	-0.64733100	3.61369800	-3.62399400
C	-0.76679500	4.77593400	-2.76487100
C	-6.43002700	-1.69280500	0.97712400
O	-6.02140800	-1.60073000	2.31996500
C	-2.05489400	-2.60894900	8.19284900
C	-1.37168600	-2.50931800	6.81463700
C	-2.10429600	-1.62049200	5.80551700
C	-1.63212200	-1.82661200	4.37397400
N	-2.35447500	-0.88777800	3.48115900
C	-2.01688000	2.90896800	4.81065200
S	-0.94260900	1.65526100	4.00003600
C	0.94770200	-5.42527500	4.27522900
C	1.97418100	-5.28941700	3.08484400
O	3.11378300	-4.83499100	3.35338900

O	1.56680900	-5.66928600	1.95652400
C	4.33000000	-6.48961900	0.48283200
C	3.70838200	-6.83863200	-0.84264800
N	4.42504400	-7.24551200	-1.96196700
C	2.39609200	-6.81979800	-1.21626700
C	3.58210800	-7.47434400	-2.96471500
N	2.34525000	-7.22182800	-2.53613700
C	8.21836900	1.42388600	3.55738800
C	7.55890900	0.02411700	3.58531100
C	6.05770700	-0.03460000	3.33779500
O	5.57931500	0.21397900	2.22839200
N	5.30609700	-0.38288500	4.39422100
C	6.33486800	-1.20722300	-0.76257400
C	4.90013400	-1.68978300	-0.94917700
C	4.42128500	-2.81144000	-0.26393600
C	4.02247400	-0.99735100	-1.78876800
C	3.10191600	-3.24246700	-0.41522700
C	2.71455700	-1.44335600	-1.97044000
C	2.24808700	-2.56409400	-1.28587700
O	3.01042600	2.18262000	-2.78967300
O	-4.85028300	-9.14187300	1.11594600
O	-0.01477800	-7.83379200	2.18642700
H	-2.93196100	-6.32671900	-1.57599700
H	-2.48850100	-4.64292100	-2.00016200
H	-1.01654700	-6.18639400	0.14560600
H	-3.78033600	-5.51471000	0.49714800
H	-3.32176600	-3.15791400	0.68327800
H	-3.03882400	-3.67055000	2.37347900
H	-0.58532400	-3.78838600	1.90003000
H	-0.89055000	0.58588100	-0.94031500
H	3.57320700	0.06668800	1.35585500
H	3.28453300	-2.96979700	3.01376100
H	4.33450200	-1.75981800	2.37077200
H	-2.23629200	1.15320700	-4.52966200
H	-0.77460600	0.34115900	-3.87185800
H	-0.45834300	3.77300400	-4.61365400
H	-0.67849400	4.43205300	-1.71605800
H	-5.60679700	-2.19105400	0.44382100
H	-6.55563100	-0.68829300	0.52289300
H	-6.72686800	-1.20223900	2.86681900
H	-1.58626900	-3.44448800	8.75159300
H	-3.11363600	-2.89089600	8.04283000
H	-1.31237600	-3.52767700	6.41318100
H	-0.33496700	-2.16658800	6.92763900
H	-3.18390500	-1.82987100	5.85893700
H	-1.96137100	-0.55542900	6.04927800
H	-1.78813800	-2.86111300	4.05293000
H	-0.56662700	-1.58963900	4.27699100
H	-2.12296100	-1.07233700	2.50097500
H	-3.36959000	-0.97356100	3.57750200
H	-2.76224900	2.43581100	5.48445500
H	-2.59001000	3.46986000	4.05029000
H	-1.91396800	0.28686600	3.73525500
H	0.04110300	-5.94281500	3.94052300
H	0.65338400	-4.38074200	4.52312600

```
H          3.66608000   -5.80039200    1.01740400
H          5.27522700   -5.95714100    0.24496300
H          5.47195600   -7.32525800   -2.04328500
H          1.51857100   -6.53533500   -0.66889300
H          3.86288100   -7.81504900   -3.95261500
H          1.46912400   -7.29482000   -3.09107600
H          8.62397300    1.65367600    4.55493300
H          7.46661600    2.20525200    3.33028600
H          7.96704400   -0.60701900    2.78049900
H          7.79313900   -0.48457500    4.52753500
H          5.71431100   -0.73070600    5.25272100
H          4.33403400   -0.66709200    4.24745700
H          6.63300900   -1.33785000    0.29569700
H          6.39180900   -0.12245500   -0.95445100
H          5.08675700   -3.34846900    0.41341300
H          4.34704000   -0.09245700   -2.29618000
H          2.70995700   -4.06531200    0.18018800
H          2.04546700   -0.88177200   -2.62317700
H          1.21992100   -2.90279100   -1.39812800
H          2.40901200    1.62256300   -3.31629900
H          2.81205600    1.91582400   -1.87128300
H         -4.93420400   -9.18918200    0.13250600
H         -4.96266500   -8.16380500    1.36902500
H          0.36091700   -6.94706800    1.97008300
H         -0.95904000   -7.68402800    2.33722700
H         -0.03200082    5.51042163   -3.02081129
H         -1.73609095    5.20497019   -2.91079325
H         -1.38513156    3.57145740    5.36463910
H         -7.32765235   -2.25328621    0.81891668
H         -3.54989593   -6.15679203    4.97232278
H         -1.19960292   -6.49860452   -3.12370351
H          1.36788414   -5.88587433    5.14482387
H         -1.99162797   -1.72770376    8.79642521
H          4.54391303   -7.35889391    1.06892273
H          9.00014135    1.43401606    2.82688860
H          7.02563903   -1.72994895   -1.39066075
H         -0.63316772    1.52164471   -5.22797533
```

Lys Activation: RC2–All   E = -3875.593005 a.u.

```
O         -0.97050000   -6.04752700   -2.33144100
C         -2.10135900   -5.58870100   -1.60738200
C         -1.64938000   -5.39272000   -0.17582800
O         -0.88042900   -4.19587700   -0.09154600
C         -2.78941800   -5.26964700    0.85233000
O         -2.42544000   -6.17435100    1.91658600
C         -2.71610300   -3.82333200    1.30905400
C         -1.23526200   -3.48598900    1.08257600
N         -0.93053000   -2.08550600    0.86168300
C         -1.54722800   -1.27362200   -0.12709800
N         -0.67102100   -0.24482300   -0.36105100
C          0.46949700   -0.39519500    0.42712700
C          1.72104400    0.27862900    0.40979600
O          2.05732000    1.26721200   -0.24217100
N          2.62297000   -0.35004100    1.28904700
```

C	2.38282500	-1.51415500	1.96618200
N	3.40967800	-2.00650200	2.71272700
N	1.22541200	-2.14193000	1.95162200
C	0.32163300	-1.55561600	1.15054300
O	-2.65459300	-1.43306200	-0.61691200
P	-3.49198400	-6.83221700	2.92143900
O	-2.87677700	-8.18647800	3.35259100
O	-4.85968700	-6.93949800	2.30165500
O	-3.40429700	-5.74886900	4.10100600
N	-0.42683400	1.62065600	-5.57159000
C	-1.14487600	1.29099300	-4.32227700
C	-1.02674300	2.38357700	-3.22646000
O	-1.34159900	2.12019200	-2.07454900
N	-0.63811300	3.62005300	-3.62144600
C	-0.75719900	4.78100800	-2.76172500
C	-6.42664700	-1.69154500	0.98541300
O	-6.02129000	-1.63544800	2.32939200
C	-2.05912500	-2.61962100	8.19726600
C	-1.46933700	-2.50431400	6.77764500
C	-2.35006600	-1.75595700	5.77378700
C	-1.91144900	-1.94235000	4.32548400
N	-2.76439300	-1.13878100	3.44020000
C	-2.05405900	2.93872500	4.83215700
S	-1.02804000	1.58283200	4.14095500
C	0.94581600	-5.42963600	4.26782500
C	1.97667100	-5.30587400	3.08006400
O	3.11488100	-4.84581400	3.34807800
O	1.57823100	-5.70378300	1.95486500
C	4.32880700	-6.49022300	0.48125100
C	3.68883700	-6.83259600	-0.83671800
N	4.39126500	-7.24950800	-1.96128200
C	2.37360400	-6.79864200	-1.19884500
C	3.53677100	-7.46990800	-2.95663200
N	2.30718500	-7.20192000	-2.51790100
C	8.22062900	1.41634500	3.56485500
C	7.55293200	0.02067900	3.59190000
C	6.05245800	-0.02988400	3.33490400
O	5.58079200	0.24056700	2.22824800
N	5.29404100	-0.39650600	4.38096100
C	6.33638200	-1.21090300	-0.76005000
C	4.90206100	-1.69213700	-0.95233100
C	4.42341700	-2.81993900	-0.27727100
C	4.02537600	-0.99431400	-1.78845500
C	3.10478800	-3.25084500	-0.43428000
C	2.71835100	-1.44056200	-1.97630000
C	2.25176000	-2.56712600	-1.30144600
O	3.00877400	2.18870100	-2.77349900
O	-4.86199300	-9.16629900	1.10694900
O	-0.02948200	-7.84880900	2.18062600
H	-2.93384600	-6.31808500	-1.61906200
H	-2.47229900	-4.62739500	-1.99550400
H	-1.03545000	-6.25194100	0.11696100
H	-3.77908300	-5.55322800	0.46959500
H	-3.31582500	-3.19718900	0.64090900
H	-3.05496400	-3.69452800	2.33741400

```
H          -0.60396600    -3.80574100     1.91738000
H          -0.90318400     0.55523600    -0.94864300
H           3.55854500     0.05908100     1.35264200
H           3.28303800    -2.98684600     2.99924000
H           4.33121500    -1.78692000     2.34346700
H          -2.22882200     1.16114400    -4.52958800
H          -0.76785500     0.34747800    -3.87197000
H          -0.44965900     3.77988900    -4.61107300
H          -0.67007800     4.43445700    -1.71375200
H          -5.60507400    -2.18090100     0.44128100
H          -6.54814700    -0.67626200     0.55476600
H          -6.70813700    -1.21208300     2.88013300
H          -1.52455700    -3.42970900     8.73436300
H          -3.11252200    -2.94607500     8.11563500
H          -1.31350600    -3.52620300     6.41218600
H          -0.47369500    -2.04238600     6.81504000
H          -3.39027600    -2.10224600     5.87746900
H          -2.35037200    -0.67585500     5.98595600
H          -1.91313900    -3.01478300     4.07994100
H          -0.87862200    -1.58590200     4.20651700
H          -2.47245700    -1.26434100     2.47188600
H          -3.73323100    -1.45876000     3.48265200
H          -2.83791200     2.52765700     5.49982100
H          -2.56174400     3.48463700     4.01934900
H          -2.02136200     0.67690800     3.86640200
H           0.03767600    -5.94456500     3.93307700
H           0.65436400    -4.38342900     4.51122000
H           3.67908800    -5.79407300     1.02411200
H           5.27819500    -5.96956600     0.23211500
H           5.43490800    -7.33918000    -2.04843500
H           1.50533800    -6.50025000    -0.64353500
H           3.80380300    -7.81528500    -3.94679200
H           1.42506600    -7.26717400    -3.06602300
H           8.62728100     1.64273400     4.56280000
H           7.47234500     2.20149300     3.33876800
H           7.96206800    -0.61465300     2.79075200
H           7.77907200    -0.48815100     4.53589600
H           5.69794800    -0.76023300     5.23512100
H           4.32682000    -0.68926300     4.21887400
H           6.63199900    -1.34509200     0.29853400
H           6.39519200    -0.12565700    -0.94871700
H           5.08835900    -3.36245300     0.39620500
H           4.35018100    -0.08529700    -2.28831300
H           2.71283200    -4.07827100     0.15445500
H           2.04971300    -0.87453900    -2.62567900
H           1.22412900    -2.90634500    -1.41733100
H           2.41101900     1.63238600    -3.30826700
H           2.80555000     1.91153100    -1.85878100
H          -4.95135100    -9.22124100     0.12466400
H          -4.97250100    -8.18547800     1.35456500
H           0.35448500    -6.96567500     1.96408900
H          -0.97266100    -7.68907300     2.32743100
H          -0.02166002     5.51550921    -3.01547761
H          -1.72588504     5.21165518    -2.90695022
H          -7.32591020    -2.24623659     0.81646641
```

H	9.00274037	1.42521356	2.83470217
H	7.02777390	-1.73323675	-1.38777980
H	4.53987315	-7.36149906	1.06539919
H	1.36278404	-5.89024854	5.13895860
H	-1.39240634	3.58089186	5.37505430
H	-1.99594185	-1.73485982	8.79568521
H	-3.56407762	-6.15515615	4.95599191
H	-1.19927438	-6.49317400	-3.15037997

Deglycosylation K249–Nuc: TS2–K$_{Nuc}$ E = –3875.586961 a.u. (408.60i cm^{-1})

O	-0.97421800	-6.02709400	-2.36237800
C	-2.10577300	-5.57716100	-1.63262200
C	-1.66141000	-5.42440000	-0.19336100
O	-0.87656200	-4.24042000	-0.07262200
C	-2.80742600	-5.31199000	0.82633800
O	-2.44785400	-6.21953000	1.89090600
C	-2.74503300	-3.86942400	1.29133300
C	-1.26348300	-3.52184300	1.08724300
N	-0.96588200	-2.12056100	0.85797900
C	-1.58144500	-1.32215700	-0.14166500
N	-0.71035200	-0.28817700	-0.37879200
C	0.42810800	-0.42745500	0.41364900
C	1.67338000	0.25608200	0.39731300
O	2.00189400	1.24732300	-0.25587500
N	2.57834600	-0.36216400	1.28123200
C	2.34338900	-1.52445400	1.96398400
N	3.37405300	-2.00493500	2.71558800
N	1.18993300	-2.15853400	1.95199300
C	0.28235300	-1.58351600	1.14572000
O	-2.68037600	-1.49610200	-0.64419000
P	-3.51897200	-6.85708100	2.90458000
O	-2.90844200	-8.20748600	3.35333800
O	-4.88507700	-6.96681200	2.28142700
O	-3.43382000	-5.75883200	4.07125900
C	-1.13615900	1.30339800	-4.32155600
C	-1.01509800	2.39191400	-3.22166300
O	-1.32664200	2.12477800	-2.06996700
N	-0.62736300	3.62996000	-3.61490000
C	-0.74545200	4.78996000	-2.75427000
C	-6.42508900	-1.68835100	0.98545900
O	-6.01622500	-1.67828500	2.32734700
C	-2.04500500	-2.65184900	8.22045400
C	-1.51972100	-2.53664300	6.77704000
C	-2.55808100	-2.02466100	5.78074100
C	-2.09386500	-2.05230600	4.32811900
N	-3.06623700	-1.35226900	3.49253000
C	-2.05942000	2.97584000	4.80920400
S	-1.20977200	1.46048200	4.23044200
C	0.93900200	-5.43689500	4.25617900
C	1.97387500	-5.31686200	3.07144900
O	3.10828600	-4.84797100	3.34069800
O	1.58365300	-5.72814100	1.94845000
C	4.32437600	-6.49312400	0.47229800
C	3.67640600	-6.82907700	-0.84320600

```
N          4.37258100   -7.25065800   -1.96987000
C          2.36041200   -6.78459400   -1.20161300
C          3.51356800   -7.46404900   -2.96305500
N          2.28750600   -7.18679900   -2.52079600
C          8.21977300    1.39979900    3.57120200
C          7.54396800    0.00729800    3.58558000
C          6.04246000   -0.03564100    3.32898200
O          5.56956300    0.24541500    2.22587800
N          5.28386600   -0.40852400    4.37344200
C          6.33824500   -1.21590400   -0.75678200
C          4.90376100   -1.69820800   -0.94635400
C          4.42495700   -2.82304600   -0.26640300
C          4.02699300   -1.00436800   -1.78583600
C          3.10699900   -3.25625600   -0.42409900
C          2.72061800   -1.45258400   -1.97359800
C          2.25463600   -2.57779200   -1.29590000
O          3.02139100    2.17624600   -2.75881100
O         -4.87756300   -9.19407700    1.08685000
O         -0.04381500   -7.85940500    2.16723900
H         -2.94584500   -6.29741700   -1.66879300
H         -2.46383200   -4.60234700   -1.99801700
H         -1.05917900   -6.29797200    0.08046600
H         -3.79266200   -5.59945600    0.43480300
H         -3.34205900   -3.24168400    0.62244400
H         -3.09269300   -3.74917400    2.31653100
H         -0.64439500   -3.82749400    1.93579400
H         -0.94046900    0.50577100   -0.97507100
H          3.51239400    0.05057400    1.34084700
H          3.25319900   -2.98535900    3.00463200
H          4.29285700   -1.78955200    2.33648900
H         -2.22043900    1.17736700   -4.52963900
H         -0.76174300    0.35729900   -3.87456800
H         -0.44123800    3.79118200   -4.60470300
H         -0.65992900    4.44141600   -1.70691800
H         -5.60805600   -2.16414000    0.42220600
H         -6.54461000   -0.66013700    0.58644700
H         -6.67099000   -1.21836700    2.88693900
H         -1.45358200   -3.42289800    8.75611100
H         -3.08375500   -3.02868200    8.19123200
H         -1.18884600   -3.53228700    6.46016100
H         -0.62538700   -1.89887500    6.74438900
H         -3.47803700   -2.62133600    5.87482900
H         -2.84957600   -0.99054800    6.02062900
H         -1.90108900   -3.09739300    4.03549600
H         -1.13108600   -1.52651200    4.24064300
H         -2.71353700   -1.26355700    2.54148200
H         -3.93844700   -1.87592800    3.42266300
H         -2.95094700    2.69595300    5.40139500
H         -2.42698400    3.51085100    3.91774800
H         -1.85620600    0.58620000    5.02335500
H          0.03074800   -5.95033900    3.91926400
H          0.65002000   -4.38989200    4.49841400
H          3.68180800   -5.79414300    1.01954700
H          5.27635500   -5.97862500    0.21949700
H          5.41470500   -7.34630600   -2.05899900
```

H	1.49629500	-6.47810700	-0.64385700
H	3.77468700	-7.81087300	-3.95431500
H	1.40321400	-7.24667300	-3.06676100
H	8.62456600	1.61641400	4.57203700
H	7.47648000	2.19072200	3.34859200
H	7.95028900	-0.62377400	2.77957500
H	7.76798100	-0.51031900	4.52525300
H	5.68793700	-0.78280100	5.22301200
H	4.31637100	-0.69896500	4.20871600
H	6.63547500	-1.35032100	0.30128500
H	6.39573200	-0.13055400	-0.94517600
H	5.08937100	-3.36221200	0.41028500
H	4.35183500	-0.09723900	-2.28915300
H	2.71493200	-4.08187700	0.16695800
H	2.05210000	-0.88951400	-2.62560900
H	1.22809500	-2.91980100	-1.41326100
H	2.42005700	1.62932100	-3.29923200
H	2.80920100	1.89567900	-1.84723200
H	-4.97460700	-9.25757700	0.10616400
H	-4.99053500	-8.21260500	1.32903600
H	0.34734500	-6.97990100	1.94903200
H	-0.98772700	-7.69275800	2.30016600
H	-1.71331926	5.22247109	-2.89941521
H	-1.38940683	3.58994511	5.37387848
H	-0.00880885	5.52409986	-3.00585602
H	-0.61554949	1.54339357	-5.22503144
H	-7.32641300	-2.23699232	0.80795481
H	-3.58036607	-6.15676032	4.93252395
H	-1.20319663	-6.47936245	-3.17762155
H	1.35368117	-5.89907713	5.12757379
H	4.53246161	-7.36638892	1.05454258
H	9.00422573	1.41014926	2.84358481
H	7.02942443	-1.73725735	-1.38555993
H	-1.99623779	-1.75309206	8.79903651

Deglycosylation K249–Nuc: RC3–K$_{Nuc}$ E = −3875.582132 a.u.

O	-0.96698400	-5.97852600	-2.52917700
C	-2.08952800	-5.53686800	-1.77738700
C	-1.65427000	-5.51323000	-0.32770400
O	-0.72284900	-4.44472500	-0.14470700
C	-2.80439700	-5.27309200	0.65444600
O	-2.46276200	-5.99824200	1.86651800
C	-2.73005500	-3.77850700	0.88746400
C	-1.22078300	-3.52872200	0.82410400
N	-0.83241600	-2.18175400	0.46580100
C	-1.39608500	-1.37753700	-0.54730200
N	-0.56090900	-0.29065000	-0.65914200
C	0.49731400	-0.40363800	0.24052400
C	1.72872900	0.29680600	0.31809600
O	2.08056900	1.31652400	-0.28006200
N	2.59446800	-0.33344400	1.23062700
C	2.34168000	-1.52057700	1.86183600
N	3.34634100	-2.00371700	2.65443700
N	1.20816600	-2.17691200	1.75963600

```
C           0.33921000     -1.59869700      0.90940800
O          -2.42373200     -1.58215600     -1.17571500
P          -3.54678800     -6.80553600      2.73579900
O          -2.87695800     -8.12951900      3.18768400
O          -4.84710800     -6.99404900      2.00570300
O          -3.67417600     -5.77174500      3.95559400
C          -1.15510800      1.34298100     -4.30942700
C          -1.03505700      2.43303100     -3.21346100
O          -1.35040000      2.16849800     -2.06095800
N          -0.64319600      3.66991600     -3.59926700
C          -0.75880100      4.81925200     -2.72419900
C          -6.43369000     -1.67554900      0.98371100
O          -6.03593700     -1.62582300      2.32455700
C          -2.15047700     -2.64862500      8.18431800
C          -0.85174700     -3.13914900      7.54490500
C          -1.19391200     -3.89165400      6.26442600
C          -1.31163600     -2.91654400      5.08965900
N          -1.95250200     -3.43706700      3.89520600
C          -2.07434400      2.95460500      4.85653600
S          -1.48142500      1.23434900      4.68331100
C           0.98959100     -5.46780400      4.18499500
C           2.04261400     -5.37305400      3.01549200
O           3.16135800     -4.87385600      3.29533600
O           1.67135800     -5.81420500      1.90005000
C           4.32878900     -6.49073600      0.41018000
C           3.65210500     -6.81937200     -0.89379500
N           4.33078100     -7.24866000     -2.02839500
C           2.33287500     -6.75599800     -1.23956800
C           3.45943300     -7.44927700     -3.01367200
N           2.24205200     -7.15603000     -2.55908400
C           8.21975800      1.39073400      3.56486800
C           7.53326300      0.00372100      3.57478300
C           6.03221800     -0.02476000      3.31153500
O           5.56459800      0.29925000      2.21850100
N           5.26870900     -0.43605200      4.33801300
C           6.32665200     -1.20052500     -0.77804500
C           4.89460300     -1.67503500     -0.99483500
C           4.41185300     -2.81753000     -0.34852900
C           4.02999400     -0.96729200     -1.83503600
C           3.10120900     -3.25649900     -0.54248500
C           2.73131500     -1.42112000     -2.05884100
C           2.26190800     -2.56552100     -1.41688900
O           2.97940100      2.27353100     -2.79593700
O          -4.93120500     -9.31434200      1.01577200
O          -0.08993400     -7.83117300      2.13093800
H          -2.96564900     -6.20922900     -1.87332400
H          -2.38874000     -4.52215500     -2.07864700
H          -1.16049300     -6.45985200     -0.08443500
H          -3.78118400     -5.62261500      0.29751100
H          -3.20950300     -3.26476300      0.04725200
H          -3.16798700     -3.44188800      1.82545200
H          -0.73956900     -3.71896300      1.78218200
H          -0.82163700      0.54118900     -1.18651400
H           3.51919500      0.08842000      1.34603500
H           3.22675600     -2.99062100      2.91827700
```

H	4.27455100	-1.79061300	2.29601400
H	-2.23920100	1.21403200	-4.51601100
H	-0.77888100	0.39677500	-3.86350000
H	-0.45197400	3.83913300	-4.58691500
H	-0.66993000	4.45765900	-1.68205500
H	-5.61369700	-2.17126700	0.44203700
H	-6.55116200	-0.66025900	0.54918800
H	-6.72107900	-1.19933300	2.87377300
H	-2.56813600	-3.48329300	8.78818900
H	-2.89715300	-2.45811700	7.39204500
H	-0.29960000	-3.77447000	8.25782100
H	-0.17918500	-2.30427000	7.30358900
H	-0.44417600	-4.65388500	6.05794200
H	-2.15166200	-4.41671900	6.39951600
H	-0.31039900	-2.54437100	4.83003300
H	-1.87983500	-2.02918000	5.40937700
H	-1.58423400	-4.36181700	3.68095200
H	-2.93340200	-3.61932700	4.09647600
H	-3.08005800	2.95218000	5.31823100
H	-2.18824000	3.33153700	3.82632900
H	-1.66626100	0.85592900	5.98281400
H	0.07659800	-5.96996300	3.83852700
H	0.73364900	-4.40735400	4.38845300
H	3.71499100	-5.77227600	0.96267600
H	5.29055700	-6.00477400	0.13484600
H	5.37005700	-7.35133000	-2.12580400
H	1.47842900	-6.42995900	-0.67693800
H	3.70509100	-7.79854400	-4.00827100
H	1.35289000	-7.20506800	-3.09679900
H	8.62953200	1.59826400	4.56570500
H	7.48000300	2.18718500	3.34994000
H	7.93720900	-0.62944200	2.76896900
H	7.75004300	-0.51845500	4.51353200
H	5.66816600	-0.83529700	5.17853000
H	4.30079200	-0.71649300	4.16123000
H	6.61395500	-1.35759600	0.27960400
H	6.39422100	-0.11255300	-0.94698800
H	5.06747900	-3.36792600	0.32749900
H	4.35736800	-0.04567300	-2.30974600
H	2.70523000	-4.09789900	0.02282700
H	2.06872500	-0.84752300	-2.70819800
H	1.24068200	-2.91365700	-1.56255500
H	2.40120700	1.70114100	-3.33571900
H	2.78572600	1.97749800	-1.88428800
H	-5.11463500	-9.50132600	0.06394300
H	-5.00405200	-8.31057300	1.14094600
H	0.33120300	-6.97394300	1.88341800
H	-1.02550100	-7.63430500	2.28420000
H	-0.02215736	5.55530049	-2.97014365
H	-1.72728000	5.25288991	-2.86170021
H	-1.39131950	3.56666405	5.40768140
H	-7.33421864	-2.22674267	0.81012036
H	9.00213513	1.40324891	2.83505337
H	7.01720729	-1.71832733	-1.41043264
H	-0.63548675	1.58833522	-5.21203160

H	4.52851240	-7.36342480	0.99620460
H	1.36961324	-5.92316939	5.07557091
H	-3.69073006	-6.17956606	4.82450593
H	-1.21004909	-6.46633952	-3.31946640
H	-2.02025666	-1.77675110	8.79076550

Deglycosylation K249–Nuc: TS3–K$_{Nuc}$ E = –3875.503694 a.u. (296.34i cm^{-1})

O	-1.23487500	-6.33478200	-1.75806000
C	-1.19766800	-5.01657100	-1.24720500
C	-1.28303500	-5.25549600	0.26433600
O	-0.82829900	-4.10511400	1.03666700
C	-2.69105800	-5.49932300	0.78150600
O	-2.46973200	-6.37883600	1.89576200
C	-3.13824300	-4.10033200	1.21333900
C	-1.82451800	-3.44368700	1.51427200
N	-1.71387600	-1.80212100	-0.16367800
C	-2.53520000	-1.11334400	-1.03202900
N	-1.85594600	0.02732700	-1.47161600
C	-0.65323300	0.11010900	-0.77395200
C	0.44742000	0.97094700	-0.84180800
O	0.62802100	2.01363700	-1.51431900
N	1.46345500	0.56737900	0.05546400
C	1.44255400	-0.58003100	0.79299800
N	2.59007400	-0.84519600	1.53899700
N	0.42822800	-1.39520700	0.83530500
C	-0.60845800	-1.05850500	0.00586600
O	-3.68293000	-1.41696800	-1.36465000
P	-3.62741300	-6.99277500	2.82736400
O	-3.10041000	-8.35644100	3.31568600
O	-4.95171100	-7.01569000	2.12488100
O	-3.53580700	-5.88817900	3.99321400
C	-1.11174100	1.38197600	-4.29468300
C	-1.33970100	2.61546200	-3.40313200
O	-2.18140700	2.58016500	-2.51391200
N	-0.55542200	3.69855000	-3.58749300
C	-0.69380100	4.82191300	-2.68774200
C	-6.42378800	-1.66242000	0.94558100
O	-5.98423100	-1.71928300	2.28007600
C	-2.12252700	-2.75175800	8.15531800
C	-1.23484900	-2.77582200	6.88843400
C	-1.80444300	-2.02829600	5.66442600
C	-2.56630200	-2.85342200	4.61447700
N	-1.71320200	-3.73107600	3.79353000
C	-2.06219200	2.92839800	4.86981900
S	-1.49151600	1.20541100	4.69289300
C	0.94555300	-5.52538200	4.17851400
C	1.97746000	-5.45304300	2.97537700
O	3.08332900	-4.94137000	3.20140400
O	1.56982800	-5.94960400	1.87903600
C	4.32923900	-6.53086200	0.40873100
C	3.70251500	-6.85103400	-0.91743800
N	4.41230900	-7.19597600	-2.05934300
C	2.38377000	-6.87065200	-1.26451800
C	3.55950100	-7.41436500	-3.05679500

```
N          2.32329400    -7.22020100    -2.59677900
C          8.27003700     1.32106500     3.67164900
C          7.33778000     0.09002200     3.62982400
C          5.97959200     0.32578200     2.97029300
O          5.86268100     1.02967800     1.97422700
N          4.93172600    -0.30531100     3.54594600
C          6.36643300    -1.27746600    -0.70780500
C          4.92667000    -1.71050100    -0.95165500
C          4.40461700    -2.87347100    -0.37066100
C          4.09017100    -0.92858300    -1.75261100
C          3.08376400    -3.25901400    -0.60175100
C          2.77879800    -1.32625400    -2.01179000
C          2.27444700    -2.49158000    -1.44167900
O          3.08318800     1.95122300    -2.86781400
O         -4.93109300    -9.27438100     0.93605300
O         -0.10204500    -8.00920000     2.11476300
H         -2.02080300    -4.37675100    -1.60187900
H         -0.24560100    -4.50665500    -1.46858100
H         -0.62022100    -6.07778400     0.52525200
H         -3.36045300    -5.96763300     0.04794100
H         -3.55940500    -3.55430500     0.35249800
H         -3.85887600    -4.06920200     2.03148900
H         -1.63356200    -2.47433300     1.93184900
H         -2.32268500     0.83200700    -1.88311700
H          2.32071800     1.10689500    -0.00835100
H          2.57138700    -1.81766700     1.84243500
H          3.44093300    -0.68234500     0.99786300
H         -2.10259700     0.94659100    -4.53480900
H         -0.54926600     0.64979600    -3.66819500
H         -0.03341800     3.80773200    -4.45252500
H         -0.61326800     4.42904400    -1.65318700
H         -5.61481900    -2.07939400     0.32653000
H         -6.56916800    -0.61501700     0.60874600
H         -6.64059100    -1.29496600     2.86433500
H         -1.85002800    -3.62802500     8.77884900
H         -3.17900100    -2.90133300     7.86305200
H         -1.05464900    -3.82504500     6.62159900
H         -0.24385200    -2.37713200     7.14103300
H         -0.99104900    -1.50658300     5.14071100
H         -2.48523400    -1.23751000     6.00936100
H         -3.08697000    -2.14749000     3.95007200
H         -3.34433300    -3.46818000     5.07966100
H         -0.73798600    -3.45604900     3.86937900
H         -1.80171300    -4.70455200     4.06142600
H         -3.07246700     2.93255700     5.32095800
H         -2.15916000     3.31983200     3.84510800
H         -1.64933100     0.84916800     6.00028300
H          0.00900500    -5.99191500     3.84526000
H          0.73280700    -4.46711100     4.43306700
H          3.69022900    -5.82807500     0.95471400
H          5.29383800    -6.03133200     0.17495300
H          5.46104100    -7.26626800    -2.15270600
H          1.50694500    -6.66313000    -0.68298000
H          3.83285800    -7.70599900    -4.06133000
H          1.43427900    -7.27351600    -3.13743300
```

H	8.75295800	1.34862400	4.66298000
H	7.65474500	2.23896000	3.57768500
H	7.79586700	-0.73141700	3.05384800
H	7.18477000	-0.30631300	4.64021000
H	5.01148000	-0.91777500	4.35351100
H	4.02001400	-0.24159900	3.10018500
H	6.65102400	-1.50744300	0.33752700
H	6.45790000	-0.18355000	-0.80916700
H	5.03111200	-3.47182800	0.29012600
H	4.44934900	0.00806500	-2.16778100
H	2.66306200	-4.12358300	-0.09106200
H	2.13765900	-0.69723900	-2.62994000
H	1.23868500	-2.77393300	-1.61086100
H	2.85234900	1.27426700	-3.53291300
H	2.22482200	2.09731900	-2.40891700
H	-5.05668400	-9.35936700	-0.03866100
H	-5.04954500	-8.29576900	1.15700800
H	0.41826500	-7.18305900	1.94422200
H	-1.02758100	-7.73048200	2.14520700
H	-1.65962124	5.26364514	-2.81798781
H	0.05013719	5.55657415	-2.91518203
H	-0.57640880	1.61718618	-5.19078322
H	-1.37299978	3.51593815	5.43965288
H	9.03073272	1.31535244	2.91918014
H	7.04660677	-1.77711101	-1.36554242
H	4.51282542	-7.41779681	0.97841747
H	1.33281993	-5.99489706	5.05855941
H	-2.03064150	-1.87874505	8.76712307
H	-3.65433384	-6.27671025	4.86303861
H	-7.32448327	-2.21180570	0.76718993
H	-1.36796147	-6.46923025	-2.69923568

Deglycosylation K249–Nuc: IC1–K_{Nuc} E = –3875.589031 a.u.

O	-1.57285300	-6.19654100	-1.74473800
C	-2.13510100	-4.95349600	-1.36053200
C	-2.13443700	-4.92346700	0.16548200
O	-2.24219700	-3.56599500	0.58069600
C	-3.31065400	-5.67448800	0.81392600
O	-2.73663200	-6.59526700	1.78327000
C	-4.13018500	-4.55533300	1.44854100
C	-3.10376900	-3.45104200	1.70425800
N	-0.87092400	-1.30818100	1.66385200
C	-1.53666600	-0.47211100	0.77144400
N	-0.56446200	0.38529500	0.28365700
C	0.68444000	0.01725600	0.79152100
C	1.99824700	0.50198600	0.59861100
O	2.39941000	1.44786900	-0.09195100
N	2.91664400	-0.26192300	1.35133500
C	2.60626900	-1.37214000	2.08432300
N	3.63785100	-2.04383000	2.67343300
N	1.38054100	-1.79377600	2.28710400
C	0.46465400	-1.05914800	1.63591400
O	-2.72701100	-0.48565600	0.49213200
P	-3.65336800	-7.19717900	2.95977000

```
O          -3.05826900    -8.56052700     3.35876500
O          -5.10130600    -7.24765900     2.53825600
O          -3.34359000    -6.05688300     4.04347000
C          -1.11035600     1.38354100    -4.31966200
C          -0.98574300     2.45559800    -3.20307800
O          -1.31103000     2.18068300    -2.05891600
N          -0.57567600     3.69275700    -3.57814100
C          -0.68828600     4.83638200    -2.69716300
C          -6.43426800    -1.64886500     0.94196000
O          -6.01100800    -1.73014700     2.27484800
C          -2.01209600    -2.69799700     8.00791200
C          -2.70654200    -2.45386800     6.62255900
C          -2.13840100    -3.24231800     5.42389900
C          -2.98345100    -3.03078700     4.14986000
N          -2.31428600    -3.53647100     2.94206100
C          -2.04503400     2.90609000     4.85153800
S          -1.45769900     1.18511500     4.66322600
C           0.91609300    -5.52502100     4.13445300
C           1.99167100    -5.36161500     2.99002400
O           3.10929200    -4.88477400     3.30277800
O           1.64803100    -5.75730400     1.84310400
C           4.30657800    -6.53193500     0.36441600
C           3.67345000    -6.83274300    -0.96136200
N           4.37730900    -7.18470600    -2.10475700
C           2.35424800    -6.82443100    -1.30696000
C           3.52172400    -7.38305100    -3.10290000
N           2.28966700    -7.16851200    -2.64045900
C           8.28123400     1.30124600     3.62866800
C           7.64324700    -0.09310200     3.76242200
C           6.16847600    -0.16125300     3.41088000
O           5.77971200     0.11290800     2.27336200
N           5.34659500    -0.51714500     4.40971100
C           6.35480200    -1.24894300    -0.78531100
C           4.90395900    -1.68203700    -0.95905800
C           4.40907900    -2.82033600    -0.31436900
C           4.01990900    -0.90471400    -1.71275000
C           3.05998800    -3.16902600    -0.39294500
C           2.67953800    -1.26672600    -1.82546000
C           2.19225700    -2.38612800    -1.15494100
O           3.03401400     2.25792100    -2.73766300
O          -4.89415000    -9.06484400     0.81428600
O          -0.05780100    -7.81927200     1.94168700
H          -3.16728700    -4.81865200    -1.73400600
H          -1.53507200    -4.09768800    -1.71013800
H          -1.18988300    -5.35872600     0.51691900
H          -3.88235400    -6.27333300     0.09090400
H          -4.83370200    -4.19500200     0.67723000
H          -4.73596600    -4.84875900     2.30126300
H          -0.74637800     1.02986200    -0.47961500
H           3.89376100     0.03394300     1.31528900
H           3.39981600    -3.00312900     2.95696000
H           4.53068500    -1.94594700     2.19949600
H          -2.19455300     1.26836700    -4.53435600
H          -0.74523400     0.42885800    -3.88419400
H          -0.37873400     3.86769800    -4.56338200
```

H	-0.60685000	4.46749900	-1.65706800
H	-5.62092600	-2.08061600	0.33817000
H	-6.56248200	-0.59775200	0.61078700
H	-6.65155800	-1.28655700	2.86299600
H	-0.95915700	-2.98902300	7.82818400
H	-2.47008100	-3.57726900	8.50021700
H	-2.63716700	-1.39915200	6.32262400
H	-3.78314600	-2.66504000	6.71946900
H	-1.11489900	-2.89533700	5.22739000
H	-2.07374600	-4.31324500	5.65063700
H	-3.14928200	-1.95235100	4.00116900
H	-3.97539700	-3.48859900	4.29579100
H	-1.27461300	-2.12983200	2.13847800
H	-2.02876000	-4.50086100	3.09791600
H	-3.05374500	2.90410300	5.30638900
H	-2.14809800	3.29622600	3.82493700
H	-1.61582600	0.81459200	5.96790400
H	0.03560600	-6.05433000	3.74996800
H	0.59812400	-4.49081700	4.38720900
H	3.66674000	-5.83299400	0.91446400
H	5.27277600	-6.03406600	0.13415800
H	5.42374100	-7.26988800	-2.19801300
H	1.47726100	-6.60883100	-0.72684100
H	3.79019600	-7.67353600	-4.10904700
H	1.40493600	-7.19887300	-3.18079000
H	8.72169700	1.58769300	4.59760000
H	7.50914100	2.05999500	3.39348200
H	8.10572400	-0.79100100	3.04828000
H	7.81263000	-0.50769800	4.76262500
H	5.70695400	-0.87843800	5.28433100
H	4.41486500	-0.86883700	4.16554300
H	6.65828600	-1.39812500	0.26963200
H	6.43792600	-0.16290600	-0.96147900
H	5.08468200	-3.43092600	0.28652600
H	4.36118000	0.00776500	-2.19401200
H	2.66844200	-4.00863800	0.17981100
H	2.00385800	-0.63635400	-2.40293100
H	1.13651300	-2.64061100	-1.20343800
H	2.43784100	1.68960900	-3.26121400
H	2.85943400	1.98660700	-1.81259200
H	-4.81099200	-8.83416500	-0.14636900
H	-5.14161100	-8.20611300	1.28763900
H	0.43244100	-6.97935000	1.77095200
H	-0.99016500	-7.60380700	1.79057200
H	-3.54268000	-2.44788800	1.67072300
H	0.05542101	5.56820506	-2.93430199
H	-1.65264637	5.27898746	-2.83503788
H	-7.33667816	-2.18922157	0.74556580
H	9.03707751	1.29024009	2.87138374
H	7.03200413	-1.77715030	-1.42350715
H	1.31052720	-6.00147818	5.00755678
H	4.48580280	-7.42572542	0.92469911
H	-3.57663804	-6.35350786	4.92625100
H	-1.36133082	3.50577918	5.41529579
H	-1.99700622	-1.87470252	8.69118244

```
H                      -1.60454127   -6.37071607   -2.68827332
H                      -0.58459447    1.63017015   -5.21835487
```

Deglycosylation K249–GB: RC3–K$_{GB}$ E = −3875.584189 a.u.

```
O                      -1.00018000   -5.95581800   -2.53428100
C                      -2.13402100   -5.56097200   -1.77473900
C                      -1.68402900   -5.49852400   -0.33219100
O                      -0.81428000   -4.37561500   -0.18132600
C                      -2.83019000   -5.31987300    0.67279900
O                      -2.46569300   -6.10368900    1.83164100
C                      -2.77345400   -3.83998200    0.98562800
C                      -1.26620800   -3.56004300    0.89056000
N                      -0.91486900   -2.18037700    0.61071700
C                      -1.50283700   -1.36184300   -0.38358700
N                      -0.64982500   -0.29600000   -0.53601600
C                       0.44864000   -0.43490700    0.30921000
C                       1.68431500    0.26200600    0.35287500
O                       2.02054200    1.27851600   -0.25883900
N                       2.56901900   -0.36985100    1.24541200
C                       2.32552900   -1.55374100    1.88792500
N                       3.34223800   -2.03608300    2.66236300
N                       1.18535900   -2.20531200    1.81542300
C                       0.29702100   -1.62323500    0.99036100
O                      -2.56515600   -1.53977000   -0.95943000
P                      -3.53105400   -6.81054400    2.79889800
O                      -2.89343600   -8.15022800    3.24642600
O                      -4.88093900   -6.95643600    2.14905600
O                      -3.52546500   -5.74040400    3.99866600
C                      -1.15459200    1.34368100   -4.31040400
C                      -1.02969400    2.42883900   -3.20899100
O                      -1.33549700    2.15860500   -2.05561000
N                      -0.64587800    3.66874100   -3.59591500
C                      -0.76161800    4.81947600   -2.72282100
C                      -6.43386400   -1.67598800    0.97339100
O                      -6.02622500   -1.62398700    2.31236400
C                      -2.15595300   -2.66700400    8.19590500
C                      -0.85105400   -3.20131200    7.60096400
C                      -1.12745200   -3.82753900    6.24096300
C                      -1.18368200   -2.73748500    5.17786900
N                      -1.64069800   -3.25242200    3.89857000
C                      -2.07173700    2.94807900    4.85405500
S                      -1.47651500    1.22572200    4.69452900
C                       0.99452000   -5.46543500    4.17868900
C                       2.03892800   -5.38662600    3.00566500
O                       3.16612300   -4.89549400    3.27376800
O                       1.66319200   -5.82526700    1.88858500
C                       4.33464200   -6.48757700    0.40523800
C                       3.66305100   -6.81604500   -0.90086700
N                       4.34465500   -7.23759200   -2.03649800
C                       2.34358900   -6.76169000   -1.24593200
C                       3.47484200   -7.44134600   -3.02232000
N                       2.25528700   -7.15788700   -2.56684700
C                       8.21710600    1.39012700    3.55860100
C                       7.53200900    0.00155700    3.56048400
```

```
C          6.03018900     -0.03333800      3.29882200
O          5.55939200      0.27714800      2.20324400
N          5.26863500     -0.43619000      4.33051300
C          6.32710800     -1.19903700     -0.78124700
C          4.89446800     -1.67776500     -0.98913400
C          4.41506600     -2.81903000     -0.33773500
C          4.02345500     -0.97084800     -1.82360100
C          3.10205300     -3.25673000     -0.52049900
C          2.72223500     -1.42296700     -2.03601000
C          2.25608400     -2.56568800     -1.38849400
O          2.98584500      2.24267300     -2.76482500
O         -4.89391100     -9.21658400      1.02552600
O         -0.08016700     -7.85715900      2.11480500
H         -2.97870600     -6.27454700     -1.85270600
H         -2.48707800     -4.56529100     -2.08182500
H         -1.14004600     -6.41603900     -0.08328100
H         -3.80854000     -5.65700500      0.30546800
H         -3.28049700     -3.28607200      0.18896300
H         -3.22820300     -3.58496800      1.94247700
H         -0.74368200     -3.83057800      1.80940700
H         -0.88810100      0.52274700     -1.09367600
H          3.49717300      0.04992800      1.34034600
H          3.22715900     -3.02300500      2.93178100
H          4.26596600     -1.81833700      2.29560800
H         -2.23947100      1.21846800     -4.51550100
H         -0.77900100      0.39543100     -3.86897700
H         -0.46115300      3.83798800     -4.58478800
H         -0.67241400      4.45904400     -1.68030600
H         -5.61370300     -2.16409700      0.42518700
H         -6.55959200     -0.66042600      0.54153500
H         -6.71596300     -1.21339300      2.86822900
H         -2.61306200     -3.47765000      8.80429600
H         -2.87852800     -2.46975300      7.38422500
H         -0.39460100     -3.92945700      8.29154500
H         -0.10383400     -2.40472900      7.48129000
H         -0.36558500     -4.56105800      5.99806200
H         -2.08883700     -4.36136000      6.27383800
H         -0.17333900     -2.32378800      5.04396200
H         -1.80493400     -1.90581000      5.56552300
H         -2.52392000     -3.74747700      4.01461200
H         -1.81556100     -2.46905300      3.26927500
H         -3.07973000      2.94632700      5.31019200
H         -2.17876500      3.31965300      3.82127300
H         -1.66824300      0.85107600      5.99490100
H          0.06169900     -5.93493000      3.84568000
H          0.74653400     -4.40122700      4.37025500
H          3.71700900     -5.77330500      0.95904800
H          5.29574300     -5.99816100      0.13374700
H          5.38477100     -7.33667400     -2.13348100
H          1.48818200     -6.44792700     -0.67856200
H          3.72305500     -7.78613600     -4.01780800
H          1.36738600     -7.20979400     -3.10562000
H          8.62407200      1.59379100      4.56130200
H          7.47767500      2.18724800      3.34517200
H          7.93745200     -0.62646700      2.75145800
```

H	7.75091700	-0.52465000	4.49648900
H	5.67003300	-0.82936600	5.17301500
H	4.30220000	-0.72326100	4.15645100
H	6.61893700	-1.35191700	0.27575700
H	6.38913100	-0.11109800	-0.95249800
H	5.07477400	-3.36961100	0.33417100
H	4.34876400	-0.05122000	-2.30350900
H	2.70941800	-4.09749400	0.04821900
H	2.05654200	-0.84990900	-2.68247600
H	1.23331200	-2.91234800	-1.52540900
H	2.39935700	1.68389100	-3.30960800
H	2.78356700	1.94594500	-1.85564000
H	-5.02797400	-9.32181200	0.05312000
H	-4.99802000	-8.22616800	1.23260600
H	0.35148700	-6.99850700	1.88873000
H	-1.00927600	-7.64243100	2.27981200
H	-0.02567953	5.55611723	-2.96910187
H	-1.73026917	5.25264963	-2.86057263
H	-0.63633242	1.59004509	-5.21351625
H	-1.39108231	3.56138586	5.40674287
H	-7.33289750	-2.23118011	0.80486656
H	9.00136158	1.40571071	2.83086456
H	7.01841904	-1.71427360	-1.41490330
H	4.53443055	-7.36167807	0.98913170
H	1.37470724	-5.92417521	5.06746067
H	-3.61524823	-6.15830780	4.85825624
H	-1.22778839	-6.45177713	-3.32410311
H	-2.01983818	-1.78852420	8.79142661

Deglycosylation K249–GB: TS3–K$_{GB}$ E = –3875.502299 a.u.

O	-1.00533500	-6.19027100	-2.12018200
C	-2.12826000	-5.76117900	-1.38193800
C	-1.87462300	-6.09274600	0.08772200
O	-1.18007000	-4.94912300	0.72736700
C	-3.10951300	-6.23229800	0.95582000
O	-2.65246400	-6.94576800	2.11196300
C	-3.39274000	-4.78258700	1.33344000
C	-2.00213800	-4.25073500	1.40024100
N	-2.21222000	-1.64933600	0.53359400
C	-2.78913500	-0.89029900	-0.46747700
N	-1.83631800	0.00229500	-0.96239800
C	-0.67088700	-0.15649500	-0.22490200
C	0.59102300	0.44445800	-0.28495200
O	0.99414300	1.39730900	-0.98342000
N	1.46872300	-0.15417400	0.65579500
C	1.17830900	-1.25154100	1.41937500
N	2.23204900	-1.75840100	2.17324700
N	-0.01250200	-1.78374000	1.49049000
C	-0.94279100	-1.21894700	0.64953800
O	-3.95065500	-0.95859400	-0.88289900
P	-3.68879400	-7.86041800	2.95300200
O	-2.82753000	-8.87178400	3.70860200
O	-4.65157300	-8.56453800	1.98641400
O	-4.51284200	-6.81902900	3.83124700

```
C            -1.06518300     1.41556400    -4.31021700
C            -1.19599700     2.59186000    -3.31822900
O            -1.91258100     2.47989700    -2.33474000
N            -0.48663400     3.72118100    -3.55015400
C            -0.64785700     4.85811600    -2.66752500
C            -6.41693200    -1.64966700     0.88545900
O            -6.01170800    -1.71851000     2.23725200
C            -2.06570600    -2.77118600     8.07793200
C            -2.16238000    -2.45399100     6.55933400
C            -3.59336700    -2.53867000     6.00215200
C            -3.91757800    -1.66245400     4.79305800
N            -3.13028000    -1.99342400     3.59303100
C            -2.05296700     2.88445300     4.86226400
S            -1.42009800     1.17545700     4.70156200
C             0.77542800    -5.55390700     4.18671500
C             1.47766200    -5.70400400     2.77549000
O             2.35720800    -4.86640900     2.48745000
O             1.08722800    -6.69658100     2.09645200
C             4.28264500    -6.53374400     0.37985100
C             3.68613100    -6.84735300    -0.96277800
N             4.41094500    -7.19668700    -2.09482400
C             2.37335100    -6.84007500    -1.33159300
C             3.57008600    -7.39548200    -3.10650100
N             2.32939700    -7.18247600    -2.66725300
C             8.26156500     1.29130600     3.71104700
C             7.34693300     0.04852200     3.67588200
C             5.96004200     0.28304900     3.07426400
O             5.78256600     1.08372700     2.16734100
N             4.97222400    -0.48808100     3.58531600
C             6.38119600    -1.24336400    -0.71787300
C             4.92736500    -1.61562400    -0.98202800
C             4.35785300    -2.74347400    -0.38291200
C             4.12483100    -0.82253200    -1.80981800
C             3.02599300    -3.09177100    -0.61917200
C             2.80281700    -1.17883700    -2.07051000
C             2.25039000    -2.31443800    -1.47919100
O             2.98584000     2.27772600    -2.72514300
O            -1.56205000    -9.31703200     1.12600000
O            -2.03101800    -4.40934200     3.69458200
H            -3.06155700    -6.27846200    -1.68320200
H            -2.29358100    -4.67867600    -1.49322600
H            -1.20474600    -6.94380400     0.17500100
H            -3.94179400    -6.75708600     0.47293500
H            -3.88476500    -4.23829300     0.50173400
H            -3.98342200    -4.63392000     2.23463300
H            -1.63923500    -3.30335800     1.75822900
H            -2.06976300     0.81701600    -1.52232600
H             2.42844300     0.17387600     0.60352700
H             2.04504200    -2.71778700     2.48080100
H             3.09831900    -1.77212100     1.63705300
H            -2.09381700     1.08427800    -4.56067300
H            -0.56449200     0.59483600    -3.74537900
H            -0.07583400     3.87255700    -4.46940300
H            -0.58425600     4.49187500    -1.62594700
H            -5.59142500    -2.05928300     0.28728500
```

```
H          -6.53473400    -0.59970000     0.55393700
H          -6.65766400    -1.25337900     2.80195600
H          -1.14174700    -3.34749900     8.27925300
H          -2.89429800    -3.44545700     8.36497600
H          -1.53818000    -3.16716300     6.01454600
H          -1.72820000    -1.46555100     6.34601000
H          -3.81021800    -3.57930400     5.74614500
H          -4.31943100    -2.27578400     6.79033000
H          -3.79784800    -0.60220800     5.06448600
H          -4.97113500    -1.81664700     4.53771000
H          -2.52100100    -3.50572200     3.68584900
H          -3.68751600    -1.82621300     2.75102900
H          -3.06567700     2.86254300     5.30685800
H          -2.15251000     3.26683500     3.83418700
H          -1.61165600     0.80841400     6.00448800
H          -0.24863600    -5.93862800     4.09289000
H           0.72076500    -4.46089000     4.39716000
H           3.60518800    -5.85783100     0.92151200
H           5.22968900    -5.99167500     0.17540000
H           5.45949200    -7.27384200    -2.17689700
H           1.49615000    -6.60787300    -0.75776900
H           3.85430800    -7.68775000    -4.10834100
H           1.45242000    -7.22843900    -3.23033400
H           8.73497500     1.34274300     4.70577700
H           7.63108200     2.19630800     3.59458900
H           7.78881000    -0.75227700     3.05956900
H           7.23792300    -0.37935500     4.67946900
H           5.08645200    -1.08681100     4.39817200
H           4.03224700    -0.42900200     3.20983600
H           6.63497900    -1.48216100     0.33319700
H           6.51570800    -0.15310100    -0.81852300
H           4.96179000    -3.35392400     0.28891400
H           4.51737500     0.09025300    -2.24805000
H           2.58276700    -3.93002700    -0.08508500
H           2.19226600    -0.53302500    -2.70099700
H           1.20847100    -2.57214600    -1.65366700
H           2.44362100     1.82627300    -3.40076300
H           2.51073600     2.01470000    -1.91090700
H          -0.88922700    -9.67665100     0.51319300
H          -1.12275700    -8.60420300     1.62476100
H          -1.12924400    -4.16992500     3.95061800
H          -2.32322600    -1.37391000     3.50073200
H          -1.61193064     5.29997451    -2.80973285
H          -1.37943810     3.48680506     5.43535283
H           0.09832495     5.59056855    -2.89473803
H           9.02759402     1.28549508     2.96400900
H           7.06233539    -1.76305100    -1.35886798
H           4.48768955    -7.42323170     0.93812365
H           1.25379120    -6.02139207     5.02189544
H          -7.32062797    -2.18783798     0.68897596
H          -4.04873056    -6.56976940     4.63378686
H          -1.20891180    -6.44363100    -3.02348992
H          -2.04647601    -1.91196141     8.71531989
H          -0.52675245     1.66241617    -5.20131551
```

Deglycosylation K249–GB: PC–K$_{GB}$ E = –3875.577054 a.u. (107.79i cm^{-1})

O	-1.12719900	-5.94924600	-2.42695800
C	-2.29465300	-5.81070200	-1.62601700
C	-1.96906600	-6.40400900	-0.26387900
O	-0.83558200	-5.74965600	0.28235700
C	-3.02331500	-6.18394400	0.81424100
O	-2.54540200	-6.97321900	1.93898000
C	-2.81032000	-4.71452300	1.13269700
C	-1.30119900	-4.52595700	0.85883800
N	-1.00561900	-1.46119400	1.13736000
C	-1.58913900	-0.62317200	0.18873200
N	-0.57398200	0.21380000	-0.22972700
C	0.59931700	-0.08665600	0.45740500
C	1.90784100	0.45068000	0.40095700
O	2.33888500	1.40112200	-0.26077900
N	2.76249300	-0.25064600	1.27226000
C	2.41104500	-1.34689000	2.00832300
N	3.41356100	-1.93595400	2.72962700
N	1.18684100	-1.81780200	2.08459300
C	0.31690800	-1.14991600	1.29806300
O	-2.75115400	-0.64268000	-0.19127200
P	-3.55516400	-7.72268500	2.94788200
O	-2.69244400	-8.69770600	3.75064100
O	-4.61169100	-8.48505800	2.13192300
O	-4.21669300	-6.52413700	3.78156400
C	-1.15027900	1.37082500	-4.32016600
C	-1.08969100	2.47272000	-3.23240000
O	-1.49332500	2.22934100	-2.10359100
N	-0.63267300	3.69406600	-3.59098800
C	-0.76443800	4.83171600	-2.70320200
C	-6.42611400	-1.71918900	0.94307600
O	-6.05610500	-1.67008700	2.29349400
C	-2.00411900	-2.79782900	8.19144700
C	-1.87390500	-2.66934300	6.66117600
C	-3.19322900	-2.44863100	5.91001500
C	-3.13681700	-2.87001000	4.43805400
N	-2.16185900	-2.14669900	3.62109600
C	-2.09585700	2.89541700	4.85946300
S	-1.48630700	1.17749800	4.71486500
C	0.99032700	-5.48988600	4.15747300
C	2.10060200	-5.31779900	3.04478000
O	3.21145100	-4.84326800	3.39187200
O	1.76921900	-5.69517900	1.89211800
C	4.35619900	-6.47591000	0.37335100
C	3.64874900	-6.77228800	-0.91948600
N	4.30732300	-7.19043200	-2.06937700
C	2.32390600	-6.68720900	-1.24275700
C	3.42003800	-7.36403400	-3.04595500
N	2.21415100	-7.06448100	-2.56840100
C	8.22464400	1.38903400	3.60523100
C	7.57821600	-0.01331800	3.64617700
C	6.08698900	-0.06921800	3.35500700
O	5.64610300	0.21303400	2.23886200
N	5.30458700	-0.43562400	4.38312400

```
C          6.35084500     -1.16563400     -0.77907400
C          4.91650200     -1.65286600     -0.94201000
C          4.45290300     -2.77025300     -0.24064400
C          4.02232900     -0.96443100     -1.76724700
C          3.12812000     -3.19635400     -0.35321700
C          2.70906200     -1.40534600     -1.91192900
C          2.25602000     -2.51592000     -1.20251300
O          2.94915500      2.39146800     -2.83083300
O         -1.38016700     -9.42862000      1.27645800
O         -0.63354700     -4.29242200      2.04608900
H         -3.19792800     -6.31247300     -2.03574700
H         -2.53146000     -4.74387400     -1.53883100
H         -1.72316700     -7.46301100     -0.38026700
H         -4.04395800     -6.48189600      0.54450800
H         -3.41010000     -4.07945800      0.46371800
H         -3.06226000     -4.45554200      2.16022100
H         -1.10825800     -3.71918200      0.13138100
H         -0.73719300      0.96628400     -0.89243400
H          3.73259500      0.07103800      1.31670400
H          3.21365400     -2.89260600      3.04304200
H          4.33042100     -1.84009000      2.30095900
H         -2.22501900      1.20077700     -4.54358900
H         -0.74927000      0.44402900     -3.85540300
H         -0.39008300      3.86924300     -4.56607700
H         -0.67848100      4.46047100     -1.66441500
H         -5.59211800     -2.20796600      0.41840100
H         -6.53752300     -0.70425800      0.50918200
H         -6.75360100     -1.24863500      2.83084900
H         -1.16166100     -3.41903600      8.56051800
H         -2.91519000     -3.38103200      8.42320200
H         -1.43284600     -3.60726300      6.30313300
H         -1.14727300     -1.88668000      6.40176500
H         -3.99757600     -3.01039300      6.41352700
H         -3.49346100     -1.39053000      5.96166200
H         -4.11996300     -2.72593500      3.97590900
H         -2.89737000     -3.93613300      4.36778100
H         -1.54720000     -2.04276300      1.79685600
H         -2.30775100     -1.14101500      3.72347900
H         -3.10688100      2.88823000      5.30780800
H         -2.19454400      3.26314200      3.82488900
H         -1.69149400      0.80273100      6.01544300
H          0.11411600     -5.99850300      3.74339800
H          0.65509500     -4.45994000      4.41187700
H          3.75783300     -5.76342600      0.94956900
H          5.31757000     -5.99481700      0.08815400
H          5.34134900     -7.30496600     -2.17738100
H          1.46986300     -6.36916500     -0.66784900
H          3.64558200     -7.69756700     -4.05051900
H          1.31369800     -7.09323200     -3.09901100
H          8.64097300      1.62463500      4.59738800
H          7.46257900      2.16273200      3.38613700
H          8.01028600     -0.65564800      2.86316800
H          7.78779900     -0.50465500      4.60311000
H          5.69431100     -0.81360900      5.23770400
H          4.34762100     -0.74545500      4.18579000
```

```
H          6.66404000   -1.29106200    0.27564700
H          6.39870500   -0.08070100   -0.97346700
H          5.13534300   -3.30905600    0.41830900
H          4.33771600   -0.06280600   -2.28618300
H          2.75711300   -4.02100000    0.25273500
H          2.02511400   -0.84712000   -2.55128300
H          1.22355200   -2.84484100   -1.29413200
H          2.39584600    1.78539300   -3.36063200
H          2.80015800    2.08321700   -1.91427300
H         -0.96932100   -9.66274900    0.41808200
H         -1.23867900   -8.46834600    1.39646700
H          0.31252600   -4.46992800    1.86929200
H         -1.20884500   -2.34995000    3.92421800
H         -0.02897869    5.57215343   -2.93932063
H         -1.73488886    5.26149796   -2.83889504
H         -7.32328438   -2.27117639    0.75520576
H          8.99773959    1.40645132    2.86569071
H          7.03660283   -1.68473536   -1.41560363
H          4.55774799   -7.36075936    0.94020161
H         -3.87347662   -6.46316591    4.67603873
H         -1.28097568   -6.40300025   -3.25885933
H          1.37985599   -5.96753238    5.03212785
H         -1.99001440   -1.89446242    8.76470948
H         -1.41804482    3.50627318    5.41832378
H         -0.62271586    1.62158739   -5.21665658
```

Deglycosylation D268–GB: RC3–D$_{GB}$ E = –3875.59852 a.u.

```
O         -0.96326000   -6.10003500   -2.23704400
C         -2.10865800   -5.71109900   -1.48860800
C         -1.67154900   -5.73125200   -0.03685800
O         -0.71027300   -4.68568200    0.16567500
C         -2.79219900   -5.48211100    0.97434400
O         -2.42039700   -6.14481500    2.21722000
C         -2.72090700   -3.98482200    1.18457500
C         -1.21472400   -3.70575900    1.05372300
N         -0.87445500   -2.36715200    0.58863200
C         -1.54224100   -1.58721400   -0.38817300
N         -0.73942200   -0.48665100   -0.59144500
C          0.39875600   -0.56738900    0.20669300
C          1.59527500    0.19882000    0.22298900
O          1.85977700    1.23096400   -0.39380900
N          2.53395100   -0.37659100    1.10304400
C          2.37230500   -1.56430400    1.76060900
N          3.40699500   -1.97966800    2.54002100
N          1.26853400   -2.28008400    1.70188300
C          0.32477700   -1.75199200    0.90279200
O         -2.61736000   -1.81760200   -0.91685800
P         -3.30735400   -7.33011100    2.84723300
O         -2.31889900   -8.30524700    3.51665200
O         -4.17165200   -8.07700400    1.83043100
O         -4.27337700   -6.59667300    3.89026500
C         -1.18345400    1.32760100   -4.31242300
C         -1.06854000    2.40441600   -3.20033500
O         -1.36442400    2.11429600   -2.04969600
```

```
N            -0.70502600    3.65373300   -3.58433200
C            -0.83450200    4.80915700   -2.71886000
C            -6.42383800   -1.75751900    0.97263600
O            -6.01691100   -1.70288700    2.31226500
C            -2.04667400   -2.75304300    8.25053000
C            -1.34113400   -2.76521200    6.89018600
C            -2.21611200   -2.26761700    5.74303600
C            -1.57953500   -2.51251600    4.37685400
N            -0.19283100   -2.05056200    4.36556300
C            -2.12873400    2.93987700    4.84594200
S            -1.53067000    1.22353500    4.69447000
C             1.00636000   -5.42339300    4.22369100
C             2.04127800   -5.28715900    3.04048600
O             3.16237800   -4.79245300    3.31129500
O             1.66953700   -5.71426900    1.91532900
C             4.38784800   -6.42750300    0.41571900
C             3.70831900   -6.75829800   -0.88519500
N             4.38590600   -7.17637400   -2.02396600
C             2.38656400   -6.70364000   -1.22411200
C             3.51087100   -7.37723000   -3.00690600
N             2.29433400   -7.09553800   -2.54523000
C             8.18562500    1.49243600    3.55758700
C             7.51480600    0.09601300    3.55692000
C             6.01605200    0.03869400    3.27955000
O             5.55063900    0.33266400    2.17650000
N             5.24953200   -0.37141900    4.30479800
C             6.32703900   -1.11667200   -0.78924500
C             4.90681100   -1.61299300   -1.03221400
C             4.43860200   -2.77350100   -0.40900100
C             4.04382700   -0.91585300   -1.88300300
C             3.14220400   -3.23858400   -0.63245900
C             2.76053300   -1.39593100   -2.13835800
C             2.30519200   -2.55702000   -1.51617600
O             2.95234600    2.29031200   -2.79139200
O            -1.30035400   -9.49216700    0.71413100
O             0.11123700   -7.78009000    2.12798700
H            -2.96218800   -6.40437900   -1.61894900
H            -2.43231900   -4.69358900   -1.76126900
H            -1.19574300   -6.69258500    0.16792200
H            -3.76876900   -5.85320900    0.64244800
H            -3.24850400   -3.47829100    0.36927800
H            -3.14348800   -3.66040000    2.13673600
H            -0.69664200   -3.81715800    2.01109300
H            -1.02688900    0.31938200   -1.14473500
H             3.43616700    0.09682500    1.17956300
H             3.33826200   -2.96287200    2.83790100
H             4.32358800   -1.68294500    2.21341500
H            -2.26730100    1.19374900   -4.51885000
H            -0.79864800    0.37947300   -3.87847300
H            -0.52857500    3.82421700   -4.57441700
H            -0.74206300    4.45612900   -1.67396300
H            -5.59734000   -2.23271000    0.42260100
H            -6.56355300   -0.74262400    0.54337200
H            -6.71163000   -1.30037300    2.86795900
H            -1.59967500   -3.55014100    8.88209100
```

```
H          -3.10803900    -3.03282100     8.11262100
H          -1.03460800    -3.79598300     6.67294800
H          -0.40628400    -2.19588600     6.91820800
H          -3.19671400    -2.76208700     5.77658400
H          -2.42566500    -1.19528700     5.87109900
H          -2.20796900    -2.05164000     3.59552200
H          -1.56899700    -3.59149900     4.18650400
H           0.29226700    -2.38899300     3.53741000
H          -0.16962300    -1.03182300     4.30529200
H          -3.13891600     2.93368200     5.29708200
H          -2.22977500     3.31475800     3.81328000
H          -1.68405200     0.87043100     6.00504600
H           0.08790100    -5.91956200     3.88925100
H           0.73299600    -4.37813600     4.50040300
H           3.76162800    -5.72664400     0.97924200
H           5.33594700    -5.91633400     0.13928500
H           5.42386800    -7.27254200    -2.12506900
H           1.52858200    -6.38135900    -0.66372100
H           3.75411800    -7.71810500    -4.00485200
H           1.39581700    -7.14426200    -3.08046800
H           8.58991600     1.69754400     4.56097200
H           7.43827100     2.28280700     3.34650500
H           7.93695400    -0.52957500     2.75458200
H           7.72961900    -0.42425700     4.49700800
H           5.64226300    -0.75049300     5.15810900
H           4.28564700    -0.65944700     4.12635500
H           6.60341800    -1.27557000     0.27064800
H           6.38267100    -0.02716600    -0.95223600
H           5.09319700    -3.31605100     0.27372500
H           4.36162100     0.01547600    -2.34476400
H           2.75469700    -4.09048100    -0.07785800
H           2.10033900    -0.83050900    -2.79762800
H           1.29488900    -2.92511100    -1.68538100
H           2.36366300     1.74467700    -3.34754600
H           2.74338500     1.97549600    -1.89091100
H          -0.97085100   -10.01768700    -0.05012600
H          -0.55556500    -8.91811800     1.02250000
H           0.49440400    -6.87896300     1.91681200
H          -0.74562900    -7.64717500     2.57305100
H          -1.80789383     5.23078152    -2.85900677
H          -0.10862995     5.55505803    -2.96713691
H           8.97043783     1.51893761     2.83076756
H           7.02773375    -1.62447476    -1.41858054
H           4.61065011    -7.30211988     0.99044026
H          -3.85699645    -6.46716731     4.74551672
H          -7.31563383    -2.32404314     0.80337115
H          -1.17339396    -6.47384586    -3.09594397
H          -1.44947400     3.54881205     5.40514139
H          -0.66779682     1.58290691    -5.21454082
H          -1.98269069    -1.83926599     8.80353788
H           1.42581773    -5.90013363     5.08489573
```

Deglycosylation D268–GB: TS3–D$_{GB}$ E = –3875.500019 a.u. (334.58i cm^{-1})

O	-1.45704000	-5.56075500	-2.61388000
C	-2.61756600	-5.39470600	-1.82006800
C	-2.33019800	-6.03183100	-0.46161600
O	-1.04612900	-5.44436800	-0.06231100
C	-3.29153500	-5.78180500	0.72307100
O	-3.45717100	-7.03902600	1.41555300
C	-2.54320700	-4.74932400	1.54543100
C	-1.13304900	-4.99397700	1.13608000
N	-0.99916500	-2.36672800	0.52812700
C	-1.73569000	-1.57743500	-0.33225300
N	-0.98592800	-0.43685700	-0.64906500
C	0.20844100	-0.49334800	0.06102100
C	1.36338200	0.30102700	0.06825000
O	1.60402800	1.37915600	-0.50796000
N	2.35322800	-0.27314400	0.90986500
C	2.23900100	-1.47369600	1.54575000
N	3.32429200	-1.86048900	2.31478300
N	1.17008900	-2.22299100	1.50979400
C	0.15171300	-1.71865600	0.74312300
O	-2.87510500	-1.80875800	-0.75847000
P	-3.72067900	-7.53204400	2.91774500
O	-2.43242900	-8.22408900	3.42819900
O	-4.82852600	-8.58730100	2.83013600
O	-4.05181300	-6.20157100	3.74726900
C	-1.15329300	1.35793100	-4.30547000
C	-1.09989500	2.45785500	-3.21436600
O	-1.51325300	2.20922700	-2.09347800
N	-0.62950500	3.68048700	-3.57322800
C	-0.76232000	4.83008600	-2.70336300
C	-6.43001800	-1.68902300	0.97277600
O	-6.04842900	-1.65521400	2.32028000
C	-2.07626000	-2.74345800	8.22862100
C	-1.34666400	-2.75626600	6.87546300
C	-2.21308800	-2.29600000	5.70341600
C	-1.59508500	-2.61147300	4.34303800
N	-0.20204100	-2.17174600	4.28344400
C	-2.08954700	2.94748900	4.85516700
S	-1.50761900	1.22451100	4.70413300
C	0.94544600	-5.40123000	4.24138300
C	1.95115800	-5.42572300	3.04160500
O	3.04194600	-4.85778200	3.15664900
O	1.59159800	-6.13305700	2.02944500
C	4.34545800	-6.47581400	0.39977700
C	3.74708200	-6.80065100	-0.94178600
N	4.48362600	-7.16307000	-2.06213100
C	2.43961300	-6.78306500	-1.33294900
C	3.65888200	-7.36278200	-3.08490900
N	2.41298700	-7.13637700	-2.66602900
C	8.22805200	1.41920900	3.60796100
C	7.49780100	0.05927900	3.66873500
C	6.03621500	0.04996100	3.22717100
O	5.70070700	0.43910200	2.10994800
N	5.15900200	-0.42527000	4.13057000

C	6.33255200	-1.16925400	-0.77923600
C	4.89512100	-1.54807700	-1.10975700
C	4.35014300	-2.74212000	-0.63007100
C	4.09732900	-0.71934200	-1.90412400
C	3.04151500	-3.10856700	-0.93887400
C	2.79738500	-1.09547800	-2.23581900
C	2.26169600	-2.28720000	-1.75351000
O	2.93718200	2.35575000	-2.76093100
O	-1.57168700	-9.34627100	0.98024700
O	-0.75112000	-6.78954800	1.92984100
H	-3.53425000	-5.85480200	-2.24271800
H	-2.78968400	-4.32058700	-1.68803100
H	-2.15407100	-7.10686900	-0.56152200
H	-4.28698400	-5.44427300	0.39002900
H	-2.75081900	-3.73738800	1.15704300
H	-2.74488000	-4.76935900	2.61051500
H	-0.25259900	-4.49920800	1.53329600
H	-1.33483000	0.36315000	-1.16639900
H	3.23216600	0.23493300	0.97523500
H	3.24538500	-2.83675200	2.60849500
H	4.21766600	-1.65429600	1.86874400
H	-2.22693200	1.17925900	-4.52867900
H	-0.74346800	0.43435300	-3.84022500
H	-0.39765500	3.84860400	-4.55176800
H	-0.68243000	4.47190600	-1.66054600
H	-5.59963100	-2.16744900	0.43061200
H	-6.54998300	-0.66909100	0.55137800
H	-6.73121800	-1.21392700	2.86093000
H	-1.65363400	-3.55445600	8.85897700
H	-3.13876800	-3.00548400	8.06840400
H	-1.01574900	-3.78410600	6.67829200
H	-0.42226000	-2.16923900	6.91335600
H	-3.20046400	-2.77478200	5.76258500
H	-2.40888200	-1.21667500	5.78296400
H	-2.22808700	-2.19349500	3.54438100
H	-1.59282600	-3.70146200	4.21614200
H	0.17929200	-2.36001300	3.35460600
H	-0.16954500	-1.15488700	4.38143000
H	-3.10163700	2.95085200	5.30231400
H	-2.18610200	3.32184200	3.82366700
H	-1.67208400	0.87718000	6.01482100
H	-0.03129300	-5.81291400	3.96040100
H	0.77970100	-4.33101500	4.50781000
H	3.69111800	-5.77722200	0.93072100
H	5.30360000	-5.95851000	0.18053700
H	5.53799900	-7.23519400	-2.13773400
H	1.54887700	-6.51946700	-0.79507000
H	3.95927800	-7.66538500	-4.07908000
H	1.54853100	-7.17689100	-3.23689900
H	8.66902600	1.62567100	4.59673200
H	7.50239200	2.23195200	3.40471700
H	7.97281300	-0.65616300	2.97918300
H	7.58315500	-0.37661800	4.67012300
H	5.44983200	-0.85011200	5.00476100
H	4.22596500	-0.69437500	3.81281600

```
H          6.55379100    -1.40027900     0.28006100
H          6.47218700    -0.07950200    -0.87777700
H          4.95913700    -3.39122100     0.00067200
H          4.47509600     0.23323500    -2.26314600
H          2.61238300    -4.01182000    -0.51159700
H          2.18410800    -0.42556000    -2.83861100
H          1.23392600    -2.56215000    -1.97788400
H          2.34511800     1.86613700    -3.36311600
H          2.63990600     2.03470700    -1.88208700
H         -1.30350700    -9.67602100     0.09547400
H         -1.24082900    -8.42575300     1.06258800
H          0.28240500    -6.60107200     2.05250700
H         -1.20904200    -7.18461700     2.70861800
H         -0.02728793     5.56886058    -2.94593254
H         -1.73071038     5.26356954    -2.84197066
H         -1.40742166     3.54988453     5.41794995
H         -0.63079672     1.60990381    -5.20458475
H          8.99864687     1.41772819     2.86561246
H          7.02309235    -1.69362246    -1.40620629
H          4.54052041    -7.35478903     0.97792365
H          1.35797373    -5.91635307     5.08362352
H         -3.83284986    -6.31682210     4.67483157
H         -7.32985519    -2.23880190     0.79129268
H         -1.49062637    -6.20747194    -3.32256128
H         -2.00844511    -1.83785745     8.79447327
```

Deglycosylation D268–GB: PC–D$_{GB}$ E = –3875.53412 a.u.

```
O         -1.40178600    -5.79074200    -2.23776200
C         -2.65996600    -5.38290300    -1.71005200
C         -2.88348200    -6.13190400    -0.39402700
O         -1.68381700    -6.05354800     0.37714300
C         -3.94638400    -5.54050100     0.52969800
O         -4.43374300    -6.57696800     1.44350900
C         -3.18807600    -4.40815900     1.19387100
C         -1.72163400    -4.85410200     1.14267600
N         -1.41784800    -1.82392200     0.42194900
C         -2.25540000    -1.25584700    -0.52138200
N         -1.63139600    -0.12841000    -1.06954900
C         -0.41926800     0.05090200    -0.41345400
C          0.65229400     0.91850100    -0.61271800
O          0.78191700     1.89851100    -1.39030000
N          1.71853100     0.61469300     0.27182200
C          1.76362200    -0.49525700     1.06668500
N          2.95267300    -0.70928900     1.75908100
N          0.77343600    -1.32138100     1.23302600
C         -0.33047100    -1.05145200     0.46612100
O         -3.37710000    -1.65247200    -0.86106800
P         -3.93190000    -7.15248700     2.82833900
O         -2.44549500    -7.59422800     2.81421300
O         -4.77654800    -8.40358400     3.11554900
O         -4.13258700    -5.91505000     3.82223400
C         -1.10761300     1.29657900    -4.30582600
C         -1.28115800     2.50166600    -3.35965000
O         -2.03446400     2.40691300    -2.40224300
```

```
N              -0.55855000     3.62112400    -3.60628600
C              -0.70188400     4.77576300    -2.74798900
C              -6.41676900    -1.66649400     0.99588000
O              -6.02055400    -1.67474300     2.34066100
C              -2.07351300    -2.66404000     8.26225700
C              -1.48277700    -2.67285700     6.83893700
C              -2.44276600    -2.17916200     5.75273500
C              -2.09354700    -2.64489500     4.33728800
N              -0.67778600    -2.43292900     4.01186000
C              -2.04948600     2.98017300     4.83033800
S              -1.44014900     1.26577300     4.67989200
C               0.86391800    -5.44527400     4.33042800
C               1.86413400    -5.30191100     3.15943200
O               3.04634000    -5.06924300     3.30767700
O               1.35831000    -5.50251100     1.94671700
C               4.30935000    -6.53292300     0.49170900
C               3.73612000    -6.87189900    -0.85898500
N               4.49668500    -7.25314400    -1.95723300
C               2.43795300    -6.85210500    -1.28369300
C               3.69497600    -7.46626800    -2.99517500
N               2.44081500    -7.22859900    -2.60902400
C               8.27527400     1.38334500     3.64831800
C               7.41681000     0.09949900     3.67292200
C               6.01817500     0.24538900     3.08264000
O               5.83450700     0.80314200     2.00344500
N               5.01468400    -0.28130000     3.81143300
C               6.36591900    -1.26407100    -0.70724700
C               4.92163400    -1.68473700    -0.94080000
C               4.39975900    -2.84115100    -0.34842500
C               4.07708100    -0.90002400    -1.72789700
C               3.07123200    -3.20895100    -0.54790700
C               2.75168700    -1.27868700    -1.94946700
C               2.24256800    -2.43193500    -1.36107000
O               3.10570400     1.95111900    -2.88631500
O              -1.43041500    -8.90074700     0.78328200
O              -1.16088200    -5.18870300     2.39304600
H              -3.51960100    -5.58609000    -2.37938600
H              -2.62400900    -4.29969500    -1.54115200
H              -3.07969800    -7.19372800    -0.59807700
H              -4.86163600    -5.22042300     0.00477400
H              -3.29497300    -3.49386900     0.58868400
H              -3.53352600    -4.17582700     2.20155100
H              -1.08168600    -4.07407600     0.71183300
H              -2.10780100     0.59487000    -1.59832900
H               2.56926200     1.13962800     0.09857300
H               3.02340500    -1.69662800     1.99437200
H               3.79103800    -0.39779500     1.26734400
H              -2.12024400     0.90847600    -4.53760600
H              -0.56458200     0.52567700    -3.70860300
H              -0.12342400     3.73978400    -4.51820000
H              -0.62494500     4.42161700    -1.70095300
H              -5.59363200    -2.12269200     0.42503500
H              -6.54160100    -0.63358100     0.60824500
H              -6.67997300    -1.21197100     2.89132400
H              -1.54621900    -3.44041800     8.85664000
```

H	−3.12769200	−2.99251500	8.20502700
H	−1.20916400	−3.71019900	6.61003900
H	−0.53832900	−2.11608000	6.79922100
H	−3.45951500	−2.53071600	5.98173100
H	−2.50390000	−1.08247200	5.77981200
H	−2.77628500	−2.14911500	3.62960500
H	−2.28186400	−3.72040500	4.26126600
H	−0.54496800	−2.61072600	3.01370000
H	−0.45896600	−1.43866500	4.11060400
H	−3.05856800	2.97247100	5.28418400
H	−2.15694800	3.35157900	3.79897500
H	−1.60163700	0.91907600	5.99014500
H	−0.02513300	−5.99602600	4.02162200
H	0.51215300	−4.41112300	4.57038900
H	3.64042800	−5.83369900	1.00307200
H	5.25823400	−5.99500400	0.28863700
H	5.55435700	−7.32576500	−2.01622500
H	1.52694100	−6.58196700	−0.78489300
H	4.01903100	−7.78622400	−3.97623700
H	1.58329900	−7.27886800	−3.19317800
H	8.75601300	1.49400000	4.63456100
H	7.61695400	2.26412600	3.50519300
H	7.89021500	−0.69326900	3.07174700
H	7.34411800	−0.29270900	4.69343300
H	5.14722400	−0.80914400	4.67041900
H	4.07677100	−0.27136600	3.41346900
H	6.64462400	−1.45951400	0.34659500
H	6.46989800	−0.17464600	−0.84190500
H	5.04010900	−3.44699000	0.29403500
H	4.43393000	0.03045400	−2.15910400
H	2.65627000	−4.07374500	−0.03615800
H	2.10683600	−0.63968000	−2.55262400
H	1.20128400	−2.70996900	−1.50082300
H	2.82519500	1.29891400	−3.55736900
H	2.29104000	2.04266900	−2.33666300
H	−1.16590600	−9.24110900	−0.10051600
H	−1.35191900	−7.92269300	0.73849000
H	0.35304300	−5.46012000	2.00931300
H	−1.60266500	−6.03073200	2.66490200
H	−1.37004053	3.59024626	5.38806954
H	−1.66685592	5.21496205	−2.89232679
H	0.03908180	5.50702455	−2.99522618
H	−0.58289610	1.52954214	−5.20876584
H	−7.32019594	−2.21044492	0.81466975
H	−3.88780503	−6.14933543	4.72045008
H	−1.44696886	−6.32110434	−3.03668271
H	1.31722847	−5.91613757	5.17759806
H	4.50996836	−7.40125515	1.08386738
H	9.03217107	1.36591145	2.89220763
H	7.04494662	−1.78757118	−1.34737906
H	−2.01141747	−1.75374820	8.82119616

Nucleobase:	**ADENINE**	**Best Interaction**		**Dimer Image**
Amino Acid:	**HISTIDINE**	R_1 (Å)	3.300	
Conformation:	**NδH CONF 1**	α (°)	120.0	
		R_2 (Å)	[0.0, -0.5]	
		BE (Best)	-27.2	
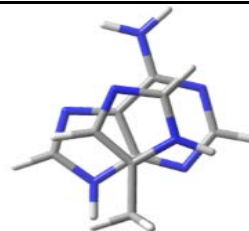
Effect of Deviation

Step 1: R_1			Step 2: α			Binding Energy Prediction	
Value	$\Delta E(R_1)$		Value	$\Delta E(\alpha)$			
(Å)	(kJ mol^{-1})		(°)	(kJ mol^{-1})		$R_{1,eq}$ =	3.100
3.0	7.99		0.0	2.7		$\Delta E(R_{1,eq})$ =	0.0
3.1	3.10		30.0	4.0		$\Delta E(\omega)$ =	0.0
3.2	0.71		60.0	3.6			
3.3	0.00		90.0	1.0		BE(sum) =	-27.2
3.4	0.40		120.0	0.0		BE(R_1) =	**-27.2**
3.5	1.48		150.0	3.3		BE(R_1,ω) =	**0.0**
3.6	2.96		180.0	7.6			↥Your pre
3.7	4.63		210.0	9.6			
3.8	6.36		240.0	10.4		**Measured Value:**	
			270.0	11.2		R_1 (P[A]···C_X[Hc1]) (Å) =	
			300.0	8.3		α (C1'–N9–Cγ–Cβ) (°) =	
			330.0	4.0		R_2 (CX[Hc1] over) (Å) =	
						ω (∠P[A]–P[Hc1]) (°) =	
							Add your va

Step 3: R_2	X-Axis (Å)						
$\Delta E(R_2)$ (kJ mol^{-1})	-1.50	-1.00	-0.50	0.00	0.50	1.00	1.50
1.50	16.0	15.1	14.2	14.2	15.3	16.2	16.5
1.00	11.0	9.8	8.7	9.0	10.7	12.2	12.7
0.50	6.7	5.0	2.9	3.3	6.7	10.0	11.4
0.00	4.9	3.1	0.1	0.2	4.8	9.6	11.6
-0.50	5.0	3.7	0.5	0.0	4.0	8.5	10.6
-1.00	4.5	3.6	1.4	1.0	3.4	6.3	8.3
-1.50	2.3	1.5	1.3	2.3	4.1	5.7	7.5

Y-Axis (Å)

R2 Grid   [0,0] in cyan
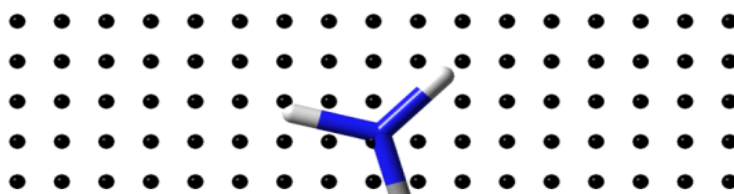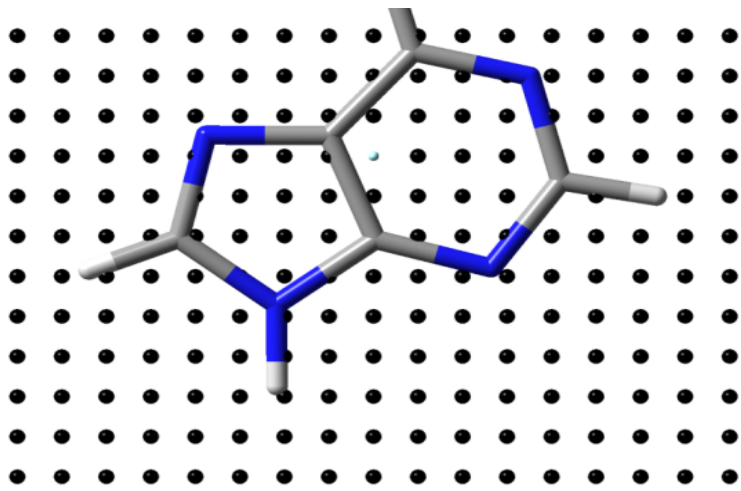
	Coefficients
a_1	2.00E-02
a_2	3.100
c_1	-2.12E-04
c_2	0.28
c_3	-0.3
b_1	31.1
b_2	1.180

$= a*\omega + b$

$= f*[1 - \exp(-g*(R_1 - R_{1,eq}))]^2$ for $(R_1 - R_{1,eq}) > -0.4$

$= c*\omega^2 + d*\omega + e$ for $\omega > 10$

$= BE(Best) + \Delta E(R_1) + \Delta E(\alpha) + \Delta E(R_2)$

$= BE(Best) + \Delta E(R_{1,eq}) + \Delta E(\alpha) + \Delta E(R_2)$

$= BE(Best) + \Delta E(R_{1,eq}) + \Delta E(\alpha) + \Delta E(R_2) + \Delta E(\omega)$

dicted binding energy in kJ mol^{-1}

	Closest	ΔE	
	0.000		From Step 1
	0.0		From Step 2
			From Step 3

lues here ⬍   ⬆Copy the corresponding ΔE here.

Appendix G: Supporting Information for Chapter 7

Predicting Binding Energies of DNA–Protein Stacking Contacts

Table of Contents

Table G1. *Test set of DNA–protein π–π contacts obtained from X-ray crystal structures.*[1]

PBD ID	Dimer		Measurements[2]					PES						Deviation Effects[3]					BE_Calc[4]	Summation		Distance Dependent		Tilt Dependent	
			ω	R_1	α	$R_2(x)$	$R_2(y)$	R_1	α	$R_2(x)$	$R_2(y)$	$R_{1,eq}$	BE_{Best}	$\Delta E(R_1)$	$\Delta E(\alpha)$	$\Delta E(R_2)$	$\Delta E(R_1,\omega)$	$\Delta E(\omega)$		BE_{Sum}	UD[5]	BE_{R1}	UD	BE_{Scan}	UD
1TDZ	A22:F111		16.2	3.678	32.9	1.5	0.0	3.700	30.0	1.5	0.0	3.664	−24.3	3.8	0.0	8.7	0.0	4.3	−15.1	−11.8	3.3	−15.6	−0.5	−11.3	3.7
1U1R	A203:F17		5.4	3.500	105.2	−1.5	0.5	3.500	0.0	−1.5	0.5	3.449	−24.3	1.2	0.0	5.2	0.1	0.0	−17.8	−17.9	−0.1	−19.0	−1.2	−19.0	−1.2
1XC8	A22:F111		16.4	3.764	35.8	1.5	0.0	3.800	30.0	1.5	0.0	3.667	−24.3	5.6	0.0	8.7	0.4	4.3	−13.8	−10.0	3.9	−15.2	−1.4	−10.9	2.9
1NNJ	A22:F111		15.3	3.669	46.5	1.5	−0.5	3.700	0.0	1.5	−0.5	3.646	−24.3	3.8	0.0	7.3	0.0	4.0	−14.7	−13.2	1.5	−17.0	−2.2	−12.9	1.8
3C58	A22:F111		19.6	3.708	32.8	1.0	0.0	3.700	30.0	1.0	0.0	3.731	−24.3	3.8	0.0	7.3	0.0	5.1	−15.1	−13.2	1.9	−17.0	−1.9	−11.9	3.2
1U1K	A203:H101	Nδ	11.6	3.606	234.2	−1.5	−1.0	3.600	240.0	−1.5	−1	3.332	−27.2	3.0	10.4	4.5	2.4	3.0	−8.4	−9.4	−1.0	−9.9	−1.6	−7.0	1.4
1U1L	A203:H101	Nδ	14.4	3.576	237.8	−1.5	−0.5	3.600	240.0	−1.5	−0.5	3.387	−27.2	3.0	10.4	5.0	1.2	3.7	−5.8	−8.8	−3.1	−10.6	−4.8	−6.8	−1.1
1U1O	A203:H101	Nδ	14.1	3.546	241.2	−1.5	−0.5	3.500	240.0	−1.5	−0.5	3.381	−27.2	1.5	10.4	5.0	1.0	3.6	−6.7	−10.3	−3.6	−10.8	−4.1	−7.2	−0.5
1U1P	A203:H101	Nδ	14.0	3.619	239.6	−1.5	−0.5	3.600	240.0	−1.5	−0.5	3.380	−27.2	3.0	10.4	5.0	1.9	3.6	−6.8	−8.8	−2.0	−9.9	−3.1	−6.3	0.5
1U1Q	A203:H101	Nδ	12.5	3.530	238.3	−1.5	−0.5	3.500	240.0	−1.5	−0.5	3.349	−27.2	1.5	10.4	5.0	1.1	3.2	−7.6	−10.3	−2.7	−10.7	−3.1	−7.5	0.1
1U1K	A203:H101	Nε	11.6	3.606	162.2	−1.5	−1.0	3.600	150.0	−1.5	−1	3.336	−29.7	2.7	1.3	7.6	2.4	1.4	−21.2	−18.1	3.0	−18.4	2.7	−17.0	4.1
1U1L	A203:H101	Nε	14.4	3.576	165.8	−1.5	−0.5	3.600	180.0	−1.5	−0.5	3.380	−29.7	2.7	0.0	8.2	1.4	2.3	−19.3	−18.8	0.5	−20.1	−0.8	−17.8	1.5
1U1O	A203:H101	Nε	14.1	3.546	169.2	−1.5	−0.5	3.500	180.0	−1.5	−0.5	3.375	−29.7	1.3	0.0	8.2	1.1	2.2	−21.4	−20.2	1.2	−20.4	0.9	−18.2	3.1
1U1P	A203:H101	Nε	14.0	3.619	167.6	−1.5	−0.5	3.600	180.0	−1.5	−0.5	3.374	−29.7	2.7	0.0	8.2	2.0	2.2	−21.3	−18.8	2.5	−19.5	1.8	−17.3	4.0
1U1Q	A203:H101	Nε	12.5	3.530	166.3	−1.5	−0.5	3.500	180.0	−1.5	−0.5	3.350	−29.7	1.3	0.0	8.2	1.2	1.7	−20.3	−20.2	0.2	−20.3	0.0	−18.6	1.7
1U1K	A203:H101	(+)	11.6	3.606	234.2	−1.5	−1.0	3.600	240.0	−1.5	−1.0	3.231	−58.4	9.7	2.9	23.2	7.4	0.1	−30.2	−22.6	7.7	−24.9	5.3	−24.8	5.4
1U1L	A203:H101	(+)	14.4	3.576	237.8	−1.5	−0.5	3.600	240.0	−1.5	−0.5	3.267	−58.4	9.7	2.9	20.9	5.5	0.7	−25.3	−25.0	0.4	−29.2	−3.9	−28.4	−3.1
1U1O	A203:H101	(+)	14.1	3.546	241.2	−1.5	−0.5	3.500	240.0	−1.5	−0.5	3.263	−58.4	6.6	2.9	20.9	4.8	0.7	−27.9	−28.1	−0.2	−29.9	−2.0	−29.2	−1.3
1U1P	A203:H101	(+)	14.0	3.619	239.6	−1.5	−0.5	3.600	240.0	−1.5	−0.5	3.262	−58.4	9.7	2.9	20.9	6.9	0.7	−28.4	−25.0	3.4	−27.8	0.6	−27.2	1.3
1U1Q	A203:H101	(+)	12.5	3.530	238.3	−1.5	−0.5	3.500	240.0	−1.5	−0.5	3.242	−58.4	6.6	2.9	20.9	4.9	0.3	−29.9	−28.1	1.8	−29.8	0.1	−29.5	0.4
2GB7	A0:W61	2	20.0	4.294	163.3	−1.0	0.0	**3.800**	150.0	−1.0	0.0	3.839	−32.0	4.2	4.5	2.8	6.3	6.7	−14.0	−20.5	−6.5	−18.5	−4.5	−11.8	2.2
3MR2	A3:W42	1	2.6	3.518	115.3	0.5	−0.5	3.500	120.0	0.5	−0.5	3.381	−35.0	0.0	6.2	5.8	0.9	0.0	−24.1	−23.0	1.1	−22.1	1.9	−22.1	1.9
3MR3	A2:W42	1	6.5	3.595	116.1	0.0	−1.5	3.600	120.0	0.0	−1.5	3.470	−35.0	0.5	6.2	3.1	0.7	0.0	−17.4	−25.2	−7.8	−25.0	−7.6	−25.0	−7.6
3MR5	A2:W42	1	3.5	3.446	121.3	0.0	−1.0	3.400	120.0	0.0	−1.0	3.400	−35.0	0.7	6.2	2.7	0.1	0.0	−21.1	−25.4	−4.3	−26.0	−4.9	−26.0	−4.9
1G38	A606:Y108	cw	14.7	3.515	278.0	0.0	0.5	3.500	270.0	0.0	0.5	3.626	−28.9	0.7	3.7	0.0	0.7	4.3	−21.6	−24.5	−2.9	−24.5	−2.9	−20.2	1.4

[1] Distances in Å; angles in degrees; energies in kJ mol⁻¹.
[2] See Section 7.2.1 for definitions.
[3] See Section 7.2.2 for definitions and calculation methods.
[4] Calculated with M06-2X/6-31+G(d,p) with CS-symmetric monomers overlayed onto crystal structure geometry.
[5] Unsigned deviation compared to BE_{Calc}.

PBD ID	Dimer		Measurements[2]					PES						Deviation Effects[3]					BE_Calc[4]	Summation		Distance Dependent		Tilt Dependent	
			ω	R_1	α	$R_2(x)$	$R_2(y)$	R_1	α	$R_2(x)$	$R_2(y)$	$R_{1,eq}$	BE_{Best}	$\Delta E(R_1)$	$\Delta E(\alpha)$	$\Delta E(R_2)$	$\Delta E(R_1,\omega)$	$\Delta E(\omega)$		BE_{Sum}	UD^5	BE_{R1}	UD	BE_{Scan}	UD
2G1P	A12:Y119	cw	6.7	3.420	250.9	−1.0	0.5	3.400	240.0	−1.0	0.5	3.395	−28.9	0.0	3.9	6.3	0.0	0.0	−18.2	−18.7	−0.6	−18.7	−0.6	−18.7	−0.6
2FR4	A13m:Y97	cw	6.5	3.453	101.6	−0.5	−0.5	3.500	90.0	−0.5	−0.5	3.389	−28.9	0.7	5.0	4.1	0.2	0.0	−23.4	−19.1	4.4	−19.6	3.8	−19.6	3.8
3MFI	A4:Y453	cw	10.8	3.660	110.4	0.0	−1.0	3.700	120.0	0.0	−1.0	3.512	−28.9	3.6	2.3	3.2	0.9	1.8	−23.4	−19.8	3.6	−22.5	0.9	−20.7	2.7
2IH2	A6:Y108	cw	8.1	3.391	283.5	0.0	1.0	3.400	270.0	0.0	1.0	3.436	−28.9	0.0	3.7	1.3	0.1	0.0	−12.1	−23.9	−11.8	−23.8	−11.7	−23.8	−11.7
1G38	A606:Y108	ccw	14.7	3.515	278.0	0.0	0.5	3.500	270.0	0.0	0.5	3.591	−30.7	0.5	3.9	4.8	0.3	1.6	−18.9	−21.5	−2.7	−21.7	−2.9	−20.1	−1.2
2G1P	A12:Y119	ccw	6.7	3.420	250.9	−1.0	0.5	3.400	240.0	−1.0	0.5	3.368	−30.7	0.0	5.1	6.8	0.1	0.0	−22.3	−18.8	3.5	−18.7	3.6	−18.7	3.6
2FR4	A13m:Y97	ccw	7.5	3.409	101.6	−0.5	−0.5	3.400	90.0	−1.0	−1.0	3.390	−30.7	0.0	11.3	5.7	0.0	0.0	−21.9	−13.7	8.2	−13.7	8.3	−13.7	8.3
3MFI	A4:Y453	ccw	10.8	3.660	110.4	0.0	−1.0	3.700	120.0	0.0	−1.0	3.481	−30.7	3.3	8.2	0.9	1.3	−0.4	−21.7	−18.3	3.4	−20.3	1.4	−20.7	0.9
2IH2	A6:Y108	ccw	8.1	3.391	283.5	0.0	1.0	3.400	270.0	0.0	1.0	3.408	−30.7	0.0	3.9	7.5	0.0	0.0	−18.7	−19.3	−0.6	−19.3	−0.6	−19.3	−0.6
3LDY	A8b:R114	cw	3.6	3.340	186.3	−2.0	0.0	3.300	180.0	−2.0	0.0	2.937	−54.8	0.0	0.0	20.9	9.2	0.0	−30.7	−33.9	−3.2	−24.7	5.9	−24.7	5.9
3LNQ	A7b:R89	cw	30.6	3.619	39.8	−1.0	−2.0	3.600	30.0	−1.0	−2.0	3.584	−54.8	6.3	8.9	15.2	0.1	19.2	−31.4	−24.5	7.0	−30.6	0.88	−11.4	20.0
3M7K	A8b:R114	cw	4.1	3.358	183.1	−2.0	0.0	3.400	180.0	−2.0	0.0	2.948	−54.8	1.0	0.0	20.9	9.4	0.0	−31.4	−33.0	−1.6	−24.5	6.8	−24.5	6.8
3MIP	A−9d:R43b	cw	7.1	3.151	297.5	−2.5	1.0	3.200	300.0	−2.5	1.0	3.020	−54.8	0.4	3.2	27.7	1.6	0.0	−25.8	−23.6	2.2	−22.4	3.4	−22.4	3.4
3MIS	A−9d:R43b	cw	13.2	3.211	283.3	−2.5	1.0	3.200	270.0	−2.5	1.0	3.167	−54.8	0.4	5.7	27.7	0.2	7.7	−21.9	−21.1	0.8	−21.2	0.6	−13.6	8.3
3Q22	A12d:R904b	cw	9.3	3.304	267.9	−2.5	−0.5	3.300	270.0	−2.5	−0.5	3.074	−54.8	0.0	5.7	25.4	4.1	0.0	−24.6	−23.8	0.8	−19.7	4.9	−19.7	4.9
3Q22	A7d:R318b	cw	20.2	3.387	69.5	−1.5	0.5	3.400	60.0	−1.5	0.5	3.335	−54.8	1.0	1.3	19.9	0.3	13.6	−29.0	−32.6	−3.6	−33.3	−4.3	−19.6	9.3
3Q22	A12c:R904	cw	10.0	3.205	269.0	−2.5	1.0	3.200	270.0	−2.5	1.0	3.090	−54.8	0.4	5.7	27.7	1.3	0.0	−22.0	−21.1	0.9	−20.2	1.8	−20.2	1.8
2WT7	A6d:R256b	ccw	0.9	3.323	272.8	−3.0	0.5	3.300	270.0	−3.0	0.5	2.871	−57.2	0.8	14.2	35.2	9.9	0.0	−20.6	−7.0	13.6	2.1	22.7	2.1	22.7
3MGH	A5e:R517c	ccw	10.4	3.497	350.4	0.0	0.0	3.500	0.0	0.0	0.0	3.099	−57.2	6.0	7.5	0.0	8.1	4.7	−45.9	−43.6	2.3	−41.5	4.4	−36.8	9.1
3MGH	A5t:R517	ccw	3.3	3.390	355.4	0.0	0.0	3.400	0.0	0.0	0.0	2.928	−57.2	2.8	7.5	0.0	10.2	0.0	−46.4	−46.8	−0.4	−39.5	7.0	−39.5	7.0
3N7Q	A4b:R387	ccw	32.1	3.553	265.0	−3.0	0.0	3.600	270.0	−3.0	0.0	3.619	−57.2	9.6	14.2	34.2	0.4	18.4	−10.5	0.8	11.3	−8.4	2.1	10.0	20.4
3ISB	C5:H34	Nd 2	3.9	3.230	93.9	−1.5	0.5	3.200	90.0	−1.5	0.5	3.266	−26.9	5.2	4.2	2.5	0.1	0.0	−27.1	−15.0	12.1	−20.1	7.0	−20.1	7.0
3H8R	C265:H171	Nd 1	10.4	3.524	277.5	1.0	−1.0	3.500	270.0	1.0	−1.0	3.417	−26.0	0.6	18.5	7.2	0.4	1.3	−5.3	0.3	5.5	0.0	5.3	1.3	6.5
3H8X	C265:H171	Nd 1	9.7	3.543	272.4	1.0	−1.5	3.500	270.0	1.0	−1.5	3.406	−26.0	0.6	18.5	8.0	0.6	0.0	−4.1	1.0	5.2	1.0	5.1	1.0	5.1
3MBY	C5:H34	Nd 2	9.1	3.311	90.3	−1.0	1.0	3.300	90.0	−1.0	1.0	3.355	−26.9	2.1	4.2	4.7	0.1	0.0	−23.3	−15.9	7.4	−18.0	5.3	−18.0	5.3
3HW8	C5:H511	Nd 1	15.7	3.374	52.9	1.0	1.0	3.400	60.0	1.0	1.0	3.502	−26.0	0.0	3.1	4.6	0.7	2.4	−13.8	−18.3	−4.5	−17.6	−3.8	−15.2	−1.4
3ISB	C5:H34	Ne	3.9	3.230	165.9	−1.5	0.5	3.200	180.0	−1.5	0.5	3.312	−26.0	1.6	20.8	0.6	0.3	0.0	−12.6	−2.9	9.6	−4.3	8.3	−4.3	8.3
3H8R	C265:H171	Ne	10.4	3.524	205.5	1.0	−1.0	3.500	210.0	1.0	−1.0	3.377	−26.9	0.0	8.1	5.9	0.7	0.5	−23.3	−12.8	10.5	−12.2	11.2	−11.7	11.7
3H8X	C265:H171	Ne	9.7	3.543	200.4	1.0	−1.5	3.500	210.0	1.0	−1.5	3.366	−26.9	0.0	8.1	5.6	0.9	0.0	−20.7	−13.1	7.6	−12.2	8.5	−12.2	8.5
3MBY	C5:H34	Ne	9.1	3.311	162.3	−1.0	1.0	3.300	150.0	−1.0	1.0	3.396	−26.0	0.2	14.8	3.2	0.3	0.0	−5.7	−7.8	−2.2	−7.7	−2.1	−7.7	−2.1

PBD ID	Dimer		Measurements[2]					PES						Deviation Effects[3]					BE_{Calc}[4]	Summation		Distance Dependent		Tilt Dependent	
			ω	R_1	α	$R_2(x)$	$R_2(y)$	R_1	α	$R_2(x)$	$R_2(y)$	$R_{1,eq}$	BE_{Best}	$\Delta E(R_1)$	$\Delta E(\alpha)$	$\Delta E(R_2)$	$\Delta E(R_1,\omega)$	$\Delta E(\omega)$		BE_{Sum}	UD[5]	BE_{R1}	UD	BE_{Scan}	UD
3HW8	C5:H511	Ne	15.7	3.374	340.9	1.0	1.0	3.400	330.0	1.0	1.0	3.467	−26.9	0.6	19.6	8.3	0.4	1.5	−11.0	1.6	12.6	1.4	12.4	2.9	13.9
3ISB	C5:H34	(+)	3.9	3.230	165.9	−1.5	0.5	3.200	180.0	−1.5	0.5	3.250	−59.9	0.2	8.3	35.9	0.0	0.0	−19.2	−15.5	3.7	−15.7	3.5	−15.7	3.5
3H8R	C265:H171	(+)	10.4	3.524	277.5	1.0	−1.0	3.500	270.0	1.0	−1.0	3.336	−59.9	2.8	2.9	5.0	1.8	2.4	−47.2	−49.2	−2.0	−50.2	−3.0	−47.8	−0.6
3H8X	C265:H171	(+)	9.7	3.543	272.4	1.0	−1.5	3.500	270.0	1.0	−1.5	3.327	−59.9	2.8	2.9	6.1	2.3	0.0	−47.8	−48.1	−0.3	−48.7	−0.9	−48.7	−0.9
3MBY	C5:H34	(+)	9.1	3.311	162.3	−1.0	1.0	3.300	150.0	−1.0	1.0	3.319	−59.9	0.0	8.7	34.9	0.0	0.0	−16.3	−16.4	−0.1	−16.4	−0.1	−16.4	−0.1
1MW8	C702:W184	1	12.5	3.509	144.0	1.5	−0.5	3.500	150.0	1.5	−0.5	3.524	−32.9	0.2	2.8	14.3	0.0	1.0	−15.6	−15.6	−0.1	−15.8	−0.3	−14.8	0.7
3MDC	C4:W274	2	6.0	3.537	97.3	−1.5	0.5	3.500	90.0	−1.5	0.5	3.363	−33.4	0.0	8.9	2.5	1.0	0.0	−21.7	−22.0	−0.3	−21.0	0.8	−21.0	0.8
3PNC	C4:W274	2	6.9	3.443	97.4	−1.5	1.0	3.400	90.0	−1.5	1.0	3.387	−33.4	0.2	8.9	3.5	0.1	0.0	−21.4	−20.8	0.6	−20.9	0.6	−20.9	0.6
3HWT	C4:W274	2	6.9	3.453	105.2	−1.5	0.5	3.500	120.0	−1.5	0.5	3.387	−33.4	0.0	11.2	2.5	0.2	0.0	−22.0	−19.7	2.3	−19.5	2.4	−19.5	2.4
3HW8	C4:W274	2	5.9	3.429	103.2	−1.5	1.0	3.400	90.0	−1.5	1.0	3.358	−33.4	0.2	8.9	3.5	0.2	0.0	−24.2	−20.8	3.4	−20.8	3.4	−20.8	3.4
2OK0	C2:Y32	cw	8.6	3.442	156.5	0.0	1.0	3.400	150.0	0.0	1.0	3.408	−24.2	1.0	3.9	4.0	0.0	0.0	−10.1	−15.3	−5.2	−16.3	−6.1	−16.3	−6.1
2FR4	C5:Y97	cw	12.0	3.388	170.4	0.0	1.0	3.400	180.0	0.0	1.0	3.510	−24.2	1.0	7.5	4.0	0.6	−1.1	−16.5	−11.7	4.8	−12.1	4.4	−13.2	3.3
1L3S	C6:Y714	cw	9.7	3.492	323.1	0.0	0.0	3.500	330.0	0.0	0.0	3.440	−24.2	0.0	0.0	3.6	0.1	0.0	−31.5	−20.6	10.9	−20.5	11.0	−20.5	11.0
2HHQ	C4:Y714	cw	17.6	3.367	313.3	1.5	−1.0	3.400	300.0	1.5	−1.0	3.677	−24.2	1.0	0.1	10.7	5.3	0.6	−19.0	−12.4	6.6	−8.1	10.9	−7.5	11.5
2HHV	C6:Y714	cw	13.3	3.543	321.8	0.0	0.0	3.500	330.0	0.0	0.0	3.548	−24.2	0.0	0.0	3.6	0.0	−0.7	−30.4	−20.6	9.8	−20.6	9.8	−21.3	9.1
2OK0	C2:Y32	ccw	8.6	3.442	156.5	0.0	1.0	3.400	150.0	0.0	1.0	3.319	−22.7	1.3	1.7	2.4	0.5	0.0	−21.1	−17.3	3.8	−18.1	3.0	−18.1	3.0
2FR4	C5:Y97	ccw	12.0	3.388	170.4	0.0	1.0	3.400	180.0	0.0	1.0	3.444	−22.7	1.3	0.0	2.4	0.1	−2.1	−29.6	−19.0	10.6	−20.2	9.5	−22.2	7.4
1L3S	C6:Y714	ccw	9.7	3.492	323.1	0.0	0.0	3.500	330.0	0.0	0.0	3.358	−22.7	0.1	7.3	1.0	0.5	0.0	−19.6	−14.3	5.2	−13.9	5.7	−13.9	5.7
2HHQ	C4:Y714	ccw	17.6	3.367	313.3	1.5	−1.0	3.400	300.0	1.5	−1.0	3.650	−22.7	1.3	8.5	9.4	4.0	−0.5	−11.7	−3.5	8.1	−0.8	10.8	−1.3	10.4
2HHV	C6:Y714	ccw	13.3	3.543	321.8	0.0	0.0	3.500	330.0	0.0	0.0	3.491	−22.7	0.1	7.3	1.0	0.1	−1.7	−18.5	−14.3	4.1	−14.3	4.1	−16.0	2.4
3G2D	C1i:R209b	cw	16.5	3.799	350.8	1.5	2.0	3.800	0.0	1.5	2.0	3.363	−57.3	10.4	10.6	21.4	7.3	3.3	−35.9	−14.9	21.0	−18.0	17.9	−14.6	21.3
3JR5	C7c:R112	cw	6.2	3.405	68.3	2.5	1.0	3.400	60.0	2.5	1.0	3.168	−57.3	1.3	8.1	10.9	2.6	0.0	−46.8	−37.0	9.8	−35.6	11.2	−35.6	11.2
3M4A	C11d:R186	cw	8.8	3.497	267.8	−3.0	0.0	3.500	270.0	−3.0	0.0	3.216	−57.3	3.1	0.7	56.1	3.5	0.0	2.0	2.6	0.6	3.0	1.0	3.0	1.0
3MIP	C−7c:R83	cw	13.6	3.374	281.7	−2.5	1.5	3.400	270.0	−2.5	1.5	3.307	−57.3	1.3	0.7	56.5	0.2	1.9	3.5	1.1	−2.4	0.1	−3.4	2.0	−1.5
3MR2	C4p:R382	cw	9.7	3.171	281.0	−2.5	1.0	3.200	270.0	−2.5	1.0	3.234	−57.3	0.0	0.7	55.3	0.3	0.0	−2.8	−1.3	1.4	−1.1	1.7	−1.1	1.7
3MX4	C10k:R169h	cw	14.7	3.493	264.2	−1.0	0.0	3.500	270.0	−1.0	0.0	3.329	−57.3	3.1	0.7	26.3	1.4	2.5	−25.1	−27.2	−2.1	−28.9	−3.8	−26.5	−1.3
3MX4	C10n:R169c	cw	2.5	3.237	262.0	−1.5	0.0	3.200	270.0	−1.5	0.0	3.097	−57.3	0.0	0.7	36.2	1.0	0.0	−18.7	−20.4	−1.7	−19.4	−0.6	−19.4	−0.6
1A1F	C3b:R174	ccw	8.9	3.399	271.5	−2.5	0.0	3.400	270.0	−2.5	0.0	3.196	−57.1	1.9	12.5	44.9	2.4	0.0	−5.5	2.2	7.7	2.8	8.3	2.8	8.3
2E42	C9c:R289	ccw	8.8	3.464	264.7	−2.5	2.5	3.500	270.0	−2.5	2.5	3.194	−57.1	4.0	12.5	53.9	3.9	0.0	1.8	13.3	11.5	13.3	11.4	13.3	11.4
2E43	C9c:R289	ccw	21.7	3.614	267.0	−1.5	2.0	3.600	270.0	−1.5	2.0	3.362	−57.1	6.7	12.5	37.6	3.5	9.9	−7.6	−0.2	7.4	−3.4	4.2	6.5	14.1
3GA6	C1h:R2209b	ccw	1.7	3.687	281.9	1.5	1.0	3.700	270.0	1.5	1.0	3.103	−57.1	9.6	12.5	6.8	12.1	0.0	−38.0	−28.2	9.9	−25.7	12.4	−25.7	12.4

PBD ID	Dimer		Measurements[2]					PES				$R_{1,eq}$	BE_{Best}	Deviation Effects[3]					BE_{Calc}[4]	Summation		Distance Dependent		Tilt Dependent	
			ω	R_1	α	$R_2(x)$	$R_2(y)$	R_1	α	$R_2(x)$	$R_2(y)$			$\Delta E(R_1)$	$\Delta E(\alpha)$	$\Delta E(R_2)$	$\Delta E(R_1,\omega)$	$\Delta E(\omega)$		BE_{Sum}	UD[5]	BE_{R1}	UD	BE_{Scan}	UD
3MGV	C12h:R259b	ccw	10.8	3.413	153.2	−3.0	−1.0	3.400	150.0	−3.0	−1.0	3.221	−57.1	1.9	17.6	49.0	2.2	6.1	4.5	11.4	6.9	11.7	7.3	17.8	13.4
3NDH	C5Ad:R171	ccw	28.8	3.920	99.6	−1.0	1.0	3.900	90.0	−1.0	1.0	3.455	−57.1	14.4	3.2	30.0	9.0	11.1	−6.7	−9.4	−2.8	−14.9	−8.2	−3.8	2.9
1BRN	G2a:F56		32.5	4.004	277.2	−0.5	1.0	3.800	30.0	−0.5	1.0	3.979	−25.3	5.3	0.1	4.5	0.0	6.3	−13.5	−15.5	−2.0	−20.7	−7.2	−14.4	−0.9
1F0V	G754:F120		35.6	4.127	90.9	−2.0	2.5	3.800	30.0	−1.5	1.5	4.054	−25.3	5.3	0.1	12.4	0.2	7.1	−3.4	−7.5	−4.1	−12.6	−9.2	−5.5	−2.1
1JB7	G9:F106		13.8	4.142	330.8	−0.5	−2.0	3.800	30.0	−0.5	−1.5	3.531	−25.3	5.3	0.1	3.0	7.9	1.8	−8.2	−17.0	−8.8	−14.4	−6.2	−12.6	−4.4
1NK7	G30:F710		25.5	4.173	63.5	−1.5	−1.0	3.800	0.0	−1.5	−1.0	3.812	−25.3	5.3	0.0	7.2	3.7	4.6	−14.2	−12.8	1.4	−14.4	−0.2	−9.7	4.4
1WTO	G103:F26		9.0	3.411	16.3	1.5	−0.5	3.400	30.0	1.5	−0.5	3.417	−25.3	0.0	0.1	6.5	0.0	0.0	−23.0	−18.7	4.3	−18.7	4.3	−18.7	4.3
2Z70	G10:F78		2.8	3.559	120.0	0.0	0.5	3.600	0.0	0.0	0.5	3.266	−25.3	1.9	0.0	1.3	2.6	0.0	−21.3	−22.1	−0.8	−21.3	0.0	−21.3	0.0
3KJP	G7:F31		3.0	3.202	174.2	0.5	−1.5	3.200	0.0	0.5	−1.5	3.272	−25.3	2.6	0.0	4.4	0.2	0.0	−23.5	−18.4	5.2	−20.7	2.81	−20.7	2.8
1RNB	G111:H102	Nd 2	4.3	3.450	202.0	0.5	−0.5	3.500	210.0	0.5	−0.5	3.173	−35.3	1.7	13.7	7.8	2.7	0.0	−21.4	−12.1	9.3	−11.1	10.3	−13.8	7.6
1RNB	G111:H102	Ne	4.3	3.450	274.0	0.5	−0.5	3.500	270.0	0.5	−0.5	3.336	−31.4	0.3	6.0	5.8	0.5	0.0	−21.8	−19.2	2.5	−19.0	2.7	−19.0	2.7
1RNB	G111:H102	(+)	4.3	3.450	274.0	0.5	−0.5	3.500	270.0	0.5	−0.5	3.118	−69.0	5.4	1.5	24.9	5.9	0.0	−34.1	−37.1	−3.0	−36.6	−2.5	−36.6	−2.5
3Q23	G16c:W129	1	9.5	3.552	72.4	0.0	−2.0	3.600	60.0	0.0	−1.5	3.458	−42.5	1.6	7.3	6.1	0.4	0.0	−24.5	−27.4	−2.9	−28.6	−4.1	−28.6	−4.1
3Q23	G16d:W129	1	8.3	3.520	71.4	0.0	−2.0	3.500	60.0	0.0	−1.5	3.424	−42.5	0.3	7.3	6.1	0.5	0.0	−24.4	−28.7	−4.4	−28.6	−4.2	−28.6	−4.2
3Q24	G16c:W129	1	8.6	3.516	70.7	0.0	−2.0	3.500	60.0	0.0	−1.5	3.433	−42.5	0.3	7.3	6.1	0.3	0.0	−25.3	−28.7	−3.4	−28.7	−3.4	−28.7	−3.4
3Q24	G16d:W129	1	7.9	3.566	69.9	0.0	−2.0	3.600	60.0	0.0	−1.5	3.413	−42.5	1.6	7.3	6.1	1.1	0.0	−24.7	−27.4	−2.7	−27.9	−3.2	−27.9	−3.2
1JB7	G2:Y103	cw	22.5	3.736	38.0	1.0	−0.5	3.700	30.0	1.0	−0.5	3.847	−32.8	2.6	6.5	5.5	0.8	5.2	−24.5	−18.1	6.4	−20.0	4.5	−14.8	9.7
1L5U	G4:Y714	cw	2.6	3.446	315.8	−1.0	−0.5	3.400	330.0	−1.0	−0.5	3.232	−32.8	0.0	8.2	1.8	1.8	0.0	−14.8	−22.8	−7.9	−21.0	−6.1	−21.0	−6.1
1NKC	G27:Y714	cw	12.7	3.529	319.4	−0.5	0.0	3.500	330.0	−0.5	0.0	3.545	−32.8	0.3	8.2	2.1	0.0	1.4	−18.7	−22.2	−3.5	−22.5	−3.8	−21.1	−2.4
1NKE	G6:Y714	cw	9.6	3.241	298.7	1.0	−1.5	3.200	300.0	1.0	−1.5	3.446	−32.8	3.5	3.4	8.6	3.0	0.0	−23.5	−17.4	6.1	−17.9	5.6	−17.9	5.6
3KJP	G12:Y223	cw	11.1	3.516	110.9	−1.0	0.0	3.500	120.0	−1.0	0.0	3.494	−32.8	0.3	0.0	1.8	0.0	0.6	−27.5	−30.7	−3.2	−30.9	−3.5	−30.3	−2.8
1JB7	G2:Y103	ccw	22.5	3.736	38.0	1.0	−0.5	3.700	30.0	1.0	−0.5	3.732	−33.4	4.1	9.0	3.4	0.0	5.1	−14.9	−17.0	−2.1	−21.0	−6.2	−16.0	−1.1
1L5U	G4:Y714	ccw	2.6	3.446	315.8	−1.0	−0.5	3.400	330.0	−1.0	−0.5	2.997	−33.4	0.0	0.0	5.8	6.2	0.0	−26.4	−27.6	−1.1	−21.4	5.0	−21.4	5.0
1NKC	G27:Y714	ccw	12.7	3.529	319.4	−0.5	0.0	3.500	330.0	−0.5	0.0	3.371	−33.4	0.8	0.0	2.3	1.0	−0.2	−30.6	−30.3	0.3	−30.1	0.6	−30.2	0.4
1NKE	G6:Y714	ccw	9.6	3.241	298.7	1.0	−1.5	3.200	300.0	1.0	−1.5	3.253	−33.4	2.2	2.0	7.7	0.0	0.0	−24.3	−21.5	2.8	−23.7	0.6	−23.7	0.6
3KJP	G12:Y223	ccw	11.1	3.516	110.9	−1.0	0.0	3.500	120.0	−1.0	0.0	3.311	−33.4	0.8	11.5	7.4	1.7	−1.1	−22.0	−13.6	8.4	−12.8	9.3	−13.8	8.2
3MGH	G11t:R549c	cw	9.1	3.514	190.3	0.5	−0.5	3.500	180.0	0.5	−0.5	3.058	−64.6	3.6	2.5	20.2	10.3	0.0	−39.6	−38.3	1.3	−31.6	8.1	−31.6	8.1
3MVA	G17e:R387o	cw	11.0	3.719	269.6	−3.0	−0.5	3.700	270.0	−3.0	−0.5	3.102	−64.6	9.4	0.1	14.5	14.7	2.8	−35.8	−40.7	−4.9	−35.3	0.5	−32.5	3.3
3OOL	G17c:R48	cw	11.5	3.054	269.9	−3.5	0.0	3.100	270.0	−3.5	0.0	3.115	−64.6	3.7	0.1	16.5	0.4	3.3	−41.5	−44.2	−2.7	−47.5	−6.0	−44.2	−2.7
3OOR	G11d:R88	cw	6.5	3.553	282.0	−3.5	1.0	3.600	270.0	−3.5	1.0	2.999	−64.6	6.5	0.1	14.0	13.1	0.0	−41.7	−44.1	−2.4	−37.5	4.2	−37.5	4.2

PBD ID	Dimer		Measurements[2]					PES				$R_{1,eq}$	BE_{Best}	Deviation Effects[3]					BE_{Calc}[4]	Summation		Distance Dependent		Tilt Dependent	
			ω	R_1	α	$R_2(x)$	$R_2(y)$	R_1	α	$R_2(x)$	$R_2(y)$			$\Delta E(R_1)$	$\Delta E(\alpha)$	$\Delta E(R_2)$	$\Delta E(R_1,\omega)$	$\Delta E(\omega)$		BE_{Sum}	UD[5]	BE_{R1}	UD	BE_{Scan}	UD
3PX7	G6c:R169	cw	30.6	3.574	106.8	2.0	0.0	3.600	120.0	2.0	0.0	3.554	−64.6	6.5	9.7	41.0	0.0	15.1	−3.4	−7.5	−4.1	−13.9	−10.5	1.2	4.6
3G00	G9h:R209b	ccw	13.9	3.363	64.5	0.5	3.0	3.400	60.0	0.5	3.0	3.169	−66.5	3.6	12.1	16.6	2.7	13.0	−50.0	−34.2	15.8	−35.1	14.9	−22.2	27.9
3GA6	G1f:R1209	ccw	8.8	3.480	29.2	1.5	1.0	3.500	30.0	1.5	1.0	3.053	−66.5	6.9	14.8	20.5	9.5	0.0	−26.4	−24.4	2.0	−21.8	4.6	−21.8	4.6
3JR5	G11b:R112	ccw	6.9	3.365	344.3	2.5	1.0	3.400	330.0	2.5	1.0	3.008	−66.5	3.6	6.1	36.1	7.3	0.0	−28.1	−20.7	7.3	−17.1	11.0	−17.1	11.0
3JTG	G107c:R331	ccw	16.1	3.354	147.5	−3.5	0.0	3.400	150.0	−3.5	0.0	3.220	−66.5	3.6	9.7	20.0	1.4	14.8	−55.6	−33.2	22.4	−35.4	20.2	−20.6	35.0
3MXB	G604e:R40	ccw	8.8	3.206	225.9	−3.5	1.0	3.200	240.0	−3.5	1.0	3.052	−66.5	0.0	15.9	16.0	1.8	0.0	−45.2	−34.7	10.5	−32.9	12.3	−32.9	12.3
3O1M	G4c:R161	ccw	38.0	3.939	289.3	−3.0	0.5	3.900	300.0	−3.0	0.5	3.723	−66.5	19.7	10.4	12.2	3.2	29.5	−46.9	−24.3	22.6	−40.7	6.2	−11.2	35.7
3NH1	G7g:E73c	(−)	23.5	4.020	119.7	2.5	1.0	4.000	120.0	2.5	1.0	3.091	−47.5	10.8	24.8	1.0	23.3	−8.7	−21.3	−10.8	10.5	1.7	23.0	−7.0	14.3
3NH1	G7g:E73c	cw	23.5	4.020	119.7	2.5	1.0	4.000	120.0	2.5	1.0	3.235	−31.0	10.2	22.5	18.6	12.5	1.6	0.1	20.3	20.3	22.6	22.5	24.1	24.1
3NH1	G7g:E73c	ccw	23.5	4.020	119.7	2.5	1.0	4.000	120.0	2.5	1.0	3.185	−30.2	7.5	14.9	8.8	15.1	0.5	−3.3	1.0	4.4	8.6	11.9	9.1	12.4
1JX4	T2:F37		5.8	3.603	189.0	1.5	−1.5	3.600	0.0	1.5	−1.5	3.544	−22.4	0.3	0.2	7.7	0.1	0.0	−14.8	−14.2	0.6	−14.4	0.4	−14.4	0.4
1QZG	T4c:F88		7.0	3.539	106.2	0.0	1.0	3.500	0.0	0.0	1.0	3.567	−22.4	0.0	0.2	3.9	0.0	0.0	−19.1	−18.3	0.8	−18.3	0.8	−18.3	0.8
1SXQ	T12c:F72		16.5	3.693	126.8	−0.5	0.0	3.700	0.0	−0.5	0.0	3.737	−22.4	1.2	0.2	1.0	0.1	3.0	−26.7	−20.0	6.7	−21.2	5.5	−18.2	8.5
1XJV	T2:F62		10.8	3.402	127.2	−1.0	0.0	3.400	0.0	−1.0	0.0	3.634	−22.4	0.5	0.2	0.3	2.6	1.9	−24.3	−21.4	3.0	−19.3	5.0	−17.5	6.8
2C62	T8:F77		3.3	3.607	46.7	1.5	−1.5	3.600	0.0	1.5	−1.5	3.500	−22.4	0.3	0.2	7.7	0.3	0.0	−14.9	−14.2	0.7	−14.2	0.7	−14.2	0.7
2ES2	T4:F17		3.9	3.647	147.2	−1.0	0.0	3.600	30.0	−1.0	0.0	3.509	−22.4	0.3	0.0	0.3	0.5	0.0	−20.8	−21.8	−1.0	−21.6	−0.8	−21.6	−0.8
2HAX	T5c:F17		8.9	3.532	85.6	0.0	0.0	3.500	30.0	0.0	0.0	3.600	−22.4	0.0	0.0	1.6	0.2	0.0	−20.7	−20.8	−0.1	−20.6	0.1	−20.6	0.1
2HAX	T4d:F27		5.9	3.601	96.7	−1.0	−0.5	3.600	30.0	−1.0	−0.5	3.545	−22.4	0.3	0.0	0.0	0.1	0.0	−24.6	−22.1	2.5	−22.3	2.3	−22.3	2.3
3JR5	T9:F114		13.5	3.482	47.2	1.5	−0.5	3.500	0.0	1.5	−0.5	3.683	−22.4	0.0	0.2	4.6	1.9	2.4	−18.4	−17.6	0.8	−15.7	2.6	−13.3	5.0
3KJP	T4:F62		4.6	3.474	124.5	−0.5	0.0	3.500	0.0	−0.5	0.0	3.522	−22.4	0.0	0.2	1.0	0.1	0.0	−25.5	−21.2	4.2	−21.2	4.3	−21.2	4.3
1A1H	T5:H149	Nd	12.7	3.385	279.1	−2.0	−0.5	3.400	270.0	−1.5	−0.5	3.416	−25.0	0.3	7.1	1.6	0.0	−0.1	−20.3	−15.9	4.3	−16.2	4.0	−16.3	4.0
1A1I	T5:H149	Nd	11.7	3.286	278.0	−2.0	−0.5	3.300	270.0	−1.5	−0.5	3.399	−25.0	1.7	7.1	1.6	0.5	−0.2	−20.2	−14.6	5.6	−15.8	4.4	−16.0	4.2
1A1J	T5:H149	Nd	12.1	3.218	278.8	−2.0	−0.5	3.200	270.0	−1.5	−0.5	3.406	−25.0	4.5	7.1	1.6	1.5	−0.2	−20.5	−11.8	8.8	−14.7	5.8	−14.9	5.7
1A1K	T5:H149	Nd	8.5	3.283	276.8	−2.0	−0.5	3.300	270.0	−1.5	−0.5	3.344	−25.0	1.7	7.1	1.6	0.1	0.0	−22.3	−14.6	7.7	−16.1	6.2	−16.1	6.2
1JK1	T5:H149	Nd	5.6	3.499	279.0	−1.5	−0.5	3.500	270.0	−1.5	−0.5	3.294	−25.0	0.0	7.1	1.6	1.1	0.0	−20.7	−16.3	4.5	−15.1	5.6	−15.1	5.6
2HAX	T3c:H29	Nd	17.6	3.798	74.9	0.5	−0.5	3.800	60.0	0.5	−0.5	3.532	−26.8	3.2	1.8	2.6	1.9	3.0	−20.1	−19.1	1.0	−20.5	−0.4	−17.4	2.7
1A1H	T5:H149	Ne	12.7	3.385	351.1	−2.0	−0.5	3.400	0.0	−1.5	−0.5	3.453	−26.8	0.0	6.7	2.6	0.2	1.8	−20.2	−17.5	2.7	−17.3	2.9	−15.5	4.7
1A1I	T5:H149	Ne	11.7	3.286	350.0	−2.0	−0.5	3.300	0.0	−1.5	−0.5	3.438	−26.8	0.7	6.7	2.6	1.1	1.6	−21.2	−16.8	4.4	−16.4	4.8	−14.8	6.4
1A1J	T5:H149	Ne	12.1	3.218	350.8	−2.0	−0.5	3.200	0.0	−1.5	−0.5	3.444	−26.8	2.8	6.7	2.6	2.8	1.7	−22.2	−14.8	7.5	−14.7	7.5	−13.0	9.2
1A1K	T5:H149	Ne	8.5	3.283	348.8	−2.0	−0.5	3.300	0.0	−1.5	−0.5	3.385	−26.8	0.7	6.7	2.6	0.5	0.0	−21.6	−16.8	4.8	−17.1	4.6	−17.1	4.6

PBD ID	Dimer		Measurements[2]					PES						Deviation Effects[3]					BE_Calc[4]	Summation		Distance Dependent		Tilt Dependent	
			ω	R_1	α	$R_2(x)$	$R_2(y)$	R_1	α	$R_2(x)$	$R_2(y)$	$R_{1,eq}$	BE_{Best}	$\Delta E(R_1)$	$\Delta E(\alpha)$	$\Delta E(R_2)$	$\Delta E(R_1,\omega)$	$\Delta E(\omega)$		BE_{Sum}	UD[5]	BE_{R1}	UD	BE_{Scan}	UD
1JK1	T5:H149	Ne	5.6	3.499	351.0	−1.5	−0.5	3.500	0.0	−1.5	−0.5	3.339	−26.8	0.2	6.7	2.6	0.8	0.0	−20.6	−17.4	3.2	−16.8	3.9	−16.8	3.9
2HAX	T3c:H29	Ne	17.6	3.798	2.9	0.5	−0.5	3.800	0.0	0.5	−0.5	3.499	−25.0	2.0	12.8	1.0	2.2	0.7	−8.3	−9.2	−0.9	−9.0	−0.7	−8.2	0.0
1A1H	T5:H149	(+)	12.7	3.385	351.1	−2.0	−0.5	3.400	0.0	−2.0	−0.5	3.432	−35.1	0.0	1.8	23.8	0.1	−1.1	−7.0	−9.5	−2.5	−9.4	−2.3	−10.4	−3.4
1A1I	T5:H149	(+)	11.7	3.286	350.0	−2.0	−0.5	3.300	0.0	−2.0	−0.5	3.421	−35.1	0.3	1.8	23.8	1.0	−1.0	−6.9	−9.2	−2.3	−8.5	−1.6	−9.5	−2.7
1A1J	T5:H149	(+)	12.1	3.218	350.8	−2.0	−0.5	3.200	0.0	−2.0	−0.5	3.425	−35.1	2.0	1.8	23.8	2.5	−1.1	−8.1	−7.4	0.7	−6.9	1.2	−8.0	0.2
1A1K	T5:H149	(+)	8.5	3.283	348.8	−2.0	−0.5	3.300	0.0	−2.0	−0.5	3.382	−35.1	0.3	1.8	23.8	0.5	0.0	−7.7	−9.2	−1.5	−9.0	−1.3	−9.0	−1.3
1JK1	T5:H149	(+)	5.6	3.499	351.0	−1.5	−0.5	3.500	0.0	−1.5	−0.5	3.347	−35.1	0.7	1.8	18.8	0.9	0.0	−10.6	−13.9	−3.3	−13.7	−3.1	−13.7	−3.1
2HAX	T3c:H29	(+)	17.6	3.798	74.9	0.5	−0.5	3.800	60.0	0.5	−0.5	3.491	−35.1	5.2	4.0	7.8	3.1	−1.1	−13.1	−18.1	−5.1	−20.3	−7.2	−21.3	−8.2
1TEZ	T7I:W286	1	13.4	3.241	186.9	−2.5	0.5	3.200	180.0	−1.5	0.5	3.505	−36.4	1.1	0.0	14.7	4.2	6.2	−20.3	−20.7	−0.4	−17.5	2.7	−11.4	8.9
2C62	T5:W89	1	9.6	3.470	142.4	−0.5	−0.5	3.500	150.0	−0.5	−0.5	3.377	−36.4	2.0	4.7	0.7	0.4	0.0	−31.5	−29.0	2.4	−30.6	0.8	−30.6	0.8
2C62	T16:W89	1	17.0	3.573	176.9	1.0	0.5	3.600	180.0	1.0	0.5	3.629	−36.4	4.0	0.0	6.7	0.2	9.0	−28.4	−25.7	2.7	−29.5	−1.1	−20.5	7.9
2OK0	T1:W50	1	5.7	3.441	209.4	1.5	0.5	3.400	210.0	1.5	0.5	3.243	−36.4	0.5	5.6	6.8	1.5	0.0	−26.8	−23.5	3.3	−22.5	4.3	−22.5	4.3
1UUT	T7:W29	2	14.4	3.914	226.2	0.0	−1.5	3.800	240.0	0.0	−1.5	3.662	−36.0	4.8	7.0	7.6	2.1	7.6	−19.6	−16.6	3.0	−19.3	0.3	−11.6	7.9
1UUT	T7d:W29	2	11.3	3.893	223.1	0.0	−1.5	3.800	210.0	0.0	−1.5	3.576	−36.0	4.8	7.2	7.6	3.2	5.5	−20.7	−16.4	4.3	−18.0	2.7	−12.5	8.2
1LAU	T3:Y90	cw	29.7	4.152	54.3	0.0	0.0	3.800	60.0	0.0	0.0	4.167	−26.1	1.9	1.2	0.3	0.0	13.5	−15.0	−22.7	−7.8	−24.6	−9.6	−11.1	3.9
2BAM	T1:Y150	cw	13.3	3.448	59.8	0.5	0.0	3.400	60.0	0.5	0.0	3.494	−26.1	1.0	1.2	0.0	0.1	3.3	−28.0	−23.9	4.1	−24.8	3.2	−21.5	6.5
1L3U	T4:Y714	cw	6.4	3.456	315.5	0.0	−0.5	3.500	330.0	0.0	−0.5	3.212	−26.1	0.0	5.8	1.3	1.7	0.0	−27.3	−19.0	8.2	−17.3	9.9	−17.3	9.9
1UUT	T9:Y65	cw	13.6	3.313	257.5	2.0	−0.5	3.300	270.0	1.5	−0.5	3.508	−26.1	3.4	0.4	6.6	1.5	3.6	−23.5	−15.7	7.8	−17.6	5.9	−14.0	9.5
2FR4	T6m:Y53	cw	9.7	3.256	117.7	−1.0	0.0	3.300	120.0	−1.0	0.0	3.346	−26.1	3.4	0.0	2.2	0.3	0.0	−22.2	−20.5	1.8	−23.6	−1.4	−23.6	−1.4
2W42	T1:Y118	cw	9.6	3.421	47.5	1.0	1.0	3.400	60.0	1.0	1.0	3.343	−26.1	1.0	1.2	7.5	0.2	0.0	−30.5	−16.5	14.1	−17.2	13.3	−17.2	13.3
3KJP	T9:Y161	cw	4.4	3.418	157.3	0.5	−1.0	3.400	150.0	0.5	−1.0	3.132	−26.1	1.0	2.1	3.2	2.2	0.0	−22.7	−19.9	2.8	−18.6	4.1	−18.6	4.1
1LAU	T3:Y90	ccw	29.7	4.152	54.3	0.0	0.0	3.800	60.0	0.0	0.0	4.199	−25.5	1.6	4.3	0.9	0.1	9.5	−10.8	−18.7	−7.9	−20.3	−9.5	−10.8	−0.1
2BAM	T1:Y150	ccw	13.3	3.448	59.8	0.5	0.0	3.400	60.0	0.5	0.0	3.591	−25.5	1.1	4.3	0.3	0.7	2.1	−23.3	−19.8	3.5	−20.2	3.1	−18.0	5.3
1L3U	T4:Y714	ccw	6.4	3.456	315.5	0.0	−0.5	3.500	330.0	0.0	−0.5	3.336	−25.5	0.0	1.2	0.2	0.4	0.0	−31.3	−24.1	7.1	−23.7	7.5	−23.7	7.5
1UUT	T9:Y65	ccw	13.6	3.313	257.5	2.0	−0.5	3.300	270.0	1.5	−0.5	3.604	−25.5	3.7	3.3	2.6	3.4	2.3	−19.5	−16.0	3.6	−16.2	3.3	−13.9	5.7
2FR4	T6m:Y53	ccw	9.7	3.256	117.7	−1.0	0.0	3.300	120.0	−1.0	0.0	3.457	−25.5	3.7	2.2	1.6	1.5	0.0	−20.7	−18.0	2.7	−20.2	0.5	−20.2	0.5
2W42	T1:Y118	ccw	9.6	3.421	47.5	1.0	1.0	3.400	60.0	1.0	1.0	3.455	−25.5	1.1	4.3	5.0	0.0	0.0	−19.3	−15.1	4.2	−16.1	3.1	−16.1	3.1
3KJP	T9:Y161	ccw	4.4	3.418	157.3	0.5	−1.0	3.400	150.0	0.5	−1.0	3.264	−25.5	1.1	0.8	1.2	0.7	0.0	−27.7	−22.4	5.3	−22.9	4.8	−22.9	4.8
2I06	T332c:R232	cw	5.6	3.376	313.8	−2.0	0.5	3.400	300.0	−2.0	0.5	3.185	−38.7	0.9	10.4	24.6	1.3	0.0	−13.1	−2.9	10.2	−2.5	10.6	−2.5	10.6
2XM3	T33k:R14d	cw	10.5	3.450	339.1	2.5	2.5	3.500	330.0	2.5	2.5	3.302	−38.7	2.5	3.7	10.8	0.8	8.3	−27.3	−21.8	5.5	−23.4	3.8	−15.2	12.1
3G73	T5c:R286b	cw	1.5	3.871	62.7	−2.5	1.0	3.900	60.0	−2.5	1.0	3.086	−38.7	10.8	4.1	24.3	12.6	0.0	−1.8	0.5	2.2	2.2	4.0	2.2	4.0

PBD ID	Dimer		Measurements[2]					PES				$R_{1,eq}$	BE_{Best}	Deviation Effects[3]					BE_{Calc}[4]	Summation		Distance Dependent		Tilt Dependent	
			ω	R_1	α	$R_2(x)$	$R_2(y)$	R_1	α	$R_2(x)$	$R_2(y)$			$\Delta E(R_1)$	$\Delta E(\alpha)$	$\Delta E(R_2)$	$\Delta E(R_1,\omega)$	$\Delta E(\omega)$		BE_{Sum}	UD[5]	BE_{R1}	UD	BE_{Scan}	UD
3KMD	T16f:R280c	cw	8.9	3.611	277.3	−2.0	0.0	3.600	270.0	−2.0	0.0	3.263	−38.7	4.7	10.4	27.8	3.6	0.0	−2.8	4.1	6.9	3.1	5.8	3.1	5.8
3LAJ	T12k:R58d	cw	25.7	4.063	301.6	−2.5	2.0	4.000	300.0	−2.5	2.0	3.668	−38.7	12.3	10.4	22.8	4.5	16.3	−5.7	6.8	12.5	−1.0	4.7	15.3	21.0
3LAP	T12j:R58b	cw	31.3	4.331	291.0	−2.5	2.0	4.000	300.0	−2.5	2.0	3.801	−38.7	12.3	10.4	22.8	7.1	17.9	−4.5	6.8	11.3	1.6	6.2	19.6	24.1
3MXB	T607v:R68r	cw	8.7	3.590	283.0	−1.0	1.5	3.600	270.0	−1.0	1.5	3.258	−38.7	4.7	24.5	13.1	3.4	0.0	−10.6	3.6	14.2	2.2	12.8	2.2	12.8
3NH1	T4e:R114b	cw	11.3	3.483	47.5	1.0	0.0	3.500	60.0	1.0	0.0	3.320	−38.7	2.5	4.1	1.9	0.9	8.8	−26.5	−30.3	−3.8	−31.8	−5.3	−23.0	3.5
2WT7	T4c:R244b	ccw	8.6	3.563	277.5	−2.5	1.5	3.600	270.0	−2.5	1.5	3.230	−33.9	5.5	4.9	19.9	4.0	0.0	−8.0	−3.6	4.4	−5.1	2.9	−5.1	2.9
2XE0	T502c:R30b	ccw	3.1	3.330	261.5	−1.0	2.5	3.300	270.0	−1.0	2.5	3.115	−33.9	0.0	4.9	10.0	2.0	0.0	−17.2	−19.0	−1.8	−16.9	0.2	−16.9	0.2
3MQ6	T12l:R31	ccw	12.2	3.364	266.9	−2.0	0.0	3.400	270.0	−2.0	0.0	3.305	−33.9	1.1	4.9	22.6	0.2	5.6	1.3	−5.2	−6.5	−6.1	−7.4	−0.5	−1.8
3MXA	T502c:R221	ccw	14.8	3.442	247.5	−1.5	2.0	3.400	240.0	−1.5	2.0	3.360	−33.9	1.1	1.0	15.7	0.4	6.8	−9.2	−16.0	−6.8	−16.8	−7.6	−10.0	−0.8
3MXB	T502c:R30b	ccw	9.1	3.258	262.8	−2.0	2.0	3.300	270.0	−2.0	2.0	3.241	−33.9	0.0	4.9	18.3	0.0	0.0	−18.2	−10.6	7.5	−10.6	7.5	−10.6	7.5
3ODH	T4h:R143f	ccw	8.4	3.302	153.4	−2.0	0.0	3.300	150.0	−2.0	0.0	3.227	−33.9	0.0	1.0	22.6	0.3	0.0	−10.2	−10.2	0.0	−9.9	0.4	−9.9	0.4
3PX7	T3c:R70	ccw	16.4	3.355	87.2	−0.5	2.0	3.400	90.0	−0.5	2.0	3.394	−33.9	1.1	0.1	8.8	0.1	7.4	−29.1	−23.8	5.3	−24.8	4.3	−17.4	11.7
3N1I	T3b:E122	(−)	5.3	3.308	225.3	−4.0	3.0	3.300	240.0	−4.0	3.0	2.982	−60.2	0.0	10.2	35.3	6.1	0.0	−16.2	−14.7	1.5	−8.6	7.6	−8.6	7.6
3N1I	T3b:E122	ccw	5.3	3.308	225.3	−4.0	3.0	3.300	240.0	−4.0	3.0	3.137	−32.0	0.5	7.9	19.7	1.2	0.0	−1.1	−4.0	−2.9	−3.2	−2.1	−3.2	−2.1
3N1I	T3b:E122	cw	5.3	3.308	225.3	−4.0	3.0	3.300	240.0	−4.0	3.0	3.019	−23.6	0.2	7.0	33.0	3.2	0.0	−5.3	16.6	22.0	19.6	24.9	19.6	24.9

Table G2. Fitting parameters for determining optimum R_1, and the effect of tilt and R_1 on the binding energy.

	Dimer		$R_{1,eq}$		$\Delta E(\omega)$			$\Delta E(R_1,\omega)$	
			a_1	a_2	c_1	c_2	c_3	b_1	b_2
A	D/E	cw	1.00E–02	3.000	–1.82E–03	0.22	–5.1	19.7	1.968
A	D/E	ccw	6.00E–03	3.050	3.30E–03	–0.08	–3.9	20.9	2.034
A	D/E	(–)	3.00E–03	3.050	1.08E–02	–0.62	–0.4	28.3	1.692
A	F		2.00E–02	3.340	–1.64E–03	0.31	–0.3	37.1	1.081
A	H	1	2.00E–02	3.100	–2.12E–04	0.28	–0.3	31.1	1.180
A	H	2	1.60E–02	3.150	–3.16E–03	0.41	–2.9	23.4	1.415
A	H	(+)	1.30E–02	3.080	–4.70E–03	0.37	–3.6	42.5	1.439
A	R	cw	2.40E–02	2.850	–1.78E–02	1.44	–8.2	30.6	1.971
A	R	ccw	2.40E–02	2.850	–1.54E–02	1.28	–6.9	52.5	1.256
A	W	1	2.30E–02	3.320	–4.24E–03	0.56	–4.5	40.3	1.146
A	W	2	2.60E–02	3.320	–7.00E–03	0.69	–4.3	53.9	0.917
A	Y	cw	2.90E–02	3.200	–9.01E–03	0.86	–6.4	32.6	1.197
A	Y	ccw	2.80E–02	3.180	–3.29E–03	0.61	–6.6	47.5	1.007
C	D/E	cw	1.00E–02	3.100	–5.70E–03	0.61	–4.1	20.6	1.533
C	D/E	ccw	1.00E–02	3.000	–4.02E–03	0.45	–4.2	24.6	1.640
C	D/E	(–)	7.00E–03	2.950	0.00E+00	0.12	–4.8	32.7	1.634
C	F		2.10E–02	3.440	–2.15E–03	0.22	–0.1	11.1	1.643
C	H	1	1.60E–02	3.250	–2.03E–03	0.28	–1.4	17.1	1.444
C	H	2	1.70E–02	3.200	0.00E+00	0.19	–1.5	17.4	1.483
C	H	(+)	1.30E–02	3.200	–6.02E–03	0.31	–0.1	32.7	1.422
C	R	cw	1.90E–02	3.050	–1.14E–02	0.83	–7.3	52.6	1.072
C	R	ccw	1.30E–02	3.080	–1.06E–02	0.70	–0.2	36.1	1.481
C	W	1	3.00E–02	3.150	–1.82E–03	0.39	–3.6	23.9	1.337
C	W	2	2.70E–02	3.200	–7.47E–04	0.29	–3.8	30.4	1.176
C	Y	cw	3.00E–02	3.150	–1.16E–03	0.33	–4.9	13.4	1.573
C	Y	ccw	3.70E–02	3.000	–5.24E–04	0.30	–5.6	24.5	1.203
G	D/E	cw	1.00E–02	3.000	0.00E+00	0.35	–6.7	20.1	1.973
G	D/E	ccw	1.00E–02	2.950	0.00E+00	0.27	–5.8	24.1	1.876
G	D/E	(–)	6.00E–03	2.950	3.03E–03	–0.14	–7.1	36.0	1.759
G	F		2.40E–02	3.200	0.00E+00	0.24	–1.6	25.9	1.312
G	H	1	1.30E–02	3.280	–2.79E–03	0.43	–2.0	24.4	1.356
G	H	2	1.70E–02	3.100	0.00E+00	0.30	–2.8	28.7	1.321
G	H	(+)	1.60E–02	3.050	–5.34E–03	0.34	–2.6	53.4	1.224
G	R	cw	2.30E–02	2.850	–1.53E–02	1.26	–9.2	31.9	1.843
G	R	ccw	2.30E–02	2.850	–7.80E–03	1.09	–0.7	42.3	1.500
G	W	1	2.70E–02	3.200	–1.16E–03	0.43	–3.5	42.6	1.139
G	W	2	3.00E–02	3.100	–5.68E–03	0.69	–5.2	42.2	1.157
G	Y	cw	3.10E–02	3.150	–5.43E–03	0.59	–5.2	26.8	1.399
G	Y	ccw	3.70E–02	2.900	–2.64E–03	0.63	–7.7	37.8	1.152
T	D/E	cw	1.30E–02	2.950	0.00E+00	0.27	–4.4	16.8	1.964
T	D/E	ccw	7.00E–03	3.100	4.25E–03	–0.11	–3.3	16.9	1.855
T	D/E	(–)	6.00E–03	2.950	3.81E–03	–0.18	–6.3	42.7	1.454
T	F		1.80E–02	3.440	0.00E+00	0.20	–0.3	18.6	1.364
T	H	1	1.60E–02	3.250	–2.00E–03	0.31	–1.8	16.4	1.542
T	H	2	1.70E–02	3.200	0.00E+00	0.16	–2.1	24.1	1.201
T	H	(+)	1.20E–02	3.280	4.50E–03	–0.13	–0.1	33.2	1.179
T	R	cw	2.40E–02	3.050	–1.16E–02	0.95	–0.5	44.0	0.974
T	R	ccw	2.10E–02	3.050	–4.33E–03	0.55	–0.4	19.3	1.816
T	W	1	3.40E–02	3.050	–8.59E–03	1.03	–6.1	44.7	1.012
T	W	2	2.80E–02	3.260	–9.48E–03	0.93	–3.8	75.1	0.729
T	Y	cw	4.10E–02	2.950	–7.69E–03	0.95	–7.9	67.9	0.702
T	Y	ccw	3.70E–02	3.100	–5.44E–03	0.68	–5.9	40.4	0.880